

出國報告（出國類別：國際會議）

第 18 屆環境系統科學及工程國際研討會
出國報告書

**(18th International Conference on
Environmental System Science and
Engineering)**

服務機關：行政院環境保護署

姓名職稱：梁淑婷薦任技正、李秋燕薦任科員

派赴國家：日本東京

出國期間：105 年 9 月 4 日至 105 年 9 月 8 日

報告日期：105 年 12 月 8 日

摘 要

近來隨著社會及經濟發展，我國在地狹人稠的天然條件限制、各種經濟、社會活動快速擴張下，環境負荷日趨沉重，面對環境系統諸多變遷及衝擊，須有完善保護方案之規劃及推動，始足以維護環境品質、保障人權；行政院環境保護署本於我國環境保護之最高行政機關，應瞭解現今國際環保科學及工程技術，爰派員出席第 18 屆環境系統科學及工程國際研討會(ICESSE 2016: 18th International Conference on Environmental System Science and Engineering)蒐集相關資料。

本署代表藉由參加本次國際研討會的互相討論，除了平日鑽研研究與查閱期刊論文所得知識，更能開闊自身眼界，瞭解國際研究趨勢與脈動，因而增進業務推廣動力與方向。

目 錄

壹、出國目的.....	1
貳、出國行程.....	2
參、第 18 屆環境系統科學及工程國際研討會.....	3
肆、心得及建議.....	10

附錄 1：論文摘要(全)

附錄 2：發表論文原文

附錄 3：新宿環境資訊學習中心活動簡章

壹、出國目的

近來隨著社會及經濟發展，我國在地狹人稠的天然條件限制、各種經社活動快速擴張下，環境負荷日趨沈重，面對環境系統諸多變遷及衝擊，須有完善保護方案之規劃及推動，始足以維護環境品質、保障人權；行政院環境保護署本於我國環境保護之最高行政機關，應瞭解現今國際環保科學及工程技術，爰派員出席第 18 屆環境系統科學及工程國際研討會(ICESSE 2016：18th International Conference on Environmental System Science and Engineering)以蒐集相關資料。

前述研討會舉辦單位為國際科學、工程與技術學會(WASET，World Academy of Science, Engineering and Technology)，於 2016 年 9 月 5 日至 9 月 6 日假日本東京成田機場東武酒店舉行，該研討會主要探討的主題包括環境問題解決及環境管理系統，屬於探討現今新興科技應用於環境系統工程之學術研討會，而本次參與發表之專家學者 20 餘人，來至日本、韓國、臺灣、中國大陸、馬來西亞、斯里蘭卡、泰國、土耳其、波蘭、德國、英國等。藉由參加本次國際研討會的互相討論，除了平日鑽研研究與查閱期刊論文所得知識外，更能開闊自身眼界，瞭解國際研究趨勢與脈動，因而增進業務推廣動力與方向。

貳、出國行程

活動日期	工作內容概要
9月4日	啟程：出發至日本千葉縣
9月5日	出席「第18屆環境系統科學及工程國際研討會」 主題：財經教育與經濟系統監控、社會與古文明、工業製程改良
9月6日	出席「第18屆環境系統科學及工程國際研討會」 主題：土木及電子材料改良、環境問題解決、環境管理系統
9月7日	整理會議資料
9月8日	返程，自日本返回台北

參、第 18 屆環境系統科學及工程國際研討會

研討會收錄論文領域涵蓋甚廣，除了經濟、歷史、社會人文領域外，土木材料改良、半導體製程優化、環境問題解決等技術性研究論文亦不少，發表研討會 2 天之議程、論文題目及作者列表如下：

9 月 5 日會議

論文題目	作者
Session I	Chair: Bożena Frączek, Atara Shrik
Usage of Internet Technology in Financial Education and Financial Inclusion by Students of Economics Universities	B. Frączek University of Economics in Katowice, Poland
Measuring Banking Systemic Risk Conditional Value-At-Risk and Conditional Coherent Expected Shortfall in Taiwan Using Vector Quantile GARCH Model	Ender Su, Kai Wen Wong, I-Ling Ju, Ya-Ling Wang National Kaohsiung First University of Science and Technology, Taiwan
Suitability Verification of Technological Project through Estimated Cost and Period Information by Technology Development Stage	Bong-Goon Seo, Do-Hyung Park, Daeheon Choi, Seung-Pyo Jun Kookmin University, Korea, Republic Of
Prevention of Ragging and Sexual Gender Based Violence (SGBV) in Higher Education Institutions in Sri Lanka	Anusha Edirisinghe University of Kelaniya, Sri Lanka
The Two Sides of Coin of Peer Review and Its Effects on Prospective Mathematics Teachers' Insights regarding Mathematical Proofs	Ilana Lavy, Atara Shriki Yezreel Valley College, Israel
Nurturing Students' Creativity through Engagement in Problem Posing and Self-Assessment of Its Development	Atara Shriki, Ilana Lavy Oranim Academic College of Education, Israel
Pedagogical Effects of Using Workbooks in English Classes for the TOEIC Test: A Study on ESL Learners in Japanese Colleges	Mikako Nobuhara Tokyo Metropolitan College of Industrial Technology, Japan

Social Support in Perception of the Youth with Cerebral Palsy from Migrating Families	Anna Gagat Matuła
Session II	Chair: Jay Prakash Singh, Riad Benelmir
Analytical Model for Columns in Existing Reinforced Concrete Buildings	Chang Seok Lee, Sang Whan Han, Girbo Ko, Debbie Kim Hanyang University, Korea, Republic Of
On Quasi Conformally Flat LP-Sasakian Manifolds with a Coefficient α	Jay Prakash Singh Mizoram University, India
Mixed Integer Programming-Based One-Class Classification Method for Process Monitoring	Younghoon Kim, Seoung Bum Kim Korea University, Korea, Republic Of
Adaptive Process Monitoring for Time-Varying Situations Using Statistical Learning Algorithms	Seulki Lee, Seoung Bum Kim Korea University, Korea, Republic O
Improved Classification Procedure for Imbalanced and Overlapped Situations	Hankyu Lee, Seoung Bum Kim Korea University, Korea, Republic Of
Feature Evaluation Based on Random Subspace and Multiple-K Ensemble	Jaehong Yu, Seoung Bum Kim Korea University, Korea, Republic Of
Process Monitoring Based on Parameterless Self-Organizing Map	Young Jae Choung, Seoung Bum Kim Korea University, Korea, Republic Of
Asynchronous Sequential Machines with Fault Detectors	Seong Woo Kwak, Jung-Min Yang Kyungpook National University, Korea, Republic Of
Implemented Cascade with Feed Forward by Enthalpy Balance Superheated Steam Temperature Control for a Boiler with Distributed Control System	Kanpop Saion, Sakreya Chitwong King Mongkut's Institute of Technology Ladkrabang, Thailand
An Indoor Guidance System Combining Near Field Communication and Bluetooth Low Energy Beacon Technologies	Rung-Shiang Cheng, Wei-Jun Hong, Jheng-Syun Wang, Kawuu W. Lin National Kaohsiung University of Applied Sciences, Taiwan
CertifHy: Developing a European Framework for the Generation of Guarantees of Origin for Green Hydrogen	Frederic Barth, Wouter Vanhoudt, Marc Londo, Jaap C. Jansen, Karine Veum, Javier Castro, Klaus Nürnberger, Matthias Altmann Hinicio, Belgium
Adsorption Cooling Using Hybrid Energy Resources	R. Benelmir, M. El Kadri, A. Donnot, D. Descieux University of Lorraine, France

9月6日會議議程

論文題目	作者
Session III	Chair: Oliver Kinnane, Yue Yongli
Judging Restoration Success of Kamisaigo River Japan	Rita Lopa, Yukihiro Shimatani Kyushu University
Acoustic Absorption of Hemp Walls with Ground Granulated Blast Slag	Oliver Kinnane, Aidan Reilly, John Grimes, Sara Pavia, Rosanne Walker Queens University Belfast, United Kingdom
Use of Geometrical Relationship in the Ancient Vihara Housing Reclining Buddha Remains of Thailand's Kamphaeng Phet World Heritage Site	Vacharee Svamivastu King Mongkut's Institute of Technology Ladkrabang, Thailand
Free Vibration Analysis of Conical Helicoidal Rods Having Elliptical Cross Sections Positioned in Different Orientation	Merve Ermis, Akif Kutlu, Nihal Eratlı, Mehmet H. Omurtag Istanbul Technical University, Turkey
Static and Dynamic Analysis of Hyperboloidal Helix Having Thin Walled Open and Close Sections	Merve Ermis, Murat Yılmaz, Nihal Eratlı, Mehmet H. Omurtag Istanbul Technical University, Turkey
Accurate Algorithm for Selecting Ground Motions Satisfying Code Criteria	S. J. Ha, S. J. Baik, T. O. Kim, S. W. Han Hanyang University, Korea, Republic Of
Effect of Bamboo Chips in Cemented Sand Soil on Permeability and Mechanical Properties in Triaxial Compression	Sito Ismanti, Noriyuki Yasufuku Kyushu University, Japan
Study of Geotechnical Characteristics of Miocene Marl in the Region of Medea North-South Highway, Algeria	Yue Yongli, M. H. Aissa The First Highway Consultants Co. Ltd., China
Session IV	Chair: Yoshio Kobayashi, Szu-Hua Wang
Effect of Surface-Modification of Indium Tin Oxide Particles on Their Electrical Conductivity	Y. Kobayashi, T. Kurosaka, K. Yamamura, T. Yonezawa, K. Yamasaki Ibaraki University, Japan
Bimetallic Cu/Au Nanostructures and Bio-Application	Si Yin Tee Institute of Materials Research and Engineering, Singapore

Characterization of Bacteria by a Nondestructive Sample Preparation Method in a TEM System	J. Shiue, I. H. Chen, S. W. Y. Chiu, Y. L. Wang Academia Sinica, Taiwan
Study of Linear Generator for Vibration Energy Harvesting of Frequency more than 50Hz	Seong-Jin Cho, Jin Ho Kim Yeungnam University, Korea, Republic Of
Ergonomics Shallow Recharge Well for Sustainable Ground Water Resources	Lilik Sudiajeng, Wiraga Wayan, Lanang Parwita I Gusti Bali State Polytechnic
Discovery of New Inhibitors for Colorectal Cancer Treatment	Kai-Cheng Hsu, Tzu-Ying Sung, Jinn-Moon Yang Graduate Institute of Cancer Biology and Drug Discovery, Taipei Medical University, Taiwan
The Effects of Weather Events and Land Use Change on Urban Ecosystems: From Risk to Resilience	Szu-Hua Wang Chinese Culture University, Taiwan
Comparative Growth Rates of <i>Treculia africana</i> Decne: Embryo in Varied Strengths of Murashige and Skoog Basal Medium	Okafor C. Uche, Agbo P. Ejiofor, Okezie C. Eziuche University of Nigeria, Nigeria
Inhibitory Effect of Lactic Acid Bacteria on Uropathogenic <i>Escherichia coli</i> -Induced Urinary Tract Infections	Cheng-Chih Tsai, Yu-Hsuan Liu, Cheng-Ying Ho, Chun-Chin Huang Hungkuang University, Taiwan
Anti-Obesity Effect of <i>Cordyceps militaris</i> Fermented Black Rice	Chih-Hung Liang, Jung-Jung Chen, Shen-Shih Chiang National Chung Hsing University, Taiwan

本報告僅挑選數篇論文進行研讀後，摘要如下：

(一) 日本九州福岡縣福津市上西鄉川(Kamisaigo River)水岸活化(Judging Restoration Success of Kamisaigo River Japan)

上西鄉川長 880 公尺，屬日本第 2 級河川，流經國道 3 號後與西鄉川匯流。上西鄉川部分河段無植被、無昆蟲、河岸河床皆由水泥覆蓋，河面不寬、坡度陡峭、常年流量低，下雨時氾濫頻繁，親水性十分低，附近居民及孩童無法接近河川遊玩或進行水上活動，居民與河川之關係盪然無存。

有鑑於此，日本政府以洪氾控制、復育河川、恢復居民親水關係三大目標，委託九州大學活化水岸；九州大學於西元 2009 年著手開始對上西鄉川進行復育前評估，當時調查到河中有 7 種本土魚類，西元 2010 年起開始選取 6 處河段、總面積 326 公頃進行無曲徑直流、人工格條加曲徑、僅有曲徑、1 公尺大岩石加曲徑、小堰加曲徑、增加淺灘降低河床坡度等不同工法來復育上西鄉川，並以魚群種類及數量作為生態指標來評估各工法的復育程度；結果發現，河道改直取彎、消除河岸水泥鋪面改種水草、於河道中設置小堰、河床鋪設岩石的方式，復育效果最佳，復育後河中本土魚類增至 11 種。

九州大學先以景觀模型讓河川管理單位（政府）及當地居民瞭解未來復育後的河川模擬全貌，並由三方（政府、居民、執行單位）組成工作小組，召開超過 40 場次諮商討論會議，不斷讓各界提供意見、參採可行意見調整作法，終於在西元 2015 年宣告復育成功。現階段上西鄉川已恢復昔日魚蝦悠游、蟲鳥飛翔、綠草如茵之景象，河川魚種數量調查仍持續進行，亦提供親水環境教育予當地中、小學生參與，工作小組並未因復育成功而解散，現仍定期以最優水岸活化為目標運作著。

(二) 發展歐洲綠色氫氣源頭保證制度(CertifHy: Developing a European Framework for the Generation of Guarantees of Origin for Green Hydrogen)

氫氣在交通、能源、石化工業等部門的低碳經濟中扮演重要的角色，然而，大眾卻認為氫氣的製造與使用，僅在對自然資源衝擊最小且溫室氣體減量大於傳統燃料的情況下，才有意義。由歐洲主要天然氣公司、化工廠、能源單位、汽車工廠等工業領導者支持的 CertifHy 計畫有 2 大目標：(1)定義可被廣泛接受的綠色氫氣，(2)為歐洲建構一個可執行且穩固的綠色氫氣源頭保證制度。

CertifHy 計畫可分為 6 個工作程序：(1)綜觀市場上綠色氫氣:驗證歐洲工業及新能源的未來趨勢、趨動者及市場評估。(2)定義綠色氫氣:採用逐步諮詢法(step-by-step consultation approach)，在歐洲取得綠色氫氣的共識。(3)檢視現存源頭保證與綠色氫氣之相互關係與平臺。(4)定義綠色氫氣源頭保證制度，包含技術規範、標準、契約並進行影響評估。(5)設定歐洲綠色氫氣源頭保證制度的發展期程，並在結案前，作為重要結果展示給支持者及股東瞭解。(6)定義綠色氫氣為由再生資源所產出的氫氣，即 CertifHy 低溫室氣體排放的氫氣。再生資源產出的氫氣是能源消耗的產品。CertifHy 低溫室氣體排放的氫氣低於定義中的 CertifHy 低溫室氣體排放閾值，即 $36.4\text{gCO}_2\text{eq/MJ}$ ，也不超過天然氣的排放密度 $91.0\text{gCO}_2\text{eq/MJ}$ 。

(三) 土地利用與氣候事件變化對都市生態系統之影響：從風險到調適(The Effects of Weather Events and Land Use Change on Urban Ecosystems: From Risk to Resilience)

都市生態系是一個極為複雜、富含天然資源、人類消耗資源的場所，都市發展對都市生態的影響極鉅，而土地利用方式亦闡述了人類活動與環境因子之間的互動，西元 2014 年 IPCC 會議已揭露人類活動及都市化是造成氣候變遷的主要因

素，因此風險評估及恢復分析是都市系統因應氣候變遷的關鍵。本研究以大臺北地區颱風降雨量之風險評估及恢復分析為起點，整合都市空間規劃，以永續發展為目的，評析都市空間規劃內容，包含都市計畫、運輸計畫、環境計畫、人口活動、營建分配等，發現皆會影響都市的發展。

(四) 利用向量定性GARCH模式分析臺灣銀行的赤字風險(Measuring Banking Systemic Risk Conditional Value-At-Risk and Conditional Coherent Expected Shortfall in Taiwan Using Vector Quantile GARCH Model)

利用 GARCH 模式分析 22 個臺灣本地銀行及 21 個外國銀行在西元 2002 年 5 月 17 日至西元 2013 年 12 月 13 日間的股價波動，所得結論為臺灣本地銀行赤字風險較外國銀行低，而赤字風險最高為歐洲地區銀行。

(五) 斯里蘭卡高等教育機構性騷擾與性暴力防範(Prevention of Ragging and Sexual Gender Based Violence (SGBV) in Higher Education Institutions in Sri Lanka)

性別暴力在斯里蘭卡高等教育機構是很常見的社會現象，顯然已成為大學校園中隱藏的犯罪行為，本研究著重於評析校園系統中性騷擾與性暴力防範方法，同時闡述國家法律及政策在高等教育機構性暴力防範所遭遇的窘境；根據西元 2016 年調查訪談 Kelaniya 大學一年級女生所得結果，建議 Grant 大學設立性暴力防治委員會；建議之後，Grant 大學已擬訂長期及短期緊急實施方案，並成立線上申訴中心，此一防護網亦有警察單位、校警及警惕委員會參與。

(六) 為永續地下水資源設計的人工補注淺井(Ergonomics Shallow Recharge Well for Sustainable Ground Water Resources)

本研究計畫始於西元 2013 年印尼巴里島 Denpasar Regency 地區，目的在於設

計一個可以保護地下水資源的人工補注家用或工業用水井。Denpasar Regency 地區的西北方近年快速發展的觀光產業，使得該區人口密度逐漸上升到極高程度，土地使用的改變造成土壤涵容雨水量降低，同時也減弱了居民保護天然資源及地下水資源的意識；研究團隊為解決此地下水危機，依當地水力學及土壤特性所設計的人工補注家用井及社區水井都必須考量環境友善、能源效率、土地取得，且配有過濾設備及沈澱池以符合地下水水質標準。

肆、心得及建議

1. 此次出席論文發表研討會，除吸收到環境工程及管理的新穎技術外，對於工業製程改善、建築材料改良、微生物應用、疾病控制等研究領域亦有涉略；來自斯里蘭卡的 E.A.D. Anusha Edirisinghe 博士談到，在她國家裡，超過 30% 女大學生在孩童時期，曾遭受到生理及心理方面的性別暴力，雖然在她的社會文化中，性別不平等是常見的社會現象，卻已造成嚴重的社會問題，因此斯里蘭卡民主社會主義共和國已立法推動性別平等，並為該政策出版規劃文件及執行成果；慶幸自己處在臺灣性別平等的社會，也建議我國各機關推動性別平等推動計畫及成果，亦可在機關網路上公開，以提升資訊透明度。
2. 本次研討會上臺報告者以大學研究所學生居多，摻雜數位民間業者及學校教授，口頭(Oral)報告時間為 15 分鐘，張貼論文(e-post)報告時間為 5 分鐘，是一個論文發表、訓練英文演講的良好平臺，建議本署同仁今後倘有業務資料欲於國際發表，可將 WASET(World Academy of Science, Engineering and Technology Conference Program) 相關會議納入考量。

3. 研討會結束次日，整理會議資料之餘，利用時間參訪附近社區，於中央公園意外發現「新宿環境情報學習中心」，性質類似新宿區區民活動中心，係由市民、民間團體、事業者及行政部門聯手成立，提供相關環境情報資訊及辦理環境教育學習活動，該中心定期舉辦各類與環境有關的學習課程，有專題講座，園藝休憩，創意發明，彩繪攝影等等相關活動，提供該區市民學習機會，間接擴大環境教育成效。



圖 1 與會者大合照



圖 2 本署代表人員與主辦單位工作人員合影



圖 3 論文發表者 1

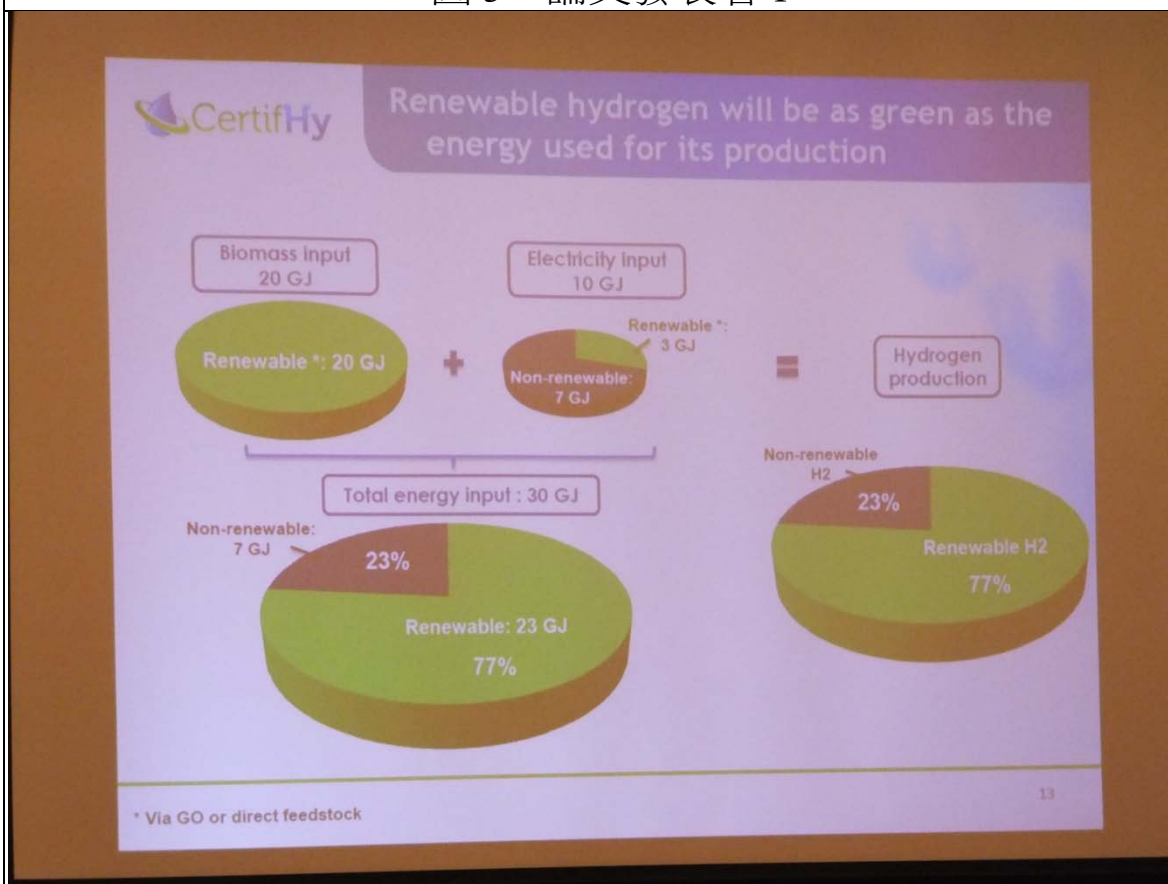


圖 4 論文發表簡報



圖 5 論文發表者 2



圖 6 研討會與會情形



圖 7 新宿環境情報學習中心



圖 8 活動成果



圖 9 活動訊息



圖 10 學習情報及相關資訊



圖 11 學習成果展示



圖 12 學習成果展示



圖 13 學習成果展示



圖 14 公園萬紫千紅綠蔭盎然

A Method of Improving Out Put Using a Feedback Supply Chain System: Case Study Bramlima

S. A Danji, V. Moleke

Abstract— The increase of globalization is a very important part of today's changing environment and due to this, manufacturing industries have to always come up with methods of continuous improvement of their manufacturing methods in order to be competitive, without which may lead them to be left out of the market due to constant changing customers requirement. Due to this, the need be an advance supply chain system which prevent a number of issues that can prevent a company from being competitive. In this work, we developed a feedback control supply chain system which streamline the entire process in order to improve competitiveness and the result shows that when applied in different geographical area, the output varies.

Keywords— Globalization, Supply chain, Improvement, Manufacturing.

S. A Danji, is with the Tshwane University of Technology, Main campus currently doing his Phd in Industrial Engineering

V. Moleke is with the Tshwane University of Technology, Main campus e-mail: malijoneskw@yahoo.com.

A Review of Manufacturing System Supply Chain Using a Fish Bone and Value Stream Mapping to Reduce Disruption and Improve Productivity: Case Study Vitro

V. Moleke, J. Temba

Abstract— Now our days, manufacturing systems are becoming very complicated due to a number of unforeseen supply chain disruption that prevent manufacturing organizations from realizing their actual or expected out-put in goods and services. Due to this, the need to be a method of overcoming this unforeseen circumstance. The production operation is subjected to a grate number of issues that need to be address, we are going to apply a number of Industrial engineering techniques which includes a fish bone diagram and value stream mapping in order to minimize the supply chain disruption and improve the productivity out. According to our result, it show that they are a number of issues that cause supply chain disruptions which includes, machine breakdown, employees absenteeism and delay of raw material supply.

Keywords—Supply chain; disruption; unforeseen; productivity; manufacturing.

A Study of Challenges Faced and Support Systems Available for Emirati Student Mothers Post-Childbirth

Martina Dickson, Lilly Tennant

Abstract—The young Emirati female university students of today are the first generation of women in the UAE for whom higher education as become not only a possibility, but almost an expectation. Young women in the UAE today make up around 77% of students in higher education institutes in the country. However, the societal expectations placed upon these women in terms of early marriage, child-bearing and rearing are similar to those placed upon their mothers and grandmothers in a time where women were not expected to go to university. A large proportion of female university students in the UAE are mothers of young children, or become mothers whilst at the university. This creates a challenging situation for young student mothers, where two weeks' maternity leave is typical across institutions. The context of this study is in one such institution in the UAE. We have employed a mixed method approach to gathering interview data from twenty mothers, and survey data from over one hundred mothers. The main findings indicate that mothers have strong desires for their institution to support them more, for example by the provision of nursery facilities and resting areas for new mothers, and giving them greater flexibility over course selections and schedules including the provision of online learning. However, the majority felt supported on a personal level by their tutors. The major challenges which they identified in returning to college after only two weeks' leave included the inevitable health and lack of sleep issues when caring for a newborn, struggling to catch up with missed college work and handling their course load. We also explored the women's' home support systems which were provided from a variety of extended family, spouses and paid domestic help.

Keywords—student mothers, challenges, supports, United Arab Emirates

Corresponding Author

Martina Dickson from Emirates College for Advanced Education,
United Arab Emirates
e-mail: mdickson@ecae.ac.ae

Accurate Algorithm for Selecting Ground Motions Satisfying Code Criteria

S. J. Ha, S. J. Baik, T. O. Kim, S. W. Han*

Abstract—For computing the seismic responses of structures, current seismic design provisions permit response history analyses (RHA) that can be used without limitations in height, seismic design category, and building irregularity. In order to obtain accurate seismic responses using RHA, it is important to use adequate input ground motions. Current seismic design provisions provide criteria for selecting ground motions. In this study, the accurate and computationally efficient algorithm is proposed for accurately selecting ground motions that satisfy the requirements specified in current seismic design provisions. The accuracy of the proposed algorithm is verified using single-degree-of-freedom systems with various natural periods and yield strengths. This study shows that the mean seismic responses obtained from RHA with seven and ten ground motions selected using the proposed algorithm produce errors within 20% and 13%, respectively.

Keywords— Algorithm, Ground motion, Response history analysis, Selection.

I. INTRODUCTION

Current seismic design provisions provides analysis procedures for all seismic design categories: equivalent lateral force analysis, modal response spectrum analysis, and linear and nonlinear response history analyses [1-3]. The equivalent lateral force analysis is permitted only for regular buildings with their heights within a specified limit and assigned as low seismic performance categories (SDC). Where the equivalent lateral force analysis cannot be used for the seismic design of a building because of its structural irregularity, high SDC and height, modal response spectrum analyses and response history analyses can be used.

The response history analysis can produce accurate seismic demands on structures with actual or simulated ground motions. The accuracy of response history analyses strongly depends on analytical models and ground motions used for analyses. According to ASCE 7-10 [1], appropriate acceleration histories for a response history analysis shall be selected and modified from records of events having magnitudes, fault distance, and source mechanism that are consistent with those that control the maximum considered

earthquake.

Araújo et al. [4] evaluated accuracy of ground selection procedures provided in various seismic provisions such as Eurocode 8 and ASCE 41-13 [2-3]. It was shown that higher number of ground motion records were required for ASCE 41-13 [4] selection procedure to compute mean structural responses, which was typically equal or greater than 10 and depends on the type of seismic action and performance objective. They also reported that the estimation of robust mean seismic demands was uncertain and depended on the ground motion selection and scaling methods adopted, and the use of the additional control of the spectral mismatch in ground motion selection improved the accuracy in predicting seismic response demands on structures.

Recently, many studies have focused on developing accurate and efficient methods developed for selecting ground motions that match a target response spectrum [5-6]. For selecting a set of ground motions that best match a target response spectrum, all possible combinations of ground motions in a ground motion library can be considered [5]. However, it requires excessive computation, particularly when the number of ground motions in a library is large. A procedure for selecting ground motions matching a target response spectrum mean and variance was first developed by Kottke and Rathje [5]. This pioneering procedure first selects ground motions that best match a target response spectrum mean, and subsequently applies individual scaling factors on the selected ground motions to match a target response spectrum variance. However, this technique does not easily scale to work with large ground motion data sets, and cannot account for the correlations of response spectral values at different periods, which are the characteristic property of ground motions.

A simulation-based selection procedure was developed by Jayaram et al. [6]. These procedures can be used for the selection of both scaled and unscaled ground motions. However, a unique set of ground motions cannot be obtained using a simulation-based selection methods since subroutines require random number generation, which may affect the results of RHA for a structure.

The objective of this study is to propose a method for accurately selecting and scaling ground motions that is applicable to the selection criteria specified in ASCE 7-10 [1]. With the proposed selection method, this study is to verify the accuracy of ground motions selected in compliance with ASCE 7-10 [1] selection criteria. For this purpose, nonlinear response history analyses are conducted with various single degree of

S. J. Ha is with the department of Architectural Engineering, Hanyang Univ., Seoul, Korea (e-mail: hasz2233@gmail.com).

S. J. Baik is with the department of Architectural Engineering, Hanyang Univ., Seoul, Korea (e-mail: baektjdwls227@gmail.com).

T. O. Kim is with the department of Architectural Engineering, the Hanyang Univ., Seoul, Korea (e-mail: tokim27@gmail.com).

S. W. Han is with the department of Architectural Engineering, the Hanyang Univ., Seoul, Korea (corresponding author to provide phone: +82-2-2220-0566; e-mail: swhan@hanyang.ac.kr).

freedom (SDF) systems.

II. ASCE 7-10 CRITERIA FOR GROUND MOTION SELECTION

In Chapter 16 of ASCE 7-10 [1], ground motion selection criteria are specified for conducting the response history analyses of structures. The minimum number of ground motions used for response history analyses is three, which can be either recorded or simulated ground motions.

For two dimensional analyses, the ground motions shall be scaled to such that the average value of 5% damped response spectra for a set of ground motions is not less than the design (target) response spectrum for the site for periods ranging from $0.2T_n$ to $1.5T_n$ where T_n is the fundamental period of a structure. For three dimensional analyses, ground motions consist of pairs of appropriate horizontal ground motion components. For each pair of horizontal ground motion components, a square root of the sum of the squares (SRSS) spectrum shall be constructed by taking the SRSS of the 5% damped response spectra for the scaled components where an identical scale factor is applied to both components. Each pair of motions shall be scaled in the period range from $0.2T_n$ to $1.5T_n$ such that the average of the SRSS spectra does not fall below the target response spectrum.

This study focuses on ground motion selection criteria for two dimensional analyses. According to Section 16.1.4 of ASCE 7-10 [1], if fewer than seven ground motions are used in analyses, design response demands shall be taken as the maximum values of response demands over all ground motions. If at least seven ground motions are used, the design response

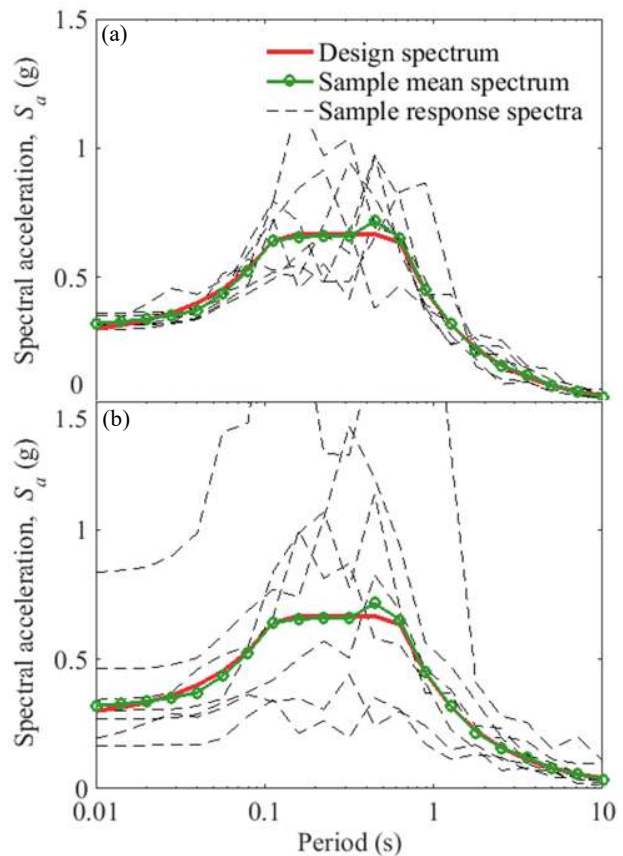


Fig. 1 Design spectrum and sample response spectra of seven ground motions calibrated with different scaling factors demands are permitted to be taken as the average value of response demands over all ground motions.

It is worthwhile noting that scaling procedure provided in Section 16.1.3.1 of ASCE 7-10 [1] does not insure a unique scaling factor for individual selected ground motions. Fig. 1 shows individual and mean spectra of three sets of seven ground motions selected and scaled to match a design (target) response spectrum according to the selection criteria in ASCE 7-10 [1]. As seen in Fig. 1(a)-(b), different combinations of scaling factors are used for ground motions of the two sets. The dispersion in response spectra for individual sets differs significantly even though their mean response spectra are similar. Therefore, unique and reliable analyses results may not be expected using ground motions selected according to selection criteria provided in ASCE 7-10 [1]. Moreover, whenever ground motions are selected using the ASCE 7-10 [1] criteria, a different set of ground motions are selected in each trial. It is also difficult to guarantee the accuracy of selection results.

III. GROUND MOTION SELECTION ALGORITHMS

In this study, an accurate and efficient method is proposed for selecting ground motions that satisfy the criteria specified in ASCE 7-10 [1]. As a first step of selection process, all ground motions in a library are scaled to match a target response spectrum. It is noted that scaling ground motions are permitted

in ASCE 7-10 [1]. However, if scaling ground motions are not allowed, this process can be skipped. A scaling factor (s) for an individual ground motion can be easily determined without iterations using (1) and (2) [10].

$$\mu_{\Delta} = \frac{1}{n_p} \sum_{i=1}^{n_p} \Delta_i = \frac{1}{n_p} \sum_{i=1}^{n_p} [\ln S_a^{\text{target}}(T_i) - \ln S_a(T_i)] \quad (1)$$

$$s = \exp(\mu_{\Delta}) \quad (2)$$

where $\ln S_a^{\text{target}}(T_i)$ and $\ln S_a(T_i)$ are the logarithmic 5% damped target and sample response spectra at period T_i , respectively, and n_p is the number of periods in a given period range. In this study, a period range between $0.2T_n$ and $1.5T_n$ is used according to Section 16.1.3.1 of ASCE 7-10.

Fig. 2(a) shows the response spectra of a ground motion before and after scaling. Fig. 2(b) shows the response spectra of 184 scaled ground motions. The dispersion in the response spectra of scaled ground motions (Fig. 2(b)) is much less than that in the response spectra of un-scaled ground motions.

According to ASCE 7-10 [1], if fewer than seven ground motions are used in analyses, the seismic response demands should be taken as the maximum value. The minimum number of ground motions is specified as three.

In this proposed procedure, a desired number of ground motions are sequentially selected for a library with scaled ground motions, which best match a target response spectrum. The fitness between a target and individual spectra is measured using the sum of squared error (SSE) calculated with (3).

$$SSE = \sum_{i=1}^{n_p} [\ln S_a^{\text{target}}(T_i) - \ln s \times S_a(T_i)]^2 \quad (3)$$

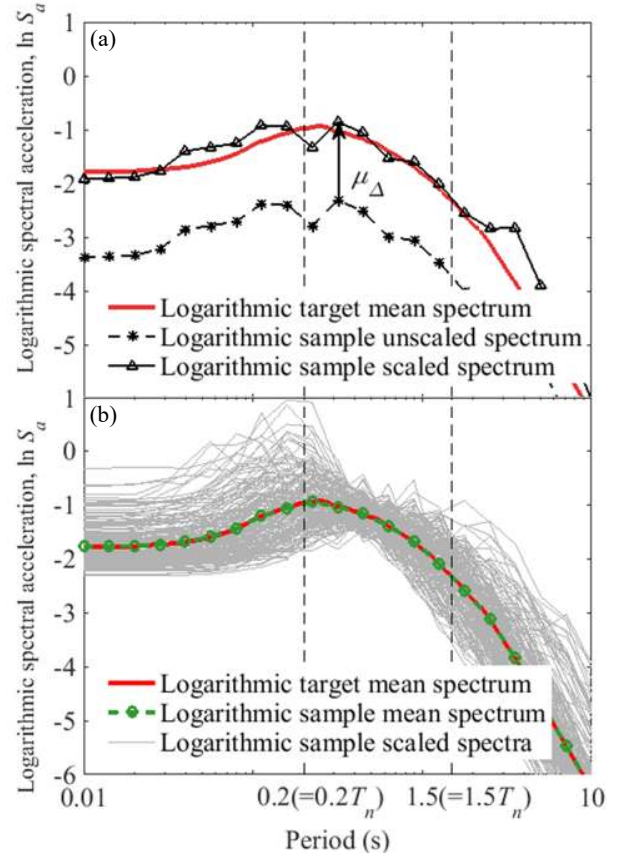


Fig. 2 Target response spectrum and scaled response spectra

where $\ln S_a^{\text{target}}(T_i)$ and $\ln s \times S_a(T_i)$ are the logarithmic target and individual scaled sample response spectra at a period T_i , respectively. A ground motion with the smallest SSE indicates that the ground motion best matches the target response spectrum among scaled ground motions in a library.

If at least seven ground motions are used in analyses, it is important to select a set of desired number of ground motions whose mean response spectrum match a target response spectrum. In this case, the first ground motion is selected from a library, which has smallest SSE [(3)] among scaled ground motions in the library. The process selecting the first ground motion is the same process used when selecting fewer than 7 ground motions. Therefore the same ground motion is selected as the first ground motion from both procedures. As mentioned previously, a ground motion with the smallest SSE best matches a target response spectrum among ground motions in a library.

After selecting the first ground motion, a ground motion is selected, which make their mean response spectrum best match a target response spectrum. This process is repeated until a desired number (n_g) of ground motions are selected. To avoid selecting the same ground motion selected previously when selecting the $k^{\text{th}} (\geq 2)$ ground motion, $k-1$ ground motions selected in previous iteration steps are removed from a library. The fitness between target and mean response spectra is measured by SSE_s calculated using (4) and (5).

$$SSE_S = \sum_{i=1}^{n_p} \left[\ln S_a^{target}(T_i) - \mu_{\ln S_a}(T_i) \right]^2 \quad (4)$$

$$\mu_{\ln S_a}(T_i) = \frac{1}{k} \sum_{j=1}^k \left[\ln s_j \times S_{aj}(T_i) \right] \quad (5)$$

where $\ln s_j \times S_{aj}(T_i)$ is the j^{th} ground motions ($j \leq k$) selected from scaled ground motions in a library. To select the k^{th} ground motion properly ($k \geq 2$), SSE_S is calculated using (4) with previously selected $k-1$ ground motions and one candidate ground motion in a library with $n_L - (k-1)$ scaled ground motions. The ground motion producing the smallest SSE_S is the one to be selected as the k^{th} ground motion.

Even though response spectra of selected ground motions in previous sections match the target response spectrum, the selected ground motions need to be re-scaled to have their mean response spectrum larger than a target response spectrum within a considered period range as required in Section 16.1.3.1 of ASCE 7-10 [1]. In order to satisfy this requirement, the distance (Δ_i) between target and mean response spectra at period T_i is calculated using (6).

$$\Delta_i = \ln S_a^{target}(T_i) - \mu_{\ln S_a}(T_i) \quad (6)$$

where $\mu_{\ln S_a}(T_i)$ is the mean value of logarithmic 5% damped response spectra of selected ground motions. The maximum of positive Δ_i [$\max(\Delta_i)$] within a considered period range becomes a re-scaling factor. If all Δ_i are negative, selected ground motions does not have to be re-scaled. In other words, re-scaling factor is 1 in this case. All ground motions selected from scaled ground motions in a library are rescaled with $\max(\Delta_i)$. Therefore, final scaling factor (s_k^*) for individual selected ground motions is calculated using (7).

$$\ln s_k^* = (\ln s_k) + \max(\Delta_i) \quad (k = 1 \sim n_g) \quad (7)$$

where s_k is the scaling factor that already applied to ground motions in a library as explained in previous section.

Fig. 3 shows selection results using a library with 184 scaled ground motions for $n_g=7$. As shown in Fig. 3, the sample mean response spectra of selected ground motions using proposed algorithm match the target response spectrum and satisfy ground motion selection criteria specified in ASCE 7-10.

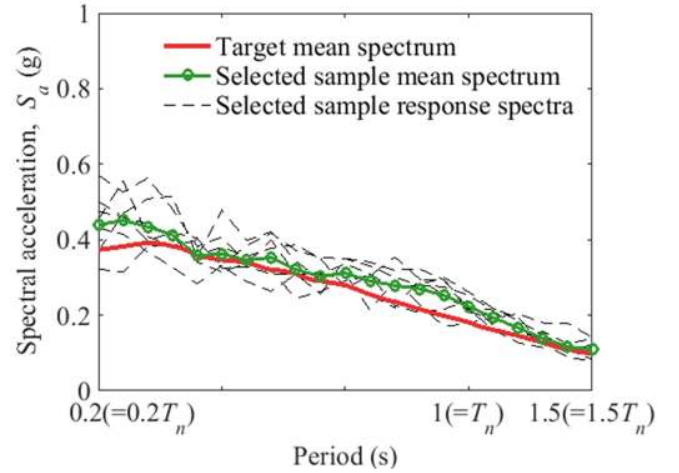


Fig. 3 Target response spectrum and sample response spectra for $n_g=7$.

IV. ACCURACY OF ASCE 7-10 CRITERIA WITH PROPOSED GROUND MOTIONS SELECTION ALGORITHM

In this study, various model SDF systems are considered, which have two different periods (1s, 2.5s) and yield strengths ($R_y=4, 8$). For evaluating the accuracy of maximum and minimum response prediction, $n_g=1\sim 6$ and $n_g = 7\sim 10$ are selected using the proposed algorithm, respectively. The maximum (u_{\max}) and mean drift responses (\bar{u}) of each system obtained under a certain number of ground motions is determined and compared with a target drift (u_{target}) that is the mean value of the drifts of the system obtained from nonlinear RHA with 184 ground motions used in this study. Errors of u_{\max} and \bar{u} in predicting u_{target} are calculated using (8).

$$\text{Error} = \left| \frac{u_{\max} \text{ (or } \bar{u}) - u_{\text{target}}}{u_{\text{target}}} \right| \times 100 \text{ [\%]} \quad (8)$$

Fig. 4 and 5 shows maximum ($n_g < 7$) and mean ($n_g \geq 7$) drifts of 4 SDF systems and corresponding target drifts. Errors calculated using (8) are also plotted.

As shown in Fig. 4, drifts obtained using fewer than 7 ground motions are always larger than corresponding target drifts. This indicates that ASCE 7-10 [1] criteria with the proposed

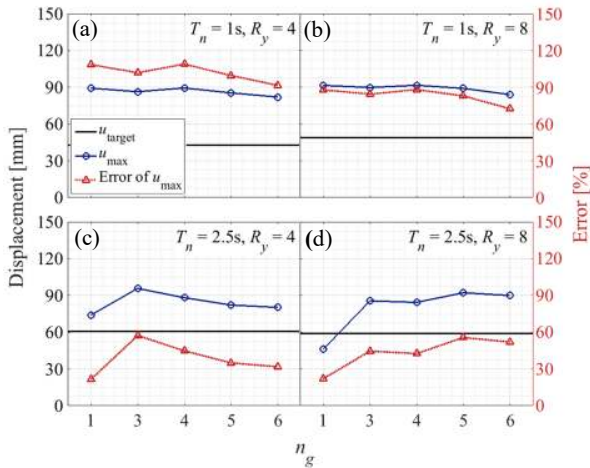


Fig. 4 Comparison between target displacements and mean displacements of 4 SDF systems according to $n_g (<7)$

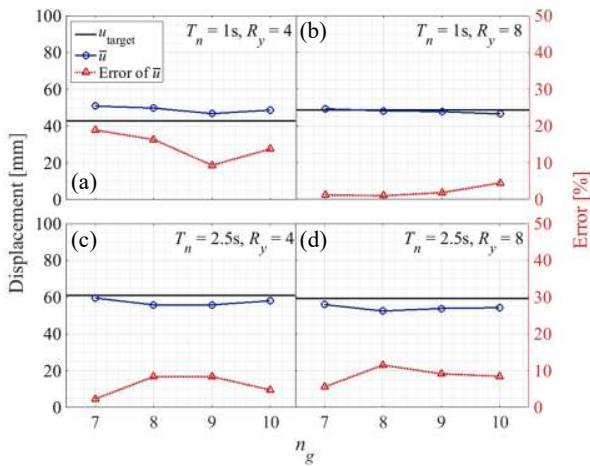


Fig. 5 Comparison between target displacements and mean displacements of 4 SDF systems according to $n_g (\geq 7)$

procedure for selecting fewer than 7 ground motions ($n_g=3\sim 6$) always overestimate target drifts. Sometimes errors for n_g of 6 are larger than n_g of 3. For a systems $T_n=2.5s$ and $R_y=8$ (Fig. 4(d)), errors for n_g of 3 are 44% but errors of the same systems associated with n_g of 6 are 55%.

In Fig. 5, Errors in predicting target displacements with at least 7 ground motions are significantly smaller than errors in predicting target displacements with fewer than 7 ground motions (Fig. 4). The largest error is observed for a system with T_n of 1s and R_y of 4 under 7 selected ground motions, which is 20% (Fig. 5(a)). As n_g increases as 9 and 10, the error decreases, which are 10% and 13%, respectively.

V.CONCLUSION

This study evaluates the accuracy of ASCE 7-10 [1] ground motion selection criteria with the proposed selection method. For this purpose, ground motion selection algorithms are proposed for applicable to ASCE 7-10 [1] selection criteria and nonlinear RHA are conducted for 4 SDF systems using ground motions selected by proposed algorithms. The conclusions based on this study are as follows:

(1) In this study, efficient and accurate ground motion selection method was proposed. For computational efficiency, a desired number of ground motions were sequentially selected from a library using the proposed method without considering all possible combinations of ground motions in a library.

(2) For fewer than 7 ground motions selected using the proposed method, maximum displacements of 4 SDF systems overestimated target displacements. For n_g of 3, errors in predicting target displacements ranges from 24% to 118%. Errors tend to increase with increasing n_g .

(3) For $n_g \geq 7$, errors were within 20%. Therefore, 7 or more ground motions selected according to ASCE 7-10 [1] criteria produced selection results more accurately matching a target response spectrum than fewer than 7 ground motions selected according to ASCE 7-10 [1].

ACKNOWLEDGMENT

Authors would like to acknowledge the financial supports provided by the National Research Foundation of Korea (No. 2014R1A2A1A11049488).

REFERENCES

- [1] ASCE, "Minimum design loads for buildings and other structures," *American Society of Civil Engineers*, Reston, VA, 2010.
- [2] CEN, "ENV 1998-1 Eurocode 8: Design of structures for earthquake resistance – Part 1: general rules, seismic actions and rules for buildings," *European Committee for Standardization*, Brussels, Belgium, 2004.
- [3] ASCE, "Seismic evaluation and retrofit of existing buildings (ASCE/SEI 41-13)," *American Society of Civil Engineers*, Reston, VA, 2014.
- [4] M. Aratj, L. Macedo, M. Marques, and J.M. Castro, "Code-based record selection methods for seismic performance assessment of buildings," *Earthquake Engng Struct. Dyn.*, vol. 45, pp. 129-148, Aug 2015.
- [5] A. R. Kottke, and E. M. Rathje, "A semi-automated procedure for selecting and scaling recorded earthquake motions for dynamic analysis," *Earthquake Spectra*, vol. 24, no. 4, pp. 911-932, Nov 2008.
- [6] N. Jayaram, T. Lin, and J. W. Baker, "A computationally efficient ground-motion selection algorithm for matching a target response spectrum mean and variance," *Earthquake Spectra*, vol. 27, no. 3, pp. 797-815, Aug 2011.

Acoustic Absorption of Hemp Walls with Ground Granulated Blast Slag

Oliver Kinnane, Aidan Reilly, John Grimes, Sara Pavia, Rosanne Walker

Abstract—Unwanted sound reflection can create acoustic discomfort and lead to problems of speech comprehensibility. Contemporary building techniques enable highly finished internal walls resulting in sound reflective surfaces. In contrast, sustainable construction materials using natural and vegetal materials, are often more porous and absorptive. Hemp shiv is used as an aggregate and when mixed with lime binder creates a low-embodied-energy concrete. Cement replacements such as ground granulated blast slag (GGBS), a byproduct of other industrial processes, are viewed as more sustainable alternatives to high-embodied-energy cement. Hemp concretes exhibit good hygrothermal performance. This has focused much research attention on them as natural and sustainable low-energy alternatives to standard concretes. A less explored benefit is the acoustic absorption capability of hemp-based concretes. This work investigates hemp-lime-GGBS concrete specifically, and shows that it exhibits high levels of sound absorption.

Keywords—Hemp, hempcrete, acoustic absorption, GGBS.

I. INTRODUCTION

Hemp-based concretes are bio-aggregate based construction materials that allow for low energy, and sustainable buildings both in construction and in use. Hemp sequesters significant quantities of CO₂ throughout its growth cycle, during which it grows up to 4 meters in 4 months with low fertilizer and irrigation requirement. In the context of building materials, hemp-based concretes exhibit good heat retention [1] and hygrothermal performance [2] primarily due to its high inherent multi-scale porosity.

This paper is focused on the acoustic capabilities of hemp construction. Specifically, it looks at the acoustic absorption of hemp composite walls using binders with hydrated lime and GGBS. These binders are proposed to offer sustainable alternatives to more commonly used cementitious based binders. Extensive investigations of a range of hemp-lime formulations have been previously undertaken that have characterized mechanical as well as moisture transfer and thermal properties [3]. As part of these studies GGBS, was identified as having potential for use in hemp-lime concretes on account of their fast setting and high reactivity [4], [5]. GGBS is a by-product of the iron and steel manufacturing

process. It is created by a polluting industry but is a waste product that would otherwise be disposed of in landfill. GGBS is not a true pozzolan but a latent hydraulic material. In the reaction of GGBS lime acts as an activator; and hydration is accompanied by the slower pozzolanic reaction; the amorphous silica and alumina in the slag react with lime forming additional hydrates [6].

Designing for acoustic comfort is often an appendix to building projects, achieved in post-occupancy by attaching noise absorbing panels to surfaces. Exposure to high levels of noise constitute risks to health and well-being [7]. Limiting acoustic exposure is particularly pertinent for people of specific age groups; including school children and the elderly. People with dementia are highly sensitive to acoustic discomfort [8]. The contemporary architectural tendency toward open-plan space, an increase in the specification of glass, smooth and polished hard surface finishes, has exacerbated the problem, with noise discomfort commonly reported in post-occupancy evaluations of buildings [9], [10]. Construction methods and building materials that exhibit inherently good sound dissipation properties can offer solutions in environments where excess and reverberated noise is a nuisance, such as classrooms [11], [12].

Highly porous construction materials have the potential to absorb sound and convert it to heat energy within the material pores. Studies have reported the absorption coefficient of fibrous materials [13], aerated autoclaved concrete [14] and concrete using recycled waste concrete aggregate [15].

Some recent studies have focused on the acoustic properties of hemp based concretes [16]. Hemp composites are characterised by high porosity in the range of 70-80% [17]. Pores of different scales exist, including macropores or inter-particle pores between the particles of hemp shiv, mesopores (intra-particle) within shiv and binder and micropores (intra-binder) in the binder. Gle et al. [16], [18] investigated the parameters of fabrication, including density, particle size distribution, type of binder and water content; and how these affect the acoustic properties of hemp concrete with hydraulic and cementitious binders. In the low frequency range, up to 500 Hz, hemp concretes were shown to offer significant sound absorption ($\alpha=0.2$ to 0.5) depending on binder type, with the quick cement binder displaying significantly lower sound absorption capabilities than hydraulic lime binders [16].

This study reports the acoustic absorption characteristics of hemp with a hydrated lime and GGBS binder across a wider range of frequencies consistent with salient frequencies of human speech.

Oliver Kinnane was previously Assist. Prof. of Façade Engineering at Trinity College Dublin when this research was undertaken. He is now with the School of Architecture at Queens University Belfast, United Kingdom (corresponding author, phone: 003535-85-7111587; e-mail: o.kinnane@qub.ac.uk).

Aidan Reilly is with the School of Architecture at Queens University Belfast, United Kingdom.

Sara Pavia, Rosanne Walker and John Grimes are with the Department of Civil, Structural and Environmental Engineering, Trinity College Dublin, Ireland.

II. METHODOLOGY

Acoustic absorption was tested on hemp lime wall sections in a laboratory with minimal background noise. Details of the materials and testing procedure are outlined below.

A. Materials

The hemp shiv used in this study is grown in Central France



Fig. 1 Hemp particles of varied scale

A hydrated lime (CL90 – calcium lime) is mixed with GGBS to form the primary binder (termed GGBS in Table I). A second mix (GGBS+WR) includes a water retainer, methyl cellulose, to retain water in the binder and reduce the water adsorbed by the hemp [19].

Wall sections measuring 900x800x300 mm were cast in timber shuttering and allowed to cure for 21 months prior to testing. Replicating common hemp concrete construction methods, the walls were tamped in the shuttering by an experienced practitioner.

TABLE I
MIX PROPERTIES

Label	Composition	Binder:Hemp:Water ratio (by weight)
GGBS	70% CL90, 30% GGBS	2:1:3.1
GGBS +WR	70% CL90, 30% GGBS 0.5% Methyl Cellulose	2:1:3.1

Density values are listed in Table III. The porosity is measured by water displacement pycnometry and ranges from 72 to 74 for the samples assessed [20].

B. Acoustic Testing Procedure

An impedance tube is tightly contacted to the wall surface. A white noise signal is generated using a B&K 1405 noise generator, attenuated with amplifier and transmitted through a speaker down the length of impedance tube.

Acoustic absorption coefficients were calculated in the frequency range 332 Hz up to 2865 Hz with cut-off frequencies defined in the standards [21] and literature [22], for the distance between the microphones (43 mm) and length of tube (963 mm).

and supplied by La Chanvrière De L'aube. Considering the significance of multi-scale porosity, the particle size distribution was evaluated for a sample of hemp used in the walls being tested.

TABLE II
IMPEDANCE TUBE GEOMETRY

Description	Notation	Dimension
Internal diameter of tube	d	70 mm
Length of tube	l	963 mm
Impedance tube wall thickness	t	3 mm
Microphone diameter	d _{microphone}	7 mm
Spacing between microphones	s	43 mm



Fig. 2 Impedance tube contacting section of hemp-GGBS wall

III. RESULTS

A scanning electron microscope (SEM) was used to analyse the hemp concrete samples. SEM images evidence their inherent pore structure [23]. Fig. 3 illustrates the pore structure of hemp concrete with GGBS binder under analysis in this study. Sound absorption was calculated across the range of frequencies to 2000 Hz and its values at key frequencies are listed in Table III.

Table III documents the sound absorption coefficient at the 1/3 octave frequencies 500 Hz, 1000 Hz and 2000 Hz.

The characteristic curves for the range of sound absorption parameters are shown in Fig. 4.

TABLE III
ACOUSTIC ABSORPTION PROPERTIES

Label	Physical Properties		Acoustic Absorption Coefficient		
	Density	Porosity	500Hz	1kHz	2kHz
GGBS	505 kg/m ³	72-74	0.49	0.42	0.44
GGBS +WR	522 kg/m ³	72-74	0.52	0.45	0.53

When the water retainer is added to the mix, a slight (3%) increase in density and decrease in porosity (1%) is observed. The sound absorption coefficient is seen to increase across the frequency range; however, it is likely insensitive to these slight physical changes and instead due to variants in casting or alterations in pore structure.

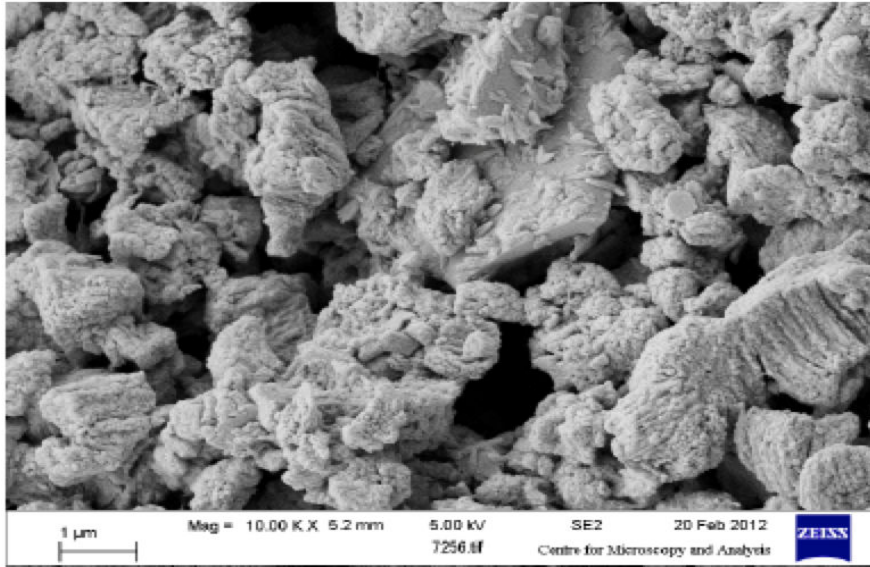


Fig. 3 SEM image of hemp concrete matrix with GGBS binder including significant macropores, carbonated lime and hydrates covering hemp particles.

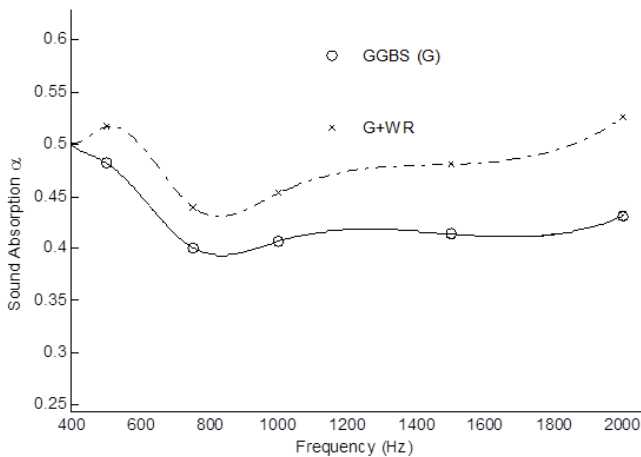


Fig. 4 Characteristic sound absorption curves for hemp concrete

IV. DISCUSSION

Hemp exhibits high sound absorption when combined with lime-GGBS binder. Values reported in this study are similar to those reported by Gle et al. (2011) for hydraulic lime binders, and higher than those reported for a binder including cement. However, values documented in this study are consistent over a wider range of frequencies tested. In a previous study, the acoustic absorption of a range of other wall types were investigated using the impedance tube method in situ [24]. These include wood finishes, fair-faced and painted cinder

block and unpainted render walls. Hemp-lime concrete displays good sound absorption when compared to other common building materials although it exhibits sound absorption coefficients slightly lower than porous concrete [15] and fair faced concrete block [24].

V. CONCLUSION

Un-rendered hemp concrete with hydrated lime and GGBS binder exhibits significant acoustic absorption, with average sound absorption of 40-50% of the normal incident signal, across the tested range of frequencies.

Further work will focus on comparing lime based hemp concretes with those containing cement and also look at the impact of lime render on bulk hemp-lime acoustic characteristics.

REFERENCES

- [1] F. Collet and S. Pretot, "Thermal conductivity of hemp concretes: Variation with formulation, density and water content," *Constr. Build. Mater.*, vol. 65, pp. 612–619, Aug. 2014.
- [2] A. Shea, M. Lawrence, and P. Walker, "Hygrothermal performance of an experimental hemp-lime building," *Constr. Build. Mater.*, vol. 36, pp. 270–275, Nov. 2012.
- [3] R. Walker and S. Pavia, "Moisture transfer and thermal properties of hemp-lime concretes," *Constr. Build. Mater.*, vol. 64, pp. 270–276, Aug. 2014.
- [4] M.-P. Boutin, C. Flamin, S. Quinton, G. Gosse, and L. Inra, "Étude des caractéristiques environnementales du chanvre par l'analyse de son cycle de vie (Study of environmental characteristics of hemp by means

- of an analysis of its lifecycle).” Ministère de l’Agriculture et de la Pêche (Ministry of Agriculture and Fishery), 2005.
- [5] R. Walker and S. Pavia, “Behaviour and Properties of Lime-Pozzolan Pastes,” 2010.
 - [6] R. Walker and S. Pavia, “Physical properties and reactivity of pozzolans, and their influence on the properties of lime–pozzolan pastes,” *Mater. Struct.*, vol. 44, no. 6, pp. 1139–1150, Nov. 2010.
 - [7] World Health Organisation, *Burden of disease from environmental noise. Quantification of healthy life years lost in Europe*. 2011.
 - [8] T. Grey, O. Kinnane, and M. Dyer, “Perceptions of thermal environments in dementia friendly dwellings. (Accepted for publication),” presented at the Windsor Conference, Windsor, UK, 2016.
 - [9] O. Kinnane, M. Dyer, and T. Grey, “Energy and environmental forensic analysis of public buildings.,” *Eng. Sustain. Proc. Inst. Civ. Eng.*, vol. 167, no. 4, 2014.
 - [10] A. Leaman and B. Bordass, “Assessing building performance in use 4: the Probe occupant surveys and their implications,” *Build. Res. Inf.*, vol. 29, no. 2, pp. 129–143, Mar. 2001.
 - [11] Department for Education, “Acoustic design of schools: performance standards 2014.” (Online). Available: <http://www.bre.co.uk/page.jsp?id=384>. (Accessed: 16-Nov-2014).
 - [12] *DIN 18041:2004-05, Acoustical quality in small to medium-sized rooms*. Beuth, 2004.
 - [13] O. Umnova, K. Attenborough, E. Standley, and A. Cummings, “Behavior of rigid-porous layers at high levels of continuous acoustic excitation: theory and experiment,” *J. Acoust. Soc. Am.*, vol. 114, no. 3, pp. 1346–1356, Sep. 2003.
 - [14] A. Laukaitis and B. Fiks, “Acoustical properties of aerated autoclaved concrete,” *Appl. Acoust.*, vol. 67, no. 3, pp. 284–296, Mar. 2006.
 - [15] S. B. Park, D. S. Seo, and J. Lee, “Studies on the sound absorption characteristics of porous concrete based on the content of recycled aggregate and target void ratio,” *Cem. Concr. Res.*, vol. 35, no. 9, pp. 1846–1854, Sep. 2005.
 - [16] P. Glé, E. Gourdon, and L. Arnaud, “Acoustical properties of materials made of vegetable particles with several scales of porosity,” *Appl. Acoust.*, vol. 72, no. 5, pp. 249–259, Apr. 2011.
 - [17] L. Arnaud and E. Gourlay, “Experimental study of parameters influencing mechanical properties of hemp concretes,” *Constr. Build. Mater.*, vol. 28, no. 1, pp. 50–56, Mar. 2012.
 - [18] P. Glé, E. Gourdon, L. Arnaud, K.-V. Horoshenkov, and A. Khan, “The effect of particle shape and size distribution on the acoustical properties of mixtures of hemp particles,” *J. Acoust. Soc. Am.*, vol. 134, no. 6, pp. 4698–4709, Dec. 2013.
 - [19] R. Walker and S. Pavia, “Impact of water retainers in the strength, drying and setting of lime hemp concrete,” in *Bridge and Concrete Research in Ireland*, Dublin, 2012.
 - [20] R. Walker, *A Study of the Properties of Lime-Hemp Concrete with Pozzolans*. Dublin, Ireland, 2013.
 - [21] *ISO 10534-2:1998 - Acoustics -- Determination of sound absorption coefficient and impedance in impedance tubes -- Part 2: Transfer-function method*. 1998.
 - [22] R. Oldfield and F. Bechwati, “Accurate low frequency impedance tube measurements,” in *Proceedings of the Institute of Acoustics*, 2008, vol. 30 (4).
 - [23] R. Walker, S. Pavia, and R. Mitchell, “Mechanical properties and durability of hemp-lime concretes,” *Constr. Build. Mater.*, vol. 61, pp. 340–348, Jun. 2014.
 - [24] J. Grimes, O. Kinnane, R. Walker, and S. Pavia, “In situ measurement of the sound absorption characteristics of existing building fabrics,” in *Proceedings of the Institute of Acoustics*, Manchester, UK, 2013, vol. 35(2).



architecture.

Dr. Oliver Kinnane is a Lecturer of Architecture at Queens University Belfast. Oliver was born in the Peoples Republic of Cork in 1977. Oliver’s experience is wide and varied, including a Ph.D. in modeling and control from the National University of Ireland Maynooth (2005), a Masters of Architecture from the Illinois Institute of Technology (2008) and a Bachelor of Electrical Engineering from University College Cork (2000). Oliver’s major field of study is

He’s research is focused on the betterment of buildings through material and technical advancement and behavioural adaptation. . Primarily his work concentrates on optimizing building skins, improving the methods by which we envelope and condition our homes and fuel our lives. He is PI of a Horizon 2020 project focused on the renovation of those least loved of buildings - the precasts from the 1950s and 60s. He has a keen interest in sustainable materials and he and Dr. Aidan Reilly are currently investigating the thermal mass potential of hemp-lime.

Dr. Aidan Reilly is also with the School of Architecture at Queens University Belfast. He graduated with a Masters degree in Energy and Environmental Engineering from the University of Cambridge (Trinity Hall, 2006), and completed his PhD in 2013 (Sidney Sussex College, Cambridge). He now works as a Research Fellow on the IMPRESS project researching materials for improved thermal performance with an emphasis on phase-change materials. Prof. Sara Pavia, Dr. Rosanne Walker are focused on historic building, renovation and sustainable materials and are based at the Department of Civil, Structural and Environmental Engineering, Trinity College Dublin.

Dr. Sara Pavia is a Professor in the Department of Civil Engineering at the University of Dublin, Trinity College. She has worked in industry and academia for twenty years and has released six books and a hundred other publications. Her main areas are sustainable materials and construction and the repair and conservation of traditional and historic fabrics.

Dr. Rosanne Walker is focused on historic building, renovation and sustainable materials and is based at the Department of Civil, Structural and Environmental Engineering, Trinity College Dublin.

Adaptive Process Monitoring for Time-Varying Situations using Statistical Learning Algorithms

Seulki Lee, Seoung Bum Kim

Abstract—Statistical process control (SPC) is a practical and effective method for quality control. The most important and widely used technique in SPC is a control chart. The main goal of a control chart is to detect any assignable changes that affect the quality output. Most conventional control charts, such as Hotelling's T^2 charts, are commonly based on the assumption that the quality characteristics follow a multivariate normal distribution. However, in modern complicated manufacturing systems, appropriate control chart techniques that can efficiently handle the nonnormal processes are required. To overcome the shortcomings of conventional control charts for nonnormal processes, several methods have been proposed to combine statistical learning algorithms and multivariate control charts. Statistical learning-based control charts, such as support vector data description (SVDD)-based charts, k -nearest neighbors-based charts, have proven their improved performance in nonnormal situations compared to that of the T^2 chart. Beside the nonnormal property, time-varying operations are also quite common in real manufacturing fields because of various factors such as product and set-point changes, seasonal variations, catalyst degradation, and sensor drifting. However, traditional control charts cannot accommodate future condition changes of the process because they are formulated based on the data information recorded in the early stage of the process. In the present paper, we propose a SVDD algorithm-based control chart, which is capable of adaptively monitoring time-varying and nonnormal processes. We reformulated the SVDD algorithm into a time-adaptive SVDD algorithm by adding a weighting factor that reflects time-varying situations. Moreover, we defined the updating region for the efficient model-updating structure of the control chart. The proposed control chart simultaneously allows efficient model updates and timely detection of out-of-control signals. The effectiveness and applicability of the proposed chart were demonstrated through experiments with the simulated data and the real data from the metal frame process in mobile device manufacturing.

Keywords—Multivariate control chart, nonparametric method, support vector data description, time-varying process

Seulki Lee is with the Department of Industrial Management Engineering, Korea University, Seoul, Korea (phone: 82-2-3290-3769; fax: 82-2-929-5888; e-mail: seulki.lee.316@gmail.com).

Seoung Bum Kim is with the Department of Industrial Management Engineering, Korea University, Seoul, Korea (phone: 82-2-3290-3397; fax: 82-2-929-5888; e-mail: sbkim1@korea.ac.kr).

Aerodynamic Performance of a Forward Bent Frame in a High Speed Bicycle

Paritosh Prakhar, Musfera S. Javed

Abstract—With growing demand for transportation medium with minimum fuel consumption and maximum efficiency, often the most economical medium is overlooked i.e. a bicycle. A bicycle is one of the most primitive yet one of the most efficient mode of transport with the 97% power transmission efficiency. A new design with double reduction chain drive transmission system claims to attain speeds as high as 300 km/h at practical cadence of 130 rpm. However the aerodynamic stability of such a bike with a conventional frame is a questionable issue. Moreover the human body itself is not designed to counter such high air flow velocities on its ventral side. The large ventral area combined with the very small lateral area leads to formation of low pressure zones as well as vortices behind the dorsal surface which tends to increase the overall drag while bending the upper torso to counter this drag leads to the generation of a lift force on the body of the ride. Moreover the bending of upper torso still leaves the lower part of the body to attack the air in the same way as an upright body. Thus, a new frame that can reduce the drag forces without causing an uplift is a desirable venture. Here, a new frame design where the seating position is kept ahead of the pedaling shaft is proposed, i.e. the entire body from the feet to the head lie in along a curve to minimize air drag along with uplift forces. The designing of the frame will be initiated with a simulation of the conventional frame under high speed conditions (speeds above 100km/h) and the simulation of various seating positions with respect to the pedaling shaft and the handle to compare the improvements. The wheel speed, crank speed, chain movement and the pedaling motion will all be taken into account while doing the simulation. The simulations will be carried out in no wind, moderate axial wind, high speed axial wind and moderate cross wind conditions. The results of the best design attained from the simulation will then be verified experimentally to ensure the integrity of the results. The overall research is aimed at the creation of a bicycle design that is aerodynamically efficient at speeds higher than the motorized bikes and thus offers an alternative to the fast gasoline powered bikes as well as to the slow human powered vehicles (battery powered).

Keywords—air drag, cadence, uplift, vortices

Corresponding Author

Paritosh Prakhar from Zakir Hussain College of Engineering and Technology, Aligarh Muslim University, India
e-mail: pp95aw@gmail.com

An Indoor Guidance System Combining NFC and BLE Beacon Technologies

Rung-Shiang Cheng, Wei-Jun Hong, Jheng-Syun Wang, Kawuu W. Lin

Abstract—Users rely increasingly on Location-Based Services (LBS) and automated navigation / guidance systems nowadays. However, while such services are easily implemented in outdoor environments using Global Positioning System (GPS) technology, a requirement still exists for accurate localization and guidance schemes in indoor settings. Accordingly, the present study proposes a based on GPS, Bluetooth Low Energy (BLE) beacons, and Near Field Communication (NFC) technology. Through establishing graphic information and the design of algorithm, this study develops a guidance system for indoor and outdoor on smartphones, with aim to provide users a smart life through this system. The proposed system is implemented on a smartphone and evaluated on a student campus environment. The experimental results confirm the ability of the proposed app to switch automatically from an outdoor mode to an indoor mode and to guide the user to the requested target destination via the shortest possible route.

Keywords—Beacon, BLE, Dijkstra algorithm, indoor, GPS, near field communication technology.

I. INTRODUCTION

ACCORDING to statistics published by the International Telecommunication Union (ITU), the number of mobile devices in the world reached 6.835 billion at the end of 2013. Furthermore, the number of devices is still growing. As wireless technology continues to improve, and wireless networks are ever more extensively deployed, the feasibility of developing Location-Based Services (LBS) has attracted growing interest [1]. LBS have many advantages from a user perspective, including convenience, efficiency and fun. As a result, they are now widely applied in social networks, traffic and geographic search systems, and even public safety [2], [3]. Of the many functions offered by LBS, those of positioning localization and guidance are some of the most useful. According to previous research, adults spend around 86.9% of their time indoors, 5.5% in vehicles and 7.6% outdoors [4]. Thus, in realizing seamless LBS applications, it is necessary to develop localization and guidance schemes capable of working

Rung-Shiang Cheng is with the Department of Computer and Communication, Kun Shan University, No.195, Kunda Rd., Yongkang Dist., Tainan City 710, Taiwan (R.O.C.) (e-mail: rscheng@mail.ksu.edu.tw).

Wei-Jun Hong is with the Department of Computer Science and Information Engineering, National Kaohsiung University of Applied Sciences, No.415, Jiangong Rd., Sanmin Dist., Kaohsiung City 807, Taiwan (R.O.C.) (e-mail: 1103405117@gm.kuas.edu.tw).

Jheng-Syun Wang is with the Department of Computer and Communication, Kun Shan University, No.195, Kunda Rd., Yongkang Dist., Tainan City 710, Taiwan (R.O.C.) (e-mail: a.way612101@gmail.com).

Kawuu W. Lin is with the Department of Computer Science and Information Engineering, National Kaohsiung University of Applied Sciences, No.415, Jiangong Rd., Sanmin Dist., Kaohsiung City 807, Taiwan (R.O.C.) (e-mail: linwc@kuas.edu.tw).

in both indoor and outdoor environments, and switching between the two modes automatically as required.

Global Positioning System (GPS) technology is used widely in the navigation, tourism, measurement, and engineering fields. However, the success of GPS depends on a strong signal between the user and the navigational satellite. Thus, while GPS functions well in open outdoor environments, its performance suffers dramatically in mountainous areas or build-up urban areas. Furthermore, the signals are unable to penetrate through building structures, and hence GPS is of only limited use in indoor environments.

The literature thus contains various alternative proposals for performing indoor localization. For example, in [5], [6], the user position is estimated using a wireless communication signal, while in [7], a visible light communication system is used. The authors in [8] performed indoor positioning using radio-frequency identification (RFID) tags. In [9], user positioning was performed by mapping the activities of the user to the positions in the indoor environment at which these activities were known to be performed. Finally, in [10], multiple indoor positioning technologies were combined in order to improve the localization accuracy.

Although mobile devices are invaluable in daily life nowadays, their usefulness is limited by their short battery lives, which prompts the need for frequent recharging. To address this problem, many mobile devices use Bluetooth Low Energy (BLE) technology to realize wireless communication connections. BLE has many advantages as a connection technology, including a stable signal, an ease of distribution, a low cost, and widespread compatibility with existing wireless devices. Furthermore, BLE beacons have an operating life of several months using only a simple button cell battery [11]. As a result, BLE has significant potential as an enabling technology for indoor LBS applications.

Owing to indoor environment is a complicated space. The spreading of wireless or GPS signals are easily affected by the interior structure of the building, therefore, it urgently needs precise technologies and a lot of spherical auxiliary electronic devices, leading to the difficulty in indoor precise positioning. Thus, for many years, these well-known positioning technologies such as GPS positioning system or Google map services are usually applied in public construction fundamental facilities, road or outdoor large area; however, along with the urbanization of living environment, there are more and larger complex buildings, increasing the need for indoor positioning. Near Field Communication (NFC) is a short-range wireless connectivity standard which enables communications to be achieved between devices simply by touching them together or

bringing them into very close proximity of one another (typically, less than 10 cm). NFC has found widespread use nowadays for such applications as loyalty schemes, home healthcare, public transport payment, ticketing, mobile workforce management, and so on. With the ability it provides to infer the user position with an ultra-high degree of precision, NFC also has significant potential for indoor localization purposes.

Thus, to enhance the application of the positioning system and enable smartphones to become a key equipment of augmented humanity which can effectively enhance the convenience, this study is based on short-distance wireless communication technology, combining NFC, BLE Beacon and GPS technology to develop a positioning guidance system which is suitable for indoor buildings. This study combines GPS, BLE and NFC technologies to realize a seamless indoor-outdoor user localization and guidance app suitable for implementation on a smart mobile device. In the proposed scheme, user localization is performed using conventional GPS technology in the outdoor environment. However, when the user enters an indoor space, the app switches automatically to an indoor mode, and user positioning is performed by means of BLE beacons and NFC tags. The positioning information obtained via the various technologies is combined with map information (outdoor and indoor) to realize a guidance system capable of leading the user to the requested target destination via the shortest available route.

The design of the system includes "storage data design", "positioning method design", "algorithm design" and "graphic design." In between, for indoor map establishment, this study designs a method which can assist in establishing positioning point storage function through wireless signal exploration (indoor space area as unit positioning base). Outdoor maps use GPS as positioning base to obtain the location information, using route maps to display the guidance results. When users are outdoors, this app will automatically adopt "outdoor mode" to obtain GPS positioning to provide users with guidance information.

The remainder of this paper is organized as follows. Section II reviews the GPS, BLE and NFC technologies used for localization purposes in this study and introduces the path-finding algorithm used to realize the indoor guidance system. Section III describes the system framework and implementation. Section IV presents and discusses the experimental evaluation results. Finally, Section V provides some brief concluding remarks.

II. BACKGROUND KNOWLEDGE

This section commences by describing the GPS, BLE beacon and NFC technologies used in the present study to develop the proposed positioning and guidance system. The shortest-path algorithm used to accomplish indoor guidance is then briefly introduced. Fig. 1 presents a schematic illustration of the respective communication distances of the GPS, Beacon and NFC technologies.

A. GPS

GPS is a middle-distance global tracking satellite guidance system with a coverage area of more than 98% of the earth's surface. GPS can be used by any enabled device capable of receiving its signals and has the advantage of anonymity in that the user's position is not recorded as part of the communication process. However, GPS relies on the availability of a clear Line of Sight (LOS) between the user device and the satellite system. As a result, it provides only a limited positioning capability in indoor environments.

B. BLE

Bluetooth Low Energy (BLE) is a communication standard designed to enable short-range wireless devices to operate for months or even years on a single coin cell battery. When combined with beacon technology, BLE provides a highly effective method for estimating the position of the user relative to certain predefined monitoring spots. BLE operates over a distance of up to 50 m and provides the means to customize the LBS offered to the user based on their physical location. For example, certain advertisements can be pushed to the user device as the user approaches a particular sales counter in a store. Similarly, the user may be presented with different notification messages and application events as he or she moves across the boundary separating one monitored area from another.

The literature contains various proposals for integrating the BLE standard with beacon technology in order to support user localization, including iBeacon, Gimbal, and AltBeacon. The beacons used in such systems periodically broadcast a wireless radio signal advertising their presence. As described above, BLE operates over a range of up to 50 m. Hence, in the event that the signal is detected (sighted) by a proximity-enabled user device, the user position can be inferred with an error of no more than 50 m. As a result, BLE/beacon technology provides a low-cost and energy-efficient solution for performing user localization with a medium degree of accuracy. The localization system proposed in the present study utilizes the Gimbal Series 10 beacon produced by Qualcomm.

C. NFC

Near Field Communication (NFC) is an ultra-short distance wireless communication technology based on radio-frequency identification (RFID). NFC utilizes signal attenuation technology to enable devices to conduct non-contact point-to-point data transmissions over distances of up to approximately 10 cm (3.9 inches). NFC is currently used for such applications as automated payment, ticketing, loyalty schemes, and so forth. However, with its high bandwidth and low energy consumption, NFC (see Fig. 3) also has significant potential for highly-precise indoor positioning. As with the Gimbal beacon, each NFC chip has a unique ID number assigned to it by the manufacturer. Thus, by associating the ID with a physical location, and storing this information in a database, the position of the user can be inferred with an extremely high degree of precision each time a sensing event occurs.

D. Shortest-Path Algorithm

Determining the shortest route between a start point and an target end point given the availability of multiple paths between them is a common problem in many walks of life [12]. The guidance system proposed in this study utilizes the algorithm proposed by Dijkstra [13] since, of the various algorithms available, it has the advantages of being a concise algorithm and the optimal solution can be obtained.

III. SYSTEM FRAMEWORK AND IMPLEMENTATION

The app proposed in this study provides the user with a seamless positioning and guidance service as he or she moves from an outdoor environment to a target destination in an indoor environment or vice versa. In other words, the app switches automatically not only from an outdoor mode to an indoor mode, but also from an indoor mode to an outdoor mode. As described in the Introduction section, positioning in the outdoor environment is performed using conventional GPS technology, while in the indoor environment it is performed using BLE beacon and NFC technologies. For both environments, the guidance function is achieved using map information stored in a remote server and downloaded to the user device as required. For illustration purposes, the present study considers the localization / guidance problem for the case of a student campus environment containing many buildings scattered over a wide geographic area with many floors and rooms within each building. As described in the following sections, the system framework comprises four design components, namely (1) storage data design, (2) positioning method design, (3) shortest-path algorithm design, and (4) map structure design.

A. Positioning Method Design

To simplify the data storage and management task, four different data structures are used to support the different functionalities of the system, namely an outdoor map structure, an indoor map structure, a Beacon positioning data structure, and an NFC positioning data structure. The localization / guidance app proposed in this study resides by default in the "outdoor mode" and uses conventional GPS technology to locate the position of the user. More specifically, the system acquires the current latitude and longitude information from the GPS system and uploads this information together with the Device ID to a remote server. On receiving this information, the server interrogates the coordinate information and returns the appropriate outdoor map to the user device using the JavaScript Object Notation (JSON) format, as shown in Fig. 5.

The JSON message sent back includes the name, address, latitude and longitude and building introduction of the destination whose format is shown in Fig. 5.

When the user moves from the outdoor environment to an indoor environment, the app switches automatically to an "indoor mode" and launches an indoor positioning routine. If the user is within wireless range of a Beacon, a sighting event occurs and the device uploads both its own ID and that of the beacon to the server. Utilizing the Factor ID as a key, the server retrieves the approximate location of the user and returns this

information to the user device. When the user's smartphone approaches an NFC tag, the user can send tag ID along with the Device ID back to the server after the mobile reads the set NFC tag. The server will conduct indexing from the NFC data list and send the index results back the app to obtain the user's location and conduct indoor positioning.

```
{
  "id": 1,
  "name": "School",
  "address": "No.195, Kunda Rd.",,
  "latitude": "22.996175",
  "longitude": "120.252970",
  "info": "Kun Shan University"
}
```

Fig. 5 JSON data format

B. Shortest-Path Algorithm Design

After obtaining the user location, the app downloads the map from the server. Specifically, the app informs the server of the Device ID and the required map ID and the server searches its database for the corresponding map and returns it to the user device.

Let $G = (V, E)$ denote an indoor map, where V is the set of nodes in the map and E is the set of connecting edges (paths). In constructing the map, the server hosts a database with four columns, namely ID (primary index key), node ID, adjacent node ID and Distance Between Adjacent Nodes. Taking Node 2 in Fig. 6 as an example, let the nodes adjacent to Node 2 be denoted as Node 0, Node 1, Node 3 and Node 4, respectively. Furthermore, let the distances of these nodes from Node 0 be equal to 4, 2, 9 and 2, respectively.

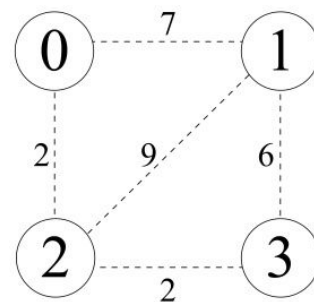


Fig. 6 Node layout scheme

The information provided in the JSON message, provides the app with the relevant indoor Shortest-path map. However, the Dijkstra shortest-path algorithm requires the input information to be presented in the form of a matrix. Therefore, in implementing the indoor guidance function, the JSON map information must first be converted into a matrix form. For example, the illustrative layout in Fig. 6 contains five nodes, and should therefore be converted to a 5×5 matrix of the form shown in Table I.

TABLE I
DIJKSTRA ADJACENT MATRIX

Node	0	1	2	3
0	0	7	2	INF
1	7	0	9	6
2	2	9	0	2
3	INF	6	2	0

Accordingly, in the app proposed in this study, the matrix construction task is performed automatically using the function shown in (1), in which i is the number of the current node, v is the number of the adjacent node, and e is the cost of the path between them. When presented with the node map (constructed manually by the system developer), the matrix construction algorithm takes the current node and adjacent node information as an input and uses (1) to automatically generate the corresponding $n \times n$ adjacent matrix with a time complexity of $O(n)$.

`graph[i].adjacentEdge(v, e)` (1)

For example, taking Node 2 in Fig. 6 for illustration purposes once again, the relation between Node 2 and its adjacent nodes

has the form shown in (2). Taking the i , v and e information given in (2), the algorithm automatically constructs the matrix shown in Fig. 11.

`graph[2].adjacentEdge(0, 4)`
`graph[2].adjacentEdge(1, 2)` (2)
`graph[2].adjacentEdge(3, 9)`
`graph[2].adjacentEdge(4, 2)`

C. Map Structure Design

In general, the success of any app is determined to a large extent by the appearance and intuitiveness of its graphical user interface (GUI). For a guidance system such as that is proposed in the present study, a pictorial map with too much detailed information will serve simply to confuse the user. Consequently, in the proposed app, the indoor and outdoor maps are presented in the form of metro-like maps, in which the key locations (e.g., buildings, offices, classrooms, toilets, and so on) are represented as nodes and the distances between them are indicated by numerals placed alongside the corresponding paths (see Fig. 8).

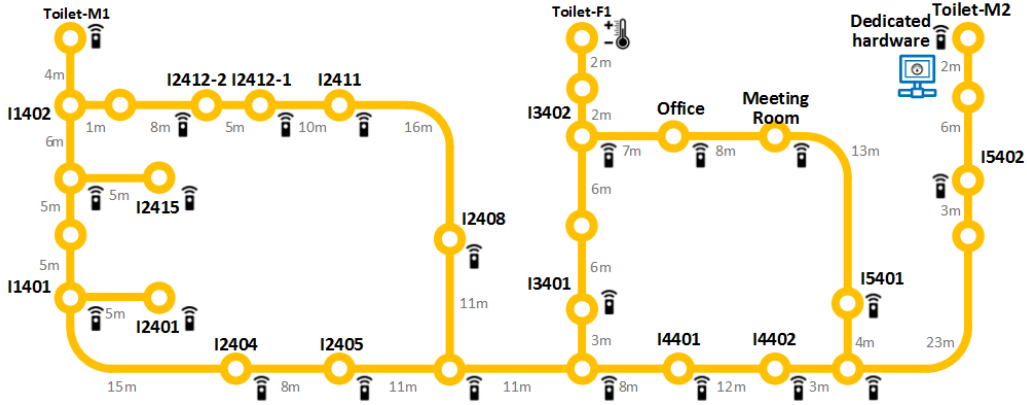


Fig. 8 Map representation

As discussed above, having determined the user's current location, the app requests the appropriate map from the server and then stores the received map in the device. Notably, the map is downloaded in its entirety, and hence the need for repeated download events is avoided. Having downloaded the map, the user then selects the target destination (i.e., node) for which they require routing information. To ensure smooth node selection, the app stores an acceptable touch range error in addition to the coordinates of each node center.

When the user touches the screen to select a particular destination node, the app determines the intended node in accordance with Eq. (3), in which X_1 and Y_1 are the stored coordinates of the node center, X_2 and Y_2 are the coordinates of the point at which the user touches the screen, and r is the allowable touch range error.

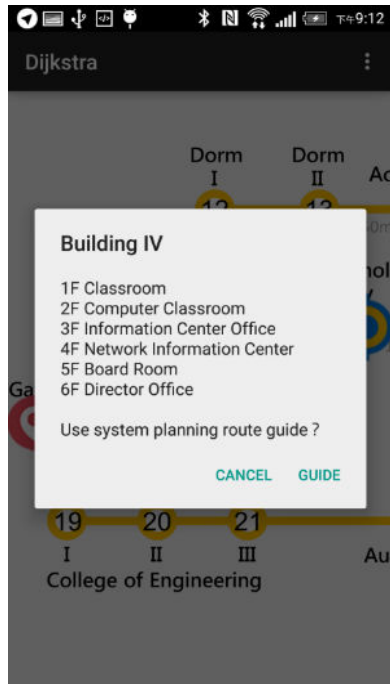
$$|X_1 - X_2|^2 + |Y_1 - Y_2|^2 < r^2 \quad (3)$$

Having established the user's present location, and his or her intended destination, the app invokes Dijkstra's shortest-path algorithm and marks the suggested route pictorially on the node map.

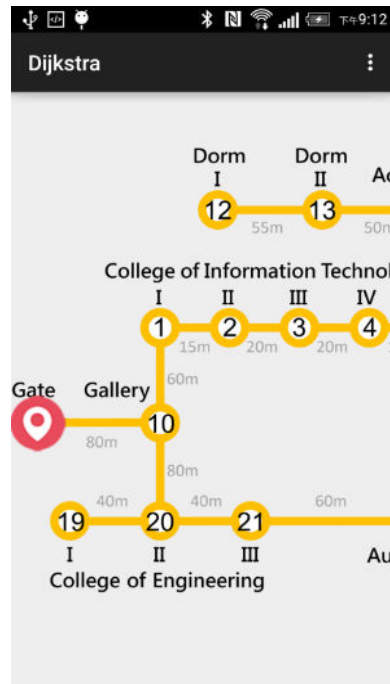
IV. IMPLEMENTATION RESULTS

A. System Implementation and Function Display

Performance evaluation trials were performed on a university campus in Taiwan, with the aim being to guide the user to a specific target in the building shown in Fig. 11. As shown, seven beacons and 31 NFC tags were placed at appropriate points throughout the experimental field, e.g., on the doors of the main rooms in the building, at the entrances to staircases, at forks or corners in the corridors, and so on. Due to their lower cost, the NFC tags greatly outnumbered the beacons, and were placed with an approximate spacing of 2 ~ 15 m.



(b) Nearby building information



(c) Position of user

Fig. 13 User located outside

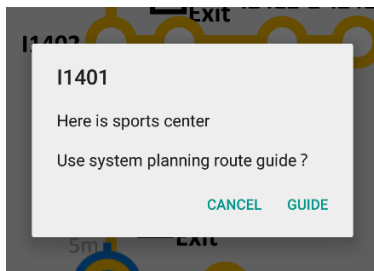
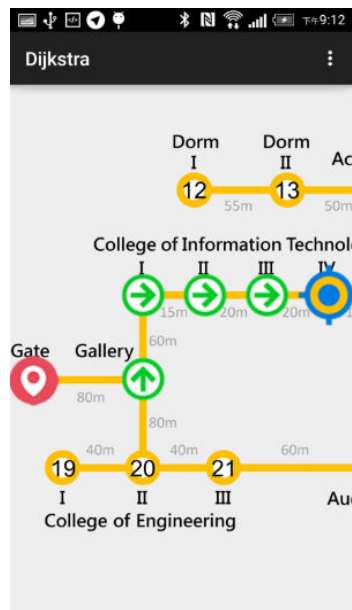
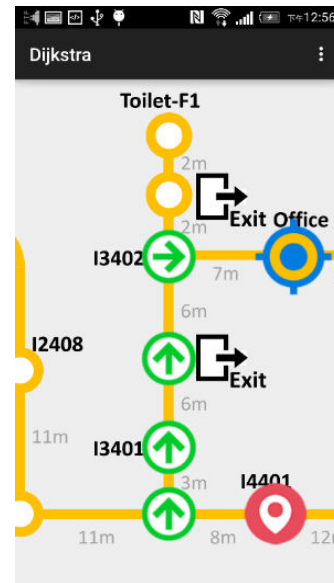


Fig. 14 Guidance notification



(a) Outdoor navigation aid



(b) Indoor navigation aid

Fig. 15 Navigation aid

B. Experimental Design and Results

The performance of the proposed app was evaluated by comparing the time spent by four users in finding their way from the main campus entrance to a particular classroom within a certain building with and without the assistance of the localization / guidance system, respectively. In performing the experiments, the process of navigating to the classroom was separated into six steps, namely (1) looking for campus map;

(2) find the target building; (3) search for indoor floor layout; (4) reach the floor; and, (5) reach the destination. Thus, we record the spent time in various steps as reference. As shown in Figs. 16 and 17, the total time spent by each user in reaching the target was divided into four separate times, namely the time taken in moving from the main campus gate to the first destination sign at Spot A; the time spent in moving from Spot A to the target building (Spot B); the time spent in walking from Spot B to the destination sign located in the building at Spot C; and the time taken in moving from Spot C to the target classroom at No 14401.

Tables II-A and B show the timing results obtained for the four users. Note that Users 1 and 2 performed the search process in a non-assisted manner, while Users 3 and 4 both used the app. As shown, Users 1 and 2 completed the search process in 281.7 s and 333.9 s, respectively (i.e., an average search time of 307.8 s). Since Users 3 and 4 used the guidance app, they did not need to locate the direction signs at Spots A and C, respectively. Consequently, the total search times for the two users were just 206.48 s and 202.3 s, respectively (i.e., an average search time of 204.39 seconds). In other words, the mean time of the assisted users was 33.59% shorter than that of the two non-assisted users.

TABLE II-A
TIMES SPENT BY FOUR USERS IN COMPLETING EACH STAGE OF SEARCH
PROCESS: SEARCH TIMES OF FOUR USERS (UNIT: S)

Name	Spot A	Spot B	Spot C	Spot D
Subject 1	43.87	113.93	118.97	4.93
Subject 2	23.4	153.6	128	28
Subject 3	N/A	109.43	N/A	97.05
Subject 4	N/A	129.9	N/A	72.4

TABLE II-B
TIMES SPENT BY FOUR USERS IN COMPLETING EACH STAGE OF SEARCH
PROCESS:(B) TOTAL SEARCH TIMES OF FOUR USERS AND AVERAGE SAVED
TIME (UNIT: S)

Name	Total	Percentage of Time Saving
Subject 1	281.7	0%
Subject 2	333.9	-18.53%
Subject 3	206.48	26.8%
Subject 4	202.3	28.18%

V. CONCLUSION

With the emergence of Location-based Services (LBS), the need to locate the position of the user with a high degree of accuracy has emerged as an important concern. Accordingly, this study has proposed an app based on GPS, Bluetooth Beacon and NFC technology for providing both a user localization service and an automatic guidance function. Importantly, the app functions in both outdoor and indoor environments, and thus provides a seamless localization / guidance function as the user moves from one environment to the other. The feasibility of the proposed system has been demonstrated by means of localization and guidance tests on a typical student campus building.

VI. CONCLUSION

A conclusion section is not required. Although a conclusion may review the main points of the paper, do not replicate the abstract as the conclusion. A conclusion might elaborate on the importance of the work or suggest applications and extensions.

ACKNOWLEDGMENT

The authors would like to thank the National Science Council, Taiwan, R.O.C. for the financial support of this study under Contract No. MOST 103-2627-E-168-001.

REFERENCES

- [1] S. Ray, R. Blanco, A.K. Goel, "Supporting Location-Based Services in a Main-Memory Database," 2014 IEEE 15th International Conference on Mobile Data Management (MDM), pp. 3-12, 2014.
- [2] A. Chandra, S. Jain and M.A. Qadeer, "GPS Locator: An Application for Location Tracking and Sharing Using GPS for Java Enabled Handhelds," 2011 International Conference on Computational Intelligence and Communication Networks (CICN), pp. 406-410, 2011.
- [3] F. Liu and Z. Yang, "Study on Applications of LBS Based on Electronic Compass," WiCom '09. 5th International Conference on Wireless Communications, Networking and Mobile Computing, 2009, pp. 1-4, 2009.
- [4] Neil E. Klepeis, William C. Nelson, Wayne R. Ott, John P. Robinson, Andy M. Tsang, Paul Switzer, Joseph V. Behar, Stephen C. Hern, William H. Engelmann, "The National Human Activity Pattern Survey (NHAPS): a resource for assessing exposure to environmental pollutants," Journal of Exposure Analysis and Environmental Epidemiology 11, pp. 231-252, 2001.
- [5] I. Yamada, T. Ohtsuki, T. Hisanaga, Li Zheng, "An indoor position estimation method by maximum likelihood algorithm using RSS," 2007 Annual Conference SICE, pp. 2927-2930, 2007.
- [6] J.S. Leu, H.J. Tzeng, "Received Signal Strength Fingerprint and Footprint Assisted Indoor Positioning Based on Ambient Wi-Fi Signals," 2012 IEEE 75th Vehicular Technology Conference (VTC Spring), pp. 1-5, 2012.
- [7] M.G. Moon, S.I. Choi, "Indoor position estimation using image sensor based on VLC," 2014 International Conference on Advanced Technologies for Communications (ATC), pp. 11-14, 2014.
- [8] E. Nakamori, T. Tsukuda, M. Fujimoto, Y. Oda, T. Wada, H. Okada, K. Mutsuura, "A new indoor position estimation method of RFID tags for continuous moving navigation systems," 2012 International Conference on Indoor Positioning and Indoor Navigation (IPIN), pp. 1-8, 2012.
- [9] S. Khalifa, M. Hassan, "Evaluating mismatch probability of activity-based map matching in indoor positioning," In 2012 International Conference on Indoor Positioning and Indoor Navigation (IPIN), pp. 1-9, 2012.
- [10] A. Baniukevic, D. Sabonis, Jensen, S. Christian, Hua Lu, "Improving Wi-Fi Based Indoor Positioning Using Bluetooth Add-Ons," 2011 12th IEEE International Conference on Mobile Data Management (MDM), pp. 246-255, 2011.
- [11] Myungin Ji, Jooyoung Kim, Juil Jeon, Youngsu Cho, "Analysis of positioning accuracy corresponding to the number of BLE beacons in indoor positioning system," 2015 17th International Conference on Advanced Communication Technology (ICACT), pp. 92-95, 2015.
- [12] David Eppstein. "Finding the k Shortest Paths", March 1997.
- [13] Thomas H. Cormen, Charles E. Leiserson, Ronald L. Rivest, and Clifford Stein. "Introduction to Algorithms", Second Edition. MIT Press and McGraw-Hill, Section 24.3: Dijkstra's algorithm, pp. 595-601, 2001.

An Integrated Visualization Tool for Heat Map and Gene Ontology Graph

Somyung Oh, Jeonghyeon Ha, Kyungwon Lee, Sejong Oh

Abstract—Microarray is a general scheme to find differentially expressed genes for target concept. The output is expressed by heat map, and biologists analyze related terms of gene ontology to find some characteristics of differentially expressed genes. In this paper, we propose integrated visualization tool for heat map and gene ontology graph. Previous two methods are used by static manner and separated way. Proposed visualization tool integrates them and users can interactively manage it. Users may easily find and confirm related terms of gene ontology for given differentially expressed genes. Proposed tool also visualize connections between genes on heat map and gene ontology graph. We expect biologists to find new meaningful topics by proposed tool.

Keywords—heat map, gene ontology, microarray, differentially expressed gene

Corresponding Author

Somyung Oh from Ajou University, Korea, Republic Of
e-mail: somyungoh@hotmail.com

Analysis of Global Social Responsibilities of Social Studies Pre-Service Teachers Based on Several Variables

Zafer Cakmak, Birol Bulut, Cengiz Taskiran

Abstract—Technological advances, the world becoming smaller and increasing world population increase our interdependence with individuals that we maybe never meet face to face. It is impossible for the modern individuals to escape global developments and their impact. Furthermore, it is very unlikely for the global societies to turn back from the path they are in. These effects of globalization in fact encumber the humankind at a certain extend. We succumb to these responsibilities for we desire a better future, a habitable world and a more peaceful life. In the present study, global responsibility levels of the participants were measured and the significance of global reactions that individuals have to develop on global issues was reinterpreted under the light of the existing literature. The study was conducted with general survey model, one of the survey methodologies General survey models are surveys conducted on the whole universe or a group, sample or sampling taken from the universe to arrive at a conclusion about the universe, which includes a high number of elements. The study was conducted with data obtained from 350 pre-service teachers attending 2016 spring semester to determine 'Global Social Responsibility' levels of social studies pre-service teachers based on several variables. Collected data were analyzed using SPSS 21.0 software. T-test and ANOVA were utilized in the data analysis.

Keywords—social studies, globalization, global social responsibility, education

Corresponding Author

Birol Bulut from Firat University, Turkey
e-mail: birolbulut1@gmail.com

Analysis of Global Social Responsibilities of Social Studies Pre-Service Teachers Based on Several Variables

Zafer Cakmak, Birol Bulut, Cengiz Taskiran

Abstract—Technological advances, the world becoming smaller and increasing world population increase our interdependence with individuals that we maybe never meet face to face. It is impossible for the modern individuals to escape global developments and their impact. Furthermore, it is very unlikely for the global societies to turn back from the path they are in. These effects of globalization in fact encumber the humankind at a certain extend. We succumb to these responsibilities for we desire a better future, a habitable world and a more peaceful life. In the present study, global responsibility levels of the participants were measured and the significance of global reactions that individuals have to develop on global issues was reinterpreted under the light of the existing literature. The study was conducted with general survey model, one of the survey methodologies General survey models are surveys conducted on the whole universe or a group, sample or sampling taken from the universe to arrive at a conclusion about the universe, which includes a high number of elements. The study was conducted with data obtained from 350 pre-service teachers attending 2016 spring semester to determine 'Global Social Responsibility' levels of social studies pre-service teachers based on several variables. Collected data were analyzed using SPSS 21.0 software. T-test and ANOVA were utilized in the data analysis.

Keywords—social studies, globalization, global social responsibility, education

Corresponding Author

Birol Bulut from Firat University, Turkey
e-mail: birolbulut1@gmail.com

Analytical Model for Columns in Existing Reinforced Concrete Buildings

Chang Seok Lee, Sang Whan Han, Girbo Ko, Debbie Kim

Abstract—Existing reinforced concrete structures are designed and built without considering seismic loads. The columns in such buildings generally exhibit widely spaced transverse reinforcements without using seismic hooks. Due to the insufficient reinforcement details in columns, brittle shear failure is expected in columns that may cause pre-mature building collapse mechanism during earthquakes. In order to retrofit those columns, the accurate seismic behavior of the columns needs to be predicted with proper analytical models. In this study, an analytical model is proposed for accurately simulating the cyclic behavior of shear critical columns. The parameters for pinching and cyclic deterioration in strength and stiffness are calibrated using test data of column specimens failed by shear.

Keywords—analytical model, cyclic deterioration, existing reinforced concrete columns, shear failure

Corresponding Author

Chang Seok Lee from Hanyang University, Korea, Republic Of
e-mail: mtsonicc@gmail.com

Anti-obesity effect of *Cordyceps militaris* fermented black rice

Chih-Hung Liang, Jung-Jung Chen and Shen-Shih Chiang^{c*}

Abstract—Obesity are defined as abnormal or excessive fat accumulation that presents a risk to health, which are major risk factors for a number of chronic diseases, including diabetes, cardiovascular diseases and cancer. *Cordyceps militaris* (CM) is a well-known traditional medicine in Asian countries and a rich source of biologically active components. Black rice (*Oryza sativa* L.) is a special cultivar of rice that contains rich anthocyanins and regarded as a health-promoting food in China and other Eastern. The aim of this study was to investigate the anti-obesity effect of *Cordyceps militaris* fermented black rice (CB) on HFD-induced BALB/c mice model. The results indicated that administration of low and high dosage of CB powder significantly reduced the body weights (7.38% and 7.78%), body fat ratio (2.37% and 2.78%), aspartate aminotransferase (AST) and alanine aminotransferase (ALT) levels compared to the HF group ($p<0.05$). Histopathological analysis showed that the score of fatty liver in HF group (5.0) was significantly higher than CB groups (2.1 and 3.6) ($p<0.05$). In conclusion, *Cordyceps militaris* fermented black rice can reduce the body weight via inhibition of the fat accumulation in liver and body and possess the anti-obesity potency.

Keywords—*Cordyceps militaris*, black rice, obesity, HFD-induced mice

Chih-Hung Liang is with the Department of Food Science, Tunghai University, 1727, Sec.4, Taiwan Boulevard, Xitun District, Taichung 40704, Taiwan (phone: 886-4-2359-0120 ex 37332; e-mail: liang200@thu.edu.tw).

Jung-Jung Chen is with Department of Food Science, Tunghai University, 1727, Sec.4, Taiwan Boulevard, Xitun District, Taichung 40704, Taiwan (phone: 886-9-6314-4269; e-mail:candy3215777@hotmail.com).

Shen-Shih Chiang is with the Department of Food Science and Biotechnology, and NCHU-UCD Plant and Food Biotechnology Program, Biotechnology Center, 250 Kuokuang Road, Taichung City 40227, Taiwan National Chung Hsing University (phone: 886-4-2285-7797 ; e-mail: sschiang@hotmail.com).

Anticancer Effects of MicroRNA-1275 in Human Nasopharyngeal Carcinoma by Targeting HOXB5

Cheng-Cao Sun¹, Shu-Jun Li^{1,2}, and De-Jia Li¹

¹ Department of Occupational and Environmental Health, School of Public Health, Wuhan University, Wuhan, P. R. China; ² Wuhan Hospital for the Prevention and Treatment of Occupational Diseases, 430071 Wuhan, P. R. China;

Corresponding author: De-Jia Li; No.115 Donghu Road, Wuchang District, Wuhan, China; Tel: (86)18271470520; Fax: (86)02768778695; E-mail: lodjlwhu@sina.com

Abstract

Through analysis of a published micro-array-based high-throughput assessment, we discovered that miR-1275 was markedly down-regulated in nasopharyngeal carcinoma (NPC) tissues. However, little is known about its effect and mechanism involved in NPC development and progression. In this study, we investigated the role of miR-1275 on the development of NPC. The results indicated that miR-1275 was significantly down-regulated in primary NPC tissues and very low levels were found in NPC cell lines. Ectopic expression of miR-1275 in NPC cell lines significantly suppressed cell growth as evidenced by cell viability assay and colony formation assay, through inhibition of HOXB5. In addition, miR-1275 suppresses G1/S transition through inhibition of HOXB5. Further, oncogene *HOXB5* was revealed to be a putative target of miR-1275, which was inversely correlated with miR-1275 expression in NPC. Collectively, our study demonstrates that as a tumor suppressor, miR-1275 played a pivotal role on NPC through inhibiting cell proliferation, and suppressing G1/S transition by targeting oncogenic *HOXB5*.

Key words: microRNA-1275 (miR-1275), HOXB5, nasopharyngeal carcinoma, proliferation

Asynchronous Sequential Machines with Fault Detectors

Seong Woo Kwak, Jung-Min Yang

Abstract—A strategy of fault diagnosis and tolerance for asynchronous sequential machines is discussed in this paper. With no synchronizing clock, it is difficult to diagnose an occurrence of permanent or stuck-in faults in the operation of asynchronous machines. In this paper, we present a fault detector comprised of a timer and a set of static functions to determine the occurrence of faults. In order to realize immediate fault tolerance, corrective control theory is applied to designing a dynamic feedback controller. Existence conditions for an appropriate controller and its construction algorithm are presented in terms of reachability of the machine and the feature of fault occurrences.

Keywords—Asynchronous sequential machines, corrective control, fault diagnosis and tolerance, fault detector.

I. INTRODUCTION

CORRECTIVE control theory is a novel research approach to controlling the stable state behavior of asynchronous sequential machines. The basic configuration of corrective control is similar to that of traditional feedback control for continuous-time systems, but the way the control input is made is significantly different. As asynchronous sequential machines are classified as finite state discrete-event systems, generation of the control input and the operation of the closed-loop system must be considered in discrete mathematics and switching and finite automata theory. In the operation of asynchronous sequential machines working without no global synchronizing clock, only stable states are noticeable and practically meaningful [1]. Thus we say that a corrective controller achieves its control objective if the stable state behavior of the closed-loop system matches that of a pre-specified model.

Since first developed for general sequential machines in the mid 1990's [2], [3], corrective control theory has been mainly applied to tolerating or eliminating various deficiencies in asynchronous sequential machines. Reference [4] addresses the model matching problem for input/state

asynchronous machines with critical races. Here, input/state asynchronous machines are referred to as those machines in which the current state is given as the output value. References [5], [6] extend the work of [4] to input/output asynchronous machines, where the output value is different from the machine's state. Reference [7] further generalizes the former studies by incorporating the information on the output burst. Reference [8] solves the model matching problem for input/state asynchronous machines subject to infinite cycles. References [9], [10] develop corrective controllers for diagnosing and tolerating transient faults that cause a violation of state transition characteristics of asynchronous machines. Reference [11] demonstrates that the control mechanism for transient faults can be implemented in real-world digital systems. In [12], a corrective controller is presented to realize model matching with the constraint that some external input characters are uncontrollable. A similar study with the application to error counters can be found in [13]. References [14], [15] present fault tolerant corrective control schemes for tolerating permanent faults occurring to input/output machines. Finally, [16] addresses identification and corrective control of asynchronous machines with unspecified transition parts based on an adaptive control law.

The objective of this paper is to present a scheme of fault diagnosis and tolerance for input/state asynchronous sequential machines subject to permanent state transition faults. Permanent state transition faults are defined as perpetual transformation of the feature of a transient pair to stable one caused by an occurrence of the adversarial input. Due to the absence of a global synchronizing clock, it is impossible for a corrective controller to diagnose permanent state transition faults only based on the state feedback. Hence, we propose a *fault detector* comprised of a timer and a set of static functions to determine the occurrence of faults. Note that in the case of transient faults [9]-[11], no fault detector is required since the change of the state feedback indicates an occurrence of an adversarial input. In order to realize immediate fault tolerance, corrective control theory is applied to designing a dynamic feedback controller. Existence conditions for an appropriate controller and its construction algorithm are presented in terms of reachability of the machine and the feature of fault occurrences.

The rest of this paper is organized as follows. In Section II, starting with background material on dynamics of asynchronous sequential machines, we present a model of permanent state transition faults and the basic configuration of the fault tolerant corrective controller. In Section III, we propose the structure of the fault detector and show that

The research of S. W. Kwak was supported by Basic Science Research Program through the National Research Foundation of Korea (NRF) funded by the Ministry of Education (No. NRF-2016R1D1A1B02012959). The research of J.-M. Yang was supported in part by Basic Science Research Program through the National Research Foundation of Korea (NRF) funded by the Ministry of Science, ICT and future Planning (No. NRF-2015R1A2A1A15054026), in part by Basic Science Research Program through the National Research Foundation of Korea (NRF) funded by the Ministry of Education (No. NRF-2015R1D1A1A01056764), and in part by the Bio & Medical Technology Development Program of the National Research Foundation (NRF) funded by the Korean government (MSIP) (No. NRF-2015M3A9A7067220).

S. W. Kwak is with the Department of Electronic Engineering, Keimyung University, Daegu, 42601, Republic of Korea (e-mail: ksw@kmu.ac.kr).

J.-M. Yang is with the School of Electronics Engineering, Kyungpook National University, Daegu, 41566, Republic of Korea (corresponding author; e-mail: jmyang@ee.knu.ac.kr).

the proposed fault detector can diagnose any occurrence of permanent state transition faults, which can be utilized to realize fault tolerant corrective controllers. Finally, Section IV summarizes the main contributions of the paper.

II. PRELIMINARIES

A. Modeling of Asynchronous Machines

An input/state asynchronous machine Σ is modeled by the following deterministic finite-state machine.

$$\Sigma = (A, X, x_0, f)$$

where A is the input set, X is the state set, $x_0 \in X$ is the initial state, and

$$f : X \times A \rightarrow X$$

is the state transition function partially defined on $X \times A$. Owing to the lack of a synchronizing clock, a valid state–input pair $(x, v) \in X \times A$ is either stable or transient according to $f(x, v)$:

$$(x, v) = \begin{cases} \text{stable} & f(x, v) = x \\ \text{transient} & f(x, v) \neq x \end{cases}$$

Σ stays at a stable pair (x, v) indefinitely unless the external input changes. If the input is switched to a new character v such that $f(x, v) \neq x$, then (x, v) is a transient pair and Σ initiates a chain of transient transitions, e.g.,

$$\begin{aligned} f(x, v) &= x_1, \\ f(x_1, v) &= x_2, \\ &\vdots \end{aligned}$$

while the input v remains fixed. Under the asynchronous mechanism, Σ traverses transient states x_1, x_2, \dots , instantaneously. If Σ has no infinite cycle, this chain of transitions will end at a stable state x' such that $f(x', v) = x'$. x' is called the next stable state of (x, v) .

It is often convenient to express the dynamics of Σ only in terms of stable states, since transient states are unnoticeable from the viewpoint of outer users. The *stable recursion function*

$$s : X \times A \rightarrow X$$

[4] is defined for this purpose. For a valid state–input pair (x, v) ,

$$s(x, v) := x'$$

where x' is the next stable state of (x, v) . If (x, v) is a stable pair, $s(x, v) = x$. The chain of transitions from (x, v) to (x', v) , represented by $s(x, v) = x'$, is termed a *stable transition*. For later usage, define two input sets $U(x), T(x) \subset A$ with respect to $x \in X$ as

$$\begin{aligned} U(x) &:= \{v \in A | s(x, v) = x\} \\ T(x) &:= \{v \in A | s(x, v) \neq x\}. \end{aligned}$$

$U(x)$ and $T(x)$ denote the set of input characters that make a stable and transient pair with x , respectively. We can extend the domain of s from input characters to strings. For $x \in X$

and $v_1 v_2 \dots v_k \in A^+$, where A^+ is the set of all non-empty strings of characters in A ,

$$s(x, v_1 v_2 \dots v_k) := s(s(x, v_1), v_2 \dots v_k).$$

If an input string $t \in A^+$ exists for two states x and x' such that $x' = s(x, t)$, x' is said to be *stably reachable* from x in Σ [4].

To represent the underlying transient states that are traced from a given transient pair (x, v) , we define a partial function

$$\tau : X \times A \rightarrow P(X),$$

where $P(X)$ is the power set of X :

$$\tau(x, v) := \begin{cases} \{x, x_1, \dots, x_{k-1}\} & s(x, v) \neq x \\ \emptyset & s(x, v) = x \end{cases} \quad (1)$$

$\tau(x, v)$ is the set of all transient states traversed by Σ when it goes on a chain of transitions starting from (x, v) . Since a stable pair does not involve any transient state, $\tau(x, v) = \emptyset$ if $s(x, v) = x$.

In this paper, we assume that Σ suffers from permanent state transition faults, namely by an occurrence of a fault input, a transient state–input pair is transformed into a stable one. To describe permanent state transition faults, we introduce the following definition.

Definition 1: Given $\Sigma = (A, X, x_0, f)$, let

$$F := \{f_1, \dots, f_r\}$$

be the set of permanent state transition faults, and let

$$H := \{(z_1, w_1), \dots, (z_r, w_r)\} \subset X \times A$$

be the set of associated transient state–input pairs. f_i , the i th permanent state transition fault, alters perpetually the transition characteristics of (z_i, w_i) from transient to stable, i.e.,

$$s(z_i, w_i) \neq z_i \xrightarrow{\text{fault } f_i} s(z_i, w_i) = z_i.$$

Each f_i is supposed to be distinctive with one another. On the other hand, z_i and z_j are not necessarily disjoint with each other. If $z_i = z_j$, however, w_i must differ from w_j ; otherwise, f_i and f_j would correspond to the same state–input pair.

B. Closed-Loop System

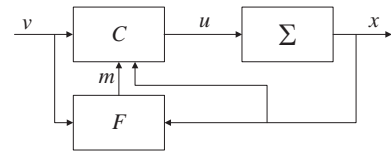


Fig. 1 Corrective control system with a fault detector

Fig. 1 shows the configuration of the proposed corrective control system for Σ . C is a corrective controller having the form of an input/output asynchronous machine. $v \in A$ is the external input, $u \in A$ is the control input provided by C , and x is the state feedback of Σ . D denotes a *fault detector* positioned in the feedback path to detect occurrences of fault inputs F . Receiving x and v , D provides C with a logical value $m \in \{0, 1\}$, called the *fault indicator signal*, that

indicates whether a permanent state transition fault occurs. Let us denote by Σ_c the closed-loop system comprised of C , D , and Σ . With no synchronizing clock, the external input v also varies asynchronously. In this study, we assume that any interval between two consecutive external inputs is greater than or equal to the *minimum interval* T_v . In other words, the external input must not change too quickly, which fits into common operations of sequential machines.

When Σ shows the normal behavior, C relays the external input v to the control input channel u without modification. When a permanent state transition fault occurs, the notification of the fault occurrence is transmitted to C via the signal $m = 1$. C generates an appropriate control input sequence so that Σ_c seems to maintain the normal operation despite the fault occurrence. In this paper, we study the single fault scenario [17] in which at most one of the fault events f_1, \dots, f_r may occur at a time.

When working with asynchronous machines, it is important to comply with the principle of fundamental mode operations [18], an operating policy that prohibits the simultaneous change of two or more system variables. This policy is intended to prevent any unpredictable outcome that attributes to asynchronous mechanisms. Adapting the results of [11], we obtain the following conditions to ensure fundamental mode operations of the closed-loop system Σ_c in Fig. 1.

Condition 1: The closed-loop system Σ_c in Fig. 1 operates in fundamental mode if and only if all the following requirements are met:

- (a) Σ is at a stable state when C undergoes transitions.
- (b) C is at a stable state when Σ undergoes transitions.
- (c) The variables v and m change their values only when Σ and C are both at stable states, and then only one at a time.

According to Condition 1.(b), C must be designed so that it commences transitions only after verifying Σ has reached a stable pair, and must adopt a stable pair immediately prior to providing the control input u to Σ . Similarly, the fault detector D must generate the fault indicator signal m only when both Σ and C are at stable states and v does not change its value. C and D will be designed so as to satisfy all these requirements (Condition 1.(c)). The fundamental mode operation assures that all transitions of Σ_c are unambiguous and deterministic.

III. FAULT DETECTOR

A. Structure of Fault Detector

Consider a state-input pair (z_i, w_i) at which Σ may experience the permanent state transition fault f_i . Since the moment that f_i occurs to Σ is indeterminate in general, we must examine as below all the possible instances to derive detectability.

- (i) First, assume that Σ has been staying at a stable pair (z_i, v) with $v \in U(z_i)$ when the fault f_i happens. The fault occurrence is not perceived at this instant because no explicit change of the system variables is observed. Suppose further that the external input changes to w_i . Were it not for the fault f_i , Σ would go through the normal stable transition from z_i to $s(z_i, w_i)$. With the

incidence of f_i , however, Σ does not respond to w_i ; it is stuck at z_i unless a fault-tolerant control scheme is activated. If the fault is not recovered immediately, further change of the external input would drive Σ to an incorrect next stable state, possibly leading to total breakdown of the machine.

- (ii) Next, assume that for a transient pair (x, w_i) with $x \neq z_i$, z_i is an element of $\tau(x, w_i)$ where $\tau(x, w_i)$ is defined in (1). This implies that Σ passes through the transient pair (z_i, w_i) during the course of the stable transition from x to $s(x, w_i)$. Note that $s(x, w_i) = s(z_i, w_i)$ if $z_i \in \tau(x, w_i)$. If f_i has occurred before Σ begins this transition, Σ falls into z_i instead of reaching the next stable state $s(x, w_i)$. Likewise, further change of the external input would cause incorrect subsequent behaviors.

In both (i) and (ii), the result of the fault occurrence is the same: Σ does not respond to the last changed variable, either it is z_i or w_i . In case (i), for instance, if Σ has been staying at the stable state z_i , it does not carry out the innate transition from z_i to $f(z_i, w_i)$ in response to the changed input w_i after the fault occurrence. Thus we can know the occurrence of f_i by measuring the dead-lock time that lapses away from the instant that the last changed variable of (z_i, w_i) enters Σ . If the dead-lock time is greater than the prescribed threshold, we regard that f_i occurs.

The fault detector D in Fig. 1 plays the role of detecting faults using the foregoing criterion. It records the entrance time of the last changed variable among z_i and w_i , and it measures the duration during which neither the state nor input changes its value after the entrance time of the last changed variable. The fault indicator signal m is generated by the following function.

$$\begin{aligned} \nu &: X \times A \times T \rightarrow \{0, 1\} \\ m &= \nu(x, v, t) := \begin{cases} 1 & (x, v) \in H \text{ and } t \geq T_h \\ 0 & \text{otherwise} \end{cases} \quad (2) \end{aligned}$$

where t is the measured dead-lock time and T_h is the pre-determined threshold. Consider again case (i) where w_i enters Σ that has been stuck at z_i by the fault f_i . In view of Fig. 1, D records the entrance time of w_i and measures the dead-lock time t thereafter. If f_i does not occur, Σ would transfer to $f(z_i, w_i)$ instantaneously and the state feedback x would change to $f(z_i, w_i)$ right after the entrance of w_i . According to (2), we have

$$\begin{aligned} \nu(z_i, w_i, t) &= 0 & \because t \ll T_h \\ \nu(f(z_i, w_i), w_i, t) &= 0 & \because (f(z_i, w_i), w_i) \notin H. \end{aligned}$$

Hence the fault indicator signal m remains 0. On the other hand, after the occurrence of f_i , the dead-lock time t is prolonged indefinitely. At the moment that t becomes equal to T_h , D generates the indicator signal of fault detection, namely $m = 1$. The fault detection procedure in case (ii) is analyzed in a similar manner. Recalling that T_v is the minimum interval between two consecutive external inputs, we must select T_h such that

$$T_h < T_v.$$

Otherwise, the external input might change its value before the dead-lock time accumulates to the threshold value T_h .

B. Fault Tolerant Control

We first review the existence condition and the operation of corrective controllers solving model matching problems addressed in the prior work [4]. The objective is to design a controller C so that the closed-loop system Σ_c in Fig. 1 (without D) can transfer from a state z to the desired state z' in response to an external input a . This implies that the next stable state of (z, a) is not equal to z' , i.e., $s(z, a) \neq z'$, or (z, a) may not be even a valid pair of Σ . In the framework of corrective control, the necessary and sufficient condition for realizing the desired stable transition from z to z' is that z' is stably reachable from z [4], that is,

$$[\Sigma_c : z \rightarrow z'] \Leftrightarrow \quad (3)$$

$$[\exists \alpha = u_1 \cdots u_k \in A^+ \text{ s.t. } s(z, \alpha) = z'].$$

C utilizes α to make a correction trajectory from z to z' . Under the principle of fundamental mode operations, Σ must stay at the stable state z when the external input changes to a (see Condition 1.(a)). In view of Fig. 1, C suppresses the incoming input a and instead generates the first input character u_1 of α . Σ then transfers to the next stable state $s(z, u_1)$. Receiving $s(z, u_1)$ as the state feedback, C undergoes its own state transition and generates the second character u_2 , in response to which Σ moves to the second next stable state $s(s(z, u_1), u_2)$ and so on. The interaction between C and Σ is conducted very fast due to the lack of a synchronizing clock. Hence the closed-loop system Σ_c seems to move from z to z' instantaneously in response to a , which accomplishes the objective of model matching.

The condition (3) is equally applied to fault-tolerant control for permanent state transition faults with little modification. We can regard fault recovery as another model matching problem. When we detect an occurrence of f_i by observing that Σ is stuck at the transient state z_i longer than T_h , a control law must be activated that takes Σ_c immediately toward the desired state $s(z_i, w_i)$. The existence condition for the controller is easily derived from (3) as

$$\exists \alpha_i \in A^+ \text{ such that}$$

$$s(z_i, \alpha_i) = s(z_i, w_i) \text{ and } \alpha_i \neq w_i, \quad \forall w_i \in W_i. \quad (4)$$

$\alpha_i \neq w_i$ means that the correction trajectory must detour the faulty transient pair (z_i, w_i) . The procedure of the correction procedure will be constructed in a similar manner to the previous results [11], [14].

IV. SUMMARY

We have presented a corrective control scheme for asynchronous sequential machines with permanent state transition faults. Main consideration is devoted to proposing a fault detection and tolerance scheme for permanent state transition faults. Necessary and sufficient conditions for the existence of the fault detector and corrective controller are analyzed in the framework of corrective control.

REFERENCES

- [1] J. Sparsø and S. Furber, *Principles of Asynchronous Circuit Design — A Systems Perspective*, Kluwer Academic Publishers, 2001.
- [2] J. Hammer, “On the corrective control of sequential machines,” *Int. J. Control*, vol. 65, no. 2, pp. 249–276, 1996.
- [3] J. Hammer, “On the control of sequential machines with disturbances,” *Int. J. Control*, vol. 67, no. 3, pp. 307–331, 1997.
- [4] T. E. Murphy, X. Geng, and J. Hammer, “On the control of asynchronous machines with races,” *IEEE Trans. Autom. Control*, vol. 48, no. 6, pp. 1073–1081, 2003.
- [5] J. Peng and J. Hammer, “Input/output control of asynchronous sequential machines with races,” *Int. J. Control*, vol. 83, no. 1, pp. 125–144, 2010.
- [6] X. Geng and J. Hammer, “Input/output control of asynchronous sequential machines,” *IEEE Trans. Autom. Control*, vol. 50, no. 12, pp. 1956–1970, 2005.
- [7] J. Peng and J. Hammer, “Bursts and output feedback control of non-deterministic asynchronous sequential machines,” *European J. Control*, vol. 18, no. 3, pp. 286–300, 2012.
- [8] N. Venkatraman and J. Hammer, “On the control of asynchronous sequential machines with infinite cycles,” *Int. J. Control*, vol. 79, no. 7, pp. 764–785, 2006.
- [9] J.-M. Yang, “Corrective control of input/output asynchronous sequential machines with adversarial inputs,” *IEEE Trans. Autom. Control*, vol. 55, no. 3, pp. 755–761, 2010.
- [10] J.-M. Yang and J. Hammer, “Asynchronous sequential machines with adversarial intervention: the use of bursts,” *Int. J. Control*, vol. 83, no. 5, pp. 956–969, 2010.
- [11] J.-M. Yang and S. W. Kwak, “Realizing fault-tolerant asynchronous sequential machines using corrective control,” *IEEE Trans. Control Syst. Technol.*, vol. 18, no. 6, pp. 1457–1463, 2010.
- [12] J.-M. Yang and S. W. Kwak, “Model matching for asynchronous sequential machines with uncontrollable inputs,” *IEEE Trans. Autom. Control*, vol. 56, no. 9, pp. 2140–2145, 2011.
- [13] J.-M. Yang and S. W. Kwak, “Corrective control of asynchronous machines with uncontrollable inputs: application to single-event-upset error counters,” *IET Control Theory Appl.*, vol. 4, no. 11, pp. 2454–2462, 2010.
- [14] J.-M. Yang, “Fault tolerance in asynchronous sequential machines using output feedback control,” *IEEE Trans. Autom. Control*, vol. 57, no. 6, pp. 1604–1609, 2012.
- [15] J.-M. Yang and S. W. Kwak, “Fault diagnosis and fault-tolerant control of input/output asynchronous sequential machines,” *IET Control Theory Appl.*, vol. 6, no. 11, pp. 1682–1689, 2012.
- [16] J.-M. Yang, T. Xing, and J. Hammer, “Adaptive control of asynchronous sequential machines with state feedback,” *European J. Control*, vol. 18, no. 6, pp. 503–527, 2012.
- [17] S. Shu and F. Lin, “Fault-tolerant control for safety of faulty discrete event systems,” *IEEE Trans. Auto. Sci. Engr.*, vol. 11, no. 1, pp. 78–89, 2014.
- [18] Z. Kohavi and N. K. Jha, *Switching and Finite Automata Theory*, 3rd ed. Cambridge University Press: Cambridge, UK, 2010.

Bimetallic Cu/Au Nanostructures and Bio-Application

Si Yin Tee

Abstract—Bimetallic nanostructures have received tremendous interests as a new class of nanomaterials which may have better technological usefulness with distinct properties from those of individual atoms and molecules or bulk matter. They excelled over the monometallic counterparts because of their improved electronic, optical and catalytic performances. The properties and the applicability of these bimetallic nanostructures not only depend on their size and shape, but also on the composition and their fine structure. These bimetallic nanostructures are potential candidates for bio-applications such as biosensing, bioimaging, biodiagnostics, drug delivery, targeted therapeutics, and tissue engineering. Herein, gold-incorporated copper (Cu/Au) nanostructures were synthesized through the controlled disproportionation of Cu⁺-oleylamine complex at 220 °C to form copper nanowires and the subsequent reaction with Au³⁺ at different temperatures of 140, 220 and 300 °C. This is to achieve their synergistic effect through the combined use of the merits of low-cost transition and high-stability noble metals. Of these Cu/Au nanostructures, Cu/Au nanotubes display the best performance towards electrochemical non-enzymatic glucose sensing, originating from the high conductivity of gold and the high aspect ratio copper nanotubes with high surface area so as to optimise the electroactive sites and facilitate mass transport. In addition to high sensitivity and fast response, the Cu/Au nanotubes possess high selectivity against interferences from other potential interfering species and excellent reproducibility with long-term stability. By introducing gold into copper nanostructures at a low level of 3, 1 and 0.1 mol% relative to initial copper precursor, a significant electrocatalytic enhancement of the resulting bimetallic Cu/Au nanostructures starts to occur at 1 mol%. Overall, the present fabrication of stable Cu/Au nanostructures offers a promising low-cost platform for sensitive, selective, reproducible and reusable electrochemical sensing of glucose.

Keywords—bimetallic, electrochemical sensing, glucose oxidation, gold-incorporated copper nanostructures

Corresponding Author

Si Yin Tee from Institute of Materials Research and Engineering,
Singapore
e-mail: teesy@imre.a-star.edu.sg

CertifHy: Developing a European Framework for the Generation of Guarantees of Origin for Green Hydrogen

Frederic Barth¹, Wouter Vanhoudt^{1*}, Marc Londo, Jaap C. Jansen², Karine Veum², Javier Castro³, Klaus Nürnberger³ and Matthias Altmann⁴

¹ *Hinicio SA, RUE DES PALAIS 44, B-1030 Brussels, Belgium*

² *Sticchting Energieonderzoek Centrum Nederland, WESTERDUINWEG 3, 1755 LE Petten, Netherlands*

³ *Tiiv Sud Industrie Service GmbH, WESTENDSTRASSE 199, 80686 Munchen, Germany*

⁴ *Ludwig-Boelkow-Systemtechnik GmbH Daimlerstr. 15, 85521 Ottoburn Germany*

(*) certifhy@hinicio.com

Hydrogen is expected to play a key role in the transition towards a low-carbon economy, especially within the transport sector, the energy sector and the (petro)chemical industry sector. However, the production and use of hydrogen only make sense if the production and transportation are carried out with minimal impact on natural resources, and if greenhouse gas emissions are reduced in comparison to conventional hydrogen or conventional fuels. The CertifHy project, supported by a wide range of key European industry leaders (gas companies, chemical industry, energy utilities, green hydrogen technology developers and automobile manufacturers, as well as other leading industrial players) therefore aims to: 1. Define a widely acceptable definition of green hydrogen. 2. Determine how a robust Guarantee of Origin (GoO) scheme for green hydrogen should be designed and implemented throughout the EU. It is divided into the following work packages (WPs). 1. Generic market outlook for green hydrogen: Evidence of existing industrial markets and the potential development of new energy related markets for green hydrogen in the EU, overview of the segments and their future trends, drivers and market outlook (WP1). 2. Definition of “green” hydrogen: step-by-step consultation approach leading to a consensus on the definition of green hydrogen within the EU (WP2). 3. Review of existing platforms and interactions between existing GoO and green hydrogen: Lessons learnt and mapping of interactions (WP3). 4. Definition of a framework of guarantees of origin for “green” hydrogen: Technical specifications, rules and obligations for the GoO, impact analysis (WP4). 5. Roadmap for the implementation of an EU-wide GoO scheme for green hydrogen: the project implementation plan will be presented to the FCH JU and the European Commission as the key outcome of the project and shared with stakeholders before finalisation (WP5 and 6). Definition of Green Hydrogen: CertifHy Green hydrogen is hydrogen from renewable sources that is also CertifHy Low-GHG-emissions hydrogen. Hydrogen from renewable sources is hydrogen belonging to the share of production equal to the share of renewable energy sources (as defined in the EU RES directive) in energy consumption for hydrogen production, excluding ancillary functions. CertifHy Low-GHG hydrogen is hydrogen with emissions lower than the defined CertifHy Low-GHG-emissions threshold, i.e. 36.4 gCO₂eq/MJ, produced in a plant where the average emissions intensity of the non-CertifHy Low-GHG hydrogen production (based on an LCA approach), since sign-up or in the past 12 months, does not exceed the emissions intensity of the benchmark process (SMR of natural gas), i.e. 91.0 gCO₂eq/MJ.

Characterization of Bacteria by a Nondestructive Sample Preparation Method in A TEM System

J. Shiue, I-H. Chen, S. W.-Y. Chiu, Y.-L. Wang

Abstract— In this work, we present a nondestructive method to characterize bacteria in a TEM system. Unlike the conventional TEM specimen preparation method, which needs to thin the specimen in a destructive way, or spread the samples on a tiny millimeter sized carbon grid, our method is easy to operate without the need of sample pretreatment. With a specially designed transparent chip that allows the electron beam to pass through, and a custom made chip holder to fit into a standard TEM sample holder, the bacteria specimen can be easily prepared on the chip without any pretreatment, and then be observed under TEM. The centimeter sized chip is covered with Au nanoparticles in the surface as the markers which allow the bacteria to be observed easily on the chip. We demonstrate the success of our method by using *E. coli* as an example, and show that high resolution TEM images of *E. coli* can be obtained with the method presented. Some *E. coli* morphology characteristics imaged using this method are also presented.

Keywords— bacteria, chip, nanoparticles, TEM

J. Shiue is with the Institute of Physics, Academia Sinica, Taipei 11529, Taiwan (e-mail: yshiue@phys.sinica.edu.tw).

I-H. Chen is with the Research Program on Nanoscience and Nanotechnology, Academia Sinica, Taipei 11529, Taiwan (e-mail: ihchen@gate.sinica.edu.tw).

S. W.-Y. Chiu and Y.-L. Wang are with the Institute of Atomic and Molecular Sciences, Academia Sinica, Taipei 10617, Taiwan (e-mail: shirleywchiu@gmail.com; ylwang@pub.iams.sinica.edu.tw).

CO₂ Adsorption on the Activated Klaten-Indonesian Natural Zeolite in a Packed Bed Adsorber

Sang Kompiang Wirawan, Chandra Purnomo

Abstract—Carbon dioxide (CO₂) adsorption on the activated Klaten-Indonesian natural zeolite (AKINZ) in a packed bed adsorber has been studied. Experiment works consisted of acid activation and adsorption experiments. The natural zeolite sample was activated using 0.3 M HCl at the temperature of 353 K. In the adsorption experiments the feed gas concentrations were 40 and 80 % CO₂ in helium within various temperatures of 303; 323 and 373 K. The experiments were conducted by using transient step change adsorption and 20 % Ar/He tracer experiment was conducted to measure dispersion and time lag effect of the packed bed system. A mathematical model of CO₂ adsorption had been set up by assuming plug flow; isothermal; isobaric and no gas film mass transport resistance. Single site Langmuir physisorption and Maxwell Stefan mass transport in micropore were applied. All the data were then optimized to get the best value of modified fitted parameter. The model was in a good agreement with the experiment data. Diffusivity tended to increase by increasing temperatures.

Keywords—adsorption, Langmuir, Maxwell-Stefan, natural zeolite, surface diffusion

Corresponding Author

Sang Kompiang Wirawan from Gadjah Mada University, Indonesia
e-mail: skwirawan@ugm.ac.id

Comparative Growth Rates of *Treculia africana* Decne: Embryo in Varied Strengths of Murashige and Skoog Basal Medium

Okafor C. Uche, Agbo P. Ejiofor, Okezie C. Eziuche

Abstract—This study provides a regeneration protocol for *Treculia africana* Decne (an endangered plant) through embryo culture. Mature zygotic embryos of *T. africana* were excised from the seeds aseptically and cultured on varied strengths (full, half and quarter) of Murashige and Skoog (MS) basal medium supplemented. All treatments experienced 100±0.00 percent sprouting except for half and quarter strengths. Plantlets in MS full strength had the highest fresh weight, leaf area, and longest shoot length when compared to other treatments. All explants in full, half, quarter strengths and control had the same number of leaves and sprout rate. Between the treatments, there was a significant difference ($P>0.05$) in their effect on the length of shoot and root, number of adventitious root, leaf area, and fresh weight. Full strength had the highest mean value in all the above-mentioned parameters and differed significantly ($P>0.05$) from others except in shoot length, number of adventitious roots, and root length where it did not differ ($P<0.05$) from half strength. The result of this study indicates that full strength MS basal medium offers a better option for the optimum growth for *Treculia africana* regeneration *in vitro*.

Keywords—Medium strengths, Murashige and Skoog, *Treculia africana*, zygotic embryos.

I. INTRODUCTION

TRECVLIA africana Decne, commonly called African breadfruit (also known as “Ukwa” by the Igbo tribe), is a member of the taxonomic family Moraceae, genus *Treculia* and a multipurpose tree crop in Nigeria and Africa as a whole [1]. Propagation is by seed, but it can also be propagated vegetatively through cuttings and shield grafting. The seeds are highly nutritious and constitute a cheap source of vitamins, minerals, proteins, carbohydrates, and fats [2]. Despite its importance, little or no effort has been made to propagate the species as this valuable plant is being lost because of deforestation and urbanization, and nothing is being done about replanting the species. This, however, results in the plant declining at an alarming rate, and thus, needs priority conservation. This decline is due to non-improvement and non-cultivation of the species since it takes ten years or more to fruit. Hence, the need for mass propagation is necessary [3].

Plant tissue culture, precisely embryo culture, has been found to be the best means of mass propagating for the declining plants. Zygotic embryo culture is a technique which involves isolating and culturing of immature or mature zygotic

embryos on a nutrient media under aseptic conditions. This technique helps in understanding the concepts related to nutrient requirements of the growing zygotic embryo. Murashige and

Skoog (MS) medium is a plant basal medium mainly used in the laboratory for the cultivation of plant cell *in vitro*. It is the most widely used culture medium because most plant cell cultures react to it favorably. It is classified as a high salt medium in comparison to other formulations with high level of nitrogen, potassium, and some of the micro nutrients, particularly boron and manganese [4].

Different studies have been conducted on growth response of *T. africana* seeds to the factors such as organic nutrient (poultry manure) [5], storage method [6], [7], but there is no literature as regards *in vitro* (seed or embryo) growth of the plant.

Thus, the objective of this study is to establish an *in vitro* regeneration protocol from the mature zygotic embryo explant of *Treculia africana* seeds in varied strengths of MS (Murashige and Skoog) basal medium.

II. MATERIALS AND METHODS

A. Site of Experiment

This study was conducted at the Tissue Culture and Molecular Biology Laboratory of the National Biotechnology Development Agency (NABDA) located at University of Nigeria, Nsukka.

B. Source of Explant

Mature fruits (Fig. 2) of *Treculia africana* Decne. were collected from a tree (Fig. 3) in Umunkpume, Orba in Udenu Local Government Area of Enugu state. They were identified in the Herbarium of Department of Plant Science and Biotechnology, University of Nigeria, Nsukka. The seeds (Fig. 4) were manually separated from fruits and were soaked in water for 24h then were dissected to excise the embryos which served as the explants for the study. Embryo excision was done under a dissecting microscope. Embryo explants were measured between 1.1 and 1.5 cm.

C. Stock Solutions

Stock solutions (macro elements-stock A, CaCl_2 - stock B, Na_2EDTA -stock C, micro element- stock D, Myo-inositol-stock E, Vitamins- stock F) of [4] were used to formulate MS medium (full strength), while the composition of various stock solutions A-F was divided into two and four for $\frac{1}{2}$ and $\frac{1}{4}$ MS

Okafor C. Uche is with the Department of Plant Science and Biotechnology, University of Nigeria, Nsukka, Nigeria (e-mail: uche.okafor1287@unn.edu.ng).

medium, respectively. Appropriate volumes of stock solutions were measured and transferred to a beaker containing 700 ml of distilled water. Sucrose (3% w/v) was added to the media. The pH of the medium was adjusted to 5.8 with 1M NaOH or HCL, and each medium was solidified by using Fluka agar at 7.0 g l^{-1} prior to autoclaving by steam sterilization at 103 kN M^{-2} pressure and $121 \text{ }^\circ\text{C}$ for 15 mins. The embryos were cultured singly in Pyrex test tubes at $27 \pm 2 \text{ }^\circ\text{C}$ under 16h light/8h dark photoperiod at a photon flux density of $60 \mu\text{mol m}^{-2}\text{S}^{-1}$ provided by cool white fluorescent tubes. All operations starting from the preparation of explants to establishment of cultures were carried out in a Laminar flow hood previously kept sterile by exposure to ultraviolet light for 30 min. The cultured embryos were left to grow for three weeks after which they were scored for the requisite growth parameters. Ten replicate tubes containing an embryo each were randomly selected under each treatment and scored for the following: percent sprouting (%), sprout rate (sprout rate is obtained as the reciprocal of the number of days to 50% sprouting), mean length of shoots and roots, mean fresh weight of sprouts produced, number of roots and area of leaves produced in culture.

D. Experimental Design and Statistical Analysis

This study was carried out in a completely randomized design that involves four treatments (full MS, $\frac{1}{2}$ MS, $\frac{1}{4}$ MS and control) with ten cultures per treatment for each of the basal medium. Embryos were cultured one per vessel. One-way analysis of variance (ANOVA) was used to analyze data collected from the germination studies. Gen-Statistical package was used for the data computation. Treatment means were tested for significance ($P < 0.05$) by using least significant difference (LSD). Error bars were represented at 5% value.

III. RESULTS AND DISCUSSION

Sprouting of the zygotic embryos started within 2-3 days of inoculation. The embryo (Fig. 5), which appeared white in colour from the onset, enlarged and began to turn green leading to the emergence of radicle from the radicular end and plumule from the plumular end within 3 days in culture. The radicle and plumule finally resulted in the root and new shoot, respectively. The addition of sucrose to the cultures was necessary for autotrophy as seen in this study. Since embryonic axis turned from white to green about 3 days from the time of inoculation, this, however, indicates that photosynthesis may have taken place. This is a clear manifestation of a transition from semiautotrophy to full autotrophy, which is a characteristic of *in vitro* systems. In mature plants (*in vivo*), photosynthesis takes place in the green leaves under favourable conditions of light intensity, temperature, water, and carbon (IV) oxide. Green plants are self-dependent because they can synthesize their own food materials. Leaves generally appear green because the wavelengths of light from the red and blue regions of the visible spectrum excite the chloroplast electrons, and unused green light is reflected [8].

The results obtained in the germination studies showed different MS salt strengths (full, half and quarter) (Figs. 6-8) had significant effect on the growth and development of *Treculia africana* cultured *in vitro*. Varied responses in terms of embryo sprouting and plantlet development were observed in the three treatments including the control (Fig. 9). For percent sprouting, explants in both full strength and control treatment had 100 ± 0.00 , while half and quarter strengths had 94 ± 0.32 and 87 ± 0.42 , respectively. The observation where all treatments had above 50% sprouting is in agreement with the findings made by [9]. The healthy seeds do not really need supplementary nutrients to germinate as they can do well with the nutrient materials from their endosperm and sometimes cotyledon. In addition, supplementing the basal medium with carbon source (sucrose) at 3% in all the media may have also caused the explants to sprout including the one devoid of mineral nutrient (control). Full strength was found to have the longest root ($5.00 \pm 0.54 \text{ cm}$), average number of adventitious roots 18.30 ± 1.44 as well as maximum fresh weight of $0.10 \pm 0.00 \text{ g}$. In addition, it had the highest leaf area $1.11 \pm 0.17 \text{ cm}^2$ and longest shoot length $2.60 \pm 0.30 \text{ cm}$ when compared to the explants cultured on half strength, quarter strength, and the control (Table I). Also, it was obvious from the data that quarter strength MS medium gave the lowest results in root length (3.20 ± 0.41), leaf area ($0.67 \pm 0.93 \text{ cm}^2$), number of adventitious root (12.80 ± 1.95), fresh weight (0.89 ± 0.01), and shoot length (1.91 ± 0.14). The explants in all the treatment had the same number of leaves 2.00 ± 0.00 and the same sprout rate of 0.33 ± 0.00 . Generally, the obtained results indicate that full strength MS medium improved in most growth parameters investigated. This is in line with the work of [10] which reported that among the different strengths of media, the highest growth (shoot height and number, leaf area and number, root length and number) was recorded in apple rootstocks (MM106 and B9) shoots grown in full strength MS medium for 30-60 days, while the above mentioned parameters were lowest when the shoots of both rootstocks were grown on quarter strength for the same duration. Moreover, the obtained results also agreed with [11] on *Cymbidium aloifolium* (L.) Sw. and [12] on *Prunus ameniaca*. However, in contrast to these findings, [13] reported that reduction of major salts to half strength improved the germination percentage of zygotic embryos in *Givotia rottleriformis*.

IV. CONCLUSION

T. Africana, an important forest tree species from both economical and ecological perspectives has great potentials of enhancing rural livelihoods and national food security. Therefore, contentious effort made in this study to ascertain the basal medium necessary for its growth ushers the preliminary steps in developing appropriate conservation measures for this highly valuable plant. These results as described in this study have the potentials for the mass production and shortening the germination time required to obtain *Treculia africana* plantlets. The plantlets, after hardening, would be raised *ex vitro* for ensuring a steady

supply of seeds important for food and other products derivable from it.

TABLE I
LEAF AREA, SHOOT LENGTH, NUMBER OF ADVENTITIOUS ROOT, ROOT LENGTH AND FRESH WEIGHT OF *TRECVLIA AFRICANA* EMBRYO EXPLANTS IN VARIED STRENGTHS OF MS (1962) MEDIUM

Treatments	Number of Leaves	Leaf Area (cm ²)	Number of Root	Root Length (cm)	Fresh Weight (g)	Shoot Length (CM)
Full MS medium	2.00 ± 0.00 ^a	1.11 ± 0.17 ^c	22.40 ± 3.11 ^b	5.24 ± 0.54 ^b	0.22 ± 0.08 ^b	2.60 ± 0.30 ^c
½ MS medium	2.00 ± 0.00 ^a	0.77 ± 0.13 ^b	18.30 ± 1.44 ^{a,b}	5.00 ± 0.54 ^b	0.10 ± 0.01 ^a	2.37 ± 0.12 ^{b,c}
¼ MS medium	2.00 ± 0.00 ^a	0.67 ± 0.93 ^b	12.80 ± 1.95 ^a	3.20 ± 0.41 ^a	0.89 ± 0.01 ^a	1.91 ± 0.14 ^b
Control	2.00 ± 0.00 ^a	0.02 ± 0.00 ^a	12.70 ± 1.27 ^a	2.61 ± 0.35 ^a	0.53 ± 0.00 ^a	0.68 ± 0.15 ^a

Different superscript lowercase letters within column indicate significant difference among treatments (Duncan's new multiple range test P≤0.05).

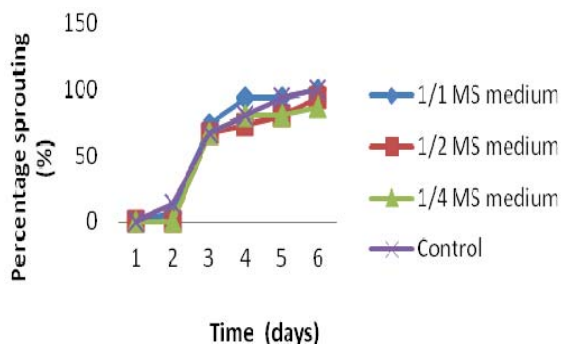


Fig. 1 Time course in percent sprouting of *Trecculia africana* plantlets in varied strengths of Murashige and Skoog basal medium



Fig. 4 Seeds of *Trecculia africana* Decne (0.2)



Fig. 2 Fruits of *Trecculia africana* Decne (0.2)



Fig. 5 Embryos of *Trecculia africana* Decne (0.2)



Fig. 3 *Trecculia africana* Decne tree (0.002)



Fig. 6 21 day-old plantlets of *Trecculia africana* in full strength MS medium



Fig. 7 21 day-old plantlets of *Treculia africana* in half strength MS medium



Fig. 8 21 day-old plantlets of *Treculia africana* in quarter strength MS medium



Fig. 9 21 day-old plantlets of *Treculia africana* in control treatment

REFERENCES

- [1] Agbogidi, O. M. and Onomeregbor, V. A. (2008). Morphological changes in the seedlings of *Treculia africana* grown in crude oil impacted soils. In: Popoola, L. (ed.). Climate Change and Sustainable Renewable Natural Resources Management. *Proceedings of 32nd Annual Conference of the Forestry Association of Nigeria*. Umuahia, Abia-State, Nigeria. 20th – 24th Oct; 2008, pp.170-182.
- [2] Osuji, J. O. and Owei, S. D. (2010). Mitotic index studies on *Treculia africana* Decne. in Nigeria. *Australian Journal of Agricultural Engineering*, 1 (1): 25-28.
- [3] Nuga, O.O. and Ofodile, E.A.U. (2010). Potentials of *Treculia Africana* Decne- An endangered species of Southern Nigeria. *Journal of Agriculture and Social Research* 10(2): 91-99.
- [4] Murashige, T. and Skoog, F. (1962). A revised medium for rapid growth and bioassays with tobacco tissue cultures. *Physiologia Plantarum*, 15: 473-497.
- [5] Aghimien, E. V., Kukogho, J., Ojo, M. O., Adams, B. A. and Akinbosoye, B. S. (2011). Effect of poultry manure, agrosorb and watering regime on the growth of *Treculia africana* (Decne.) seedlings. *Continental Journal of Agronomy*, 5 (2): 15 - 21.
- [6] Idowu, O. J., Olanite, J. A., Arigbede, O. M., Adedire, M. O., Adeoye, S. A. and Adelusi, O. O. (2013). Effect of storage methods on germination, growth and proximate composition of *Treculia africana* var. *decne*(dis cannot be a variety) seedlings. *Journal of Agriculture and Biodiversity Research*, 2 (6): 117-123.
- [7] Oboho, E. G. and Ngalum, E. L. (2014). Germination response of *Treculia africana* Decne. seeds in relation to moisture content, storage method and its duration. *Journal of Applied and Natural Science* 6 (1): 88-94.
- [8] Edwin, R. (2005). *Biology-Botany*. Tamil Nadu Textbook Corporation, Chennai India, 216pp.
- [9] Pierik, R. L. M. (1987). *In vitro* Culture of Higher Plants. Martinus Nijkost publishers, wageningen. 344 pp.
- [10] Melita, M., Ram, R. and Bhattacharya, A. (2014). A simple and cost effective liquid culture system for the micropropagation of two commercially important apple rootstocks. *Indian Journal of Experimental Biology*, 52: 748-754.
- [11] Shreeti, P., Tripti, R., Gaurav, P. and Bijaya, P. (2013). Effect of different media on *in vitro* seed germination and seedling development of *Cymbidium aloifolium* (L.) Sw. *Nepal Journal of Science and Technology*, 14 (1): 51-56.
- [12] Yildirim, H., Tilkat, E., Onay, A. and Ozen, H. C. (2007). *In vitro* Embryo Culture of Apricot, *Prunus armeniaca* L. CV. *International Journal of Science and Technology*, 2:99-104.
- [13] Samuel, K., Debashish, D., Madhumita, B., Padmaja, G., Prasad, S. R., Murthy, V. B. R. and Rao, P. S. (2009). *In vitro* germination and micropropagation of *Givotia rottleriformis* Griff. *In Vitro Cell Developmental Biology Plant*, 5: 466-473.

Comparative Performance and Emission Analysis of Diesel Engine Fueled with Diesel and Bitter Apricot Kernel Oil Biodiesel Blends

Virender Singh, Akash Deep, Sarbjot Singh Sandhu

Abstract—Vegetable oils are produced from numerous oil seed crops. While all vegetable oils have high energy content, most require some processing to assure safe use in internal combustion engines. Some of these oils already have been evaluated as substitutes for diesel fuels. In the present research work Bitter Apricot kernel oil was employed as a feedstock for the production of biodiesel. The physico-chemical properties of the Bitter Apricot kernel oil methyl ester were investigated as per ASTM D6751. From the series of engine testing, it is concluded that the brake thermal efficiency (BTE) with biodiesel blend was little lower than that of diesel. BSEC is slightly higher for Bitter apricot kernel oil methyl ester blends than neat diesel. For biodiesel blends, CO emission was lower than diesel fuel as B 20 reduced CO emissions by 18.75%. Approximately 11% increase in NO_x emission was observed with 20% biodiesel blend. It is observed that HC emissions tend to decrease for biodiesel based fuels and Smoke opacity was found lower for biodiesel blends in comparison to diesel fuel.

Keywords— Biodiesel, Transesterification, Bitter Apricot Kernel oil, Methyl esters, Performance and Emission testing, Diesel engine

I. INTRODUCTION

Vegetable oils were used as fuel for diesel engines to some extent since the invention of the compression ignition engine by Rudolf Diesel in the late 1800's. During the early stages of the diesel engine, strong interest was shown in the use of vegetable oils as fuel but this interest declined in the late 1950's after the supply of petroleum products become abundant [1]. During the early 1970's, oil shock, however, caused a renewed interest in vegetable oil fuels. This interest evolved after it became apparent that the world's petroleum reserves were declining. At present, in order to replace a part of petroleum based diesel usage, the use of vegetable oils derived biodiesel has been starting in many countries. Vegetable oils are renewable energy source and significant environmental benefit can be derived from the combustion of vegetable oil based biodiesel rather than petroleum based

diesel fuels. Mostly, biodiesel is prepared from oils like soybean, rapeseed, sunflower, safflower, etc. throughout the world [2]. These oils are essentially edible in nature. When biodiesel is produced from refined edible oils, feedstock cost contributes more than 88% to the cost of biodiesel [3]. Few attempts have been made for producing biodiesel with non-edible oils like karanja and jatropha, especially in India [4]. However, there remain a number of other tree based oilseeds with an estimated annual production potential of more than 20 Mt [4]. These oils have great potential to make biodiesel for supplementing other conventional sources.

- Production of biodiesel from Bitter Apricot Kernel oil.
- Determination of important Physico-chemical properties of produced biodiesel.
- Conducting exhaustive experiments on the diesel engine test rig to evaluate performance and emission characteristics of biodiesel-diesel blends and comparison with baseline data of diesel fuel.

II. MATERIALS AND METHODS

In the present work Bitter Apricot kernel oil (FFA <2%) is used for Biodiesel production. As the oil has low Free Fatty Acid (FFA), so it is suitable for biodiesel production through direct transesterification reaction.

A. Transesterification of Bitter Apricot kernel oil

Transesterification has been done to produce biodiesel. Transesterification is also known as alcoholysis. A mixture of bitter apricot kernel oil and methanol mixed with potassium hydroxide (used as catalyst) are heated and maintained at 60°C, while the solution is continuously stirred with the help of magnetic stirrer. Catalyst concentration, 1% (% wt. / wt. of oil) and molar ratio of, 6:1 (alcohol: oil) is used. Time taken in transesterification reaction is 5 to 60 minutes. When the reaction is over, product is poured into separating funnel. Two distinct layers are formed; the lower layer is of glycerin and the upper layer of ester. The glycerol formed is removed by density separation. The upper layer (ester) is separated out, washed with mild water and then heated to 110°C to remove any moisture present in the biodiesel. This process increases the volatility and decreases the viscosity of the oil, making it similar to the diesel fuel in these characteristics.

Virender Singh is a research scholar at Dr. B.R. Ambedkar National Institute of Technology, Jalandhar 144011 (e-mail: virendergurau@gmail.com).

Akash Deep is a research scholar at Dr. B.R. Ambedkar National Institute of Technology, Jalandhar 144011 (e-mail: akashgoeleng@gmail.com).

Akash Deep a corresponding author is an assistant professor at Dr. B.R. Ambedkar National Institute of Technology, Jalandhar 144011 (e-mail: sandhuss@nitj.ac.in).

B. Bitter Apricot kernel oil biodiesel properties

Measured physico-chemical properties of bitter apricot kernel oil biodiesel are shown in table 1

TABLE 1.
MEASURED PROPERTIES OF BITTER APRICOT KERNEL OIL BIODIESEL

Property	ASTM Method	Value
Acid Number (mg KOH/gm)	D 664	0.10
Density @ 15°C (gm/cm ³)	D 1298	0.88
Kinematic Viscosity @ 40°C (cSt)	D 445	4.32
Calorific Value (MJ/kg)		39.5
Flash Point (°C)	D 93	115
Ester Content (%)	EN 14103	95

C. Diesel engine test rig

A Kirloskar made, single cylinder, water cooled, direct injection diesel engine is selected for the present research work, which is primarily used for agricultural activities and household electricity generation. Specifications of Diesel engine are shown in Table 2.

TABLE 2.
SPECIFICATIONS OF THE DIESEL ENGINE

Make	Kirloskar
Model	TV 1
Rated Brake Power	5.2 kW @ 1500 rpm
Rated Speed (rpm)	1500
Number of Cylinder	One
Bore x Stroke (mm)	87.5 x 110
Displacement volume	661
Compression Ratio	17.5:1
Cooling System	Water Cooled
Fuel Injection	23° before TDC

III. RESULTS AND DISCUSSION

The first part deals with the results of various tests conducted for physico-chemical characterization of biodiesel and diesel fuel. The second part discusses the results of performance and emission analysis on diesel engine.

A. Evaluation of physico-chemical properties

All the fuels, namely neat diesel and diesel- bitter apricot kernel oil biodiesel blends were analyzed for several physical, chemical properties. Density and viscosity of

biodiesel- diesel blends were found to be higher than those of diesel fuel. Blending of biodiesel derived from bitter apricot kernel oil in diesel reduces calorific value of the blend due to lower heating value of biodiesel. Table 3 shows the Physico-Chemical properties of fuels used in engine:

TABLE 3.
PHYSICO-CHEMICAL PROPERTIES OF FUEL USED

Sample	Density (g/cm ³)	K.V. (cSt)	Cal. Val. (MJ/kg)	Flash Point (°C)
Diesel	0.85	2.95	42	65.5
B 10	0.855	3.087	41.75	70.5
B 20	0.857	3.224	41.5	75.5
B 30	0.86	3.361	41.25	80.5
B 50	0.865	3.635	40.75	90.5

B. Performance Characteristics

The performance characteristics of the test engine on neat diesel and biodiesel- diesel blends are summarized below:-

a. Brake Thermal Efficiency

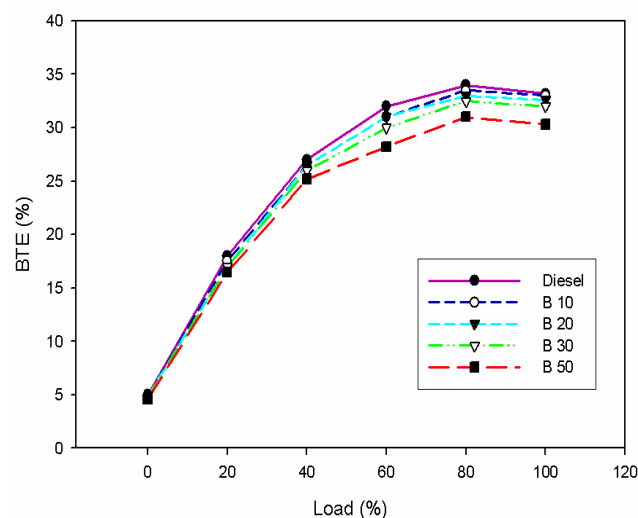


Fig. 1 Variation of Brake thermal efficiency with Engine load

The variation of brake thermal efficiency with respect to engine load for different test fuels is shown in Figure 1. In all the cases, brake thermal efficiency has the tendency to increase with increase in applied load reaching a maximum somewhere at 80 per cent load and then decreases. The peak brake thermal efficiency in case of diesel, B10, B20, B30 and B50 are 34.1%, 33.6%, 33%, 32.4% and 31% respectively. It can be seen that brake thermal efficiency with biodiesel blend was little lower than neat diesel fuel [5-7].

b. Brake Specific Energy consumption

Brake specific energy consumption (BSEC) is an ideal parameter for comparing engine performance of fuels having different calorific values and densities. The variation of BSEC with engine load for different test fuels is shown in Figure 2. It is observed that for all the fuels, the BSEC decreases with increase in load. This is due to higher percentage increase in brake power with load as compared to increase in the fuel consumption. For biodiesel and its blend the BSEC is slightly higher than diesel fuel. This is due to lower calorific value with increase in biodiesel percentage in the blends [8].

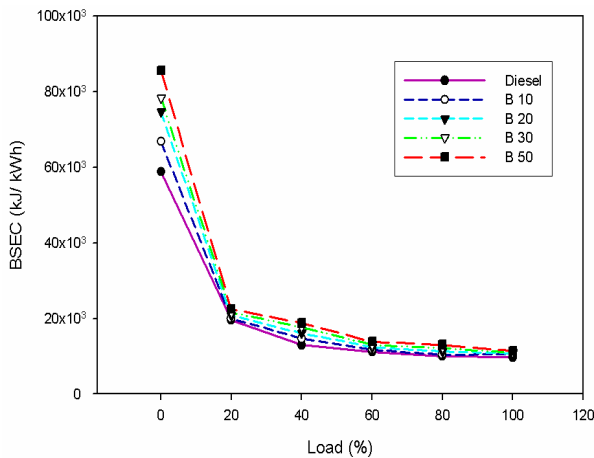


Fig. 2 Variation of Brake specific energy consumption with Engine load

c. Exhaust temperature

Figure 3 shows the variation of exhaust gas temperature with engine load for diesel and biodiesel- diesel blends. The results show that the exhaust gas temperature increases with the increase in load for all the test fuels. The amount of fuel injected increases with the engine load in order to maintain the power output and hence the heat release and the exhaust gas temperature rise with increase in load. Exhaust gas temperature is an indicative of the quality of combustion in the combustion chamber. At all loads, diesel was found to have the lowest temperature and the temperature for the different blends showed the upward trend with increasing concentration of biodiesel in the blends [5,6].

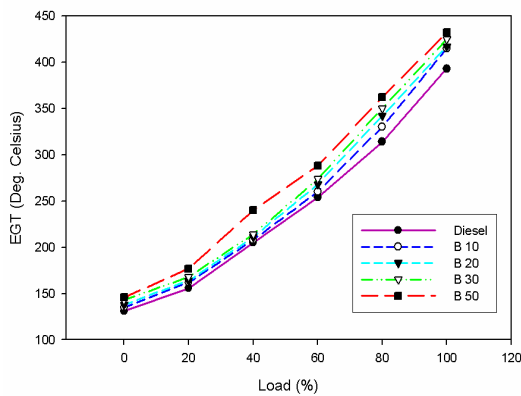


Fig. 3 Variation of Exhaust gas temperature with Engine load

C. Emission Characteristics

The emissions characteristics of the test engine on neat diesel and biodiesel- diesel blends are summarized in this section.

a. CO Emissions

Figure 4 shows the CO emissions of the diesel fuel and blends of biodiesel. CO is an intermediate combustion product and is formed mainly due to incomplete combustion of fuel. If combustion is

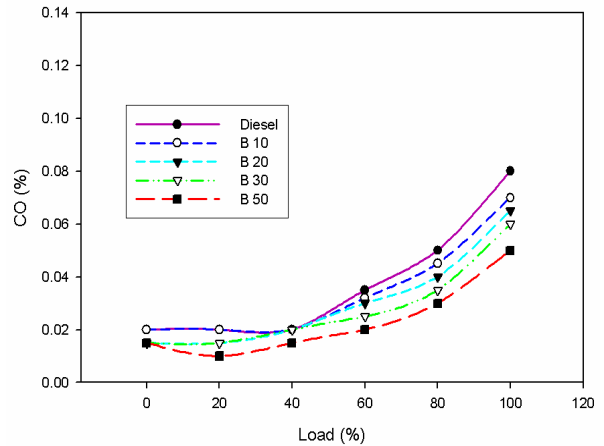


Fig. 4 Variation of CO emission with Engine load

b. CO₂ Emissions

Figure 5 compares the CO₂ emissions of various test fuels. The CO₂ emission increases with increase in load, as richer air- fuel mixture burns at higher loads. The biodiesel- diesel blends emits more amount of CO₂, as compared to neat diesel operation. Due to inbuilt oxygen in biodiesel, more amount of CO₂ in exhaust emission is an indication of the complete combustion of fuel. This supports the higher value of exhaust gas temperature. The CO₂ emission using neat diesel as fuel is lower because of the inferior combustion as compared to biodiesel blends [5-6].

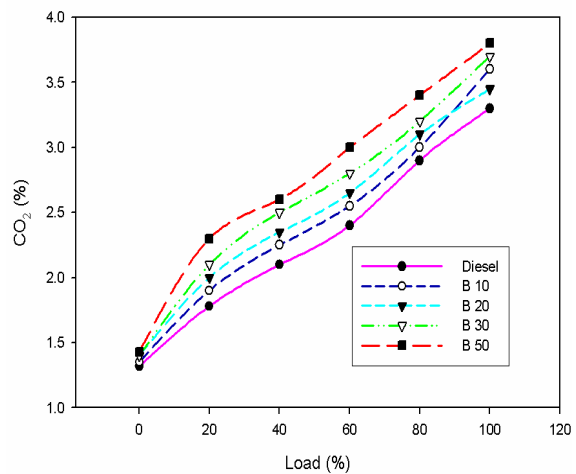


Fig. 5 Variation of CO₂ emission with Engine load

c. NO_x Emissions

The variation of NO_x emission for different fuels is indicated in Figure 6. Naturally NO_x emission increases with the increase in load. It is well known that nitrogen is an inert gas, but it remains inert up to a certain temperature (1100 °C) and above this level, it does not remain inert and participate in chemical reaction. At the end of combustion, gas temperature inside cylinder arises around 1500 °C. At this temperature, oxidation of nitrogen takes place in presence of oxygen inside the cylinder. So with increasing load more fuel burns which lead to higher combustion temperature thus higher NO_x formation takes place. NO_x level was higher for biodiesel blends than diesel fuel at the same load. This can be explained due to the presence of extra oxygen in the molecules of biodiesel blends. This additional oxygen was responsible for higher NO_x emission [5-7, 9]. Around 11% increase in NO_x emission was observed with 20% biodiesel blend at full load.

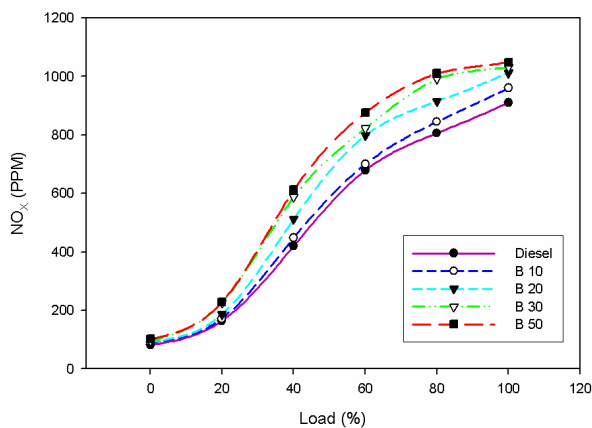


Fig. 6 Variation of NO_x emission with Engine load

d. HC Emissions

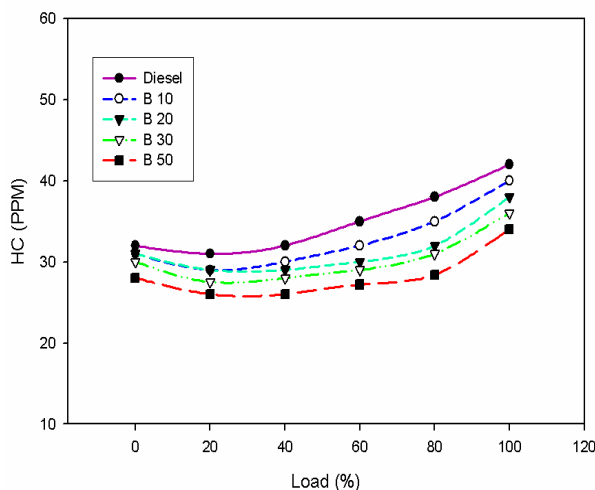


Fig 7 Variation of HC emission with Engine load

Figure 7 depicts the variation of HC emissions for different fuels with load. It can be seen that hydrocarbon emissions tend to increase for all fuels with increasing load. This is because of less oxygen available for the reaction when more fuel is

injected into the engine cylinder at high engine load which makes the fuel mixture to become very rich at certain points in combustion chamber. As a result, proper combustion does not take place at those points and fuel goes off in the exhaust as hydrocarbons. It can also be seen that with increasing amount of biodiesel in blends, HC emissions tend to decrease and are lower compared to diesel fuel. This is due to inbuilt oxygen content in biodiesel which is responsible for more complete combustion [10- 12].

e. Smoke opacity

The variation of smoke opacity with engine load for diesel fuel and biodiesel blends is shown in Figure 8. It can be seen that smoke is high mainly at high power outputs for all the fuels. High loads imply that more fuel is injected into the combustion chamber and hence incomplete combustion of fuel is enhanced. Reduction of smoke emissions for different biodiesel based fuels in comparison to diesel fuel has been achieved for all load conditions [13].

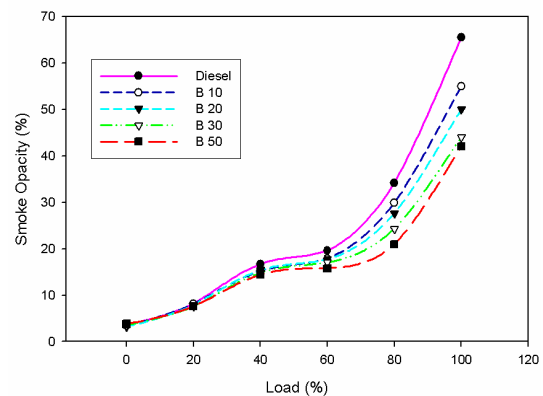


Fig 8 Variation of smoke opacity with Engine load

IV. CONCLUSIONS

The bitter apricot kernel oil was taken as a feedstock in the present research work mainly to evaluate the potential suitability of bitter apricot kernel oil for conversion into biodiesel and subsequent engine application. From the series of exhaustive experiments, the following conclusions can be derived.

- The brake thermal efficiency with biodiesel blend was little lower than that of diesel. The slight reduction of brake thermal efficiency with increase of biodiesel content in blends can be attributed to lower heating value, high viscosity.
- The BSEC decreases with increase in load. For B5, B10, B20, B30 and B50 the BSEC is slightly higher than neat diesel.
- The exhaust gas temperature increases with the increase in load for all the test fuels. At all loads, diesel was found to have the lowest temperature and the temperature for the

different blends showed the upward trend with increasing concentration of biodiesel in the blends.

- CO emission is found to increase with increase in load for all test fuels. For biodiesel blends, CO emission was lower than diesel fuel as B 20 reduced CO emissions by 18.75% at full load.
- The biodiesel- diesel blends emits more amount of CO₂, as compared to neat diesel operation.
- The NO_x level was higher for biodiesel blends than conventional diesel fuel. Approximately 11% increase in NO_x emission was observed with 20% biodiesel blend at full load.
- It is observed that HC emissions tend to decrease for biodiesel based fuels. It was also seen that as concentration of biodiesel in biodiesel- diesel blends increases, a downward trend in HC emission is observed.
- Smoke opacity was found lower for biodiesel blends in comparison to diesel fuel.

It can be concluded from the research work that B20 blend can be successfully used in Diesel engine without sacrificing much performance and improve emissions.

REFERENCES

- [1] G. Knothe, "Cetane numbers-The History of Vegetable Oil-based Diesel Fuels," The Biodiesel Handbook, American Oil Chemist's Society Press, 2005.
- [2] X. Lang, A.K. Dalai, N.N. Bakhshi, M.J. Reany, P.B. Hertz, "Preparation and characterization of bio-diesels from various bio-oils," *Bioresource Technology* 2001; 80: 53–62.
- [3] Michael J. Hass, Andrew J. McAloon, Winnie C. Yee and A. Thomas Foglia, "A process model to estimate biodiesel production costs," doi:10.1016/j. biortech. 2005.03.039.
- [4] S. Kaul, A. Kumar, A.K. Bhatnagar, H.B. Goyal, A.K. Gupta, "Biodiesel: a clean and sustainable fuel for future. Scientific strategies for production of non-edible vegetable oils for use as biofuels,," All India seminar on national policy on non-edible oils as biofuels, SUTRA, IISc Bangalore, 2003.
- [5] B.S. Chauhan, N. Kumar, H.M. Cho, H.C. Lim, "A study on the performance and emission of a diesel engine fuelled with Karanja biodiesel and its blends," *Energy* 2013; 56: 1–7.
- [6] B.S. Chauhan, N. Kumar, H.M. Cho, "A study on the performance and emission of a diesel engine fuelled with Jatropha biodiesel oil and its blends," *Energy* 2012; 37: 616–22.
- [7] M. Canakci, A.N. Ozsezen E. Arcaklioglu, A. Erdil, "Prediction of performance and exhaust emissions of a diesel engine fuelled with biodiesel produced from waste frying palm oil," *Expert Syst Appl* 2009; 36: 9268–80.
- [8] B. Baiju, M.K. Naik, L.M. Das, "A comparative evaluation of compression ignition engine characteristics using methyl and ethyl esters of Karanja oil," *Elsevier, Renewable Energy*, Vol. 34, pp.1616–1621, 2009.
- [9] C.D. Rakopoulos, D.C. Rakopoulos, D.T. Hountalas, E.G. Giakoumis, E.C. Andritsakis, "Performance and emissions of bus engine using blends of diesel fuel with biodiesel of sunflower or cottonseed oils derived from Greek feedstock," *Fuel* 2008; 87: 147–57.
- [10] G. Labeckas, S. Slavinskas, "Performance and emission characteristics of a direct injection diesel engine operating on KDV synthetic diesel fuel," *Energy Convers Manage* 2013; 66: 173–88.
- [11] S.W. Kruczynski, "Performance and emission of CI engine fuelled with camelina sativa oil," *Energy Convers Manage* 2013; 65: 1–6.
- [12] D.J.P. Selvam, K. Vadivel, "Performance and emission analysis of DI diesel engine fuelled with methyl esters of beef tallow and diesel blends", In: International conference on modelling optimization and computing. *Proc Eng.* 2012; 38: 342–58.
- [13] A.K. Agarwal, "Biofuels (alcohols and biodiesel) applications as fuels for internal combustion engines," *Prog Energy Combust Sci* 2007; 33: 233–71.

Compared of Pbs/Zns quantum dots synthesis methods

Mahbobeh bozhmehrani¹- Afshin farah bakhsh*

1. Department of Chemical Engineering Quchan branch, Islamic Azad University Quchan, Iran

*Afshin.farahbakhsh@gmail.com

ABSTRACT

Nanoparticles with PbS core of 12 nm and shell of approximately 3 nm were synthesized at PbS:ZnS ratios of 1.01:0.1 using Merca Ptopropionic Acid as stabilizing agent. PbS/ZnS nanoparticles present a dramatically increase of Photoluminescence intensity, confirming the confinement of the PbS core by increasing the Quantum Yield from 0.63 to 0.92 by the addition of the ZnS shell. In this case, the synthesis by microwave method allows obtaining nanoparticles with enhanced optical characteristics than those of nanoparticles synthesized by colloidal method.

KEYWORDS: Pbs/Zns, quantum dots, colloidal Method, microwave.

1-Introduction

During the past decades, quantum confined semiconductor nanoparticles (quantum dots, QDs) have found widespread interest in the field of electronics, solar cells, sensors and diagnostics [1]. In troductionA quantum dot (QD) is composed of a few hundred to severalthousand atoms, and the size of a QD typically ranges from 1 to20 nm [2]. They have a wide range of physical applications such as light-emitting diodes, biomedical labelling, photo-catalysis, optical wave guide, photo-conductive devices, solar cells, lasers and sensors [3].

Lead sulfide (PbS) nanoparticles exhibit a large Bohr radius (18 nm) and a small band gap (0.41 eV), therefore, it is relatively easy to prepare particles of size smaller than the Bohr radius that show strong quantum confinement effects. This effect, besides other properties such as photo multiplication of charges, makes PbS a semiconductor widely studied and applied in photovoltaic, bio analytical and micro-electronic device. PbS nanoparticles are very unstable in oxidizing conditions and they must be stabilized. One of the attempts to stabilize PbS nanoparticles is to cover them with an outer shell of a more stable component [4].

the surface modification of ZnS and PbS by interfacing PbS on ZnS, and ZnS on PbS, nanoparticles, generating In this way core-shell nano composites ZnS/PbS and PbS/ZnS by the colloidal method and varying the amount of shell precursor. They conclude that the nucleation of ZnS on PbS produces a

core-shell structure, which induces the separation of charge and enhances the lifetime. The optical, photo physical, and electronic properties of the generated nanoparticles can be manipulated by changing the surface environment [5].

Microwave radiation perform selective heating of compounds in the reaction mixture with a greater reaction and as a consequence of rates, produce smaller particles with high homogeneity [5]. Traps Microwave radiation allows a selective heating of compounds in the reaction mixture with reaction rate acceleration as a consequence of high heating rates, obtaining smaller particles with high homogeneity[6]. In addition, this method has proved to be environmental friendly, as shorter reaction times are used, compared to the traditional method, saving energy.

This work present the results of the synthesis of PbS/ZnS core/shell system by microwave heating and their comparison with the optical properties of the same material synthesized by colloidal method the size and under reflux conditions [6].

2- PbS/ZnS Nanoparticles traditional colloidal Method

In a typical synthesis, 50.0 mL of sodium citrate 3.0 mM were prepared, and then 2.0 mL of PbCl₂ 30.0 mM and 2.0 mL of TAA 30.0 mM were added to the reaction vassal. The pH was adjusted to 7.0 with NaOH 1.0 M. The reaction mixture was placed under reflux conditions for 30 min, obtaining a dark brown solution. Then, 1.0 mL of MPA 0.18 M was added to the PbS previously synthesized, and kept under stirring for 10 minutes; the solution turned to a light brown. After that, 10.0 mL of TAA 1.0 mM were added and pH adjusted to 8.0 with NaOH. The solution was kept into reflux conditions for 30 min; meanwhile Zn (OAc)₂ 1.0 mM was added with a constant flux of 0.3 mL/min. The mixture was kept under reflux conditions for six hours. The obtained nanoparticles were centrifuged, washed with acetone and acetonitrile, and then re-dispersed in water for further characterization [5].

Fig1a shows PbS nanoparticles with an average size of 20 nm for the PbS synthesized by colloidal method, those particles form agglomerates with size above 50 nm.fig1c the particle size distribution of the PbS synthesized by colloidal method with a disperse distribution obtained by DSL analysis.

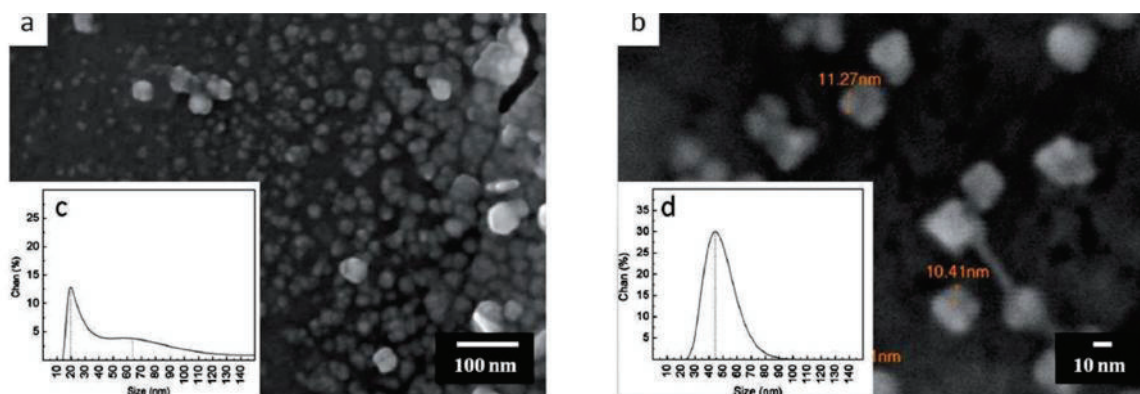


Figure 1. SEM images and particle size distribution for PbS nanoparticles synthesized by (a, c) colloidal synthesis and (b, d) microwave synthesis methods for PbS 2 experiment.

3- PbS/ZnS nanoparticles by microwave method

The same experimental conditions as in the traditional method. In this case the microwave heating was applied on the reaction mixture in cycles of on/off radiation with a total heating time of 60 s, Table I show the different heating rates of the experiments. The microwave system used for the synthesis of the desired nanoparticles operates at 1100 W, 2.45 GHz, working at 80% of power under the described conditions (see Table I). After the microwave exposition, 1.0 mL of MPA 0.18 M was added to the PbS previously synthesized, and it was kept under magnetic stirring for 10 minutes; the solution turned light brown. The pH adjusted to 8.0 with NaOH 1.0 M. The solution was placed into the microwave system and Zn(OAc)₂ and TAA 30.0 mM were added in portions of 2.0 mL during the on/off cycling the total microwave heating time was 15 min, Table 1 shows the experimental conditions les by microwave method for the synthesis. The obtained nanoparticles were centrifuged, washed with acetone and acetonitrile, and then re-dispersed in water for further characterization [5].

Fig1b shows nanoparticles synthesized by microwave heating with an average size of 11 nm. Those particles are interacting among them in order to form agglomerates of four particles with an average size of 33 nm. Fig1d shows the particle size distribution of the PbS synthesized by microwave heating method acquired by DSL analysis.

Table 1. Heating methods used for the experiments of PbS and PbS/ZnS nanoparticles synthesized by microwave method

PbS nanoparticles		PbS/ZnS nanoparticles			
Experiment	Microwave on/off profile (s)	[Zn ²⁺] (mM)	[TAA] (mM)	Microwave on/off profile (s)	Pb:Zn ratio
PbS1	10/5	-	-	-	-
PbS2a	20/5	1	1	10/50	1.0 : 0.1
PbS 2b		2	2		1.0 : 0.3
PbS3	60/0	-	-	-	-

Size distribution of the PbS synthesized by colloidal method with a disperse distribution obtained by DSL analysis. The wide distribution could be attribute to the synthesis method, since in the colloidal method, the walls of the reactor are heated by convection or conduction and the center of the flask filled with the reaction temperature, resulting in a non-homogeneous temperature profiles within the reaction flask. This gives different size of the particles and a wide size distribution. Figure 1b shows an image of nanoparticles synthesized by microwave heating with an average size of 11 nm. Those particles are interacting among them in order to form agglomerates of four particles with an average size of 33 nm. Figure 1d shows the particle size distribution of the PbS synthesized by microwave heating method acquired by DSL analysis. The distribution for the microwave method is narrower than the one for colloidal synthesis and it's centered around 40 nm, which correspond to the size of the agglomerates observed by FESEM. Microwave process induces a rapid and homogeneous heating of the reaction mixture to the desired temperature, which saves time and energy because of the faster energy transfer mechanism. This allows to the formation of smaller nuclei and the presence of the sodium citrate which acts as completing and electrostatic stabilizer helps to segregate the particles and maintain the size of the particle constant giving a better size distribution [5]. Thelma Serrano et al., Highly Luminescent PbS/ZnS Nanoparticles Synthesized by Microwave Method.

3. Conclusions

The synthesis of PbS nanoparticles was achieved by both, colloidal and microwave heating methods, where the synthesized PbS nanoparticles presented the best optical characteristics when they were synthesized at pH = 7 and on/off heating profile of 20/5ms. Those nanoparticles present absorption in the visible electromagnetic spectra and they present higher luminescent properties than those particles generated by colloidal method. The particles size was 11 nm for the PbS nanoparticles. The generated PbS nanoparticles were used as core, in order to produce PbS/ZnS nanoparticles. The best optical characteristics were obtained when the PbS:ZnS ratio was kept to 1.0:0.1 during the synthesis, leading to nanoparticles with PbS core of 12 nm and shell of

approximately 3 nm. PbS/ZnS nanoparticles present a dramatically increase of PL intensity, this can be observed by the increment from 0.63 to 0.92 of the QY when adding the ZnS shell, confirming the confinement of the PbS core.

ACKNOWLEDGEMENTS

Financial supports from the Islamic azad university of quchan experts, friends and colleagues are gratefully acknowledged.

REFERENCES

- 1-D. Segets, W. Peukert, From In Situ Characterization to Process Control of Quantum Dot Systems, *Procedia Engineering* 102 (2015) 575 – 581
- 2- B R. Liua, J G. Winiarzb, J Moonb, S Loc, Y Huangd, , Robert S. Aronstamd, H-Jung Leea, Synthesis, characterization and applications of carboxylated and polyethylene-glycolated bifunctionalized InP/ZnS quantum dots in cellular internalization mediated by cell-penetrating peptides *Colloids and Surfaces B: Biointerfaces* 111 (2013) 162– 170
- 3- M. Sookhakian,n, Y.M.Amin, W.J.Basirun, M.T.Tajabadi, N.Kamarulzaman, Synthesis, structural, and optical properties of type-II ZnO–ZnS core–shell nanostructure *Journal of Luminescence* 145(2014)244–252
- 4- A. Sharma, V. Kameswara Rao, D. Kamboj, R. Gaur, S. Upadhyay, M. Shaik, Relative efficiency of zinc sulfide (ZnS) quantum dots (QDs) based electrochemical and fluorescence immunoassay for the detection of Staphylococcal enterotoxin B (SEB), *Biotechnology Reports* 6 (2015) 129–136.
- 5-T. Serrano, A. Vazquez, I. Gómez, Highly Luminescent PbS/ZnS Nanoparticles Synthesized by a Microwave Method, *Journal of Microwave Power and Electromagnetic Energy*, 47 (2), 2013, pp. 102-109.
- 6- T. SERRANOa, L. CAVAZOSb, Y. PEÑAA, I. GÓMEZa, SYNTHESIS AND CHARACTERIZATION OF PbS/ZnS CORE/SHELL NANOPARTICLES BY MICROWAVE METHOD, *Chalcogenide Letters*, January 2014, p. 21 – 28.

Comparison of the Effects of Fresh Leaf, Septum and Peel Extracts of Walnut on Blood Glucose and Pancreatic Structure

Tahmineh Hasanzadeh, Afshin Farahbakhsh*

Tahmineh hasanzadeh, Department of Chemical Engineering, quchan Branch, Islamic Azad University, quchan, Iran (phone: +98-936-7320409; e-mail: tahminehhasanzadeh67@gmail.com).

*Afshin Farahbakhsh, Department of Chemical Engineering, Qochan Branch, Islamic Azad University, Qochan, Iran (afshin.farahbakhsh@gmail.com) (corresponding).

Abstract— There is some report about the hypoglycemic effect of *Juglans regia* L. leaf in alloxan induced diabetic rats and hypoglycemic effect of its fruit peel administered intra peritoneally. In Iranian traditional medicine, septum of walnut shell (SWS) was recommended to reduce blood glucose. For this purpose, 41 male bulb/C mice 25-30 gm were divided into five groups. All the animals received IP injection of streptozotocin (STZ) (220 mg/kg). Two weeks later, the diabetic animals were received daily oral treatment of normal saline and aqueous extract of SWS (200, 400, 600 and 800 mg/kg) respectively for four weeks. Blood samples were taken from retro orbital sinus before the start of the experiment and repeated each two week. At the end of experiment, the animals were sacrificed and the pancreatic tissues were fixed, prepared and stained by Hematoxylin-Eosin for light microscope studies. The results showed that in each group, the SWS extract reduced blood glucose in long time ($p < 0.05$). metabolic extract in STZ- induced diabetic rats, which was accompanied by hypoglycemic effect of leaf extract. But this effect should be determined with scientific researches. Therefore, the aim of this study is to evaluate the effect of the aqueous extract of SWS on blood glucose and histopathological structure of pancreas.

Keywords— Septum of walnut, Blood Glucose, Pancreas, Diabetes, Walnut leaf, Walnut peel, Insulin

1. INTRODUCTION

Diabetes mellitus is a metabolic disease characterized by hyperglycemia together with impaired metabolism of glucose and other energy-yielding fuels, like lipids and proteins [1]. These metabolic disorders are the result of insulin deficiency or tissue insulin resistance, or both. More than 220 million people worldwide suffer from diabetes and this number is likely double by the year of 2030. Walnut (*Juglans regia*) is a plant in the family Juglandaceae. Useful parts of walnut tree are leaves, second peel and fleshy part of green fruit and its wood [2].

Different parts of *Juglans regia* L. such as peel, leaves and septum have shown significant hypoglycemic effects. Green peel of walnuts fruit, epicure contains emulsion, glucose, organic acids such as citric acid, malic acid, phosphates, and calcium oxalate. Hydro alcoholic extract of *Juglans regia*'s leaves has an anti-hyperglycemic effect in diabetic rats. Walnut leaf, similar to the walnut peels has some antioxidant, antifungal, astringent, and wart liquidator properties used for skin diseases and anemia [3].

Regulation of blood glucose concentration plays an important role in diabetic patient. The degree of oxidative stress in

diabetes makes them prone to oxidative injury [1]. Studies have shown that pancreatic damage occurs following STZ injection in animal model. STZ increased oxidative stress in diabetes through free radical generation [1,2]. So, it needs to explore methods for oxidative damage protection in this syndrome [2]. Hypoglycemic effects have been proved for some plants containing phenolic compounds. Therefore, the aim of this study is to evaluate the effect of septum of walnut shell (SWS) on blood glucose and histopathological changes in pancreas in diabetic mouse [4].

2. AQUEOUS EXTRACT OF WALNUT SEPTUM

2.1 Extract Preparation

Walnut (*Juglans regia*) in the family Juglandaceae was obtained from a local supplier in Shiraz, Iran, during September-October, and identified by specialized botanist [5]. Septum of walnut shell (300g) was separated and shed dried (at 25 °C) ground and mixed with water by blender. After 24 h, the mixture was filtered through Watt man filter, evaporated by rotator evaporator and dried in a desiccators. The extract was obtained with the percolation method. The final yield was 30 g powdered extract [6].

2.2 DIABETES INDUCTION

The animals were fasted for 24 h, with free access to water. Diabetes was induced by intraperitoneal injection of a single dose of Streptozotocin (STZ, Sigma, Aldrich, 220 mg/kg in 0.1 M citrate buffer, pH 4.4). Blood samples were taken from retro-orbital sinus before the start of the experiment and repeated each two week. The fasting blood glucose levels were estimated on days 1, 14, 28 and 42. Mice with blood glucose (fasting) level >300 mg/dl for 2 weeks or longer and before day 28 after injection of STZ were considered diabetic and used for the study. The blood glucose (mg/dl) was measured by 'One Touch-ULTRA' glucometer (Johnson & Johnson Company, USA). Blood sampling in all animals were done by a micropipette from retro-orbital sinus under deep anesthesia [6,7].

3. AQUEOUS EXTRACT OF WALNUT LEAF

3.1 Extract Preparation

Fresh ripe Walnuts and leaves of *Juglans regia* L. were collected from a garden near Eize (31°48'N, 049°54'E; the South-West of Iran) and were authenticated by Department of Pharmacognosy (Faculty of Pharmacy, Ahvaz Jundishapur

University of Medical Sciences).[7] The walnut fruits and leafes were cleaned and the green coat of the walnut fruits peeled. Peels and leaves were powdered by mill. Methanol was added to cover the surface of each powder. Seventy two hr later the solutions were filtered through filter paper. The leaf extract was concentrated by rotary evaporator at 40 °C and lyophilized to get a powder. To overcome to it's rather insolubility the leaf extract was decanted by chloroform. Then the obtained extract was concentrated by rotary evaporator at 40 °C and dried [8].

3.2 Diabetes Induction

Diabetes was induced by IV injection of STZ (Alexis Corporation, Switzerland; 50 mg kg⁻¹) dissolved in 0.1 M citrate buffer (pH=4.5). Negative control group received equal volume of citrate buffer, with no manipulation during the study. One week later, the FBS of negative control and diabetic animals were measured by commercial glucose kit (Parsazmun, Karaj, Iran). Survived rats with marked hyperglycemia (FBS > 300 mg dL⁻¹) were selected as diabetic rats, divided into 4 diabetic groups. A solution of distilled water and propylene glycol (3/2: v/v) was used to dissolve the extracts. Positive control group, peel extract group and leaf extract group were fed through a tube with daily administration 2 mg kg⁻¹ of extract solvent, 200 mg kg⁻¹ of leafe extract and 200 mg kg⁻¹ of leaf extract,21, 26 respectively. Insulin group treated with daily SC injection of 5 IU kg⁻¹ of neutral protamine Hagedorn (NPH) insulin [9,10].

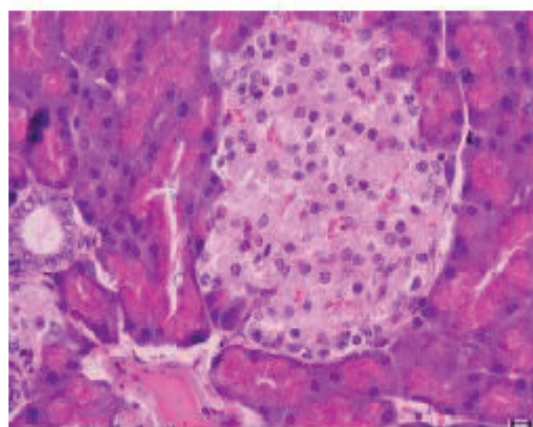
4. AQUEOUS EXTRACT OF WALNUT PEEL

4.1 Extract Preparation

The peel extract was concentrated by rotary evaporator at 40 °C and lyophilized to get a powder. To overcome to it's rather insolubility the peel extract was decanted by chloroform), and its oil fraction was extracted with hexane.

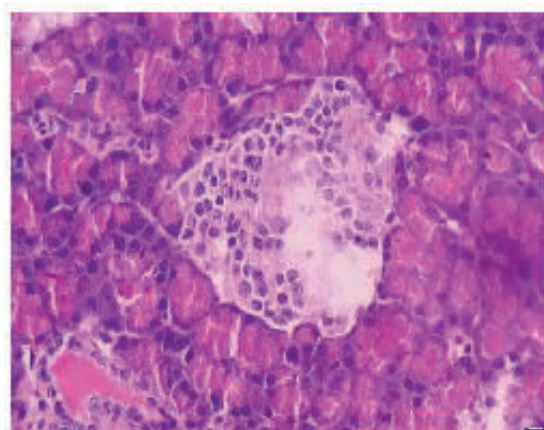
4.2 Diabetes Induction

A solution of distilled water and propylene glycol (3/2: v/v) was used to dissolve the extracts. Positive control group, peel extract group were fed through a tube with daily administration 2 mg kg⁻¹ of extract solvent, 200 mg kg⁻¹ of peel extract. Insulin group treated with daily SC injection of 5 IU kg⁻¹ of neutral protamine Hagedorn (NPH) insulin.



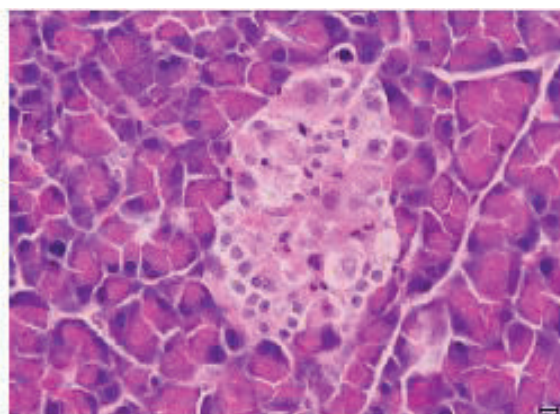
(a)

(Fig 1 a): shows normal islet with normal β -cells that were at the center of langerhans' islands



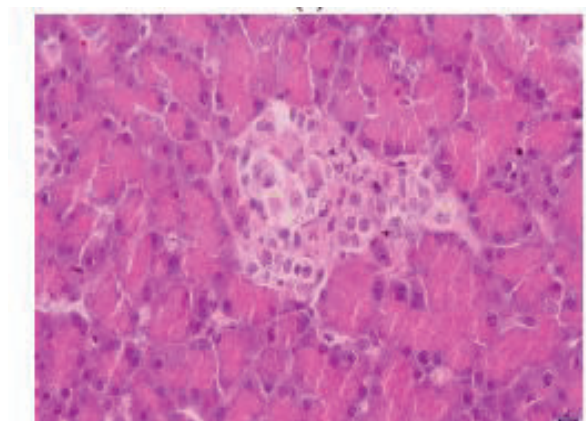
(b)

(Fig1 b): In untreated animals, the sections showed intense degenerative necrotic cells
Some β -cells had vacuolated cytoplasm with pyknotic nucleus



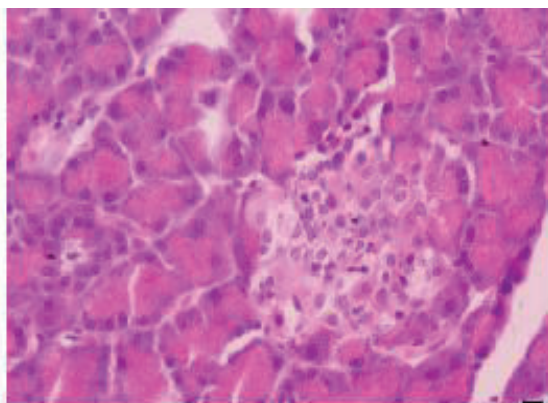
(c)

(Fig1 c): Two islets of Langerhans from pancreas of diabetic rat, treated with walnut peel extract



(d)

(Fig1 d) Two islets of Langerhans from pancreas of diabetic rat treated with walnut leaf extract



(e)

(Fig1 e) An islet of Langerhans from pancreas of diabetic rat treated with NPH insulin

5. CONCLUSION

The septum of walnut shell (SWS) extract reduced blood glucose in long time ($p < 0.05$), but this effect was not dose-dependent between groups. Hemoglobin (HbA1c) decreased in leaf extract and insulin groups. The β -cells number increased in leaf and peel extract groups. Insulin increased moderately in all treatment groups. There was no significant decrease in fast blood sugar (FBS) of peel extract and insulin groups compared to pretreatment level, but HbA1c significantly decreased in insulin group ($p < 0.05$). There was no significant decrease in FBS of peel extract and insulin groups compared to pretreatment level, but HbA1c significantly decreased in insulin group ($p < 0.05$).

ACKNOWLEDGMENTS

This study was supported by the vice-chancellor for Research of quchan University of chemical engineering. We appreciate the support of the dr. Farahbakhsh for drafting this article.

REFERENCES

- [1] Somey Javidanpour1, Seed Reza Fatima Tabtabaei1, Amir Siahpoosh, Hasan Morovati1, Ali Shahriari. Comparison of the effects of fresh leaf and peel extracts of walnut (*Juglans regia* L.) on blood glucose and β -cells of streptozotocin-induced diabetic rats. *Veterinary Research Forum*. 2012; 3 (4) 251 - 255

- [2] Forzani dehghani, There mashhoody, Mohammadreza panjehshahin, Effect of Aqueous Extract of Walnut Septum on Blood Glucose and Pancreatic Structure in Streptozotocin-Induced Diabetic Mouse, For author affiliations, see end of text. Received April 12, 2011; Revised July 9, 2011; Accepted September 5, 2011
- [3] Teimori M, Montasser Kouhsari S, Ghafarzadegan R, Hajiaghace R. Study of Hypoglycemic Effect of *Juglans regia* Leaves and its Mechanism. *J Med Plants* 2010; 9:57-65.
- [4] Esmacili MA, Yazdanparas R. Hypoglycemic effect of *Teucrium polium* studies with rat pancreatic islets. *J Ethnopharmacol* 2004; 95:27-30.
- [5] Sharma SB, Nasir A, Prabhu KM, Murthy PS. Antihyperglycemic effect of the fruit-pulp of *Eugenia jambolana* in experimental diabetes mellitus. *J Ethnopharmacol* 2006;104:367-73.
- [6] Soliman MM, Attia HF, El-Shazly SA, Saleh OM. Biomedical effects of cinnamon extract on obesity and diabetes relevance in Wistar Rats. *Am J Biochem Mol Biol* 2012; 2:133-45.
- [7] Okpuzor J, Ogbunugafor H, Kareem GK, Igwo-Ezikpe MN. In vitro investigation of antioxidant phenolic compounds in extracts of *Senna alata*. *Res J Phytochem* 2009; 3:68-76.
- [8] Mallick Ch, Maiti R, Ghosh D. Antidiabetogenic Effects of separate and composite extract of seed of Jamun (*Eugenia jambolana*) and root of Kadali (*Musa paradisiaca*) in streptozotocin-induced diabetic male Albino rat. A comparative study. *Int J Pharmacol* 2006; 2:492-503.
- [9] Chigozie II, Chidinma IC. Hypoglycemic, hypocholesterolemic and ocular-protective effects of an aqueous extract of the Rhizomes of *Sansevieria senegambica* Baker (Agavaceae) on alloxan-induced diabetic Wistar rats. *Am J Biochem Mol Biol* 2012; 2:48-66.
- [10] Mohana priya E, Gothandam KM, Karthikeyan S. Antidiabetic activity of *Feronia limonia* and *Artocarpus heterophyllus* in streptozotocin-induced diabetic rats. *Am J Food Technol* 2012; 7: 43-9.
- [11] Jelodar GH, Maleki M, Shahram S. Effect of walnut leaf, coriander and pomegranate on blood glucose and histopathology of pancreas of alloxan-induced diabetic rats. *Afr J Trad CAM* 2007; 4:299-305.
- [12] Shirdel Z, Madani H, Mirbadalzadeh R. Investigation into the hypoglycemic effect of hydroalcoholic extract of *Ziziphus Jujuba* Leaves on blood glucose and lipids in Alloxan-Induced diabetes in rats Iran. *J Diabet Lipid Disord*; 2009; 13-9.

Control of Underactuated Biped Robots Using Event Based Fuzzy Partial Feedback Linearization

Omid Heydarnia, Akbar Allahverdizadeh, Behnam Dadashzadeh, M. R. Sayyed Noorani

Abstract—Underactuated biped robots control is one of the interesting topics in robotics. The main difficulties are its highly nonlinear dynamics, open-loop instability, and discrete event at the end of the gait. One of the methods to control underactuated systems is the partial feedback linearization, but it is not robust against uncertainties and disturbances that restrict its performance to control biped walking and running. In this paper, fuzzy partial feedback linearization is presented to overcome its drawback. Numerical simulations verify the effectiveness of the proposed method to generate stable and robust biped walking and running gaits.

Keywords—Underactuated system, biped robot, fuzzy control, partial feedback linearization.

I. INTRODUCTION

RESEARCHERS are still interested in biped robots because of their friendly and human-like appearance and their capability to move in uneven environments. Through three decades of research on biped robots, effective control methods are sought to improve stability and robustness of biped walking like human or animals. Underactuated biped robots walking and running have been noticed by many researchers [1], [2].

Systems that have fewer number of actuators than the degree of freedom (DOF) are defined as underactuated systems. Control of these systems is more challenging than fully actuated systems and it is an open research problem. Second order sliding mode controller [3], sliding mode tracking control [4], and optimal sliding mode [5] were designed for the underactuated systems. The hierarchical sliding mode is designed to overcome uncertainty and disturbances of a class of the underactuated systems [8]. Partial feedback linearization was also proposed by Spong [6], [7] as a base to control the underactuated systems. A collocated form of partial feedback linearization was applied to a flexible link, and asymptotic stability of its zero dynamic was proved [9].

Biped robots can be divided into three classes: 1- passive bipeds, 2- underactuated bipeds and 3- fully actuated bipeds. There are no actuators in passive robots, and they use gravity force to continue walking. Engineers usually use springs to improve performance of these robots [10], [11]. A robot with

point feet provides an example of a common underactuated bipeds, since there is no actuation on ankle. While flat feet biped robots are often controlled by zero moment point (ZMP) stability criterion showing unnatural and slow walking and running gaits [12], underactuated robots demonstrate more natural dynamics and faster gaits [2].

Tzafestas et al. [13] showed that for a 5-link biped robot sliding mode controller is more robust than feedback linearization. A robust tracking control algorithm was presented for underactuated biped robots, making them self-balance in presence of disturbances. Then, stability criteria were derived based on linearization of the one nonlinear equation [14]. An adaptive controller was developed for underactuated biped locomotion in which recursive least square error was used for parameter estimation [15]. Stability analysis of compass gait walking has been investigated with the partial feedback linearization in [1], [16], and the convergence of its state vector to a reference limit cycle for both feedback linearization and partial feedback linearization was investigated. Poincaré map is one of the best tools for analysing the stability of periodic orbits of dynamic systems. It converts the hybrid dynamic model of biped walking or running to a discrete map. The fixed point of the map corresponds to periodic walking or running gait of the robot. The method of Poincaré has been used to study the stability of underactuated motion in several studies [17], [18]. Poincaré map has been used to study the stability of both passive and underactuated bipeds [18], [19].

Initiating by Zadeh's pioneering work [25], fuzzy logic has been utilized in control engineering for four decades. As a consequence, an Adaptive Network Based Fuzzy Interface System (ANFIS) control strategy has been proposed based on a hierarchy of walking gait planning and joint control level which do not require detailed kinematics and dynamics biped models [20]. Fuzzy logic has been used to eliminate chattering phenomena in classic sliding mode and was applied to a biped robot [21].

In this paper, a fuzzy partial feedback linearization controller is presented for biped models to enhance controller performance and improve its disturbance rejection. This controller is applied to a compass gait biped and a 5-link biped robot. We use two different gait generation methods to investigate the effect of gait generation method on controller performance. The rest of this paper is organized as follows. Section II describes dynamic modelling of the considered biped robots, including dynamic model of stance phase and touch-down. Section III describes reference trajectories generation for walking. Section IV discusses controller design

Omid Heydarnia was MSc student at the School of Engineering-Emerging Technologies, University of Tabriz, Tabriz, Iran (e-mail: omid.heidarnia92@ms.tabrizu.ac.ir).

Akbar Allahverdizadeh, Behnam Dadashzadeh and M. R. Sayyed Noorani are with the School of Engineering-Emerging Technologies, University of Tabriz, Tabriz, Iran. (e-mail: allahverdizadeh@tabrizu.ac.ir, b.dadashzadeh@tabrizu.ac.ir, smrs.noorani@tabrizu.ac.ir).

using fuzzy logic and its implementation on biped models. Section V provides simulation results of our control strategy for walking on flat ground, for both compass gait and 5-link biped robot. Finally, Section VI is the conclusion that discusses about effect of fuzzy logic on enhancement of partial feedback linearization in walking of biped robots.

II. DYNAMIC MODELLING

At this paper, we study dynamic model of two biped robots in sagittal plane. Walking gait includes two phases, single support phase (SSP) and double support phase (DSP). Here, it is assumed that transition from SSP to DSP occurs instantaneously. So, dynamic model of this type of biped walking gait is divided in two parts as following:

- Stance phase
- Touch-down (collision of leg with ground)

Walking dynamic model of an n -DOF biped robot with point feet can be expressed as follows. Let q be a vector of generalized coordinates in n -dimensional configuration space Q , and u be a vector of forces and torques, which is $(n-1)$ -dimensional.

$$\begin{cases} M(q)\ddot{q} + C(q, \dot{q})\dot{q} + G(q) = B(q)u & \text{for } q \notin \mathfrak{S} \\ q^+ = \Delta_q q^- \\ \dot{q}^+ = \Delta_{\dot{q}}(q^-)\dot{q}^- \end{cases} \quad \text{whenever } q^- \in \mathfrak{S} \quad (1)$$

where $M(q)$ is inertia matrix, $C(q, \dot{q})$ is matrix of Coriolis and centrifugal terms, $G(q)$ is the gradient of the potential energy field, and $B(q)$ describes the effects of actuators on the generalized coordinates. The set of \mathfrak{S} represents switching surface which is chosen to be:

$$\mathfrak{S} = \{q \in Q, \dot{q} \in Q \mid P_e^v = 0, P_e^h > 0\} \quad (2)$$

where P_e^v and P_e^h denote the vertical and horizontal position of the end of the swing leg, respectively.

Several assumptions are considered for touch-down phase [22]. To find angular velocities after collision, Lagrange Impact equation and two additional equations coming from no slip and rebound constraint has been used. So, we have:

$$\Delta_{\dot{q}_e}(q_e^-) = \begin{bmatrix} I_{1 \times N} & -D_a^{-1} J_a^T \cdot (J_a \cdot D_a^{-1} \cdot J_a^T)^{-1} J_a \end{bmatrix} \quad (3)$$

where D_a is the inertia matrix of biped robot when both legs in the air and we need to add the Cartesian coordinates of the robot body. (x_p, y_p) is the robot position which can be located at the end of swing leg, center of mass, or hip. Also,

$$J_a = \frac{\partial p_e}{\partial q_e} \quad \text{and} \quad q_e = [q, x_p, y_p]^T$$

$$\dot{q}_e^+ = \Delta_{\dot{q}_e}(q_e^-)\dot{q}_e^- \quad (4)$$

The vector of \dot{q}^+ in (1) is the first n element of \dot{q}_e^+ in (4).

More details about dynamic modelling of biped robots can be found in Refs. [13], [23].

A. Compass Gait Biped Robot

This robot has two DOF and there is only one actuator on the hip which makes this robot an underactuated system. Dynamic model of compass gait can be derived using Lagrange method and is available in literature [23], [24].

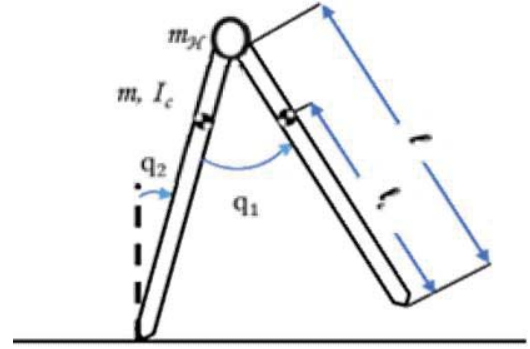


Fig. 1 Schematic of compass gait

We denote $q = [q_1, q_2]^T$ as configuration vector of the robot so $M(q) \in R^{2 \times 2}$, $C(q, \dot{q}) \in R^{2 \times 2}$, $G(q) \in R^{2 \times 1}$, $B = [1 \ 0]^T$.

B. 5-Link Biped Robot

One of the famous anthropomorphic biped models is 5-link biped robot. Various prototypes have been made for this robot like RABBIT and MABEL [23]. Fig. 2 depicts a schematic view of this robot.

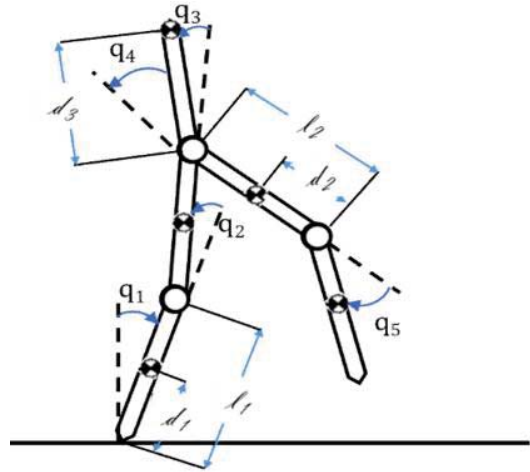


Fig. 2 Schematic of 5-link biped robot

Vector of generalized coordinate is considered as $q = [q_1 \ q_2 \ q_3 \ q_4 \ q_5]^T$ and dimension of matrixes in (1) are as $M(q) \in R^{5 \times 5}$, $C(q, \dot{q}) \in R^{5 \times 5}$, $G(q) \in R^{5 \times 1}$, $B = \begin{bmatrix} 0_{1 \times 4} \\ I_{4 \times 4} \end{bmatrix}$.

III. REFERENCE TRAJECTORY OF WALKING

In order to find reference trajectory of walking, we used two convenient methods: 1- Poincaré Map [2], 2- intellectual trajectory [13]. Here, we consider both of these methods to understand effects of reference trajectories on controller abilities. We used Poincaré map to find the reference trajectory of compass gait and intellectual method to find the reference trajectory of 5-link biped robot.

A. Active Poincaré Map

Poincaré map is a powerful mathematical tool to transform problem of finding periodic orbits into finding fixed points of a discrete map. Fixed point can be considered as equilibrium point of a specific discrete nonlinear system. Active Poincaré map can be used to find the reference trajectories of walking that consists of finding an initial condition and control commands which enables the robot to walk periodically.

$$x(k+1) = P(x(k), u(k)) \quad (5)$$

We use active Poincaré map to find reference trajectories of compass gait biped robot. Poincaré section is selected as start of stance phase, and a nonlinear optimization method is used to find the root or minimum of (6).

$$Er = x(k+1) - x(k) \quad (6)$$

Optimization parameters includes initial condition of stance phase and five points which determine motor torques during this phase. We apply these initial condition and torque to robot and save the reference trajectory of robot. The desired reference trajectory of walking is demonstrated in Fig. 3.

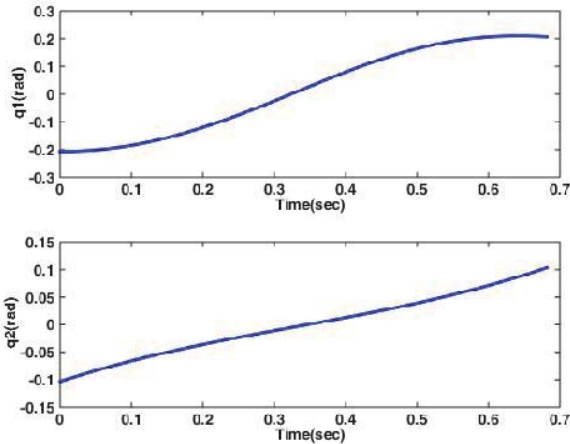


Fig. 3 Reference trajectories of compass gait

B. Intellectual Method

We name ‘‘intellectual trajectory’’ any desired reference trajectory of walking which is proposed by an expert person without using analytical tools like inverse kinematics, splines, and so on. We use this method similar to Tzafestas et al. [13] to find joints reference trajectories for the 5-link biped robot. These trajectories are designed so that torso remains vertical,

and the angular momentum of biped about support point increases by gravitational forces. Fig. 4 indicates the reference trajectories which are designed by intellectual method [13].

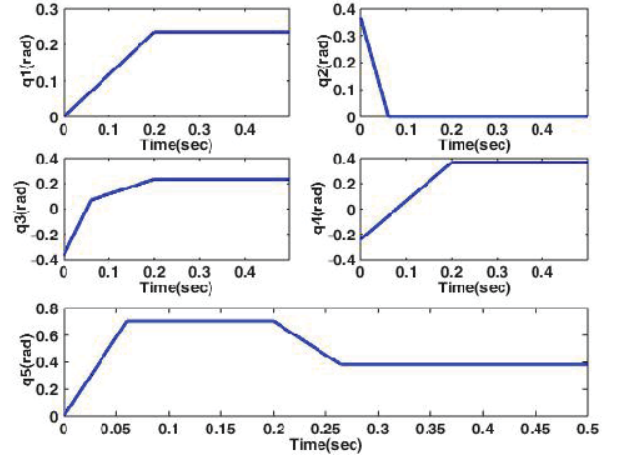


Fig. 4 Reference trajectories of 5 link biped robot

IV. FUZZY PARTIAL FEEDBACK LINEARIZATION

Linearization of underactuated systems is impossible with exact feedback linearization. So, partial feedback linearization was proposed to linearize the controllable part of underactuated systems so that it makes the remaining zero dynamic stable. Partial feedback linearization is divided into three categories: 1- Collocated form, 2- Non-collocated form and 3- Task space form.

In the collocated form, control signal linearizes dynamics of actuated degrees of freedom. Non-collocated form refers to linearizing dynamics of passive degrees of freedom, and in task space form, a combination of some active and passive degrees of freedom are linearized and controlled. Here, we used fuzzy logic to enhance capabilities of collocated partial feedback linearization abilities.

General form of underactuated systems can be written as

$$\begin{cases} M_{aa}\ddot{q}_a + M_{a0}\ddot{q}_0 + H_a(q, \dot{q}) + G_a(q) = \tau \\ M_{a0}^T \ddot{q}_a + M_{00}\ddot{q}_0 + H_0(q, \dot{q}) + G_0(q) = 0 \end{cases} \quad (7)$$

where q_a and q_0 represent actuated and unactuated variables, respectively. Note that because M is uniformly positive definite, M_{aa} and M_{00} are also positive definite and hence invertible.

$$\ddot{q}_0 = -M_{00}^{-1} (M_{a0}^T \ddot{q}_a + H_0 + G_0) \quad (8)$$

By substituting (8) into first term of (7), the dynamic equation of the system can be expressed as

$$N\ddot{q}_a = \tau - D \quad (9)$$

where

$$N = M_{aa} - M_{a0}M_{00}^{-1}M_{a0}^T$$

$$D = H_a(q, \dot{q}) + G_a(q) - M_{a0}M_{00}^{-1}(H_0 + G_0).$$

A feedback linearization control law can linearize the actuated subsystem. Therefore, it can be defined for (9) according to

$$\tau = Nv + D \quad (10)$$

where v is an additional outer loop control input. Similar to Ref. [7], v can be defined as:

$$v = \ddot{q}_a^d - K_d(\dot{q}_a - \dot{q}_a^d) - K_p(q_a - q_a^d) \quad (11)$$

with $K_d, K_p > 0$.

The complete dynamic model of the system can be written as

$$\ddot{q}_a = v$$

$$M_{00}\ddot{q}_0 + H_0 + G_0 = -M_{a0}^T v \quad (12)$$

Similar to [6], we define new variables as

$$z_1 = q_a - q_a^d, \quad \dot{z}_1 = z_2 = \dot{q}_a - \dot{q}_a^d$$

$$\eta_1 = q_0, \quad \dot{\eta}_1 = \dot{q}_0 \quad (13)$$

So, we have

$$\dot{z} = Az$$

$$\dot{\eta} = \omega(\eta, z, t) \quad (14)$$

Matrix A is Hurwitz because we defined $K_d, K_p > 0$. So, there is a zero dynamics $\dot{\eta} = \omega(\eta, 0, t)$ in our problem.

Stability of this zero dynamics is discussed in Ref. [6].

Because of highly nonlinear dynamics and presence of a discrete event at the end of the gait, control of a point feet biped robot is more difficult than other underactuated systems. So choosing control parameters properly is very important. As depicted in Fig. 5, we use a supervisory fuzzy controller to adjust the partial feedback linearization controller parameters.

The supervisory controller finds λ which will be used in partial feedback linearization as:

$$k_d = 2\lambda$$

$$k_p = \lambda^2 \quad (15)$$

The fuzzy controller will be updated at the beginning of SSP which has less computational effort. The membership functions of input variables e, \dot{e} and the membership functions of output linguistic variable λ are shown in Fig. 6 (a) and Fig. 6 (b), respectively.

The input variables of fuzzy controller are defined as weighted combination of actuated and non-actuated states

$$e = \|q_a - q_a^d\|_2 + \alpha \|q_0 - q_0^d\|_2$$

$$\dot{e} = \|\dot{q}_a - \dot{q}_a^d\|_2 + \beta \|\dot{q}_0 - \dot{q}_0^d\|_2 \quad (16)$$

where α, β are positive constants. The fuzzy rule base is designed as Table I, and a general form is used to describe the fuzzy rules as:

If $e(t)$ is E^j and $\dot{e}(t)$ is D^k then λ is Y^s ,

where E^j, D^k and Y^s are triangular membership functions that are depicted in Fig. 6.

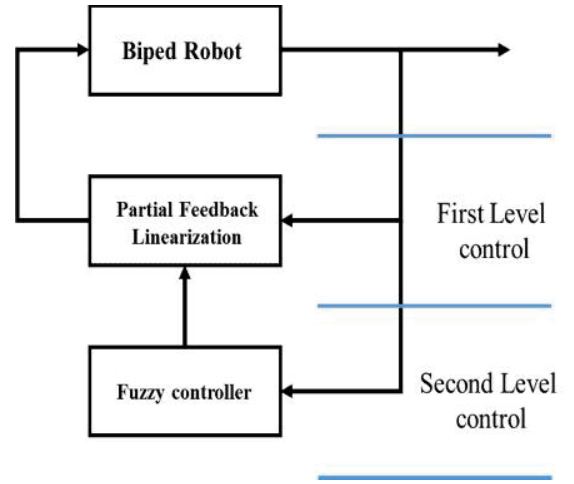


Fig. 5 Structure of fuzzy partial feedback linearization

TABLE I
RULE TABLE OF FUZZY PFL

λ'		e (j index)				
		E^{-2}	E^{-1}	E^0	E^1	E^2
$\frac{d}{dt}e$ (k index)	D^{-2}	B	B	B	M	S
	D^{-1}	B	B	M	M	S
	D^0	B	M	S	M	B
	D^1	S	M	M	B	B
	D^2	S	M	B	B	B

V. SIMULATION RESULTS

Validity of our designed controller is checked by simulations. We apply our controller on “compass gait biped robot” and “5-link biped robot”. In order to be sure about our controller performance, two different methods are used to find the reference trajectories of walking.

A. Compass Gait Biped Robot

Dynamic model of compass gait is expressed in Refs. [23], [24] and biped characteristics are chosen similar to Ref. [24]. A non-constrained optimization approach (OPTIMSEARCH) is used to find the Poincaré map fixed point. Stick diagram of 10 steps of walking is showed in Fig. 7.

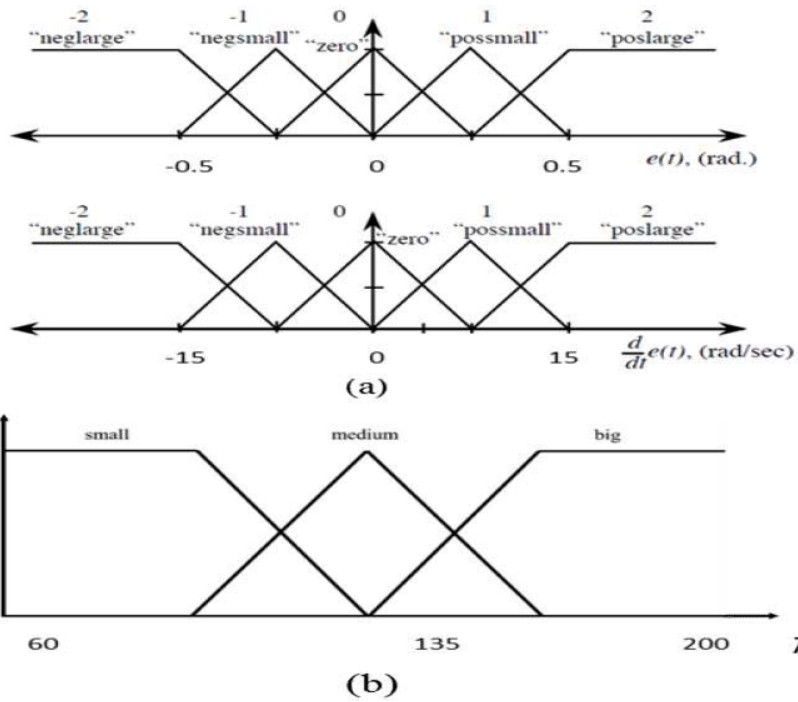


Fig. 6 (a) Membership function of input variables, (b) Membership function of output variable

Phase plane of one leg during 10 steps is shown in Fig. 8. At the beginning of stance phase, a 30% deviation of state vector from reference trajectory is considered. Our fuzzy partial feedback linearization controller is able to stabilize it, whereas a conventional partial feedback linearization controller can stabilize initial deviations up to 20%. As shown in Fig. 8, the system state converges to a stable limit cycle.

Fig. 9 depicts the control torque at the hip that has rational magnitudes in Newton-meters considering robot size and mass.

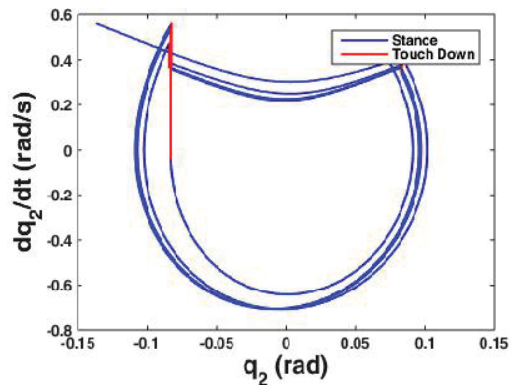


Fig. 8 Phase plane of one leg for 10 steps walking

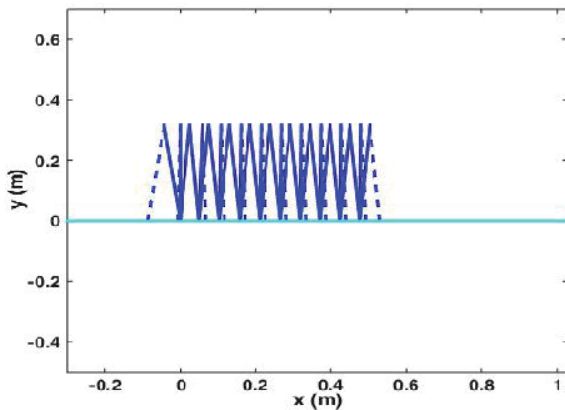


Fig. 7 Stick Diagram of 10 step walking for compass gait biped robot

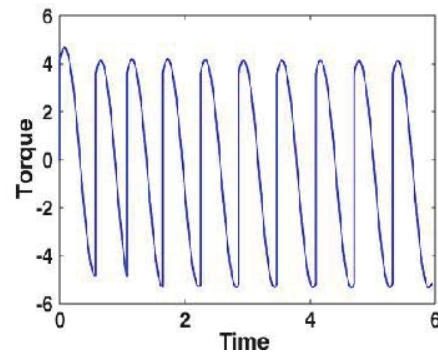


Fig. 9 Torque of hip actuator

B. 5-link Biped Robot

Dynamic model and characteristics of 5-link biped model are illustrated in Refs. [13], [23]. Again, we apply both convenient partial feedback linearization and fuzzy partial feedback linearization controllers to this robot and we obtain

similar results to compass gait biped robot. Stick Diagram of stable walking of this model using our designed controller is shown in Fig. 10.

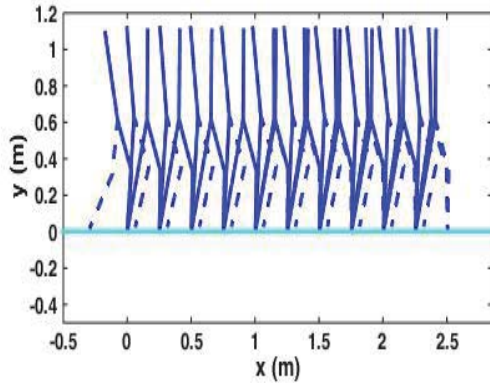


Fig. 10 Stick diagram of 10 steps walking for 5-link biped robot

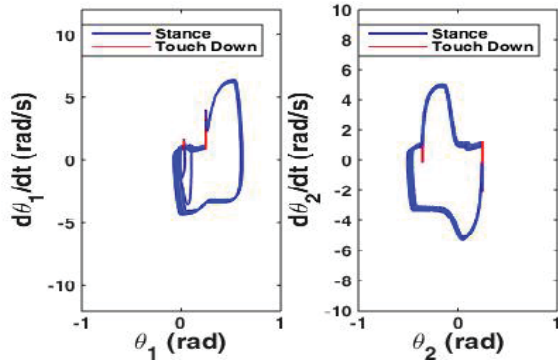


Fig. 11 Phase plane of one leg for 10 steps walking of 5-link biped robot

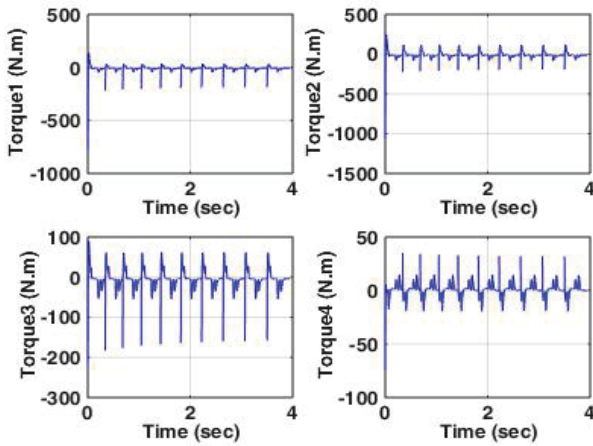


Fig. 12 Driving torques of 5-link biped robot

In the phase portraits shown in Fig. 11, absolute angles of the links belonging to the stand leg with respect to the vertical axis has been considered to investigate the stability of the limit cycles well. Clearly, they are taken as:

$$\begin{aligned}\theta_1 &= q_1 \\ \theta_2 &= q_1 - q_2.\end{aligned}\quad (17)$$

Phase diagram convergence of these angles to a stable limit cycle is obvious in Fig. 11. Fig. 12 shows the required actuator torques at the hip and knee joints. These actuation torque profiles are comparable to the previous published numerical results using the other non-fuzzy controller results [13], and their magnitudes are reasonable for a biped robot with the mass of 50 kg and the length of 1.3 m.

VI. CONCLUSION

Fuzzy partial feedback linearization controller was proposed and applied to underactuated biped robots walking. We used fuzzy logic as supervisory controller to enhance the capabilities of partial feedback linearization controller. According to the simulation results, the fuzzy partial feedback linearization showed better performance in comparison with a convenient partial feedback linearization controller. Two types of reference trajectories of walking including fixed point of active Poincaré map and intellectual method were considered. The designed controller was able to stabilize the desired walking gait in both models. The basin of attraction was larger with the fuzzy partial feedback linearization method.

REFERENCES

- [1] S. Kochuvila, S. Tripathi, and T. Sudarshan, "Stability of an Underactuated Passive Biped Robot Using Partial Feedback Linearization Technique," *Applied Mechanics and Materials*, vol. 394, pp. 456-462, 2013.
- [2] B. Dadashzadeh, M. Mahjoob, M. Nikkhah Bahrami, and C. Macnab, "Stable active running of a planar biped robot using Poincaré map control," *Advanced Robotics*, vol. 28, pp. 231-244, 2014.
- [3] S. Kurode, P. Trivedi, B. Bandyopadhyay, and P. Gandhi, "Second order sliding mode control for a class of underactuated systems," in *Variable Structure Systems (VSS), 2012 12th International Workshop on*, 2012, pp. 458-462.
- [4] R. Yu, Q. Zhu, G. Xia, and Z. Liu, "Sliding mode tracking control of an underactuated surface vessel," *IET control theory & applications*, vol. 6, pp. 461-466, 2012.
- [5] K. R. Muske, H. Ashrafuon, S. Nersesov, and M. Nikkhah, "Optimal sliding mode cascade control for stabilization of underactuated nonlinear systems," *Journal of Dynamic Systems, Measurement, and Control*, vol. 134, p. 021020, 2012.
- [6] M. W. Spong, "Partial feedback linearization of underactuated mechanical systems," in *Intelligent Robots and Systems '94. Advanced Robotic Systems and the Real World, IROS'94. Proceedings of the IEEE/RSJ/GI International Conference on*, 1994, pp. 314-321.
- [7] M. W. Spong, "Underactuated mechanical systems," in *Control problems in robotics and automation*, ed: Springer, 1998, pp. 135-150.
- [8] W. Wang, J. Yi, D. Zhao, and D. Liu, "Design of a stable sliding-mode controller for a class of second-order underactuated systems," *IEE Proceedings-Control Theory and Applications*, vol. 151, pp. 683-690, 2004.
- [9] Z. Zhang and S. S. Ge, "Partial feedback linearization control of space flexible-link manipulator with geometric nonlinearity," in *Information and Automation (ICIA), 2014 IEEE International Conference on*, 2014, pp. 1102-1107.
- [10] Y. Akutsu, F. Asano, and I. Tokuda, "Passive dynamic walking of compass-like biped robot with dynamic absorbers," in *Intelligent Robots and Systems (IROS 2014), 2014 IEEE/RSJ International Conference on*, 2014, pp. 4855-4860.
- [11] R. M. Alexander, "Three uses for springs in legged locomotion," *The International Journal of Robotics Research*, vol. 9, pp. 53-61, 1990.
- [12] C. Chevallereau, G. Bessonnet, G. Abba, and Y. Aoustin, *Bipedal robots: modeling, design and walking synthesis* vol. 78: John Wiley & Sons, 2010.
- [13] S. Tzafestas, M. Raibert, and C. Tzafestas, "Robust sliding-mode control applied to a 5-link biped robot," *Journal of Intelligent and Robotic Systems*, vol. 15, pp. 67-133, 1996.

- [14] M. Nikkhah, H. Ashrafiuon, and F. Fahimi, "Robust control of underactuated bipeds using sliding modes," *Robotica*, vol. 25, pp. 367-374, 2007.
- [15] L. M. Liu and W. Liang, "Adaptive asymptotic stable biped locomotion," in *Control Conference (CCC), 2014 33rd Chinese*, 2014, pp. 8375-8380.
- [16] S. Kochuvila, S. Tripathi, and T. Sudarshan, "Control of a Compass Gait Biped Robot Based on Partial Feedback Linearization," in *Advances in Autonomous Robotics*, ed: Springer, 2012, pp. 117-127.
- [17] B.-K. Cho and J.-H. Oh, "Running pattern generation with a fixed point in a 2D planar biped," *International Journal of Humanoid Robotics*, vol. 6, pp. 241-264, 2009.
- [18] A. D. Kuo, "Stabilization of lateral motion in passive dynamic walking," *The International journal of robotics research*, vol. 18, pp. 917-930, 1999.
- [19] C. E. Bauby and A. D. Kuo, "Active control of lateral balance in human walking," *Journal of biomechanics*, vol. 33, pp. 1433-1440, 2000.
- [20] C. Zhou and K. Jagannathan, "Adaptive network based fuzzy control of a dynamic biped walking robot," in *Intelligence and Systems, 1996., IEEE International Joint Symposia on*, 1996, pp. 109-116.
- [21] A. Takhmar, M. Alghooneh, and S. A. A. Moosavian, "Chattering Eliminated and Stable Motion of Biped Robots Using a Fuzzy Sliding Mode Controller," *Majlesi Journal of Electrical Engineering*, vol. 7, 2012.
- [22] Y. Hurmuzlu and D. B. Marghitu, "Rigid body collisions of planar kinematic chains with multiple contact points," *The international journal of robotics research*, vol. 13, pp. 82-92, 1994.
- [23] E. R. Westervelt, J. W. Grizzle, C. Chevallereau, J. H. Choi, and B. Morris, *Feedback control of dynamic bipedal robot locomotion*: Citeseer, 2007.
- [24] I. Manchester, U. Mettin, F. Iida, and R. Tedrake, "Stable dynamic walking over rough terrain: Theory and experiment," in *ISRR 2009*, 2009, pp. 1-16.
- [25] L.A. Zadeh, "Fuzzy sets," *Information and Control*, Volume 8, Issue 3, Pages 338-353, June 1965.

Cultural Influence Health and Safety to the Performance of Construction Project Toll Roads above Sea

Sri Kristinayanti Wayan, Mas Pertiwi I. G. Ag Istri, Suryanegara R. S. Dwipa

Abstract—Construction project toll roads above sea (Nusa Dua - Ngurah Rai - Benoa) in the Province of Bali is a big project that can not escape from a variety of hazards due to do the work piling some point in the middle of the sea is a big risk, so the focus of the contractor is to create good conditions of safety and health in the project. Occupational health and safety culture plays as a very important part in shaping the behavior of workers to safety and health, which affects the performance of the construction project. This study is conducted to identify and analyze the factors that influence the health and safety culture, especially in highway construction projects over the sea, as well as to analyze the influence of cultural factors on the occupational safety and health performance of the construction project. Various research data is taken from the assessment of respondent's answers to the questionnaire by workers in the research sample. Regression analysis is used to explain the influence of the culture of safety and health on the performance of highway construction projects over the sea. The results showed that simultaneously and partially independent variables consisting of management policies, rules and procedures of health and safety, communication, worker competency, work environment, worker participation, compliance worker, a significant effect on performance variables construction projects. Results also showed that the regression coefficient influence party policies on the performance of construction project management is positive, indicating that the influence of both unidirectional.

Keywords—culture occupational health and safety, work accidents, project performance construction, toll road above the sea

Corresponding Author

Wayan Sri Kristinayanti from Bali State Polytechnic, Indonesia
e-mail: yantie_5977@yahoo.com

Different Methods Anthocyanins Extracted from Saffron

Hashem Barati ¹, Dr Afshin farahbakhsh ^{1*}

1. Department of Chemical Engineering Quchan branch, Islamic azad University of Quchan, Iran

*Afshin.farahbakhsh@gmail.com

Abstract

The flowers of saffron contain anthocyanins. Generally, extraction of anthocyanins takes place at low temperatures (below 30 °C), preferably under vacuum (to minimize degradation) and in an acidic environment. In order to extract anthocyanins, the dried petals were added to 30 ml of acidic ethanol (pH=2). Amount of petals, extraction time, temperature, and ethanol percentage which were selected. Total anthocyanin content was a function of both variables of ethanol percent and extraction time. To prepare SW with pH of 3.5, different concentrations of 100, 400, 700, 1,000, and 2,000 ppm of sodium metabisulfite were added to aqueous sodium citrate. At this selected concentration, different extraction times of 20, 40, 60, 120, 180 min were tested to determine the optimum extraction time. When the extraction time was extended from 20 to 60 min, the total recovered anthocyanins of sulfur method changed from 650 to 710 mg/100 g. In the EW method Cellubrix and Pectinex enzymes were added separately to the buffer solution at different concentrations of 1%, 2.5%, 5%, 7%, 10%, and 12.5% and held for 2 hours reaction time at an ambient temperature of 40 °C. There was a considerable and significant difference in trends of Acys content of tepals extracted by pectinex enzymes at 5% concentration and AE solution.

Keywords Saffron. Anthocyanins. Acidic environment. Acidic ethanol. Pectinex enzymes. Cellubrix enzymes, Sodium metabisulfite.

Introduction

The flowers of saffron (*Crocus sativus* L.) contains anthocyanins. It has a mixture of natural colorants and is used as a food additive. Saffron (*Crocus sativus*) is used as a food additive for its pleasant smell and antioxidants activity (M.hamedi et al.2013). Owing to the high consumption of synthetic colorants in food processing and risks associated with it, intensive research has been focused on extraction, purification, and stabilization of natural pigments. Some researchers could separate the polyphenols from the needles of two plant pigments (*pinus taiwensis* and *pinus morrissonicola*) successfully when they used mixed enzymes of cellulose, hemicellulose, pectinase, and protease, and also hot pressurized water for extraction (L.lotfi et al.2015). The color properties and stability of these pigments depends on several factors, including their structure, concentration, pH, temperature, light intensity, attached pigment metallic ions, enzymes, oxygen, ascorbic acid, sugars, degradation products, and sulfur dioxide in the solution (L.lotfi et al.2015). Anthocyanins as natural pigments are found in roots, leaves, fruits, and flowers of plants. Attractive color and functional properties (like prevention of neuronal and cardiovascular, cancer, and diabetes illnesses) of anthocyanins make them a suitable substitute for synthetic pigments in the food

industry has cyanic color flowers with major colorant of anthocyanins. There are different sources of anthocyanins like grapes, berries, red cabbage, apples, red potatoes, and black carrots (M.sarfarazi et al.2015). Saffron (*Crocus Sativus*) which produces largely in Iran, with a share of annually more than 90 % of total saffron in the world (M.sarfarazi et al.2015). In the past, different solvents and acidifying solutions have been used to extract anthocyanins from wine pomace, radish, black carrot, Jaboticaba and grape seeds. The type of solvent used for anthocyanins extraction depends on chemical composition of the plant tissue and ratio of solid-liquid extraction. (M.hamedi et al.2013) . . Among the various solvents, ethanol is usually preferred for its low toxicity (M.sarfarazi et al.2015). Use of mineral acids such as hydrochloric acid preserves this pigment through extraction in its stable form (ion flavylum) by reducing pH of solvents. Generally, in solutions with pH>5, monomeric anthocyanins significantly ($P<0.05$) decreased. Temperature is another factor in conventional solvent extraction of anthocyanins. Saffron petals consist a large portion of saffron flower total weight. Then, these petals could be a good source of natural anthocyanins. Generally, extraction of anthocyanins takes place at low temperatures (below 30 °C), preferably under vacuum (to minimize degradation) and in an acidic environment (M. sarfarazi et al.2015). Solvents like ethanol, methanol, 1,N-butanol, cold acetone, propylene glycol, mixture of methanol-acetone and water, or boiled water can be used in extraction of anthocyanins. According to Einstein's equation, ($D \propto T / \eta$) rising temperature increases diffusion coefficient, and thus, ingredients can be extracted faster (M.sarfarazi et al.2015). However, the vulnerability of anthocyanins to heat and deterioration of these pigments into brown or colorless polymeric pigments and disappearance of desired color of extract exposed to heat treatment cannot be easily ignored (M.sarfarazi et al.2015). The aim of this study was to compare different methods of anthocyanin extracted from saffron and the impact of the time factor on rates of anthocyanin extraction.

Extraction of Anthocyanins by Response Surface Methodology

Saffron flowers were collected before sunlight from a farm near Torbat-E-Heydariyeh (Iran) on November 2013. After removing stigmas and anther, the petals were dried in a dark and warm room (37 °C) in front of a fan. This method of drying was compared with three other methods of drying in oven, 70 °C for 6 h, vacuum oven drying, 40 °C for 24 h, and conventional drying, 25 °C for 3 days, and mentioned that method was chosen due to the most stability of anthocyanins

through drying. Dried petals were crushed and sieved (16 meshes) and were kept in airtight bags in around 5 °C. Analytical grade hydrochloric acid (HCL) and ethanol were purchased from Merck (Darmstadt, Germany). Distilled water was used for preparation of all solutions. Potassium chloride buffer pH 1.0 and sodium acetate buffer pH 4.5 used in this study were of analytical grade.

In order to extract anthocyanins, the dried petals were added to 30 ml of acidic ethanol (pH=2). Amount of petals, extraction time, temperature, and ethanol percentage which were selected. Experiments were done in brown color bottles with screwed caps. After extraction, samples were filtered through filter paper (Whatman No. 1). Total anthocyanins of extracts were measured with pH differential method which was adopted from Giusti and Wrolstad (2001). In this method, the extracts were added to buffers 1.0 and 4.5 and allowed to equilibrate for 20 min. The absorbance of each equilibrated solution was then measured at 520 nm (λ max) and 700 nm for haze correction, using an UV-Vis spectrophotometer (Shimatzu-160A, Japan). Pigment content in acidic ethanol was calculated based on cyanidin-3-glucoside (Lee et al 2008). The absorbance of the diluted sample (A) was calculated as follows:

$$A = (A_{\lambda_{vis-max}} - A_{\lambda 700nm})_{pH 1.0} - (A_{\lambda_{vis-max}} - A_{\lambda 700nm})_{pH 4.5} \quad (1)$$

The total anthocyanin content in the original sample was calculated using the following formula:

$$\text{Total anthocyanin content (mg/L)} = (A \times MW \times DF \times 1000) / (\alpha \times L) \quad (2)$$

where MW is the molecular weight of delphinidin. Since major anthocyanin content of saffron petal was not clear, we used delphinidin MW (Giusti and Wrolstad 2001). DF is the dilution factor, and α is the molar absorptivity.

Total anthocyanin content was a function of both variables of ethanol percent and extraction time. In the first 12 h of extraction, as the percentage of ethanol solvent was increased, total anthocyanin content increased too. In contrast, in the second 12 h of extraction, total anthocyanin content decreased with increasing the ethanol concentration (fig.1)

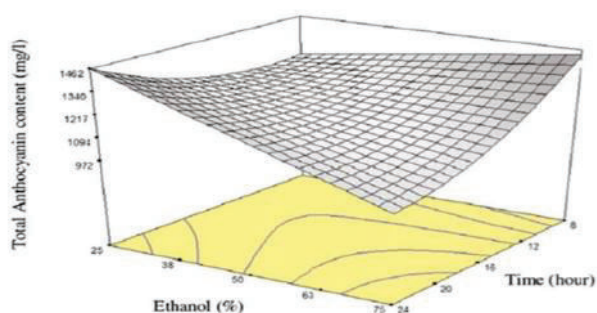


Fig.1 Response surface plots for the effect of extraction parameters on total anthocyanin content of saffron petals extract Ethanol percent and extraction time (temperature 35 °C and solvent ratio 50 ml/g).

Extraction of Anthocyanins by acidified ethanol (AE) solution and sulfur water solution (SW)

All chemicals and reagents used in this study were of analytical grade and obtained from chemical Merck Chemical Co (Germany). After detaching stigmas (real saffron) from saffron flowers (harvested from a farm located in the northeast of Iran), the remaining part (mainly tepals) were sorted (carefully), collected and transferred quickly to a cold storage at less than 5 °C. Then they were frozen in a kitchen freezer at less than -10 °C. Next, the frozen tepals were defrosted at room temperature and dried in a thermostatic vacuum oven at 40 °C for 36 h to around 3 % moisture. Dried tepals were crushed in a Moulinex Coffee Grinde (Moulinex International Corp., France) and passed through a 40 mesh sieve. The resulting fine powder was placed in brown vials and stored at -20 °C.

AE solution (with pH~1) was prepared by mixing hydrochloric acid (1.5 mol/L) with ethanol (95%) in ratio 15:85. The tepal powder was mixed with this solution at solid liquid ratio of 1:10 and held in a thermostatic chamber at 40 °C for various duration times (5, 10, 20, 60, 120, and 180 min). After washing the sediment of each sample with ethanol, a Hettich Universal 320 Centrifuge (Buckinghamshire, England) at 4,000 rpm for 15 min was used to separate the sediment phase of the mixture. The supernatant was collected and transferred into a 25 mL volumetric flask. A rotary evaporator (Laboratorium-Technic AG, Swiss) used to separate the ethanol portion of crude tepals at 40 °C and negative pressure of 0.1 MPa. The stock of alcohol free solution was stored at 0–5 °C for the anthocyanins determination.

Buffer solution was prepared by adding 200 mL NaOH (1 N) to 21.01 g of citric acid. Then 20 mL of the resulting solution was mixed with 80 mL of HCl (0.1N) to make a solution with pH of 3.5. To prepare SW with pH of 3.5, different concentrations of 100, 400, 700, 1,000, and 2,000 ppm of sodium metabisulfite were added to aqueous sodium citrate. Next 1 g of pulverized tepals were mixed with 10 mL of each prepared solution and maintained at 40 °C. The anthocyanins recovery of each sulfur solution was measured after 1 h extraction time and based on the highest yield, the best sulfur concentration treatment was chosen. At this selected concentration, different extraction times of 20, 40, 60, 120, 180 min were tested to determine the optimum extraction time. The highest rate of anthocyanins recovery was at 40 °C. Each sample solution was centrifuged at similar conditions, and its supernatant was collected and transferred into a 25 mL volumetric flask. After washing the residue and centrifugation of the supernatant, it was stored at 0–5 °C for further analysis. The extraction time affected the total anthocyanins recovery of tepals in sulfur (at concentration of 700 ppm) and ethanol solutions. While the SW recovered an anthocyanins yield of 650 mg/100 g after 20 min of extraction time, the anthocyanins yield extracted by AE with the same extraction time was about 580 mg/100 g. When the extraction time was extended from 20 to 60 min, the total recovered anthocyanins of sulfur method changed from 650 to 710 mg/100 g (fig.2). However, when the extraction time increased more than one hour, the change in anthocyanins recovery was insignificant.

Hence, it was not useful to extend the extraction time for more than 60 min. The negative coefficient of trendline equation for anthocyanin extracted by AE method showed clearly that the increasing of extraction time did not improve the anthocyanins removal of tepal powder, and diminished the recovered anthocyanins considerably due to degradation.

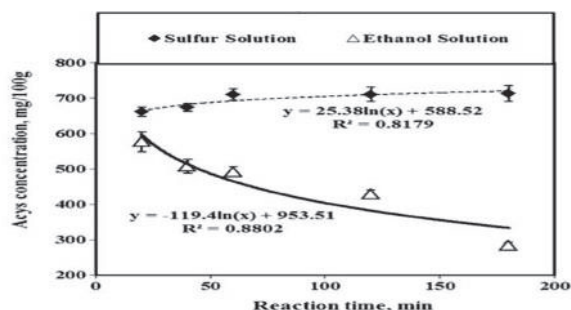


Fig.2 Effects of extraction time on anthocyanins recovery of saffron tepals by using SW(with sulfur concentration of 700 ppm) and AE methods

Extraction of Anthocyanins by enzymes

After detaching stigmas (real saffron) from saffron flowers harvested from a farm located in the Northeast of Iran, the remaining parts (mainly tepals) were carefully sorted, collected, and transferred quickly to a cold storage at $<5^{\circ}\text{C}$ and frozen in a kitchen freezer at -20°C . Later, the frozen tepals were defrosted at room temperature and dried in a thermostatic vacuum oven (Townson & Mercer, England) at 40°C for 36 hours to $<3\%$ moisture. Dried tepals were crushed in a coffee grinder (Moulinex International Goro., France) and passed through a 40 mesh sieve. The resulting fine powder was placed in a brown vial and stored at -20°C . The Pectinex Ultra SP-L was produced from the strain of *Aspergillus aculeatus* and had several enzymes including pectinase, cellulose, hemicellulose, pectinesterase, protease, fructosyltransferase, and β -galactosidase. Cellubrix was a liquid from of two mixed enzymes of cellulose and cellobiase produced by separate fermentation of a *Tichoderma* and *Aspergillus* strains. Both Pectinex Ultra SP-L and Cellubrix were supplied by Novozymes (Bagsverd, Denmark). All chemicals and reagents used in this study were analytical grade and obtained from Merck Chemical Co.

Extraction of Acys available in saffron tepals was done with separate acidified ethanol(AE) and enzymatic water(EW). In the AE method 1 g of the sample was mixed with 10 mL solution of 1.5N hydrochloric acid in ethanol (15:85 v/v) and held in a thermostatic chamber at 40°C for various duration times of 5, 10, 20, 60, 120 and 180 minutes. After ethanol washing of solid sediments, the resulting solution of each sample was centrifuged and then its ethanol portion (containing Acys) was evaporated at negative pressure of 0.1 MPa at 40°C . The stock of alcohol free thick solution was kept in a refrigerator at $0-5^{\circ}\text{C}$ for the Acys determination. In the EW method, again 1g powder of saffron tepals was mixed with 10 mL of prepared buffer solution. The buffer solution was prepared by adding 21.01 g of citric acid to 200 mL NaOH

(1N). Then 20 mL of resulting solution was mixed with 80 mL of HCl(0.1N) to make an aqueous solution with pH of 3.5. Then Cellubrix and Pectinex enzymes were added separately to the buffer solution at different concentrations of 1%, 2.5%, 5%, 7%, 10%, and 12.5% and held for 2 hours reaction time at an ambient temperature of 40°C . Although the optimum temperature for extraction of phenolic compounds from plant materials is around 50°C , the temperature was adjusted at 40°C in our experiment to prevent its degradation during the recovery process. The Acys yields extracted by pectinex Ultra SP-L and Cellubrix samples were measured at different enzyme concentrations. Then, the highest content of Acys yield between two groups of enzymes and among different concentrations was chosen to find out the most suitable extraction time. In this stage, the Acys experiment was repeated with different extraction times of 20, 40, 60, 120, and 180 minutes. After centrifugation of each sample, its supernatant was collected, and after washing the resulting sediment with enough AE, its Acys content was determined in three replicates and quantified in cyanidin by using the following formulae and its updated version for Acys measurement.

There was a considerable and significant difference in trends of Acys content of tepals extracted by pectinex enzymes at 5% concentration and AE solution. While the Acys content of EW solution increased very quickly after 20 minutes and reached 675 mg/100 g of solution after 3 hours of extraction, the Acys extracted by AE solvent decreased sharply ($>60\%$) at parallel conditions (Fig. 3). Furthermore, the enzyme extracted Acys of saffron tepals was resistant against browning and decomposition processes and had much better color values (less lightness and more chroma) and more stability (less degradation and less polymerization) than the ones extracted with AE solution.

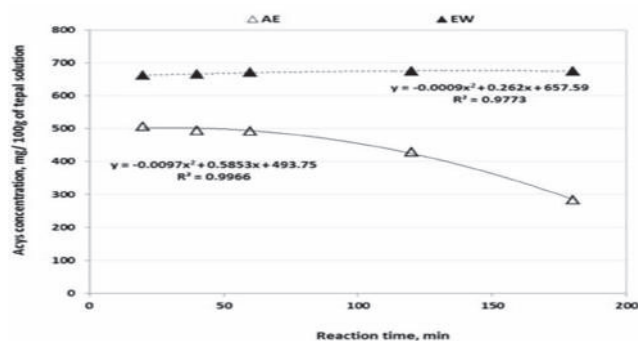


Fig.3 Effect of reaction time on anthocyanins (Acys) content of saffron tepals extracted by acidified ethanol (AE) and enzymatic water (EW)

Conclusion:

The results showed that the process variables, including temperature, extraction time, solvent ratio, and the percentage of ethanol, had statistically significant effects on anthocyanin extraction from the saffron petal. Maximum anthocyanin content was obtained in 24 h extraction time, 25.8°C , 20 ml/g solvent, and 25.02 % ethanol, and extracted anthocyanins was 1609.11 mg/l.

Although 700 ppm sodium metabisulfite was used in aqueous solution of saffron tepals to dissociate its cells and release anthocyanins upto 7 mg/g (significantly higher than acidified ethanol solution), only part of sulfur compound was necessary to shield this pigment from degradation or gradual decomposition. is a valuable and promising tool to rapidly extract high quantity and quality anthocyanins and also phenolic pigments from the freshly harvested and discarded tepals of saffron and avoid using expensive and sometimes toxic organic solvents.

The mixed enzymes of Pectinex Ultra SP-L with 5% concentration in aqueous solution were able to extract Acys of saffron tepals with significantly higher efficiency than the ones extracted by ethanol solution. Overall, the enzyme method utilizes saffron tepals (as a low-cost raw material) to produce a completely natural and healthy Acys with a valuable source of antioxidants and attractive natural color.

Acknowledgments The authors wish to thank Islamic Azad University of Quchan (Faculty of Engineering) and for their assistances and supports that they made for this project.

References

1. Lotfi L , Kalbasi-Ashtari A , Hamed M , Ghorbani F (2013) Effects of sulfur water extraction on anthocyanins properties of tepals in flower of saffron (*Crocus sativus* L). *J Food Sci Technol* DOI 10.1007/s13197-013-1058-z
2. Mahdavee Khazaei K , Jafari S. M , Ghorbani M , Hemmati Kakhki A, Sarfarazi M (2015) Optimization of Anthocyanin Extraction from Saffron Petals with Response Surface Methodology. *Food Anal. Methods* DOI 10.1007/s12161-015-0375-4
3. L. Lotfi , A. Kalbasi-Ashtari , M. Hamed , F. Ghorbani (2015) Effect of enzymatic extraction on anthocyanins yield of saffron tepals (*Crocus sativus*) along with its color properties and structural stability. *J of food and drug analysis* 23(2015) 210-218
4. Byamukama R, Jordheim M, Kiremire B, Namukobe J, Andersen ØM (2006) Anthocyanins from flowers of *Hippeastrum* cultivars. *Sci Hortic* 109:262–266
5. Cacace JE, Mazza G (2002) Extraction of anthocyanins and other phenolics from black currants with sulfured water. *J Agric Food Chem* 50:5939–5946
6. Freitas V, Mateus N (2006) Chemical transformations of anthocyanins yielding a variety of colours (review). *Environ Chem Lett* 4:175– 183
7. Gould K, Davies K, Winefield C (2008) *Anthocyanins: biosynthesis, functions, and applications*. Springer
8. Sarfarazi M, Jafari SM, Rajabzadeh G (2015) Extraction optimization of saffron nutraceuticals through response surface methodology. *Food Anal Methods* 8:2273–2285
9. Montes C, Vicario IM, Raymundo M, Fett R, Heredia FJ (2005) Application of tristimulus colorimetry to optimize the extraction of anthocyanins from jaboticaba (*Myrcia Jaboticaba* Berg.). *Food Res Int* 38(8–9):983–988
10. Fatehi M, Rashidabady T, Fatehi-Hassanabad Z (2003) Effect of *Crocus sativus* petals' extract on rat blood pressure and on responses induced by electrical field stimulation in the rat isolated vas deferens and guinea-pig ileum. *J Ethnopharmacol* 84(2–3):199–203
11. Hadizadeh F, Khalili N, Hosseinzadeh H, Khair-Aldine R (2003) Kaempferol from saffron petals. *Iran J Pharm Res* 2:251–252
12. Hemmati Kakhki A et al (2001) Optimization of effective parameters of production of food color from saffron petal. *Agric Sci* 13(20):16–23
13. Kafi M (2006) *Saffron (Crocus Sativus) production and processing*. Science Publishers
14. Karimi G, Hosseinzadeh H, Khaleghpanah P. Study of antidepressant effect of aqueous and ethanolic of *Crocus sativus* L. in mice. *Iran J Basic Med Sci* 2001;4:11-5.

Different methods of Fe₃O₄ nano particles synthesis

Arezoo hakimi¹, Dr Afshin farahbakhsh^{2*}

1. Department of Chemical Engineering, Quchan branch, Islamic azad University, Quchan, Iran.

2. University Of Applied Science And Technology, Shirvan Center, Shirvan, North Khorasan, Iran.

*Afshin.farahbakhsh@gmail.com

Abstract—Herein, we comparison synthesized Fe₃O₄ using , hydrothermal method, Mechanochemical processes and solvent thermal method. The Hydrothermal Technique has been the most popular one, gathering interest from scientists and technologists of different disciplines, particularly in the last fifteen years. In the hydrothermal method Fe₃O₄ microspheres, in which many nearly monodisperse spherical particles with diameters of about 400nm, in the mechanochemical method regular morphology indicates that the particles are well crystallized and in the solvent thermal method Fe₃O₄ nanoparticles have good properties of uniform size and good dispersion.

Keywords—Fe₃O₄ nanoparticles, hydrothermal method, Mechanochemical processes, solvent thermal method

1. Introduction

Recently, researchers have focused on the synthesis of the low cost nano-sized metal oxides.[1] Magnetic material is of great importance in the fields of chemistry, biology, and medical sciences as well as in biotechnology[2]. Control of the size and different morphologies (spherical, octahedral and cubic) of monodisperse Fe₃O₄ NPs is very important because these various structures generate distinct properties. To understand magnetic behavior and to improve applications, careful research related to synthetic strategies and growth mechanisms of Fe₃O₄ NPs are essential.[3]

the hydrothermal synthesis of iron pyrite has gained much attention due to its facile process, low operating temperature as well as inexpensive reactants (i.e., water is used as the main solvent).[4] Hydrothermal synthesis offers many advantages over conventional and non conventional synthesis methods. Unlike many advanced methods that can prepare a large variety of forms, the respective costs for instrumentation, energy and precursors are far less for hydrothermal methods[5].

Mechanochemical processes are used to prepare different kinds of nano-structures of metal oxides, hydrogen storage materials, composites and so on. Since no toxic liquid solvent have been used in these reactions, they do not pollute the environment and therefore these reactions can be considered as green chemistry methodologies.[6] in the present study we have compered three different sizes of Fe₃O₄ nanoparticles by using three different methods.

2. Methods Of Synthesis Fe₃O₄

2.1. Hydrothermal Method

The synthesis was carried out through a hydrothermal process according to a previous report. Typically, 1.35 g of iron chloride (III) hexahydrate was dissolved in 40mL ethylene glycol to form a clear solution, then 1.0 g of polyethylene glycol (Mw= 4000) and 3.6 g of sodium acetate trihydrate was

added subsequently. The mixture was stirred until the reactants were fully dissolved. After that, the mixture was transferred into a Teflon lined autoclave with a capacity of 50mL and heated at 200 °C for 8 h. The products were collected and fully rinsed with deionized water and absolute ethanol with the help of an external magnet. Finally, the products were dried under vacuum at 60 °C for 2 h for further use.[7]

The morphology and size of the prepared samples were examined by FESEM. Fig. 1a shows a FESEM image of the Fe₃O₄ microspheres, in which many nearly monodisperse spherical particles with diameters of about 400nm can be seen.

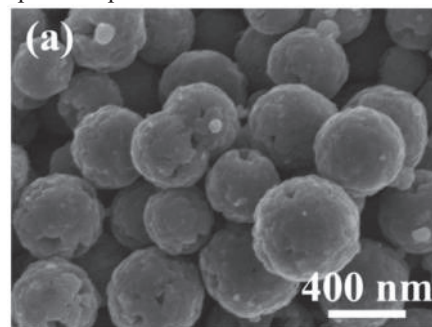
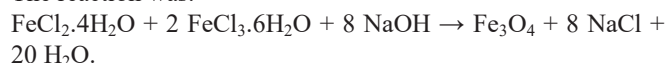


Fig. 1. FESEM images of (a) Fe₃O₄ microspheres

2.2. Mechanochemical Method

The Fe₃O₄ nanoparticles were synthesized by mechanochemical reaction of FeCl₂.4H₂O, FeCl₃.6H₂O and NaOH. The excess of NaCl powder was added to avoid the aggregation of Fe₃O₄ particles. First, 0.43 g FeCl₃.6H₂O, 0.3 g of FeCl₂.4H₂O and 3 g NaCl were mixed together and were put in a stainless steel cylinder (10 mL) with two small balls of 10 mm diameter by utilizing a mass ratio of 8:1 ball-to-powder. Milling was carried out for 10 min with a rate of 30 Hz (1800 rpm) at room temperature. Then 0.25 g of NaOH was added and the process of ball-milling was repeated for another 10, 30, 50 and 70 min.[1]

The reaction was:



Sampling was carried out at different ball milling time that resulted to three type of Fe₃O₄ nanoparticles, Fe₃O₄-10, Fe₃O₄-30, Fe₃O₄-50 and Fe₃O₄-70.

Figs. 2 show SEM images of Fe₃O₄ nanoparticles synthesized by mechanochemical route at times of 50min. Small particle size, uniform morphology and narrow size distribution of Fe₃O₄ particles prepared at 50 (Fe₃O₄-50 and Fe₃O₄-70) is obvious that show the optimum time is 50 min for ball-milling

process. The regular morphology indicates that the particles are well crystallized.

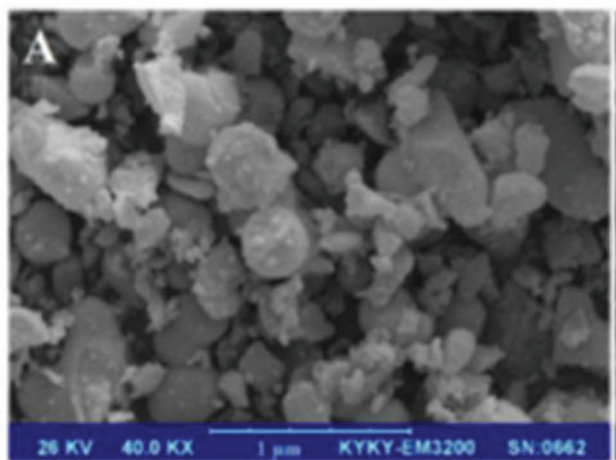


Fig.2. To confirm the crystal structure of the formed Fe_3O_4 -50 nanoparticles, XRD experiments were performed.

2.3. solvent thermal method

Fe_3O_4 nanoparticles were synthesized through the solvent thermal method. Specific synthesis steps were as follows: firstly, 1.35g of ferric chloride hexahydrate, 1g of PEG 4000 and 3.6g of sodium acetate were completely dissolved in 72ml of ethylene glycol. The mixed solution was under ultrasonic dispersion for 20 min, forming a pale yellow homogeneous solution. Then, the mixed solution was transferred to a hydrothermal reaction kettle, with the temperature setting at $200\text{ }^\circ\text{C}$ and time setting at 16h. After the completion of this action, the kettle was cooled to room temperature and the black products were washed with deionized water and ethanol each for three times. Subsequently, the products were put in to the vacuum drying oven in $50\text{ }^\circ\text{C}$ for drying. Finally, we obtained the Fe_3O_4 nanoparticles we wanted.[8]

To further characterize the morphology and size of the as prepared Fe_3O_4 nanocomposites, SEM observations were carried out as shown in Fig. 3. Notably, it can be seen that Fe_3O_4 nanoparticles have good properties of uniform size and good dispersion.

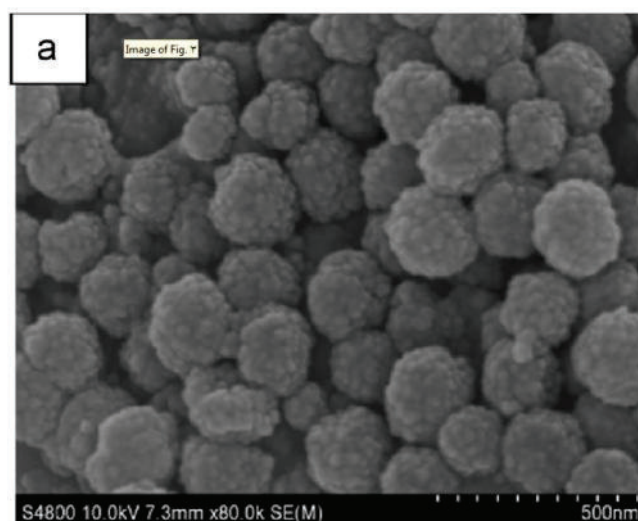


Fig.3. SEM images of (a) Fe_3O_4

3. conclusion

This report has showed that Fe_3O_4 nanoparticles can be synthesis by a fast and facile mechanochemical method at only 50 min. The Fe_3O_4 microspheres are composed of many smaller nanoparticles, and their surfaces are rough in the hydrothermal method. Fe_3O_4 nanoparticles with uniform particle size, good monodispersity, and average particle size were prepared via hydrothermal reaction.

Acknowledgments

Financial supports from the Islamic azad university of Quchan, experts, friends and colleagues are gratefully acknowledged.

Reference

- [1] M. Rabbani, F. Rafiee, H. Ghafuri, R. Rahimi, Synthesis of Fe_3O_4 nanoparticles via a fast and facile mechanochemical method: Modification of surface with porphyrin and photocatalytic study, *Materials Letters*, S0167-577X(15)31042-9.
- [2] H. Peng, G. Liu, X. Dong, J. Wang, W. Yu, J. Xu, Magnetic, luminescent and core-shell structured $\text{Fe}_3\text{O}_4@YF_3:\text{Ce}^{3+}, \text{Tb}^{3+}$ bifunctional nanocomposites, *Powder Technology*, 215-216 (2012) 242–246.
- [3] L. Jiang, X. Zhou, G. Wei, X. Lu, W. Wei, J. Qiu, Preparation and Characterization of Poly(glycidyl methacrylate)-grafted Magnetic Nanoparticles: Effects of the Precursor Concentration on Polyol Synthesis of Fe_3O_4 and [PMDETA]0/[CuBr₂]0 Ratios on SI-AGET ATRP, *APSUSC*, S0169-4332(15)02442-3.
- [4] A. Azarafza, M. Ziarati, N. Khandanc, J. Aminian, H. Kazemi Esfeh, M. Setarekokab, Experimental and numerical study of iron pyrite nanoparticles synthesis based on hydrothermal method in a laboratory-scale stirred autoclave, *Powder Technology*, 287 (2016) 177–189.
- [5] Hydrothermal Method, Chapter 2, page 18
- [6] S. Shahbazi, S. Afshar, A facile, green, one pot synthesis of cuprous iodide nanoparticles using the mechanochemical method, *Materials Letters*, 115 (2014) 190–193.
- [7] Z. Wang, S. Zhu, S. Zhao, H. Hu, Synthesis of core-shell $\text{Fe}_3\text{O}_4@SiO_2@MS$ (M= Pb, Zn, and Hg) microspheres and their application as photocatalysts, *Journal of Alloys and Compounds*, 509 (2011) 6893–6898.
- [8] L. Yu, G. Hao, J. Gu, S. Zhou, N. Zhang, W. Jiang, $\text{Fe}_3\text{O}_4/\text{PS}$ magnetic nanoparticles: Synthesis, characterization and their application as sorbent so foil from waste water, *Journal of Magnetism and Magnetic Materials*, 394(2015)14–21.

Different methods of producing bioemulsifier by *Bacillus licheniformis* strains

Saba Pajuhan^a, Afshin Farahbakhsh^{b*}, S.M.M Dastgheib^c

^aDepartment of Chemical engineering, Islamic Azad University, Quchan branch, Quchan, Iran

^bDepartment of Chemical engineering, Islamic Azad University, Quchan branch, Quchan, Iran

^cEnvironment and Biotechnology Department, research institute of Petroleum industry

* Email: afshin.farahbakhsh@gmail.com

Abstract

Biosurfactants and bioemulsifiers are a structurally diverse group of surface-active molecules synthesized by microorganisms, they are amphiphilic molecules which reduce surface and interfacial tensions and widely used in pharmaceutical, cosmetic, food and petroleum industries. In this paper, several methods of bioemulsifier synthesis and purification by *Bacillus licheniformis* strains (namely ACO1, PTCC 1595 and ACO4) were investigated. strains were grown in nutrient broth with different conditions in order to get maximum production of bioemulsifier. the purification of bio emulsifier and the quality evaluation of the product was done by adding sulfuric acid (H₂SO₄) (98%), Ethanol or HCl to the solution followed by centrifuging. To determine the optimal conditions yielding the highest bioemulsifier production, the effect of various carbon and nitrogen sources, temperature, NaCl concentration, pH, O₂ levels, incubation time are indispensable and all of them were highly effective in bioemulsifiers production.

Key words: biosurfactant, bioemulsifier, purification, surface tension, interfacial tension

1.introduction

Biosurfactants are amphiphilic biological compounds produced extracellularly or as part of the cell membranes by a variety of yeast, bacteria and filamentous fungi from various substances including sugars, oils and wastes.[3] Biosurfactants are a diverse group of surface-active chemical compounds produced by a wide variety of microorganisms and can be divided into two categories: low-mass molecules that act to lower surface and interfacial tensions and high-molecularmass polymers, also known as bioemulsifier, that are more effective in stabilizing oil–water emulsions without remarkable surface tension reduction.[4]Bioemulsifiers are amphiphilic molecules secreted by microorganisms facilitates uptake of insoluble substrate.studies on bioemulsifier are fast gaining ground due to their widespread application.[10]high-molecularmass polymers, also known as bioemulsifier, that are more effective in stabilizing oil–water emulsions without remarkable surface tension reduction.[4] Biosurfactants can reduce the surface tension between two liquids, and bioemulsifiers induce a dispersion of undissolved material throughout the liquid, by formation and stabilization of droplets of the dispersed phase. biopolymers are less effective on lowering the surface tension, but are highly effective on the production of emulsions, and have a considerable specificity for the substrate.[5] Bioemulsifiers reduce the interfacial tension between

immiscible liquids, or at the solid-liquid interface.[6]Bio emulsifiers can be divided into three categories: 1. Bio emulsifiers were produced exclusively with alkenes as a carbon source, such as *Corynebacterium* sp., 2. Bio emulsifiers were produced only with water-soluble substrates as the carbon source, such as *Bacillus* sp., and 3. Bio emulsifiers were produced with alkenes and water-soluble substrates as carbon sources, such as *Pseudomonas* sp.[7]Unlike their synthetically produced counterparts, emulsifiers of natural origin are biodegradable and have reduced toxicity, which is in agreement with the concept of environmental sustainability. In addition, they can remain effective even at extreme conditions of pH, temperature, and salinity.they can be produced in situ, at the contaminated site.[7]In the field of bioremediation, the application of bioemulsifiers as natural alternatives to synthetic production is an efficient strategy for removing hydrocarbons from contaminated soils and Sediments.[2] Bio emulsifiers are not only of interest for bioremediation processes in the petroleum industry. These compounds can be used to enhance oil recovery from wells, reduce the heavy oil viscosity, clean oil storage tanks, increase flow through pipelines and stabilize fuel water–oil emulsions.[7]A diverse microorganisms (including bacteria, filamentous fungi, and yeasts[2]) can emulsify hydrocarbons even in the absence of cell growth or uptake of hydrocarbons. Surface-active compounds produced by microorganisms are of two main types, those that reduce surface tension at the air–water interface (bio surfactants) and those that reduce the interfacial tension between immiscible liquids, or at the solid–liquid interface (bio emulsifiers).[7] diversity of microorganisms are able to produce a wide range of amphiphilic compounds that exhibit surface activities at interfaces, such as bioemulsifiers Although a wide diversity of bioemulsifiers has been produced up until now using a large variety of microorganisms, only a few reports have appeared in relation to actinobacteria emulsifier producers such as *Streptomyces* sp., isolated from marine environments, or *Streptomyces* sp. S22, isolated from garden soil. *Streptomyces* sp. MC1, an actinobacteria isolated from sugar cane, has shown the ability to reduce hexavalent chromium [Cr(VI)] to less toxic species with this biological reduction seeming to occur largely on the cell surface.[1] *Bacillus licheniformis* produces a lipopeptide called lichenysin. Lichenysin is a cyclic lipopeptide and belongs to the most effective biosurfactant discovered so far. Bioemulsifier produced by *B. licheniformis* JF-2 exhibits a critical micelle concentration of

10 mg/l and reduces the interfacial tension against decane to 6×10^{-3} dyne cm^{-1} , which is one of the lowest interfacial tensions ever reported for a microbial surfactant [8]. Despite their potential applications in multiple biotechnological areas, the commercial availability of bioemulsifiers is currently limited. This is mainly due to economic obstacles to their sustainable production at industrial levels. The production of new biomolecules and strains could therefore be key for overcoming these limitations and challenges, especially if inexpensive substrates can be used. It is important to remark that substrates represent 10–30% of total production costs [2]. This review however aims to provide a quick glance into obtain microbial cultures producing BE with several bacteria and the main techniques employed for their purification, and Concentration.

2.1 . Bioemulsifier Production by *B.licheniformis* (ACO1)

Isolated bacteria was cultivated in a flask containing a 50 ml mineral salt (MS) solution supplemented with 2% (w/v) glucose and was incubated at 45C for 7 days. The MS solution was used as the basic medium. A crude bioemulsifier preparation was obtained by centrifuging (10000g, 15 min, 4C) a stationary-phase culture to remove the cells. Three volumes of cold ethanol were added to the supernatant and kept at 4C overnight. Crude bioemulsifier precipitate was collected after centrifugation at 3000g for 5 min and was washed with ethanol. Dried emulsifier was dissolved in 100 ml distilled water to prepare a crude extract solution and was tested for emulsifying activity.

To determine the optimal conditions yielding the highest bioemulsifier production, the effect of various carbon and nitrogen sources was analyzed. The highest emulsifier production was obtained when yeast extract was used in the medium. Among the nitrogen sources tested, sodium nitrate was shown to be the best substrate for emulsifier production. The optimum temperature, NaCl concentration and pH for its bioemulsifier production were 45C, 4% (w/v) and 8.0, respectively. Strain ACO1 was able to grow under different O_2 levels but emulsifier production was optimal in the static condition [9].

2.2 .Bioemulsifier production by *B. licheniformis* PTCC 1595

After the bacterial cells were removed from the liquid culture by centrifugation (13000 g, 15 min) in a HEPTICH centrifuge mod., the crude bioemulsifer was isolated by adding concentrated HCl to the supernatant. A flocculated precipitate was formed at pH 2.0 that could be collected by centrifugation (20000 g, 20 min). The precipitate was dried under vacuum in dessicator and kept overnight at 4°C. The crude product was resuspended in dichloromethane. After stirring for one night, the suspension filtered through Whatman No. 1 filter paper to remove the coarse impurities. The filtrate was extracted twice with equal volumes of distilled water (pH 8.0) while stirring for 20 min. After this period, it was left 3 h in a separating funnel to allow the two phases to separate. The aqueous phases containing the bioemulsifer were collected and then were lyophilized overnight [8].

Maximum of bioemulsifer production was achieved in 48 h of incubation and CMD values were minimal at this point. Emulsification index values followed a similar pattern as surface tension lowering. According to these data, 37°C and 300 rpm were selected as best conditions. The production yield of bioemulsifer was improved by addition of FeSO_4 , MnSO_4 and starch while CaCl_2 and MgSO_4 decreased it. The addition of hydrocarbons, such as almond, castor oil and olive oil to the culture medium increased the bioemulsifer production while maximum of yield was achieved with olive oil [8].

2.3 .Bioemulsifier production by *B. licheniformis* (ACO4)

In the first stage of the separation process, the incubated culture was sterilized with humid heat and Centrifuged at 10000 rpm and 4°C for 15 min. The supernatant was collected and then sterilized by the same procedure previously described. In the second stage of the separation process, 1mL of H_2SO_4 (98%) was added per 200 mL of supernatant and Centrifuged at 10000 rpm and 4°C for 15 min. The collected precipitate was separated from supernatant layer and dissolved in 8 mL water to form an aqueous solution bio emulsifier. Thereafter, the solution was sterilized with humid heat [7].

To achieve the enhance growth of the strain. Optimized incubation time and temperature are indispensable. For the strain in this paper, these parameters are 7 hr and 30 °C, respectively. Furthermore, sterilizing the medium after the incubation and growth stage is necessary to extract the emulsifier from the strain wall. Sterilizing facilitates the rupture of the linkage between the emulsifier and the strain wall. Besides, to complete the extraction of the emulsifier and remove the inactive microorganisms, centrifugation in 10000 rpm and 4°C for 15 min is necessary [7].

3. Conclusions

ACO1 showed a high capacity for bioemulsifier production and grew up to 60C with NaCl at 180 g l^{-1} . The optimum NaCl concentration, pH and temperature for bioemulsifier production were 4% (w/v), 8.0, and 45C, respectively. *B. licheniformis* PTCC 1595 was grown in nutrient broth with different conditions in order to get maximum production of bioemulsifer. The best culture medium was found to be nutrient broth medium supplemented with starch, Fe^{2+} , Mn^{2+} and olive oil. For the strain of ACO4, Optimized incubation time and temperature are 7 hr and 30 °C, respectively.

Acknowledgment

This work was financially supported by Iranian Oil Pipeline and Telecommunication Company and Islamic Azad University, Quchan branch, Iran. The authors would like to express their sincere gratitude to all those who contributed to this research.

References

- [1] Veronica Leticia Colin, Claudia Elizabeth Pereira, Liliana Beatriz Villegas, Maria Julia Amoroso, Carlos Mauricio Abate, Production and partial characterization of bioemulsifier from a chromium-resistant actinobacteria, *Chemosphere* 90 (2013) 1372–1378
- [2] Veronica Leticia Colina, b, Marçsa Fernanda Castroa, Maria Julia Amoroso, Liliana Beatriz Villegasa, Production of bioemulsifiers by *Amycolatopsis tucumanensis* DSM 45259 and their potential application in

remediation technologies for soils contaminated with hexavalent chromium, *Journal of Hazardous Materials* 261 (2013) 577– 583

- [3] C. R. Suresh Chander, T. Lohitnath, D. J. Mukesh Kumar and P. T. Kalaichelvan, Production and characterization of biosurfactant from *Bacillus subtilis* MTCC441 and its evaluation to use as bioemulsifier for food bio – preservative, *Advances in Applied Science Research*, 2012, 3 (3):1827-1831
- [4] Chenggang Zheng, Jianglin He, Yongli Wang, Manman Wang, Zhiyong Huang, Hydrocarbon degradation and bioemulsifier production by thermophilic *Geobacillus pallidus* strains, *Bioresource Technology* 102 (2011) 9155–9161
- [5] Sabina Viramontes-Ramos, Martha Cristina Portillo-Ruiz, María de Lourdes Ballinas-Casarrubias, José Vinicio Torres-Muñoz, Blanca Estela Rivera-Chavira, Guadalupe Virginia Nevárez-Moorillón
- [6] Afshin Farahbakhsh, Majid Taghizadeh, Bagher Yakhchali, Kamyar Movagharnejad, Stabilization of Heavy Oil-Water Emulsions using a Bio/Chemical Emulsifier Mixture, *Chemical Engineering and Technology*, 2011, 10.1002/ceat.201100169
- [7] Afshin Farahbakhsh, Majid Taghizadeh, Bagher Yakhchali, Kamyar Movagharnejad, Hassan Ali Zamani, Production of a New Emulsifier Material for the Formation Heavy Hydrocarbon/Water Emulsion, *Int. J. Ind. Chem.*, Vol. 2, No. 1, 2011, pp.xxxx-xxxx
- [8] Gholamreza Dehghan Noudeh, Mohammad Hasan Moshafi, Payam Kazaeli, and Farideh Akef, Studies on bioemulsifier production by *Bacillus licheniformis* PTCC 1595. *African Journal of Biotechnology* Vol. 9(3), pp. 362-366, 18 January 2010
- [9] S. M. M. Dastgheib, M. A. Amoozegar, E. Elahi, S. Asad, I. M. Banat, Bioemulsifier production by a halothermophilic *Bacillus* strain with potential applications in microbially enhanced oil recovery, *Biotechnol Lett* (2008) 30:263–270
- [10] Javed P Maniyar, Dhawal V Doshi, Smita S Bhuyan & Shilpa S Mujumdar, Bioemulsifier production by *Streptomyces* sp.S22 isolated from garden soil, *Indian Journal of Experimental Biology* Vol.49, April 2011, pp.293-297

Discovery of New Inhibitors for Colorectal Cancer Treatment

Kai-Cheng Hsu, Tzu-Ying Sung, Jinn-Moon Yang

Abstract—Colorectal cancer (CRC) is one of the main causes of cancer death in the world. Although several drugs have been developed to treat colorectal cancer, such as Regorafenib and 5-FU, their efficacy is often limited by the development of drug resistance. Therefore, development of new drugs with new scaffolds is necessary to treat CRC. Here, we used site-moiety maps to identify inhibitors against PIM1, LIMK1, SRC, and mTOR, which are often overexpressed in CRC. A site-moiety map represents physicochemical properties and moiety preferences of a binding site through anchors. An anchor contains three elements: (1) conserved interacting residues of a binding pocket; (2) moiety preference of the binding pocket; and (3) the type (e.g., hydrogen-bonding or van der Waals interactions) of interaction between the moieties and the binding pocket. Then, we performed a structure-based virtual screening of ~260,000 compounds and selected compound candidates with high site-moiety map scores for bioassays. Among these candidates, compound 1 and compound 2 inhibited the growth of CRC cells with IC_{50} values of $<10 \mu\text{M}$. The experimental result of enzyme-based assays indicated that compound 1 is a dual inhibitor against PIM1 (IC_{50} $6 \mu\text{M}$) and LIMK1 (IC_{50} $11 \mu\text{M}$). Compound 2 was predicted as a SRC inhibitor and will be further validated. The compounds inhibited different protein targets compared to the current drugs. We believe that the compounds provide a starting point to design new drugs for CRC treatment.

Keywords—Colorectal cancer, drug discovery, site-moiety map, virtual screening, PIM1, and LIMK1.

Kai-Cheng Hsu is with the Graduate Institute of Cancer Biology and Drug Discovery, Taipei Medical University, Taipei, Taiwan. (e-mail: piki@tmu.edu.tw).

Tzu-Ying Sung is with the Institute of Bioinformatics and Systems Biology, National Chiao Tung University, Hsinchu, Taiwan (e-mail: tzyying34@gmail.com).

Jinn-Moon Yang is with the Institute of Bioinformatics and Systems Biology, National Chiao Tung University, Hsinchu, Taiwan (e-mail: moon@faculty.nctu.edu.tw).

Effect of Bamboo Chips in Cemented Sand Soil on Permeability and Mechanical Properties in Triaxial Compression

Sito Ismanti, Noriyuki Yasufuku

Abstract—Cement utilization to improve the properties of soil is a well-known method applied in field. However, its addition in large quantity must be controlled. This study presents utilization of natural and environmental-friendly material mixed with small amount of cement content in soil improvement, i.e. bamboo chips. Absorbability, elongation, and flatness ratio of bamboo chips were examined to investigate and understand the influence of its characteristics in the mixture. Improvement of dilation behavior as a problem of loose and poorly graded sand soil is discussed. Bamboo chips are able to improve the permeability value that affects the dilation behavior of cemented sand soil. It is proved by the stress path as the result of triaxial compression test in the undrained condition. The effect of size and content variation of bamboo chips, as well as the curing time variation are presented and discussed.

Keywords—Bamboo chips, permeability, mechanical properties, triaxial compression.

I. INTRODUCTION

BAMBOO is a kind of natural resource that has ability to grow in varying conditions, especially in tropical and sub-tropical countries. In the form of bamboo chips combined with cement. References [1] and [2] investigated bamboo utilization to improve the soft ground with low bearing capacity and to increase erosion resistance, respectively. Moreover, [3] studied bamboo chips and flakes utilization in high water content of excavated mud. However, the combination between pozzolanic content of cement and high water absorbability of bamboo chips in the poorly graded sand under saturated condition has not been investigated yet.

Characteristic of loose and poorly graded sand in saturated condition has been investigated in some studies. In undrained condition, sand has three main behaviors in monotonic triaxial test, i.e. dilative, limited/partially-contractive, and fully contractive [6]-[11]. In this case, contractive behavior can also be interpreted as a static liquefaction phenomenon. Liquefaction is a destructive phenomenon subjected to either cyclic or monotonic loading. The main concept of this phenomenon is the generation of high pore water pressure that affects shear strength significantly.

There are some conditions and properties that affect the dilation behavior of sand. One of them is the coefficient of permeability. Reference [4] conducted some simulations using

numerical analysis on liquefaction phenomenon. They concluded about the importance of soil permeability coefficient to predict the pore pressure and displacement. Moreover, [5] showed the sensitivity of loose and poorly graded sand behavior due to permeability value. The higher the soil permeability, the weaker the soil dilation. But, if the coefficient of permeability becomes too high, the excessive pore pressure is significantly reduced.

Dilation tendency of sand might be studied using a triaxial compression test to understand the mechanism. The effective stress path as result of the test shows the tendency. The dilation is shown by “elbow” shape that is formed by reaching the maximum deviator stress then together with the strain softening emerged at a certain stage of shear to a minimum deviator stress before turned and ascended along the failure line [6]-[11]. The elbow is observed in this study as comparison of dilation tendency.

II. MATERIAL AND EXPERIMENTAL PROGRAM

A. Soil Sample

Liquefaction phenomenon was occurred in several sites in Yogyakarta City in Java Island, Indonesia after Mid Java Earthquake on May 27, 2006. Japanese Geotechnical Society (JGS) survey team investigated on geotechnical issues. Selection of soil type in this paper is based on this investigation result in [12]. Toyoura sand is fine sand used in this study. There are compatibility properties of Toyoura sand with liquefied soil in several sites. Fig. 1 shows that the grain size distribution curve of Toyoura sand is located among the other curves. The index properties of Toyoura sand are $G_s = 2.64$, $D_{50} = 0.17$ mm, $U_c = 1.75$, $e_{max} = 0.953$, $e_{min} = 1.352$. This sand is at a relative density (D_r) of 35%.

B. Bamboo Chips

Bamboo chips are made from bamboo rod produced by using cutting machine. In this study, there are two types of bamboo chips based on the longest size of chips, i.e. 6 mm and 10 mm. In addition, there is physical characterization of bamboo chips performed by elongation and flatness ratio. Elongation ratio is a ratio between intermediate and shortest length of bamboo flakes particle, whereas flatness ratio is the ratio between shortest and longest length. Particle length measurement was conducted by using a digital caliper.

Sito Ismanti and Noriyuki Yasufuku are with the Faculty of Engineering, Kyushu University, Japan (e-mail: sitoismanti88@gmail.com, yasufuku@civil.kyushu-u.ac.jp).

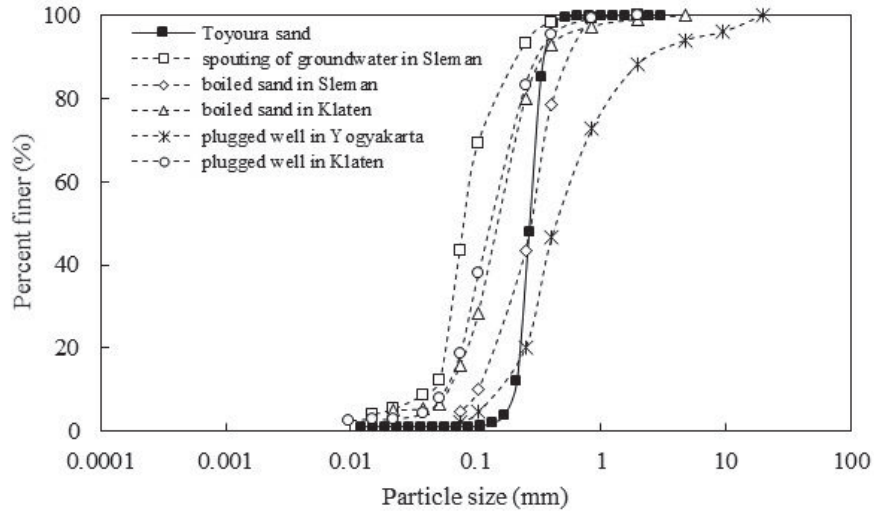


Fig. 1 Particle size distribution curve of the liquefied soil in several sites in Indonesia (modified after [12])



Fig. 2 Bamboo chips (a) 6 mm and (b) 10 mm

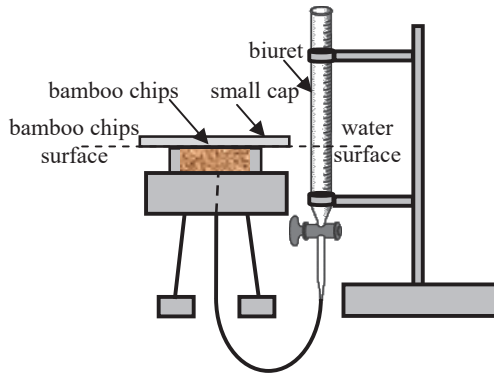


Fig. 3 Concept of absorbability test apparatus

Water absorbability test was conducted to obtain absorbed water in a constant volume of cylinder sample. The dimensions of sample are 6 cm diameter and 1.5 cm height. The initial water content was kept less than 5%. Bulk density of the bamboo chips is about 0.2 gram/cm³. A simple procedure of the absorbability test was conducted by connecting the bamboo chips cylinder with biuret contains distilled water. Water flowed to the bottom of bamboo chips. At the same time, upper part of bamboo chips was detained in order to keep the volume by using small cap to avoid the over pressure. Pressure of the cap is 0.03 kPa. Water surface in

biuret was maintained as high as bamboo chips surface during the test. The decreasing water in biuret is the absorbed water volume. Tests were conducted for 90 minutes. Result of this test provides the absorbability tendency in short term. Calculation of absorbed water index was conducted to provide understanding and comparison between both of the bamboo chips types. Absorbed water index is ratio between the decreasing water in biuret and volume of bamboo chips.

C. Test Method and Procedure

In this paper, specimen is mixture between Toyoura sand with 35% of D_r, and variation of bamboo chips and cement. The dimensions of specimen are 50 mm diameter and 100 mm height in cylinder. Cement used in this study is Ordinary Portland Cement (OPC). The variations are presented in Table I. Water addition of 20% was decided based on the preliminary trial considering the workability reason. The percentages of bamboo chip, cement, and water are referenced to dry mass of Toyoura sand. Specimen was prepared by mixing soil, cement, and bamboo chips in dry condition into a homogeneous color mixture then pour into the mixture. Compaction was conducted in acrylic cylinder. The specimens were cured for 7 and 14 days. After curing, acrylic cylinder was removed.

TABLE I
SPECIMEN VARIATIONS

Type of the test	Curing time (days)	Specimen variations
	0	Toyouira sand (T)
Triaxial, constant head permeability	7, 14	T:1% 6 mm bamboo chips (TB ₆ 1)
		T:2% 6 mm bamboo chips (TB ₆ 2)
		T:1% 10 mm bamboo chips (TB ₁₀ 1)
		T:2% 10 mm bamboo chips (TB ₁₀ 2)
		T:4% OPC (TC4)
		T:4% OPC:1% 6 mm bamboo chips (TC4B ₆ 1)
		T:4% OPC:2% 6 mm bamboo chips (TC4B ₆ 2)
		T:4% OPC:1% 10 mm bamboo chips (TC4B ₁₀ 1)
T:4% OPC:2% 10 mm bamboo chips (TC4B ₁₀ 2)		

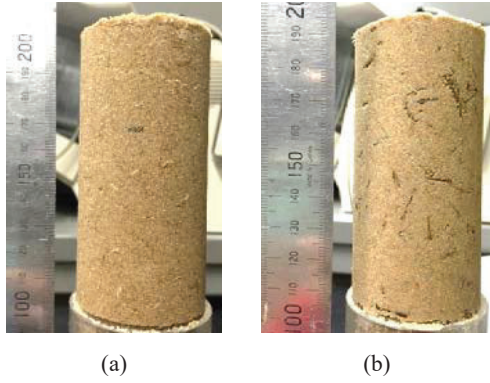


Fig. 4 Specimens with 2% of (a) 6 mm bamboo chips (TB₆₂) and (b) 10 mm bamboo chips (TB₁₀₂)

Permeability and triaxial test were conducted by using constant head method (ASTM 2434-68) and consolidated-undrained method with the pore water pressure measurement during loading (ASTM 4767-02), respectively. In triaxial test, to obtain a high degree of saturation, deaired water was circulated in the specimen by using double negative pressure method. In addition, back pressure of 200 kPa was applied. B-values of more than 0.9 were observed in all. The test was performed at 50, 100, and 150 kPa of confining pressure. Strain was controlled after isotropic consolidation. The samples were executed by applying a monotonic axial load with a strain rate of 0.1%/min. Stress parameters p' and q are used for representing the effective mean principal stress, $p' = (\sigma'_1 + 2\sigma'_3)/3$, and the deviator stress, $q = \sigma'_1 - \sigma'_3$, respectively.

III. RESULT AND DISCUSSION

A. Bamboo Chips Properties

1. Elongation and Flatness Ratio

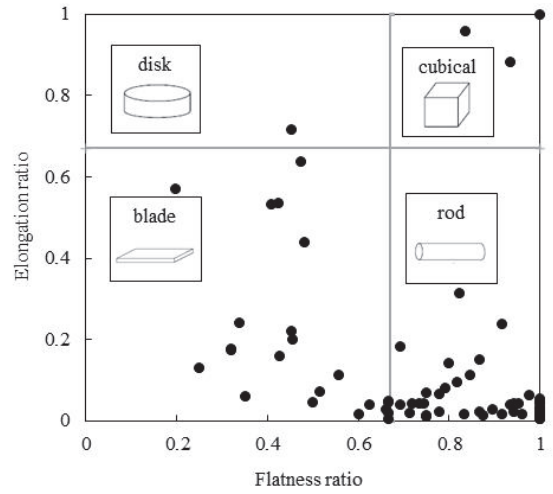
Based on the elongation and flatness ratio parameters, particles are divided to be four shapes, i.e. disk, cubical, blade, and rod. The limit of these shapes is $2/3$ value of each parameter [13]. In the densification process, each shape of particle has typical characteristic in mixture. But, in compaction process, cubical is the best shape in the workability reason.

Both types of bamboo chips have same dominant shape, i.e. blade and rod. It can be seen in Fig. 5 that depicts the elongation and flatness ratio of bamboo chips. However, 6 mm bamboo chips have cubical shape and its size is smaller, so the compaction process of specimen with 6 mm bamboo chips content is easier.

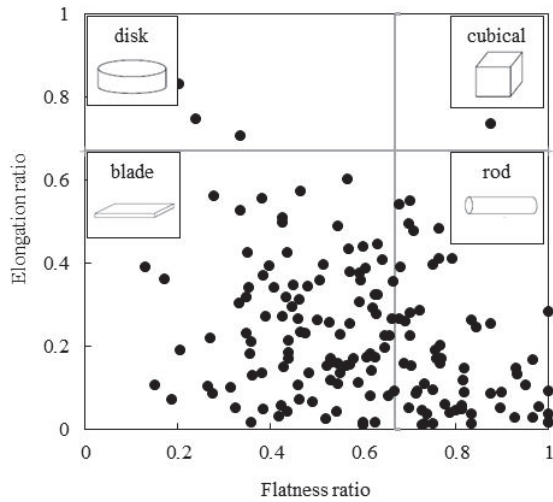
2. Absorbability

As an important parameter, absorbability of bamboo chips was investigated. The absorbability of bamboo chips provides potential to decrease the excess pore water pressure of soil mixture in undrained condition during loading. Fig. 6 shows the tendency of bamboo chips absorbability. Based on the test result, absorbed water of 6 mm bamboo chips is higher than 10 mm bamboo chips. In the larger size, water requires longer

time to saturate the bamboo chips. This result proves that shape factor has significant effect to the water absorbability.



(a)



(b)

Fig. 5 Elongation and flatness ratio of (a) 6 mm and (b) 10 mm bamboo chips

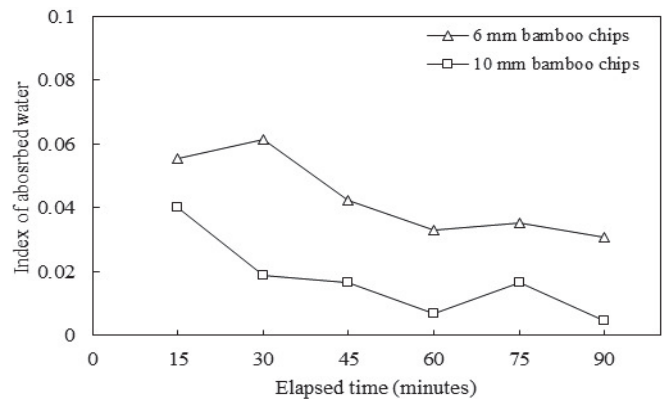
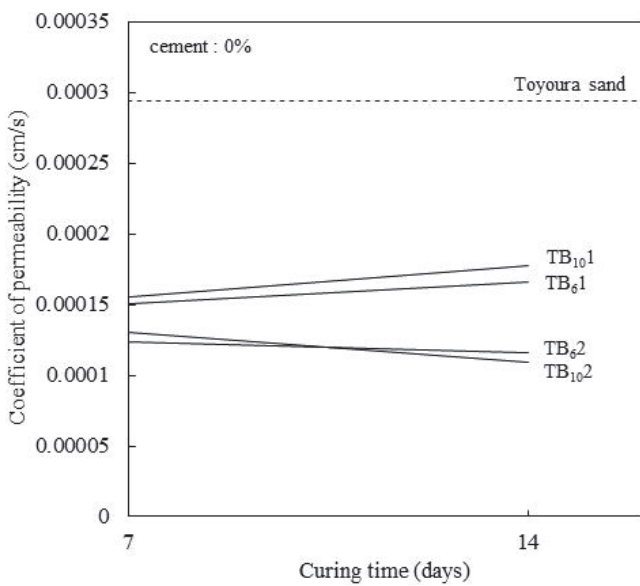


Fig. 6 Absorbed water index of bamboo chips in 90 minutes

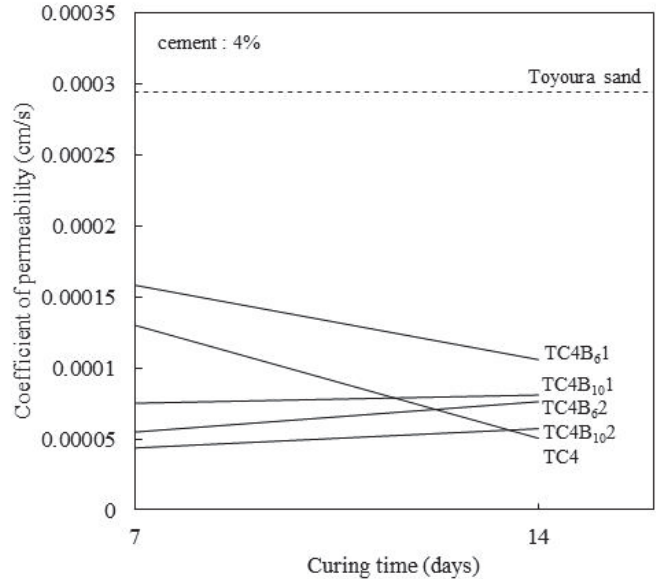
B. Coefficient of Permeability

In the mixture without cement, bamboo chips addition provides significant effect to the coefficient of permeability. Fig. 7 shows the decreasing of permeability coefficient about 47-58% and 40-63% of bamboo chips addition after 7 days and 14 days curing time compared to Toyoura sand, respectively. Based on this result, size factor of bamboo chips provides slight effect. It can be seen from adjacent lines between 6 mm and 10 mm of bamboo chips on the same percentage content in Fig. 7 (a). However, the quantity factor and curing time have an influence on the coefficient of permeability. This is indicated by the different slope of the curve between 1% and 2% of cement content in Fig. 7 (a). The higher content of bamboo chips, the lower of permeability coefficient. Based on the influence of curing time, there is also information that the addition of 1% of bamboo chips gives a negative effect over time. This is because small amount of bamboo chips allows water to saturate in a short time. There is intersected curve in the 2% of bamboo chips content. It might be due to the human error in the experimental stage during specimen preparation.

Pozzolanic content in cement presents different tendency. This information can be seen in Fig. 7 (b). The decreasing permeability of the cemented sand soil provides that cementation reaction was occurred. The decreasing void of sand is an effect of the bonding reaction between cement and water. Moreover, bamboo chips additions provide varying tendency. After 7 days curing time, permeability coefficient of the specimen with 1% and 2% content of 10 mm bamboo chips and 2% content of 6 mm bamboo chip are low compared to the cemented sand. Yet, after 14 days curing time, there are increasing tendency. It can be approved that cementation reaction might be hampered due to the presence of the bamboo chips as additive material in large quantities. Based on this result, factor of size and content of bamboo chips presents significant effect on the coefficient of permeability.



(a)



(b)

Fig. 7 Coefficient of permeability (a) without cement and b) with 4% cement in mixture

C. Undrained Monotonic Triaxial Compression Behavior

Dilation behavior of sand soil can be interpreted by using the stress path as a result of the monotonic triaxial test. Figs. 8 and 9 depict result of cemented sand soil test. Elbow shape in Fig. 8 that indicates the softening behavior is not fine. It can be approved that the cemented sand soil has dilative behavior. Based on this result, addition of the bamboo chips in the mixture has to be investigated to obtain the optimum type and content as proposed additive material in the cemented loose and poorly graded sand soil improvement

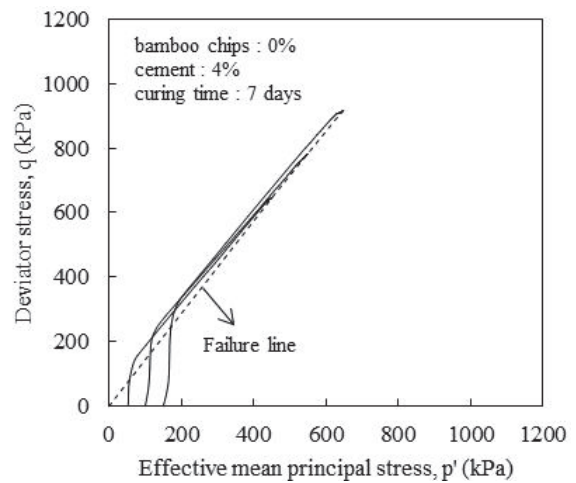


Fig. 8 Stress path of the cemented sand soil

In this study, the comparison of the properties contained in the specimen is presented only on the application of 100 kPa of confining pressure. This boundary provides focus discussion in order to provide understanding of each parameter effect. There are three parameters compared, i.e.

variation of bamboo chips size and content, curing time, and cement content. Observation is focused on the stress path behavior, especially on the elbow characteristic line that depicts the dilation behavior of specimen.

1. Effect of Bamboo Chips Size and Content

In the dilation behavior of cemented sand soil, factor of size and content of bamboo chips has main effect. Based on Fig. 10, after 7 days curing time, it can be seen that the highest stress path is reached by addition of 1% content of 10 mm bamboo chips. However, the upright curve is reached by addition of 2% content of 6 mm bamboo chips. It proves that 10 mm bamboo chips in small amount are able to improve the strength of the specimen using its form, while bamboo chips of 6 mm allow cement to react with water due to its small size. In accordance with the absorbability test, water can be easily absorbed by small bamboo chips. This can be concluded that cemented reaction is the main factor in addition of small bamboo powder.

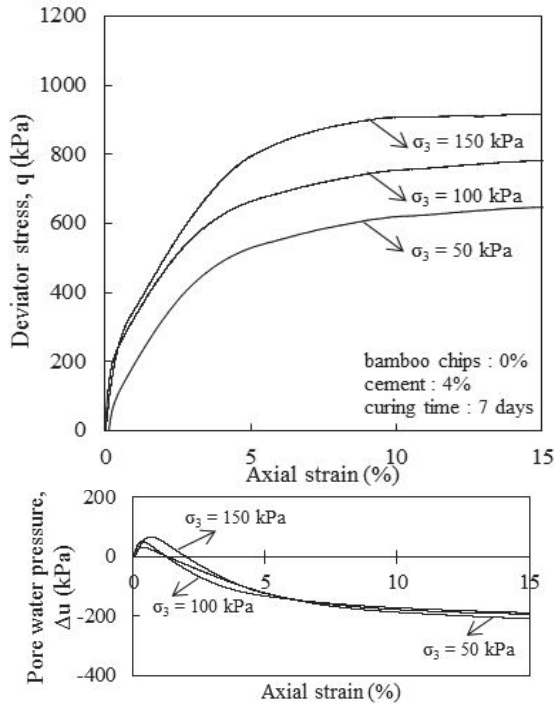


Fig. 9 Stress-strain relationship and pore water pressure of cemented sand soil

2. Effect of Curing Time

Variation of the curing time can be seen in Figs. 12-15. This information provides slight differences based on the adjacent curve. Based on observation of elbow shape and characteristic of stress path in Figs. 12 and 14, after 14 days curing time, improvement of specimen is shown by both types of bamboo chips. Positive tendency of the curing time is also shown in the stress-strain relationship curve in Figs. 13 and 15. This variation result shows that time dependency is also the main factor of this improvement of the loose and poorly sand.

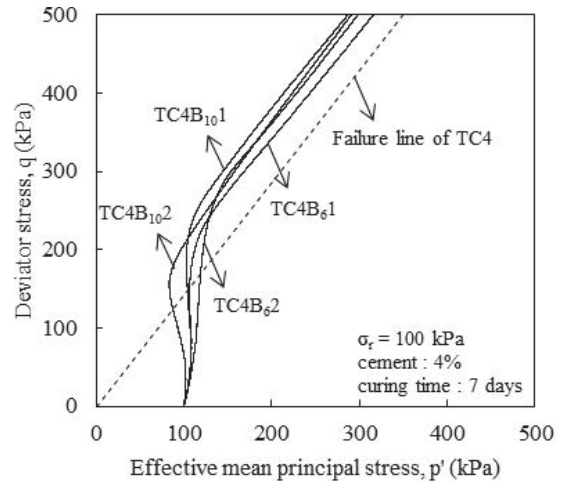


Fig. 10 Stress path in variation of bamboo chips size and content in cemented soil

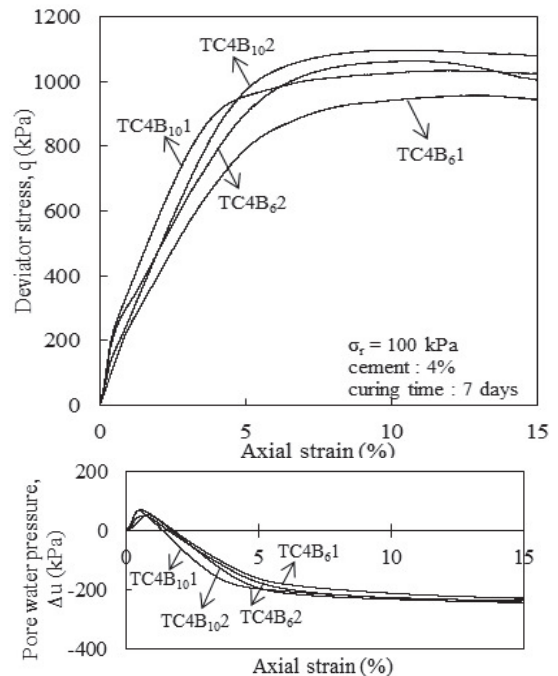


Fig. 11 Comparison of stress-strain relationship and pore water pressure in variation of size and content of bamboo powder

3. Effect of Cement Content

Variation of cement content is shown in Fig. 16. It shows that cement addition provides higher result compared to the utilization of bamboo chips only. This can be concluded that bamboo chips are not suitable as a substitute of cement material. However, addition of bamboo chips improves the strength of cemented sand. This statement is approved by the comparison of results that can be seen in Fig. 17. Curve in Fig. 17 is the comparison of deviator stress increment at 15% of strain between each specimen variation and cemented sand soil at the same curing time period. It shows that the higher content of bamboo chips, the higher strength of the cemented sand.

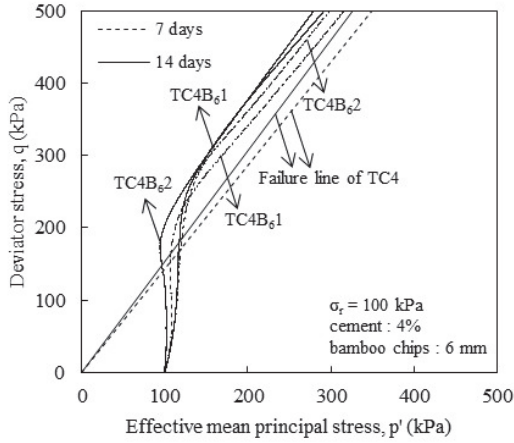


Fig. 12 Stress path in variation of curing time (6 mm bamboo chips)

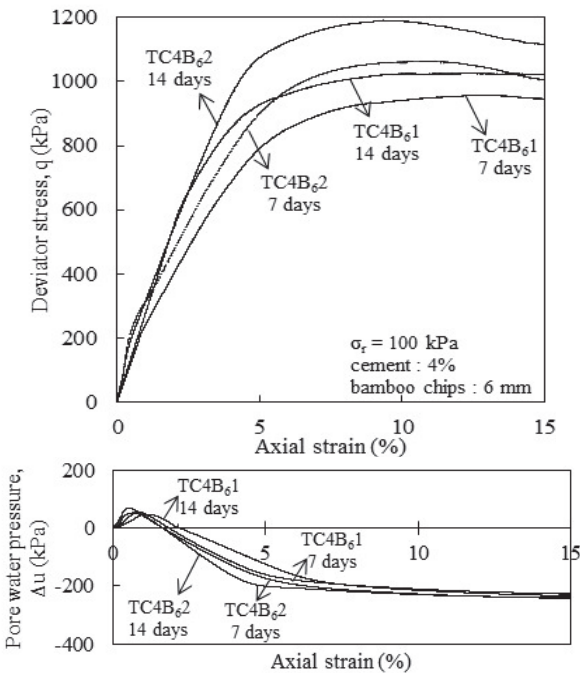


Fig. 13 Comparison of stress-strain relationship and pore water pressure in variation of size and content of bamboo powder (6 mm bamboo chips)

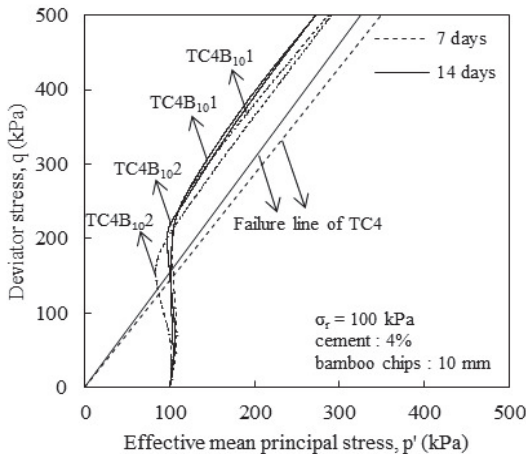


Fig. 14 Stress path in variation of curing time (10 mm bamboo chips)

IV. CONCLUSIONS

In environmental issues, restriction of cement utilization becomes the main focus in soil improvement. Cement replacement by bamboo chips is not the purpose of this study. Yet, the addition of bamboo chips as environmental-friendly material is proposed to be an additive material in cemented sand soil to provide positive tendency to its mechanical properties in order to reduce amount of cement content.

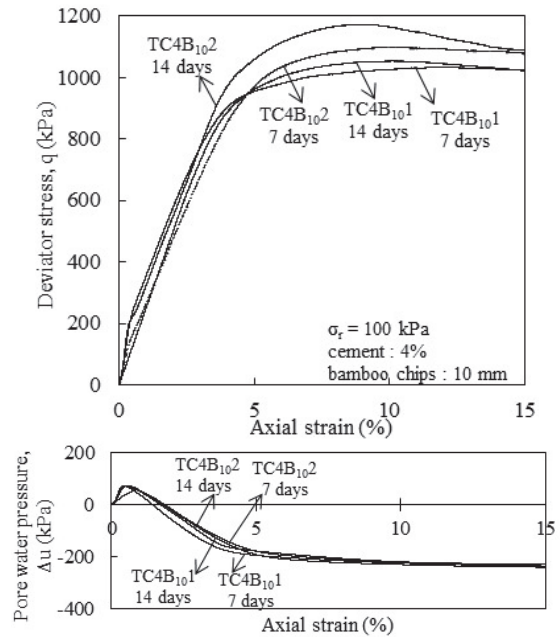


Fig. 15 Comparison of stress-strain relationship and pore water pressure in variation of size and content of bamboo powder (10 mm bamboo chips)

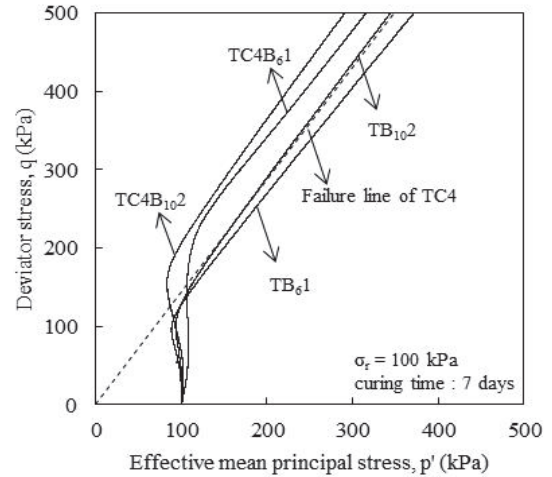


Fig. 16 Stress path in variation of cement

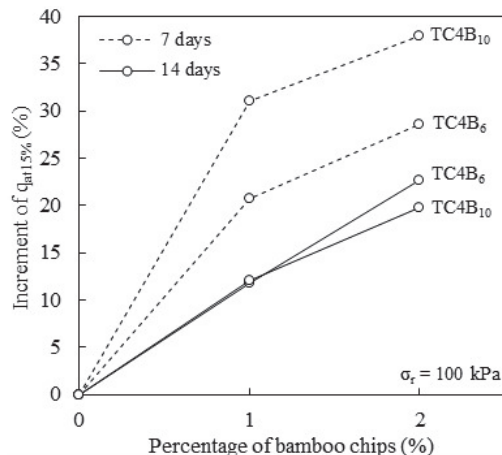


Fig. 17 Increment deviator stress at 15% of strain compared to cemented sand soil

ACKNOWLEDGMENT

The authors would like to thank Nouken Sangyou Co. Ltd for provide bamboo chips, Mr. Michio Nakashima as technical assistance in laboratory, and all members of Geotechnical Engineering Laboratory Kyushu University for their supports.

REFERENCES

- [1] H. Huang, S. Jin, and H. Yamamoto, "Study on strength characteristics of reinforced soil by cement and bamboo chips", *Applied Mechanics and Materials*, vol. 71-78, 2011, pp. 1250-1254.
- [2] K. Saki, R. Kitamura, T. Kawaji, and T. Yotsuda, "Erosion resistant properties of improved soil using bamboo chips for erosion prevention of Alameda in historic places", *Disaster Mitigation of Urban Cultural Heritage Papers*, vol. 7, 2013. (in Japanese)
- [3] K. Sato, T. Fujikawa, and C. Koga, "Improved effect of the high water content clay using the water absorptivity of bamboo", *Geosynthetic Papers*, vol. 29, 2014. (in Japanese)
- [4] A. Rahmani, O. G. Fare, and A. Pak, "Investigation of the influence of permeability coefficient on the numerical modeling of the liquefaction phenomenon," *Scientia Iranica, Transactions A: Civil Engineering* 19, 2012, pp. 179-187.
- [5] J. M. Ramirez, "Influence of soil permeability on liquefaction-induced lateral pile response," *Electronic Theses and Dissertations, University of California, San Diego*, 2010.
- [6] M. Hyodo, H. Tanimizu, N. Yasufuku, and H. Murata, "Undrained cyclic and monotonic triaxial behaviour of saturated loose sand," *Soils and Foundation*, vol. 34, no. 1, Japanese Society of Soil Mechanics and Foundation Engineering, 1994, pp. 19-32.
- [7] Y. Jafarian, A. Ghorbani, S. Salamatpoor, and S. Salamatpoor, "Monotonic triaxial experiments to evaluate steady-state and liquefaction susceptibility of Babolsar sand," *Journal of Zhejiang University-SCIENCE A (Applied Physics & Engineering)*, ISSN 1673-565X (print); ISSN 1863-1775 (online), 2013.
- [8] O. Igwe, K. Sassa, and H. Fukuoka, "Liquefaction potential of granular materials using differently graded sandy soils," *Annals of Disaster Prevention Research Institute, Kyoto University*, no. 47 B, 2004.
- [9] K. Ishihara, F. Tatsuoka, and S. Yasuda, 1975, "Undrained deformation and liquefaction of sand under cyclic stresses," *Soils and Foundation*, vol. 15, no. 1, Japanese Society of Soil Mechanics and Foundation Engineering, Mar 1975.
- [10] R. Mohamad and R. Dobry, "Undrained monotonic and cyclic triaxial strength of sand," *Journal of Geotechnical Engineering*, vol. 112, no. 10, ASCE, 1986.
- [11] L. B. Ibsen, "The mechanism controlling static liquefaction and cyclic strength of sand," *Aalborg: Geotechnical Engineering Group, AAU Geotechnical Engineering Papers: Soil Mechanics Paper*, vol. R9816, no. 27, 1998.
- [12] J. Koseki, M. Yoshimine, T. Hara, T. Kiyota, R. I. Wicaksono, S. Goto, and Y. Agustian, "Damage survey report on May 27, 2006, Mid Java

Earthquake, Indonesia", *Soils and Foundations*, vol. 47, no. 5, Japanese Geotechnical Society, Oct. 2007, pp. 973-989.

- [13] J. S. Chen, M. K. Chang, and K. Y. Lin, "Influence of coarse aggregate shape on the strength of asphalt concrete mixtures," *Journal of the Eastern Asia Society for Transportation Studies*, vol. 6, 2005, pp. 1062-1075.

Effect of Surface-Modification of Indium Tin Oxide Particles on Their Electrical Conductivity

Y. Kobayashi, T. Kurosaka, K. Yamamura, T. Yonezawa, K. Yamasaki

Abstract—The present work reports an effect of surface-modification of indium tin oxide (ITO) particles with chemicals on their electronic conductivity properties. Examined chemicals were polyvinyl alcohol (nonionic polymer), poly(diallyl dimethyl ammonium chloride) (cationic polymer), poly(sodium 4-styrene-sulfonate) (anionic polymer), (2-aminopropyl) trimethoxy silane (APMS) (silane coupling agent with amino group), and (3-mercaptopropyl) trimethoxy silane (MPS) (silane coupling agent with thiol group). For all the examined chemicals, volume resistivities of surface-modified ITO particles did not increase much when they were aged in air at 80 °C, compared to a volume resistivity of un-surface-modified ITO particles. Increases in volume resistivities of ITO particles surface-modified with the silane coupling agents were smaller than those with the polymers, since hydrolysis of the silane coupling agents and condensation of generated silanol and OH groups on ITO particles took place to provide efficient immobilization of them on particles. The APMS gave an increase in volume resistivity smaller than the MPS, since a larger solubility in water of APMS providing a larger amount of APMS immobilized on particles.

Keywords—Indium tin oxide, particles, surface-modification, volume resistivity.

I. INTRODUCTION

TIN-DOPED indium oxide, or indium tin oxide (ITO), is electro-conductive, and its film is transparent in the visible region. These properties are applicable to opto-electronic devices such as display, solar cell, and sensor [1]-[3]. The ITO faces a problem: Electrical conductivity of ITO is reduced under exposure to air; that is, the ITO is unstable as for its electrical conductivity. According to Yu et al. [4], oxygen and moisture molecules adsorbed on ITO film surface diffuse into inside of the film, which controls the mobility of carriers. The control provides the reduction of electrical conductivity of ITO. Based on the mechanism of the reduction, the oxygen-adsorption should be controlled to stabilize the electrical conductivity. Covering of ITO surface with chemicals, or surface-modification might work for the stabilization since the covering chemicals prevent the ITO surface from contacting with air. In fabrication of metallic copper nanoparticles in aqueous solution, oxidation of the

nanoparticles could be controlled with the presence of CTAB and citric acid in the aqueous solution [5], [6]. Adsorption of these chemicals on particle surface is considered to make the particle surface not contact with oxygen molecules in air. This result expects that use of chemicals acting on particle surface solves the problem on unstable electrical conductivity.

There are various chemical agents for surface-modification, in which representatives are the chemical agents such as cationic polymer, anionic polymer, non-ionic polymer and silane coupling agent. The present work examines various chemical agents for surface-modification to find chemical agents suitable to stabilization of electrical conductivity of ITO.

II. EXPERIMENTAL

A. Chemicals

ITO particles suspended in ethanol (25 wt.%) were supplied from Mitsubishi Materials Corporation. Their morphology is explained in a section of Results and Discussion. Polymers examined for surface-modification of ITO particles were polyvinyl alcohol (polymerization degree: 2000, Kanto Chemical) a nonionic polymer, poly (diallyl dimethyl ammonium chloride) (PDADMAC) (20 wt.% in H₂O, Mw: 100000-200000, Sigma-Aldrich) as a cationic polymer, and poly (sodium 4-styrene-sulfonate) (PSS) (Mw: ca. 70000, Sigma-Aldrich) as an anionic polymer. Silane coupling agents examined for the surface-modification were (2-aminopropyl) trimethoxy silane (APMS) (97%, Sigma-Aldrich) and (3-mercaptopropyl) trimethoxy silane (MPS) (95%, Sigma-Aldrich). Ethanol (99.5%, Kanto Chemical) was used as solvent for the examined chemicals. All the chemicals were used as received. Water that was ion-exchanged, distilled, sterilized with an ultra-violet lamp and filtrated with Advantec RFD270NC was used in all preparations.

B. Methods

For surface-modification using the polymers, ethanol and polymer/ethanol solution were added to the ITO suspension. The mixture was stirred at room temperature for 24 h. The concentrations of ITO and polymer in the mixture were 2.5 wt.% and 1 g/L, respectively. For surface-modification using the silicone alkoxides, silane coupling agent/ethanol solution, ethanol and water were added to the ITO suspension. The mixture was stirred at room temperature for 24 h. The concentrations of ITO and silane coupling agent in the mixture were 2.5 wt.% and 1 g/L, respectively. The H₂O concentration was adjusted to 0, 20, 40, 60 and 80 vol.% by varying the amounts of ethanol and water. The surface-modified ITO particles were washed by repeated centrifugation, supernatant

Y. Kobayashi is with Department of Biomolecular Functional Engineering, College of Engineering, Ibaraki University, Hitachi, Ibaraki 316-8511 Japan (phone: +81-294-38-5052; fax: +81-294-38-5078; e-mail: yoshio.kobayashi.yk@vc.ibaraki.ac.jp).

T. Kurosaka and K. Yamamura are with Department of Biomolecular Functional Engineering, College of Engineering, Ibaraki University, Hitachi, Ibaraki 316-8511 Japan.

T. Yonezawa and K. Yamasaki are with Central Research Institute, Mitsubishi Materials Corporation, Naka, Ibaraki 311-0102, Japan (e-mail: yonezawa@mmc.co.jp, kazuyama@mmc.co.jp).

removal via decantation, ethanol addition and sonication. This procedure was repeated three times. To obtain a concentrated ITO particle colloid solution, the amount of added ethanol was reduced by 1/10, which resulted in an ITO concentration of 25 wt.% in the final colloid solution. The ITO particles surface-modified with PVA, PDADMAC, PSS, MPS and APMS are indicated as ITO/PVA, ITO/PDADMAC, ITO/PSS, ITO/MPS and ITO/APMS, respectively.

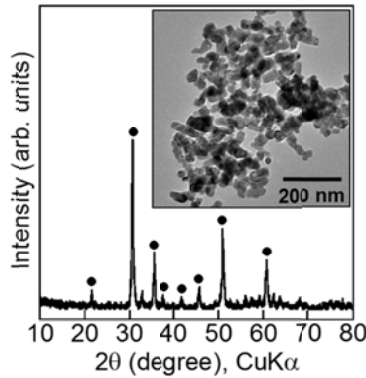


Fig. 1 XRD pattern of ITO nanoparticles. An inset shows their TEM image

The particles were characterized by using transmittance electron microscopy (TEM) and X-ray diffractometry (XRD). The TEM was performed by using a JEOL JEM-2000FX II microscope at 200 kV. The TEM samples were prepared by dropping and evaporating the particle suspensions onto a colloid-coated copper grid. The XRD patterns of the particle powder samples were obtained with a Rigaku Ultima IV X-ray diffractometer at 40 kV and 30 mA with $\text{CuK}\alpha$ radiation (λ : 0.154056 nm).

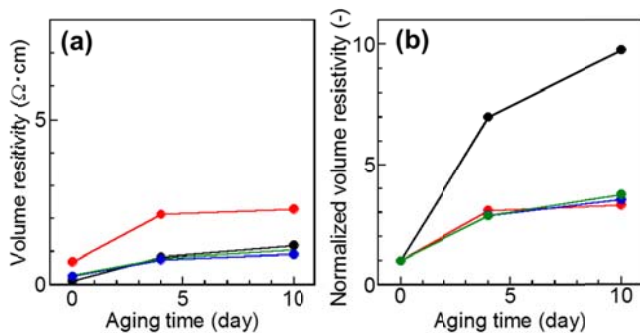


Fig. 2 Volume resistivities of various particle powders (a) and normalized volume resistivities (b) versus time after surface-modification. The volume resistivities were normalized with that for 0 day. Black plot: ITO (un-surface-modified). Red, blue and green plots: ITO surface-modified with PVA, PDADMAC and PSS, respectively

The volume resistivities of the particle powders were measured by using a 4-pin probe to determine the electrical resistivity of the particles. The concentrated ITO particle colloid solution was dropped on a substrate (polyethylene terephthalate (PET) (Toyobo: COSMOSHINE® A4100)) with

sizes of 5 cm \times 5 cm, spread by spin-coating with a Mikasa 1H-DS spinner at 1000 rpm for 30 s, and dried at room temperature. The ITO/PET film was covered with a polyimide film (Du Pont-Toray: Kapton®), and pressed with a Thank Metal 3t/hydraulic roll press at a linear pressure of 1000 kgf/cm and a rolling speed of 1.0 m/s. Film thicknesses were measured with an SFT-9400 SII X-ray fluorescent analysis thickness meter. The measurements of volume resistivities were performed by using a Mitsubishi Chemical Analytech MCP-T370 resistivity meter. The as-pressed ITO/PET film was aged at 80 °C in air with an As-One OFW-600B drying chamber.

III. RESULTS AND DISCUSSION

A. Morphology of ITO Nanoparticles

The inset of Fig. 1 shows a TEM image of the ITO particles. The ITO particles were quasi rod-shaped, and had longitudinal and lateral sizes of 40.6 ± 15.0 and 25.7 ± 7.7 nm, respectively. Fig. 1 shows an XRD pattern of the ITO particles. Several peaks were mainly recorded at 30.6, 35.5, 50.9 and 60.7 degrees. They were assigned to the (222), (400), (440) and (622) phases of cubic ITO according to references [7], [8] and the standard data (ICSD 01-089-4597). Their crystal size was calculated as 7.7 nm by applying Scherrer equation to the XRD line broadening of the 30.6° peak. The average particle size was larger than the crystal size. Accordingly, the ITO particles were polycrystallites of cubic ITO.

B. Volume Resistivities of Particles Surface-Modified with Polymers

Fig. 2 (a) shows the volume resistivities of particles surface-modified with various polymers as a function of aging time. A volume resistivity of ITO particles, or ITO particles that were not surface-modified, is also shown. The volume resistivity of ITO particles was $0.12 \Omega \cdot \text{cm}$ at an aging time of 0 day. The volume resistivity increased from 0.12 to $1.17 \Omega \cdot \text{cm}$ monotonously with an increase in aging time from 0 to 10 days, because of exposure to air. The volume resistivities of surface-modified particle powders at 0 day were larger than that for the ITO particle powder. The polymer molecules were immobilized through their adsorption on particle surface due to intermolecular force and/or electrostatic interaction to cover the particles. The covering prevented the particle surface from contacting directly with surface of other particles, which controlled electric conductivity of particles. The volume resistivities also increased monotonously with the increase in aging time. Fig. 2 (b) shows normalized volume resistivities of the surface-modified particles as a function of aging time. A normalized volume resistivity of the ITO particles increased from 1 to 9.8 with the increase in aging time from 0 to 10 days. For all the surface-modified ITO particles examined, their normalized volume resistivities also increased with increasing the aging time. The normalized volume resistivities were around 3.5 at the aging time of 10 days. These values were smaller than that of the ITO particles at 10 days, which indicated that the surface-modification with polymer controlled

the increase in volume resistivity. Accordingly, the surface-modification was confirmed to have an ability to protect the ITO particles and to make the particles stable as for electric resistivity.

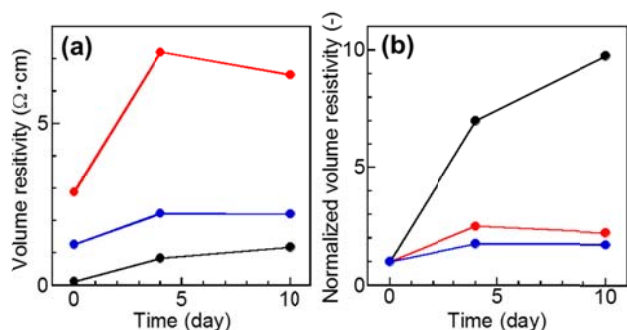


Fig. 3 Volume resistivities of various particle powders (a) and normalized volume resistivities (b) versus time after surface-modification. The volume resistivities were normalized with that for 0 day. Black plot: ITO particles (un-surface-modified). Red and blue plots: ITO particles surface-modified with MPS and APMS, respectively. H_2O concentrations in surface-modification were 20 and 80 vol% for MPS and APMS, respectively

C. Volume Resistivities of Particles Surface-Modified with Silane Coupling Agents

Fig. 3 (a) shows volume resistivities of the particles surface-modified with different silane coupling agents as a function of aging time. The volume resistivity of ITO particles that were not surface-modified is also shown, which is the same as in Fig. 2 (a). The volume resistivities of surface-modified particle powders at 0 day were also larger than that for the ITO particle powder, due to effect of the covering of the ITO particles with the silane coupling agents on electric conductivity of particles. Volume resistivities increased remarkably with an increase in aging time to 4 days due to exposure to air. Over 4 days, the volume resistivities tended to level off. Fig. 3 (b) shows normalized volume resistivities of the surface-modified particles as a function of aging time. For the surface-modified ITO particles examined, their normalized volume resistivities were 2.3 for ITO/MPS and 1.7 for ITO/APMS at the aging time of 10 days. These values were smaller than those for the polymers: the surface-modification using silane coupling agents controlled electric conductivity of ITO particles more dominantly. The silane coupling agent was hydrolyzed to form silanol groups. The silanol groups acted on hydroxide groups on particle surface. The groups were condensed to form chemical bond like Si-O-Sn and Si-O-In, and then the silane coupling agent molecules were immobilized on particle surface. The formation of chemical bonds was considered to immobilize the surface-modifying agents more efficiently than the adsorption in the case of polymers. Thus, the efficient immobilization for silane coupling agents controlled interaction between particle surface and air, and kept the electric conductivities of ITO particles.

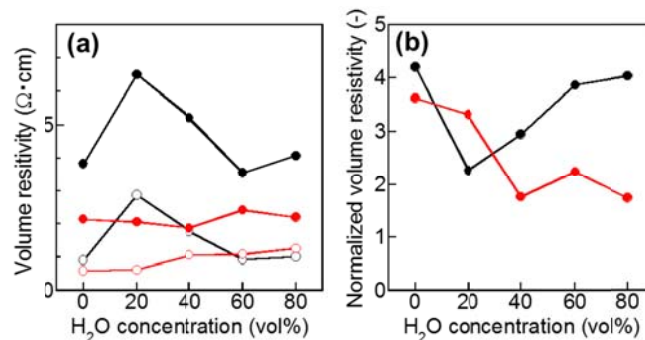


Fig. 4 Volume resistivities of various particle powders versus H_2O concentration in surface-modification (a graph (a)). Open and closed circles: ITO particles for 0 and 10 days after surface-modification, respectively. A graph (b) shows normalized volume resistivities versus H_2O concentration. The volume resistivities were normalized with that for 0 day. Black and red plots: ITO particles surface-modified with MPS and APMS, respectively

D. Effect of Water Concentration in Surface-Modification Using Silane Coupling Agent on Volume Resistivity

Figs. 4 (a) and (b) show volume resistivities and normalized volume resistivities of particles surface-modified with different silane coupling agents as a function of H_2O concentration in surface-modification, respectively. For ITO/MPS, a volume resistivity at an H_2O concentration of 0 vol.% was $0.91 \Omega \cdot \text{cm}$ for the 0 day-film. The volume resistivity was a maximum of $2.88 \Omega \cdot \text{cm}$ at 20 vol.%. This result implied that the MPS was immobilized on particle surface most efficiently at 20 vol.% among the H_2O concentrations examined, because of the maximum volume resistivity. Over 20 vol.%, the volume resistivity decreased with increasing the H_2O concentration. Because MPS is organic compound, the amount of MPS in the ethanol/water solution is expected to be small at the high water concentrations. Accordingly, the particle surface was not covered with MPS well at the high water concentrations because of loss of undissolved MPS, so that the volume resistivities were low compared to at the concentration as low as 20 vol.%. The aging for 10 days increased the volume resistivity for all the H_2O concentrations. A normalized volume resistivity was a minimum of 2.3 at 20 vol.% among all the H_2O concentrations. The amount of MPS on particles was the largest at 20 vol.%, according to the implication on efficient immobilization at 20 vol.%. The covering with the large amount of MPS controlled the contact of ITO particle surface with air. As a result, the change in volume resistivity was the smallest at 20 vol.%.

For ITO/APMS, a volume resistivity at an H_2O concentration of 0 vol.% was $0.59 \Omega \cdot \text{cm}$ for the 0 day-film. The volume resistivity increased with increasing the H_2O concentration, and reached $1.26 \Omega \cdot \text{cm}$ at 80 vol.%, which was the largest among the H_2O concentrations examined. This result implied that the APMS was immobilized on particle surface the most efficiently at the water concentration as high as 80 vol.% because of the maximum volume resistivity. It is known that amino organofunctional trialkoxysilanes are readily soluble in water to give solutions of unlimited solubility [9]. Accordingly, many APMS molecules were considered to be dissolved in water, and

be consumed for the immobilization, which provided efficient covering of particle surface. Consequently, the largest volume resistivity was recorded at the high water concentration. The volume resistivity increased with the aging for 10 days for all the H₂O concentrations as well as the ITO/MPS. A normalized volume resistivity tended to decrease with the increase in H₂O concentration, and was the smallest value of 1.7 at 80 vol.%. The largest amount of APMS was present on particle surface at 80 vol.%, which was implied from the result on the largest volume resistivity at 80 vol.%. The covering with the large amount of APMS controlled the contact of ITO particle surface with air. As a result, the change in volume resistivity was the smallest at 80 vol.%. The normalized volume resistivity of 1.7 for ITO/APMS at 80 vol.% was smaller than 2.3 for ITO/MPS at 20 vol.%. The results on the volume resistivities implied that the amount of APMS on particle surface was larger than that of MPS. This indicated that the smaller volume resistivity was attained with smaller amount of silane coupling agent for ITO/APMS. Accordingly, it was demonstrated that the APMS was suitable to control the resistivity of ITO particles, compared to MPS, although a mechanism on the different abilities to control the resistivity is still unclear.

IV. CONCLUSIONS

The ITO particles were surface-modified with various chemicals such as polymers (PVA as the nonionic polymer, PDADAMC as the cationic polymer and PSS as the anionic polymer) and silane coupling agents (MPS as the silane coupling agent with thiol group and APMS as the silane coupling agent with thiol group). Volume resistivities of particles increased with aging in air at 80 °C. Any chemicals examined had the ability to reduce the increase in volume resistivity of ITO particles, due to covering their surfaces with the chemicals. Increases in volume resistivities of ITO particles were controlled dominantly for the surface-modifications with the silane coupling agent, since the silane coupling agents were efficiently immobilized on the ITO particle surface through hydrolysis of the silane coupling agents and condensation of generated silanol and OH groups on ITO particles. In particular, the surface-modification using APMS was more effective against the increase in volume resistivity than MPS, since the APMS was more soluble in water, and more APMS molecules were immobilized on particles.

ACKNOWLEDGMENT

This work was partially supported by the Mitsubishi Materials Corporation.

REFERENCES

- [1] M. Aleksandrova, N. Kurtev, V. Videkov, S. Tzanova, and S. Schintke, "Material alternative to ITO for transparent conductive electrode in flexible display and photovoltaic devices," *Microelectron. Eng.*, vol. 145, pp. 112–116, September 2015.
- [2] S. Marikkannu, M. Kashif, N. Sethupathy, V.S. Vidhya, Shakkthivel Piraman, A. Ayeshamariam, M. Bououdina, Naser M. Ahmed, and M. Jayachandran, "Effect of substrate temperature on indium tin oxide (ITO) thin films deposited by jet nebulizer spray pyrolysis and solar cell application," *Mater. Sci. Semicond. Process.*, vol. 27, pp. 562–568, November 2014.
- [3] V. S. Vaishnav, S. G. Patel, and J. N. Panchal, "Development of ITO thin film sensor for detection of benzene," *Sensor Actuat. B*, vol. 206, pp. 381–388, January 2015.
- [4] S. Yu, W. Yang, L. Li, and W. Zhang, "Improved chemical stability of ITO transparent anodes with a SnO₂ buffer layer for organic solar cells," *Solar Energ. Mater. Solar Cells*, vol. 144, pp. 652–656, January 2016.
- [5] S.-H. Wu, and D.-H. Chen, "Synthesis of high-concentration Cu nanoparticles in aqueous CTAB solutions," *J. Colloid Interface Sci.*, vol. 273, pp. 165–169, May 2004.
- [6] Y. Kobayashi, T. Shirochi, Y. Yasuda, and T. Morita, "Preparation of metallic copper nanoparticles in aqueous solution and their bonding properties," *Solid State Sci.*, vol. 13, pp. 553–558, March 2011.
- [7] S. Li, X. Qiao, J. Chen, H. Wang, F. Jia, and X. Qiu, "Effects of temperature on indium tin oxide particles synthesized by co-precipitation," *J. Cryst. Growth*, vol. 289, pp. 151–156, March 2006.
- [8] H.-C. Lu, J.-W. Mao, and Y.-C. Chiang, "Low temperature preparation of ITO thin films by the coating solutions containing solvothermally synthesized ITO nanoparticles," *Surf. Coat. Technol.*, vol. 231, pp. 526–530, September 2013.
- [9] E. P. Plueddemann, *Silane Coupling Agents*. New York: Plenum Press, 1982, ch. 3.

Effects of Propolis on Immunomodulatory and Antibody Production in Broilers

Yu-Hsiang Yu

Abstract—The immunomodulatory effect of propolis has been widely investigated in the past decade. However, the beneficial effects in broilers are still poorly understood. The aim of this study was to evaluate the effect of propolis added in drinking water on immunomodulatory and antibody production in broiler. Total of 48 chicks were randomly allocated into four groups with 12 broilers per group. All birds were intranasal inoculated with Newcastle Disease vaccine at 4 and 14 days old of age. Four groups, including control without any treatment, groups of A, B and F [3 days of anterior (A), 3 days of posterior (P) and 6 days of full (F)] were supplied the propolis at 300 ppm in drinking water when vaccination was performed, respectively. Our results showed that no significant difference was found in growth performance, antibody production and immune organ index among groups. However, propolis treatments in broilers significantly reduced IL-4 expression in spleen at 14 days-old of age and bursa at 28 days-old of age compared with control group. The expression of IFN-gamma in spleen (A, P and F group) and bursal (F group) were elevated compared with control group at 28 days-old of age. In conclusion, our results indicated that propolis-treated birds could bear the capability for immunomodulatory effects by change Th1 subset cytokine expression in vaccination.

Keywords—propolis, broiler, immunomodulatory, vaccination

Corresponding Author

Yu-Hsiang Yu from National Ilan University , Taiwan
e-mail: yuyh@niu.edu.tw

Ergonomics Shallow Recharge Well for Sustainable Ground Water Resources

Lilik Sudiajeng, Wiraga Wayan, Lanang Parwita I Gusti

Abstract—This is the ongoing research started in 2013 with the final aim is to design the recharge wells both for housing and industry for ground water conservation in Bali - Indonesia. The research started in Denpasar Regency, one of the strategic areas in Bali. The research showed that there is some critical area of ground water resources, especially in north and west part of Denpasar Regency. It driven by the rapid increase of the tourism industry which is followed by the high rate of population, change of land use that leads to the decreasing of rain water catchment areas, and less awareness on preserve natural resources, including ground water. Focus Group Discussion concluded that in order to solve the problem of groundwater crisis, requires the contribution of all parties, started from making simple recharge well for housing. Because of the availability of land is limited and expensive, it is necessary to present an ergonomic shallow recharge well in accordance with the ability of the family or community. The ergonomics shallow recharge well is designed based on the data of hydrology and the characteristics of soil. The design is very flexible depending on the availability of land, environmentally friendly, energy efficient, culture-based, and affordable. To meet the recommended standard of ground water quality, then it equipped with a filtration and sedimentation ponds. Before design recharge wells is disseminated to the public, it is necessary to analyze the effectiveness of the wells to harvest and absorb rainwater into the ground.

Keywords—ergonomics, ground water resources, recharge well, sustainable

Corresponding Author

Lilik Sudiajeng from Bali State Polytechnic, Indonesia
e-mail: liliksudiajeng@gmail.com

Experimental and Analytical Dose Assessment of Patient's Family Members Treated with I-131

Marzieh Ebrahimi, Vahid Changizi, Mohammad Reza Kardan, Seyed Mahdi Hosseini Pooya, Parham Geramifar

Abstract—Radiation exposure to the patient's family members is one of the major concerns during thyroid cancer radionuclide therapy. The aim of this study was to measure the total effective dose of the family members by means of thermoluminescence personal dosimeter, and compare with those calculated by analytical methods. Eighty-five adult family members of fifty-one patients volunteered to participate in this research study. Considering the minimum and maximum range of dose rate from 15 $\mu\text{Sv/h}$ to 120 $\mu\text{Sv/h}$ at patients' release time, the calculated mean and median dose values of family members were 0.45 mSv and 0.28 mSv, respectively. Moreover, almost all family members' doses were measured to be less than the dose constraint of 5 mSv recommended by Basic Safety Standards. Considering the influence parameters such as patient dose rate and administrated activity, the total effective doses of family members were calculated by TEDE and NRC formulas and compared with those of experimental results. The results indicated that, it is fruitful to use the quantitative calculations for releasing patients treated with I-131 and correct estimation of patients' family doses.

Keywords—Effective dose, thermoluminescence, I-131, Thyroid cancer.

I. INTRODUCTION

DIFFERENTIATED thyroid carcinoma (DTC) occurs as one of the common endocrine tumor, with an annual incidence of 1.2-2.6 per 100,000 males and 2.0-3.8 per 100,000 females [1]. Radioiodine therapy (^{131}I) is one of the most effective and partly inexpensive treatment modality for DTC after thyroidectomy operation. The objective of radioiodine therapy is to ablate the thyroid or treat the metastatic region. It should be noted DTC is treated with 3700 MBq to 7400 MBq of radioiodine [2], [3].

Since the radioiodine is a beta/gamma emitter, the potential radiation risks always exist due to both external and internal irradiation. Internal exposures in consequence of radioactive secretions/excretions from patient may be prevented via staying away from a closed contact of the patient during the first few days after treatment [4]-[6]. However, the radiological hazards due to external irradiation to other individuals (e.g. staff of the hospital, the patient's family

members and public) causes serious concern in radioiodine therapy and may not be reduced easily. Hospitalization is an effective solution decreasing the integral effective dose to the other individuals as low as reasonably achievable [4].

The International Commission of Radiological Protection (ICRP) has recommended 1 mSv/year as the general population dose limit [7]. However, according to the Basic Safety Standards (BSS) recommendations, individuals such as the patient's family members who "knowingly and willingly" help in the support and comfort of patients undergoing medical treatment is excused from aforementioned dose limit [8]. BSS permits a dose limit of 5 mSv per episode of treatment for the patient's family members. However, in order to keep the dose as low as reasonably achievable, dose constraints have been suggested by European Commission (EC) to family members and close friends of patients treated with radioiodine [9].

Some consensuses of international guidelines about the release of patients treated with radioiodine from hospital are as follows [4], [10]-[12]:

- I. Retained activity of ^{131}I within a patient's body should be less than 1110 MBq.
- II. Measured dose rate of patient should be less than 70 $\mu\text{Sv/h}$ at 1 meter.
- III. The total effective dose equivalent from the patient to the other individuals should be retained less than 5 mSv (Patient-specific calculation).

In some countries (e.g. Germany, Switzerland and the Czech Republic) the released dose rate guidelines are stricter [13]. Also the other European countries and the United States prefer to use the patient-specific calculation [6]. Therefore, some investigators have endeavored to improve patient-specific calculations, and several researches have been conducted assessing the integral effective dose of the patient's family members [14], [15].

Mathieu et al. [16] measured the effective dose of family members (adult and children) of thyroid cancer patients using TLD, and reported the effective doses of less than 0.5 mSv in all cases. Barrington et al. [17] carried out a same study, in which adults' dose was ranged from 0.2 to 5.8 mSv with the children's doses ranged from 0.2 to 7.2 mSv. Grigsby et al. [18] reported the dose range of 0.01 mSv to 1.09 mSv for family members.

According to the national regulations in Iran, patients receiving over than 1110 MBq should be quarantined in hospital. Furthermore, according to the current national guidelines, if the external dose rate at 1 meter away from the patient was less than 70 $\mu\text{Sv/h}$, the patient could be released.

Vahid Changizi is with the Department of Radiology and Radiotherapy, Allied Medical Sciences School, Tehran University of Medical Sciences, No:17, Faredanesh Alley, Ghods Ave, BLW Keshavarz, Tehran, Iran (corresponding author, e-mail: changizi@sina.tums.ac.ir).

Marzieh Ebrahimi is with the Department of Technology of Radiology and Radiotherapy, Allied Medical Sciences School, Tehran University of Medical Sciences, Tehran, Iran.

Mohammad Reza Kardan and Seyed Mahdi Hosseini Pooya are with the Radiation Application Research School, Nuclear Science and Technology Research Institute, AEOL, Tehran, Iran.

Parham Geramifar is with the Research Center for Nuclear Medicine, Shariati Hospital, Tehran University of Medical Sciences, Tehran, Iran.

The objective of this study is to assess the effective dose of family members whose patients undergo the radioiodine therapy. The assessments have been carried out by thermoluminescence personal dosimeters and the results were compared with the total effective doses obtained from the proposed formulas by the Nuclear Regulatory Commission (NRC) and the Total Effective Dose Equivalent (TEDE) approaches.

II. MATERIALS AND METHODS

The family members of fifty-one self-caring DTC patients treated with ^{131}I were studied at Research Center for Nuclear Medicine (RCNM), Shariati hospital, Iran. Table I illustrates the characteristics of patients and their family members.

Detailed recommendations about restriction of behavior were given to the patients and their family members at release time. The restriction time period was two weeks, independent of the release external dose rate. The given advices were presented in Table II.

The administered activity of radioiodine was ranged from 100 to 200 mCi. The external dose rate at 1 meter away from the patient was measured by a Geiger-Moller counter (Radiation Alert, Monitor 5, SE International Co., USA) within 2, 12, 24, 36 and 48 hours after ^{131}I administration. Radioiodine treated in-patients could be released if their measured external dose rates were less than $70 \mu\text{Sv/h}$ (except those of patients who participated in the dose rate study).

The analytical calculation approaches were based on TEDE and NRC formulas. The TEDE formula can be obtained via the integration coming as:

$$TEDE = \int_{t_1}^{\infty} a \times e^{-\lambda_{eff} t} \quad (1)$$

where; t_1 is the time interval between radioiodine administration and release time, λ_{eff} is effective decay constant which is derived from the exponential curve of measured dose rate as shown in Fig. 1, and a is the patient's dose rate at maximum uptake.

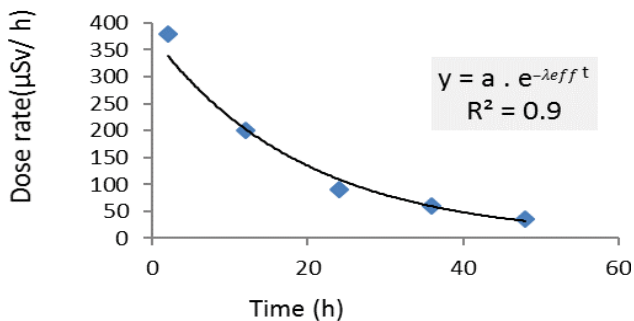


Fig.1 Exponential curve of patient external dose rate. The curve is used for calculating the effective decay constant (λ_{eff})

Also, the NRC [12] has suggested the following formula to determine infinite dose of family members as:

$$D(\infty) = \left[\frac{34.6\Gamma Q_0}{100} \right] \left[E_1 T_p (0.8) \left(1 - e^{-\frac{0.693(0.33)}{T_p}} \right) \right] + (E_1 F_1 T_{1eff} + E_2 F_2 T_{2eff}) e^{-\frac{0.693(0.33)}{T_p}} \quad (2)$$

where: $D(\infty)$ is family member dose (rem), Γ is the exposure rate constant for ^{131}I (2.2 R/mCi-h at 100 cm), Q_0 is the administered activity of ^{131}I (mCi), E_1 and E_2 are the occupational factors for the extra thyroidal and intra thyroidal components, respectively; and they are assumed to be 0.125 and 0.25 according to duration of hospitalization, F_1 and F_2 are the uptake fractions of the extra thyroidal and intra thyroidal components, respectively, and they are assumed to be 0.95 and 0.05 according to duration of hospitalization, T_p is physical half-life for ^{131}I (8.04 days), T_{1eff} and T_{2eff} are effective half-lives (in days) for the extra thyroidal and intra thyroidal components, respectively.

In order to measure the actual total effective dose of family members, one personal TLD dosimeter (TLD-100) was delivered to each family member wearing it on their chest region for a continues limited period of 7 to 21 days.

The measured dose value by TLD was adjusted to the infinite time (i.e. total effective dose) using:

$$D_{infinite} = \frac{D_{TLD}}{1 - e^{-\lambda_{eff} t}} \quad (3)$$

where $D_{infinite}$ is the total effective dose, D_{TLD} is the measured personal dose equivalent by TLD, and t is the number of days that the TLD was worn.

The minimum measured dose (MMD) of the TLD-100 was calculated to be 0.1 mSv, therefore TLD values less than aforementioned value were excluded from this study. The statistical analysis consisted of Kolmogorov-Smirnov test, Kruskal-Wallis test, Wilcoxon rank sum test and Spearman Correlation test was performed using SPSS v.17 software.

III. RESULTS AND DISCUSSION

A. Comparative Study of TEDE and NRC Dose with TLD Measurements

According to Kolmogorov-Smirnov test, as the TLD, TEDE and NRC dose values did not follow a normal distribution, statistical analysis should be performed with non-parametric test. The appropriate parameters for exploratory analysis were median, minimum and maximum values of the range.

A descriptive analysis was presented in Table III. The results demonstrate that generally the TEDE formula gives better estimation of TLD doses than the NRC formula.

Statistically significant differences were observed between the effective doses of family members in the three methods (i.e. $P < 0.001$ in Kruskal-Wallis analysis). The range of variations in estimated dose by NRC was higher than that of TEDE and TLD methods in the analysis (Fig. 2).

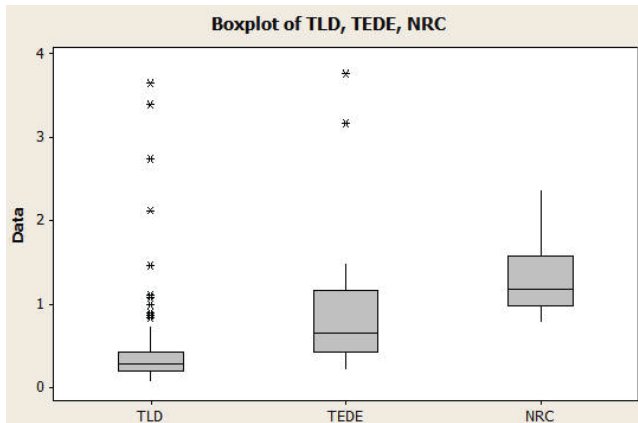


Fig. 2 Box-plot showing the distribution of the calculated (NRC and TEDE) and measured TLD dose values

The measured TLD dose values were less than those calculated by both analytical methods, because:

- Analytical methods estimate each patient's family member doses at a fix distance (e. g 100 cm).
- Patients and their family members' self-absorption were often being neglected in analytical methods.

Moreover, the calculated dose values were not the same in NRC and TEDE methods, since the effective half-life in (2) was a presumptive value in NRC method, whereas has been derived from actual patient's dose rate curve (i.e. Fig. 1) in TEDE method. Moreover, in 85% of cases, NRC dose value was greater than TEDE as the result of Wilcoxon signed-rank statistical test ($Z = -6.2$, $p < 0.001$).

B. Effect of Half Life

Fig. 3 shows the distribution of in the NRC, TEDE and TLD doses values versus the effective half life.

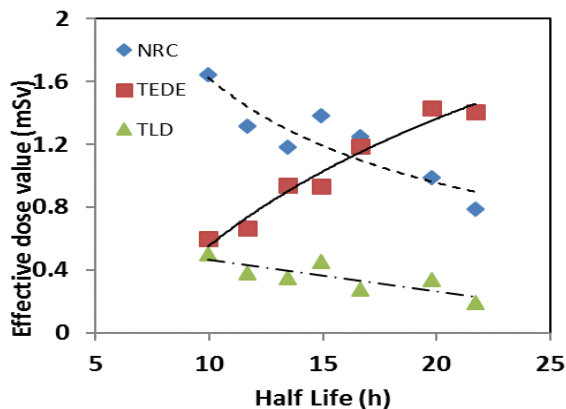


Fig. 3 Calculated (NRC and TEDE) and measured TLD dose values of family members vs. radioiodine effective half life in patients

The results indicate that both the NRC and TEDE formula were greater than TLD dose values. However, with the assumption of an acceptable value of 100% in overestimation, the TEDE formula may be a better estimation at the half life values less than 17 h, whereas the NRC formula would be better at the values greater than 17 h. Thus neither TEDE nor

NRC formula could be an ideal estimation for the effective dose of family members alone. Moreover, there was a significant negative correlation between the subtraction of the TEDE from NRC dose Value [Diff (NRC-TEDE)] and the effective half life (the Spearman's $r = 0.81$, $P < 0.001$).

C. Effect of Dose Rate

Table IV presents the mean and median dose values of estimated (TEDE, NRC) and measured (TLD) at release external dose rates of patients.

It was found a statistically significant differences between the dose rate groups and the NRC, TEDE and TLD doses (Kruskal-Wallis, $P < 0.001$). Further analysis shows a positive correlation between the release external dose rate and dose values of obtained by NRC, TEDE and TLD approaches (Spearman's $r = 0.69$, 0.81 and $.028$, $p = 0.001$, 0.001 and 0.009 , respectively). The results indicate that TEDE gives a better estimation of dose at external dose rate values less than $70 \mu\text{Sv/h}$.

According to the definition of TEDE dose, the positive correlation was predictable. However, it may be explained in NRC method by the residual activity in the patients' body which affects the dose rate values. It should be noted, higher release dose rate may increase the radiation exposure hazard and potential dose to other individuals as demonstrated in TLD dose values.

D. Effect of Administrated Activity

It was found a statistical significant difference between administered activity in NRC and TEDE dose values (Kruskal- Wallis, $P = 0.001$ and 0.05 , respectively). The administered activity in NRC and TEDE dose were positively correlated. (Spearman's $r = 0.47$ and 0.31 , $p < 0.001$ and $= 0.004$, respectively). However, there was not any correlation between the TLD dose and administered activity.

Table V presents a descriptive analysis about administered activity and dose values.

According to the definition of NRC formula, the positive correlation was predictable. However, it may be explained in TEDE method by release external dose rate related to the administrated activity and effective half-life. TLD dose values show no relationship with administered activity, because it may be strongly influenced by how the individuals followed the precaution instructions, the time spent close to the patient or the degree of patient's care requirements.

IV. CONCLUSION

By following the precaution restrictions, all of the measured total effective doses were found to be well below the recommended dose limits for adult family members of patients treated with radioiodine therapy.

This study has provided information on the criteria for patient release based on TEDE and NRC analytical dose estimation of family members. TEDE or NRC approach could not be an ideal estimation for the effective dose of family members alone. Patient specific release dose calculation is strongly affected by radioiodine effective half life and patient

external dose rate that could be helpful in choosing the suitable method. The NRC may be a better estimation than TEDE at the half life values greater than 17h. On the other hand, TEDE is more useful in external dose rates less than 70 $\mu\text{Sv/h}$.

TABLE I
AGE AND SEX CHARACTERISTIC OF PATIENTS AND THEIR FAMILY MEMBERS

	Mean age (Years)	Gender	
		Female	Male
Patients	39.55	40	11
Adult of Family –members	42.98	30	55

TABLE II
RESTRICTION INSTRUCTIONS TO PATIENTS AND THEIR FAMILY MEMBERS

1. Do not use public transportation for getting back to your home after release
2. Keep 2 meters distance away from others
3. Avoid close contact with children under 2 years old
4. Sleep alone in a separate bed for 1 week after releasing
5. Postpone returning to work for 1 week after releasing
6. Avoid attending at public places such as cinema for 2 weeks after releasing

TABLE III
DESCRIPTIVE ANALYSIS OF NRC, TEDE AND TLD DOSE VALUES

		Statistical value	SD
Mean		1.35	.05
Median		1.19	
NRC Dose (mSv)	Std. Deviation	.45	
	Minimum	.79	
	Maximum	2.37	
	Skewness	1.1	.26
	Kurtosis	.84	.52
Mean		.83	.07
Median		.66	
TEDE Dose (mSv)	Std. Deviation	.65	
	Minimum	.22	
	Maximum	3.75	
	Skewness	2.69	.26
	Kurtosis	8.5	.52
Mean		.45	.05
Median		.28	
TLD Dose (mSv)	Std. Deviation	.46	
	Minimum	.1	
	Maximum	3.64	
	Skewness	4.94	.26
	Kurtosis	29.91	.52

TABLE IV
COMPARISON OF THE MEAN AND MEDIAN DOSE VALUES OF NRC, TEDE AND TLD IN FOUR PREDEFINED EXTERNAL DOSE RATE GROUPS

Dose Rate	NRC Dose(mSv)	TEDE Dose(mSv)	TLD Dose(mSv)
Mean	1	.43	.28
Median	1.19	.38	.26
30 to 50 $\mu\text{Sv/h}$	Mean	1.37	.89
Median	1.19	.73	.29
50 to 70 $\mu\text{Sv/h}$	Mean	2.24	1.12
Median	2.37	1	.43
> 70 $\mu\text{Sv/h}$	Mean	1.38	3.31
Median	1.58	3.16	.8

TABLE V
COMPARISON OF THE MEAN AND MEDIAN DOSE VALUES OF NRC, TEDE AND TLD IN FIVE ADMINISTERED ACTIVITY GROUPS

Administered activity	doseNRC	doseTEDE	doseTLD
100 mCi	Mean	1.06	.68
	Median	.79	.53
125 mCi	Mean	1.37	.89
	Median	.99	.64
150 mCi	Mean	1.41	.73
	Median	1.19	.63
175 mCi	Mean	1.38	.95
	Median	1.38	1.16
200 mCi	Mean	1.58	1.96
	Median	1.58	1.09

ACKNOWLEDGMENT

This study has been supported by Tehran University of Medical Sciences

REFERENCES

- [1] Kitagawa W, Shimizu K, Akasu H, Tanaka S. (Endocrine surgery. The ninth report: the latest data on and clinical characteristics of the epidemiology of thyroid carcinoma). Journal of Nippon Medical School = Nippon Ika Daigaku zasshi. 2003;70(1):57-61.
- [2] Maxon HR. Quantitative radioiodine therapy in the treatment of differentiated thyroid cancer. The quarterly journal of nuclear medicine: official publication of the Italian Association of Nuclear Medicine. 1999; 43(4):313-23.
- [3] American Thyroid Association Guidelines Taskforce on Thyroid N, Differentiated Thyroid C, Cooper DS, Doherty GM, Haugen BR, Kloos RT, et al. Revised American Thyroid Association management guidelines for patients with thyroid nodules and differentiated thyroid cancer. Thyroid: official journal of the American Thyroid Association. 2009; 19(11):1167-214.
- [4] American Thyroid Association Taskforce On Radioiodine S, Sisson JC, Freitas J, McDougall IR, Dauer LT, Hurley JR, et al. Radiation safety in the treatment of patients with thyroid diseases by radioiodine 131I: practice recommendations of the American Thyroid Association. Thyroid: official journal of the American Thyroid Association. 2011; 21(4):335-46.
- [5] Barrington SF, Anderson P, Kettle AG, Gadd R, Thomson WH, Batchelor S, et al. Measurement of the internal dose to families of outpatients treated with 131I for hyperthyroidism. European journal of nuclear medicine and molecular imaging. 2008;35(11):2097-104.
- [6] Grundel M, Kopka B, Schulz R. 131I exhalation by patients undergoing therapy of thyroid diseases. Radiation protection dosimetry. 2008; 129(4):435-8.
- [7] Watanabe H. (Explanation of the draft, "release of patients after therapy with unsealed radionuclides" of the International Commission on Radiological Protection: the 2nd report). Nihon Hoshasen Gijutsu Gakkai zasshi. 2004;60(5):689-97.
- [8] Collins BJ, Chiappetta G, Schneider AB, Santoro M, Pentimalli F, Fogelfeld L, et al. RET expression in papillary thyroid cancer from patients irradiated in childhood for benign conditions. The Journal of clinical endocrinology and metabolism. 2002;87(8):3941-6.
- [9] Frigen S. Radiation Protection following Iodine-131 therapy (exposures due to out-patients or discharged in-patients) Directorate-General Environment, Nuclear Safety and Civil Protection. 1998(European Commission).
- [10] International Commission on Radiological P. Release of patients after therapy with unsealed radionuclides. Annals of the ICRP. 2004;34(2):v-vi, 1-79.
- [11] Criteria for the release of individuals administered radioactive materials-NRC. Final rule. Federal register. 1997;62(19):4120-33.
- [12] Fesenko SV, Voigt G, Spiridonov SI, Sanzharova NI, Gontarenko IA, Belli M, et al. Analysis of the contribution of forest pathways to the radiation exposure of different population groups in the Bryansk region of Russia. Radiation and environmental biophysics. 2000;39(4):291-300.
- [13] Authorities HotERpC. 131I therapy: Patient release criteria

- [14] Likhtarev IA, Kovgan LN, Vavilov SE, Gluvchinsky RR, Perevoznikov ON, Litvinets LN, et al. Internal exposure from the ingestion of foods contaminated by ¹³⁷Cs after the Chernobyl accident. Report 1. General model: ingestion doses and countermeasure effectiveness for the adults of Rovno Oblast of Ukraine. *Health physics*. 1996;70(3):297-317.
- [15] Fatome M. (Management of accidental internal exposure). *Journal de radiologie*. 1994;75(11):571-5.
- [16] Mathieu I, Caussin J, Smeesters P, Wambersie A, Beckers C. Recommended restrictions after ¹³¹I therapy: measured doses in family members. *Health physics*. 1999;76(2):129-36.
- [17] Barrington SF, Kettle AG, O'Doherty MJ, Wells CP, Somer EJ, Coakley AJ. Radiation dose rates from patients receiving iodine-131 therapy for carcinoma of the thyroid. *European journal of nuclear medicine*. 1996;23(2):123-30.
- [18] Grigsby PW, Siegel BA, Baker S, Eichling JO. Radiation exposure from outpatient radioactive iodine (¹³¹I) therapy for thyroid carcinoma. *Jama*. 2000;283(17):2272-4.

Experimental Investigation on the Behavior of Steel Fibers Reinforced Concrete under Impact Loading

Feng Fu, Ahmad Bazgir

Abstract—This study aimed to investigate and examine the structural behaviour of steel fibre reinforced concrete slabs when subjected to impact loading using drop weight method. A number of compressive tests, tensile splitting tests, as well as impact tests were conducted. The experimental work consists of testing both conventional reinforced slabs and SFRC slabs. Parameters to be considered for carrying out the test will consist of the volume fraction of steel fibre, type of steel fibres, drop weight height and number of blows. Energy absorption of slabs under impact loading and failure modes were examined in-depth and compared with conventional reinforced concrete slab are investigated.

Keywords—steel fibre reinforce concrete, compressive test, tensile splitting test, impact test

Corresponding Author

Feng Fu from City University London, United Kingdom
e-mail: cenffu@yahoo.co.uk

Feature Evaluation and Applications of Various Advanced Conductors with High Conductivity and Low Flash in Overhead lines

Atefeh Pourshafie, Homayoun Bakhtiari

Abstract—In power transmission lines, electricity conductors are main tools to carry electric power. Thus, other devices such as shield wires, insulators, towers, foundations etc. should be designed in a way that the conductors be able to successfully do their task which is appropriate power delivery to the customers. Non-stop increase of energy demand has led to saturated capacity of transmission lines which, in turn, causing line flash to exceed acceptable limits in some points. An approach which may be used to solve this issue is replacement of current conductors with new ones having the capability of withstanding higher heating such that reduced flash would be observed when heating increases. These novel conductors are able to transfer higher currents and operate in higher heating conditions while line flash will remain within standard limits. In this paper, we will attempt to introduce three types of advanced overhead conductors and analyze the replacement of current conductors by new ones technically and economically in transmission lines. In this regard, progressive conductors of transmission lines are introduced such as ACC (Aluminum Conductor Composite Core), AAAC-UHC (Ultra High Conductivity, All Aluminum Alloy Conductors), and G(Z)TACSR-Gap Type.

Keywords -ACC- AAAC-UHC- Gap Type-Transmission lines.

I. INTRODUCTION

Today, in the world, various types of overhead conductors are used according to their functional needs. These conductors may be different from each other in terms of mechanical properties, electrical properties, structure, manufacturing process, and the materials used in alloys or other geometric principles. To design overhead lines process, the type of the conductor – which transmits electrical energy- is considered as an important indicator which also allocates 25 to 30 percent of all costs of lines construction to itself. Conductors can be made of different types of metals, including copper, aluminum, steel, or various alloys, but in power transmission lines that the goal is to transmit electrical energy with the lowest cost, it is attempted to produce them using suitable metals and alloys whose have electrical and mechanical properties as well as relative advantage from an economic perspective. Various types of conductors, which have been used so far, are as follows:

GS conductors, AS conductors, AW conductors, AZ conductors, OPGW conductors, ACSR/GS conductors,

ACSR/AS conductors, ACSR/AW conductors, ACSR/AZ conductors, TACSR conductors, SLAC conductors, AAAC conductors (All Aluminum Alloy Conductor), ACAR conductors (Aluminum Conductor Reinforced Steel), and AAC conductors (All Aluminum Conductor).

A. Copper Conductors

These conductors are not used in overhead power transmission lines but they are widely used in distribution lines and cables. Copper conductors compared to aluminum conductors have less electrical resistance and more mechanical resistance. Therefore, to transmit a specific amount of power, if a copper conductor is used, its cross-section can be smaller. In spite of the major benefits of this type of conductor, its relative high price and limited mechanical strength, compared to steel and aluminum conductors, limit its use in overhead transmission lines.

B. Conductors Properties

Conductors' properties are as follows:

B.1. conductor cross-sectional area

B.2. conductor diameter: When the conductor's diameter is more, its wind age and the weight of ice around it (in cold areas) get more which accordingly leads to impose additional mechanical loads on conductors and towers. On the other hand, the conductor's large diameter has some positive features including reducing Corona losses and increasing conductor's acceptable current.

B.3. mechanical resistance

B.4. electrical resistance: This is another important conductor's property, which has a very significant and effective role in an electrical load and the amount of energy losses.

In overhead transmission lines, aluminum, as the most popular metal conductor, has been replaced with copper. Although to equalize the amount of losses in aluminum with copper the cross-sectional area should be more, aluminum is lighter and cheaper. In addition, it is possible to provide abundant aluminum while providing copper is limited.

One of the most popular conductors is Aluminum Conductor Steel-Reinforced (ACSR) which contains some layers of aluminum strands in which steel strands surround the central core.

Atefeh Pourshafie is a Post graduate in power engineering and is power expert in Lorestan province electric power distribution company, Iran (phone: 00989161610281; fax:0986633208564; e-mail: a.pourshafie@gmail.com).

Producing stranded conductors is easier and their size can be increased by adding successive layers of strands. Such conductors are easier to use and especially in bigger sizes than a single-stranded conductor, they have more flexibility. Using steel strands in ACSR conductors enhances strength-to-weight ratio. To dissipate the heat, the conductors used in overhead transmission lines are not insulated.

Another kind of conductor called developed ACSR, with a buffer such as fiber or paper between steel and aluminum, has been also produced. The buffer increases the conductor's diameter, decreases the electrical field on the conductor's surface, and thereby reduces the corona. Increasing electricity in overhead lines increases the temperature which itself increases the conductor's length and finally the flash lines which sometimes go beyond the safety limit. This has been shown in figure 1.

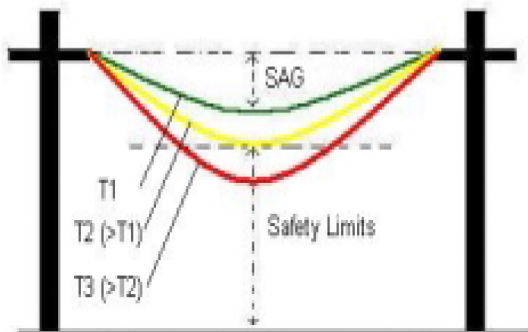


Figure 1: Flash and space constraints: T1 and T2 and T3 are the temperature of the conductor ($^{\circ}C$)

II. ARTICLE DETAILS

In this section, we introduce three types of conductors with high temperature and low flash (or HTLS: High Temperature and Low Sag). Replacing existing conductors with such conductors is considered as repairs of lines and there is no need to taking new ways. Moreover, HTLS conductors do not increase the environmental impacts.

2.1. Aluminum Conductor Composite Core:

In such conductors, annealed aluminum with a sector trapezoidal cross-section is placed around a core made of composite with ultra-high tensile strength [1].



Figure 2: a sample of a conductor with a composite core

Such conductors, compared to steel-core conductors, can double the current carrying capacity in transmission and distribution lines, increase the system reliability by eliminating the curvature caused by overload and additional temperature, and eliminate the Bi-Metal corrosion process. They also need fewer structures during newly built lines and as a result, they reduce the time, cost and compared to conductors with the same diameter, and operating temperature, reduce lines losses [2].

This fact that aluminum conductors with composite core are lighter allows us to add aluminum in any desired diameter without any weight gain. This property simultaneously increases transmission lines capacity and reduces transmission lines losses. ACCC conductors have been designed to increase energy efficiency and work at high working temperature. In contrast to the conductor with the same diameter, weight and transmission power, the ACCC conductor's temperature is lower [3].

2.2. All Aluminum Alloy Conductor with High Conductivity:

Undoubtedly, UHC-AAAC is one of the most effective overhead conductor today. Such conductors decline releasing CO₂ and increase the production capacity to compensate the network losses. Each kilogram of conductor contains aluminum alloy with high conductivity of electric current. They, compared to AAAC conductors, work with higher efficiency and lower temperature (cooler).

Using such conductors as a double bundle in a double-circuit 100 km route, annually saves 2.5 million euros and they, compared to AAAC conductors with the same size and weight, decrease the losses up to 9 percent. By replacing ACSR conductors with UHC-AAAC, line capacity increases up to 35 percent. To replace such conductors, just the conductors are exchanged and there is no need to change the equipment of transmission lines. Due to high conductivity, low weight, and high mechanical strength, compared to ACSR with the same size, the curvature of lines is less [3].

3- Gap Type Conductors:

One type of HTLS conductors is called GTACSR that is known Gap Type. Their geometry shape is like ACSR and it has been shown in figure 3.

Zirconium aluminum wires have thermal resistance around a steel core with high tensile strength. In Type Gap conductors' basic design, there are several layers of Al_{zr} round wires around a layer of sector wires [1]. Aluminum wires in the inner layers are trapezoidal cross-section. There is also a gap between layers and the steel core which is filled with grease. Grease reduces the friction between these two layers and it makes the GTACSR conductor has a high capacity in removing vibrations [4].

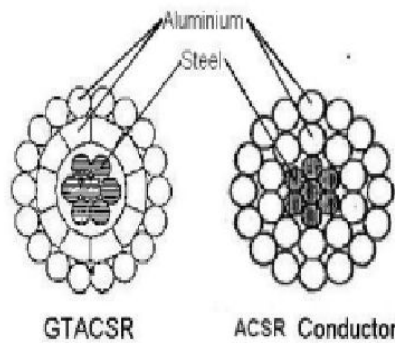


Figure 3: GTACSR and ACSR conductors

Reducing friction allows the GTACSR conductors to be tightened only with a steel core. There is no need to tighten the aluminum conductors. It means that the elongation of GTACSR conductors just depends on the steel conductor's properties and thereby when the temperature increases, the flash line increases too.

Accordingly, the power transmission increased without fitting with flash. Under normal statuses, GTACSR conductors with the same flash as ACSR conductors work at 150 °C. It means that GTACSR conductors have the capacity of a 1.6 time-electric current [4].

Different types of ALZr alloys can be used and each one has its various properties. A steel core with a high tensile strength along with an appropriate galvanization, a high thermal resistance above 250 °C, and high-temperature greases are used to allow the aluminum move around the steel core easily. It prevents steel core corrosion in a long time and increases the thermal resistance up to 300 °C. A wide range of zirconium aluminum alloys are used in domestic products. All layers with a trapezoidal-shaped aluminum increase the Fill Factor up to 98.5% [1].

Gap type conductor is the best way to optimize the overhead lines. ACSR conductors can be easily replaced with Gap Type conductors with the capacity increase of over two times. Excellent mechanical properties and the thermal flash substantial reduction under various loads allow us to construct overhead lines with low cost and in a short time [1]. Because such conductors are similar to ACSR conductors. The only concern about using such conductors is high-temperature performance that may have negative effects on clamps. So the first step before using such conductors is to check the temperature of conductors and their performance effects on the old clamps.

2.3.1. Introduction of Clamp Systems:

Clamp systems are a part of overhead lines, which hold the conductors. And also, if the conductor is not insulated, a clamp system must be chain insulated. The primary objective of the dielectric system (insulator) is to isolate the electric current from lines to pylons. However, this property strongly depends on the temperature reaches to the insulator. In thermal analysis, insulator is one of very sensitive components in the clamp system. In high-pressure overhead lines, conductors are not usually insulated. In ACSR conductors, such points are not

important because the maximum temperature is around 80 and such temperature does not have a negative impact on the insulator. However, GTACSR may be a problem. High temperature (150 °C) may have a negative impact on insulators. That is why it is very important to consider heat distribution during a clamp system in general and especially in insulator chain when GTACSR conductors are being applied.

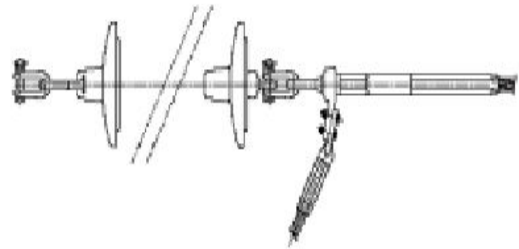


Figure 4: a sample of a simple under pressure clamp system for a simple guide[5]

There are various combinations of clamp systems: single chains for one conductor, single chains for double conductors, two chains for two conductors, a double V-shaped chain for three conductors and etc. Each of these modes can be used in accordance with technical requirements. However, Figure 3 shows a simple clamp system for a conductor and it is a state in which the highest temperature in the insulations produced because in this state, there is the shortest gap between the first insulator and the conductor.

Hence, the system shown in Figure 3 represents the most restrictions. That is why this particular case of a clamp system has been examined.

In order to do a thermal analysis in reference [4], first a three-dimensional model of a clamp system is designed using CAD software, then the clamp system modeled is transferred to thermal analysis software. Such software has a computing tool to do the thermal analysis using Finite Element Method (EFM) method. In this simulation, undesirable statuses have been studied because if the system works properly in the most unfavorable status, it will work properly in other normal statuses. Because of natural convection heat transfer and when the ambient temperature reaches to 40 °C and there is no wind, the temperature of GTACSR conductor reaches to its maximum operating temperature or 150 °C which is the most undesirable status. After the simulation, this system is tested in laboratory to measure the difference between results in the simulation and the practical test.

This analysis aims to examine the maximum temperature of the first insulated plate, when such conductor is used in overhead transmission lines. Considering the theoretical and experimental results, we can be sure that high temperature in GTACSR neither affects clamp system performance nor insulation capacity. Thus, replacing the previous conductors may change the critical temperature only up to 20 °C.

After the first test, we can be sure that the under-pressure clamp applied for ACSR conductors, is valid for GTACSR conductors with the same size because the insulation does not

reach its critical temperature at all. Therefore, the high temperature of the insulation has no negative effect on its correct operation.

On the other hand, the comparison between experimental and theoretical results, ensure that the actual behavior of the system with a high level of reliability has only 5% difference with the obtained results.

III. CONCLUSION

Since nowadays demands for energy are constantly rising, its direct effect is to saturate transmission lines, especially overhead lines. That is why the problems of overhead lines should be considered. Therefore, this article discussed three kinds of conductors with high temperature and low flash.

Compared to ACSR conductors, such conductors have very significant properties and they can constantly work in high temperature –with no losses; and also using these conductors, rated current can be increased.

Since on the one hand ,the materials of composite core has a very low coefficient of thermal expansion and on the other hand such materials determine the curvature of lines, conductors with composite core can decrease the curvature of lines.

In general, due to this fact that to replace the introduced conductors with current conductors there is no need to change the systems of pylons, clamps etc., it is suggested that the regional electricity companies in Iran put such replacement on their agenda

REFERENCES

- [1] Karim Roshan Milani, Innovations of Distribution Networks of Cired Conference 2009 report for Iran distribution power companies.
- [2] The Energy Blog ,ACCC (Aluminum Conductor Composite Core) cable , October 03, 2006 at 12:42 AM in Electric Power
- [3] Lamifil Overhead Conductors, Fredric Shidlaan, 2620 Hemiksem, Belgium
- [4] A.J.Mazon ,I.Zamora,"Gap-type Conductors : influence of high tempreture in the compression clamp systems". 2003 IEEE Bologna Power Tech conference :23th-26thjune , Italy
- [5] A. J. Mazon ; P. Eguia ; R. Criado ; C. Alonso ; J. Iglesias ; J. R. Saenz High-temperature conductors: A solution in the uprating of overhead transmission lines, Conference: Power Tech Proceedings, 2001 IEEE Porto, Volume: 4 Dept. of Electr. Eng., Univ. of the Basque Country, Bilbao, Spain, <https://www.researchgate.net>

Feature Evaluation based on Random Subspace and Multiple- k Ensemble

Jaehong Yu, Seoung Bum Kim

Abstract—Clustering analysis can facilitate the extraction of intrinsic patterns in a dataset and reveal its natural groupings without requiring class information. For effective clustering analysis in high dimensional datasets, unsupervised dimensionality reduction is an important task. Unsupervised dimensionality reduction can generally be achieved by feature extraction or feature selection. In many situations, feature selection methods is more appropriate than feature extraction methods because of their clear interpretation with respect to the original features. The unsupervised feature selection can be categorized as feature subset selection and feature ranking method, and we focused on unsupervised feature ranking methods which evaluate the features based on their importance scores. Recently, several unsupervised feature ranking methods were developed based on ensemble approaches to achieve their higher accuracy and stability. However, most of ensemble-based feature ranking methods require the true number of clusters. Furthermore, these algorithms evaluate the feature importance depending on the ensemble clustering solution, and they produce undesirable evaluation results if the clustering solutions are inaccurate. To address these limitations, we proposed an ensemble-based feature ranking method with random subspace and multiple- k ensemble (FRRM). The proposed FRRM algorithm evaluates the importance of each feature with the random subspace ensemble, and all evaluation results are combined with the ensemble importance scores. Moreover, FRRM does not require the determination of the true number of clusters in advance through the use of the multiple- k ensemble idea. Experiments on various benchmark datasets were conducted to examine the properties of the proposed FRRM algorithm and to compare its performance with that of existing feature ranking methods. The experimental results demonstrated that the proposed FRRM outperformed the competitors.

Keywords—Clustering analysis, multiple- k ensemble, random subspace-based feature evaluation, unsupervised feature ranking

Jaehong Yu is with the Department of Industrial Management Engineering, Korea University, Seoul, Korea (phone: 82-2-3290-3769; fax: 82-2-929-5888; e-mail: dreamer7744@korea.ac.kr).

Seoung Bum Kim is with the Department of Industrial Management Engineering, Korea University, Seoul, Korea (phone: 82-2-3290-3397; fax: 82-2-929-5888; e-mail: sbkim1@korea.ac.kr).

Free Vibration Analysis of Conical Helicoidal Rods Having Elliptical Cross Sections Positioned in Different Orientation

Merve Ermis, Akif Kutlu, Nihal Eratlı, Mehmet H. Omurtag

Abstract—In this study, the free vibration analysis of conical helicoidal rods with two different elliptically oriented cross sections is investigated and the results are compared by the circular cross-section keeping the net area for all cases equal to each other. Problems are solved by using the mixed finite element formulation. Element matrices based on Timoshenko beam theory are employed. The finite element matrices are derived by directly inserting the analytical expressions (arc length, curvature, and torsion) defining helix geometry into the formulation. Helicoidal rod domain is discretized by a two-noded curvilinear element. Each node of the element has 12 DOFs, namely, three translations, three rotations, two shear forces, one axial force, two bending moments and one torque. A parametric study is performed to investigate the influence of elliptical cross sectional geometry and its orientation over the natural frequencies of the conical type helicoidal rod.

Keywords—Conical helix, elliptical cross section, finite element, free vibration.

I. INTRODUCTION

THE number of researches about circular or non-circular helicoidal geometry has been increased and some of these studies are about double helix-DNA [1], carbon nanotubes [2], fibers [3], polymers [4], dampers [5], and staircases [6] *etc.* Helicoidal rods are also preferred for various applications, such as, to support mechanical equipment, to transfer the forces, absorb the energy or reduce the vibration in structural system, to be used as steam generators in nuclear industries, and helical actuators used to manage thermal heating in smart material applications, etc. In the literature, the theoretical and numerical studies exist on the static/dynamic analyses of elastic helices having circular or rectangular cross-sections. In some of these studies, reference [7] studied the dynamic analysis of helical rods based on the exact differential equations governing static behavior of an infinitesimal element by using the finite element method (FEM). The static analysis of circular and non-circular helices having rectangular cross-section is investigated by using the mixed FEM in [8]. References [9], [10] applied to investigate the static or dynamic analysis of helices by the transfer matrix method. The free vibration analysis of a circular helicoidal bar is studied by using both the dynamic transport matrix method and the finite element method in [11]. Reference [12] employed the exact

element method for the static analysis of helicoidal structures of variable cross section. The pseudospectral method is used to investigate the free vibration analysis of cylindrical helical springs with circular cross-sections in [13]. Considering the warping deformations of the cross-section, free vibration analysis of naturally curved and twisted beams are investigated by using the analytical study in [14]. The cylindrical and non-cylindrical helicoidal rods having thin-thick walled circular and non-circular cross sections, equilateral triangular, cruciform and composite cross sections are studied by using the mixed FEM in [15], [16].

In this study, the both curvatures and the arc length of helicoidal geometry are directly taken into account in the mixed FE formulation, and it is applied to dynamic analysis of viscoelastic helicoidal rods in [17], [18]. By using the Timoshenko beam theory adapted mixed FE formulation, the free vibration analysis of conical helicoidal rods having elliptical cross sections is solved. As a parametric study, the influence of the orientation of elliptical cross-sections on the natural frequencies is investigated. Also, the fundamental natural frequencies of elliptical cross sections are compared with the circular cross section keeping the cross sectional area constant for both cases. Some benchmark examples are presented for the literature.

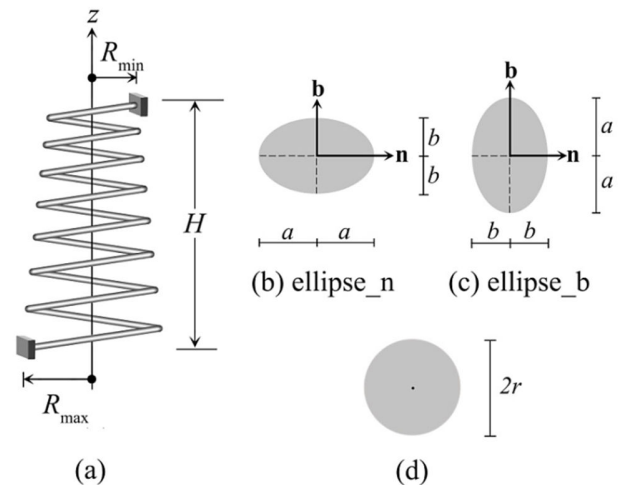


Fig. 1 Conical helix and cross-sectional geometries $a = 5 \text{ mm}$, $b = 2.5 \text{ mm}$ and $r = 3.53553 \text{ mm}$

M. Ermis, A. Kutlu, N. Eratlı, and M. H. Omurtag are with the Faculty of Civil Engineering, Istanbul Technical University, Maslak 34469, Turkey (phone: +90-212-2856551; e-mail: ermism@itu.edu.tr, e-mail: kutluak@itu.edu.tr, e-mail: eratli@itu.edu.tr, e-mail: omurtagm@itu.edu.tr).

II. FORMULATION

A. Helix Geometry and Functional

The parametrical representation of helical geometry can be given as: $x = R(\varphi)\cos\varphi$, $y = R(\varphi)\sin\varphi$, $z = p(\varphi)\varphi$, $p(\varphi) = R(\varphi)\tan\alpha$, horizontal angle φ , the pitch angle and the centerline radius $R(\varphi)$, the step for unit angle of the helix $p(\varphi)$. By using $c(\varphi) = \sqrt{R^2(\varphi) + p^2(\varphi)}$, the infinitesimal arc length becomes $ds = c(\varphi)d\varphi$. The radius of conical helix

$$R(\varphi) = R_{\max} + (R_{\min} - R_{\max})\varphi/2n\pi \quad (1)$$

where R_{\max} and R_{\min} are the bottom and top radius, respectively (see Fig. 1).

In the Frenet coordinate system for the helix geometry, based on Timoshenko beam theory the field equations, exist in [10], can be given in the form

$$\left. \begin{aligned} -\mathbf{T}_{,s} - \mathbf{q} + \rho A \ddot{\mathbf{u}} &= \mathbf{0} \\ -\mathbf{M}_{,s} - \mathbf{t} \times \mathbf{T} - \mathbf{m} + \rho \mathbf{I} \ddot{\boldsymbol{\Omega}} &= \mathbf{0} \end{aligned} \right\} \quad (2)$$

$$\left. \begin{aligned} \mathbf{u}_{,s} + \mathbf{t} \times \boldsymbol{\Omega} - \mathbf{C}_\gamma \mathbf{T} &= \mathbf{0} \\ \boldsymbol{\Omega}_{,s} - \mathbf{C}_\kappa \mathbf{M} &= \mathbf{0} \end{aligned} \right\} \quad (3)$$

where the accelerations of the displacement $\ddot{\mathbf{u}}$ and rotations $\ddot{\boldsymbol{\Omega}}$ vectors, the displacement vector $\mathbf{u}(u_t, u_n, u_b)$, the rotational vector $\boldsymbol{\Omega}(\Omega_t, \Omega_n, \Omega_b)$, the force vector $\mathbf{T}(T_t, T_n, T_b)$, the moment vector $\mathbf{M}(M_t, M_n, M_b)$, the material density ρ , the area of the cross section A , the moments of inertia \mathbf{I} , and compliance matrices, \mathbf{C}_γ and \mathbf{C}_κ , the distributed external force \mathbf{q} and moment \mathbf{m} vectors, respectively. In the free vibration analysis, considering the harmonic motion, it is obvious that $\mathbf{q} = \mathbf{m} = \mathbf{0}$. Incorporating Gâteaux differential with potential operator concept [19] yields the functional in terms of(2)-(3)

$$\begin{aligned} \mathbf{I}(\mathbf{y}) = & - \left[\mathbf{u}, \frac{d\mathbf{T}}{ds} \right] + \left[\mathbf{t} \times \boldsymbol{\Omega}, \mathbf{T} \right] - \left[\frac{d\mathbf{M}}{ds}, \boldsymbol{\Omega} \right] - \frac{1}{2} \left[\mathbf{C}_\kappa \mathbf{M}, \mathbf{M} \right] \\ & - \frac{1}{2} \left[\mathbf{C}_\gamma \mathbf{T}, \mathbf{T} \right] - \frac{1}{2} \rho A \omega^2 \left[\mathbf{u}, \mathbf{u} \right] - \frac{1}{2} \rho \omega^2 \left[\mathbf{I} \boldsymbol{\Omega}, \boldsymbol{\Omega} \right] \\ & - \left[\mathbf{q}, \mathbf{u} \right] - \left[\mathbf{m}, \boldsymbol{\Omega} \right] + \left[\left(\mathbf{T} - \hat{\mathbf{T}} \right), \mathbf{u} \right]_\sigma + \left[\left(\mathbf{M} - \hat{\mathbf{M}} \right), \boldsymbol{\Omega} \right]_\sigma \\ & + \left[\hat{\mathbf{u}}, \mathbf{T} \right]_\varepsilon + \left[\hat{\boldsymbol{\Omega}}, \mathbf{M} \right]_\varepsilon \end{aligned} \quad (4)$$

where square brackets indicate the inner product, the terms with hats are known values on the boundary and the subscripts ε and σ represent the geometric and dynamic boundary conditions, respectively.

B. The Mixed FE Method and Free Vibration Analysis

Linear shape functions, $\phi_i = (\varphi_j - \varphi) / \Delta\varphi$ and $\phi_j = (\varphi - \varphi_i) / \Delta\varphi$ are employed, where $\Delta\varphi = (\varphi_j - \varphi_i)$. A two-noded curvilinear element is used to discretize the helicoidal

rod domain, where the subscripts i and j shows the node numbers of the element. The degree of freedom (DOF) of the curved element is 24, where each node of the element has 12 DOFs. The variable vectors are $\mathbf{u}, \boldsymbol{\Omega}, \mathbf{T}, \mathbf{M}$ for per node. The curvatures and arc length of the helix are directly taken into consideration through the mixed FE formulation[11-12].

The problem of determining the natural frequencies of a structural system reduces to the solution of a standard eigenvalue problem $([\mathbf{K}] - \omega^2[\mathbf{M}])\{\mathbf{u}\} = \{\mathbf{0}\}$, where the system matrix $[\mathbf{K}]$, the mass matrix $[\mathbf{M}]$, the eigenvector (mode shape) \mathbf{u} and the natural angular frequency ω of the system. In the mixed formulation, the explicit form of standard eigenvalue problem can be given as follows

$$\left(\begin{bmatrix} [\mathbf{K}_{11}] & [\mathbf{K}_{12}] \\ [\mathbf{K}_{22}] & [\mathbf{K}_{22}] \end{bmatrix} - \omega^2 \begin{bmatrix} [\mathbf{0}] & [\mathbf{0}] \\ [\mathbf{0}] & [\mathbf{M}] \end{bmatrix} \right) \begin{Bmatrix} \{\mathbf{F}\} \\ \{\mathbf{U}\} \end{Bmatrix} = \begin{Bmatrix} \{\mathbf{0}\} \\ \{\mathbf{0}\} \end{Bmatrix} \quad (5)$$

where the nodal force and the moment vectors $\{\mathbf{F}\}$, and, the nodal displacement and rotation vectors $\{\mathbf{U}\} = \{\mathbf{u} \ \boldsymbol{\Omega}\}^T$. In order to attain consistency between (5) and $([\mathbf{K}] - \omega^2[\mathbf{M}])\{\mathbf{u}\} = \{\mathbf{0}\}$, the $\{\mathbf{F}\}$ is eliminated in (5), which yields to the condensed system matrix $[\mathbf{K}^*] = [\mathbf{K}_{22}] - [\mathbf{K}_{12}]^T [\mathbf{K}_{11}]^{-1} [\mathbf{K}_{12}]$. In the mixed formulation, the eigenvalue problem becomes $([\mathbf{K}^*] - \omega^2[\mathbf{M}])\{\mathbf{U}\} = \{\mathbf{0}\}$.

III. NUMERICAL EXAMPLE

This is a parametric study of a conical helix, which has three different cross-sections (circular and two different elliptical orientations), three different number of active turns ($n = 2, 4, 6$), and three different pitch angles. The objective of this study is to investigate the influence of the above cited geometric properties on the natural frequency of the conical helix. Helicoidal rod is clamped at both ends. The orientations of the two different elliptical cross sections are as shown in (see Figs.1(b)-(c)). The abbreviations "ellipse_n" and "ellipse_b" are used elliptical cross sections with long side oriented horizontal and vertical direction, respectively. The natural frequencies of the conical helix having the elliptical cross sections are compared with the results of the circular cross section. The net areas of the all three cross-sectional geometries are equal to each other.

The material and geometric properties of the helix are as follows: the modulus of elasticity is $E = 206$ GPa, Poisson's ratio is $\nu = 0.3$, density of material is $\rho = 7850$ kg/m³, the taper ratio $R_{\min} / R_{\max} = 0.5$ where $R_{\max} = 100$ mm. The three different number of active turns and the height of the helix are $n = 2, 4, 6$, and $H = 200, 400, 600$ mm, respectively. The cross-sectional dimensions of the circular and elliptical cross sections are $a = 5$ mm and $b = 2.5$ mm; $r = 3.53553$ mm (see Figs.1(b)-(d)). The torsional moment of inertia [14] for an elliptical cross section is given as follows

$$I_t = \pi \frac{a^3 b^3}{a^2 + b^2} \quad (6)$$

The natural frequencies of the conical helix having circular cross section are obtained via the mixed finite element and these results are compared for first six natural frequencies with the commercial program SAP2000 and verified. The convergence by the present study and the SAP2000 is given for the fundamental natural frequency in Fig.2. In this study 200 mixed finite element results are compared by the 1000 displacement type SAP2000 elements. The normalized percent differences between these two finite elements models are calculated and the results are tabulated in Tables I-III, where the absolute maximum percent difference is 0.38%. The natural frequencies of elliptical cross sections ("ellipse_n", "ellipse_b") and the percent differences normalized in case of "ellipse_n" with respect to "ellipse_b" are also given in Tables IV-VI.

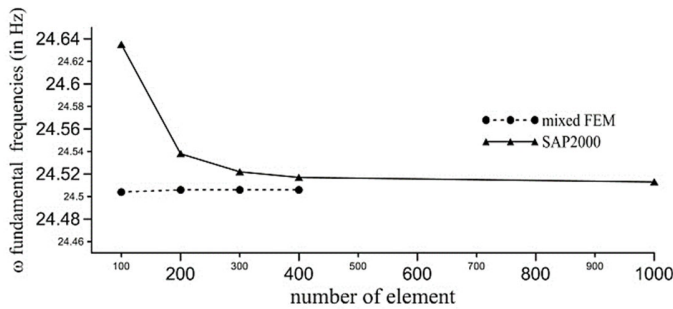


Fig.2 The convergence analysis for ω fundamental frequency of the conical helix having circular cross section for the number of active turn $n=4$ and the height $H=400$ mm (see Table II.)

The fundamental natural frequencies decrease by increasing the number of active turns n for each value of $H = 200, 400, 600$ mm (see Tables I-VI). The fundamental natural frequency values of $n = 4, 6$ are normalized with respect to $n = 2$ that correspond $H = 200, 400, 600$ mm and the decrease of the percent differences are given in Table VII for all type of cross-sections. The fundamental natural frequencies decrease by increasing the height H for each value of $n = 2, 4, 6$ (see Tables I-VI). The fundamental natural frequency values of $H = 400, 600$ mm are normalized with respect to $H = 200$ mm that correspond $n = 2, 4, 6$ and the decrease of the percent differences are tabulated in Table VIII for all type of cross-sections.

The fundamental natural frequencies of the conical helix are normalized with respect to the results of circular cross-section and the normalized percent differences are given in Table IX. It is observed that the fundamental natural frequencies of the elliptical cross sections ("ellipse_n", "ellipse_b" see Fig.1(b)-(c)) decreased with respect to the circular cross section ("circle") in the range of 9.6%~15.4% and 11.0%~ 31.7%, respectively. When the fundamental frequencies of the elliptical cross-section ("ellipse_b") are compared with the respective results of the elliptical cross-section ("ellipse_n") to investigate the effect of the orientation of the long axis of the ellipse, the reductions by increasing the helix height are observed. These reductions are approximately 14.7%~15.2%,

7.4%~12.2% and -3.7%~-2.3%, respectively (see Tables IV-VI).

TABLE I
THE NATURAL FREQUENCIES OF CONICAL HELIX HAVING CIRCULAR CROSS SECTION FOR THE DIFFERENT NUMBER OF ACTIVE TURNS ($H = 200$ mm)

n		ω (in Hz)					
		1	2	3	4	5	6
2	this study	46.9	52.8	63.3	80.9	89.5	120.3
	SAP2000	47.0	52.8	63.3	80.8	89.6	119.9
	diff.%	-0.21	0.00	0.00	0.12	-0.11	0.33
4	this study	26.6	28.4	34.5	37.0	46.6	49.2
	SAP2000	26.7	28.4	34.6	37.0	46.6	49.3
	diff.%	-0.38	0.00	-0.29	0.00	0.00	-0.20
6	this study	18.3	19.5	23.8	24.8	33.6	35.1
	SAP2000	18.3	19.5	23.8	24.8	33.6	35.2
	diff.%	0.00	0.00	0.00	0.00	0.00	-0.28

diff. % = (This study-SAP2000) \times 100/This study)

TABLE II
THE NATURAL FREQUENCIES OF CONICAL HELIX HAVING CIRCULAR CROSS SECTION FOR THE DIFFERENT NUMBER OF ACTIVE TURNS ($H = 400$ mm)

n		ω (in Hz)					
		1	2	3	4	5	6
2	this study	39.4	44.9	55.8	68.3	100.7	115.8
	SAP2000	39.4	44.9	55.8	68.1	100.5	115.4
	diff.%	0.00	0.00	0.00	0.29	0.20	0.35
4	this study	24.5	25.8	29.3	30.0	44.7	49.5
	SAP2000	24.5	25.8	29.3	30.0	44.8	49.4
	diff.%	0.00	0.00	0.00	0.00	-0.22	0.20
6	this study	17.3	18.0	19.6	19.9	33.4	35.1
	SAP2000	17.3	18.0	19.6	19.9	33.4	35.1
	diff.%	0.00	0.00	0.00	0.00	0.00	0.00

diff. % = (This study-SAP2000) \times 100/This study)

TABLE III
THE NATURAL FREQUENCIES OF CONICAL HELIX HAVING CIRCULAR CROSS SECTION FOR THE DIFFERENT NUMBER OF ACTIVE TURNS ($H = 600$ mm)

n		ω (in Hz)					
		1	2	3	4	5	6
2	this study	31.5	34.4	47.3	60.0	84.0	116.4
	SAP2000	31.6	34.4	47.3	59.9	83.7	116.2
	diff.%	-0.32	0.00	0.00	0.17	0.36	0.17
4	this study	20.1	20.4	26.4	28.8	40.4	43.1
	SAP2000	20.1	20.4	26.4	28.8	40.4	43.1
	diff.%	0.00	0.00	0.00	0.00	0.00	0.00
6	this study	14.1	14.2	18.3	19.5	30.6	30.9
	SAP2000	14.1	14.2	18.3	19.5	30.6	30.9
	diff.%	0.00	0.00	0.00	0.00	0.00	0.00

diff. % = (This study-SAP2000) \times 100/This study)

TABLE IV

THE NATURAL FREQUENCIES OF CONICAL HELIX HAVING ELLIPTICAL CROSS SECTIONS FOR THE DIFFERENT NUMBER OF ACTIVE TURNS
($H = 200\text{mm}$)

n	ω (in Hz)						
	1	2	3	4	5	6	
2	ellipse_n	42.8	61.7	71.3	92.0	115.5	124.1
	ellipse_b	36.3	45.3	49.2	63.4	73.1	108.9
	diff.%	15.19	26.58	31.00	31.09	36.71	12.25
4	ellipse_n	23.8	35.2	37.2	40.6	44.0	53.1
	ellipse_b	20.2	24.1	26.5	28.9	38.8	41.1
	diff.%	15.13	31.53	28.76	28.82	11.82	22.6
6	ellipse_n	16.3	24.9	25.5	27.9	30.7	37.3
	ellipse_b	13.9	16.4	18.4	19.3	27.2	29.8
	diff.%	14.72	34.14	27.84	30.82	11.40	20.11

diff. % = (ellipse_n - ellipse_b) × 100 / ellipse_n

TABLE V

THE NATURAL FREQUENCIES OF CONICAL HELIX HAVING ELLIPTICAL CROSS SECTIONS FOR THE DIFFERENT NUMBER OF ACTIVE TURNS
($H = 400\text{mm}$)

n	ω (in Hz)						
	1	2	3	4	5	6	
2	ellipse_n	35.2	43.3	64.3	75.8	115.2	137.9
	ellipse_b	32.6	38.2	45.3	56.1	79.3	93.2
	diff.%	7.39	11.78	29.55	25.99	31.16	32.41
4	ellipse_n	22.0	24.5	27.4	39.6	40.8	47.8
	ellipse_b	19.6	21.8	23.5	26.0	36.5	41.6
	diff.%	10.91	11.02	14.23	34.34	10.54	12.97
6	ellipse_n	15.6	17.0	18.0	27.5	29.8	34.8
	ellipse_b	13.7	15.2	16.0	17.1	26.5	29.7
	diff.%	12.18	10.59	11.11	37.82	11.07	14.66

diff. % = (ellipse_n - ellipse_b) × 100 / ellipse_n

TABLE VI

THE NATURAL FREQUENCIES OF CONICAL HELIX HAVING ELLIPTICAL CROSS SECTIONS FOR THE DIFFERENT NUMBER OF ACTIVE TURNS
($H = 600\text{mm}$)

n	ω (in Hz)						
	1	2	3	4	5	6	
2	ellipse_n	27.3	31.1	47.8	72.9	86.5	138.2
	ellipse_b	28.3	30.4	38.6	50.1	68.4	94.4
	diff.%	-3.66	2.25	19.25	31.28	20.92	31.69
4	ellipse_n	17.6	17.9	23.9	35.6	38.3	41.0
	ellipse_b	18.0	18.4	20.5	24.7	34.0	37.7
	diff.%	-2.27	-2.79	14.23	30.62	11.23	8.05
6	ellipse_n	12.3	12.4	16.4	26.9	27.4	28.8
	ellipse_b	12.7	12.9	14.0	16.6	25.4	27.0
	diff.%	-3.25	-4.03	14.63	38.29	7.30	6.25

diff. % = (ellipse_n - ellipse_b) × 100 / ellipse_n

TABLE VII

THE PERCENT DECREASE OF THE FUNDAMENTAL NATURAL FREQUENCIES OF CONICAL HELIX HAVING CIRCULAR AND ELLIPTICAL CROSS SECTIONS IN THE CASE OF $n = 4, 6$ WITH RESPECT TO $n = 2$

$H(\text{mm})$	n	circle	ellipse_n	ellipse_b
200	4	43.3%	44.4%	44.4%
	6	61.0%	61.9%	61.9%
400	4	37.8%	37.5%	37.5%
	6	56.1%	55.7%	55.7%
600	4	36.2%	35.5%	35.5%
	6	55.2%	54.9%	54.9%

TABLE VIII

THE PERCENT DECREASE OF THE FUNDAMENTAL NATURAL FREQUENCIES OF CONICAL HELIX HAVING CIRCULAR AND ELLIPTICAL CROSS SECTIONS IN THE CASE OF $H = 400, 600\text{mm}$ WITH RESPECT TO $H = 200\text{mm}$

n	$H(\text{mm})$	circle	ellipse_n	ellipse_b
2	400	16.0%	17.8%	10.2%
	600	32.8%	36.2%	22.0%
4	400	7.9%	7.6%	3.0%
	600	24.4%	26.1%	10.9%
6	400	5.5%	4.3%	1.4%
	600	23.0%	24.5%	8.6%

TABLE IX

THE PERCENT DECREASE OF THE FUNDAMENTAL NATURAL FREQUENCIES OF CONICAL HELIX HAVING ELLIPTICAL CROSS SECTIONS WITH RESPECT TO CIRCULAR CROSS SECTION

$H(\text{mm})$	n	ellipse_n	ellipse_b
200	2	9.6%	29.2%
	4	11.8%	31.7%
	6	12.3%	31.7%
400	2	11.9%	20.9%
	4	11.4%	25.0%
	6	10.9%	26.3%
600	2	15.4%	11.3%
	4	14.2%	11.7%
	6	14.6%	11.0%

IV. CONCLUSIONS

The free vibration analysis of conical helicoidal rod circular and elliptical cross sections is investigated using the mixed finite element formulation. Curved finite element is derived based on Timoshenko beam theory. The analytical functions of both curvatures and arc length defining the helix geometry are directly inserted into the mixed finite element formulation. The results of this formulation are compared with the commercial program SAP2000 for circular cross section. Some parametric studies are performed to observe the effects of the number of active turns, the height of helix and the orientation of the elliptical cross-section on the natural frequencies of the conical helix. The increase in the number of active turns n and the helix vertical height decreased the natural frequencies of the conical helix.

REFERENCES

- [1] A. A. Lucas and P. Lambin, "Diffraction by DNA, carbon nanotubes and other helical nanostructures", *Rep. Prog. Phys.*, vol. 68, pp. 1181-1249, 2005.
- [2] J. Cherusseri, R. Scharma and K.K. Kar, "Helically coiled carbon nanotube electrodes for flexible supercapacitors", *Carbon*, vol. 105, pp.113-125, 2016.
- [3] D. Tentori, A. Garcia-Wadner and J.A. Rodriguez-Garcia, "Use of fiber helical coils to obtain polarization insensitive fiber devices", *Opt. Fiber Technol.*, vol. 31, pp.13-19, 2016.
- [4] E.H. Egelman, "Three-dimensional reconstruction of helical polymers", *Arch. Biochem. Biophys.*, vol. 581, 54-58, 2015.
- [5] N. Barbieri, R. Barbieri, R.A. de Silva, M.J. Mannala and L.D.S.V. Barbieri "Nonlinear dynamic analysis of wire-rope isolator and Stockbridge damper", *Nonlinear Dyn.*, doi: 10.1007/s11071-016-2903-1, 2016.
- [6] A. Baratta and I. Corbi, "Equilibrium models for helicoidal laterally supported staircases", *Comput. Struct.*, vol. 124, pp. 21-28, 2013.
- [7] J.E. Mottershead, "Finite elements for dynamical analysis of helical rods", *Int. J. Mech. Sci.*, vol. 22, pp. 267-283, 1980.

- [8] M.H. Omurtag and A.Y. Aköz, “The mixed finite element solution of helical beams with variable cross-section under arbitrary loading”, *Comput. Struct.*, vol. 43, pp. 325–331, 1992.
- [9] V. Haktanır and E. Kıral, “Statical analysis of elastically and continuously supported helicoidal structures by the transfer and stiffness matrix methods”, *Comput. Struct.*, vol. 49, pp. 663–677, 1993.
- [10] V. Yıldırım, “Investigation of parameters affecting free vibration frequency of helical springs”, *Int. J. Numer. Methods Eng.*, vol. 39, pp. 99–114, 1996.
- [11] S.A. Alghamdi, M.A. Mohiuddin and H.N. Al-Ghamedy, “Analysis of free vibrations of helicoidal beams”, *Eng. Comput.*, vol. 15, pp. 89–102, 1998.
- [12] W. Busool and M. Eisenberger, “Exact static analysis of helicoidal structures of arbitrary shape and variable cross section”, *J. Struct. Eng.*, vol. 127, pp. 1266–1275, 2001.
- [13] J. Lee, “Free vibration analysis of cylindrical helical springs by the pseudospectral method”, *J. Sound Vib.*, vol. 302, pp. 185–196, 2007.
- [14] A.M. Yu, C.J. Yang and G.H. Nie, “Analytical formulation and evaluation for free vibration of naturally curved and twisted beams”, *J. Sound Vib.*, vol. 329, pp. 1376–1389, 2010.
- [15] N. Eratlı, M. Ermis and M.H. Omurtag, “Free vibration analysis of helicoidal bars with thin-walled circular tube cross-section via mixed finite element method”, *Sigma Journal of Engineering and Natural Sciences*, vol. 33(2), pp. 200-218, 2015.
- [16] N. Eratlı, M. Yılmaz, K. Darılmaz and M.H. Omurtag, “Dynamic analysis of helicoidal bars with non-circular cross-sections via mixed FEM”, *Struct. Eng. Mech.*, vol. 57(2), pp. 221-238, 2016.
- [17] M. Ermis, *The dynamic analysis of non-cylindrical viscoelastic helical bars using mixed finite element*, Msc Thesis, Istanbul Technical University, Istanbul, 2015.
- [18] M. Ermis, N. Eratlı, Argeso H., A. Kutlu and M.H. Omurtag, “Parametric Analysis of Viscoelastic Hyperboloidal Helical Rod”, *Adv. Struct. Eng.*, doi: 10.1177/1369433216643584, 2016.
- [19] J.T. Oden and J.N. Reddy, *Variational Method in Theoretical Mechanics*, Springer-Verlag, Berlin, 1976.
- [20] S. Timoshenko and J.N. Goodier, *Theory of elasticity*, McGraw-Hill, New York, 1951.

Gender Mainstreaming in Kazakhstan: A University Audit as the First Stage to Inform Policy

A. S. CohenMiller, Jenifer Lewis, Gwen McEvoy, Kristy Kelly

Abstract—This international, interdisciplinary study presents the first stage of a gender mainstreaming project within one university as a microcosm of society in Kazakhstan to make concrete policy recommendations and set up the potential for new research to monitor change over time. Local, regional, and UN representatives have noted the critical need and interest in gender related issues in Kazakhstan. Gender mainstreaming has been noted as a strategy to understand and address gender equality and equity such as within the academy in exploring and examining organizational/management issues, university decision-making and leadership, assessing the overall academic climate, discrimination issues, hiring and promotion, and student recruitment and retention. This presentation provides preliminary findings from the university gender audit, highlighting key elements for moving forward in gender mainstreaming. The full study analyzes findings from the full gender audit including interview with key stakeholders, time-use surveys, participant-observations and interviews with female students, staff and faculty, and reviews of formal organizational policies and practices.

Keywords—academia, equity, Eurasia, gender audit, gender mainstreaming, Kazakhstan, policy, time-use survey

Corresponding Author

Anna Cohenmiller from Nazarbayev University, Kazakhstan
e-mail: anna.cohenmiller@nu.edu.kz

Handle-Bar Design for High Speed Bikes

Musfera Javed, Paritosh Prakhar

Abstract—Abstract— Current times have seen the introduction of high speed human powered and battery powered bikes to counter the impact of road traffic on climatic changes. A recently developed design that claims speeds as high as 200 kilometers per hour (km/h) for a bicycle, need aerodynamically designed handlebars for reduction of the effect of airflow about the rider. Bicycle handle bars suffer from an inherent defect that is absent in modern-day sports bikes. The absence of a front cover causes the air to flow directly about the body of the rider, giving rise to instability at speeds as high as 200 km/h. Thus to make the bicycle achieve such high speeds on road conditions, the handle-bar design needs to be altered so that it guides the airflow without having the rider brace the effect of pressure disturbances and vortex formations due to the airflow. Thus, a new design will be able to keep the bicycle stability at high speeds as well as strong wind conditions. To prepare the design, the previously available handlebars are simulated in road-ride conditions and all the aspects of instability are identified. The instability inducing parts are identified and a new design to eliminate the instability will be prepared and simulated in different riding conditions. Further the simulation is done for different environmental conditions as well as different designs for each one of them at such high speeds. Also experimental verification of the design will follow to check the practical usability of the bike. The end products will contain a range of handle-bar designs that will ensure a high speed aerodynamic ride in all formats of riding, from road race to time trial and even to casual bicycling. **Keywords**—airflow, handlebar, pressure differences, Vortex creations.

Keywords—airflow, pressure differences, handlebar, Vortex creations

Corresponding Author

Musfera Javed from Aligarh Muslim University, India
e-mail: musferaj@gmail.com

High-Performance Thin-layer Chromatography (HPTLC) Analysis of Multi-Ingredient Traditional Chinese Medicine Supplement

Martin Cai, Khadijah B. Hashim, Leng Leo, Edmund F. Tian

Abstract—Analysis of traditional Chinese medicinal (TCM) supplements has always been a laborious task, particularly in the case of multi-ingredient formulations. Traditionally, herbal extracts are analysed using one or few markers compounds. In the recent years, however, pharmaceutical companies are introducing health supplements of TCM active ingredients to cater to the needs of consumers in the fast-paced society in this age. As such, new problems arise in the aspects of composition identification as well as quality analysis. In most cases of products or supplements formulated with multiple TCM herbs, the chemical composition, and nature of each raw material differs greatly from the others in the formulation. This results in a requirement for individual analytical processes in order to identify the marker compounds in the various botanicals. Thin-layer Chromatography (TLC) is a simple, cost effective, yet well-regarded method for the analysis of natural products, both as a Pharmacopeia-approved method for identification and authentication of herbs, and a great analytical tool for the discovery of chemical compositions in herbal extracts. Recent technical advances introduced High-Performance TLC (HPTLC) where, with the help of automated equipment and improvements on the chromatographic materials, both the quality and reproducibility are greatly improved, allowing for highly standardised analysis with greater details. Here we report an industrial consultancy project with ONI Global Pte Ltd for the analysis of LAC Liver Protector, a TCM formulation aimed at improving liver health. The aim of this study was to identify 4 key components of the supplement using HPTLC, following protocols derived from Chinese Pharmacopeia standards. By comparing the TLC profiles of the supplement to the extracts of the herbs reported in the label, this project proposes a simple and cost-effective analysis of the presence of the 4 marker compounds in the multi-ingredient formulation by using 4 different HPTLC methods. With the increasing trend of small and medium-sized enterprises (SMEs) bringing natural products and health supplements into the market, it is crucial that the qualities of both raw materials and end products be well-assured for the protection of consumers. With the technology of HPTLC, science can be incorporated to help SMEs with their quality control, thereby ensuring product quality.

Keywords—traditional Chinese medicine supplement, high performance thin layer chromatography, active ingredients, product quality

Corresponding Author

Edmund Tian from Temasek Polytechnic , Singapore
e-mail: ftian@tp.edu.sg

Impact of Climate Change on Forest Ecosystem Services: In situ Biodiversity Conservation and Sustainable Management of Forest Resources in Tropical Forests

Rajendra Kumar Pandey

Abstract—Forest genetic resources not only represent regional biodiversity but also have immense value as the wealth for securing livelihood of poor people. These are vulnerable to ecological due to depletion/deforestation and /or impact of climate change. These resources of various plant categories are vulnerable on the floor of natural tropical forests, and leading to the threat on the growth and development of future forests. More than 170 species, including NTFPs, are in critical condition for their survival in natural tropical forests of Central India. Forest degradation, commensurate with biodiversity loss, is now pervasive, disproportionately affecting the rural poor who directly depend on forests for their subsistence. Looking ahead the interaction between forest and water, soil, precipitation, climate change, etc. and its impact on biodiversity of tropical forests, it is inevitable to develop co-operation policies and programmes to address new emerging realities. Forests ecosystem also known as the 'wealth of poor' providing goods and ecosystem services on a sustainable basis, are now recognized as a stepping stone to move poor people beyond subsistence. Poverty alleviation is the prime objective of the Millennium Development Goals (MDGs). However, environmental sustainability including other MDGs, is essential to ensure successful elimination of poverty and well being of human society. Loss and degradation of ecosystem are the most serious threats to achieving development goals worldwide. Millennium Ecosystem Assessment (MEA, 2005) was an attempt to identify provisioning and regulating cultural and supporting ecosystem services to provide livelihood security of human beings. Climate change may have a substantial impact on ecological structure and function of forests, provisioning, regulations and management of resources which can affect sustainable flow of ecosystem services. To overcome these limitations, policy guidelines with respect to planning and consistent research strategy need to be framed for conservation and sustainable development of forest genetic resources.

Keywords—climate change, forest ecosystem services, sustainable forest management, biodiversity conservation

Corresponding Author

Rajendra Kumar Pandey from State Forest Research Institute, India
e-mail: bicasrpk@gmail.com

Implemented Cascade with Feed Forward by Enthalpy Balance Superheated Steam Temperature Control for a Boiler with Distributed Control System

Saion K., Chitwong S.

Abstract— Control of superheated steam temperature in steam generation is essential for the efficiency safety and increment age of the boiler. Conventional cascade PID temperature control in the super heater is known to be efficient to compensate disturbance. However, the complex of thermal power plant due to nonlinearity, load disturbance and time delay of steam of superheater system is bigger than other control systems. The cascade loop with feed forward steam temperature control with energy balance compensator using thermodynamic model has been used for the compensation the complex structure of superheater. In order to improve performance of steam temperature control. The experiment is implemented for 100% load steady and load changing state. The cascade with feed forward with energy balance steam temperature control has stabilize the system as well.

Keywords—Cascade with feed forward, boiler, superheated steam temperature control, enthalpy balance.

Nomenclature

C	specific heat (kJ/kg K)
h	specific enthalpy (kJ/kg)
m	mass (kg)
\dot{m}	mass flow (kg/s)
P	pressure (MPa)
Q	heat transferred (MJ)
T	temperature (°C)
γ	Dimensionless Gibbs free energy, $\gamma = g / (RT)$
Δ	Difference in any quantity
δ	Reduced density, $\delta = \rho / \rho^*$
i	Serial number; Exponent
j	Serial number; Exponent
k	Boltzmann's constant
n	Coefficient
R	Specific gas constant
π	Reduced pressure, $\pi = p / p^*$
σ	Reduced entropy, $\sigma = s / s^*$
τ	Inverse reduced temperature, $\tau = T^* / T$
ϕ	Dimensionless Helmholtz free energy, $\phi = f / (RT)$

K. Saion and S. Chitwong are with the Instrumentation and Control Engineering Department, Faculty of Engineering, King Mongkut's Institute of Technology Ladkrabang, ladkrabang, Bangkok 10520 Thailand (e-mail: sakreya.ch@kmitl.ac.th).

Superscripts

- o Ideal-gas part; ideal gas
- r Residual part

I. INTRODUCTION

SUPERHEATED steam temperature is essentially important for running boiler safety and efficiency. Superheated steam temperature control is one of challenged parameter to control thermal power plant. It is a difficult control application because of slow process response and many potential disturbance sources. The temperature needs to be controlled strictly with unspecified range[1]. There are many literature that research to control the superheated steam because of complexly process characterize by nonlinearity, uncertainty and load disturbance[2,3] and superheated steam temperature control is slow process response because it have high time constant. It is necessary to have excellent temperature control system to control steam temperature in acceptance range. If steam temperature is too high, it will effect to boiler tube, piping and steam turbine assembly. If steam temperature is too low, it will condense and also make damage to steam turbine blade. Effectively control temperature is to increase boiler performance, to reduce energy consumption and to reduce emission that will effect to surrounding environment. This research purposes to learn superheated temperature control by cascade PID controller because cascade PID controller have efficiency to control high disturbance system[4]. By improving performance of the control system by enthalpy balance calculation, the control process response and behavior during steady state load and load variable are studied.

II. STEAM TEMPERATURE CONTROL PROCESS DESCRIPTION

Boiler steam attemperator system is consisted of steam attemperator, temperature measurement devices, pressure measurement devices, flow measurement devices, flow control valves and distributed control system. The superheated steam from primary superheater through steam attemperator and steam flow to platen superheater are controlled. Attemperator uses spray water to decrease steam temperature control water flow by spray water valve. Schematic view is shown in fig 1.

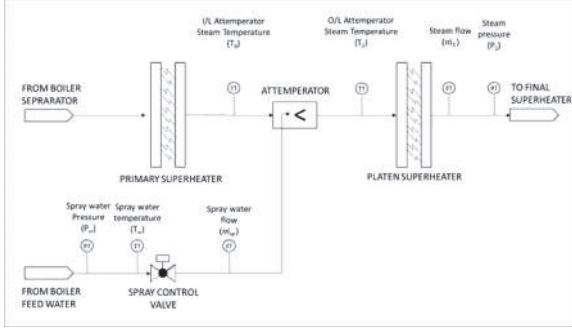


Fig. 1 . Superheated steam temperature control schematic

The steam coming from the boiler steam separator passes through the primary superheater and receives a spray water injection before passing through the platen superheater to the final superheater. From final superheater, the steam is for steam turbine. The control system uses PID cascade controller with energy balance compensator consisted of temperature controller being “Primary controller” (outer loop) and flow controller being “Secondary controller” (inner loop) to control spray water flow injected to steam attemperator. The “Enthalpy balance” is calculated by thermodynamic energy balance principle. The control model is shown in fig 2.

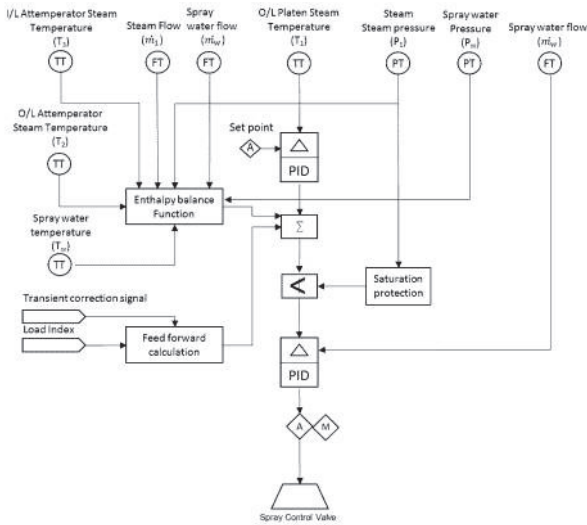


Fig. 2 superheated steam temperature control model

The inner loop is controlled by manipulating the valve command, the outer loop is controlled by manipulating the set point of the inner loop. This set point is also affected by the energy enthalpy balance calculation equation. The inner loop prevents disturbances affecting the fast part of the plant (mainly the valve and water/steam mixing) from propagating to the slower part (mainly the platen superheater dynamics). The enthalpy balance effects provide rejection of accessible disturbances. The outer loop compensates for the errors due to plant/model mismatching in the enthalpy balance terms and rejects the unmeasurable disturbances[5]. PID cascade controller with energy balance compensator block diagram is shown in Fig. 3.

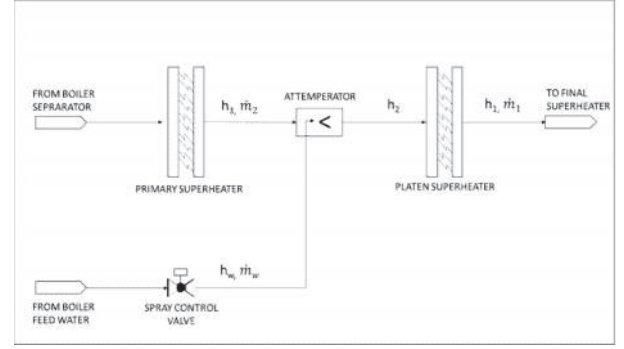


Fig. 3 Control parameter.

III. CONTROL MODEL

A. Energy Balance Model Calculation

Before attemperature superheated steam flow is \dot{m}_2 and after attemperature superheated steam flow is spray water s, \dot{m}_1 flow istemperature a Before. h_w is pray water enthalpys, \dot{m}_w superheated steam enthalpy is h_3 , after attemperature superheated steam enthalpy is h_2 and after platen superheater superheated steam enthalpy is3 Fig. ingsee, h_1 Form mass balance at attemperator

$$\dot{m}_2 + \dot{m}_w = \dot{m}_1 \quad (1)$$

From energy conservation at attemperator

$$\dot{m}_2 h_3 + \dot{m}_w h_w = \dot{m}_1 h_2 \quad (2)$$

From equation (1) and (2)

$$0 = (\dot{m}_1 - \dot{m}_w) h_2 + \dot{m}_w h_w - \dot{m}_1 h_2 \quad (3)$$

$$\dot{m}_1 (h_2 - h_2) = (h_2 - h_w) \dot{m}_w \quad (4)$$

$$\dot{m}_w = \frac{(h_3 - h_2) \dot{m}_1}{(h_3 - h_w)} \quad (5)$$

Equation (5) is spray water flow (\dot{m}_w) used to control steam temperature from Energy conservation law. Inlet attemperature superheated steam enthalpy value (h_2) can be calculated by ($h_2 = f(P, T_2)$). Outlet attemperature superheated steam enthalpy value $f(P, T_2) = (h_2)$ can be calculated by (h_2) and spray water enthalpy-refered to IAPWS $f(P_w, T_w) = (h_w)$ IF97 in Section B.

B. Superheated steam and spray water enthalpy calculation

Superheated steam and spray water enthalpy can calculate from IAPWS-IF97 [6]–basic equation region 1 for water spray enthalpy calculation and basic equation region 2 for superheated steam enthalpy calculation.

B.1 Spray water enthalpy calculation

Enthalpy equation from IAPWS-IF97 in basic equation region 1 are

$$h = g - T \left(\frac{\partial g}{\partial T} \right)_p \text{ is } \frac{h(\pi, \tau)}{RT} = \tau \gamma_\tau \quad (6)$$

and

$$\gamma_\tau = \sum_{i=1}^{24} n_i (7.1 - \pi)^{i_1} J_i (\tau - 1.222)^{i_2 - 1} \quad (7)$$

Where $\pi = p/p^*$, $T^* = 16.53$ MPa, p^* and $\tau = T^*/T$ 1386 K; $R = 0.461526$ KJkg⁻¹K⁻¹ coefficient n_i , exponent I_i and J_i show in IAPWS-IF97 table 1.

B.2 Superheated steam enthalpy calculation

Enthalpy equation form IAPWS-IF97 in basic equation region 2

$$h = g - T \left(\frac{\partial g}{\partial T} \right)_p \text{ is } \frac{h(\pi, \tau)}{RT} = \tau(\gamma_c^o + \gamma_c^r) \quad 8$$

$$\gamma_c^o = \sum_{i=1}^9 n_i^o J_i^o \tau^{I_i^o - 1} \quad 9$$

and

$$\gamma_c^r = \sum_{i=1}^{43} n_i^r \pi^{I_i^r} J_i^r (\tau - 0.5)^{J_i^r - 1} \quad 10$$

where $\pi = p/p^*$, $T^* = 540$ K; $T^* = 1$ MPa, p^* and $\tau = T^*/T$ $R=0.461526$ KJkg⁻¹K⁻¹ coefficient n_i , exponent I_i and J_i show in IAPWS-IF97 in table 2 and 3

TABLE 1
Coefficients and exponents of equation 7

i	I _i	J _i	n _i	i	I _i	J _i	n _i
1	0	-	0.146 329 712	18	2	3	-0.441 418 453
		2	131 67				308 46 × 10 ⁻⁵
2	0	-	-0.845 481 871	19	2	17	-0.726 949 962
		1	691 14				975 94 × 10 ⁻¹⁵
3	0	0	-0.375 636 036	20	3	-4	-0.316 796 448
			720 40 × 10 ¹				450 54 × 10 ⁻⁴
4	0	1	0.338 551 691	21	3	0	-0.282 707 979
			683 85 × 10 ¹				853 12 × 10 ⁻⁵
5	0	2	-0.957 919 633	22	3	6	-0.852 051 281
			878 72				201 03 × 10 ⁻⁹
6	0	3	0.157 720 385	23	4	-5	-0.224 252 819
			132 28				080 00 × 10 ⁻⁵
7	0	4	-0.166 164 171	24	4	-2	-0.651 712 228
			995 01 × 10 ⁻¹				956 01 × 10 ⁻⁶
8	0	5	0.812 146 299	25	4	10	-0.143 417 299
			835 68 × 10 ⁻³				379 24 × 10 ⁻¹²
9	1	-	0.283 190 801	26	5	-8	-0.405 169 968
			238 04 × 10 ⁻³				601 17 × 10 ⁻⁶
10	1	-	-0.607 063 015	27	8	-	-0.127 343 017
			7 658 74 × 10 ⁻³			11	416 41 × 10 ⁻⁸
11	1	-	-0.189 900 682	28	8	-6	-0.174 248 712
			1 184 19 × 10 ⁻¹				306 34 × 10 ⁻⁹
12	1	0	-0.325 297 487	29	21	-	-0.687 621 312
			705 05 × 10 ⁻¹			29	955 31 × 10 ⁻¹⁸
13	1	1	-0.218 417 171	30	23	-	0.144 783 078
			754 14 × 10 ⁻¹			31	285 21 × 10 ⁻¹⁹
14	1	3	-0.528 383 579	31	29	-	0.263 357 816
			699 30 × 10 ⁻⁴			38	627 95 × 10 ⁻²²
15	2	-	-0.471 843 210	32	30	-	-0.119 476 226
			3 732 67 × 10 ⁻³			39	400 71 × 10 ⁻²²
16	2	0	-0.300 017 807	33	31	-	0.182 280 945
			930 26 × 10 ⁻³			40	814 04 × 10 ⁻²³

17	2	1	0.476 613 939	34	32	-	-0.935 370 872
			069 87 × 10 ⁻⁴			41	924 58 × 10 ⁻²⁵

TABLE 2
Coefficients and exponents of equation 9

i	I _i	n _i	i	I _i	n _i
1	0	-0.969 276 865	6	-2	0.142 408 191
		002 17 × 10 ¹			714 44 × 10 ¹
2	1	0.100 866 559	7	-1	-0.438 395 113
		680 18 × 10 ²			194 50 × 10 ¹
3	-5	-0.560 879 112	8	2	-0.284 086 324
		830 20 × 10 ⁻²			607 72
4	-4	0.714 527 380	9	3	0.212 684 637
		814 55 × 10 ⁻¹			533 07 × 10 ⁻¹
5	-3	-0.407 104 982			
		239 28			

TABLE 3
Coefficients and exponents of equation 10

i	I _i	J _i	n _i	i	I _i	J _i	n _i
1	1	0	-0.177 317	23	7	0	-0.590 595
			424 732 13 ×				643 242 70
			10 ⁻²				× 10 ⁻¹⁷
2	1	1	-0.178 348	24	7	11	-0.126 218
			622 923 58 ×				088 991 01
			10 ⁻¹				× 10 ⁻⁵
3	1	2	-0.459 960	25	7	25	-0.389 468
			136 963 65 ×				424 357 39
			10 ⁻¹				× 10 ⁻¹
4	1	3	-0.575 812	26	8	8	0.112 562
			590 834 32 ×				113 604 59
			10 ⁻¹				× 10 ⁻¹⁰
5	1	6	-0.503 252	27	8	36	-0.823 113
			787 279 30 ×				408 979 98
			10 ⁻¹				× 10 ¹
6	2	1	-0.330 326	28	9	13	0.198 097
			416 702 03 ×				128 020 88
			10 ⁻⁴				× 10 ⁻⁷
7	2	2	-0.189 489	29	10	4	0.104 069
			875 163 15 ×				652 101 74
			10 ⁻³				× 10 ⁻¹⁸
8	2	4	-0.393 927	30	10	10	-0.102 347
			772 433 55 ×				470 959 29
			10 ⁻²				× 10 ⁻¹²
9	2	7	-0.437 972	31	10	14	-0.100 181
			956 505 73 ×				793 795 11
			10 ⁻¹				× 10 ⁻⁸
10	2	36	-0.266 745	32	16	29	-0.808 829
			479 140 87 ×				086 469 85
			10 ⁻⁴				× 10 ⁻¹⁰

11	3	0	0.204 817	33	16	50	0.106 930
			$376\ 923\ 09 \times 10^{-7}$				318 794 09
12	3	1	0.438 706	34	18	57	- 0.336 622
			$672\ 844\ 35 \times 10^{-6}$				505 741 71
13	3	3	- 0.322 776	35	20	20	0.891 858
			$772\ 385\ 70 \times 10^{-4}$				453 554 21
14	3	6	- 0.150 339	36	20	35	0.306 293
			$245\ 421\ 48 \times 10^{-2}$				168 762 32
15	3	35	- 0.406 682	37	20	48	- 0.420 024
			$535\ 626\ 49 \times 10^{-1}$				676 982 08
16	4	1	- 0.788 473	38	21	21	- 0.590 560
			$095\ 593\ 67 \times 10^{-9}$				296 856 39
17	4	2	0.127 907	39	22	53	0.378 269
			$178\ 522\ 85 \times 10^{-7}$				476 134 57
18	4	3	0.482 253	40	23	39	- 0.127 686
			$727\ 185\ 07 \times 10^{-6}$				089 346 81
19	5	7	0.229 220	41	24	26	0.730 876
			$763\ 376\ 61 \times 10^{-5}$				105 950 61
20	6	3	- 0.167 147	42	24	40	0.554 147
			$664\ 510\ 61 \times 10^{-10}$				153 507 78
21	6	16	- 0.211 714	43	24	58	- 0.943 697
			$723\ 213\ 55 \times 10^{-2}$				072 412 10
22	6	35	- 0.238 957				$\times 10^{-6}$
			$419\ 341\ 04 \times 10^2$				

IV. IMPLEMENTATION

Implementing cascade with feed forward by enthalpy balance superheated steam temperature control model is shown in Fig. 4 to control superheated steam temperature by applying the logic to Distributed Control System (DCS) shown in Fig. 5 for studying in steady state and load variable situation

V. RESULT AND DISCUSSION

A. Steady state load

Experimental results of cascade with feed forward by enthalpy balance superheated steam temperature control model to control steam temperature in 100% steady state load,

are shown in Fig. 6

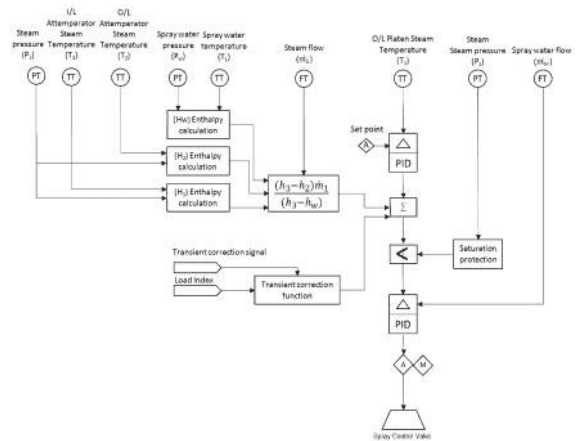


Fig. 4 Cascade with feed forward by enthalpy balance superheated steam temperature control model

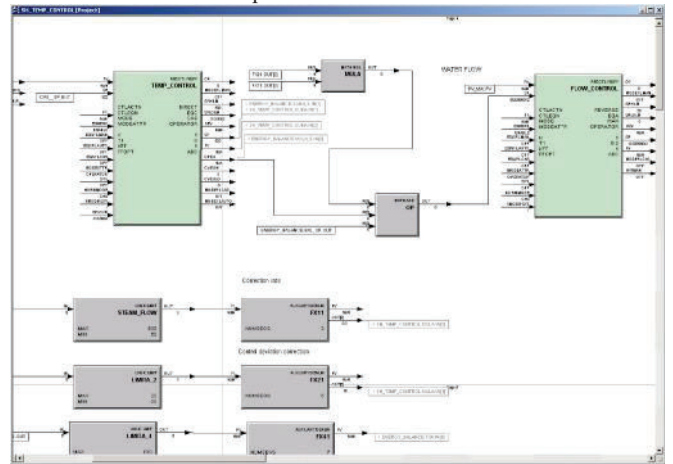
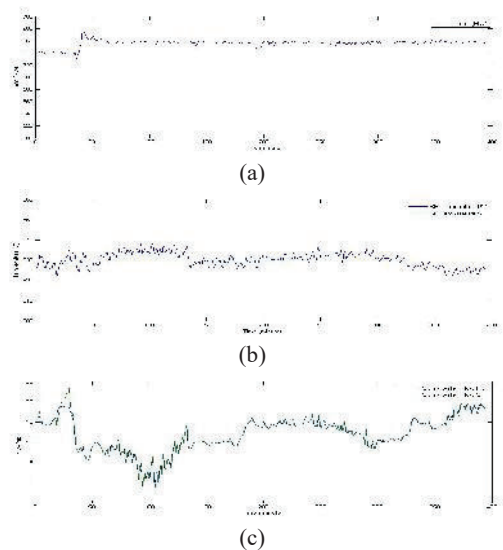


Fig. 5 Cascade with feed forward by enthalpy balance superheated steam temperature control model in DCS



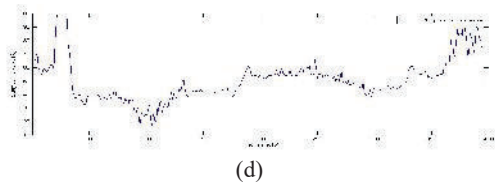


Fig. 6 Steady state load situation

(a) Boiler load, (b) Superheated steam temperature, (c) Spray water flow and (d) Spray water control valve position

The Fig. 6 being steady state temperature control and temperature set-point $^{\circ}\text{C}$ 530 steam temperature is showed significantly steady while fuel energy and small load variable are disturbed. The maximum and minimum of steam temperature is 535. $^{\circ}\text{C}$ 06 and 526., respectively, was $^{\circ}\text{C}$ 18 oscillated in steady state equal to ± 5 Spray water control. $^{\circ}\text{C}$ with cascade with feed forward by enthalpy balance model in steady state situation shows good performance to control superheated steam temperature.

B. Increase and decrease load

Results of studying cascade with feed forward by enthalpy balance superheated steam temperature control model to control in increase and decrease load testing between 100% load and 85% load are showed in Fig. 7.

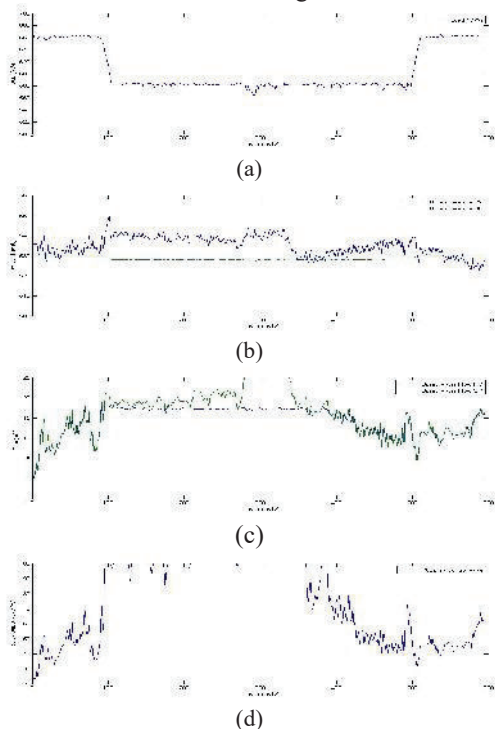


Fig. 7 Increase and decrease load situation

(a) Boiler load, (b) Superheated steam temperature, (c) Spray water flow and (d) Spray water control valve position

Fig. 7 shows superheated steam temperature control response during load variable form 100% to 85% and back to 100% suddenly. The steam temperature set point was changed from 530 $^{\circ}\text{C}$ to 528 $^{\circ}\text{C}$ effecting to spray water flow set point

increased by load disturbance effect. However superheated steam energy is too many and make control signal reach the flow control valve high limit and spray water flow reach maximum limit. In case of steam temperature cannot decrease to set point in period of time until steam enthalpy decrease to control range and the steam temperature decrease to set point. It is controllable in this situation. That is showing that spray water control valves is not enough to handle because of huge energy from the coal fired boiler. However, the temperature control system by cascade with feed forward by enthalpy balance superheated steam temperature control model can handle superheated steam temperature to set-point significantly after huge energy was decreased to controllable range.

VI. CONCLUSIONS

Superheated steam temperature control by cascade with feed forward by enthalpy balance superheated steam temperature control model was showed significantly control in steady state load situation. Similarly during boiler load increasing and decreasing suddenly. The control model was showed fast response to control temperature even though load disturbance was too huge and acting the spray water flow control valve was reached maximum limit. However the control model can handle superheated steam temperature to set-point effectively after huge energy was decreased to controllable range.

REFERENCES

- [1] Geng Liang, Wen Li, Zhijun Li, "Control of superheated steam temperature in large-capacity generation units based on active disturbance rejection method and distributed control system," *Control Engineering Practice*, vol. 21, pp. 268–285, 2013
- [2] Jianhua Zhang, Fenfang Zhang, Mifeng Ren, Guolian Hou, Fang Fang, "Cascade control of superheated steam temperature with neuro-PID controller," *ISA Transactions*, vol. 51, pp. 778–785, 2012
- [3] A. Sanchez-Lopez, G. Arroyo-Figueroa, A. Villavicencio-Ramirez, "Advanced control algorithms for steam temperature regulation of thermal power plants," *Electrical Power and Energy Systems*, vol. 26, pp. 779–785, 2004
- [4] O-Shin KWON, Jin-Sung KIM, Sung-Man PARK, "MIMO Controller with Compensator via Gain tuning method for Steam Temperature Control of Thermal Power Plant," *Korea University Anam-dong, Seongbuk-gu, Seoul*, pp. 136-713
- [5] R. N. Silva, P. O. Shirley, J. M. Lemos, A. C. Goncalves, "Adaptive regulation of super-heated steam temperature: a case study in an industrial boiler," *Control Engineering Practice*, vol. 8, pp. 1405-1415, 2000
- [6] Wolfgang Wagner, Hans-Joachim Kretzschmar, *Properties of Water and Steam Based on the Industrial Formulation IAPWS-IF97*, International Steam Tables, Second edition

Implication of Soil And Seismic Ground Motion Variability On Dynamic Pile Group Impedance For Bridges

Tariq A. Chaudhary, PhD, PE
Civil Engineering Department, Kuwait University, Kuwait.
Email: tariq.chaudhary@ku.edu.kw

ABSTRACT

Bridges constitute a vital link in a transportation system and their functionality after an earthquake is critical in reducing disruption to social and economic activities of the society. Bridges supported on pile foundations are commonly used in many earthquake prone regions. In order to properly design or investigate the performance of such structures, it is imperative that the effect of soil-foundation-structure interaction be properly taken into account. This study focused on the influence of soil and seismic ground motion variability on dynamic impedance of pile-group foundations typically used for medium span (about 30 m) urban viaduct bridges. Soil profiles corresponding to various AASHTO soil classes were selected from actual data of such bridges and / or from the literature. The selected soil profiles were subjected to 1-D wave propagation analysis to determine effective values of soil shear modulus and damping ratio for a suite of properly selected actual seismic ground motions varying in PGA from 0.01g to 0.64g, and having variable velocity and frequency content. The effective values of the soil parameters were then employed to determine the dynamic impedance of pile groups in horizontal, vertical and rocking modes in various soil profiles. Pile diameter was kept constant for bridges in various soil profiles while pile length and number of piles were changed based on AASHTO design requirements for various soil profiles and earthquake ground motions. Conclusions were drawn regarding variability in effective soil shear modulus, soil damping, shear wave velocity and pile group impedance for various soil profiles and ground motions and its implications for design and evaluation of pile-supported bridges. It was found that even though the effective soil parameters underwent drastic variation with increasing PGA, the pile group impedance was not affected much in properly designed pile foundations due to the corresponding increase in pile length or increase in number of piles or both when subjected to increasing PGA or founded in weaker soil profiles.

Keywords—bridge, pile foundation, dynamic foundation impedance, soil profile, shear wave velocity, seismic ground motion, seismic wave propagation

Improved Classification Procedure for Imbalanced and Overlapped Situations

Hankyu Lee, Seoung Bum Kim

Abstract—The issue with imbalance and overlapping in the class distribution becomes important in various applications of data mining. Imbalanced dataset is a special case in classification problems in which the number of observations of one class (i.e., major class) heavily exceeds the number of observations of the other class (i.e., minor class). Overlapped dataset is the case where many observations are shared together between the two classes. Imbalanced and overlapped data can be frequently found in many real examples including fraud and abuse patients in healthcare, quality prediction in manufacturing, text classification, oil spill detection, remote sensing, and so on. The class imbalance and overlap problem is the challenging issue because this situation degrades the performance of most of standard classification algorithms. In this study, we propose a classification procedure that can effectively handle imbalanced and overlapped datasets by splitting data space into three parts: nonoverlapping, light overlapping, and severe overlapping and applying the classification algorithm in each part. These three parts were determined based on the Hausdorff distance and the margin of the modified support vector machine. An experiments study was conducted to examine the properties of the proposed method and compared it with other classification algorithms. The results showed that the proposed method outperformed the competitors under various imbalanced and overlapped situations. Moreover, the applicability of the proposed method was demonstrated through the experiment with real data.

Keywords—Classification, imbalanced data with class overlap, split data space, support vector machine

Hankyu Lee is with the Department of Industrial Management Engineering, Korea University, Seoul, Korea (phone: 82-2-3290-3769; fax: 82-2-929-5888; e-mail: koogi303@gmail.com).

Seoung Bum Kim is with the Department of Industrial Management Engineering, Korea University, Seoul, Korea (phone: 82-2-3290-3397; fax: 82-2-929-5888; e-mail: sbkim1@korea.ac.kr).

Influence of Dietary Inclusion of *Bacillus Licheniformis* on Laying Performance, Egg Production, Hatching Eggs and Mortality of Broiler Breeder Hens

Mohammad Khosravi, Ali Kiani

Keywords—*Bacillus licheniformis*, Broiler breeder performance, Hatching egg, Mortality.

Abstract—Abstract According to the definition proposed in 2002 by FAO/WHO experts, probiotics are “live microorganisms which, when administered in adequate amounts, confer a health benefit on the host”. Probiotics stimulates the growth of beneficial microorganisms and reduces the amount of pathogens thus improving the intestinal microbial balance of the host. Numerous studies have concluded that probiotics used as feed additives exert a beneficial influence on egg production and the physiological parameters of birds. Probiotics contained in laying hen diets contribute to improving egg quality, increasing laying rates and reducing feed costs. This experiment was conducted to evaluate the effects of dietary inclusion of *Bacillus licheniformis* on laying performance, egg production, hatching eggs and mortality of broiler breeder hens. This experiment used 30,000 Ross 308 broiler breeders (27,300 female and 2,700 males) that were 26 wk old and they were kept for 10weeks. The birds were divided into 2 groups, each group with 4 replications (n = 3750). All birds were fed iso-nitrogenous and iso-caloric diets, and had free access to water. The control group received the basal diet formulated with maize and soybean meal. The treatment groups received the same basal diets supplemented with 0.003% *Bacillus licheniformis* powder (2×10^{10} cfu/g) for a 10-wk trial. The birds were weighed at the beginning (26 weeks of age) and at the end of every week till the end of the trial (35 weeks of age). Eggs were collected from each cage six times per week to determine the total number of eggs laid. The average weight of eggs laid was determined by weighing eggs from each cage every week. Feed intake and feed conversion were recorded at four-week intervals. The data on hatchability on total eggs set (TES) was calculated for weekly hatches. The mortality for each group was recorded daily and was calculated at the end of trial. The results showed that dietary supplementation with 0.003% *B. licheniformis* did not have a significant effect on laying performance ($P < 0.05$). Panda et al. (2003, 2008) observed no differences in the weight gains of hens fed diets supplemented with probiotic bacteria. Gallazzi et al. (2008) demonstrated that dietary supplementation with *Lactobacillus acidophilus* had no influence on the weight gains of layers. In our experiment, a probiotic preparation containing *B. licheniformis* had no significant effect on production parameters such as ,egg production, hatching eggs and mortality. Gallazzi et al. (2008) did not note any improvements in laying performance, egg weight, feed intake or feed efficiency in hens fed diets supplemented with *Lactobacillus acidophilus*.

Corresponding Author

Mohammad Khosravi from Gorgan University, Iran, Islamic Republic Of
e-mail: mohammad.khosravi121@gmail.com

Inhibitory Effect of Lactic Acid Bacteria on Uropathogenic Escherichia coli-Induced Urinary Tract Infections

Cheng-Chih Tsai, Yu-Hsuan Liu, Cheng-Ying Ho, Chun-Chin Huang

Abstract—The aim of this study evaluated the in vitro and in vivo antimicrobial activity of selected lactic acid bacteria (LAB) against Uropathogenic Escherichia coli (UPEC) for prevention and amelioration of UTIs. We screened LAB strains with antimicrobial effects on UPEC using a well-diffusion assay, bacterial adherence to the uroepithelium cell line SV-HUC-1 (BCRC 60358), and a coculture inhibition assay. The results showed that the 7 LAB strains (*Lactobacillus paracasei*, *L. salivarius*, two *Pediococcus pentosaceus* strains, two *L. plantarum* strains, and *L. crispatus*) and the fermented probiotic products produced by these multi-LAB strains exhibited potent zones of inhibition against UPEC. Moreover, the LAB strains and probiotic products adhered strongly to the uroepithelium SV-HUC-1 cell line. The growth of UPEC strains was also markedly inhibited after co-culture with the LAB strains and probiotic products in human urine. In addition, the enhanced levels of IL-6, IL-8 and lactic acid dehydrogenase were significantly decreased by treatments with the LAB strains and probiotic products in UPEC-induced SV-HUC-1 cells. Furthermore, oral administration of probiotic products reduced the number of viable UPEC in the urine of UPEC-challenged BALB/c mice. Taken together, this study demonstrates that probiotic supplementation may be useful as an adjuvant therapy for the treatment of bacterial-induced urinary tract infections.

Keywords—lactic acid bacterium, SV-HUC-1 uroepithelium, urinary tract infection, uropathogenic Escherichia coli, BALB/c mice

Corresponding Author

Cheng-Chih Tsai from Hungkuang University, Taiwan
e-mail: tsaicc@sunrise.hk.edu.tw

Investigating the Impact of the Operation of Car Adaptive Headlights on the Amount of Fuel Consumption Reduction

Mohammad Reza pishkar Mohammad Ali nezhad

1&2*

Abstract

Car industry is considered as one of the most important and most active industries in the world in which car safety is one of the most important issues of the day. Headlights play a special role among all the constituent parts of a car because as well as the direct impact they have on the safety of the passengers in the car they are on, they clearly play an important role in relation to the safety of pedestrians and the front cars. This collection should have both important parameters of observing and being observed at once. In terms of operation, car headlights are considered as parts with first-degree safety. One of the dangers intimidating the passengers in a car is accidents at night. Lighting at night to create the best vision for the driver can be a key to solve the problems of accidents at night. On the one hand, it should be noted that the suitable car should have the capabilities of optimized performance in different, complex, and inappropriate conditions. In recent years, technology has always come to help humans in many cases such as the methods of lighting the roads. Shining road signs and signposts at night and road lights that turn on whenever they identify a car according to which the headlights operated based on driver's eyes tracking. The front lights are known as adaptive forward lighting system. This system has nine particular lighting functions including complete automatic beam activating, different lighting patterns for different driving conditions and shining towards the sides and the corners according to steering the car. Until recent years in Iran, the amount of cars fuel consumption had not been attended to because of gas supply at a low price. Today, big car factories spend extravagant have paid much expenses to research on fuel consumption reduction because they are aware of the tendencies of their customers to use those types of cars. This issue has been extended to the point that car manufacturers are considering fuel consumption reduction even in developing car lighting systems such as LED lights.

Keywords: Lights, Adaptive, Car, Fuel Consumption Reduction

1. Introduction

Designing and manufacturing guided headlights resulted from normal headlights. The constant movement of headlights from the left to the right or vice versa is related to a sensor. One of the advantages of the developed headlight system with high compatibility is that the configuring can be easily performed within the space of different designs of vehicles (Baker and Hariri, 2010). Some modern cars are very smart. There are some computers within those cars that superintend all of their electrical and mechanical systems. But despite all of the advances, car headlights do not have very high IQs. In the last century, their light resources evolved into Tungsten filaments and LED lights from acetylene and oil lights. But, except for

1. Department of Mechanical Engineering, Science and Research Branch of East Azerbaijan, Islamic Azad University, Tabriz, Iran

2. Department of Mechanical Engineering, Tabriz Branch, Islamic Azad University, Tabriz, Iran

*Corresponding Author: Mohammad Reza pishkar

Mohammad Ali nezhad, E-mail: m.r.pishkar@gmail.com

few developed headlights that have been installed in luxury cars, the only work they perform is to shine light upon the objects in front of them (Zahedi, 2015). The natural tendency of eyes to blink and movement from side to side leads to the disorderly movements of the beams. This problem is solved by the algorithm that causes a little delay in responsiveness and leads to smoother movements of the beams.

The researches done on accidents indicate that most serious accidents happen at night. In most cases, drivers are not able to see the curve of the twists in the darkness to adjust their speed accordingly. About 54% of the cars that have had accidents deviated from the twists and more than a quarter (26%) had head-on accidents. For the importance of the issue, the engineers investigated a modern lighting system with regard to which the normal lights of cars activate automatically and perform the following actions in reaction to the received data of the sensors responsible for controlling the movements and the traffic (Ghaderi & Daei, 2014): 1) City and roads lightings 2) Lighting at the twists of the roads 3) Freeways lightings 4) Lightings in bad and inappropriate weather

2. Statement of the Problem

The main issue of investigating the programmable headlights solves the issue of shining the glaring light onto the face of the front driver. This system identifies the approaching cars and turns of the beams moving towards the other drivers. With that property, the headlights can always remain on the high beam mode. Tamburo et al., are working on a method that the headlights can illuminate the road ahead using GPS data. The key to this problem is increasing the light intensity in a way to illuminate the road ahead lighter than the side lanes. The camera of this system is also able to identify and track the barriers such as wild animals. The camera of this system can detect barriers at the speed of 80 km/h and with the distance of 5 meters from the headlights. Years should be passed so that such adaptive lights are applied in most vehicles extensively (Zahedi, 2015). According to Shree Nayar, the manager of computer lab vision in Columbia University, this issue is completely dependent upon the investment of car manufacturers to produce and apply that technology. As Nayar said, this belief should be created that it is time to use programmable headlights because in the area of technology, there is no problematic barrier on the way to this system.

Normal, sport, xenon, and LED lights, etc. The topics under question in this study are important and general parameters in the area of manufacturing and designing and are factors which emphasize both the technical and engineering issues of the collection and also the aesthetic science of the car, harmonizing the lines, and the overall shape of the car that is considered by customers.

3. Research Background

Joseph Swan put the first light lamp on display in England in 1878. The first lights (big front lights) used in the early cars resembled the lights of horse-drawn carriages and Daimler cars in 1886 were equipped with the light in which candles were lit (Ghaderi & Daei, 2014). A lot of progress has been made since then. The history of the evolution of light sources is divided into some periods. 1892 to 1912 is a period in which cars did not have lighting devices. At the end of that period, cars were equipped with a type of light called acetylene lamps. The second period lasted from 1912 to 1932 in which cars had separable electric lamps which were installed within the reflector system plus lens. 1939 to 1979 was the period of sealed lights in which all the system should have been changed if the lamp burned out.

In 1902 not every car had lights. In those days, the cars in the absence of lights at night changed into carriages without horses with the difference that they could not go back home at home. Later, kerosene was used as the fuel of the car lights. That system was like that of normal lanterns a lot. Oil lamps were common until 1906 but gradually the need to create change in them was felt because of their inadequacy in producing light. In 1906, stronger lamps were supplied.

Those lamps were still non-electrical and acetylene was used in them as fuel. That system included a flat and transparent lens that gave an appropriate extensiveness to the light. From then on and with the increase in the level of the light of the front lamps, the issues concerning the glare resulting from the too bright light were considered. Then, acetylene headlights with oil side lights were installed on the car of Ford company model 1909. About 1908, electric lamps with carbon filaments were supplied to be applied in cars. In 1911, some cars used electric lamps and in 1912, using electric lamps in cars were pervasive of course with some exceptions. In those years, no actions were taken to distribute the produced lights in lights and the light of the headlights of the cars were like shining spotlights shone on the road. In 1912, half-transparent lenses and patterned lenses on which there were small prisms and grooves were supplied and the purpose of using them was light distribution. The year 1915 was ambiguous in some ways in the history of lighting. Before that year, the used lamps were those in which filaments reached inflammation temperature in the relative vacuum environment by passing an

electric current. That year the lamps which had been filled by neutral gasses (nitrogen or argon) were supplied. One filament became hot in the presence of a neutral gas that did not react with tungsten. That change increased the lifetime of the lamps and in 1915 lenses changed and changed into the active optical parts in the lamp light distribution. Those changes continued for years and many steps were taken to seek the best pattern on the lenses (Esmaeili et al., 2008). In 1924 another evolution happened and the headlights were supplied with two high and low beam modes. That was performed by two-filament lamps. In 1915, low beam headlights were introduced by Guide Lamp 5 Company. In that time, Cadillac introduced a system by which the low beam mode could be selected by the driver through a handle. In 1924 a system was supplied in the market in which high and low beam modes were placed in one bulb which was standardized as foot dimmer. In 1930, many types of headlights with patterned lenses were used in different models of Cadillac cars. In 1932, headlights with asymmetrical low beams were supplied. Before that time, the created beam pattern by the lamp system, reflector, and the lens was symmetric and as a result driving at night was accompanied by too much glaring light that caused a lot of dangers. By that progress, more light was conducted to the opposite direction of the driver and driving safety improved. In 1934, pre-concentrated lights were supplied in which there was a special cover at the point where the lamp was placed in the reflector and when the lamp was placed in it, filament orienteering and also its distance from the center of the reflector could be adjusted properly. That was the last major progress until the advent of current halogen lamps. In 1954, Cadillac introduced a system that could be selected by a high or low beam switch. In 1940, 7-inch round sealed beam headlamps (178mm) were introduced in the U.S. which were obligatory for all the cars on sale in a short while. That system was confirmed in Japan and Australia while it was not received very well in Europe and subsequently the headlight designing became different in the U.S. and Europe (Babaei, 2015). HID headlight system was introduced for the first time in the mid-90s in some Japanese and European luxury cars. That technology could not find a place rapidly in the market for its high price. However, its high efficiency and transcendence in the area of the driver's vision and the advantage that it prepared in terms of high safety gradually raised the demands for it even for the cars with medium prices (Yazdi Moghadam, 2015).

The innovation of XENON glowing gas that was used in different Class E Mercedes Benz's since 1995 had many advantages the most important of which was very low electricity consumption that was equal to 35 Watt. Xenon lamps had twice as much as the lighting power of normal 55-Watt halogen lamps (Ghaderi & Daei Zadeh, 2014).

The issue of fuel consumption and its reduction is not new in car industry and it attracted special attention in non-Iranian countries especially after the oil crises in 1973 that resulted in the extinction of big and high-fuel consumption American cars.

4. The Purpose of the Study

- One of the important purposes in the effective factors of safe movements of vehicles at intersections is the existence of an adequate field of view.
- A brief look at the modality of performance and new innovations of adaptive headlights and investigating their difference with normal lights
- The impact of the program based on “The theory of developed programmed behavior” on the using method of appropriate headlights to prevent accidents.
- Offering solutions to boost the use of appropriate car lights.
- Increasing safety (car disasters and accidents).
- Increasing car welfare equipment.
- The purpose of this system is to illuminate the road for the driver, visibility of the car itself, and presenting information including size, the location of the car, and its speed.

5. The Questions of the Study

- Using which type of adaptive lights helps reduce the fuel consumption?
- How investigating the operation and innovation of the lights is different from that of normal lights?
- What type of lights helps reduce the number of accidents and is appropriate to increase the safety for drivers?

6. Hypothesis

- It seems using adaptive lights helps reduce fuel consumption reduction.
- It seems that investigating the operation and new innovations of lights is different from that of normal lights.
- It seems using adaptive lights helps reduce the number of accidents and is appropriate to increase the safety for drivers.

7. Theoretical Basics

7.1. Different lights used in cars:

7.1.1. Headlights

They are the front lighting system of cars that are used as high and low beam modes. The front lighting system of cars might be accompanied by side lights and anti- fog lights.

- Low Beam

In this mode adequate vision is created for the driver by light scattering without the driver’s gaze.

- High Beam

This mode is designed for conditions that there is no other car in the road. At high beam mode the amount of lighting is not controlled. According to the international laws, using high beam with North American standard specifications is permissible.

- Anti Fog

Anti-fog lights shine a strip of light upon the surface of the road that is generally adjusted facing down. These lights are usually produced in white or yellow and are designed to be used at low speeds. The main reason for designing these lights is to compensate for the inadequate vision of the driver in rainy, snowy, or foggy weather conditions.

- Side Lights

Side lights are mostly used for more illumination while the car is turning or changing its direction. These lights are also connected to turn signals or to the reversing lights. Side lights have been used in some models of Saab and Corvette cars.

- Turn Signals

Turn signals or in general term blinkers or flashers are the lights that are installed on the front and back corners of the car and are used when changing directions. In some car models they are installed at the side of cars which are used when changing lanes. Using electric turn signals obligatory for all car manufacturers and its manual type are still installed on bicycles (Ghaderi, 2012).

7.1.2. Lamp Types

Most lamps are used in the headlights and of cars in the past and the present which are mainly halogens. Before oil , acetylene, and electric lights and after halogens, HID, xenon, LED, AFS and finally laser lights had the most use respectively (Farahani, 2015).

1. Oil and Acetylene Lights

The first type of lights that were used in cars with the property of illuminating roads was acetylene lights (Carbide lights). Acetylene (C₂H₂) is obtained from the reaction of Calcium Carbide (CaC₂) and water the burning of which produces the desired light. In the early twentieth century the mobile type of this light was also used in mines. These lights were popular because of their appropriate resistance against wind or rain (Mosaheb, 2015).

2. Electric Lights

In 1908, electric lights were used in the American car, Peerless, for the first time in a standard way. From then on, car lighting has undergone a lot of changes. Options that are used in most cars have been strange from a long time ago. For example, the smart system of light turning of headlights at twists that are known today as AFS (Mosaheb, 2015).

3. AFS System

In AFS systems, the lighting of the passing direction has improved in relation to common systems by 90%. Normal lights are only able to illuminate the direction with the distance of 30 meters when they enter a twist with a 190-meter radius. New lights illuminate 55 meters of the direction by 25 meters increase in the length. There are some shortages in the above-mentioned systems. In this system, steering wheel angle, car speed, pivot sensors (accelerometer sensors indicating the speed difference between the speeds of the front wheels), GPS, and the fast camera that increase the safety while passing a twist have been used (Ghaderi & Daeizadeh, 2014).

AFS Features

- Rotational dynamic lights operate quickly at sharp turns.
- Light is completely appropriate for sharp twists and their inner parts.
- Higher efficiency by using a combination of dynamic and static light systems
- Usefulness of Xenon lamp technology with high power or halogen lamps.
- Simple electronic control by car data network.
- Designing ECU with algorithm for sensors.
- Installing ECU in each unit of headlights.
- The completely changed appearance (Ghaderi & Daeizadeh, 2014).

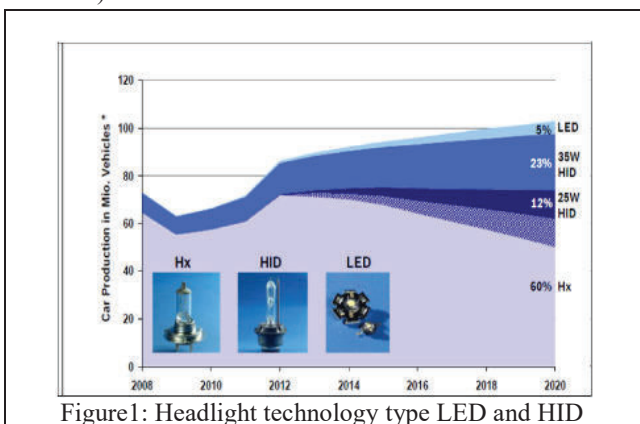


Figure1: Headlight technology type LED and HID

7.1.3. Investigating the Advantages and the Defects of Lamps

Table 1. Advantages and defects of lamps.				
Rows	Lamp Type	Advantages	Defects	Source
1	Oil and acetylene lights	The mobile type of this light was also used in mines. These lights were popular because of their appropriate resistance against wind or rain	They did not have adequate light to illuminate the road ahead and merely helped the visibility of vehicles to others.	(Mosaheb, 2015)
2	Halogen lamps	This technology was used in Europe for its higher efficiency in producing more light in relation to non-halogen filament at the same consumption power. Energy consumption reduction, simpler structure, reduction in wiring and the relative switches are the advantages of this technology.		(Babaei, 2015)
3	HID lamps	Technical advantages of HID lightings are consuming less power, longer lifetime, and the better output light in terms of quantity and quality. A 35-Watt HID lamp produces light twice as much as 60-watt halogen lamps.	The defects of this system are the produced ultra violet light percentage and reduction of the shining of the lights by the erosion and oldness of electrodes. Nevertheless, they produce more light than halogen lamps.	(Babaei, 2015)
4	LED lamps	The advantages of LED lamps are their small volume of the lamp (their shallowness), longer lifetime of LEDs in relation to the car lifetime, low fuel consumption, and the increase in efficiency (Babaei, 2015).	The defect of LEDs is the management of heat. Heat is not sent out with beams and should be eliminated separately. Also, the relative lighting of LEDs (Radius intensity for every hour unit) is low. The efficiency of anti-fog lamps has improved by using LED Technology in a way that from 6 to 8 powerful LEDs are used in projectors (Ghaderi and Daeizadeh, 2014).	(Ghaderi & Daeizadeh, 2014) (Babaei, 2015)

5	AFS system	<p>1- More lighting at night 2- reduction of stress and tiredness of drivers at road twists and intersections 3- Light scattering according to the steering wheel angle as a result of the increase in the received light at the twists of the roads 4- increasing the safety in roads</p>	<p>This system is used for lenses with plastic covers to prevent any scratch.</p>	(Ghadiri & Daeizadeh, 2014)
---	------------	---	---	-----------------------------

beams moving towards other drivers. By that property, the headlights can always remain on the high beam mode (Zahedi, 2015).

7.1.4. Adaptive Headlights

Standard headlights shine their light straightly regardless of the direction in which the car is moving. At twists, the headlights illuminate the roadsides more than the road itself. Adaptive headlights are harmonious with the steering wheel and the speed of the car and automatically concentrate the light on the road. The cars that are equipped with adaptive headlights use electronic sensors to specify the speed of the car in order to perform their job. Also these sensors are very useful in specifying the amount of the rotation of the steering wheel and the car deviation. For example, the amount of deviation changes when the car is turning around it. In fact, these sensors put into motion the small engine within the headlights that causes the beam to turn. In that system, the lighting beams of the car turn to the angel of 15 degrees from the center. It should be said that adaptive headlights can have free rotation as much as 30 degrees (Tahoori, 2013). The headlights of future cars change the amount, direction, and concentration of the light intelligently according to the landscape ahead and the barriers on the way. These lights can help the driver's vision to improve by adapting to different situations. A group of researchers are making headlights in lighting and filming laboratories to prevent shining light upon rain drops or snowflakes in adverse weather conditions to shine light upon the road ahead more than the side lanes to make the driver aware of the barriers on the way. The adaptive headlights can change the amount, type, and the direction of light according to different situations. This smart headlights system constantly assesses the different driving conditions and reacts to them. A camera placed at the front of the car registers the pictures in the front. After that, a computer processor processes those pictures. This processor uses the obtained information to control the spatial light modulator and dividing a light beam to millions of smaller beams each of which can turn on or off when needed (Zahedi, 2015).

This programmable headlight solves the problem of the glaring light shining upon the face of the opposite driver. This system identifies the approaching cars and turns of the light

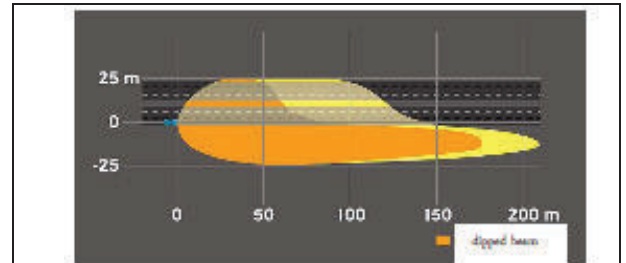


Figure 2: Highway lighting

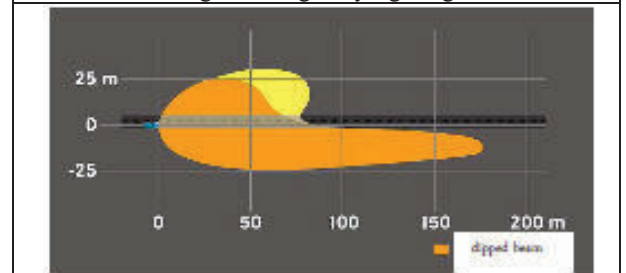


Figure 3: Light country

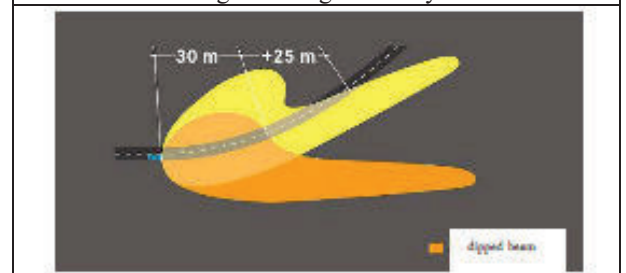


Figure 4: Deflection of light

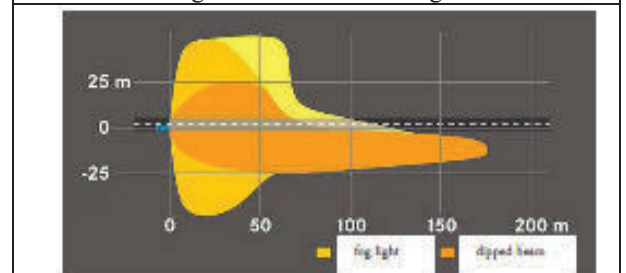


Figure 5: Fog lights long

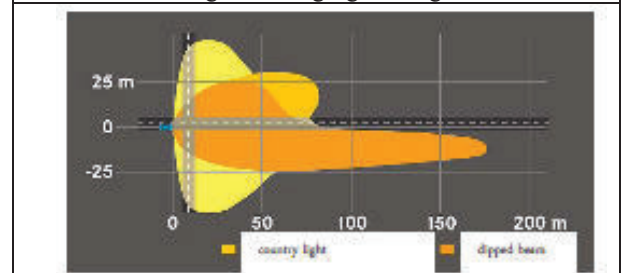


Figure 6: Static bending light

(mueller, 2010)

7.1.5. Modern Technologies of Headlight Lighting

More safety and lighting is the demand of every driver especially at night. Smart headlight lighting systems provide appropriate and compatible operation with regard to the course of the road and the direction even in adverse weather conditions such as rain and fog and increase the driver's vision significantly. Most operations of smart lighting systems have been mentioned as follows:

- Curved Lighting System

This system causes more safety, relief, and tranquility in interstate roads with many turns and twists by creating more vision for the drivers. By applying this system, the cone of the driver's vision increases by 70% in relation to the normal lighting.

- Roadside Lighting System

This system consists of fixed lights that can begin to work automatically while the cars enter the twists slowly and at low speeds. In that situation, the resolution of the roadside is more than normal systems by 30 or 60 meters.

- Camera-based Advanced Front Lighting System

This technology is able to automatically change the amount of the light of the headlights when needed to illuminate a wider space on the road. In order to do so, Ford system identifies the traffic signs and then combines them with GPS data.

Ford believes that this technology can be very useful especially when the driver is going to confront a turn. It is interesting to know that Ford smart system is able to identify the pits ahead and shine the needed light upon them before the car reaches them. Designing and development of this technology by an international team of Ford engineers and the provider associates were performed for Ford adaptive headlights and its automatic high beam system. This system adjusts the angle of headlights angle and its intensity with regard to speed, environment light, steering wheel angle, the distance from the front vehicle, and the active wiper of the windshield.

- Spot Lighting System

This system has been designed for urban roads in which there is not enough light. Spot lighting by infrared cameras that are placed at the front filters of the car can identify humans and big animals according to their body temperature. After detecting the possible barriers on the way, the high beam of the car shines upon them automatically so that the driver can observe what he or she has in the front. In addition, the barriers are observable on the interior monitor of the car with yellow

color. That system can simultaneously track and detect up to eight objects within a distance of 120 meters by infrared cameras.

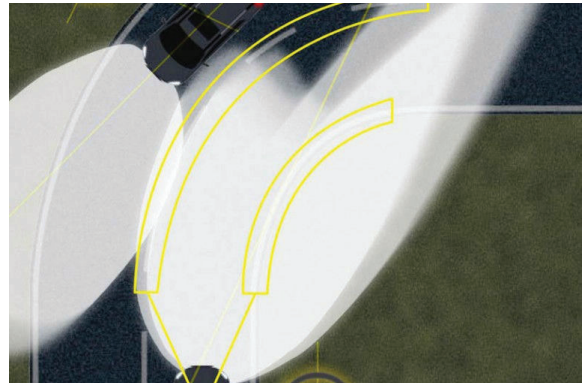


Figure7: Screw on the road



Figure 8: Spot Lighting System

8. Analysis of AFS and LED Lights in terms of Fuel Consumption

The braking intensity of the driver behind impacts the car fuel consumption a lot.

1. Because the fuel within the combustion chamber is able to continue to combust which enters the environment while it is not combusted by braking.
2. By a sudden braking or an intensive braking, the amount of friction between the tires and the road reaches its maximum amount. In this situation, in order to start again, the friction force should be zeroed and overcome for which the maximum power of the car is needed.
3. Selecting the right direction and having adequate vision on the part of the driver especially at night causes a better and correct driving and finally fuel consumption is reduced by 20%.

For every 6 kilometers per hour at night or in the darkness, 6 meters of the depth of vision is reduced.

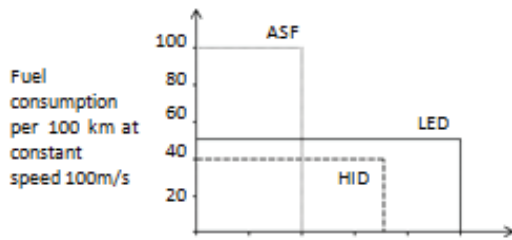


Diagram1: Fuel consumption

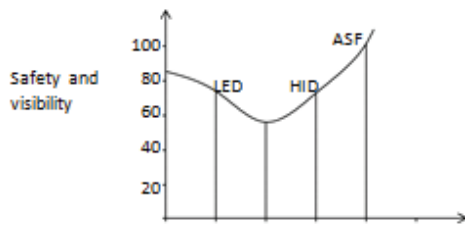


Diagram 2: Driver safety and better visibility

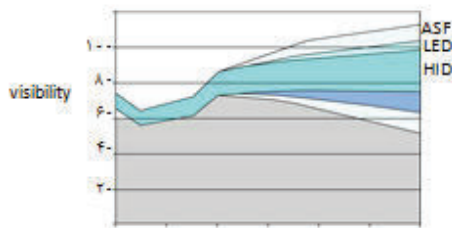


Diagram 3: visibility

9. Conclusion

According to the study it is concluded that the light should be adjusted to prevent the irritation of the eyes of the opposite driver. The adaptive braking lights of the front car provide the possibility that the driver can see the amount intensity of the front car and prevent possible disaster while adjusting one's breaking intensity. When the driver puts on the brake slowly those lights warns the drivers behind by indicating a weak shine that the barrier ahead is not very serious, thus, there is no need to reduce speed much. Generally, the force exerted upon the brake pedal specifies the intensity by which the adaptive backlights should turn on which can be a great help to the drivers behind. Car industry is considered as one of the most important and most active industries in the world in which car safety is one of the most important issues of the day. One of the threats intimidating the passengers in a car is accidents at night and as a result adaptive lights help the safety of the car and the passengers at night.

1. Improving the driver's vision by 90%;

2. Reduction of the number of accidents at night by 50%;
3. Fuel consumption reduction by 35%;
4. Reduction in the brake lining consumption by 15%;
5. Increasing the life of tires by 13%

References

- Babaei A, 2015. The role of boosting the technology of car lights in the correspondence of geometric pattern of roads and safety improvement. The magazine of mechanic and vibrations. 6(2).
- Cherati M, 2015. Development of eye-tracking lighting system for cars. Technology news. WWW.Gizma.com
- Farahani M, 2015. The comparison of the technology of headlights, which is better?
- Ghaderi H, Daeizadeh H, 2014. General familiarity with the headlights of cars and specifications of each of them.
- Ghaderi Y, 2012. Car lighting system, side turn signals.
- Hrairi M, Abu Bakar B , 2010. Development of an Adaptive Headlamp Systems. International Conference on Computer and Communication Engineering, Kuala Lumpur, Malaysia.
- Mosaheb M, 2015. The technology of car lightings over time.
- Mueller F, 2010, Adaptive Lighting System Today and Tomorrow, Mercedes Benz.
- Neumann R, 2011. Automotive Front Lighting. GTB Document. CE-4563.
- Salcianu Monica, Foslau C, Hariton A, 2011. Simulation of an intelligent-adaptive front lighting system. Buletinul institutului poly technic din iasi Publicat de Universitatea Tehnică Gheorghe Asachi" din Iasi Tomul LVII (LXI), Fasc.
- Tahoori A, 2013. The operation of adaptive headlights. Traffic regulations, 2005. 20873-29169.
- Yazdi Moghadam A, 2015. HID car lights and new standards.
- Zahedi E, 2015. Adaptive headlights, the future ahead of the cars. Scientific American.

Judging Restoration Success of Kamisaigo River Japan

Rita Lopa, Yukihiro Shimatani

Abstract—The focus of this research is 880m extension development along the Kamisaigo River. The river is flowing tributary of grade 2 rivers Fukutsu City, Fukuoka Prefecture. This river is a small-scale urban river and the river was formerly a straight concrete sea wall construction. The river runs through National Highway No. 3 from the confluence of Saigo River. The study covers the river basin about 326 ha with a catchment area of 20.63 ha and 4,700 m³ capacity regulating pond. The river is not wide, shallow, and has a straight alignment with active (un-vegetated) river channel sinuosity (ratio of river length to valley length) ranging between 1 and 1.3. However, the alignment of the low-flow river channel does have meandering or sinuous characteristics. Flooding is likely to occur. It has become difficult to live in the environment for organisms of the river. Hydrophilic is very low (children cannot play). There is little connection with the local community. Overall, the Kamisaigo River watershed is heavily urbanized and from a morphological, biological and habitat perspective, Kamisaigo River functions marginally not well. For river improvement and maintenance of the Kamisaigo River, the workshop was conducted in the form of planning for the proposed model is presented by the Watershed Management Laboratory. This workshop showed the relationship between citizens, City Government, and University of mutual trust has been established, that have been made landscape, environment, usage, etc: retaining wall maintenance, hydrophilic zone, landscape zone, nature walks zone: adjacent medical facilities and adjacent to large commercial facilities. Propose of Nature walks zone with point of the design: provide slope that the wheelchair can access and walking paths to enjoy the scenery, and summary of the Kamisaigo River workshop: creating a multi-model study and creation of natural rivers.

Keywords—River restoration, river improvement.

Introduction

Rivers confer benefits on human beings in various forms. Rivers also contribute in creating landscape, nature and culture. Another reason why the rivers become a key element of all of civilization is that the rivers that support the commercial and social activities, such as shipping transportation and fisheries and so on. For example, by utilizing the Nile River of Egypt to achieve progress in the

fields of culture and civilization, also including the main water source of the Arabs at that time. In addition to significant gains in social and commercial fields, the beauty of the scenery of a river is another gift to the human conscience. Water sources that pleased the eye and ear give a beautiful landscape/aesthetical value, and makes neighborhoods like it more valuable but the landscape of rights of access and management of water resources is changing rapidly, both for hydrological and political reasons.

River restoration is the harmony of the arts and the engineering to enhance a scenery and function of the river. U.S. Environmental Protection Agency ~USEPA, (2000) defined restoration refers to the return of a degraded ecosystem to a close approximation of its remaining natural potential. Society for Ecological Restoration (2002) also stated that restoration as the process of assisting the recovery of an ecosystem that has been degraded, damaged, or destroyed and may be thought of as an attempt to return an ecosystem to its historic pre-degradation trajectory. River restoration, which is defined as the process of returning a river section to a near-natural state (Bradshaw, 1996; Palmer *et al.*, 2005; Roni, 2005). We define river restoration as assisting the recovery of ecological integrity in a degraded watershed system by reestablishing natural hydrologic, geomorphic, and ecological processes, and replacing lost, damaged, or compromised biological elements (Ellen Wohl *et al.*, 2004). Restoration to improve physical and ecological conditions of degraded streams and rivers has become a key component of watershed management (Hassett *et al.*, 2005; Jansson *et al.*, 2007).

Yukihiro Shimatani (2000) stated that there are seven basic concepts of river restoration: 1) Consider defining flood control, 2) Clearly recognize the current environmental state based on historical data, 3) Establish deterministic objectives,

Rita Lopa, is with associate professor of River Engineering Laboratory of the Civil Engineering Department, University of Hasanuddin, Indonesia (phone: +6281381266719; e-mail: ritalopa04@yahoo.com).

Yukihiro Shimatani, is with professor of Watershed Management Laboratory of the Urban and Environmental Engineering Department, Kyushu University, Japan (phone: +819062915901; e-mail: shimatani@civil.kyushu-u).

4) Correctly understand the targets to be conserved and restored with their scales, 5) Accept expected changes, 6) Take full use of natural energy, and 7) Understand living things having homes there. Whilst Rosgen (2011) have revealed restoration basics including: 1) Understand the cause of problems, 2) Identify the degree and nature of impairment, 3) Evaluate departure from stability, 4) Examine potential of river systems 5) How to fix, stabilize, enhance amongst great complexity and risk, and 5) Appropriate.

The nine step guides for stream restoration by USDA NRCS (2012) are follows : 1) Identify problems and opportunities: What stream characteristics should be changed? 2) Determine objectives: What are the desired physical, chemical and biological changes? 3) Inventory resources: Study the stream to understand the dominant physical processes, impacts on water quality, and abundance and distribution of biological populations, 4) Analyze resource data: Evaluate the collected information and decide what processes most influence the desired stream condition, 5) Formulate alternatives: Determine which processes can be changed. Include a no action option, 6) Evaluate alternatives: Which alternatives are sustainable and cost effective? 7) Make decisions: Develop a consensus-based decision by the stakeholders and interdisciplinary team regarding which alternative to implement, 8) Implement the plan and 9) Evaluate the plan: Perform post project monitoring, to assess performance and revise practices.

EPA Watershed Ecology Team revealed that restoration principles are: 1) Preserve and protect aquatic resources, 2) Restore ecological integrity, 3) Restore natural structure and function 4) Address causes of degradation, 4) Develop clear, achievable and measurable goals, 5) Focus on feasibility, 6) Use reference sites, 7) Anticipate future changes, 8) Involve a multidisciplinary team, 9) Design for self sustainability, 10) Plant native species, 11) Use natural fixes and bioengineering, and 12) Monitor and adapt where changes are necessary.

Civilizations have been developed along the river since early times. Restoration of urban rivers is a new endeavor. Restoring rivers are combination between art and technical or

scientific challenge. River restoration and waterfront development are in the mode, ranging from Europe over the American continent to Australia, Japan and many other countries, there have been many restoration practices for small river ecosystems with mature restoration technology. The earliest river restoration projects are launched in Europe. River restoration started in Europe in the 1980ies, ranging from landscape gardening (improving the aesthetic value) and river training using bio-engineering approaches to restoring historical conditions (e.g. re-meandering river) or natural processes (e.g. adding wood to initiate natural channel dynamics), include the creation of secondary channels along the Rhine (Simons et al. 2001). Generally the number of urban river rehabilitation schemes across Europe is still small. A total of about fifty urban river rehabilitation schemes, mainly from Europe, was identified. It became obvious, that there is an uneven distribution of potentially appropriate rehabilitation projects across the European countries. For instance, in Austria, France, Germany and Great Britain a comparatively high number of projects could be identified. The US started the activities in 1976, and later in China (Ren, 2001). South of Korea started the big revitalization for the four river restoration in 2008, which is enhancing restoration along 929 km of ecological streams and wetlands including Han River, Nakdong River, Geun River and Yeong san River, hence the typhoon naemi in 2003 afflicted this country.

Nishikawa Sukenobu was born in 1671 and *between 1710 and 1722, Sukenobu published some fifty erotic works. This study contends that these works were an expression of political disaffection.* Therefore, with Sukenobu being based in the imperial city of Kyoto this provided him with more freedom and his thinking would be influenced by the environment he resided in (Lee Jay Walker, 2012).

Japanese rivers are unique. They are steep, short, flashy and sediment rich (Yoshimura et.al, 2005). 70% of Japan is mountains, hence rivers are short and steep and flow rapidly and violently. It has a narrow surface area, rapid run-off of precipitation, and high population density. Moreover, Japan has twice precipitation as much as that of the world average. Most of Japanese cities are susceptible to flooding because

they lie in lowland which is below the flood water level of the rivers. In Japan, 109 river systems that are especially important in terms of national land conservation and the nation's economy are defined as Class A water systems, and they are managed mainly by the Ministry of Land, Infrastructure, Transport and Tourism (partly by prefectures). Furthermore, other river systems that play an important role in the public interest are called Class B river systems. Class B and other river systems except for Class A river systems are managed mainly by prefectures.

After the Second World War Japan experienced a period of rapid industrialization and urbanization, this caused serious pollution of many rivers. Some devastating typhoons led to the initiation of a massive flood control project with a boom of large dam constructions and river channelization works. At least three endemic fish species have totally disappeared, and about 60 fish species are listed as endangered (Yoshimura 2005). The chemical water quality started to return to acceptable levels, but the physical condition remained poor, especially in lowland rivers. A rating system used in Japan to evaluate the condition of the river based upon assessments of river, river cover and habitat diversity. In 1970, the term "easy-access-to-water" used for the first time in Japan. It is that in order to create a variety of conservation and river scenery, and river management. Notification will be issued in 1990 for the promotion of "natural type river development" many natural rivers making this multi various efforts have been made in various parts of the country. In response to that, such as the improvement of river development remains challenging has been pointed out as a center small river, basic guidelines have been created. Although it is specified by the planning technical standards for erosion control rivers River Bureau Ministry of Land, Infrastructure and Transport. The idea of channel planning, and specific techniques of small and medium-sized river plan was unclear.

Then, Naturally-diverse river works (Japanese river restoration) officially started in 1990 by MOC (the Ministry of Construction) now MLIT (The Ministry of Land, Infrastructure and Transport and Tourism) with a purpose:

Ecosystem with high biodiversity and beautiful landscape, and then river restoration activities have increased significantly. Based on a comprehensive database of >37,000 river restoration projects across the Japan country. The Itachi River restoration project was one of the earliest such project in Yokohama Japan starting in 1982 in order to restore the waterfront to its natural state (re-naturalization of waterway). A part of the riverbed of the cross sectional waterway was dug out. At the ends of the waterway, banking is done. This case is so famous that it is called the Itachi River method. There were several goals for this river restoration plan to maintain sufficient water depth (ie. to restore the water depth to pre-construction levels), to restore water front vegetation, to revive the riverbed micro-topography in both rapid and slow streams, and to develop the river-walk. Through experimentation with various construction method, the waterfront environment has now regained its natural vitality and once again attracts the local people (Shimatani 2000).

Then, in 1998, "technical standards for river plan for small and medium-sized rivers," which summarized the considerations and basic idea of the preparation of small rivers river plan has been proposed. By 2010, incorporate the technical standards for the design and planning of the waterfront, seawall, the banks of the small rivers in the revision of the "technical standards on small river river plan" has been made. In urban river, this is even more pronounced. For this reason, only the natural river, thereby playing a clear structure abyss is difficult rapids, some construction methods during construction, and regenerating the abyss rapids is required. Thus, for the regeneration of deep structure, small urban rivers, various construction methods have been tried. However, currently, the repair process is still at the stage of trial and error in Japan.

The Kamisaigo River is not wide, shallow, and has a straight alignment with active (un-vegetated) river channel sinuosity (ratio of river length to valley length) ranging between 1 and 1.3. However, the alignment of the low-flow river channel does have meandering or sinuous characteristics. Flooding is likely to occur. It has become difficult to live in the environment for organisms of the river. Hydrophilic is

very low (children cannot play). There is little connection with the local community. Overall, the Kamisaigo River watershed is heavily urbanized and from a morphological, biological and habitat perspective, Kamisaigo River functions marginally not well.

Methodology

The focus of this research is 880m extension development along the Kamisaigo River (Figure 1). The river is flowing tributary of grade 2 rivers Fukutsu City, Fukuoka Prefecture. This river is a small-scale urban river and the river was formerly a straight concrete sea wall construction. Effect of straightening of the Kamisaigo River is high riverbanks that, the river improvement now proceed, using a variety of construction methods for each interval, the structure has been tried playing rapids. The river runs through National Highway No. 3 from the confluence of Saigo River. The study covers the river basin about 326 ha with a catchment area of 20.63 ha and 4,700 m³ capacity regulating pond.

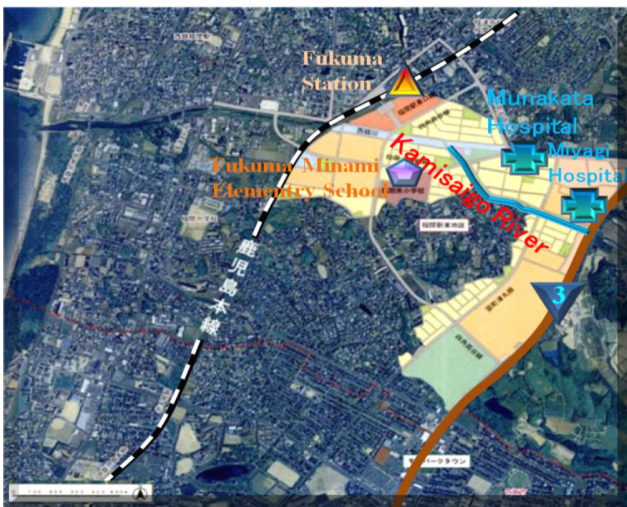


Figure 1. There is 880m extension development along the Kamisaigo River

For river improvement and maintenance of the Kamisaigo River, based on the basic proposal is summarized in 2005, and is intended to create a better plan was introduced the concept of Nature-friendly river. Redevelopment of the site required that the river be improved to create an attractive public amenity, because the site is prominently located in the

heart of Fukutsu City. The workshop was hold to participate in both the valley district, the city council building south Fukuma Township Elementary School District, Kamisaigo River workshop members in 2005: Watershed Management Laboratory, Kyushu University, civil engineering office Munakata, design consultants and local beneath.

Result and Discussion

The relationship between citizens, City Government, and University of mutual trust has been established. The workshop was conducted in the form of planning for the proposed model is presented by the Watershed Management Laboratory (Figure 2), that have been made landscape, environment, usage, etc: 1) November 10, 2007 Description of Kamisaigo River workshop, 2) March 14, 2008, retaining wall maintenance, 3) May 7, 2008, hydrophilic zone, 4) June 13, 2008, hydrophilic zone, 5) July 16, 2008, landscape zone, 6) September 1, 2008, Nature walks zone: adjacent medical facilities and adjacent to large commercial facilities, 7) October 20, 2008. Propose of Nature walks zone with point of the design: provide slope that the wheelchair can access and walking paths to enjoy the scenery, 8) November 26, 2008, Summary of the Kamisaigo River workshop: creating a multi-model study and creation of natural rivers. Construction plans cross linked change with Shiroumaru Bridge in 2008, Sakura Bridge in 2010, Kifune Bridge in 2010, and Himaki Bridge in 2012.



Figure 2. The landscape model of Kamisaigo River

The Kamisaigo River recently completed a third major river restoration project. One of the primary goals of this most recent project was the variety of the natural habitat river scenery. The restoration specifically involved placing logs and/or a series of boulders into the river. The restoration work has been started since November 2009. The first phase of the Kamisaigo River Restoration Project began at the Station 3 and ended about 70 m upstream in the winter of 2009. The second phase of the project began in the summer of 2010 and was completed during the winter of 2011. The third phase of the project began in the summer of 2011 and was completed during the winter of 2012. This second phase covered about 500 m of river from station 2 to 5, and was the primary focus of this research, Figure 3.



Figure 3. The first and the second phase of the Kamisaigo River Restoration Project.

What happened to a particular landscape in an effort to help the Kamisaigo River became stable. Rock gabions have been used to stabilize and protect steep banks. Gabions are made out of a small meshed wire grid filled with coarse gravel. Living sticks or sprouted plants are incorporated. Stabilization is enhanced through the roots of vegetation and the connection of all elements. Gabions are rectangular wire baskets made of heavy galvanized or coated wire mesh. They are filled with small to medium sized rock and soil. Gabions are laced together to form terraces or a wall. Placing live branches between each layer of rock filled baskets incorporates vegetation, Figure 4. The resultant design gave the erosion protection and increased flood capacity required while also greatly enhancing the habitat over the 300m.



Figure 4. Erosion control mats in the Kamisaigo River.

Restoration of native vegetation in the Kamisaigo River, retained for further consideration such as planting trees and shrubs, which has provided free or low cost native plants. Encouraging the growth of riparian vegetation would provide habitat cover for fish. The planting strategy employs groups and clusters of vegetation to increase chances of success with patchy development rather than randomization. Similar species will be planted together particularly with regard to the shrub species. *Salix gracilistyla* is a species of willow native to Japan known in English as *Rosegold Pussy Willow*. It blooms which appear in early Spring. It's shape is described as arching. It grows to a height of 3m and 4m in width. It has oval foliage that is gray/green. It produces flowers and this hardy plant grows with a strong and distinct shape and grows into a large and dominant plant. It requires a moist and rich soil, preferring full sun, and a position free standing, in water or by the side of water. This plant is likely to need pruning. It is susceptible to and should be protected from scale insects, rust, leaf spot, caterpillars and aphids. Bio-habitats provides habitat and is an aesthetic attraction.

In the future, it should be a harmony between citizens and the river. Many private citizens have been endeavors to nurturing the Kamisaigo River. By 2005, the Fukutsu government and Ministry of Land, infrastructure, Transportation and Tourism of Fukutsu Bureau, academia (university researchers and other experts) and citizens active

in this effort and joined to create a network. Every season the stakeholders who initiate river restoration projects include private individuals, non-governmental organizations (NGOs), governmental organizations and various collaborative combinations of the above and the restoration community (practitioners, decision makers and scientists) conduct comprehension workshop for this river, which administrative organizations perform discussion and cooperation each other for constructing and coordinating an agreement toward success this river, Figure 5. Such activities are designed to love this river, such as education for elementary school students in which students played with aquatic life in the Kamisaigo River, clean up, cut the grass and plant the flower that a key to keeping this river beautiful, and other various events, Figure 6.



Figure 5. The stakeholder and the restoration community conduct comprehension workshop every season



Figure 6. Education on river environment

Conclusion

This workshop showed the relationship between citizens, City Government, and University of mutual trust has been established, that have been made landscape, environment, usage, etc: retaining wall maintenance, hydrophilic zone, landscape zone, nature walks zone: adjacent medical facilities and adjacent to large commercial facilities. Propose of Nature walks zone with point of the design: provide slope that the wheelchair can access and walking paths to enjoy the scenery, and summary of the Kamisaigo River workshop: creating a multi-model study and creation of natural rivers.

Acknowledgements

Thank you for opportunity to write this paper at 18th International Conference on Civil and Environmental Engineering (ICCEE 2016). This work was supported by a grant from the Japan Bank International Corporation and by the Watershed Management Laboratory, Department of Urban and Environmental Engineering, Kyushu University.

Literature cited

Chihiro Yoshimura, Tatsuo Omura, Hiroaki Furumai, and Klement Tockner, 2005. *Present state of rivers and streams in Japan*, River Research and Application, 21:93-112. (www.interscience.wiley.com).

David L Rosgen, 2011. *Natural Channel Design: Fundamental Concepts, Assumptions, and Methods. (Stream restoration in the Dynamic Fluvial System: Scientific, Approaches, Analyses, and Tools)* Geophysical monograph Series 194 American Geophysical Union.

Ellen Wohl, Paul L. Angermeier, Brian Bledsoe, G. Matthias Kondolf, Larry MacDonnell, David M. Merritt, Margaret A. Palmer, N. Leroy Poff, and David Tarboton, 2004. *River Restoration*. Draft ms, 9/04, version 2.4. www.cuahsi.org/.../Wohl-20040923-paper.pdf

Kazuo Okayama and Noboru Maruoka, *Conservation and restoration of river environment*. IWRA. www.mlit.go.jp/river/trash.../english.html

Kenji Kanao, Hisanobu Sato, and Tomomi Tanikawa, *The Effort to Improve River Environments in Japan*. River Bureau, Ministry of Land, Infrastructure and Transport.

P.H. Nienhuis, A.D. Buijse, R.S.E.W. Leuven, A.J.M. Smits, R.J.W. De Nooij & E.M. Samborska, 2002. *Ecological rehabilitation of the lowland basin of the river Rhine (NW Europe)*. *Hydrobiologia* 478: 53–72

Republic of Korea, The river revitalization of Korea, *The four river restoration project of Korea*.

Sophia Jane Findlay and Mark Patrick Taylor, 2006. *Why rehabilitate urban river systems?* Area 38.3, 312–325.

Stephen Darby and David Sear, 2007. *River Restoration. Managing the Uncertainty in Restoring Physical Habitat*. John Wiley and Sons, Ltd. ISBN 978-0-470-86706-8

The River Restoration Centre, 2002. *Manual of River Restoration Techniques, RRC – Web Edition*.

USDA NRCS, 2012. *Guidance for Stream Restoration*. Technical Notes USDA Natural Resources Conservation Service. Colorado. Engineering No 27.1

U.S. Department of the Interior Bureau of Reclamation, 2002. *Physical Processes, Human Impacts, and Restoration Issues of the Lower Dungeness River Clallam County, Washington*.

Yukihiro Shimatani. 2007. *Restoration of rivers and lakes in Japan*. Arranged by Keigo Nakamura, River Restoration Team, Water Environment Research Group Public Works Research Institute. <http://www.pwri.go.jp/team/kasenseitai/eng/index.htm>

Y. W. Zhao, Z. F. Yang, and F. Xu, 2007. *The theoretical framework of the urban river restoration planning*. Environmental Informatics Archives, Volume 5, 241- 247

Measuring Banking Systemic Risk CoVaR and CoES in Taiwan Using Vector Quantile GARCH Model

Ender Su, Kai Wen Wong, I-Ling Ju, Ya-Ling Wang

Abstract—In this study, the systemic risk change of Taiwan's banking sector is analyzed during the financial crisis. The risk expose of each financial institutions to the whole Taiwan banking systemic risk or vice versa under financial distress are measured by conditional Value-at-Risk (CoVaR) and conditional coherent expected shortfall (CoES). The CoVaR and CoES are estimated by using vector quantile autoregression (MVMQ-CaViaR) with the daily stock returns of each banks included domestic and foreign banks in Taiwan. The daily in-sample data covered the period from 05/20/2002 to 07/31/2007 and the out-of-sample period until 12/31/2013 spanning the 2008 U.S. subprime crisis, 2010 Greek debt crisis, and post risk duration. All banks in Taiwan are categories into several groups according to their size of market capital, leverage and domestic/foreign to find out what the extent of changes of the systemic risk as the risk changes between the individuals in the bank groups and vice versa. The final results can provide a guidance to financial supervisory commission of Taiwan to gauge the downside risk in the system of financial institutions and determine the minimum capital requirement hold by financial institutions due to the sensibility changes in CoVaR and CoES of each banks.

Keywords—bank financial distress, vector quantile autoregression, CoVaR, CoES

Associate Professor of Risk Management and Insurance, National Kaohsiung First University of Science and TechnologyNo.2, Jhuoyue Rd., NansihDistrict,KaohsiungCity811,Taiwan, R.O.C.Phone:886-7-6011000-3022; Email: suender@ccms.nkfust.edu.tw

Corresponding author, Master Program of Risk Management and Insurance, National Kaohsiung First University of Science and TechnologyNo.2, Jhuoyue Rd.,NansihDistrict,KaohsiungCity811,Taiwan,R.O.C.Phone:886-7-6011000-3022; Email: kelvin1189@gmail.com

Master Program of Risk Management and Insurance, National Kaohsiung First University of Science and TechnologyNo.2, Jhuoyue Rd., Nansih District, Kaohsiung City 811, Taiwan, R.O.C.Phone:886-7-6011000-3022; Email: lovenow1113@gmail.com

Master Program of Risk Management and Insurance, National Kaohsiung First University of Science and TechnologyNo.2, Jhuoyue Rd., Nansih District, Kaohsiung City 811, Taiwan, R.O.C.Phone:886-7-6011000-3022; Email: iris110902@gmail.com

Method Development for the Determination of Gamma-Aminobutyric Acid in Rice Products by LC-MS-MS

Cher Rong Matthew Kong, Edmund Tian, Seng Poon Ong, Chee Sian Gan

Abstract—Gamma-aminobutyric acid (GABA) is a non-protein amino acid that is a functional constituent of certain rice varieties. When consumed, it decreases blood pressure and reduces the risk of hypertension-related diseases. This has led to more research dedicated towards the development of functional food products (e.g. germinated brown rice) with enhanced GABA content, and the development of these functional food products has led to increased demand for instrument-based methods that can efficiently and effectively determine GABA content. Current analytical methods require analyte derivatisation, and have significant disadvantages such as being labour intensive and time-consuming, and being subject to analyte loss due to the increased complexity of the sample preparation process. To address this, an LC-MS-MS method for the determination of GABA in rice products has been developed and validated. This developed method involves a relatively simple sample preparation process before analysis using HILIC LC-MS-MS. This method eliminates the need for derivatisation, thereby significantly reducing the labour and time associated with such an analysis. Using LC-MS-MS also allows for better differentiation of GABA from any potential co-eluting compounds in the sample matrix. Results obtained from the developed method demonstrated high linearity, accuracy, and precision for the determination of GABA (1ng/L to 8ng/L) in a variety of brown rice products. The method can significantly simplify sample preparation steps, improve the accuracy of quantitation, and increase the throughput of analyses, thereby providing a quick but effective alternative to established instrumental analysis methods for GABA in rice.

Keywords—functional food, gamma-aminobutyric acid, germinated brown rice, method development

Corresponding Author

Matthew Kong from Temasek Polytechnic, Singapore
e-mail: kongcr@tp.edu.sg

Microwave Assisted for Synthesize of Polysulfide Urethane Acrylate

Zohreh Khoshnevisan, Behzad Shirkavand Hadavand

Abstract—In the recent decades the use of microwave irradiation has become a common heat source in chemical reactions such as preparation of organic compounds and polymer synthesis. The importance of this method is using low energy and short reaction times. This study looks at the synthesis of polysulfide urethane acrylate by microwave radiation. At first the polymerization carries out in a small vessel using 2 mol isophorone diisocyanate (IPDI), 1 mol polysulfide polymer in presence of dibutyltin dilaurate (DBTDL) as catalyst and then 2 mol of 2-hydroxyethyl methacrylate (HEMA) were added to the prepared urethane polysulfide for acrylation. After characterization by FTIR spectroscopy, the effect of microwave power and reaction time were studied and discussed. Also the conversion of the reaction was followed by FTIR spectroscopy.

Keywords—microwave irradiation, UV-cure, polymerization, urethane acrylate, polysulfide polymer

Corresponding Author

Zohreh Khoshnevisan from Tehran Payame Nour University, Iran,
Islamic Republic Of
e-mail: z_khoshnevisan@yahoo.com

Mineral Status of Feeds And Fodder and Its Subsequent Effect On Plasma Of Livestock and Its Products in Red Lateritic Zone Of West Bengal, India

S.K.Pyne¹, M.Mondal² and G.Samanta³

¹Professor in Animal Science, Deptt. of ASEPAN, Palli Siksha Bhavana (Institute of Agriculture), Sriniketan, Visva-Bharati, Birbhum, West Bengal, India .

²Assistant Superintendent of Livestock, State Poultry Farm, Kakdwip, South 24 Parganas, West Bengal, E-mail. mmondal64@yahoo.co.in, Ph. +919800363744.

³Professor, Deptt. of Animal Nutrition, F/O, Vety. and Animal Sciences. West Bengal University of Animal and Fishery Sciences, Kolkata-37, West Bengal, India.

ABSTRACT

A survey was carried out in red lateritic zone of West Bengal to compare the mineral status in plasma of livestock grazing over red lateritic region. Sufficient number of samples of soil, feeds, fodder and blood were collected from four districts of red lateritic zone namely, West Midnapore, Birbhum, Bankura and Purulia respectively. The samples were analysed for Calcium (Ca), Phosphorus (P), Copper (Cu), Zinc (Zn), Manganese (Mn) and Iron (Fe). Concentration of Cu, Mn and Fe in soil were above the minimum critical level, whereas, Zn deficiency is wide spread in red lateritic soil. Paddy straw is deficient in Ca, P, Zn and Mn in the region. Green fodders are also deficient in P, Cu, Zn. Richness of iron (Fe) in soil, feeds, fodder and tree leaves is the characteristics of this region. Phosphorus is deficient in plasma of all categories of livestock with the exception of bullock. Cu is deficient in plasma of calf. Plasma Mn and Fe were higher ($p < 0.01$) in the animals of red lateritic zone. The study reveals that the overall deficiency of phosphorus in different categories of livestock and there is need of dietary supplementation.

Key words: Mineral, Red lateritic zone, Grazing livestock, Plasma

Mixed Integer Programming-based One-Class Classification Method for Process Monitoring

Younghoon Kim, Seoung Bum Kim

Abstract—One-class classification plays an important role in detecting outlier and abnormality from normal observations. In the previous research, several attempts were made to extend the scope of application of the one-class classification techniques to statistical process control problems. For most previous approaches, such as support vector data description (SVDD) control chart, the design of the control limits is commonly based on the assumption that the proportion of abnormal observations is approximately equal to an expected Type I error rate in Phase I process. Because of the limitation of the one-class classification techniques based on convex optimization, we cannot make the proportion of abnormal observations exactly equal to expected Type I error rate: controlling Type I error rate requires to optimize constraints with integer decision variables, but convex optimization cannot satisfy the requirement. This limitation would be undesirable in theoretical and practical perspective to construct effective control charts. In this work, to address the limitation of previous approaches, we propose the one-class classification algorithm based on the mixed integer programming technique, which can solve problems formulated with continuous and integer decision variables. The proposed method minimizes the radius of a spherically shaped boundary subject to the number of normal data to be equal to a constant value specified by users. By modifying this constant value, users can exactly control the proportion of normal data described by the spherically shaped boundary. Thus, the proportion of abnormal observations can be made theoretically equal to an expected Type I error rate in Phase I process. Moreover, analogous to SVDD, the boundary can be made to describe complex structures by using some kernel functions. New multivariate control chart applying the effectiveness of the algorithm is proposed. This chart uses a monitoring statistic to characterize the degree of being an abnormal point as obtained through the proposed one-class classification. The control limit of the proposed chart is established by the radius of the boundary. The usefulness of the proposed method was demonstrated through experiments with simulated and real process data from a thin film transistor-liquid crystal display.

Keywords—control chart, mixed integer programming, one-class classification, support vector data description.

Younghoon Kim is with the Department of Industrial Management Engineering, Korea University, Seoul, Korea (phone: 82-2-3290-3769; fax: 82-2-929-5888; e-mail: younghoon.kim11@gmail.com).

Seoung Bum Kim is with the Department of Industrial Management Engineering, Korea University, Seoul, Korea (phone: 82-2-3290-3397; fax: 82-2-929-5888; e-mail: sbkim1@korea.ac.kr).

Nurturing Students' Creativity through Engagement in Problem Posing and Self-Assessment of its Development

Atara Shriki, Ilana Lavy

Abstract— In a rapidly changing technological society, creativity is considered as an engine of economic and social progress. No doubt the education system has a central role in nurturing all students' creativity, however it is normally not encouraged at school. The causes of this reality are related to a variety of circumstances, among them: external pressures to cover the curriculum and succeed in standardized tests that mostly require algorithmic thinking and implementation of rules; teachers' tendency to teach similarly to the way they themselves were taught as school students; relating creativity to giftedness, and therefore avoid nurturing all students' creativity; lack of adequate learning materials and accessible tools for following and evaluating the development of students' creativity; and more. Since success in academic studies requires, among other things, creativity, lecturers in higher education institutions should consider appropriate ways to nurture students' creative thinking and assess its development.

Obviously, creativity has a multifaceted nature, numerous definitions, various perspectives for studying its essence (e.g., process, personality, environment, and product), and several approaches aimed at evaluating and assessing creative expressions (e.g., cognitive, social-personal, and psychometric).

In this framework, we suggest to nurture students' creativity through engaging them in problem posing activities that are part of inquiry assignments. In order to assess the development of their creativity, we propose to employ a model that was designed for this purpose, based on the psychometric approach, viewing the posed problems as the "creative product". The model considers four measurable aspects- fluency, flexibility, originality and organization, as well as a total score of creativity that reflects the relative weights of each aspect. The scores given to learners are of two types:

- (1) Total scores- the absolute number of posed problems with respect to each of the four aspects, and a final score of creativity;
- (2) Relative scores- each absolute number is transformed into a number that relates to the relative infrequency of the posed problems in student's reference group.

Through converting the scores received over time into a graphical display, students can assess their progress both with respect to themselves and relative to their reference group. Course lecturers can get a picture about the strengths and weaknesses of each student as well as the class as a whole, and to track changes that occur over time in response to the learning environment they had generated. Such tracking may assist lecturers in making pedagogical decisions about emphases that should be put on one or more aspects of creativity, and about the students that should be given a special attention.

Our experience indicates that schoolteachers and lecturers in higher education institutes find the combination of engaging learners

in problem posing along with self-assessment of their progress through utilizing the graphical display of accumulating total and relative scores has the potential to realize most learners' creative potential.

Keywords—Creativity, problem posing, psychometric model, self-assessment.

Atara Shriki is with Oranim- Academic College of Education, ISRAEL (e-mail: atrashriki@gmail.com).

Ilana Lavy is with the Academic College of Yezreel Valley, ISRAEL. (Phone: 972-4-6423519; fax: 972-4-6423517; e-mail: ilanal@yvc.ac.il).

**ON QUASI CONFORMALLY FLAT LP-SASAKIAN
MANIFOLDS WITH A COEFFICIENT α**

JAY PRAKASH SINGH

DEPARTMENT OF MATHEMATICS AND COMPUTER SCIENCE
MIZORAM UNIVERSITY
TANHRIL, AIZAWL-796004, INDIA.
e-mail: jpsmaths@gmail.com

ABSTRACT. The notion of Lorentzian almost Paracontact manifolds with a coefficient α has been introduced and studied by De et al [2]. The object of the present paper is to study some properties of Quasi Conformally flat LP-Sasakian manifolds with a coefficient α .

1. INTRODUCTION

The notion of LP-Sasakian manifolds has been introduced by Matsumoto [4]. Then in this line Mihai and Rosca [5] introduced the same notion independently and obtained several results in this manifolds. In 2002, De et al [2] introduced the notion of LP-Sasakian manifolds with a coefficient α which generalizes the notion of LP-Sasakian manifolds. In [3], De et al studied this manifolds with conformally flat curvature tensor and then Bagewadi et al [1] investigated it with pseudo projectively flat curvature tensor.

In 1968, Yano and Sawaki [8] defined and studied a tensor field W of type $(1, 3)$ which includes both the conformal curvature tensor and the concircular curvature tensor as special cases and called Quasi conformal curvature tensor which is given as

$$\begin{aligned} W(X, Y)Z &= aR(X, Y)Z + b[S(Y, Z)X - S(X, Z)Y + g(Y, Z)QX \\ &\quad - g(X, Z)QY] - \frac{r}{n} \left(\frac{a}{n-1} + 2b \right) \{ g(Y, Z)X \\ &\quad - g(X, Z)Y \}, \end{aligned} \tag{1.1}$$

where R, S, Q, r denotes curvature tensor, Ricci tensor, Ricci operator, scalar curvature tensor respectively and a, b are arbitrary constant not simultaneously zero. Motivated by these studies in this paper, we have studied some properties of Quasi conformally flat LP-Sasakian manifolds with a coefficient

Mathematics Subject Classification (2010). 53C50, 53D15.

Keywords and Phrases. LP-Sasakian manifolds with a coefficient α , Quasi conformal curvature tensor, concircular vector field, torse forming vector field, η -Einstein manifold

α . Here we prove that in a Quasi conformally flat LP-Sasakian manifolds with a coefficient α , the characteristic vector field ξ is a concircular vector field if and only if the manifold is η -Einstein. Finally we prove that Quasi conformally flat LP-Sasakian manifolds with a coefficient α is a manifold of constant curvature if the scalar curvature r is constant.

2. PRELIMINARIES

Let M be an n -dimensional differentiable manifold endowed with a $(1, 1)$ tensor field ϕ , a contravariant vector field ξ , a covariant vector field η and a Lorentzian metric g of type $(1, 2)$ such that for each point $p \in M$, the tensor $g_p : T_p M \times T_p M \rightarrow \mathbb{R}$ is a non degenerate inner product of signature $(-, +, +, \dots, +)$ where $T_p M$ denotes the tangent vector space of M at p and \mathbb{R} is real number space, which satisfies

$$\eta(\xi) = -1, \quad \phi^2 X + X + \eta(X)\xi \quad (2.1)$$

$$g(X, \xi) = \eta(X), \quad g(\phi X, \phi Y) = g(X, Y) + \eta(X)\eta(Y), \quad (2.2)$$

for all vector fields X, Y . The structures (ϕ, ξ, η, g) is said to be Lorentzian almost paracontact structure and the manifold M with the structures (ϕ, ξ, η, g) is called Lorentzian almost paracontact manifold [4]. In the Lorentzian almost paracontact manifold M , the following relations hold [4]:

$$\phi\xi = 0, \quad \eta(\phi X) = 0, \quad (2.3)$$

$$\Omega(X, Y) = \Omega(Y, X) \quad \text{where} \quad \Omega(X, Y) = g(X, \phi Y). \quad (2.4)$$

In the Lorentzian almost Paracontact manifold M , if the relations

$$\begin{aligned} (D_Z \Omega)(X, Y) &= \alpha \{ \{ g(X, Z) + \eta(X)\eta(Z) \} \eta(Y) \\ &+ \{ g(Y, Z) + \eta(Y)\eta(Z) \} \eta(X) \}, \quad (\alpha \neq 0), \end{aligned} \quad (2.5)$$

$$\Omega(X, Y) = \frac{1}{\alpha} (D_X \eta)(Y), \quad (2.6)$$

hold where D denotes the operator of covariant differentiation with respect to the Lorentzian metric g , then M is called an LP-Sasakian manifold with a coefficient α [2]. An LP-Sasakian manifolds with a coefficient $\alpha = 1$ is an LP-Sasakian manifold [4].

If a vector field V satisfies the equation

$$D_X V = \beta X + T(X)V,$$

where β is a non zero scalar function and T is a covariant vector field, then V is called a torse forming vector field [7]. In a Lorentzian manifold M , if we assume that ξ is a unit torse forming vector field, then we have the following equation

$$(D_X \eta)(Y) = \alpha [g(X, Y) + \eta(X)\eta(Y)], \quad (2.7)$$

where α is a non zero scalar function. Hence the manifold admitting a unit torse forming vector field satisfying (2.7) is an LP-Sasakian manifolds with a coefficient α . Especially, if η satisfies

$$(D_X\eta)(Y) = \epsilon [g(X, Y) + \eta(X)\eta(Y)], \quad \epsilon^2 = 1 \quad (2.8)$$

then M is called an LSP-Sasakian manifold [4]. In particular if α satisfies (2.7) and the following equation

$$\alpha(X) = p \eta(X), \quad \alpha(X) = D_X\alpha, \quad (2.9)$$

where p is a scalar function, then ξ is called a concircular vector field.

Let us consider an LP-Sasakian manifolds $M(\phi, \xi, \eta, g)$ with a coefficient α . Then we have the following relations [4]

$$\begin{aligned} \eta(R(X, Y)Z) &= -\alpha(X)\Omega(Y, Z) + \alpha(Y)\Omega(X, Z) \\ &+ \alpha^2\{g(Y, Z)\eta(X) - g(X, Z)\eta(Y)\}, \end{aligned} \quad (2.10)$$

$$S(X, \xi) = -\Psi \alpha(X) + (n-1)\alpha^2\eta(X) + \alpha(\phi X), \quad (2.11)$$

where $\Psi = \text{Trace}(\phi)$.

We now state the following results which will be needed in the later section.

Lemma 2.1. [2] *In an LP-Sasakian manifolds M with a coefficient α , one of the following cases occur:*

- i) $\Psi^2 = (n-1)^2$
- ii) $\alpha(Y) = -p \eta(Y)$, where $p = \alpha(\xi)$.

Lemma 2.2. [2] *In a Lorentzian almost paracontact manifold M with its structure (ϕ, ξ, η, g) satisfying $\Omega(X, Y) = \frac{1}{\alpha}(D_X\eta)(Y)$, where α is a non-zero scalar function, the vector field ξ is a torse forming if and only if the relation $\Psi^2 = (n-1)^2$ holds good.*

3. QUASI CONFORMALLY FLAT LP-SASAKIAN MANIFOLDS WITH A COEFFICIENT α

Let us consider a Quasi conformally flat LP-Sasakian manifold $M(n > 3)$ with a coefficient α . Then, since the quasi conformal curvature tensor W vanishes, the equation (1.1) reduces to

$$\begin{aligned} R(X, Y, Z, U) &= -\frac{b}{a}[S(Y, Z)g(X, U) - S(X, Z)g(Y, U) + S(X, U)g(Y, Z) \\ &- g(X, Z)S(Y, U)] \\ &+ \frac{r}{n}\left(\frac{1}{n-1} + \frac{2b}{a}\right)(g(Y, Z)g(X, U) - g(X, Z)g(Y, U)). \end{aligned} \quad (3.1)$$

Putting $U = \xi$ in (3.1) and using (2.10) and (2.11), we get

$$\begin{aligned}
 -\alpha(X)\Omega(Y, Z) &+ \alpha(Y)\Omega(X, Z) + \alpha^2\{g(Y, Z)\eta(X) - g(X, Z)\eta(Y)\} \\
 &= -\frac{b}{a}\{S(Y, Z)\eta(X) - S(X, Z)\eta(Y)\} \\
 &+ g(Y, Z)\{-\Psi\alpha(X) + (n-1)\alpha^2\eta(X) + \alpha(\phi X)\} \\
 &- g(X, Z)\{-\Psi\alpha(Y) + (n-1)\alpha^2\eta(Y) + \alpha(\phi Y)\} \\
 &+ \frac{r}{n}\left(\frac{1}{n-1} + \frac{2b}{a}\right)(g(Y, Z)\eta(X) - g(X, Z)\eta(Y)). \quad (3.2)
 \end{aligned}$$

Again putting $X = \xi$ in (3.2) and using (2.3) and (2.11), we obtain by straightforward calculations

$$\begin{aligned}
 S(Y, Z) &= \left\{\frac{ar}{n(n-1)b} + \frac{2r}{n} - p\Psi - (n-1)\alpha^2 - \frac{a}{b}\alpha^2\right\}g(Y, Z) \\
 &+ \left\{\frac{ar}{n(n-1)b} + \frac{2r}{n} - 2(n-1)\alpha^2 - \frac{a}{b}\alpha^2\right\}\eta(Y)\eta(Z) \\
 &+ \{\Psi\alpha(Z) - \alpha(\phi Z)\}\eta(Y) + \{\Psi\alpha(Y) - \alpha(\phi Y)\}\eta(Z) \\
 &- \frac{a}{b}p\Omega(Y, Z), \quad (3.3)
 \end{aligned}$$

where $p = \alpha(\xi)$.

If an LP-Sasakian manifolds M with a coefficient α satisfies the relation

$$S(X, Y) = c g(X, Y) + d \eta(X) \eta(Y),$$

where c, d are associated functions on the manifold, then the manifold M is said to be an η -Einstein manifold. Now, we have [2]

$$\begin{aligned}
 S(X, Y) &= \left[\frac{r}{n-1} - \alpha^2 - \frac{p\Psi}{n-1}\right]g(X, Y) \\
 &+ \left[\frac{r}{n-1} - \alpha^2 - \frac{np\Psi}{n-1}\right]\eta(X)\eta(Y). \quad (3.4)
 \end{aligned}$$

Contracting (3.4), we obtain

$$r = n(n-1)\alpha^2 + np\Psi. \quad (3.5)$$

By vitue of (3.3) and (3.4), we get

$$\begin{aligned}
 &\left[\frac{\{a + (n-2)b\}r}{n(n-1)b} - \{a + (n-2)b\}\frac{\alpha^2}{b} + \frac{(2-n)p\Psi}{n-1}\right]g(Y, Z) \\
 &+ \left[\frac{\{a + (n-2)b\}r}{n(n-1)b} - \{a + (n-2)b\}\frac{\alpha^2}{b} + \frac{np\Psi}{n-1}\right]\eta(Y)\eta(Z) \\
 &+ \{\Psi\alpha(Z) - \alpha(\phi Z)\}\eta(Y) + \{\Psi\alpha(Y) - \alpha(\phi Y)\}\eta(Z) \\
 &- p \cdot \frac{a}{b}\Omega(Y, Z) = 0. \quad (3.6)
 \end{aligned}$$

Putting $Z = \xi$ in (3.6) we obtain

$$\Psi\alpha(Y) - \alpha(\phi Y) = -\Psi p \eta(Y), \quad (3.7)$$

for all vector fields Y . In consequence of (3.5) and (3.7) the equation (3.6) becomes

$$\frac{a}{b} \left[\frac{\Psi}{n-1} \{g(Y, Z) + \eta(Y) \eta(Z)\} - \Omega(Y, Z) \right] = 0. \quad (3.8)$$

If $p = 0$, then from (3.7) we have $\alpha(\phi Y) = \Psi \alpha(Y)$. Thus since Ψ is an eigenvalue value of the matrix ϕ , Ψ is equal to ± 1 . Hence by lemma(2.1), we get $\alpha(Y) = 0$ for all Y and hence α is constant which contradict to our assumption.

Consequently, we have $p \neq 0$ and hence from (3.8) we get

$$\frac{a}{b} \left[\frac{\Psi}{n-1} \{g(Y, Z) + \eta(Y) \eta(Z)\} - \Omega(Y, Z) \right] = 0. \quad (3.9)$$

Replacing Y by ϕY in (3.9) and using (2.3) we get

$$\frac{a}{b} \left[\Omega(Y, Z) - \frac{\Psi}{n-1} \{g(Y, Z) + \eta(Y) \eta(Z)\} \right] = 0. \quad (3.10)$$

Combining (3.9) and (3.10), we get

$$\{\Psi^2 - (n-1)^2\} [g(Y, Z) + \eta(Y) \eta(Z)] = 0,$$

which gives by virtue $n > 3$

$$\Psi^2 = (n-1)^2. \quad (3.11)$$

Hence lemma (2.2) proves that ξ is torse forming.

We have

$$(D_X \eta)(Y) = \beta \{g(X, Y) + \eta(X) \eta(Y)\}.$$

Now from (2.6) we get

$$\Omega(X, Y) = \frac{\beta}{\alpha} \{g(X, Y) + \eta(X) \eta(Y)\} = g\left(\frac{\beta}{\alpha}(X + \eta(X) \xi), Y\right),$$

and $\Omega(X, Y) = g(X, \phi Y)$.

Since g is non singular, we have

$$\phi(X) = \frac{\beta}{\alpha}(X + \eta(X) \xi)$$

and

$$\phi^2(X) = \left(\frac{\beta}{\alpha}\right)^2 (X + \eta(X) \xi).$$

It follows from (2.1) that $\left(\frac{\beta}{\alpha}\right)^2 = 1$ and hence $\alpha = \pm\beta$. thus, we have

$$\phi(X) = \pm (X + \eta(X) \xi).$$

By virtue of (3.7) we see that $\alpha(Y) = -p \eta(Y)$. Thus we conclude that ξ is a concircular vector field.

Conversely suppose that ξ is a concircular vector field. Then we have the following equation

$$(D_X\eta)(Y) = \beta\{g(X, Y) + \eta(X) \eta(Y)\},$$

where β is certain function and $D_X\beta = q \eta(X)$ for a certain scalar function q . Hence by virtue of (2.6), we have $\alpha = \pm\beta$. Thus

$$\Omega(X, Y) = \epsilon\{g(X, Y) + \eta(X) \eta(Y)\}, \quad \epsilon^2 = 1,$$

$$\Psi = \epsilon (n - 1), \quad D_X\alpha = \alpha(X) = p \eta(X), \quad p = \epsilon q.$$

Using these relations and (3.7) in (3.3), it can be easily seen that M is η -Einstein manifold. This leads to the following theorem:

Theorem 3.1. *In a Quasi conformally flat LP-Sasakian manifold M ($n > 3$) with a non constant coefficient α , the characteristic vector field ξ is a concircular vector field if and only if M is η -Einstein manifold.*

Next we consider the case when α is constant. In this case the following relations hold:

$$\eta(R(X, Y)Z) = \alpha^2\{g(Y, Z)\eta(X) - g(X, Z)\eta(Y)\}, \quad (3.12)$$

$$S(X, \xi) = (n - 1) \eta(X). \quad (3.13)$$

Putting $U = \xi$ in (3.1) and then using (3.12) and (3.13) we get

$$\begin{aligned} & \alpha^2\{g(Y, Z)\eta(X) - g(X, Z)\eta(Y)\} \\ &= -\frac{b}{a}[S(Y, Z)\eta(X) - S(Y, Z)\eta(Y) \\ &+ (n - 1) \alpha^2 g(Y, Z)\eta(X) \\ &- (n - 1) \alpha^2 g(X, Z)\eta(Y)] \\ &+ \frac{r}{n}(\frac{1}{n - 1} + \frac{2b}{a})(g(Y, Z)\eta(X) - g(X, Z)\eta(Y)). \end{aligned}$$

Again putting $X = \xi$ in above and making use of (3.13) we get

$$\begin{aligned} S(Y, Z) &= [\frac{\{a + 2b(n - 1)\}r}{b n(n - 1)} - \frac{\alpha^2}{b}\{a + b(n - 1)\}]g(Y, Z) \\ &+ [\frac{\{a + 2b(n - 1)\}r}{b n(n - 1)} - \frac{\alpha^2}{b}\{a \\ &+ 2 b(n - 1)\}]\eta(Y) \eta(Z). \end{aligned} \quad (3.14)$$

Thus , we can state the following theorem:

Theorem 3.2. *A Quasi conformally flat LP-Sasakian manifold M ($n > 3$) with a constant coefficient α is an η -Einstein.*

Differentiating covariantly (3.14) along X and making use of (2.6) we obtain

$$\begin{aligned} (D_X S)(Y, Z) &= \frac{dr(X)}{b(n-1)n} \{a + 2b(n-1)\} \cdot \{g(Y, Z) + \eta(Y)\eta(Z)\} \\ &+ \frac{\alpha\{a + 2b(n-1)\}}{b} \left(\frac{r}{n(n-1)} - \alpha^2\right) \times \\ &\quad \{\Omega(X, Y)\eta(Z) + \Omega(X, Z)\eta(Y)\}, \end{aligned} \quad (3.15)$$

where $dr(X) = D_X r$.

This implies that

$$\begin{aligned} (D_X S)(Y, Z) - (D_Y S)(X, Z) &= \frac{dr(X)}{n} \left(2 + \frac{a}{b(n-1)}\right) \{g(Y, Z) + \eta(Y)\eta(Z)\} \\ &- \frac{dr(Y)}{n} \left(2 + \frac{a}{b(n-1)}\right) \{g(X, Z) + \eta(X)\eta(Z)\} \\ &+ \frac{\alpha}{b} \{a + 2b(n-1)\} \left(\frac{r}{n(n-1)} - \alpha^2\right) \times \\ &\quad \{\Omega(X, Z)\eta(Y) - \Omega(Y, Z)\eta(X)\}. \end{aligned} \quad (3.16)$$

On the other hand we also have for a Quasi conformally flat curvature tensor [6]

$$\begin{aligned} (D_X S)(Y, Z) - (D_Y S)(X, Z) &= \frac{\{2a - (n-1)(n-4)b\}}{2(a+b)n(n-1)} [dr(X)g(Y, Z) \\ &- dr(Y)g(X, Z)], \end{aligned} \quad (3.17)$$

provided $a + 2b(n-1) \neq 0$.

From (3.16) and (3.17) it follows that

$$\begin{aligned} &\frac{dr(X)}{n} \left(2 + \frac{a}{b(n-1)}\right) \{g(Y, Z) + \eta(Y)\eta(Z)\} \\ &- \frac{dr(Y)}{n} \left(2 + \frac{a}{b(n-1)}\right) \{g(X, Z) + \eta(X)\eta(Z)\} \\ &+ \frac{\alpha}{b} (a + 2(n-1)b) \left(\frac{r}{n(n-1)} - \alpha^2\right) \times \\ &\quad \{\Omega(X, Z)\eta(Y) - \Omega(Y, Z)\eta(X)\} \\ &= \frac{\{2a - (n-1)(n-4)b\}}{2(a+b)n(n-1)} [dr(X)g(Y, Z) \\ &- dr(Y)g(X, Z)]. \end{aligned} \quad (3.18)$$

If r is constant then equation (3.18) yields

$$r = n(n-1)\alpha^2.$$

Hence from (3.1) it follows that

$$R(X, Y, Z, U) = \alpha^2[g(Y, Z)g(X, U) - g(X, Z)g(Y, U)],$$

which shows that the manifold is of constant curvature. Thus we can state the following:

Theorem 3.3. *In a quasi conformally flat LP-Sasakian manifold M ($n > 3$) with a constant coefficient α if the scalar curvature tensor is constant then M is of constant curvature.*

REFERENCES

- [1] Bagewadi, C.S.,Prakasha,D.G. and Venkatesha, On pseudo projectively flat LP-Sasakian manifold with a coefficient α ,Ann. Univ. Mariae C.S. Lubin-Polonia LXI (2007), 1-8.
- [2] De,U.C., Shaikh,A.A. and Sengupta,A., On LP-Sasakian manifold with a coefficient α ,Kyungpook Math.J. **42** (2002),177-186.
- [3] De,U.C., Jun,J.B. and Shaikh,A.A., On Conformally flat LP-Sasakian manifold with a coefficient α ,Nihonkai Math.J.**13**(2002), 121-131.
- [4] Matsumoto,K., On Lorentzian para contact manifolds,Bull.of Yamagata Univ. Nat. Sci.**12** (1989),151-156.
- [5] Mihai,I. and Rosca,R., On Lorentzian P-Sasakian manifolds, Classical Analysis, World Sci.Pub.Singapore (1992),155-169.
- [6] Shaikh,A.A.,Hui,S.K. and Bagewadi,C.S., On Quasi conformally flat almost pseudo ricci symmetric manifolds, Tamsui oxford J. of math.Sci. **26** (2) (2010),203-219.
- [7] Yano,K., On the torse forming direction in Riemannian spaces, proc.Imp. Acad.Tokyo **20** (1944),340-345.
- [8] Yano,K. and Sawaki,S., Riemannian manifolds admitting a conformal transformation group,J.Diff.Geo.(1968),161-184.

On the Transition of Europe's Power Sector: Economic Consequences of National Targets

Geoffrey J. Blanford, Christoph Weissbart

Abstract—The prospects for the European power sector indicate that it has to almost fully decarbonize by 2050 in order to reach the economy-wide target of an 80% CO₂-emission reduction. We apply the EU-REGEN model to explain the penetration of RES from an economic perspective, their spatial distribution, and the complementary role of conventional generation technologies. Furthermore, we identify economic consequences of national energy and climate targets. Our study shows that onshore wind power will be the most crucial generation technology for the future European power sector. Its geographic distribution is driven by resource quality. Gas power will be the major conventional generation technology for backing-up wind power. Moreover, a complete phase out of coal power proves to be not economically optimal. The paper demonstrates that existing national targets have a negative impact, especially on the German region with higher prices and lower revenues. The remaining regions profit are hardly affected. We encourage an EU-wide coordination on the expansion of wind power with harmonized policies. Yet, this requires profitable market structures for both, RES and conventional generation technologies.

Keywords—European decarbonization pathway, power market investment, public policies, technology choice

I. MOTIVATION AND RELATED WORK

SINCE the beginning of the century the energy policy of the European Union (EU) is mainly driven by the decarbonization of the supply side. Studies showed that the power sector will be one of the main leverages to reach the ambitious decarbonization targets. On the one hand, sector coupling and the conversion of power to other energy commodities (e.g. power-to-gas) will result in soaring electricity demand [1], [2]. On the other hand, the electricity generation-mix has to reduce its CO₂-intensity.

Currently, there are three technology options that allow addressing both of the above-mentioned developments: Application of renewable energy sources, nuclear power, or conventional fuel-based generation in combination with carbon capture and storage (CCS).

The 1997, the Kyoto Protocol laid the ground for the first obligatory greenhouse gas (GHG) reduction target. For the member states of that time, the agreement was translated into a mandatory reduction target of 8% compared to 1990 levels. This was followed by the “Energy and Climate Package” in 2008, which resulted in the “20-20-20” targets [3]. Comprising a 20% share of renewable energy sources in

energy consumption, a 20% reduction of GHG emissions compared to 1990 levels, and a 20% reduction of final energy consumption compared to a business-as-usual scenario. Furthermore, each member state had to translate those EU-wide targets into national targets.

To address, the mid- and long-run perspective, the European Commission released “A roadmap for Moving to a Competitive Low Carbon Economy in 2050”, emphasizing a GHG emission-reduction target of at least 80% compared to 1990 levels [1], [4]. In 2014, this decarbonization path was further specified by targets for 2030: a 27% share of renewable energy sources in energy consumption, a 40% reduction of GHG emissions compared to 1990 levels, and a 27% decrease of final energy consumption.

The EC's energy system-wide scenarios indicate that growth of existing load patterns, combined with the above-mentioned electrification and conversion of power, will double electricity generation in 2050 compared to 1990, an increase of 50% compared to the current level. At the same time, most scenarios assume a limited potential of GHG reduction in other sectors. Meaning, the electricity sector has to contribute 98% CO₂-emission reduction in its generation-mix by 2050 to reach the economy-wide target of 80% [2]. *Fig. 1* indicates the required and contrary development of both – electricity generation and CO₂-emissions in the power sector. Moreover, Article 4 of the recently signed Paris agreement points at this by emphasizing the balancing of emissions and sinks by the middle of the century [5].

Simultaneously, we see member countries of the EU announcing additional national climate and energy targets. For instance, Germany targets a reduction of economy-wide emissions of 40% by 2020 and 80% by 2050. Electricity generation from RES should sum up to a share of 35% by 2020 and 80% by 2050. Recently, France introduced a law on the transition of its power sector limiting the share of generation from nuclear power to 50% from 2025 on, setting the share of generation from RES to at least 40% from 2030 on, and targeting a CO₂-emission reduction of 50% by 2030 and 80% by 2050.

Most existing studies on the European power sector emphasize the future role of RES along this path. Their potential, especially for variable renewable energy sources (vRES), is vast and future cost estimates suggest economic viability [6], [7]. Yet, the resources are geographically dispersed and their quality is spatially varying.

A strong strand of literature emphasizes the future role of transmission grid extensions. References [8], [9] look into the role of transmission capacity expansion for the integration of

Christoph Weissbart is with the Ifo Center for Energy, Climate and Exhaustible Resources, Ifo Institute, Munich, Germany (e-mail: weissbart@ifo.de).

Geoffrey J. Blanford is with the Electric Power Research Institute, Pao Alto, U.S.A. (e-mail: gblanford@gmail.com).

high shares of vRES and show the advantages and costs. The authors in [10], [11] point at the benefits of electricity exchange and transmission capacity expansion in a fully RES-powered sector. Similarly, the general importance of transmission grid expansion for the future European power system is analyzed in [12]–[14] looking into the impact of the EC’s RES generation targets for 2030 and the relationship between transmission capacity and RES capacity additions.

Moreover, a pure resource perspective on vRES is taken in [15] by looking at correlations of time-profiles at different spatial locations within Europe. The authors propose to utilize the resulting balancing effect for the integration of vRES. The economics of vRES are analyzed in detail in [16] by emphasizing their market value. We add to this research by showing generation and capacity investment results in the EU-REGEN model.

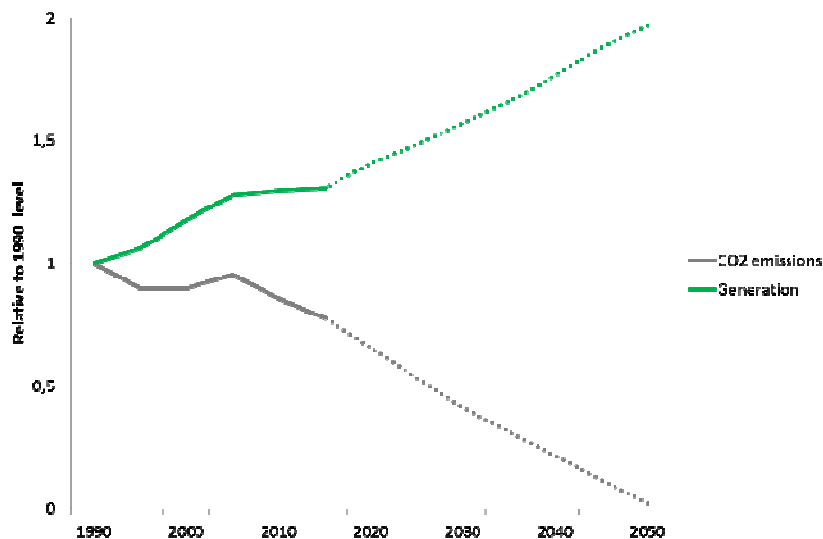


Fig. 1 Path of CO₂-emissions and generation relative to 1990

References [17], [18] focus on the supporting role of flexibility options in the European power system with high levels of vRES generation. This paper adds to this by looking at the sole target of decarbonization and analyzing the importance of CCS or nuclear power in allowing high shares of vRES.

The current political debate in Europe, and Germany especially, sees arguments for an early retirement of lignite and hard coal power plants to reach short- and mid-run climate targets [19], [20]. A recent policy letter on the phase out of coal power in Germany claims that the national climate targets cannot be met with any coal unit remaining online after 2040 [21]. Yet, there is little research on the optimal retirement schedule of conventional generation technologies across Europe with regard to the targeted decarbonization path. In that field, we contribute by analyzing the complementary role of fossil-fuel-based generation technologies and their optimal retirement path.

Additionally, the EC’s long-run climate targets are only specified for Europe as a whole. This means a cost-efficient realization of the EU decarbonization will require the integration of national electricity markets and EU-wide coordination on climate and energy policy. Reference [22] looks at the economics of alternative policy measures for decarbonizing the European power sector. The impact of national policies on supranational power sectors for the example of Germany is analyzed in [23], [24].

With respect to that, we analyze the economic benefits of coordination along Europe’s decarbonization path. This is done by comparing the default scenario that comprises EU-wide targets only with a scenario that additionally includes existing national energy and climate targets. Moreover, we identify regions that profit and suffer from the national targets.

Current national targets as a whole do not go beyond the established EU-wide targets. Therefore, the later target still determines the sum of system-wide emissions and national targets will not result in a reduction of overall emissions. A geographic shift of CO₂-emission from regions with national targets to neighboring regions will be expected. If binding, those national targets impose an additional constraint on the EU decarbonization path, disturb the least-cost capacity- and generation-distribution among countries, and finally result in additional economic costs.

To begin, Section II introduces the EU-REGEN model and the scenario set-up. Then, Section III presents the results of our analysis and a quantification of sensitivities. Finally, we close with a discussion of results and conclusions in Section IV.

II. METHODS

This chapter describes the EU-REGEN model used for this analysis, the scenarios set-up, and relevant data base.

A. The EU-REGEN Model

The EU-REGEN is a long-term dispatch and investment model for the European power sector. The model structure is based on the US Regional Economy, Greenhouse Gas, and

Energy (US-REGEN) model [25], [26]. EU-REGEN was built to generate quantitative scenarios that represent an optimal and consistent decarbonization path for the European power system towards 2050.



Fig. 2 EU-REGEN model regions and transmission links in the base year

It minimizes total system costs with respect to conventional and RES generation capacity investment, generation capacity conversion and retirement, generation dispatch and curtailment, transmission capacity investment, physical electricity exchange, storage capacity investment and operation, and carbon capture and storage capacity investment and operation. The model is set-up as a partial equilibrium model that assumes complete markets with perfect information and is subject to a wide range of constraints.

The model represents the entire European power sector. Its geographic scope includes all countries of the European Union (EU28) - except for the island countries of Malta and Cyprus. Additionally, we include Switzerland and Norway, which have a central position in the European system or are endowed with

great resource potential. To reduce the size of the model we group those 28 countries into 13 model regions.

Fig. 2 shows the EU-REGEN model regions.

The model horizon in this paper is 2050. The model starts at the base year 2015 and optimize dispatch and investment is set at five-year time intervals to 2050, which results in eight time steps. The model knows 25 different types of generation capacity. To account for different characteristics of power plants of the same type and varying resource quality of RES, we further distinguish each type into generation blocks. Resulting in 73 different generation blocks.

One specific characteristic of the EU-REGEN model is the detailed representation of the variable vRES wind and solar. We apply different resource quality classes to both resources,

which is reflected in separate temporal availability profiles and capacity potentials for each quality class.^a In addition to the constraints in [27], we introduce a carbon policy and respective market for this analysis.

B. Scenarios

1. Coordination Scenario

The coordination scenario (COOR) is the default case in this analysis and assumes the current state of energy and climate policies brought forward by the EC. For 2020, the national CO₂-emission reduction targets and RES-shares in electricity generation, representing the “20-20-20” strategy have to be fulfilled by each country. For the years 2030 and 2050, the EU-wide targets (40% and 80% GHG-emission reduction, respectively) have to be reached by the whole European electricity system. This scenario allows for quantifying the development of the European power sector with ongoing and more intense coordination between countries.

Since the EC energy and climate policies are formulated as energy sector-wide targets only, for 2020, we assume the national targets set by each member state as implementation of the “20-20-20” strategy. For the remaining time horizon, we use power-market-specific values from the EC’s “Impact Assessment on energy and climate policy up to 2030”. Here, the “GHG40” scenario provides a first overview of the impacts on the power sector when reaching the 2030 and 2050 energy and climate policy targets. According to this assessment, the RES-share by 2030 and 2050 has to be at least 49.3% and 54.2%, respectively. The level of CO₂-emission has to reach a 56% reduction by 2030 and a 98% decrease of emissions by 2050. Furthermore, annual electricity generation in 2050 sums up to 5,040 TWh. For the time-steps in between we assume linearly increasing/decreasing targets for CO₂-emission reduction, RES-shares and electricity demand.

2. National Policy Scenario

The second scenario (NAT) models existing energy and climate policies as scenario COOR. Yet, we additionally include the national energy and climate targets set by countries. An overview on currently existing energy and climate targets by country can be found in [27]. This setup tries to model the economic costs of nationalization and covers the case where EU member countries fail in agreeing on how to share the burden from reaching the long-run targets.

C. Data Base

The input data used in the EU-REGEN model is described in [27].

III. RESULTS

This chapter presents the major results of our analysis. We start off with looking at Europe’s future generation- and capacity-mix in the default scenario COOR. An analysis of the role of vRES follows this. In a second step, we present results

on the optimal retirement of existing fuel-based generation capacity and describe the future relevance of dispatchable low-carbon technologies. The chapter closes with comparing the COOR and NAT scenarios and analyzing the economic consequences of national policies.

A. Default Scenario COOR

1. vRES Generation and Capacity

The generation mix for the scenario COOR is depicted in Fig. In addition to simulation results, the paper outlines the development of the historical generation mix from 1990 on. Moreover, Fig. 3 shows the regional generation mixes. From this (Figs. 3 and 4) it can be derived:

- Wind power is the dominating generation technology for the EU decarbonization path. Between 2015 and 2050, installed capacity and generation increase from 124 GW to 586 GW and 302 TWh to 1,536 TWh, respectively. The attractiveness of wind power can be explained by cost estimates, increasing availability factors, and its positive correlation with load. The latter one reflects the seasonal correlation of availability factors with demand. Both, maximum generation from wind power and demand peak, appear during winter periods. Note that new investments in wind power take place from the first model period on, where cost estimates are close to current numbers and connected to less uncertainty. The bulk of additions are from onshore capacity. New investment in wind offshore installations proves to be hardly economically viable with its accumulated capacity constantly staying below 10 GW.
- vRES as a whole increase their share in generation over the model horizon. The share in electricity generation of vRES more than triples from 12% in 2015 to 38% in 2050. Yet, this is mainly driven by wind power. The generation share of all solar power technologies increase from 3% in 2015 to 8% in 2050 only. This weak market penetration is motivated in analogy to the attractiveness of wind power. In general, solar power technologies have lower availability factors and reduced investment costs are not able to compensate for that. Furthermore, we find a negative seasonal correlation with load in most model regions. A look at the timing of photovoltaic investments reveals the importance of decreasing investment costs. The majority of photovoltaic capacity is added in the mid- and long-run, where investment costs experience a strong decrease. In terms of technology, we only find photovoltaic power as an economically attractive technology. CSP does not penetrate the European power sector at all. Meaning, higher availability factors and flexibility though storage is not able to compensate for additional investment costs.
- We find the quality of wind and solar resources as the main driver for the geographic distribution of new wind and solar capacities. The model region “Britain” becomes dominating in wind power application, reaching a capacity and generation of 134 GW and 399 TWh in 2050 (compared to 11 GW and 140 TWh in 2015). Moreover,

^a A detailed model description can be found in [27].

France and Scandinavia experience a significant increase in wind power capacity and reach an accumulated capacity of 94 GW and 69 GW. New solar power capacity is mainly added in southern regions. Since the regional quality of solar resources correlates with latitude, the majority of new capacity is added in Italy, Iberia, and France. Those three regions reach capacities of 62 GW, 56 GW, and 48 GW in 2050.

2. Role of Dispatchable Generation Technologies

An overview on the development of conventional generation capacities is provided in *Fig. 4*. This figure depicts the net investments in each model period with columns above and below the x-axis representing positive net investments and a reduction in accumulated capacity, respectively. We want to emphasize the following key points:

- Gas power becomes the major conventional generation technology for backing-up the strong market penetration of wind power. After retiring excess-capacity in the short-run, the accumulated gas-power capacity increases from 171 GW to 488 GW and contributes 1,102 TWh of electricity in 2050. This is mainly driven by the need for flexible generation technologies as a complementary to vRES. Additionally, the targeted CO₂-emission reduction requires dispatchable generation technologies with low emission-intensity. In terms of gas power technologies, combined-cycle gas turbine is the dominating technology, reaching a capacity of 330 GW in 2050.

The capacity development of emission-intense coal power is clearly restricted by the decarbonization path. There are no additions to lignite and hard coal power capacity. Meaning, accumulated capacity is monotonically decreasing and

characterized by retirement of old vintage capacities. The 181 GW of current coal power capacity is expected to decrease to 28 GW by 2050.

- We find nuclear power capacity to stay at a level constantly above 100 GW. Starting with 132 GW in 2015 and decreasing to 114 GW by 2050. The timing of new investment in nuclear power is simultaneous to the retirement of old vintages.
- The market penetration of CCS is limited to combined biomass-CCS capacity. Capacity additions start from 2040 on and reach an accumulated capacity of 58 GW by the end of the model horizon.

B. Consequences of National Policies in Scenario NAT

1. Changes in Generation

Scenario COOR showed the optimal geographic distribution of power capacity and generation for the EU-wide decarbonization path. We analyze the consequences of national policies in scenario NAT by looking at general system-wide effects and take a deeper look at the regions of France and Germany with the most ambitious national targets.

Fig. 5 depicts the system-wide generation mix for scenario NAT. Comparing this to generation in the COOR scenario (*Fig*) shows minor differences. For 2050, current national policies reduce generation from gas power, bio-CCS, and wind onshore power by 53 TWh, 13 TWh, and 16 TWh. This is mainly substituted by an increased contribution by nuclear power (31 TWh) and PV (57 TWh).

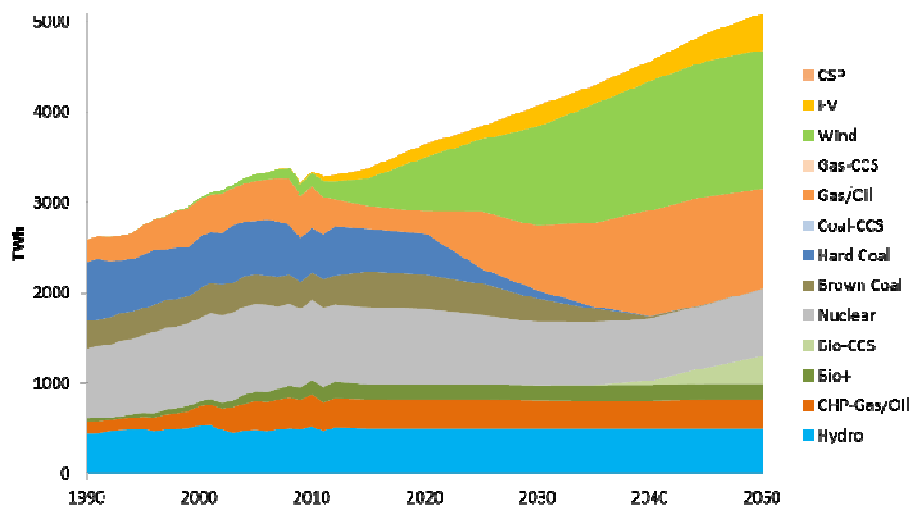


Fig. 3 System-wide generation mix in scenario COOR in [TWh]

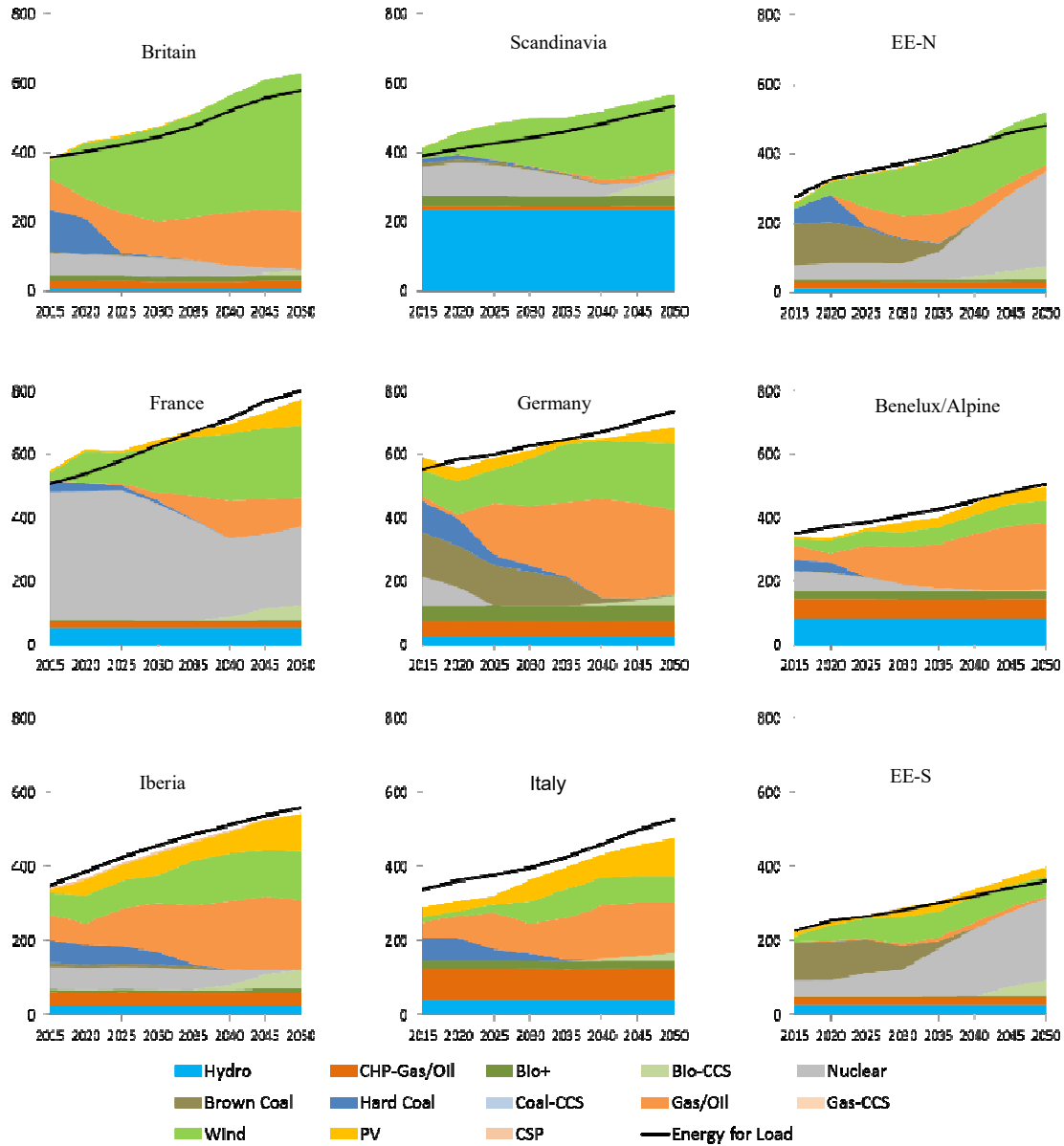


Fig. 3 Regional generation-mix in scenario COOR in [TWh]

Yet, comparing the regional generation patterns in *Fig. 3* and *Fig. 6* reveals the following:

- Germany's target of an 80% RES-share in generation is mainly reached by reducing its gas power generation. This is compensated by additional generation from PV power. Yet, accumulated generation decreases significantly. Consequently, we find a geographic shift of generation from gas power to Norway, the north-eastern region, and Italy.
- The 50% upper bound on nuclear generation appears to be the binding feature of French policy. This constraint leads to an increased generation from gas and PV power in France. From a system perspective, we find a shift of generation from nuclear power to the south-east region.

2. Impact on Cross-Border Transmission Capacities

Furthermore, changing regional generation-mixes impact the optimal grid infrastructure. We find values for the NTCs in 2050 to hardly vary between scenario COOR and NAT. We can only identify a significant difference for the link between Benelux and Germany-N. The level of transmission capacity for this connection is 3 GW and 9 GW in scenario COOR and NAT, respectively. Though, it is important to note, that we apply upper bounds on the additions to each connection. This is done to account for the political and technical feasibility of grid-extensions. Since, the upper bound is already reached in the default scenario for most of the connections, the level of transmission capacity has only limited explanatory power. In that case, the shadow price on the transmission constraint could be thought of as a better indicator to compare both scenarios. The shadow prices reveal how much the total

discounted system costs would decrease if one additional kW of transmission capacity for a specific connection would be allowed. Fig. 7 and Fig. 8 present the shadow prices on each transmission link in 2050 for both scenarios. Numbers in those figures show:

- In the default scenario, high shadow prices for connections can be found either linking regions with a high wind-resource quality, such as Britain and Scandinavia, or eastern European countries, which are

subject to conservative upper bounds on additions. We calculate the highest values for the connections from Britain to France and Benelux with of 172 €/kW and 126 €/kW. Similarly, links from Scandinavia to Benelux, the north-west of eastern Europe and northern Germany, are subject to a shadow price of 99 €/kW, 86 €/kW, and 78 €/kW. Concerning the eastern regions, there is a high value of 124 €/kW for the connection from north-east to the north-west of eastern Europe.

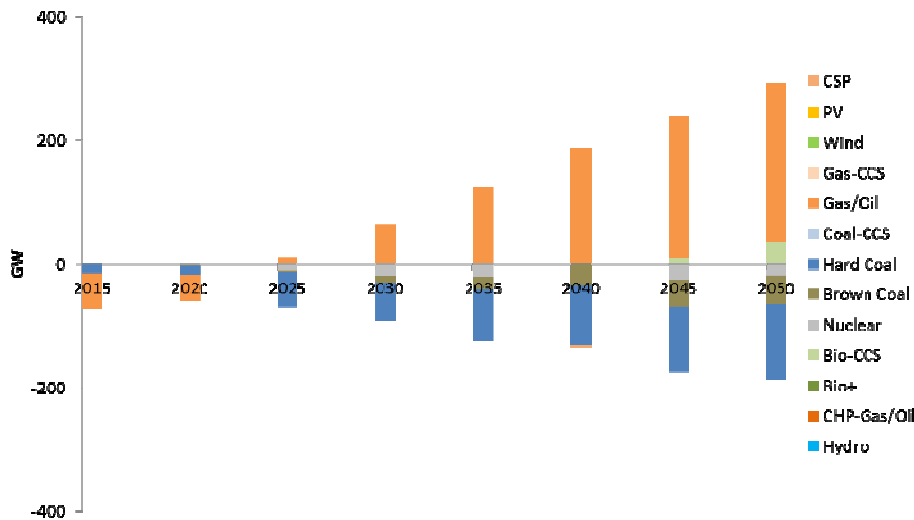


Fig. 4 Net investment in conventional generation technologies in [GW]

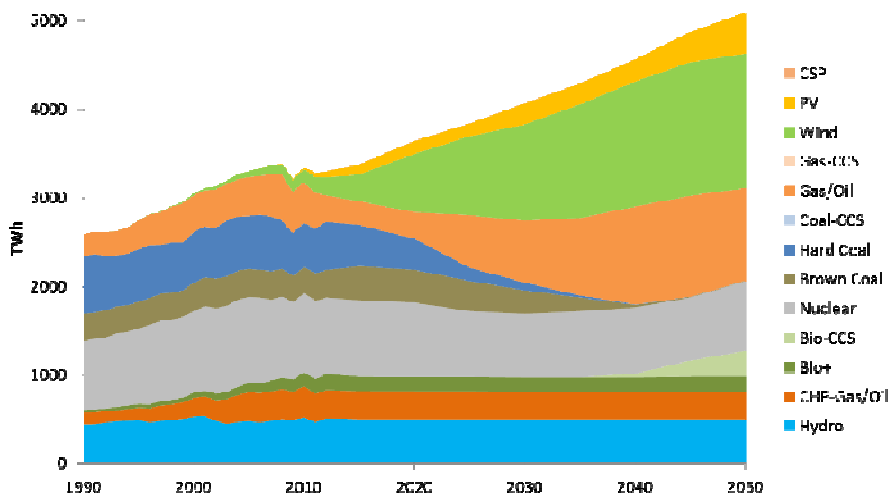


Fig. 5 System-wide generation mix in scenario NAT in [TWh]

- A comparison of values for both scenarios indicates big differences almost exclusively for connections linked to German regions. If national policies are in place, northern Germany experiences a high pressure on links from Benelux, Scandinavia, and the north-west of eastern Europe. Those shadow prices increase

to 90 €/kW (8), 137 €/kW (78), and 77 €/kW (37).^a The increase of shadow prices for connections to southern Germany is of a smaller order of magnitude. Values for links from France, Alpine, and EE-NW reach 72 €/kW (46), 46 €/kW (22), and 84 €/kW (63) in the NAT scenario. Vice versa, shadow prices for

^a Values for scenario COOR are shown in brackets.

connections from southern Germany rise as well. Links to Benelux, northern Germany, and the Alpine region have shadow prices of 35 €/kW (13), 17 €/kW (1), and 36 €/kW (12). This can be explained by a

higher generation from solar power in southern Germany that is caused by the 80 % RES-share target for the whole country

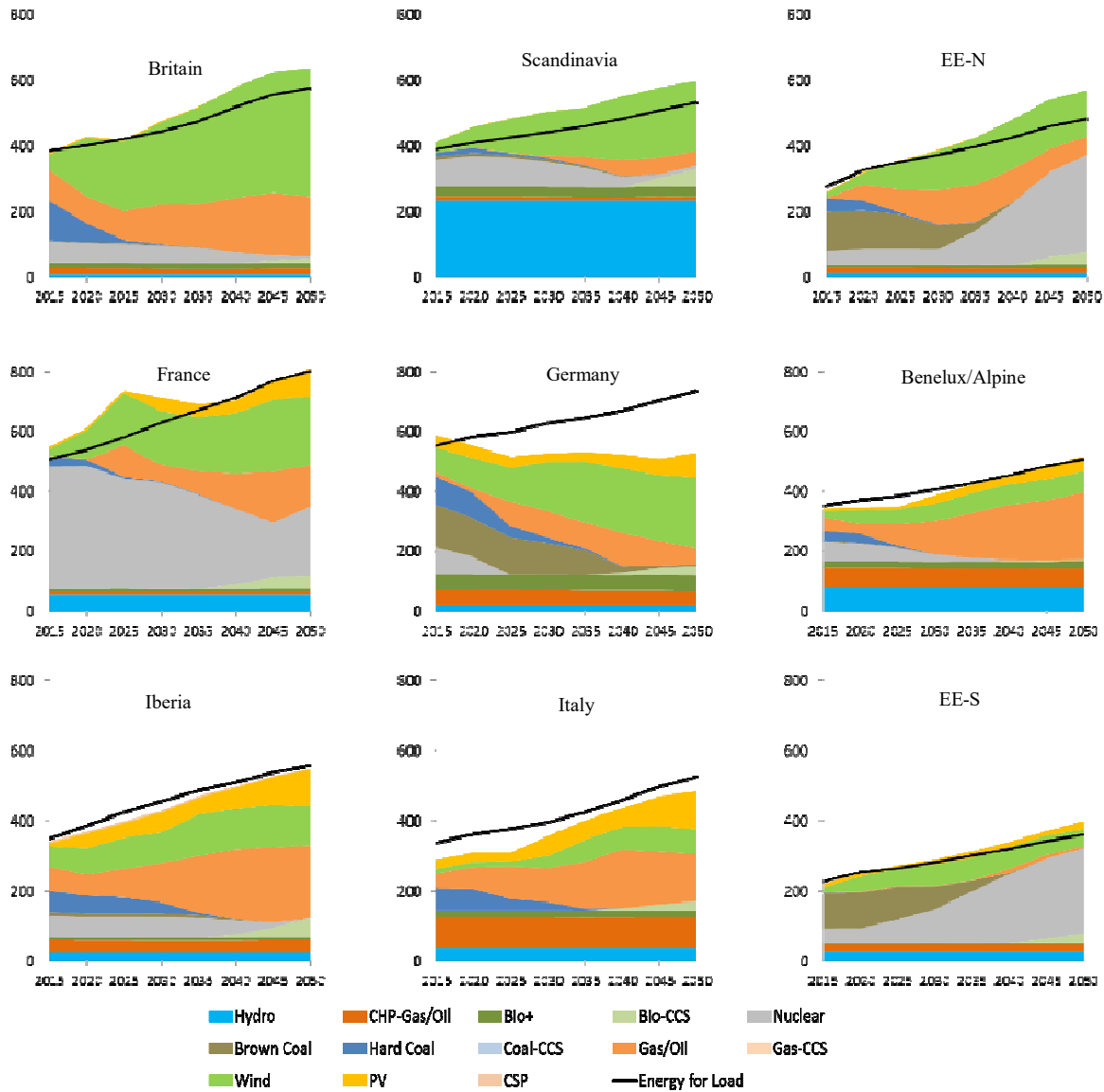


Fig. 6 Regional generation-mix in scenario NAT in [TWh]

3. Changes in Trade Flows

Consequently, also trade flows between regions change with national policies. Fig. 10 shows an analysis of the development of net exports for both the German regions and France. The measure shows to which extent a region is able to satisfy demand or depends on neighboring regions. Results indicate:

- In the COOR scenario, both German regions, especially the south, become a net importer in the long-run. Introducing additional national targets (NAT) leads to even more unbalanced trade flows. North Germany

already becomes a net importer in the mid-run and the south increases the sum of annual imports.

- In contrast, France increases exports under a national policy. We find mid-run net exports to increase significantly and almost balanced flows by 2050.

4. Economic Consequences of National Policies

We use the total discounted system costs as a first indicator for the system-wide economic consequences of national policies. A comparison of system costs in scenario COOR and NAT shows an increase of 1% with national policies. Yet, it is important to note that only a small number of countries have national long-run targets. Moreover, those policies are binding

in the long-run especially, which has less impact on the discounted system costs.

The economic perspective can be enhanced by looking at consumer and producers separately. Changing net imports are also reflected in electricity prices. Additionally, prices allow for identifying regions with consumers that win and lose from national targets. We look at average, energy only prices for consumed quantities. In general, any deviation from the cost-optimal generation pattern in scenario COOR leads to higher generation costs.

Electricity prices for both German regions in scenario NAT rise due to increased imports with higher average prices. Looking at both scenarios shows that by 2050 average prices in north and south Germany increase by 11% and 7% with national targets. We find a contrary development for France. Prices differ only in the mid-run with a reduction of up to 12% by 2030.

Finally, a changing power plant dispatch and prices impact producer's revenues. Looking at revenues allows identifying regions with producers that profit or suffer from national

targets. *Fig. 10* shows the relative change in total revenues for regions with a significant change. It can be observed that:

- Producers in both German regions suffer from a national target. Revenues of generators in northern Germany decrease by up to 25% in 2040 and reach a reduction of 18% in 2050. Revenues in south Germany drop even more with a level of -27% in 2050. This development is mainly driven by the drop of accumulated generation in both regions.
- The loss of revenues in Germany results in increased revenue streams in neighboring regions. The north-western of Eastern Europe profits the most from national targets and reaches a level of +14%. Moreover, Scandinavia and the Benelux region increase revenues by 8% and 9% in 2050.
- The French national targets have no negative impact on generators in the long-run. In the short-run revenues drop due to the cap on nuclear generation. Yet, from 2035 on, increased PV generation leads to higher revenues.



Fig. 7 Shadow prices on transmissions links in 2050 for scenario COOR in [EUR/kW]



Fig. 8 Shadow prices on transmissions links in 2050 for scenario NAT in [EUR/kW]

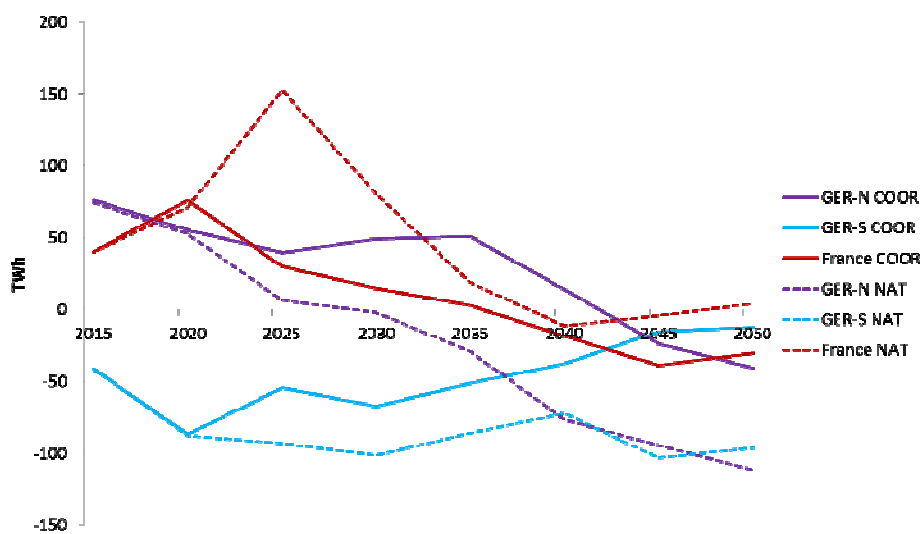


Fig. 9 Net exports in scenario COOR and NAT in [TWh]

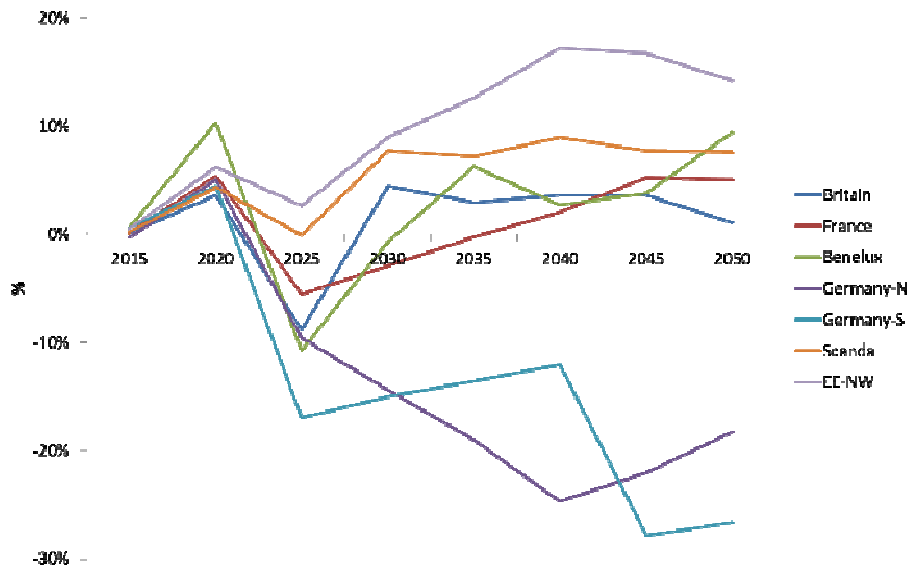


Fig. 10 Relative change in total revenues

C. Quantification of Sensitivity

Finally, we analyze the robustness of the 2050 generation-mix by a set of counter-factual scenarios. This analysis varies along two dimensions: on the one hand, the above-introduced default and policy scenario and, on the other hand, the following assumptions on transmission and generation technologies:

- Reduced investment cost for PV – 250 €/kW instead of 750 €/kW in 2050 (cheapPV)
- Reduced investment cost for nuclear power – 2,500 €/kW instead of 5,000 €/kW in 2050 (cheapNUC)
- No new transmission capacity additions (noTRANS)
- Unconstrained transmission capacity additions (unlTRANS)
- No CCS application (noCCS)
- No negative crediting of biomass-CCS (nonegCRED)
- No new nuclear power capacity (nonewNUC)

Fig. 11 shows the results with varying assumptions for scenarios COOR and NAT. The counter-factual scenarios are sorted by the order of magnitude of their change in generation-mix compared to the default parameter values. The main findings are:

- Model runs with no new transmission capacity (noTRANS), no upper bound on additions to transmission capacities (unlTRANS), and lower investment cost for PV (cheapPV) do not change the overall structure of the system generation-mix. Yet, we can note that more system flexibility through unconstrained investment into NTC leads to some substitution of generation from nuclear power by wind power. With more additions to existing NTC, more trade flows and a better utilization of low-marginal cost wind power becomes feasible. Low

investment costs for PV result in a substitution of generation from wind power by PV and electricity from nuclear power by gas power.

- A strict phase out policy on nuclear power (noNUC) results in a shift of nuclear generation to gas, bio-CCS, and wind power. Here, the increased generation from wind power is backed-up by the flexibility from gas power generators. And, negative CO₂-credits from bio-CCS generation compensate for additional CO₂-emissions from the rising gas power generation.
- In contrast, lower investment costs for nuclear power (cheapNUC), no negative crediting of biomass-CCS (nonegCRED), and No CCS application (noCCS) leads to soaring generation by nuclear generators. Furthermore, in all those three counter-factual scenarios concentrated solar power (CSP) penetrates the market with more flexibility due to its storage feature. At the same time, cheap nuclear power substitutes combined generation from gas power and biomass-CCS. Similarly, a non-decarbonized biomass supply chain with no negative credits almost completely drives biomass-CCS and gas power out of the market and triggers a higher contribution from gas-CCS.
- The case with no CCS application brings more biomass generation into the market. With no geologic storage of CO₂, gas power or other conventional generation technologies experience little generation due to the tight decarbonization path.

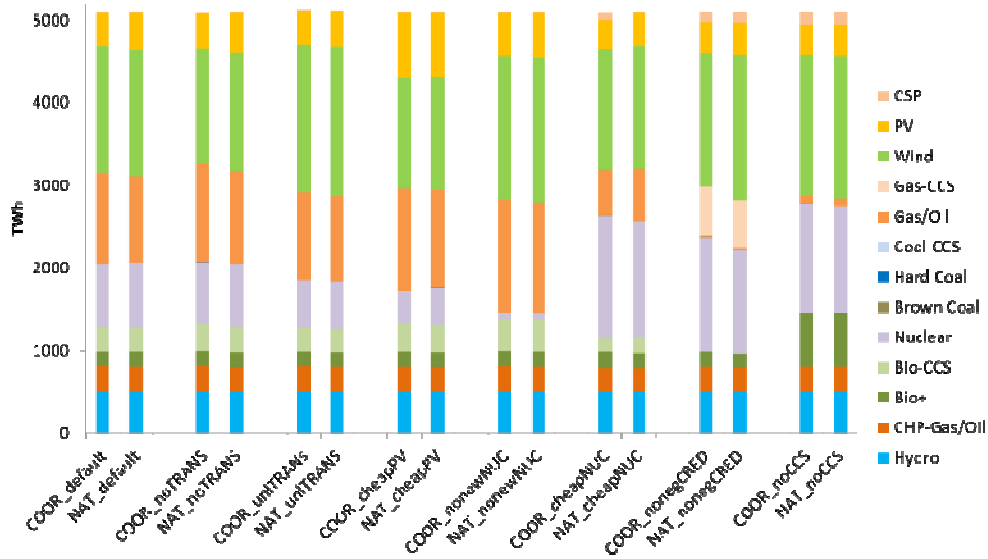


Fig. 11 Sensitivity of 2050 system generation-mix

Generally, few differences can be found between the results for scenario COOR and NAT. As mentioned above, the effect of national policies on generation is mainly reflected in regional generation-mixes. Therefore, *Fig. 12* shows the sensitivity of the overall 2050 German generation-mix, from which the following key points can be concluded:

- For all counter-factual scenarios – except for noCCS - the main difference between COOR and NAT is reduced generation from gas power or gas-CCS. Generation from vRES partly compensates for that. Yet, none of those

parameter values changes the trend of lower generation in the NAT scenario.

- Additionally, we want to point at the scenarios uniTRANS and noCCS. For both, there is even very little German generation in the COOR scenario. Those scenarios either require or support high shares of the carbon-free generation technologies nuclear power and vRES. Due to the relatively low resource quality and a legally-binding nuclear phase-out, Germany becomes a net-importing region even without its ambitious national policies.

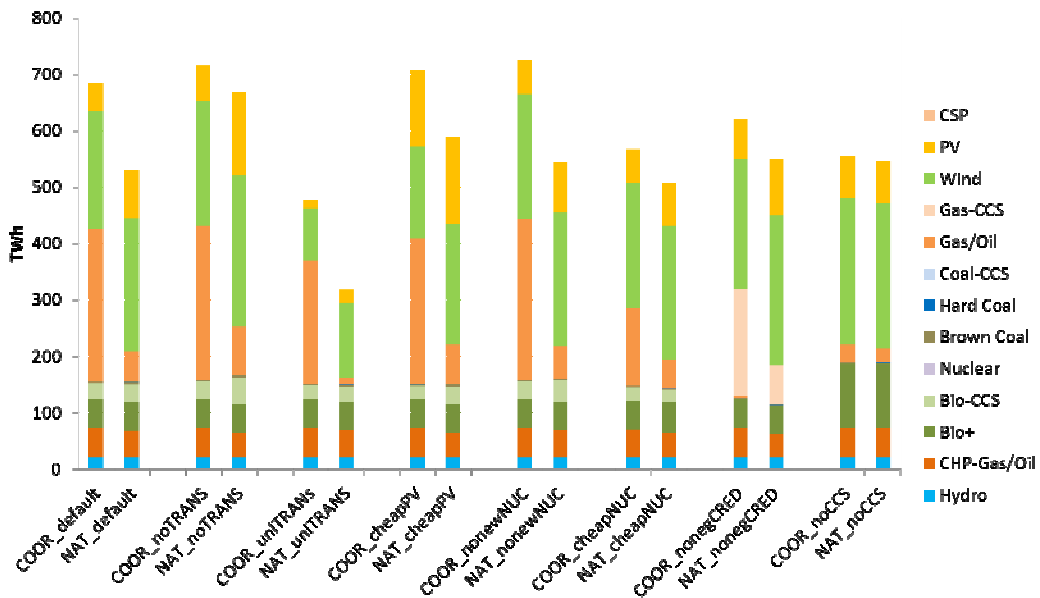


Fig. 12 Sensitivity of 2050 German generation-mix

IV. DISCUSSION AND CONCLUSION

A. Model limitations

The set-up of the EU-REGEN model captures the core dynamics that influence the long-run dispatch and investment in the European power sector. Nonetheless, the following characteristics are out of the model scope:

- EU-REGEN is a perfect foresight model that neglects uncertainty about input parameters, e.g. investment costs, fuel prices, and demand levels. Moreover, parameter values are not subject to path-dependence. Meaning that investment and dispatch decisions have no impact on parameter values in subsequent periods.
- The EU aims at an economy-wide decarbonization. With the focus on the power sector we are not able to capture the interaction with other energy sectors, EU-ETS sectors, and the economy. The results presented in this paper focus on power sector specific implications.
- As a partial equilibrium representation of the power sector with complete markets and perfect information, CO₂-emission reductions are realized where this can be done at lowest costs. EU-REGEN does not capture self-interest and motives such as protectionism.
- The model does not value benefits from introduced climate and energy policies. Any kind of policy leads to higher costs compared to a non-policy baseline scenario. Consequently, the model setting only allows for a cost-based analysis.
- EU-REGEN has a long-run perspective, which only considers political boundary conditions, e.g. the attitude towards nuclear power. Existing technology support schemes are not modeled.
- Due to computational constraints, we group the EU-28 countries to 12 model regions. The loss of a regional resolution limits our conclusions and the explanatory power on transmission and distribution grid extensions, among others.
- For the same reason, we apply a representative-hour approach with 130 time-segments instead of 8,760 hours. This means the loss of the chronological order of hours, which compromises the modeling quality of e.g. electricity storage.
- The future European power sector will be driven by the dynamics of the supply as well as demand side. With deterministic demand levels and fixed demand profiles, the current model setting does not cover the potential contribution of demand to additional system flexibility.

B. Summary of Results

Despite those shortcomings, we can draw the following conclusions on the cost-optimal infrastructure investment and electricity generation for the European power sector until 2050:

Our results reveal that onshore wind power will be the most crucial generation technology for the decarbonization of Europe's power sector. The geographic distribution of vRES capacities is driven by resource quality and not by a

geographic balancing effect as proposed by others. Great Britain, France, and Scandinavia become the dominating regions in wind power application. Concerning solar, capacity is added in the Mediterranean regions of Italy, Iberia, and France. We identify gas power as the major conventional generation technology for backing-up the strong market penetration of wind power. This is mainly driven by the need for flexible generation technologies as a complementary to vRES. Additionally, the targeted CO₂-emission reduction requires dispatchable generation technologies with low emission-intensity. Moreover, we see a smooth retirement path of coal power. Yet, in contrast to the current public debate, a complete phase out proves to be not economically optimal. Even under a 98% CO₂-emission reduction target by 2050, 15% of current capacity is still active by then. CCS takes a crucial role in providing dispatchable carbon-neutral generation.

We showed that national targets disturb the cost-optimal distribution of capacity and generation. Especially the German goals lead to a geographic shift of generation due to its target on generation from RES in combination with a relative low vRES quality. As a consequence, German consumers and generators suffer from higher prices and lower revenues. The French policy appears to be less disturbing and increases generation in the region. Missing generation from nuclear power is shifted to Eastern Europe. Moreover, those national targets have a positive impact on consumers and producers. Prices for consumption decrease and total revenues increase. Though, a sensitivity analysis shows that France would profit even more without its policy in place. The remaining regions profit or are hardly affected from announced national targets. Yet, this is due to the fact that there are no ambitious additional targets announced there.

C. Policy Implications

Based on our findings we suggest EU-wide coordination on the expansion of solar and wind power, especially. Nonetheless, profitable market structures with remuneration schemes for conventional generation technologies are required in order to back-up the market penetration of vRES. Certainty regarding the EU climate policy is essential to push the substitution of coal power by new investments into gas power. Additionally, this impacts the market conditions for CCS. Prices in the EU-ETS have to be high enough to create a business case for its application. Since CCS could become a crucial technology, uncertainties concerning its social and technical feasibility have to be addressed. If not so, a decarbonization path based on a different technology-mix has to be realized.

Furthermore, the current development of announcing national energy and climate targets should be reversed. EU-wide policies are needed to keep the costs for the transition of the European power sector at a bearable level.

REFERENCES

- [1] European Commission, "Impact Assessment: A Roadmap for moving to a competitive low carbon economy in 2050," 2011.
- [2] European Commission, "Impact Assessment: A policy Framework for climate and energy in the period from 2020 to 2030," 2014.
- [3] European Commission, "An Energy Policy for Europe," 2007.
- [4] European Commission, "Energy Roadmap 2050," 2011.
- [5] United Nations, "Adoption of the Paris Agreement," 2015.
- [6] Marcel Šúri, Thomas A. Huld, Ewan D. Dunlop, and Heinz A. Ossenbrink, "Potential of solar electricity generation in the European Union member states and candidate countries," *Solar Energy*, vol. 81, no. 10, pp. 1295–1305, 2007.
- [7] European Environment Agency, "Europe's onshore and offshore wind energy potential: An assessment of environmental and economic constraints," 2009.
- [8] K. Schaber, F. Steinke, P. Mühlich, and T. Hamacher, "Parametric study of variable renewable energy integration in Europe: Advantages and costs of transmission grid extensions," *Energy Policy*, vol. 42, pp. 498–508, doi:10.1016/j.enpol.2011.12.016, 2012.
- [9] K. Schaber, F. Steinke, and F. Hamacher, "Transmission grid extensions for the integration of variable renewable energies in Europe: Who benefits where?," *Energy Policy*, vol. 43, pp. 123–135, doi:10.1016/j.enpol.2011.12.040, 2012.
- [10] S. Becker, R. A. Rodriguez, G. B. Andresen, S. Schramm, and M. Greiner, "Transmission grid extensions during the build-up of a fully renewable pan-European electricity supply," *Energy*, vol. 64, pp. 404–418, doi:10.1016/j.energy.2013.10.010, 2014.
- [11] R. A. Rodriguez, S. Becker, G. B. Andresen, D. Heide, and M. Greiner, "Transmission needs across a fully renewable European power system," *Renewable Energy*, vol. 63, pp. 467–476, doi:10.1016/j.renene.2013.10.005, 2014.
- [12] M. Fürsch, S. Hagspiel, C. Jägermann, S. Nagel, D. Lindenberg, and E. Tröster, "The role of grid extensions in a cost - efficient transformation of the European electricity system until 2050," 2012.
- [13] B. Knopf, P. Nahmmacher, and E. Schmid, "The European renewable energy target for 2030 – An impact assessment of the electricity sector," *Energy Policy*, vol. 85, pp. 50–60, doi:10.1016/j.enpol.2015.05.010, 2015.
- [14] E. Schmid and B. Knopf, "Quantifying the long-term economic benefits of European electricity system integration," *Energy Policy*, vol. 87, pp. 260–269, doi:10.1016/j.enpol.2015.09.026, 2015.
- [15] D. Heide, L. von Bremen, M. Greiner, C. Hoffmann, M. Speckmann, and S. Bofinger, "Seasonal optimal mix of wind and solar power in a future, highly renewable Europe," *Renewable Energy*, vol. 35, no. 11, pp. 2483–2489, doi:10.1016/j.renene.2010.03.012, 2010.
- [16] L. Hirth, "The market value of variable renewables," *Energy Economics*, vol. 38, pp. 218–236, doi:10.1016/j.eneco.2013.02.004, 2013.
- [17] A. S. Brouwer, M. van den Broek, W. Zappa, W. C. Turkenburg, and A. Faaij, "Least-cost options for integrating intermittent renewables in low-carbon power systems," *Applied Energy*, vol. 161, pp. 48–74, doi:10.1016/j.apenergy.2015.09.090, 2016.
- [18] K. Schaber, F. Steinke, and T. Hamacher, "Managing Temporary Oversupply from Renewables Efficiently: Electricity Storage Versus Energy Sector Coupling in Germany," 2013.
- [19] F. Reitz, C. Gerbaulet, C. Kemfert, C. Lorenz, P.-Y. Oei, and C. von Hirschhausen, *Szenarien einer nachhaltigen Kraftwerksentwicklung in Deutschland*. Berlin: Deutsches Institut für Wirtschaftsforschung, 2014.
- [20] P.-Y. Oei, C. Kemfert, F. Reitz, and C. von Hirschhausen, *Braunkohleausstieg - Gestaltungsoptionen im Rahmen der Energiewende*. Berlin: Deutsches Institut für Wirtschaftsforschung, 2014.
- [21] Agora Energiewende, "Eleven Principles of Reaching a Consensus on Coal: Summary," 2016.
- [22] C. Jägermann, M. Fürsch, S. Hagspiel, and S. Nagl, "Decarbonizing Europe's power sector by 2050 — Analyzing the economic implications of alternative decarbonization pathways," *Energy Economics*, vol. 40, pp. 622–636, doi:10.1016/j.eneco.2013.08.019, 2013.
- [23] T. Sattich, "Germany's Energy Transition and the European Electricity Market: Mutually Beneficial?," *Journal of Energy and Power Engineering*, vol. 8, pp. 264–273, doi:10.1109/EEM.2013.6607323, 2014.
- [24] S. Kirsten, "Renewable Energy Sources Act and Trading of Emission Certificates: A national and a supranational tool direct energy turnover to renewable electricity-supply in Germany," *Energy Policy*, vol. 64, pp. 302–312, doi:10.1016/j.enpol.2013.08.030, 2014.
- [25] EPRI (Electric Power Research Institute), "PRISM 2.0: Regional Energy and Economic Model Development and Initial Application: US-REGEN Model Documentation," 2013.
- [26] G. J. Blanford, J. H. Merrick, and D. Young, "A Clean Energy Standard Analysis with the US-REGEN Model," *The Energy Journal*, vol. 35, pp. 137–164, doi:10.5547/01956574.35.S11, 2014.
- [27] G. J. Blanford and C. Weissbart, "Modeling the Dynamics of the Future European Power Sector: The EU-REGEN Model," 2016.

Oncogenic Functions of Long Non-Coding RNA XIST in Human Nasopharyngeal Carcinoma by Targeting MiR-34a-5p

Cheng-Cao Sun¹, Shu-Jun Li^{1,2}, and De-Jia Li¹

¹ Department of Occupational and Environmental Health, School of Public Health, Wuhan University, Wuhan, P. R. China; ² Wuhan Hospital for the Prevention and Treatment of Occupational Diseases, 430071 Wuhan, P. R. China;

Corresponding author: De-Jia Li; No.115 Donghu Road, Wuchang District, Wuhan, China; Tel: (86)18271470520; Fax: (86)02768778695; E-mail: lodjlwhu@sina.com

Abstract

Long non-coding RNA (lncRNA) X inactivate-specific transcript (XIST) has been verified as an oncogenic gene in several human malignant tumors, and its dysregulation was closely associated with tumor initiation, development and progression. Nevertheless, whether the aberrant expression of XIST in human nasopharyngeal carcinoma (NPC) is correlated with malignancy, metastasis or prognosis has not been elaborated. Here, we discovered that XIST was up-regulated in NPC tissues and higher expression of XIST contributed to a markedly poorer survival time. In addition, multivariate analysis demonstrated XIST was an independent risk factor for prognosis. XIST over-expression enhanced, while XIST silencing hampered the cell growth in NPC. Additionally, mechanistic analysis revealed that XIST up-regulated the expression of miR-34a-5p targeted gene E2F3 through acting as a competitive ‘sponge’ of miR-34a-5p. Taking all into account, we concluded that XIST functioned as an oncogene in NPC through up-regulating E2F3 in part through ‘sponging’ miR-34a-5p.

Key words: X inactivate-specific transcript; hsa-miRNA-34a-5p, miR-34a-5p; *E2F3*, nasopharyngeal carcinoma, tumorigenesis

Oncogenic Role of MicroRNA-346 in Human Non-Small Cell Lung Cancer by Regulation of XPC/ERK/Snail/E-Cadherin Pathway

Cheng-Cao Sun¹, Shu-Jun Li^{1,2}, and De-Jia Li¹

¹ Department of Occupational and Environmental Health, School of Public Health, Wuhan University, Wuhan, P. R. China; ² Wuhan Hospital for the Prevention and Treatment of Occupational Diseases, 430071 Wuhan, P. R. China;

Corresponding author: De-Jia Li; No.115 Donghu Road, Wuchang District, Wuhan, China; Tel: (86)18271470520; Fax: (86)02768778695; E-mail: lodjlw@whu.edu.cn

Abstract

Determinants of growth and metastasis in cancer remain of great interest to define. MicroRNAs (miRNAs) have frequently emerged as tumor metastatic regulator by acting on multiple signaling pathways. Here, we report the definition of miR-346 as a oncogenic microRNA that facilitates non-small cell lung cancer (NSCLC) cell growth and metastasis. XPC, an important DNA damage recognition factor in nucleotide excision repair was defined as a target for down-regulation by miR-346, functioning through direct interaction with the 3'-UTR of XPC mRNA. Blocking miR-346 by an antagomiR was sufficient to inhibit NSCLC cell growth and metastasis, an effect that could be phenol-copied by RNAi-mediated silencing of XPC. *In vivo* studies established that miR-346 overexpression was sufficient to promote tumor growth by A549 cells in xenografts mice, relative to control cells. Overall, our results defined miR-346 as an oncogenic miRNA in NSCLC, the levels of which contributed to tumor growth and invasive aggressiveness.

Key words: microRNA-346, miR-346, XPC, non-small cell lung cancer, oncogenesis

Orthophthalic Polyester Composite Reinforced with Sodium Alginate-Treated Anahaw (*Saribus rotundifolius*) Fibers

Terence Tumolva, Johannes Kristoff Vito, Joanna Crystelle Ragasa, Renz Marion Dela Cruz

Abstract—Natural fiber reinforced polymer (NFRP) composites have been the focus of various research projects due to their advantages over synthetic fiber-reinforced composites. For this study, anahaw is used as the fiber source due to its abundance throughout the Philippines. A problem addressed in this study is the need for an environment-friendly method of fiber treatment. The use of sodium alginate to treat fibers was thus investigated. The fibers were immersed in a sodium alginate solution and then in a calcium chloride solution afterwards. The treated fibers were used to reinforce orthophthalic unsaturated polyester (ortho-UP) resin. The mechanical properties were tested using a universal testing machine (UTM), and the fracture surfaces were characterized using scanning electron microscope (SEM). Results showed that the sodium alginate treatment had increased the tensile and flexural strength of the composite. The increase in fiber load had also been found to increase the stiffness of the composite. However, sodium alginate treatment did not provide any significant improvement in the wet mechanical properties of the NFRP. The composite is comparable to some commercially available polymeric materials.

Keywords—NFRP, composite, alginate, anahaw, polymer

Corresponding Author

Terence Tumolva from University of the Philippines Diliman,
Philippines
e-mail: terence.tumolva@coe.upd.edu.ph

Pedagogical Effects of Using Workbooks in English Classes for the TOEIC Test: A Study on ESL Learners in Japanese Colleges

Mikako Nobuhara

Abstract—The Test of English for International Communication (TOEIC) test, conducted by the Institute for International Business Communication (IIBC), has a huge impact on education in Japan. Almost all college students have to submit their TOEIC test scores when applying for entry-level jobs at companies. In addition, an increasing number of colleges are encouraging students to have a global vision. For this specific reason, studying for the TOEIC test is essential for English as a second language (ESL) learner to develop English communication skills. This study shows that studying by using some workbooks about the listening section of the TOEIC test clearly helps ESL learners to develop their listening skills. For this purpose, the listening test scores before and after classroom sessions were analyzed for each student. Students obtained higher scores in the listening section of the test and improved their English listening skills at the end of all the classroom sessions. In conclusion, it is important for English teachers to achieve the following objectives: (1) facilitate the learning of effective methods for correctly solving questions based on listening skills and (2) prepare listening tasks for reading aloud so as to keep up with the original speed, which is required for solving questions in the TOEIC test.

Keywords—education, ESL, listening skills, TOEIC test

Corresponding Author

Mikako Nobuhara from Tokyo Metropolitan College of Industrial Technology, Japan
e-mail: mikako.carpediem@gmail.com

Performance Evaluation of Prototype Power Operated Ride on Type Paddy Weeder

Basavaraj¹ and Surendrakumar.A²

¹Teaching Associate, College of Agricultural Engineering, PJTSAU, Sangareddy-502001

²Professor, Agricultural Machinery Research Centre, AEC & RI, TNAU, Coimbatore-03

Corresponding mail id: basu.py009@gmail.com

Abstract—A study was conducted for performance evaluation of prototype ride on type paddy weeder in evaluated in M-4 plot of wetland field, Tamil Nadu Agricultural University, Coimbatore, India. The field experiments were conducted in Field No M-4 of the Wetlands, Tamilnadu Agricultural University, Coimbatore. The experimental site is geographically situated at 11° North latitude and 77° East longitude and at an altitude of 427 m above MSL. Weed is inevitable part of farming. Ever since man started growing crops, he had come up with the problems of weed. SRI system of rice cultivation naturally weed growth is more in the fields because there is no stagnated water. So, it is very necessary to use proper weeding implements to reduce drudgery and cost of cultivation. Performance evaluation of prototype ride on type paddy weeder was done in the paddy field. In field evaluation the of developed ride on type paddy weeder the following evaluated parameters were wheel slip 15%, effective field capacity 0.03004 hah⁻¹, theoretical field capacity 0.0375 ha h⁻¹, field efficiency 80.35 %, plant damage 3.33% and weeding efficiency 84.04% and fuel consumption of the weeder was 0.6 lit h⁻¹.

Key words: Paddy weeder, Effective field capacity, Plant damage and Weeding efficiency

1. Introduction

Rice is an important staple food for about 50 per cent of the world's population providing 66-70 per cent body calories intake to the consumers (Barah and Pandey, 2005). The world paddy production was 614.65 million tones covering an area of 153.51 million hectare with an average yield of 3.87 tonnes per hectare. India has the largest area under rice in the world which comprises about 44 per cent of the total area under cereals in India and its production reached to a record high of 104.32 million tonnes in 2011-12.

Weed is inevitable part of farming. Ever since man started growing crops, he had come up with the problems of weed. Farmers and researchers have been putting up a combined front to tackle the menace of weeds. Weeds are serious threat to all crops. Weeds, instead of harbouring insects, compete with the crop for water, light and plant nutrients and adversely affect the microclimate around the plant. Weeding is an important but equally labour intensive agricultural unit operation. Weeding accounts for about 25 per cent of the total labour requirement during a cultivation season (Nag and Dutta, 1979). In developing countries it is estimated that

reduction in yield due to weeds alone is 20 to 30 per cent depending on the crops, weed infestation intensity and location, which might increase up to 50 per cent if adequate crop management practices were not observed.

1.1 Weeding in paddy cultivation

Human energy is predominantly used in most of the rice farming operations starting from seedbed preparation to threshing. It is estimated that nearly 145 man-days are required per hectare of rice. Among these crop, care is highly labour intensive operation accounting for 24.3 per cent of total human power requirement (Fig 1). Hand weeding is the most common method of weed control in rice but it requires high labour input. Normally two or three manual weeding is done in rice per crop.

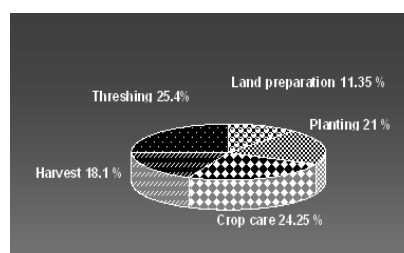


Fig.1 Labour requirement in rice farming

Among various farm operations in rice cultivation i.e. growing of seedlings, transplanting of seedlings, weeding, harvesting etc are labor intensive operations and one of the major laborious and time consuming operations in rice cultivation is weeding. The yield loss ranges from 10-50 % in transplanted rice depending on the extent of weed infestation (Pathak et al.1976). India is the second largest rice producing country in the world and represents about 10% (225 million) of the total workforce in agriculture (Nag and Nag, 2004). Even though, Rice cultivation is facing severe labour problem. It is estimated that one third to one-half of the labour used in rice cultivation is for weed control with an average figures of 30-40% labour days per hectare and 8-10 man-hour per day (Hobbs and Belinder, 2004). It is also observed that the yield is reduced from 10-50% in transplanted rice depending on the extent of weed infestation (Pathak *et al.*1976). In Transplanted paddy cultivation, Traditional seedbed-based rice cultivation consumes higher energy for weed management in India (15.3 - 23.7 %) compared to stale seedbed because traditional farmers give their higher priority to hand weeding (Chaudhary *et al.*, 2006). It is very clear that the estimates of time and cost for hand weeding are variable and dependent on weed flora, weed intensity, cropping season, labour availability and efficiency of weeding methods.

In SRI system of rice cultivation naturally weed growth is more in the fields because there is no stagnated water. So, it is very necessary to use proper weeding implements to reduce drudgery and cost of cultivation. Performance evaluation of prototype ride on type paddy weeder was done in the paddy field.

2. MATERIALS AND METHODS

The developed prototype ride on type paddy weeder evaluated in M-4 plot of wetland field, Tamil Nadu Agricultural University, Coimbatore, India. The field experiments were conducted in Field No M-4 of the Wetlands, Tamilnadu Agricultural University, Coimbatore. The experimental site is geographically situated at 11° North latitude and 77° East longitude and at an altitude of 427 m above MSL. The soil of the experimental site was sandy clay loam as per the textural classification (USDA).

Weeding was done on 25th DAS. The spacing of paddy was 25 × 25cm. The field trials were carried out at a soil moisture content of 37 %. The size of the plot was 0.25 acre. The trials were conducted between 9.00 AM 11.00 AM during the month of June 2015.

The performance of the machine was evaluated in terms of wheel slip, weeding efficiency, plant damage, field capacity, field efficiency and fuel consumption and Specification of ride on type paddy weeder has given Table 1

Table 1 Specification of ride on type paddy weeder

S. No.	Particular	Specification power weeder
1.	Name of machine	Self-propelled ride on type paddy weeder
2.	Make	TNAU Coimbatore
3.	Model	Prototype
4.	Type of machine	Self-propelled
5.	Overall length of machine (mm)	1500
6.	Overall height of machine (mm)	950
7.	Overall width of machine (mm)	250
8.	Overall weight of machine (Kg)	52
10.	Width of blade (mm)	15
11.	No. of blades on wheel	28
12.	Diameter of weeder (mm)	600
13.	Weight of float (kg)	6
14.	Length of float (mm)	850
15.	Width of float (mm)	150

2.1 Wheel slippage

Wheel slip for power weeder was measured by monitoring the number of revolutions of the wheel over a specified distance under load and zero load conditions. The slip was calculated by using the following formula.

$$S' = \frac{n_1 - n_0}{n_0} \times 100 \dots\dots\dots (1)$$

Where,
 S' = wheel slip, per cent
 n₁ = number of revolution of wheel under load conditions for specified distance.
 n₀ = number of revolution of wheel under no load conditions for specified distance

In most of the cases the tool has no effect of slip at different levels of forward speed but fuel consumption increases considerably.

2.2 Effective field capacity

The weeding machine was operated in the different test fields. The area covered during the test was calculated. The effective field capacity was calculated by using following formula

$$\text{Effective field capacity (ha/h)} = \frac{\text{Area covered (ha)}}{\text{Time required (h)}} \dots\dots\dots (2)$$

2.3 Theoretical field capacity

It is always greater than actual field capacity. The theoretical field capacity was calculated by using following formula.

$$\text{T.F.C. (ha h}^{-1}\text{)} = \frac{W_t \times S}{10} \dots\dots\dots (3)$$

Where,

- T.F.C. = Theoretical field capacity, ha/h.
- W_t = Theoretical width of operation, m.
- S = Speed of operation, km/h.

2.4 Field Efficiency

The field efficiency was calculated from theoretical and effective field capacity by using following formula.

$$\text{Field efficiency (\%)} = \frac{\text{E.F.C.}}{\text{T.F.C.}} \times 100 \dots\dots\dots (4)$$

Where,

- E.F.C. = Effective field capacity, ha h⁻¹.
- T.F.C. = Theoretical field capacity, ha h⁻¹.

2.5 Weeding Efficiency

The developed weeder was operated in the experimental plot. Before operation of the weeder the numbers of weeds in the plot were counted. After the operation the number of weeds left in the plot was also counted. This procedure was repeated at different depth. The forward speed was maintained at constant in all the field tests. Weeding efficiency was calculated by the following expression.

$$E = \frac{W_1 - W_2}{W_1} \dots\dots\dots (5)$$

Where,

- E = weeding efficiency,%
- W₁ = number of weeds counted before operation in square metre area
- W₂ = number of weeds counted after operation, in square metre area

2.6 Plant damage

The quality of work done is the measure of damage on crop during weeding operation. It is calculated using the following expression (Remesean *et al.*, 2007).

$$DF = \frac{Q_2}{Q_1} \times 100 \quad (6)$$

Where

- DF -Damage factor, per cent
- Q1 -Number of plants in 10 m row before weeding
- Q2 -Number of plants damaged in 10 m row after weeding

2.7 Fuel consumption

The fuel consumption has direct effect on economics of the weeder. It was measured by Top fill method. The fuel tank was filled to full capacity before the testing at level condition. After completion of test operation, amount of fuel required to top fill again is the fuel consumption for the test duration. This observation was used for computation of fuel consumption in L/h.

3. RESULTS AND DISCUSSION

3.1 Field evaluation of ride on type paddy weeder

The developed prototype self-propelled ride on type paddy weeder was evaluated in paddy field having cone index 0.14 to 2 kg cm⁻².

3.1.1 Wheel slippage

Wheel slip for power weeder was measured by monitoring the number of revolutions of the wheel over a specified distance under load and zero load conditions. Number of revolutions of wheel in 10 m row under no load was 11.

Number of revolutions of wheel in 10 m row under load was 13.

$$S' = \frac{n_1 - n_0}{n_0} \times 100 = \frac{13-11}{13} = 15 \%$$

The determined wheel slip of the prototype ride on type paddy weeder was 15%.

3.1.2 Effective field capacity

The effective field capacity of the self-propelled ride on type weeder obtained from the experiments varied between 0.03 ha/h to 0.0306 ha/h and the average effective field capacity of the weeder was 0.03004 ha/h. The results are presented in Table 2 and Field view of paddy weeder shown in Figure 2



Fig.2 Field view of ride on type paddy weeder

3.1.3 Theoretical field capacity

It is always greater than effective field capacity
Width of weeder is 0.15 m and speed of operation is 2.5 kmh⁻¹

$$\begin{aligned} \text{T.F.C. (ha h}^{-1}\text{)} &= \frac{W_s \times S}{10} \\ &= \frac{0.15 \times 2.5}{10} = 0.0375 \text{ ha h}^{-1} \end{aligned}$$

3.1.4 Field Efficiency

The field efficiency was calculated from theoretical and effective field capacity by using following formula.

$$\begin{aligned} \text{Field efficiency (\%)} &= \frac{\text{E.F.C.}}{\text{T.F.C.}} \times 100 \\ &= \frac{0.03004}{0.0375} \\ &= 80.35 \% \end{aligned}$$

The field efficiency of the prototype weeder was 80.35 % and effective field capacity and field efficiency of the weeder is given in Table 2

Table 2 Field capacity and efficiency of ride on paddy weeder

Observations	Area of field in (m ²)	Ride on paddy weeder	
		Effective field capacity	Field efficiency (%)
1	300	0.03064	81.73
2	300	0.02998	79.95
3	300	0.0295	79.39
Average	300	0.03004	80.35

3.1.5 Weeding efficiency

The weeding efficiency of developed self-propelled weeder was determined and presented in Table 3. Weeding operation of the experimental plot shown in Fig 3 and 4.

Table 3 Weeding efficiency of weeder at 22 DAS

Observation	Ride on type paddy weeder		Weeding efficiency %
	Number of weeds in 1 sq.m area Before weeding	After weeding	
1	123	21	82.93
2	131	23	82.44
3	140	19	86.43
4	151	23	84.77
5	132	26	80.30
6	127	19	85.04
7	119	21	82.35
8	163	20	87.73
9	134	21	84.33
Average			84.04



Fig.3 View of the field before weeding



Fig.4 View of the field after weeding

Plant damage

The plant damage was measured in paddy field and furnished in Table 4

Table 4 Plant damage by weeder at 22 DAS

Observations	Ride on type paddy weeder		
	Number of plants in 10 m row length		Plant damage %
	Before weeding	Plants damaged after weeding	
1	40	2	5.0
2	40	1	2.50
3	40	1	2.50
4	40	1	2.50
5	40	1	2.50
6	40	1	2.50
7	40	2	5.0
8	40	1	2.50
9	40	2	5.0
Average			3.33

3.1.6 Fuel consumption

Fuel consumption of the weeder was calculated by “topping method”. It was observed that the fuel consumption of the self-propelled ride on type paddy weeder varied between 0.557 L/h to 0.635 L/h and the average fuel consumption was 0.6 L/h and given Table 5

Table 5 Performance evaluation of prototype ride on type paddy weeder

S.No.	Parameters	Values
1.	Wheel slip, %	15
2.	Weeding efficiency, %	84.4 %
3.	Plant damage, %	3.33
4.	Field capacity, ha h ⁻¹	0.0306
5.	Field efficiency, %	80.35
6.	Fuel consumption, lit h ⁻¹	0.6

4. CONCLUSION

In field evaluation the of developed ride on type paddy weeder the following evaluated parameters were wheel slip 15%, effective field capacity 0.03004 hah-1, theoretical field capacity 0.0375 ha h-1, field efficiency 80.35 %, plant damage 3.33% and weeding efficiency 84.04%. Fuel consumption of the weeder was 0.6 lit h-1 and cost of operation of developed weeder was Rs. 2741.11 ha-1. From performance evaluation of ride on type paddy weeder found better than hand weeding and power operated paddy

weeder in rice cultivation.

5. REFERENCES

- Barah, B.C. and Pandey, S., 2005. Rainfed rice production systems in Eastern India: An on farm diagnosis and policy alternatives. *Indian Journal of Agricultural Economics*, **60**(1): 110-136.
- Chaudhary V. P., S. K. Sharma., D. K. Pandey and B. Gangwar .2006. Energy Assessment of Different Weed Management Practices for Rice-Wheat Cropping System in India.
- Hobbs, P.R. and R.R. Bellinder. 2004. Weed management in less developed countries. *Encyclopedia of Plant and Crop Science*. Marcel Dekker, Inc. NY: 1295-1298.
- Nag, P.K and P. Dutt. 1979. Effectiveness of some simple agricultural weeder with reference to physiological responses. *Journal of Human Ergology*, 8.1, 13:21.
- Nag, P.K. and Nag. A. 2004. Drudgery, accidents and injuries in Indian agriculture. *Industrial Health*: 42, 149–162.
- Pathak, M.D., Ou, S.H. and S.K. de Datta .1976. *Pesticides and Human Welfare*.(Eds D.L.Gunn and J.G.R. Stephens). Oxford University Press.
- R. Remesan, M.S. Roopesh, N. Remya and P.S. Preman. “Wet Land Paddy Weeding- A Comprehensive Comparative Study from South India”. *Agricultural Engineering International: the CIGR Ejournal. Manuscript PM 07 011. Vol. IX. December, 2007*

Presence of an Epibiont *Epistylis* sp. (Protozoa, Ciliophora) on Some Zooplankton

Hilal Bulut, Serap Saler

Abstract—Protozoan ciliate epibionts infestation on zooplankton in Cip Dam Lake were studied seasonally, between spring 2014-winter 2015. The ciliates peritrich Epibiont *Epistylis* sp. (Protozoa, Ciliophora) was found as colony form on some individuals of different zooplanktonic groups, especially rotifers and copepods. Totally 23 zooplankton species (19 species from Rotifera, 3 species from Cladocera and 1 species from Copepoda in Cip Dam Lake) were investigated. Rotifers were the most important zooplanktonic group (82.7 % of total) and the taxa observed with epibionts were *Keratella*, *Polyarthra*, and *Brachionus*. The highest densities of infected zooplankton were observed in winter (14265 ind.m⁻³), the lowest densities of infected zooplankton were found in summer (3056 ind.m⁻³). Rotifers were the most infected groups with 75% in this study. *Epistylis* sp. was found on three species of rotifers and one copepod species. Infestation of *Epistylis* sp. has been registered for the first time in Cip Dam Lake.

Keywords—copepoda, epibiosis, peritrich, rotifera

Corresponding Author

Hilal Bulut from Firat University, Turkey
e-mail: hilalhaykir@gmail.com

Prevention of Ragging and Sexual Gender Based Violence (SGBV) in Higher Education Institutions in Sri Lanka

Anusha Edirisinghe

Abstract—Sexual Gender based violence is a most common social phenomenon in higher education institutions. It has become a hidden crime of the Universities. Masculinities norms and attitudes are more influential and serve as key drivers and risk for ragging and SGBV. Several studies have shown that in Sri Lankan universities, SGBV takes from the violence and murder of women students, assault and battery coerced sex, sexual harassment including harassment via information technology. This study focus is to prevention of ragging and SGBV in University system. Main objective of this paper describes and critically analyses of plight of ragging and SGBV in higher education institutions and legal and national level policy implementation to prevent these crimes in society. This paper is with special reference to ragging case from University of Kelaniya 2016. University Grant commission introduced an Act for the prevention of Ragging and gender standing committee established in Sri Lanka in 2016. And each university has been involved in the prevention of SGBV and ragging in higher education institutions. Case study from first year female student, reported sexual harassment was reported to the police station in May in 2016. After this case, the university has been implementing emergency action plan, short term and long term action plan. Ragging and SGBV task force was established and online complaint center opened to all students and academic and non- academics. Under these circumstances student complained to SGBV and other harassment to the university. University security system was strong support with police and marshals, and vigilant committees including lecturers. After this case all universities start to several programmes to stop violence in university

Keywords—higher Education, ragging, sexual gender-based violence, Sri Lanka

Corresponding Author

Anusha Edirisinghe Arachchige from University of Kelaniya, Sri Lanka
e-mail: anusha_edirisinghe@yahoo.com

Prevention of Ragging, Sexual and Gender Based Violence in Higher Education Institutions in Sri Lanka

Anusha Edirisinghe

edirsinghe@kln.ac.lk

Abstract— Sexual Gender based violence is a most common social phenomenon in higher education institutions. It has become a hidden crime of the Universities. Masculinities norms and attitudes are more influential and serve as key drivers and risk for ragging and SGBV. Several studies have shown that in Sri Lankan universities, SGBV takes from the violence and murder of women students, assault and battery coerced sex, sexual harassment including harassment via information technology. This study focus is to prevent ragging and SGBV in University system.

Main objective of this paper describes and critically analyses the plight of ragging and SGBV in higher education institutions and delves on legal and national level policy implementation to prevent these crimes in society. This paper is with special reference to ragging case from University of xxxxxxxx 2016. It is noteworthy, that the University Grant commission of Sri Lanka has introduced an Act for the prevention of ragging and established a gender standing committee in 2016. Each university is involved in the prevention of SGBV and ragging in higher education institutions in the country.

Case study from first year female student with regard to her complaint on sexual harassment came to light in May, 2016. After this case, the university has implemented emergency action plan, both short term and long term. To prevent ragging and SGBV, a task force was established in the recent past and an online complaint center is now open to all students, academics and non-academics. Under these circumstances, every student is given the liberty & opportunity to complain on incidents relating to sexual and gender based violence and other harassment to the university authority. University security system has been further strengthened with the strong support of police and marshals, and with the appointment of vigilant committees headed by lecturers. After this incident, Universities across the country have commenced several programmes to stop violence in university.

Keywords— Higher Education, Ragging, Sri Lanka, Sexual Gender Based Violence

I. INTRODUCTION

Sexual gender based violence, is a common social phenomenon across the globe. It has become a more serious issue to both men & women, irrespective of gender, caste,

Dr.E.A.D.Anusha Edirisinghe, Senior Lecturer in Criminology, Dept. of Sociology,. Author special thanks to financial supported from University.

religion, ethnicity and social background. In most occasions, it is children, women and elders who are victimized in the society under the gender based violence. Women from different cultures across the world are subjected to violence on a daily basis due to community violence, violence by state and domestic violence. Maintenance of law and order in any society is strenuous. Ragging and gender based violence are identified as grave crimes and are hidden practices in Sri Lankan society.

Ragging and SGBV can lead to physical damage, psychological impact, loss of bodily function, suicide and other health related issues. And it also violates criminal law in society and human rights.

Ragging is thought to have begun in educational institutions in the 18th Century and was very much in vogue in European countries. The concept was then adopted in the US in a milder form known as 'hazing', and spread across the world during the era of colonization, entering the Indian sub-continent along with the British education system. Stern laws against ragging have resulted in its eradication from the West and most of the rest of the world. However, it remains in Sri Lankan educational institutions. (Groundviews:25/07/2016).

Ragging is defined as an act that "causes or is likely to cause physical or psychological injury or mental pain or fear to a student or a staff member". Sexual gender based violence and ragging violence have become a serious threat to higher education institutions as well as mass society. Statistics show 15 students have died, two students have committed suicide, 25 students have been disabled, and six sexually abused and more than 6,000 students have left universities All incidents mentioned above are results of ragging by seniors and the failure of university and state authorities to take effective countermeasures or to implement the law strictly.

Reported cases from the University history in Sri Lanka, In 1975 Peradeniya University was the first to report a major ragging related incident when a fresher of the Faculty of Agriculture became paralyzed as a result of having jumped from the second floor of the hostel to escape the physical ragging by seniors. (University World News:2016). Year 1997 a female student committed suicide due to the sexual harassment from senior students, also 2011, undergraduate from first year, semi paralyzed due to the physical ragging in the University. (Goonarathne:2016). According to the studies and reported cases under ragging and SGBV in Universities, it

is evident that discrimination and gender based violence is targeted mainly on female students. Some students have given up their academic life. Both male and female students were confronted with brutal ragging and sexual gender based violence. Therefore this issue should be identified as a social issue and such gruesome practices should be eradicated from the society.

Most scholars have identified ragging as an issue which isn't dependent entirely on gender as both men & women are subjected to SGBV in educational institutions. It is universally accepted that violence against women is a main subject of human rights activism. Physical, sexual and psychological violence occurring in the higher educational institutions carried out by senior students to freshers of the university. Under these circumstances gender based discrimination is committed mainly by the super seniors/senior students in the university. In Sri Lanka, Prevention of Ragging Act was introduced to the educational institutions in 1998. As result of the ragging and sexual gender based violence, university system will be disorganized while all types of degree programs will be annulled.

Most of sociologists and other scholars from different disciplines have conducted research studies based on sexual gender violence and ragging in universities. Sexual Gender based harassment takes the form of brutal violence leading to murder of female students, assaults, battering, rape, sexual abuse etc...with the use of IT (University Grand Commission, Care International & University Teacher's Association, 2013:21). One study was presented for the 10th National Convention of women Studies titled "Gender based harassment among medical students conducted by Jennifer Perera SD Abeyanayake and DP Galabada have highlighted following conclusions: as for the report 55.6% males and females (72.2%) has forced the gender based violence during the university study period (University Grand Commission, Care International & University Teacher's Association, 2013:21). Student faced gender based violence in lecture time and in the common room and canteen. Based on statistics, 21.6% of Students don't know how to report this to proper place in University.

Another study on Gender based violence in University conducted by Gunawardene, Lalini Rajapaksha, Prabashi Wijesekara and PW Chathurangana (2011), Most of students victimized sexual and physical abuse in university premises. A previous study conducted by Asvini Fernando and Wasantha Karunasekara (2009) at the University of Kelaniya, One thousand three hundred twenty two (1322) students participated as the respondents of the study and 44% students had been sexually abused in their childhood while 36% physically abused during their childhood.

Another study conducted in 2008, respondents from Dental Students in Sri Lankan Universities, 50% reported, they have confronted some form of harassment namely verbally and emotionally. Minority of 18% respondents expressed abuse of sexual nature (Rodrigo, Lekamwasam: 2015). Sexual gender based violence is identified in ragging activities.

II. GENDER EQUALITY AND SEXUAL GENDER BASED VIOLENCE

Unequal, unfair, masculinities directly linked to the ragging and sexual gender based violence. It is with no doubt, that both men and women to obtain gender justice. Gender equality is described as equal visibility, empowerment, and participation of women and men in all spheres of public and private life (United Nations Population Fund:2012). Gender equality refers to equal rights, responsibilities, treatment and opportunities men and women, girls and boys of all ages. It is an integral part of human rights and aims to promote the full and equal male and female participation in society.

Sexual gender based violence based on gender and sexuality. United Nation Declaration on the Elimination of Violence against Women (DEVAW) (1993) has described the GBV following statement. "Any act of gender based violence that result in, or likely to result in physical sexual and psychological harm or suffering to women, including threats of such acts, coercion or arbitrary deprivation of liberty, whether it occurs in public or in private life. Article 2, United Nations Declaration on the Elimination of Violence against women (1993), highlights sexual or gender based violence occurred at the home, general community and state. Gender discrimination causal link between genders based violence.

III MASCULINITIES AND POLITICS IN HIGHER EDUCATION INSTITUTIONS

Gender refers to the socially constructed expectations, assumptions about differences roles behaviors activities, attitudes, personality traits and attributes, physical and instinctual capacities that a given society considers appropriate for men and women based solely on their identity as men or woman (Ministry of Women Affairs:2013). Male and female are sex categories, feminine and masculine are gender categories. According to incidents of ragging and sexual gender based violence in Universities, masculinity ideology has shown in these cases. Kamal Basin has described, the ideology and practice of masculinities is produced by social institutions and through every day interactions (University Grand Commission, Federation of Teachers Association and Care International: 2015). Masculinities show every cultural zone in the society. In higher education institutions and in various parts of society hegemonic ideology survives even to this day. In Sri Lanka, Care International has done a research on Masculinities in the society. Major concept of masculinities cause to increase the higher rate of ragging and gender based violence. Unequal gender relationship is a reason for violence against women or men.

University students Associations are more politicized & the University students are actively involved in politics in mass society. In their years of study at the University the students support general politics in the country & use the inhuman ragging and gender based violence to support the party politics. They have expressed ragging as an important tool to socialization in the university premises. Socialization means internalizing norms in relevant institutions. However ragging

and gender based violence in University is more supportive tools for surviving sub cultural norms (Interviews: 2016).

IV LEGAL FRAMWORK ON PREVENTION ON RAGGING AND GENDER BASED VIOLENCE

There are international standers, & criminal law to help support & stop gender based violence in society. The penal code of Sri Lanka deals with the sexual violence by community, domestic premises or state. Several provisions have related to sexual gender based violence. Rape, sexual harassment, grievous sexual abuse, Molestation, unnatural sexual offence define the penal code new amendments 1995 and 1998. Prevention of domestic violence Act (2005), has recognized the domestic violence as a punishable offence in the society. The Prohibition of ragging and of other Forms of Violence in Educational Institutions Act No 20 of 1998 introduced for ragging prevention and control.

A. THE PROHIBITION OF RAGGING AND OF OTHER FORMS OF VIOLENCE IN EDUCATIONAL INSTITUTIONS ACT NO 20 OF 1998

Above Act, Section 2 (2) is of specific importance to universities as it has been drafted to prevent and punish sexual harassment that can occur during the course of ragging. Whoever, by assault or use of criminal force, sexually harasses another person, or by the use of words or actions, causes sexual annoyance, harassment or commits the offence of sexual harassment, in such circumstances conviction is allowed with imprisonment of either description for a term which may extend to five years or with fine or with both and may also be ordered to pay compensation of an amount determined by court to the person in respect of whom the offence was committed for the injuries caused to such person.

Acts of ragging of both men and women often amounts to sexual violence ranging from sexual harassment to grave sexual abuse. Possibly rape though not reported Gender boundaries are unclear, women are both perpetrators and victims, attitudinal problems of authorities. Under the Ragging Act, highlight offenses are high Criminal intimidation, hostage taking, wrongful restraint, Unlawful confinement, Forcible occupation and damage to property in higher educational institutions. A person who, whilst committing ragging causes sexual harassment or grievous hurt to any student or a member of the staff, of an educational institution shall be guilty of an offence under this Act and shall on conviction after summary trial before a Magistrate be liable to imprisonment for a term not exceeding ten years and may also be ordered to pay compensation of an amount determined by court, to the person in respect of whom the offence was committed for the injuries caused to such person. Perpetrators and victims can be both students and staff in educational institutions such as schools, universities or any other higher educational institutions. According to the Prevention of Ragging Act, offences are non - bail able offence and only a High Court judge can give a bail order and also called cognizable offence – person can be arrested without a warrant under the provisions, perpetrators and victims can be both students and staff.

Commission Circular No. 919 of 15th January 2010, guidelines to be introduced to curb the menace of ragging in the Universities or Higher Educational Institutes, Sets out the actions which amount to ragging including sexual harassment,

Sets out the preventive measures to be taken and procedures to be followed in the event of ragging taking place. University of xxxxxxxx, 27th of April of 2016 implemented prevention of ragging act for victimized first year female student. Academics from all faculties agreed to respect & uphold the zero tolerance approach to stop ragging and sexual gender based violence.

B. CASE STUDY OF VICTIMIZED FEMALE STUDENT

A first year female student was subjected to ragging at the University of xxxxxx on the 27th of April 2016. The ragging has involved verbal, physical and mental abuse and threats and therefore violates the Prohibition of Ragging and other Forms of Violence in Educational Institutions Act, No 20 of 1998. The victimised girl reported this incident to the nearest police station and submitted digital evidences of verbal threaten involving sexual harassment. Under the Prevention of ragging act, the police arrested 04 female and 07 male students.

V. PREVENTION OF RAGGING AND SGBV IN UNIVERSITY

A. ACTION PLAN

After this complaint, the university has prepared the action plan for safeguarding the victim and her family. Centre for gender studies in University of xxxxxxxx facilitates the implementation of several programmes in university. Centre for Gender Studies conducted a consultative workshop for all university senior academics and has prepared strategies for universities in 2013. Under these circumstances university Grand Commission has established gender standing committee in 2015 and has commenced awareness programmes for academics.

The goal of the action plan is to institute a dynamic, peaceful and liberal atmosphere in the university that is conducive to high academic productivity. As for the case of academics it is essential to establish such an environment in university premises. The objective of the action plan are to provide physical protection and psychological empowerment for the female students who are currently under threat, to provide back up support for staff members who may come under threat for initiating anti-ragging measures, to operation a grievance redress mechanism and a hotline with appropriate working procedures, to empower university staff and students to deal with the inevitable backlash, to ensure that there is zero tolerance for ragging – no ragging at the University of xxxxxxxx from the year 2016 (University of xxxxxxxx:2016).

After this particular incident of sexual violence against the female student, the university has established a Task Force for Ragging and SGBV in May of 2016, with the support extended by representatives from Police, community leaders, senior academics, teachers associations, student unions, and non-academic staff. It is chaired by the vice chancellor of the University and other office bearers are working to stop any form of gender based violence in university. Due to the fact that ragging activities are common in hostels, further new rules were introduced on behalf of the students to prevent such happenings in the future. I have gathered information from students about ragging incidents. Most of students said that senior male students ragging the juniors at night in hostels.

Basically, Task force for Prevention of ragging and sexual gender based violence has implemented a tree type action plan to the university, emergency action plan, middle term plan and long term action plan.

Immediate action plan was prepared for the protection and safety of the female victims of SGBV. Recently, a permanent staff of 08 female and male marshals from retired police, Navy, Army and Department of Prisons were recruited to protect the students and to patrol university premises. A chief security officer from the Army, recruited to overlook the security section. Action plan has been proposed to assist the victimized students with psychiatric counseling and to ensure the health and mental wellbeing of the students, further measures have been drawn. Based on reported cases & inquiries, students have been suspended due to their misconducts such as ragging and sexual gender based violence. Students those who are accused or convicted of ragging will be allowed to sit for exams at the prison department. All students are requested to wear their identity cards in university premises. As a long term action plan, there are several steps that have been identified to stop & prevent ragging in university.

Signing a declaration with students unions, regular awareness programmes such as lectures and training related to law, social impact and psychological impact of ragging and SGBV are carried out on a regular basis to educate the students. Posters, plays, songs, dances, advertisements and films will be produced to prevent incidents of ragging, sexual & gender based violence. Academic unions and senior academics have been participating in social and mainstream media programmes to create further awareness concerning SGBV. Members of student's unions have used social media (Face book and Email) to blame those accused and in support of the victims. It has been proposed to compile a student directory and an on-line student data base for the case of dissemination to all students.

The students who wish to report any incident could raise their complaints online. Vigilant groups and student counselors have started programmes to encourage and empower staff to deal with sensitive issues such as ragging and sexual gender based violence. University task force and administration have discussed with the student union and human rights groups in society. They have supported to conduct awareness programme and other activities. Furthermore, authorities have proposed to discuss the issues with political leaders. All students are entitled to report his/her complaints concerning unjustly happenings such as ragging by contacting the on line complaint centers. As for the sake of emergency, phone numbers have been distributed to all marshals and directors of student affairs.

University of xxxxxxx has implemented several steps to combat sexual gender based violence and ragging. Victimized girl reported the incident to police station, and the accused students were arrested & produced to the court and to prevent incidents of ragging happening in the future new rules and regulations have been implemented. After this situation various backlashes were jumped to the society by students. The High court is working on the case since three months & has implemented the act of prevention of ragging, while most of student are expected to support the new laws &

implementations in the university and within the interuniversity system. University action plan has been conducted successfully to stop violence in University. Long term action plan will be implemented based on level of years, level of Faculties..

ACKNOWLEDGMENT

The Author thanks to Vice-Chancellor Prof xxxxxx and Dean, Prof xxxxxx Faculty of Social Sciences, University of xxxxxxx, Sri Lanka. And also Author takes this opportunity to gratitude loving her family members.

REFERENCES

- [1] Commission Circular No. 919 of 15th January 2010, University Grand Commission, Colombo, 2010.
- [2] Fonseka N. Ragging in our universities: a symptom or a disease? *Groundviews.org* [Internet]. Available from: <http://groundviews.org/2009/11/30/ragging-in-our-universities-a-symptom-or-a-disease/>, officers among students affairs2009 Nov 30 [cited 2015 Jul 6].
- [3] Goonaratna C. Legal framework on Sexual Gender Based Violence and Ragging in Universities, Presented at the University of Kelaniya, Sri Lanka, 2016.
- [4] Hennayake SK. The fundamental threat to Sri Lankan University education. *Asian. Tribune* [Internet]. Available from: <http://www.asiantribune.com/?q=node/14294>, 2008 Nov 20 [cited 2015 Jul 6].
- [5] Premadasa IG, Wanigasooriya NC, Thalib L, Ellepola AN. Harassment of newly admitted undergraduates by senior students in a Faculty of Dentistry in Sri Lanka. *Med Teach*. 2011; 33(10):e556-63.
- [6] Prohibition of Ragging and other forms of Violence in Educational Institutions Act No. 20 of 1998.
- [7] Lekamwasam s., Rodrigo M, Wickramathilake, M., Wijesinghe, C, Wijerathne, G., Silva, A.D., Napagoda, Attanayake, A., Perera, C., Preventing Ragging: outcome of an integrated programme in a medical faculty in Sri Lanka, *Indian Journal of Medical Ethics*. August 30, 2015.
- [8] United Nations Populations Fund, Sri Lanka Law Directory on Protection of Women and Girl Children, Ministry of Women, Nawala, Nugegoda, Sri Lanka, 2012.
- [9] University Grand Commission, Federation of University Teacher's Association & Care International, Colombo, Sri Lanka, 2015.
- [10] University of xxxxxx, Action Plan to Prevent Ragging at the University, Unpublished document, 2016.
- [11] University World News, University Ragging rages on despite Law, Issue 204, 2012.

Process Monitoring based on Parameter-less Self Organizing Map

Young Jae Choung, Seoung Bum Kim

Abstract—Statistical Process Control (SPC) is a popular technique for process monitoring. A widely used tools in SPC is a control chart, which is used to detect the abnormal status of a process and maintain the controlled status of the process. Traditional control charts, such as Hotelling's T^2 control chart, are effective techniques to detect abnormal observations and monitor processes. However, many complicated manufacturing systems exhibit nonlinearity because of the different demands of the market. In this case, the unregulated use of a traditional linear modeling approach may not be effective. In reality, many industrial processes contain the nonlinear and time-varying properties because of the fluctuation of process raw materials, slowing shift of the set points, aging of the main process components, seasoning effects, and catalyst deactivation. The use of traditional SPC techniques with time-varying data will degrade the performance of the monitoring scheme. To address these issues, in the present study, we propose a parameter-less self-organizing map (PLSOM)-based control chart. The PLSOM-based control chart not only can manage a situation where the distribution or parameter of the target observations changes, but also address the nonlinearity of modern manufacturing systems. The control limits of the proposed PLSOM chart are established by estimating the empirical level of significance on the percentile data using a bootstrap method. Experimental results with simulated data and actual process data from a thin-film transistor-liquid crystal display process demonstrated the effectiveness and usefulness of the proposed chart.

Keywords—Control chart, parameter-less self-organizing map, self-organizing map, time-varying property

Young Jae Choung is with the Department of Industrial Management Engineering, Korea University, Seoul, Korea (phone: 82-2-3290-3769; fax: 82-2-929-5888; e-mail: youngjae8734@gmail.com).

Seoung Bum Kim is with the Department of Industrial Management Engineering, Korea University, Seoul, Korea (phone: 82-2-3290-3397; fax: 82-2-929-5888; e-mail: sbkim1@korea.ac.kr).

Programmed Cell Death in *Datura* and Defensive Plant Response toward Tomato Mosaic Virus

Asma Alhuqail, Nagwa Aref

Abstract—Programmed cell death resembles a real nature active defense in *Datura metel* against TMV after three days of virus infection. Physiological plant response was assessed for asymptomatic healthy and symptomatic infected detached leaves. The results indicated H₂O₂ and Chlorophyll-a as the most potential parameters. Chlorophyll-a was considered the only significant predictor variant for the H₂O₂ dependent variant with a P value of 0.001 and R-square of 0.900. The plant immune response was measured within three days of virus infection using the cutoff value of H₂O₂ (61.095 μ mol/100 mg) and (63.201 units) for the tail moment in the Comet Assay. Their percentage changes were 255.12% and 522.40% respectively which reflects the stress of virus infection in the plant. Moreover, H₂O₂ showed 100% specificity and sensitivity in the symptomatic infected group using the receiver-operating characteristic (ROC). All tested parameters in the symptomatic infected group had significant correlations with twenty-five positive and thirty-one negative correlations where the P value was <0.05 and 0.01. Chlorophyll-a parameter had a crucial role of highly significant correlation between total protein and salicylic acid. Contrarily, this correlation with tail moment unit was ($r = -0.930$, $P < 0.01$) where the P value was < 0.01. The strongest significant negative correlation was between Chlorophyll-a and H₂O₂ at $P < 0.01$, while moderate negative significant correlation was seen for Chlorophyll-b where the P value < 0.05. The present study discloses the secret of the three days of rapid transient production of activated oxygen species (AOS) that was enough for having potential quantitative physiological parameters for defensive plant response toward the virus.

Keywords—programmed cell death, plant-adaptive immune response, hydrogen peroxide (H₂O₂), physiological parameters

Corresponding Author

Asma Alhuqail from King Saud University, Saudi Arabia
e-mail: Huqail@hotmail.com

Public Universities in Africa: Disjuncture and Fracture in Mission

Ogutu Miruka

Abstract—The paper addresses the following question: What ought to be the mission of a public university in Africa today? The keyword here is CRISIS. The crisis in public universities whereby there is disjuncture in vision (between the managers of universities and the statespersons as well as industry) and fractures (or discontinuities) in thinking in both student and lecturer as well as manager due to uncertainties borne out of being owned by government. There is also the issue of different expectations among different stakeholders of the public universities leading to tension and friction in the wheels of the higher education institutions. These developments demand that we re-assess cross-institutional missions for fitness of purpose. This lecture presents my humble contribution to the task. On the face of it, one would assume that the more African countries advance economically, the easier it becomes to establish and efficiently run public universities the way it would be with say hospitals or roads and so on. But this is not so for a number of reasons. For one, universities have historically evolved lock-i-step with civilization. What I mean by this is that human societies are synonymous with knowledge. Societies produce knowledge that in turn spurs more learning to advance even greater knowledge. Traditionally, universities have been at the centre of this knowledge creation. Indeed, with the exception of some very old religious orders, the university is one of the oldest bureaucratic organizations known to man. So while economic development might allow a country to build and sustain a growing number of universities, it is equally true that a well-functioning university could also be an instrument of economic growth as well as a source of good governance ideas and practices. The present crisis in public universities presents us with a classical wicked problem. The famed Canadian educator, Laurence Johnston Peters famous quip that some problems are so complex that you have to be highly intelligent and well informed just to be undecided about them would be indicative of the present crisis. The same gentleman also lent Management the Peter principle: Anything that works will be used in progressively more challenging applications until it fails. We need to avoid the temptation to use what has worked before when it becomes clear that present challenges may have exceeded its effective scope.

Keywords—Africa, higher education policy and management, crisis, engaged scholarship

Corresponding Author

Ogutu Miruka from Vaal University of Technology, South Africa
e-mail: ogutu.miruka@gmail.com

Recaptualization, Conceptual Foundations and Objectives of Internationalization of Higher Education

Ali Khorsandi Taskoh

Abstract—Internationalization of higher education has been the most important agent of change across the wide variety of countries and settings over the last three decades. There is not an academic evidence that internationalization has been a core element of universities' strategic plans in Iran, as it has never been a significant trend in the area of higher education research and studies. In the absence of either a strategic trend or a collection of significant research resources in Farsi, this paper first re-conceptualizes the idea of internationalization and addresses its relationship with globalization. The paper, then, addresses the key question of what goals and rationales impact policy makers and universities presidents to engage in internationalization activities. This study used a qualitative methodology with a descriptive-analytical method and critical-documentary analysis. This study showed that internationalization is conceptually changing and evolving as there may be a significant gap between its perceptions in theory and its experiences in practice. The paper also showed that the decision to acknowledge internationalization as a priority is based on different objectives ranging from instrumental-functional (such as branding and revenue generating) to idealistic (such as peacebuilding and global citizen development) components.

Keywords—Higher Education, Internationalization, Policy Analysis, Globalization.

Corresponding Author

Ali Khorsandi Taskoh from Allameh Tabataba'i University, Tehran,
Iran, Islamic Republic Of
e-mail: khorsandi@gmail.com

Recycling of Poultry Waste as an Economic and Effective Aqua-Feed

Saroj Kumar Pyne, Pratyush Bhaskar, Arun Kumar Ray

Abstract—India is gifted with immense livestock wealth and it is growing at the rate of > 6% per annum. The input of livestock production including poultry and fish is increasing significantly in Gross Domestic Product (GDP) of the country which accounts for > 40% of the total agricultural sector and > 12% of GDP. Thus, a huge amount of poultry wastes such as litter, viscera, skin, feathers and dead parts could appear as major environmental pollutants. However, no such cost-effective technologies are yet to be identified to recycle the waste as useful products which could show direct impact on the economy and environmental pollution of the country. Simultaneously, the provisions of fishmeal are not satisfactory to sustain the current growth rate of aquaculture industry. Various studies have reported possibilities of alternative low cost and available sources to replace fishmeal without affecting fish performance. This experiment was aimed to assess the effect of different poultry wastes as an alternative dietary protein source, on the carcass characteristics of *Clarias batrachus* after 60 days feeding period. Feed ingredients were processed through cleaning, salting, fumigation and sun drying respectively, before stored in refrigerator. Feeding trials were performed in 42-L circular fibre tanks with water recirculation system. Triplicate groups of fingerlings each were fed four iso-nitrogenous compound diets, at 5% of wet body weight basis. 25 fingerlings were randomly sampled for each treatment. Control diet was based on fishmeal as major protein source, while the other three experimental diets were prepared with poultry skin, poultry intestine and poultry viscera respectively, as major protein sources, though other ingredients remained same for all the compound diets. Feed readjusted biweekly. Biweekly changes were recorded. As a result, poultry viscera were appeared as one of the most effective feed ingredient containing 60.67% protein and 12.25% lipid. Feed production charge was decreased >20% and >14% extra weight gain should be attained in fish body, by using poultry viscera meal replacing fishmeal, at 100% replacement level in compound diet. It is hoped that the ending results will reveal more clues that will justify poultry viscera as a potential recycle-able waste material in aquaculture industry.

Keywords—fishmeal, poultry waste, proximate composition, protein

Corresponding Author

Saroj Kumar Pyne from Visva-Bharati University, India
e-mail: sarojpyne@yahoo.com

Remote Sensing and GIS-Based Environmental Monitoring by Extracting Land Surface Temperature of Abbottabad, Pakistan

Malik Abid Hussain Khokhar, Muhammad Adnan Tahir, Hisham Bin Hafeez Awan

Abstract—Continuous environmental determinism and climatic change in the entire globe due to increasing land surface temperature (LST) has become a vital phenomenon nowadays. LST is accelerating because of increasing greenhouse gases in the environment which results of melting down ice caps, ice sheets and glaciers. It has not only worse effects on vegetation and water bodies of the region but has also severe impacts on monsoon areas in the form of capricious rainfall and monsoon failure extensive precipitation. Environment can be monitored with the help of various geographic information systems (GIS) based algorithms i.e. SC (Single), DA (Dual Angle), Mao, Sobrino and SW (Split Window). Estimation of LST is very much possible from digital image processing of satellite imagery. This paper will encompass extraction of LST of Abbottabad using SW technique of GIS and Remote Sensing over last ten years by means of Landsat 7 ETM+ (Environmental Thematic Mapper) and Landsat 8 vide their Thermal Infrared (TIR Sensor) and Optical Land Imager (OLI sensor less Landsat 7 ETM+) having 100 m TIR resolution and 30 m Spectral Resolutions. These sensors have two TIR bands each; their emissivity and spectral radiance will be used as input statistics in SW algorithm for LST extraction. Emissivity will be derived by Normalized Difference Vegetation Index (NDVI) threshold methods using 2-5 bands of OLI with the help of e-cognition software and spectral radiance will be extracted TIR Bands (Band 10-11 and Band 6 of Landsat 7 ETM+). Accuracy of results will be evaluated by weather data as well. The successive research will have a significant role for all tires of governing bodies related to climate change departments.

Keywords—Environment, Landsat8, SW Algorithm TIR

Malik Abid Hussain Khokhar is with Department of Military Geography PMA, National University of Science and Technology, Islamabad 44000 Pakistan (phone: +923337237137; e-mail: abidmalikgeo@gmail.com).

Muhammad Adnan Tahir is with the Department of Environmental Sciences, COMSAT Institute of Information Technology Abbottabad 22010, Pakistan.

Hisham Bin Hafeez Awan is with Department of Military Geography PMA, National University of Science and Technology, Islamabad 44000 Pakistan.

Rheological Evaluation of Wall Materials and β -Carotene Loaded Microencapsules

Gargi Ghoshal, Ashay Jain, Deepika Thakur, U. S. Shivhare, O. P. Katare

Abstract—The main objectives of this work were the rheological characterization of dispersions, emulsions at different pH used in the microcapsules preparation and the microcapsules obtain from gum arabic (A), guar gum (G), casein (C) and whey protein isolate (W) to keep β -carotene protected from degradation using the complex coacervation microencapsulation technique (CCM). The evaluation of rheological properties of dispersions, emulsions of different pH and so obtained microencapsules manifest the changes occur in the molecular structure of wall materials during the encapsulation process of β -carotene. These dispersions, emulsions of different pH and formulated microencapsules were subjected to go through various conducted experiments (flow curve test, amplitude sweep, and frequency sweep test) using controlled stress dynamic rheometer. Flow properties were evaluated as a function of apparent viscosity under steady shear rate ranging from 0.1 to 100 s⁻¹. The frequency sweep test was conducted to determine the extent of viscosity and elasticity present in the samples at constant strain under changing angular frequency range from 0.1 to 100 rad/s at 25°C. The dispersions and emulsion exhibited a shear thinning non-Newtonian behavior whereas microencapsules are considered as shear-thickening respectively. The apparent viscosity for dispersion, emulsions were decreased at low shear rates 20 s⁻¹ and for microencapsules, it decreases up to ~50 s⁻¹ besides these value, it has shown constant pattern. Oscillatory shear experiments showed a predominant viscous liquid behavior up to crossover frequencies of dispersions of C, W, A at 49.47 rad/s, 57.60 rad/s and 21.45 rad/s emulsion sample of AW at pH 5.0 it was 17.85 rad/s and GW microencapsules 61.40 rad/s respectively whereas no such crossover was found in G dispersion, emulsion with C and microencapsules still it showed more viscous behavior. Storage and loss modulus decreases with time also a shift of the crossover towards lower frequencies for A, W and C was observed respectively. However, their microencapsules showed more viscous behavior as compared to samples prior to blending.

Keywords—viscosity, gums, proteins, frequency sweep test, apparent viscosity

Corresponding Author

Gargi Ghoshal from Dr. S.S. Bhatnagar University Institute of Chemical Engineering & Technology, India
e-mail: gghoshal@yahoo.com

River Profile: A Balutakay River Profiling

Melanie Pecision

Abstract—Rivers are paramount importance to life whether considered in terms of human health, ecosystem health or spiritual. River degradation is particularly dramatic in some urban and rural areas. It has been the focus of human activity throughout ancient and modern times. And so necessary is the protection against floods and river disasters, that pursuit for knowledge of the systems overtime. A lot of rivers in Davao del Sur were definitely in its critical condition. As per observation one of these rivers which are suffering from a poor situation is Balutakay river water course. As an area increases in its size and density the magnitude effects on river ecosystem also increases. Development of these areas tends to alter the geometry and bank erosion, water quality and geodiversity aspects of the watercourse. Profiling of this river was done through a process of rapid assessment and laboratory tests on its physical, morphological and microbiological aspects. Appraisal of geoinicator conditions were allocated in points system with 1 = poor, 2 = moderate, and 3 = good. Results were being recorded after the mean of every assessment done by the researcher based on the qualitative description of the condition of the variables. Laboratory test results were assessed based on the normal values given. The study shows that Balutakay river is still on its good standing, moderate to poor depending on the area where the sample has been taken, in terms of its physical attributes in geometry and bank erosion the mean score is 2.44 which means that it is in between moderate to good score, riverbanks must be planted with more trees and should not be denuded so that it can add up to the sustainability of the river. In terms of water quality, the score is in its moderate state with a mean score is 2.0 which means that it is now alarming so the government must take its part in making a thorough survey of the area. With the geodiversity result it shows that it is in its moderate score that is may be due to human activities. With microbiological result, it shows that water contains high E-coli contaminants which are alarming to the residents of this Barangay. Geomorphic and Microbiological aspects has been degraded and contaminated over time. All properties of Balutakay river must be taken care of. Water is life; river is one of the sources of water to sustain living organisms. If we cannot take good care of this it may run dry and may be a cause of a devastating life. Everything is a cycle so we must do our part to maintain and balance this cycle. Future generation needs a responsible older generation. Let us be responsible, be the next generations inspiration.

Keywords—conservation, healthy ecosystem, preservation, responsibility

Corresponding Author

Melanie Pecision from University of Mindanao, Philippines
e-mail: pecisionmelaniem@yahoo.com

Role of Long Noncoding RNA HULC on Colorectal Carcinoma Progression through Epigenetically Repressing NKD2 Expression

Shu-Jun Li^{1,2}, Cheng-Cao Sun¹, and De-Jia Li¹

¹ Department of Occupational and Environmental Health, School of Public Health, Wuhan University, Wuhan, P. R. China; ² Wuhan Hospital for the Prevention and Treatment of Occupational Diseases, 430071 Wuhan, P. R. China;

Corresponding author: De-Jia Li; No.115 Donghu Road, Wuchang District, Wuhan, China; Tel: (86)18271470520; Fax: (86)02768778695; E-mail: lodjlwhu@sina.com

Abstract

Recently, long noncoding RNAs (lncRNAs) have been emerged as crucial regulators of human diseases and prognostic markers in numerous of cancers, including colorectal carcinoma (CRC). Here, we identified an oncogenetic lncRNA HULC, which may promote colorectal tumorigenesis. HULC has been found to be up-regulated and acts as oncogene in gastric cancer and hepatocellular carcinoma, but its expression pattern, biological function and underlying mechanism in CRC is still undetermined. Here, we reported that HULC expression is also over-expressed in CRC, and its increased level is associated with poor prognosis and shorter survival. Knockdown of HULC impaired CRC cells proliferation, migration and invasion, facilitated cell apoptosis *in vitro*, and inhibited tumorigenicity of CRC cells *in vivo*. Mechanistically, RNA immunoprecipitation (RIP) and RNA pull-down experiment demonstrated that HULC could simultaneously interact with EZH2 to repress underlying targets NKD2 transcription. In addition, rescue experiments determined that HULC oncogenic function is partly dependent on repressing NKD2. Taken together, our findings expound how HULC over-expression endows an oncogenic function in CRC.

Key words: long noncoding RNA, HULC, NKD2, colorectal carcinoma, proliferation, apoptosis

Rural Livelihood under a Changing Climate Pattern in the Zio District of Togo, West Africa

Martial Amou

Abstract—This study was carried out to assess the situation of households' livelihood under a changing climate pattern in the Zio district of Togo, West Africa. The study examined three important aspects: (i) assessment of households' livelihood situation under a changing climate pattern, (ii) farmers' perception and understanding of local climate change, (iii) determinants of adaptation strategies undertaken in cropping pattern to climate change. To this end, secondary sources of data, and survey data collected from 235 farmers in four villages in the study area were used. Adapted conceptual framework from Sustainable Livelihood Framework of DFID, two steps Binary Logistic Regression Model and descriptive statistics were used in this study as methodological approaches. Based on Sustainable Livelihood Approach (SLA), various factors revolving around the livelihoods of the rural community were grouped into social, natural, physical, human, and financial capital. Thus, the study came up that households' livelihood situation represented by the overall livelihood index in the study area (34%) is below the standard average households' livelihood security index (50%). The natural capital was found as the poorest asset (13%) and this will severely affect the sustainability of livelihood in the long run. The result from descriptive statistics and the first step regression (selection model) indicated that most of the farmers in the study area have clear understanding of climate change even though they do not have any idea about greenhouse gases as the main cause behind the issue. From the second step regression (output model) result, education, farming experience, access to credit, access to extension services, cropland size, membership of a social group, distance to the nearest input market, were found to be the significant determinants of adaptation measures undertaken in cropping pattern by farmers in the study area. Based on the result of this study, recommendations are made to farmers, policy makers, institutions, and development service providers in order to better target interventions which build, promote or facilitate the adoption of adaptation measures with potential to build resilience to climate change and then improve rural livelihood.

Keywords—climate change, rural livelihood, cropping pattern, adaptation, Zio District

Corresponding Author

Martial Amou from University of Lomé, Togo
e-mail: aaamartio@yahoo.fr

Science of Social Work: Recognizing Its Existence as a Scientific Discipline by a Method Triangulation

S. Mendes

Abstract—Social Work has encountered over time with multivariate requests in the field of its action, provisioning frameworks of knowledge and praxis. Over the years, we have observed a transformation of society and, consequently, of the public who deals with the social work practitioners. Both, training and profession have needed to adapt and readapt the ways of doing, bailing up theories to action, while action unfolds emancipation of new theories. The theoretical questioning of this subject lies on classical authors from social sciences, and contemporary authors of Social Work. In fact, both enhance, in the design of social work, an integration and social cohesion function, creating a culture of action and theory, attributing to its method a relevant function, which shall be a promoter of social changes in various dimensions of both individual and collective life, as well as scientific knowledge. On the other hand, it is assumed that Social Work, through its professionalism and through the academy, is now closer to distinguish itself from other Social Sciences as an autonomous scientific field, being, however, in the center of power struggles. This paper seeks to fill the gap in social work literature about the study of the scientific field of this area of knowledge.

Keywords—Field Theory, knowledge, science, social work.

I. INTRODUCTION

THIS paper intends to be the beginning of the framework construction to shape the science of Social Work. The aim is to demonstrate which terms we need when we want to talk about Social Work Science and why this dimension is so important for the field of a scientific discipline. We begin with a revue of social transformation to understanding why social work is a so important field, but also to understand in its definition its scientific research identity. We rescue from “structural social work theory” the idea of a constant transformation in social work. The perspective of some authors about Social Work and the contemporaneity where research appears as a “traditional thing” give a historical power to begin a legitimacy of social work as a dominant scientific discipline in the scientific field. In a second part we approach the field theory of Pierre Bourdieu to understand why social work does not have power as scientific discipline in the scientific field, however without losing its place in this board game forces. Then, we take a look on the discussion about the epistemology of Social Work, reminding classical authors from philosophy of sciences and contemporary authors who shaped epistemological debates in Social Work. In the fourth part we question, by a research that we are working in,

what scientific elements are important in order to social work be growing and legitimated by the scientific social world. In the end, we conclude with a Portuguese perspective (our perspective) about science in/for/of social work.

II. TRAVELING IN A NEW ERA

We are traveling through profound social changes with the developing of technology and social networks, which allow the possibility to have cultural experiences via the virtual world. Today we can watch a Rolling Stones concert direct live in Cuba from our living room or read the latest news from the New York Times without leaving home. Without realizing it, this virtual experience created in us new emotional and cultural dispositions, which produced new emotional needs in individuals, namely in a sensitive point of view. The “new” place of this sensitive dimension in social perspective has accompanied the beginnings of Social Work, both the pole of praxis, as well as the scientific one.

Social Work, as a profession and as a science, has progressively been the object of attention by the actors of the national and international social work field. Methods such as action-research or Evidence Based Practice (EBP) have advocated an approach where theory and practice maintain a unison relationship, so hold [16], [12], [9]. Additionally, [15] addresses the need of an alternative vision of society (more and more transformed and structured) from social work, which is in better agreement with the social, emotional, cultural, physical and spiritual well-being of all people (and not just a minority). In recent decades, there have been major events, such as the transformation of capitalism. We were all witnesses of the nation-states power decline to intervene in their own economies, or the rise of terrorism both in the growing Eastern societies and Western societies as well. Inequalities have not stopped growing between individuals and countries. All of us saw the Berlin Wall fall and the dismantling of socialist regimes, national trade union movements, the virtual collapse of left policies in developed nations and the continued oppression on the basis of class distinction, gender, culture, sexuality, age, ethnicity, geographical origin, etc. Social institutions function in a certain way that discriminate people. When [15] uses the term “structural”, it is prescriptive of social work practice and indicates that the focus for change is predominantly in the structures of society and not just the person. If we rescue the new definition of social work adopted in Melbourne in 2014, it recognizes that one’s professional practice is defined as a social intervention, but also as a source of theoretical construction by scientific research. Besides these perspectives,

S. Mendes is a social worker and a PhD Social Work student at School of Sociology and Public Policy, ISCTE- University Institute of Lisbon. Is also with the Centre for Research and Studies in Sociology (CIES), University Institute of Lisbon (e-mail: Sandra_Raquel_Mendes@iscte.pt).

some years before, [14] found that research in social work is not a contemporary framework at all. The investigative tradition goes back, according to the author, to the late nineteenth century, when the profession was looking for an organization.

III. SOCIAL WORK, A SCIENTIFIC FIELD

To realize the scientific field of social work, and therefore our research field, we appeal Pierre Bourdieu's proposal, specifically the theory of scientific field [3]. This theory presents us the scientific field as a system of objective relationships between acquired positions within the inner struggles to the field, and the place of a competitive struggle. The main goal of any scientific field is to obtain the monopoly of scientific authority, also defined as technical capacity and as social power. In his theory, Bourdieu shows us how each specific field is distinguished from others by the volume, structure, and trajectory of the capital. In this case, this capital is the monopoly of scientific ability, as the legitimate science talking and acting ability, which is socially recognized to a certain agent. To analyze the scientific field of social work it requires an analysis of these three dimensions.

The scientific field of social work is a structured space of positions and positions taken by individuals, but also by institutions, which are, in present, fighting for the monopoly of scientific authority at the same time that it tries to become autonomous. Accordingly to [3], participants engage struggles for the value of their work which is determined by the predominant principle of scientific perception. In addition, a struggle field is also a battlefield, where players are fighting for a change in the relative weight of the different types of "scientific capital".

The operation of the field produces and assumes some specific form of scientific interest and scientific authority. The fact that all practices are geared toward the acquisition of scientific authority (prestige, recognition, celebrity, etc.), lead the interest for a scientific activity always in double ways, as well as the strategies that tend to ensure the satisfaction of this interest. It is the scientific field, as a place of political struggle for scientific domination, who assigns to each researcher, depending on the position one occupies, its political and scientific problems that by reference to the system of political and scientific positions constituents of the scientific field are at the same time political strategies. Indeed, this is one of the powers that each science brings with itself. If we look at social work, it is not difficult to see that in the same way it is influenced by public policies, it also influences these same policies.

When Bourdieu addresses the scientific authority, he addresses a clear form of social capital that ensures power over the basic mechanisms of the field and that can be converted into other forms of capital. Within the scientific field, this strongly autonomous field, a particular producer cannot expect the recognition of the value of one's products (reputation, prestige, authority and competence) unless by other producers who, paradoxically, are also one's competitors and less likely to give value to such producer. This fact will

lead us to think that social work should have within its field, cohesion and authority in its accreditation as a scientific field concern, since as Bourdieu states "... one that appeals to an authority outside the field can only attract discredit " [3].

The struggle in which each agent must commit to impose the value of one's products and one's own legitimate production of authority has always as the ultimate goal, the power to impose the definition of science, by the way, the most consistent to their specific interests, i.e. the one that best allows them to take quite rightly the dominant position. In order for social work to get its recognition with legitimacy in the scientific field, it needs, in addition, to impose standards, scientific methods and theories to ensure its accuracy. Thus, to seek scientific authority in its field, the research in Social Work needs to deal within itself and only then should seek to impose itself to the other sciences of the scientific field. Indeed, the claims of legitimacy have its legitimacy in the relative strength of the groups in which interests are expressed, to the extent that the definition of evaluation criteria and the principles of hierarchy are also a fighting space where no one judges without thereby satisfying one of their own interests, becoming therefore partial parts.

IV. EPISTEMOLOGY OF SOCIAL WORK: A GREAT DEBATE

On the other hand, epistemologically speaking, and taking into account the work of [1], it is subsumed that scientific objectivity is possible only when it breaks with the immediate object and when it contradicts the thoughts that germinate from the practice. This is why scientific objectivity in social work emerges from reflective practice and rational social reality, when the real is questioned beyond what it is believed to be seen. Therefore, more than a recreation of a social control process, the methodological process, which is at the heart of the questioning process in social work, searches to look with scientific objectivity to its real problem, the person in its dimension of singular subject of rights and human dignity in its environment.

Social work epistemological questions or even ethical and professional ones were discussed throughout the theoretical production developed between the 40's and 60's, whose influence was proved to be pivotal in the dominant role that social work acquired in the mid-twentieth century, in the management of social problems. Engaged in and not undervaluing social work in the face of other professions, the intellectual and practical work of those social workers was focused in the fruitful relationship between knowledge about society, developed in the social sciences, and empirical knowledge, acquired through experimentation and observation, and putting into practice in the field of professional practice of social workers which is historically settled. [14]

More recently, [7], [8], [4], [5] enhance the design of social work as having an integration and social cohesion function, as creating a culture of action and theory, as attributing to its method a relevant function which promotes social change in several dimensions of individual and collective life, as well as the production of scientific knowledge. Indeed, Brekke defines

science in Social Work as “a combination of theory and empirical method rooted in ontological and epistemological context, applied to a defined set of phenomena” [5], while [7] demonstrates the existence of an epistemological social work way, based on the relationship of theory and practice, where the discipline uses the theoretical frameworks of social sciences and humanities, guided by four groups of values: humanistic, democratic, political and economic, and educational.

Moreover, [13] claims, in this dialogue that to understand the practice of social work, as it unfolds in open systems, it takes a certain epistemological break with positivism. They agree with [4], [21] about the proposals of critical realism as a solution to the crisis of knowledge in social work. In their perspective, the critical realist philosophy of science allows properly to think the practice of Social Work, as it provides a consistent reflection on the place of values in knowledge production, allowing to re-think the positivists and conventional assumptions about the relationship between fact and value [13]. In addition, [20] stated in an article published in response to Brekke, that the meeting of social work as a science currently seems to be much less utopian or far-reaching. Even if ambiguous, it is in fact what Sommerfeld shows us, when he questions the American social work (with a high scientific productivity in the field and a long university tradition) “What did you do for a 100 years at university if it was not scientific work? And how can it be that there are high-level social work research articles if there is no science of social work?” [21]. In this article he demonstrates the perspective of German-speaking countries, where scientific social work is now an assumed identity almost unquestioned.

V. WHAT IS THE SCIENTIFIC DIMENSION OF SOCIAL WORK IN CONTEMPORANEITY?

We consider that the attention given to social work shifts from a traditional professional activity to an activity that contemplates, simultaneously, an investigative exercise, giving birth to the marriage of action and theory. In Europe, as we have seen in society the end of the '60s, more precisely at the time of intense social movement from May '68, there are some questions that, again, rise in social work, namely its professionalization, the legitimacy of its activity, and its ability to produce knowledge. Recalling [17], it was the alternative and experimental approaches that took social work, not only as a hostage, but also as an empirical field which led to a cultural crisis contributing to its illegitimacy in the scientific sphere. For this author, the scientific field of social work was taken over by other scientific disciplines (as dominant in the scientific field), such as sociology, political science, social economy, social psychology, among others. Therefore, with Bourdieu we can understand that in order to resurge social work as a dominant scientific discipline in scientific field, we need to recognize its legitimacy within its own scientific subfield, and to do that, we have to discuss its scientific dimension.

To answer the question about what is the scientific dimension of Social Work in Contemporaneity, we need to

consider to systematize the scientific field of social work through the predominance of a qualitative paradigm and to analyze the significance of research in this area of knowledge as a producer of theory in social work from the complex analysis of the relationship between theory and practice, through a technical and methodological triangulation. In our perspective, these wide-ranging perceptions need to be developed through the interpretation of contemporary social work on the foundations of social science paying attention to its historical background. We also need to analyze the production of knowledge in Social Work having as a starting point, the scientific research conducted in this area. We pretend to identify both guiding epistemological dimensions of research in Social Work and theoretical frameworks already produced, as well as characterize the behavior, attitudes and expectations of researchers in Social Work towards the relationship between social work and science.

Authors like Brekke, Shaw, Sommerfeld, Floersch & Longhoffer have demonstrated the absence of a detailed study of the scientific dimension of social work, therefore, that is why we are doing a research to answer to this gap.

VI. A TROJAN HORSE TO ANSWER TO AN ACHILLES' HEEL

This paper follows the academic and scientific debate on the relevance and existence of social work to be distinguished as a scientific discipline, with a trajectory, a method and a set of theories through which it can legitimate its autonomy as a scientific discipline. Although [4] argues that the scientific methodologies and relevant scientific knowledge for social work have expanded over the last 30 years, demonstrating an advanced American standpoint regarding the perspective of science in Social Work, the Portuguese thought on this issue is something still new and consequently worthy of careful questioning.

In the social sciences subfield, social work faces contradictory arguments to be claim as a dominant scientific discipline. A dimension to remember is that all social sciences have a very fluid border with other social sciences. With regard to social work, the fact that it uses theories from other disciplines, both in practice, as in scientific production to understand the social world in which individuals are placed, it has often been revealed as its Achilles' heel. Throughout the research that we have been developing, we have noticed that this vulnerability becomes at the same time a Trojan horse that allows to social work play in the scientific field, recognizing its existence as a scientific discipline.

We recap Brekke when the author is careful about the fact that social work should have regard to the piggyback approach. Effectively, identity is likely to be committed to adopt the scientific perspectives of other disciplines, especially with the use of theories from other scientific disciplines of social sciences. Therefore, the use of these theories should be used only by taking into account the multidisciplinary nature that the social study must have when it comes to understanding the individual in their relationship with the environment. Indeed, the individual can only be understood as a whole if one is disassembled in different parts

under the understanding of different social sciences. However, it is through social work that we can understand the individual as a whole, through the values and ethical issues and focusing on one's change and social transformation, without forgetting the constant reflection and adjustment of the practice of social work. Social work's theory helps social workers to give sense to the complex and difficult human situation. They generate different understandings of human behavior and social situations without losing the focus in social transformation. We believe as Howe [6], that theory comes from the social work context, and from the social psychology and sociology but, for us, also from political sciences. Understanding the Howe perspective with our complementary view, social work produces scientific knowledge by reading reality and human behavior to social change, through structural and explanation perspectives (psychology and sociology married with political sciences). The first social work aim is to understand "how is it?", "why is it like that?" and "how to transform that?" We have to remind the reader that this discipline works with people, with the human side, with the collective and the individual dimension. Other professionals have one (or more) lif(v)e(s) in their hands like a surgeon performing a risky surgery. We, the social workers, have to know the body like a fragmented puzzle which can only work if every part of it is okay. When we have to deal with something like that we have to know human nature, the knowledge response and development process, and we have to be concerned with political context, and the economic and material environment where people live. Those are the objectives of the three sciences which we have mentioned before, but in social work they only can work in a marriage if they have an anti-oppressive and an anti-discriminatory perspective which we rescue from social work values. We can only understand someone if we see not only the human nature, but also the emotional condition and the capacity to a rational action to empowerment, understanding in that process past experiences. If we can talk now about a science of social work, we should talk about an emotional human science in the social sciences field devoted not only to praxis but also with ability to produce knowledge to the social work field and to other disciplines as well. Every single professional should be ready to think about "why my client is like this?", "why do I have to understand without being a social controller?" no matter if one is in natural sciences or in social sciences.

VII. CONCLUSION

To heed the prospect of [4], [5], [17]-[19], [21], we understand that the legitimacy of social work in the scientific field is, as in the past, an international issue. With [11] we can identify historical marks as moments of international scientific debate on social service dating back to the late twenties - 1928. These events have an important place when we reflect on the scientificity of the social work profession, since as [20] says, science is not discovered, but in our perspective which is consistent with the philosophy of science, it too can be found in its own history. We recall the three waves in the scientific accuracy of social work that have been thought out and

discussed in different international conferences. The first happened in 1928, after the World War II, and the third in the 80's and 90's. In this sequence, we believe that after achieving the technological advances of the last century where intellectual capital predominated over the emotional one, the 21st century gives new place to individual singularities. Here, the person is understood under ethical and humanitarian values given an environment in which virtual social networks take up as much or more space than real social network. In this context of change, social work has also at its heart, new concerns, new understandings and new practices which brings new crises. Lining identity crisis, ideologies crises, crises in conservative and avant-garde profession perspectives, the arena for the discussion of the legitimacy of social work as a knowledge scientifically recognized is open again - the 21st century as the fourth wave. In fact, there is an urgent need to discuss the issues of consolidation and legitimation of social work's science. Through [2] we can understand legitimation as an important process that objectifies a significance of a second order. It produces new meanings already connected to unrelated institutional processes. The essential function is to turn accessible, in an objective form and plausible mode, the objectivities from the first order which were already institutionalized.

To heed the perspective of [3]-[5], we understand that the challenge for him was to reflect and discuss the science emergence as a cannonball that ignites a new struggle of subfields (understood as the struggle between the scientific disciplines by achieving greater scientific power). Perhaps these struggles are seen as an obstacle to the emancipation of social work, but are however those that prove social work existence as a scientific discipline. Discuss its rigor, discuss different schools of social work, conservative views and avant-garde visions, among others, is no more than to do and to feed science in social work's science.

Believing in it as a scientific discipline, we conclude this paper with the questions that started our next research: How is configured social work science as a profession? What is social work's study? How, for what, and, for who? Who are the researchers? How does social work have legitimacy in the scientific field? For this last question we would refer to [10] "Science is dangerous; we have to keep it most carefully chained and muzzled."

REFERENCES

- [1] G. Bachelard, *A Epistemologia*. Lisboa Ed. 70, 1971.
- [2] P. Berger, T. Luckmann, *The Social Construction of Reality*. New York: Random House, 1966.
- [3] Bourdieu Pierre. *Le champ scientifique*. In: *Actes de la recherche en sciences sociales*. Vol. 2, n 2-3, juin 1976. La production de l'idéologie dominante. pp. 88-104.
- [4] J. Brekke, "Shaping a Science of Social Work.", *Research on Social Work Practice*, Vol. 22, No. 5, pp. 455-464, 2012.
- [5] J. Brekke, "The Role Quantitative Research Plays in Shaping the Science of Science of Social Work" in *The Society for Social Work and Research*, 2014.
- [6] M. Davies, *Modern Social Work Theory*. London: Palgrave Macmillan Ed. 4th, 2014
- [7] J. M. Ferreira, "Contributos para o debate da epistemologia em Serviço Social", *Trabajo Social Global*, Vol. 2, No. 3, pp. 63-77, 2011.

- [8] J. M. Ferreira, "Serviço Social: profissão e ciência Contributos para o debate científico nas ciências sociais", *Cuadernos de Trabajo Social* Vol. 21, No. 2, pp. 329-341, 2014.
- [9] C. K. Fraga, "A atitude investigativa no trabalho do assistente social", *Serviço Social & Sociedade*, No. 101, pp. 40-64.
- [10] A. Huxley, *Brave New World*. London: Vintage, 1932.
- [11] J. Kuilema, "Lessons from the first international conference on social work", *International Social Work*, pp. 1-13, 2014.
- [12] R. Lara, "Pesquisa e Serviço Social: da concepção burguesa de ciências sociais à perspectiva ontológica", *Rev. Katálysis* Vol. 10, pp. 73-82, 2007.
- [13] J. Longhoffer, J. Floersch, "The coming crisis in Social Work: Some thoughts on social work and science", *Research on Social Work Practice*, Vol. 22, No. 5, pp. 499-519, 2012.
- [14] H. Mouro, "A Investigação no Serviço Social: Os Anátemas de uma Velha Questão", *Interacções*, Vol. 7, pp. 100-109, 2004.
- [15] B. Mullaly, *The new structural social work*. Canada, Oxford University Press, 2007.
- [16] N. Parton, "Some thoughts on the relationship between theory and practice in and for social work", *British Journal of Social Work*, Vol. 30, No. 4, pp. 449-463, 2000.
- [17] S. Rullac, "De la scientificité du travail social. Quelles recherches pour quels savoir?", *Pensée plurielle*, Vol. 1, No. 26, pp. 111-128, 2011.
- [18] S. Rullac, *La science du travail social. Hypothèses et perspectives*. Issy-les Moulineaux: ESF éditeur, 2012.
- [19] S. Rullac, *La scientification du travail social*, Rennes: Presses de L'EHESP, 2014.
- [20] I. Shaw, "A science of social work? Response to John Brekke.", *Research on Social Work Practice*, Vol. 24, No. 5, pp. 524-526, 2014.
- [21] P. Sommerfeld, "Social work as an action science: A perspective from Europe.", *Research on Social Work Practice*, Vol. 24, No. 5, pp. 586-600, 2014.

Smart Cooling Using Hybrid Energy Resources

R. Benelmir, M. El Kadri, A. Donnot, D. Descieux

1

Abstract— HVAC represents a significant part of energy needs in buildings. Integrating renewable energy in cooling processes contributes to reduce primary energy consumption. Sorption refrigeration allows cold production through the use of solar/biomass/geothermal energy or even valuation of waste heat. This work present an analysis of an experimental bench incorporating an adsorption chiller driven by hybrid energy resources associating solar thermal collectors with a cogeneration gas engine and a geothermal heat pump.

Keywords— solar cooling – cogeneration - geothermal heat pump - hybrid energy resources.

I. INTRODUCTION

The technological platform ENERBAT was designed and realized by the research laboratory LERMAB of the University of Lorraine in order to conduct experimental investigation in dynamic operating mode of the coupling of an energy tri-generation system to a wooden two-zone sample building.

A bunch of solar thermal collectors, a geothermal heat pump and a cogeneration internal combustion gas engine are combined to produce heat through hot water for the needs of the sample building (heating floor of the hot zone) and also to drive an adsorption refrigeration machine which provides cold water to the sample building (cooling ceiling of the cold zone).

Moreover, the central partitioning of the cold and hot zone provides a space for the insertion of a sample construction or isolation material in order to consider studies of this material through specific temperature gradients.

II. DESCRIPTION OF THE PLATFORM ENERBAT

A. The global system

The heat requested for the operation of the platform is provided by the assembly of hybrid energy sources: solar, geothermal and gas.

Heat is stored in a stratified storage tank. A network of pipes allows the transmission of heat and cold to the equipment of the platform. The adsorption refrigeration machine uses a part of stored heat to produce cold necessary to maintain the temperature of the cold room at 10 °C. Other part of stored heat is transmitted to the hot room to keep its

temperature at 40 °C. Residual heat or cold is dissipated through dry heater/cooler.

B. The solar field

The solar field is the renewable energy source of the system. It's installed on the roof and composed of 16 solar panels Sun Win Energy Systems AF24VE2 with a total absorbing surface of 36 m². Its role is to feed the stratified storage tank with hot water. The solar panels are south oriented with an azimuthal angle of 49°, the latitude of Nancy. In well free sky, the maximum power is about 27 kW (Fig. 1).



Fig. 1: solar field

C. The stratified storage tank

With a storage capacity of 1500 liters, the storage tank collects heat provided mainly by the solar field (94°C max) and if needed by the cogeneration gas engine (95°C max). It consists of two heat exchangers in series for the solar water loop and a shell for the cogeneration engine hot water inlet and hot water supply leaving the tank. The hot water finds its target through the exchangers according to sunlight conditions. In case of good conditions ($T > 75^{\circ}\text{C}$) the thermal power produced by the solar field is sufficient for the operation of the platform. The hot water flows through both heat exchangers. Otherwise ($30^{\circ}\text{C} < T < 75^{\circ}\text{C}$), the missing power is provided by the gas cogeneration engine to respond to the needs of the adsorption refrigeration machine ($65^{\circ}\text{C} < T < 94^{\circ}\text{C}$). In such case, the hot water flows only through the lower heat exchanger in order to avoid cooling of the tank (Fig. 2).

R. Benelmir, M. El Kadri, A. Donnot, D. Descieux are with the LERMAB, Faculté des Sciences et Technologies. Bd. des Aiguillettes, BP 70239, 54506 Vandoeuvre-lès-Nancy, France. (riad.benelmir@univ-lorraine.fr).

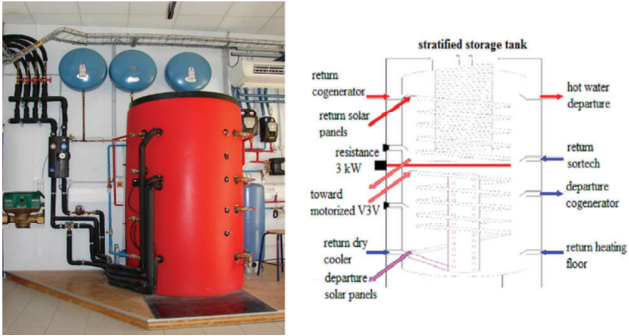


Fig. 2: stratified storage tank

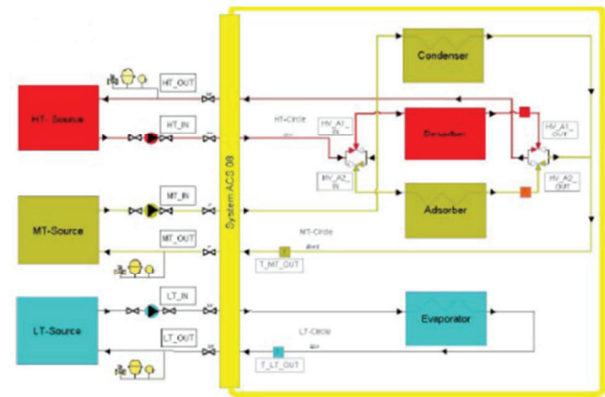


Fig. 4: operation diagram of the adsorption refrigeration machine

D. The internal combustion cogeneration gas engine

The cogenerator is a booster heat source used at low sunlight conditions. It's a dual production of energy (heat/electricity) using a single energy resource in order to improve energy efficiency. The cogenerator gas engine (Eco-power e47) has an operating regime that could be modulated between 1400 and 3400 rpm. Electric and thermal power output varies, respectively from 1.3 to 4.7 kW and 4 to 12.5 kW, with an outlet water's temperature near 85°C. The global efficiency of the cogeneration engine is about 90% (the thermal and the electrical efficiencies are respectively 60% and 30%) (Fig. 3).

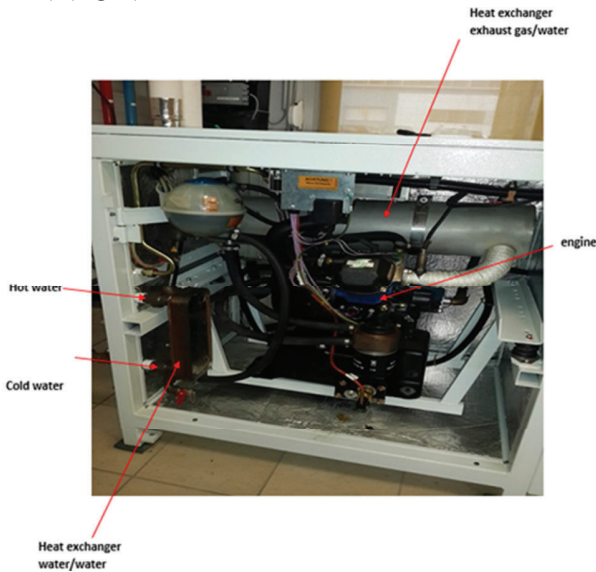


Fig. 3: internal combustion engine

The adsorption refrigeration machine (SORTECH AG), working with the silica gel/water couple, consumes heat from the storage tank to provide cold water for the cooling ceilings within the cold room (Fig. 5). Its cooling nominal power is about 8 kW for a water outlet/inlet temperature of 7/13°C and its COP is around 0.6. The adsorption refrigeration sink heat removal is operated either by a hybrid dry cooler-cooling tower (shifting to cooling tower mode at extremely warm external conditioning) or geothermal injection using the bore holes of the heat pump. Excess cold production is dissipated through a dry cooler.



Fig. 5: adsorption refrigeration machine

E. The adsorption refrigeration machine

The main difference between compression refrigeration machine and adsorption refrigeration machine is the substitution of the compressor (driven by primary energy) by a sorption system driven by heat which could be renewable or waste heat (Fig. 4).

F. The two-zone sample building

The walls and floor are made respectively of wood and concrete. The thickness of the walls and floor is 84 mm and 62 mm respectively. The sample building cover a total area of 18 m² (height of 2.3 m) and is divided into two identical cells (9 m² each). The cold cell is equipped with a cooling ceiling and the hot cell with a heating floor (Fig. 6).

The aim of the two-zone sample building is to test thermal properties of construction and insulation materials under real conditions. A space is reserved for the sample material within

the wall separating the two cells (cold/warm).



Fig. 6: sample building

The hot water provided by the storage tank (20°C to 55°C) flows in a coiled tube (heating floor) made of polyethylene (PER) to maintain the temperature of hot cell at 40°C. This tube is set over a layer of insulation material (polyurethane, 5 cm thick) and covered by a concrete screed (62 mm thick) realized with mortar fluid (Fig. 7).



Fig. 7: hot cell

The cooling ceiling is composed of 8 modules, each one consisting of a coiled copper tube welded on a rectangular steel plate. This ceiling which fills a total area of 5.76 m² and has a nominal power of 2480 W can maintain the temperature inside the cold room between 10°C and 20°C using the cold water produced in the adsorption refrigeration machine (Fig. 8).



Fig. 8: cold cell

III. NUMERICAL MODELING

A. Abbreviation list

$\frac{d}{dt}$:Derivative with respect to time
T	:Temperature (°C)
Σ	:Sum
\dot{m}	:Mass flow rate (kg/s)
o	:Outlet
h	:Enthalpy (J/kg)
E	:Internal energy (J)
I	:Inlet
\dot{Q}	:Exchanged heat (W)
\dot{W}	:Exchanged work (W)
M	:Mass (kg)
w	:Water
si	:Silica gel
eq	:Equilibrium
P	:Pressure (Pa)
sat	:Saturation
exp	:Exponential
cd	:Condenser of the adsorption refrigeration machine
des	:Desorber of the adsorption refrigeration machine
ev	:Evaporator of the adsorption refrigeration machine
ads	:Adsorber of the adsorption refrigeration machine
C_p	:Heat capacity
m	:Material in the compartment
ΔH	:Enthalpy of adsorption/desorption
ϕ	:Heat flux
U	:Thermal conductance of the heat exchanger in the compartment (W/m ² K)
A	:Surface of the heat exchanger in the compartment (m ²)
L_v	:Latent heat of water evaporation (J/kg)
hc	:Hot cell of the two-zone sample building
cc	:Cold cell of the two-zone sample building
hc → cc	:Heat flux from the hot cell to the cold cell of the two-zone sample building
sst	:Stratified storage tank
sf	:Solar field
coge	:Cogenerator
cu	:Copper
al	:Aluminum

B. The adsorption refrigeration machine

The adsorption refrigeration machine consists of four compartments: evaporator, adsorber, desorber and condenser. Each compartment contains a heat exchanger where the inlet water will heat, cool or be cooled, depending on the role of compartment.

Each compartment is considered as a thermal system. The variation of internal energy is driven according to the energy balance equation:

$$\frac{dT}{dt} + \sum_{outlet} \dot{m}_o h_o = \sum_{inlet} \dot{m}_i h_i + \dot{Q} + \dot{W} \quad (1)$$

The machine uses silica gel/water couple in its operation. The silica gel and the water are the adsorbent and the adsorbate respectively. The silica gel is attached to the external surface of the heat exchanger of the compartment. The water uptake ω is ratio of the water's mass adsorbed and the mass of silica gel.

$$\omega = \frac{m_w}{m_{si}} \quad (2)$$

The saturation point is reached when the adsorbent is unable to adsorb an additional quantity of adsorbate. The maximum uptake (called equilibrium uptake) is function of saturation pressure:

$$\omega_{eq} = 0.375 \left[\frac{P_{sat}(T_w)}{P_{sat}(T_s)} \right]^{1.6} \quad (3)$$

Saturation pressure depends of the temperature of compartment according to the equation:

$$P_{sat}(T) = \exp\left(23.5 - \frac{3984.9}{T-29.7}\right) \quad (4)$$

When the bed takes the role of desorber, the temperatures T_w and T_s in the equation (3) are the temperatures of condenser and desorber respectively. Else, in adsorption case, they represent the temperature of evaporator and adsorber. The temperature of each compartment is assumed to be homogeneous.

Desorption:

$$\omega_{eq} = 0.375 \left[\frac{P_{sat}(T_{cd})}{P_{sat}(T_{des})} \right]^{1.6} \quad (5)$$

Adsorption:

$$\omega_{eq} = 0.375 \left[\frac{P_{sat}(T_{ev})}{P_{sat}(T_{ads})} \right]^{1.6} \quad (6)$$

The derivative of the uptake can be expressed as:

$\frac{d\omega_{des}}{dt} = K_{des} (\omega_{eq,des} - \omega_{des})$	(7)
$\frac{d\omega_{ads}}{dt} = K_{ads} (\omega_{eq,ads} - \omega_{ads})$	(8)

$K_{ads/des}$ called coefficient of adsorption/desorption is a constant value depending of the type of couple adsorbent/adsorbate.

a) Energy balance of the desorber

All the compartments are assumed to be perfectly isolated, so they don't realize nor receive any heat or work. The temperature of each compartment is supposed to be homogeneous.

The hot inlet water flowing from the stratified storage tank will cause the desorption of adsorbate and heat the desorber. The variation of internal energy, the inlet and the outlet enthalpy can be written as:

$$\frac{dE}{dt} = \frac{d\Gamma_{des}}{dt} (m_{si} \omega_{des} C_{p,w} + m_{si} C_{p,si} + m_{cu} C_{p,cu} + m_{al} C_{p,al}) \quad (9)$$

$$\sum_{outlet} \dot{m}_o h_o = \dot{m}_{w,des} C_{p,w} T_{wo,des} - m_{si} \Delta H \frac{d\omega_{des}}{dt} \quad (10)$$

$$\sum_{inlet} \dot{m}_i h_i = \dot{m}_{w,des} C_{p,w} T_{wi,des} \quad (11)$$

By merging the equation (9), (10) and (11) with the equation (1):

$$\frac{d\Gamma_{des}}{dt} (m_{si} \omega_{des} C_{p,w} + m_{si} C_{p,si} + m_{cu} C_{p,cu} + m_{al} C_{p,al}) - m_{si} \Delta H \frac{d\omega_{des}}{dt} + \dot{m}_{w,des} C_{p,w} T_{wo,des} = \dot{m}_{w,des} C_{p,w} T_{wi,des} \quad (12)$$

$$\frac{d\Gamma_{des}}{dt} = \frac{\dot{m}_{w,des} C_{p,w} (T_{wi,des} - T_{wo,des}) + m_{si} \Delta H \frac{d\omega_{des}}{dt}}{m_{si} \omega_{des} C_{p,w} + m_{p,si} C_{p,si} + m_{cu} C_{p,cu} + m_{al} C_{p,al}} \quad (13)$$

The efficiency of heat exchanger is given by:

$$\varepsilon = \frac{\phi_{real}}{\phi_{max}} = 1 - \exp(-NUT) \quad (14)$$

The midterm of the equation (14) is written as:

$$\frac{\phi_{real}}{\phi_{max}} = \frac{\dot{m}_w C_{p,w} \Delta T_{real}}{\dot{m}_w C_{p,w} \Delta T_{max}} = \frac{T_{wi,des} - T_{wo,des}}{T_{wi,des} - T_{des}} \quad (15)$$

By inserting the equation (15) in the equation (14):

$$\frac{T_{wi,des} - T_{wo,des}}{T_{wi,des} - T_{des}} = 1 - \exp(-NUT) = 1 - \exp\left(\frac{-U_{des} A_{des}}{\dot{m}_{w,des} C_{p,w}}\right) \quad (16)$$

$$1 - \frac{T_{wi,des} - T_{wo,des}}{T_{wi,des} - T_{des}} = \exp\left(\frac{-U_{des} A_{des}}{\dot{m}_{w,des} C_{p,w}}\right) \quad (17)$$

$$\frac{T_{wi,des} - T_{des}}{T_{wi,des} - T_{des}} \frac{T_{wi,des} - T_{wo,des}}{T_{wi,des} - T_{des}} = \frac{T_{wo,des} - T_{des}}{T_{wi,des} - T_{des}} = \exp\left(\frac{-U_{des} A_{des}}{\dot{m}_{w,des} C_{p,w}}\right) \quad (18)$$

$$T_{wo,des} = T_{des} + (T_{wi,des} - T_{des}) \exp\left(\frac{-U_{des} A_{des}}{\dot{m}_{w,des} C_{p,w}}\right) \quad (19)$$

b) Energy balance of the condenser

The water vapor flowing from the desorber will cool and condensate in the condenser. The resulting heat flux is evacuated by the cooling water coming from the dry cooler. This water will also cause the cooling of the condenser:

$$\frac{dE}{dt} = \frac{d\Gamma_{cd}}{dt} (m_{w,cd} C_{p,w} + m_{cu} C_{p,cu}) \quad (20)$$

$$\sum_{outlet} \dot{m}_o h_o = \dot{m}_{w,cd} C_{p,w} T_{wo,cd} \quad (21)$$

$$\sum_{inlet} \dot{m}_i h_i = \dot{m}_{w,cd} C_{p,w} T_{wi,cd} - L_v m_{si} \frac{d\omega_{des}}{dt} - m_{si} C_{p,v} (T_{des} - T_{cd}) \frac{d\omega_{des}}{dt} \quad (22)$$

By merging the equation (20), (21) and (22) with the equation (1):

$$\frac{dT_{cd}}{dt} (m_{w,cd} C_{p,w} + m_{cu} C_{p,cu}) + \dot{m}_{w,cd} C_{p,w} T_{wo,cd} = -L_v m_{si} \frac{d\omega_{des}}{dt} \quad (23)$$

$$+ \dot{m}_{w,cd} C_{p,w} T_{wi,cd} - m_{si} C_{p,v} (T_{des} - T_{cd}) \frac{d\omega_{des}}{dt}$$

$$\frac{dT_{cd}}{dt} = \frac{\dot{m}_{w,cd} C_{p,w} (T_{wi,cd} - T_{wo,cd}) - m_{si} C_{p,v} (T_{des} - T_{cd}) \frac{d\omega_{des}}{dt} - L_v m_{si} \frac{d\omega_{des}}{dt}}{m_{w,cd} C_{p,w} + m_{cu} C_{p,cu}} \quad (24)$$

The water temperature at the outlet of condenser exchanger:

$$T_{wo,cd} = T_{cd} + (T_{wi,cd} - T_{cd}) \exp\left(\frac{-U_{cd} A_{cd}}{\dot{m}_{w,cd} C_{p,w}}\right) \quad (25)$$

c) Energy balance of the evaporator

The adsorption phenomena in the adsorber has as consequence a low pressure in the evaporator. Under this condition, the water in this compartment will evaporate. this endothermic reaction creates refrigeration power, the output power of this machine:

$$\frac{dE}{dt} = \frac{dT_{ev}}{dt} (m_{w,ev} C_{p,w} + m_{cu} C_{p,cu}) \quad (26)$$

$$\sum_{outlet} \dot{m}_o h_o = \dot{m}_{w,ev} C_{p,w} T_{wo,ev} + L_v m_{si} \frac{d\omega_{ads}}{dt} \quad (27)$$

$$\sum_{inlet} \dot{m}_i h_i = \dot{m}_{w,ev} C_{p,w} T_{wi,ev} - m_{si} C_{p,v} (T_{cd} - T_{ev}) \frac{d\omega_{des}}{dt} \quad (28)$$

$$\frac{dT_{ev}}{dt} (m_{w,ev} C_{p,w} + m_{cu} C_{p,cu}) + \dot{m}_{w,ev} C_{p,w} T_{wo,ev} =$$

$$-L_v m_{si} \frac{d\omega_{ads}}{dt} + \dot{m}_{w,ev} C_{p,w} T_{wi,ev} - m_{si} C_{p,v} (T_{cd} - T_{ev}) \frac{d\omega_{des}}{dt} \quad (29)$$

$$\frac{dT_{ev}}{dt} = \frac{\dot{m}_{w,ev} C_{p,w} (T_{wi,ev} - T_{wo,ev}) - m_{si} C_{p,v} (T_{cd} - T_{ev}) \frac{d\omega_{des}}{dt} - L_v m_{si} \frac{d\omega_{ads}}{dt}}{m_{w,ev} C_{p,w} + m_{cu} C_{p,cu}} \quad (30)$$

The water temperature at the outlet of evaporator exchanger:

$$T_{wo,ev} = T_{ev} + (T_{wi,ev} - T_{ev}) \exp\left(\frac{-U_{ev} A_{ev}}{\dot{m}_{w,ev} C_{p,w}}\right) \quad (31)$$

d) Energy balance of the adsorber

In the adsorber, the water vapor flowing from the evaporator will be cooled, then adsorbed by the silica gel. The heat of adsorption is evacuated by the cooling water coming from the dry cooler. The energy balance is expressed below:

$$\frac{dE}{dt} = \frac{dT_{ads}}{dt} (m_{si} \omega_{ads} C_{p,w} + m_{si} C_{p,si} + m_{cu} C_{p,cu} + m_{al} C_{p,al}) \quad (32)$$

$$\sum_{outlet} \dot{m}_o h_o = \dot{m}_{w,ads} C_{p,w} T_{wo,ads} \quad (33)$$

$$\sum_{inlet} \dot{m}_i h_i = \dot{m}_{w,ads} C_{p,w} T_{wi,ads} + m_{si} \Delta H \frac{d\omega_{ads}}{dt}$$

$$+ m_{si} C_{p,v} (T_{ev} - T_{ads}) \frac{d\omega_{ads}}{dt} \quad (34)$$

$$\frac{dT_{ads}}{dt} (m_{si} \omega_{ads} C_{p,w} + m_{si} C_{p,si} + m_{cu} C_{p,cu} + m_{al} C_{p,al}) +$$

$$\dot{m}_{w,ads} C_{p,w} T_{wo,ads} = m_{si} \Delta H \frac{d\omega_{ads}}{dt} + \dot{m}_{w,ads} C_{p,w} T_{wi,ads} +$$

$$m_{si} C_{p,v} (T_{ev} - T_{ads}) \frac{d\omega_{ads}}{dt} \quad (35)$$

$$\frac{dT_{ads}}{dt} = \frac{\dot{m}_{w,ads} C_{p,w} (T_{wi,ads} - T_{wo,ads}) + m_{si} C_{p,v} (T_{ev} - T_{ads}) \frac{d\omega_{ads}}{dt} + m_{si} \Delta H \frac{d\omega_{ads}}{dt}}{m_{si} \omega_{ads} C_{p,w} + m_{si} C_{p,si} + m_{cu} C_{p,cu} + m_{al} C_{p,al}} \quad (36)$$

The water temperature at the outlet of adsorber exchanger:

$$T_{wo,ads} = T_{ads} + (T_{wi,ads} - T_{ads}) \exp\left(\frac{-U_{ads} A_{ads}}{\dot{m}_{w,ads} C_{p,w}}\right) \quad (37)$$

C. The two-zone sample building

The two-zone sample building is constructed in the platform where the ambient temperature is about 20°C. In this model, the temperatures of the hot and cold cell are supposed to be 10°C and 40°C respectively. The heat flux spreading from the heating floor in the hot cell and toward the cooling ceiling in the cold cell can compensate the losses through the ceiling, the floor, the vertical walls, and the wall between the two cells.

For the hot cell:

$$\sum \text{losses} = \dot{m}_{wi,hc} C_{p,w} (T_{wi,hc} - T_{wo,hc}) \quad (38)$$

$$\sum \text{losses} = \phi_{ceiling} + \phi_{floor} + \phi_{walls} + \phi_{hc \rightarrow cc} \quad (39)$$

$$T_{wo,hc} = T_{wi,hc} - \frac{\sum \text{losses}}{\dot{m}_{wi,hc} C_{p,w}} \quad (40)$$

For the cold cell:

$$\sum \text{losses} = \dot{m}_{wi,cc} C_{p,w} (T_{wo,cc} - T_{wi,cc}) \quad (41)$$

$$\sum \text{losses} = \phi_{ceiling} + \phi_{floor} + \phi_{walls} + \phi_{hc \rightarrow cc} \quad (42)$$

$$T_{wo,cc} = T_{wi,cc} + \frac{\sum \text{losses}}{\dot{m}_{wi,cc} C_{p,w}} \quad (43)$$

D. Stratified storage tank

The stratified storage tank stores the power provided by both the solar collectors and the cogenerator, then transmits it to the adsorption refrigeration machine and the hot cell of the two-zone sample building. A part of the stored part is lost through the walls of the tank.

The tank is considered as thermal system; its energy balance can be written as:

$$\frac{dE}{dt} = \phi_{inlet} - \phi_{outlet} \quad (44)$$

The left member of this equation represents the variation of the temperature inside the tank. The inlet power is the power of solar collectors. The power provided to the adsorption refrigeration machine, the power consumed by the hot cell of the two-zone sample building, and the losses through the walls represent the outlet power.

$$m C_{p,w} \frac{dT_{sst}}{dt} = \phi_{sf} + \phi_{coge} - \phi_{des} - \phi_{hc} - \phi_{losses} \quad (45)$$

So the temperature of water inside the stratified storage tank is driven according to the equation below:

$$\frac{dT_{sst}}{dt} = \frac{\phi_{sf} + \phi_{coge} - \phi_{des} - \phi_{hc} - \phi_{losses}}{mC_{p,w}} \quad (46)$$

E. Cogenerator

The cogenerator is a booster which help the solar field to provide the necessary heat for the stratified storage tank. When the temperature of the last one is below 75°C, the cogenerator provides a constant power of 10 kW for the tank until its temperature reaches a maximum of 94°C. At this point the cogenerator stops working.

F. The solar field

The solar field is the renewable source of energy of the platform. Its output power depends on many factors: the sunshine, the outdoor temperature, the temperature of water circulating inside the tubes of the collectors, and the performance of its material.

The efficiency of the solar field is given by the equation below:

$$\epsilon_{sf} = 0.763 - 2.437 * 10^{-3} * (T_{sf} - T_{outdoor}) - 0.296 * 10^{-3} * (T_{sf} - T_{outdoor})^2 \quad (47)$$

G. Simulation results

The software used for this simulation is “MATLAB, Simulink”. The time of each cycle of the adsorption refrigeration machine is determined by a minimal necessary power of the evaporator which can provided to the cold cell of the two-zone sample building. This power is about 1160 W. During this simulation, the sunshine is following a sin function which starts with a minimum of 1W/m² at 6 a.m. and reach a maximum of 510 W/m² at 1 p.m. then turn back to its initial value at 9 p.m. The outdoor temperature is also following a sin function which starts with 11.75°C at 0 a.m., decreases to be 8.64°C at 6 a.m., then decreases during the day to reach its maximum of 14.86 at 18 p.m., and turns back to its initial value at 0 a.m.

The flow rates of inlet water in the evaporator, adsorber, desorber and condenser are respectively 0.56, 0.53, 0.36 and 0.5 l/s.

In our simulation, the maximum solar power is supposed to be 16 kW when sun reaches zenith with respect to summer solstice in a sunny day without nebulosity.

The purpose of our simulation is to determine the optimal incorporation between the solar system and the cogenerator, able to provide necessary power to the adsorption machine of 4 kW nominal cooling power. This power will be used to cool a building 24h/24.

The simulation starts at t₀=6 a.m., when the solar fields begins to be exposed to sunlight (Figure 9). The initial temperature of

the storage tank is 65°C. This temperature increases thanks to the power of both solar field and cogenerator. The adsorption machine starts to operate when this temperature reaches 74°C (point A in Figure 9). After 85°C (point B in Figure 9), the cogenerator stops its operation. The power of solar field is able alone to increase the temperature. The maximum allowed temperature of the tank is 94°C, so the pump between the solar field and the tank is switched off.

At 2 p.m., the power of solar field reaches its maximum. At 6 p.m., this power is no longer sufficient to compensate the power provided to the adsorption machine (point C in Figure 9). The temperature of the tank decreases. The cogenerator restarts when the temperature decreases below 65°C. After this, the power of 10 kW provided by the cogenerator is able to maintain the temperature at 65°C until the next day.

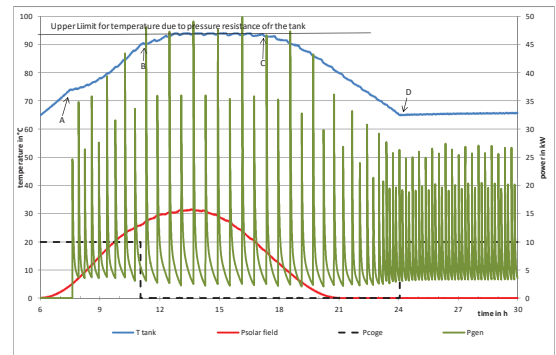


Figure 9: temperature of the storage tank, power of the generator, the cogenerator, and the solar field during 24h

Figure 9 shows the behavior of the three modules during a typical day: the cogenerator and the solar field provide together the heat power to the storage tank. The operation of the adsorption machine starts after 1h30. The cogenerator stops at 11 a.m. The solar field is able to provide sufficient power to the adsorption machine during 5h15. During the night, the cogenerator is the only provider of heat power. The temperature of the tank is maintained at the minimum level allowed to the operation of adsorption machine (65°).

By referring to Figure 9, we can prove the strong relation between the temperature of the tank and the operation of the adsorption machine: when the first one is above 74°C, the time-cycle of the second one is about 6200 s. Else it is about 600s. This difference is due to the behavior of the desorber. The high temperature of the tank leads to a high temperature of the desorber. The pressure of water vapor inside it becomes higher. Then the flow rate of water vapor flowing toward the condenser is higher leading to greater power exchanged between the compartments of the adsorption machine. The main consequence of the short time-cycle is the low cooling production of the adsorption machine (

Table I).

Table 1: mean power of the adsorption machine's generator and evaporator with and without the cogenerator (TXX and cogXX represent the initial temperature of the tank and the cut-off of the cogenerator respectively)

	Q_{gen} (cog on) kW	Q_{gen} (cog off) kW	Q_{ev} (cog on) kW	Q_{ev} (cog on) kW
T65-cog90	7.650	7.167	7.79	3.634
T65-cog85	7.638	7.213	1.543	3.685
T65-cog80	7.571	7.216	1.398	3.592

The first number in each cell of the first column of the

Table 1 represents the initial temperature of the storage tank. The second one represents the switch off temperature of the cogenerator.

The cooling power extracted at the evaporator is 3.6 kW when the switch of temperature of the cogenerator is 90°C. It becomes lower (1.6 kW) at a low temperature of the tank. It is noticeable that the variation of the power of generator is negligible (about 5%).

The challenge of this energy incorporation is to produce the possible maximum cooling with the minimum of non-renewable energy sources. To achieve this aim, we ran the simulator with different parameters:

Dispositive: solar field alone or solar field with cogenerator.
Temperatures:

- We ran the simulator with many cut off temperatures of the cogenerator.
- We ran the simulator with different several outdoor temperatures. Changing outdoor temperature has a direct effect on the outlet temperature of the dry cooler, which is the inlet temperature of condenser of the adsorption machine.

a) *Solar field alone*

The Figure 10 shows the evolution of the temperature of the storage tank starting with 3 initial temperatures: 65°C, 70°C and 75°C.

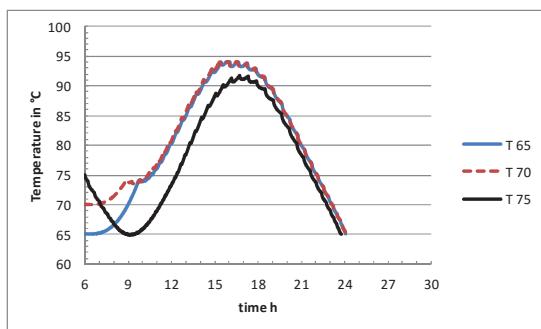


Figure 10: evolution of the temperature of the storage tank with three different initial temperatures

Without the cogenerator, the operation of the adsorption machine continues until 24h00 (12 a.m.), when the temperature of storage tank is below 65°C. The power stored in the tank provides an autonomy for the adsorption machine 3 hours after sunset.

Both 65°C and 70°C initial temperatures are not sufficient to a normal starting of the adsorption machine. To switch on this machine, we should wait about 3 hours, so the temperature of the storage tank reaches 74°C. However, when the initial temperature is 75°C, the adsorption machine can start immediately, so it consumes the power stored in the tank, and by consequence, the temperature of this last when decreases until the power of solar field become able to increase it.

The Table 2 shows the heat energy produced by the solar field, the cooling energy produced by the adsorption machine and the heat energy by the generator in the three cases of initial temperature of the storage tank.

Table 2: Energy and COP calculated for the 3 cases of initial temperature of the storage tank

	tank initial temperature 65°C	tank initial temperature 70°C	tank initial temperature 75°C
solar energy MJ/day	514	509	558
cooling energy MJ/day	173	183	174
generator used energy MJ/day	378	395	469
sortech COP	0.458	0.463	0.371
solar COP	0.337	0.360	0.312

For a high initial temperature of the storage tank (75°C) the energy of the solar field is greater than that for low initial temperature (70°) by 10%.

The quantity of the cooling energy produced is independent of the heat energy consumed by the generator which remains almost constant in the three cases. The weak COP of the adsorption machine acts against the solar energy gain, the solar COP becomes weaker.

b) *Solar field with cogenerator*

It is remarkable from the previous case that the solar field alone is unable to provide the necessary energy to the continuous operation of the adsorption machine, since the temperature of the storage tank becomes too low after 18 hours of operation. Second energy source is needed to warrant the continuous operation. It is the cogenerator.

The aim is to optimize the energy efficiency of the system during a whole day by finding the perfect coupling between the solar field and the cogenerator.

The Table 3 shows the simulation results obtained with three initial temperatures of the storage tank and three cut off temperatures of the cogenerator.

The cogenerator is switched of when the temperature of the storage tank reaches specified limit (80°C, 85°C and 90°C),

and restarts always when this temperature becomes below 65°C.

Table 3: simulation results obtained with different operation conditions of the storage tank and the cogenerator

	field energy (MJ)	cogenerator energy (MJ)	evaporator energy (MJ)	solar COP	cogenerator COP	global COP
T75-cog90	458	381	256	0.558	0.67	0.305
T75-cog85	468	351	254	0.542	0.722	0.310
T75-cog80	484	315	249	0.514	0.790	0.312
T70-cog90	460	386	245	0.533	0.634	0.289
T70-cog85	468	362	241	0.515	0.667	0.291
T70-cog80	485	323	236	0.488	0.731	0.292
T65-cog90	463	394	231	0.499	0.586	0.270
T65-cog85	470	368	230	0.488	0.625	0.274
T65-cog70	484	338	229	0.473	0.677	0.278

The thermal power of the cogenerator is constant and equal to 10 kW.

The energy produced by the solar field is independent of the initial temperature of the storage tank. However, it increases by 2MJ if the cut off temperature of the cogenerator decreases by 1°C. It depends of the cut-off temperature of the cogenerator. In fact, the tank temperature increases as fast as the cut-off temperature is higher. This increasing causes the decreasing of the solar field efficiency, then the decreasing of its energy (Figure 11).

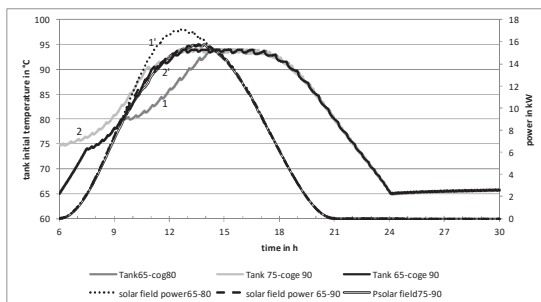


Figure 11: evolution of storage tank temperature and solar field power during a whole day

The operation of the cogenerator is shown in the Figure 12. The minimum operation time took place at lower cut off cogenerator temperature and lower initial temperature of the storage tank.

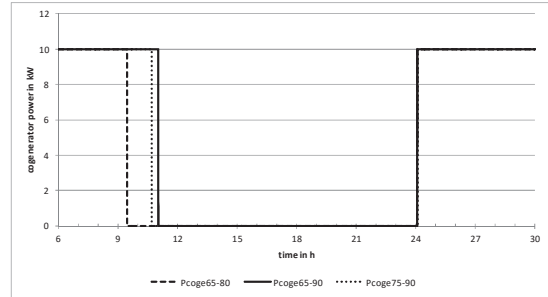


Figure 12: power produced by the cogenerator during the day

At the beginning of the day (at 6 a.m.), the energy produced by the solar field is relatively low. The major part of energy necessary for the elevation of tank temperature is provided by the cogenerator

The cooling energy produced by the evaporator of the adsorption machine depends on both initial temperature of the storage tank and cut off temperature of the cogenerator. But it is clear that the effect of the initial temperature is greater than that of cut off temperature (Table 3).

After 15 hours, the difference between parameters has no effect on the operation of the storage tank.

H. Discussion

This results show the complementarity of the two tested systems. The tank temperature reaches 65°C at the end of the day regardless of the initial temperature (65°C or 70°C). The energy required to increase the tank temperature by 5°C is 31.35 MJ. This energy must be provided by the cogenerator (nonrenewable energy) since there is no solar energy at the morning (before 6 a.m.), and this affects the efficiency of the system.

The energy required to increase the tank temperature is 4.18 MJ/m³.°C. By referring to Table 3, the increasing of cogenerator energy corresponding to the same initial tank temperature (65°) is about 4 MJ/m³.°C which is the double of that of solar field energy. Then the choice of the cogenerator cut-off temperature is very important to achieve the optimal coupling of the cogenerator and the solar field.

The Table 4 shows that the volume of the tank is one of the most important parameters in the sizing of this system.

Table 4: effect of the tank volume on the system performance

	field energy (MJ)	cogenerator energy (MJ)	evaporator energy (MJ)	solar COP	cogenerator COP	global COP
T65-cog80-5m ³	594	208	259	0.435	1.240	0.322
T65-cog80-3m ³	558	191	265	0.475	1.386	0.354
T65-cog80-1.5m ³	535	338	229	0.427	0.677	0.262
T65-cog80-1m ³	531	333	244	0.459	0.732	0.282

The optimal tank volume is that which can keep the energy requested to maintain the tank temperature above 65°C after the sunset until 6 a.m. of the next day.

IV. ACKNOWLEDGEMENT

This work was supported by national (French) and European funds (grant CPER FIBRES and CPER ENERBATIN).

V. REFERENCES

[1] R. Benelmir, M. El Kadri, A. Donnot, D. Descieux, "Numerical Investigation of the Performance of a sorption refrigerating machine", *International Journal of Energy Environment and Economics*, vol. 23 (2), 2015.

[2] Chi Yan Tso, Sau Chung Fu, Christopher Y.H. Chao Modeling a solar-powered double bed novel composite adsorbent (silica activated carbon/CaCl₂)-water adsorption chiller, Department of Mechanical Engineering, The Hong Kong University of Science and Technology, Clear Water Bay, Kowloon, Hong Kong, China

R. Benelmir graduated from Georgia Tech (Atlanta, USA) in 1989 with a PhD in Mechanical Engineering (thesis : second law analysis of combined cycle gas/steam turbine cogeneration system). He then joined the Institute of Applied Sciences of Lyon (France) from 1989 to 1991, the Institute of Technology of Longwy from 1991 to 2002, the Engineering School of Nancy (ESSTIN) from 2002 to 2007 (where he was head of studies from 2004 to 2007) and finally the Faculty of Sciences and Technology at University of Lorraine since 2007 where he conducts research activities on energy efficiency in buildings an industry within the LERMAB research laboratory. The main research programs covered substitution refrigerants (European program), vehicle HVAC's compact heat exchanger design and optimal thermal design (industrial grants), fuel cells, waste heat valuation through sorption processes (nation grant). He is also head of studies for the path "Building's Energetics" within a Master of Civil Engineering.

A. Donnot is a doctor in wood science of the University of Nancy (1989). He is specialized in thermal degradation and purification of gases. Thesis subject: catalytical cracking of tars coming from pine bark pyrolysis. Started his career at CEA France in which pyrolysis was used to reduce the volume impact of plastic waste polluted by radioisotope, and then joined SITA specialized in hazardous waste treatment (project leader). Actually researcher in LERMAB with two main themes: energy efficiency and wooddust human exposure.

D. Descieux is doctor in mechanics an energetics of the University of Lorraine (2007) (thesis: Modelling and thermo-energetics comparison of cogeneration systems). He joined LERMAB in 2008 and his research is about energy efficiency in buildings an industry. He is also the technical supervisor of the platform ENERBAT.

M. El Kadri graduated from Lebanese University (Beirut, Lebanon) in 2013 with a diplomate in mechanical engineering, Energetics path. He then worked at ENCOgroup Company as site engineer for one year, then as project manager for one year in the domain of steel tanks construction. Currently, he's continuing his studies in Master of Civil Engineering at the University of Lorraine.

Social Support in Perception of the Youth with Cerebral Palsy from Migrating Families

Anna Gagat Matuła

Abstract—The article presents social support felt by the youth with cerebral palsy whose parents migrate abroad. The study concerned 70 persons (with cerebral palsy, with normal intellectual capacity) coming from families in which at least one of parents migrates. The research used the Polish adaptation of the Interpersonal Support Evaluation List by E. Szlachta. The results show that the youth with cerebral palsy mostly experiences general support. Other essential issues include the availability of persons who they could talk to about problems and difficulties, specific material aid and the possibility of positive comparing themselves with other persons, what provides a feeling that they are accepted and valued.

Keywords—social support, migration, youth, cerebral palsy

Corresponding Author

Anna Gagat-Matuła from Pedagogical University of Cracow, Poland
e-mail: anna3006@op.pl

Sonochemical Synthesis of Ultraviolet Curable Polysulfide Urethane Acrylate Nanocomposite

Behzad Shirkavand Hadavand

Abstract—This work is focused on the optimization of reaction parameters for the synthesis of UV curable polysulfide urethane nanocomposite by ultrasound irradiation. For this purpose UV curable polysulfide urethane nanocomposite was synthesized in two steps. First the polysulfide urethane oligomer was synthesized with a reaction of a 2:1 molar ratio of diisocyanate and polysulfide polymer (PSP) in presence of dibutyltin dilaurate (DBTDL) as catalyst. Then 2 mol of 2-hydroxyethyl methacrylate (HEMA) were added to the reaction vessel and the reaction continued to the preparation of UV curable polysulfide urethane. In these two steps, the ultrasound irradiation was used instead of the traditional thermal method in various conditions. For preparation of in situ polymeric nanocomposite by ultrasound, in second step of reaction, nano particles (1, 3 and 5%) were added to the reaction vessel. At last the structure of oligomer was confirmed by FT-IR spectroscopy. Morphology and thermal characterization of nanocomposite were studied by SEM, TGA and DSC after ultraviolet curing of nanocomposite. Results indicated that the nano particles are highly dispersed in the polymer matrix. DSC thermo graphs indicated that the addition of nano particles has an alteration of the glass-transition temperature of the soft-segment phase of nanocomposite. Experimental results also confirmed that the thermal stability and mechanical properties strongly depend on the contents and the distribution of nano particles added into combination.

Keywords—urethane acrylate, polysulfide polymer, UV-cure, ultrasound irradiation, nanocomposite

Corresponding Author

Behzad Shirkavand-Hadavand from Institute for Color Science and Technology, Iran, Islamic Republic Of
e-mail: shirkavand@icrc.ac.ir

Static and Dynamic Analysis of Hyperboloidal Helix Having Thin Walled Open and Close Sections

Merve Ermis, Murat Yilmaz, Nihal Eratli, Mehmet H. Omurtag

Abstract—The static and dynamic analyses of hyperboloidal helix having the closed and the open square box sections are investigated via the mixed finite element formulation based on Timoshenko beam theory. Frenet triad is considered as local coordinate systems for helix geometry. Helix domain is discretized with a two-noded curved element and linear shape functions are used. Each node of the curved element has 12 degrees of freedom, namely, three translations, three rotations, two shear forces, one axial force, two bending moments and one torque. Finite element matrices are derived by using exact nodal values of curvatures and arc length and it is interpolated linearly throughout the element axial length. The torsional moments of inertia for close and open square box sections are obtained by finite element solution of St. Venant torsion formulation. With the proposed method, the torsional rigidity of simply and multiply connected cross-sections can be also calculated in same manner. The influence of the close and the open square box cross-sections on the static and dynamic analyses of hyperboloidal helix is investigated. The benchmark problems are represented for the literature.

Keywords—Hyperboloidal helix, squared cross section, thin walled cross section, torsional rigidity

I. INTRODUCTION

HELICOIDAL bars are important and frequently used members in civil engineering, mechanical engineering and biomechanics. They have many different forms other than their well known standard form. They have the ability to absorb energy while deforming. Although a tremendous amount of theoretical and numerical studies exist on the static/dynamic analyses of elastic helices, it can observe that only helices with limited number of cross-sections (e.g., circular and rectangular) were considered. The static analysis with rectangular cross-section [1]-[3], and, the dynamic analysis with circular cross section [4]-[7], thin-thick walled circular cross section [8], and rectangular cross-section [9] are studied.

It is straightforward to calculate the torsional rigidity of helices having a circular cross section. In the case of non-circular geometries some special treatments have to be use to determine the torsional rigidity. It is possible to find some analytical formulas in the literature expressing the torsional moment of inertia for various arbitrary cross-sections like rectangular, ellipse and equilateral triangle [10]. Some approximated analytical formulas [11], [12] and numerical

M. Ermis, M. Yilmaz, N. Eratli, M. H. Omurtag, are with the Faculty of Civil Engineering, Istanbul Technical University, Maslak 34469, Turkey (phone: +90-212-2856551; e-mail: ermism@itu.edu.tr, e-mail: yilmazmura@itu.edu.tr, e-mail: eratli@itu.edu.tr, e-mail: omurtagm@itu.edu.tr).

solutions such as finite difference [13], [14], finite element (FE)[15]-[20], and boundary element methods also exist [21], [22].

In this study, the effects of the noncircular cross-sections on the static and dynamic behavior of hyperboloidal helix are considered. The torsional rigidities of used cross-sections are calculated by finite element solution of Poisson's equation proposed by the authors [20]. The mixed FE formulation comprising the Timoshenko beam theory is employed. As a numerical investigation, the influence of the cross-sections and the boundary conditions on the static and dynamic analyses of the hyperboloidal helix is performed via the mixed FE method. These analyses are benchmark examples for the literature.

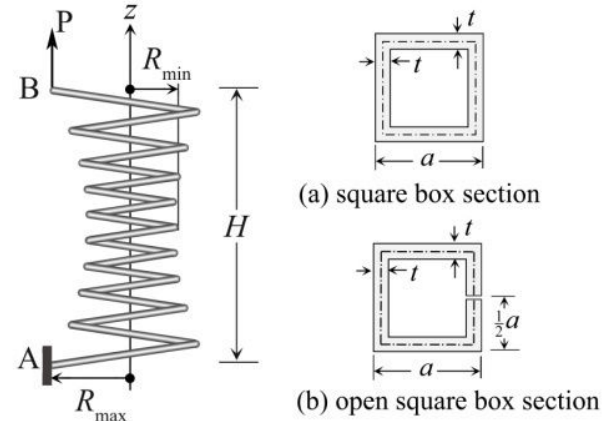


Fig. 1 Hyperboloidal helix and cross-sections

II. FORMULATION

A. Helix Geometry and Functional

The geometrical properties of the helix are $x = R(\varphi)\cos\varphi$, $y = R(\varphi)\sin\varphi$, $z = p(\varphi)\varphi$, $p(\varphi) = R(\varphi)\tan\alpha$, where α denotes the pitch angle, $R(\varphi)$ and $p(\varphi)$ signify the centerline radius and the step for unit angle, respectively, of the helix as a function of the horizontal angle φ . By letting $c(\varphi) = \sqrt{R^2(\varphi) + p^2(\varphi)}$, the infinitesimal arc length becomes $ds = c(\varphi)d\varphi$. In the case of a hyperboloidal helix, its radius

$$R(\varphi) = R_{\min} + (R_{\max} - R_{\min})(1 - \varphi/n\pi)^2 \quad (1)$$

where R_{\max} and R_{\min} are the bottom radius and the central radius, respectively (see Fig. 1).

The field equations for the elastic circular and non-circular helices, which are based on Timoshenko beam theory and refer to the Frenet coordinate system, exist in [20], these equations can be written in the form

$$\left. \begin{aligned} -\mathbf{T}_{,s} - \mathbf{q} + \rho A \ddot{\mathbf{u}} &= \mathbf{0} \\ -\mathbf{M}_{,s} - \mathbf{t} \times \mathbf{T} - \mathbf{m} + \rho \mathbf{I} \ddot{\mathbf{\Omega}} &= \mathbf{0} \\ \mathbf{u}_{,s} + \mathbf{t} \times \mathbf{\Omega} - \mathbf{C}_\gamma \mathbf{T} &= \mathbf{0} \\ \mathbf{\Omega}_{,s} - \mathbf{C}_\kappa \mathbf{M} &= \mathbf{0} \end{aligned} \right\} \quad (2)$$

where $\mathbf{u}(u_t, u_n, u_b)$ is the displacement vector, $\mathbf{\Omega}(\Omega_t, \Omega_n, \Omega_b)$ is the rotational vector, $\mathbf{T}(T_t, T_n, T_b)$ is the force vector, $\mathbf{M}(M_t, M_n, M_b)$ is the moment vector. $\ddot{\mathbf{u}}$ and $\ddot{\mathbf{\Omega}}$ are the accelerations of the displacement and rotations. ρ is the material density. A is the area of the cross section, \mathbf{I} is the moments of inertia, \mathbf{C}_γ and \mathbf{C}_κ are compliance matrices. \mathbf{q} and \mathbf{m} are the distributed external force and moment vectors, respectively. In the dynamic analysis, the motion is considered as harmonic and the conditions $\mathbf{q} = \mathbf{m} = \mathbf{0}$ are satisfied. Incorporating Gâteaux differential with potential operator concept [23] yields the functional in terms of(2)-(3)

$$\begin{aligned} \mathbf{I}(\mathbf{y}) = & - \left[\mathbf{u}, \frac{d\mathbf{T}}{ds} \right] + \left[\mathbf{t} \times \mathbf{\Omega}, \mathbf{T} \right] - \left[\frac{d\mathbf{M}}{ds}, \mathbf{\Omega} \right] - \frac{1}{2} \left[\mathbf{C}_\kappa \mathbf{M}, \mathbf{M} \right] \\ & - \frac{1}{2} \left[\mathbf{C}_\gamma \mathbf{T}, \mathbf{T} \right] - \frac{1}{2} \rho A \omega^2 \left[\mathbf{u}, \mathbf{u} \right] - \frac{1}{2} \rho \omega^2 \left[\mathbf{I} \mathbf{\Omega}, \mathbf{\Omega} \right] \\ & - \left[\mathbf{q}, \mathbf{u} \right] - \left[\mathbf{m}, \mathbf{\Omega} \right] + \left[\left(\mathbf{T} - \hat{\mathbf{T}} \right), \mathbf{u} \right]_\sigma + \left[\left(\mathbf{M} - \hat{\mathbf{M}} \right), \mathbf{\Omega} \right]_\sigma \\ & + \left[\hat{\mathbf{u}}, \mathbf{T} \right]_\varepsilon + \left[\hat{\mathbf{\Omega}}, \mathbf{M} \right]_\varepsilon \end{aligned} \quad (4)$$

where square brackets indicate the inner product, the terms with hats are known values on the boundary and the subscripts ε and σ represent the geometric and dynamic boundary conditions, respectively.

B. Calculation of Torsional Rigidity via FEM

Let's Φ is a scalar field function. The governing equations for the torsion problem is

$$\Phi_{,11} + \Phi_{,22} = -2 \quad (5)$$

with $\Phi = 0$ on Γ the boundary. Defining a vector field $\mathbf{\Xi}$ on Ω^e as $\mathbf{\Xi} = \left\{ \psi_i \Phi_{,1}^e, \psi_i \Phi_{,2}^e \right\}^T$ and using the divergence theorem the weak form of(5)can be constructed as,

$$\int_{\Omega^e} \left(\psi_{i,1} \Phi_{,1}^e + \psi_{i,2} \Phi_{,2}^e \right) d\Omega^e = 2 \int_{\Omega^e} \psi_i d\Omega^e + \int_{\Gamma^e} \psi_i \nabla \Phi^e \cdot \mathbf{n}^e d\Gamma^e \quad (6)$$

The boundary terms in (6) cancel out during the assemblage of the FE equations for adjacent element edges in the cross-section domain Ω and they are also zero on the free edges (edges without an adjacent element) to satisfy the boundary

condition of the torsion problem. The torsional constant I_t of the cross-section, in terms of the scalar field, is expressed as,

$$I_t = - \int_{\Omega} \left(\Phi_{,1} x_1 + \Phi_{,2} x_2 \right) d\Omega \quad (7)$$

which renders to the summation given with the following equation over domain elements as,

$$\mu I_3 = - \sum_{e=1}^N \mu^e \int_{\Omega_\eta^e} \mathbf{\Phi}^T \left[\partial \mathbf{\Psi} \right] \left[\mathbf{J} \right]^{-1} \left[\mathbf{X} \right] \mathbf{\Psi} \left| \det \left[\mathbf{J} \right] \right| d\Omega_\eta^e \quad (8)$$

where $\left[\partial \mathbf{\Psi} \right]$ with the definition,

$$\left[\partial \mathbf{\Psi} \right] = \begin{bmatrix} \partial \psi_1 / \partial \eta_1 & \partial \psi_1 / \partial \eta_2 \\ \partial \psi_2 / \partial \eta_1 & \partial \psi_2 / \partial \eta_2 \\ \vdots & \vdots \\ \partial \psi_9 / \partial \eta_1 & \partial \psi_9 / \partial \eta_2 \end{bmatrix} \quad (9)$$

where $\left[\mathbf{J} \right]$ (Jacobian matrix) is calculated with $\left[\mathbf{J} \right] = \left[\mathbf{X} \right] \left[\partial \mathbf{\Psi} \right]$, $\left[\mathbf{X} \right]$ being the nodal coordinates matrix, and $\mathbf{\Phi}$ is the vector with the scalar field nodal-values as its components. Integrations are performed with the $3 \times 3 = 9$ point Gauss quadrature rule. $\mu = G$ is the shear modulus and N is the total number of elements.

C. The Mixed FE Method and Dynamic Analysis

$\phi_i = (\varphi_j - \varphi) / \Delta \varphi$ and $\phi_j = (\varphi - \varphi_i) / \Delta \varphi$ are linear shape functions used in finite element formulation where $\Delta \varphi = (\varphi_j - \varphi_i)$. The subscripts represent node numbers of the curved element. The curvatures are satisfied exactly at the nodal points and linearly interpolated through the element. The curved bar element has two nodes with 2×12 degrees of freedom. The variable vectors per node are $\mathbf{u}, \mathbf{\Omega}, \mathbf{T}, \mathbf{M}$.

In the dynamic analysis, the problem of determining the natural frequencies reduces to the solution of a standard eigenvalue problem $(\left[\mathbf{K} \right] - \omega^2 \left[\mathbf{M} \right]) \{ \mathbf{u} \} = \{ \mathbf{0} \}$ where $\left[\mathbf{K} \right]$ is the system matrix, $\left[\mathbf{M} \right]$ is the mass matrix \mathbf{u} is the eigenvector (mode shape) and ω is the natural angular frequency of the system. Hence the explicit form of standard eigenvalue problem in the mixed formulation is

$$\left(\begin{bmatrix} \left[\mathbf{K}_{11} \right] & \left[\mathbf{K}_{12} \right] \\ \left[\mathbf{K}_{22} \right] & \left[\mathbf{K}_{22} \right] \end{bmatrix} - \omega^2 \begin{bmatrix} \left[\mathbf{0} \right] & \left[\mathbf{0} \right] \\ \left[\mathbf{0} \right] & \left[\mathbf{M} \right] \end{bmatrix} \right) \begin{Bmatrix} \{ \mathbf{F} \} \\ \{ \mathbf{U} \} \end{Bmatrix} = \begin{Bmatrix} \{ \mathbf{0} \} \\ \{ \mathbf{0} \} \end{Bmatrix} \quad (10)$$

where $\{ \mathbf{F} \}$ denotes the nodal force and the moment vectors and $\{ \mathbf{U} \} = \{ \mathbf{u} \mathbf{\Omega} \}^T$ signifies the nodal displacement and rotation vectors. To attain consistency between (10) and $(\left[\mathbf{K} \right] - \omega^2 \left[\mathbf{M} \right]) \{ \mathbf{u} \} = \{ \mathbf{0} \}$, the $\{ \mathbf{F} \}$ is eliminated in (10), which yields to the condensed system matrix $\left[\mathbf{K}^* \right] = \left[\mathbf{K}_{22} \right] - \left[\mathbf{K}_{12} \right]^T \left[\mathbf{K}_{11} \right]^{-1} \left[\mathbf{K}_{12} \right]$. The eigenvalue problem in the mixed formulation becomes $(\left[\mathbf{K}^* \right] - \omega^2 \left[\mathbf{M} \right]) \{ \mathbf{U} \} = \{ \mathbf{0} \}$.

III. NUMERICAL EXAMPLES

The material and geometric properties of the hyperboloidal

helix are: the modulus of elasticity is $E = 210\text{GPa}$, Poisson's ratio is $\nu = 0.3$, the number of active turns is $n = 7.5$, the height of the helix is $H = 75\text{mm}$, the ratio of the minor radius to the major radius of the helix is $R_{\min}/R_{\max} = 0.5$ where $R_{\max} = 13\text{mm}$. Closed and open square box sections that range from thin to thick with four different thickness-to-side ratios t/a (0.040, 0.125, 0.250, 0.375) where $a = 2\text{mm}$ are employed (see Figs.1(a)-(b)). The torsional rigidity moments of these closed and open sections are calculated via FE method which is verified in [20]. Referring to t/a (0.040, 0.125, 0.250, 0.375) ratios, the computed torsional inertia moments for closed square box section are $I_t = 0.0366a^4$, $0.0923a^4$, $0.1305a^4$, $0.1399a^4$ and the computed torsional moments for open square box sections are $I_t = 8.2 \times 10^{-5}a^4$, $229.6 \times 10^{-5}a^4$, $1589.2 \times 10^{-5}a^4$ and $4455.5 \times 10^{-5}a^4$, respectively.

A. Static Analysis

The behavior of the closed and open square box sections, ranging from thin to thick with four different thickness-to-side ratios, on the nodal variables at the specific points of the hyperboloidal helix are investigated. The fixed-free boundary condition is used. The helix is subjected to an external load acting at the tip of the helix (see Fig. 1, point B). The intensity of the load is $P_z = 10^{-3}\text{N}$. The hyperboloidal helix problem having thin and thick with four different t/a ratios of the closed and open square box sections is solved and the results are presented in the Cartesian coordinate system. The maximum displacements (u_z) and fixed end reactions (T_z : shear force, M_y : moment) for closed and open sections are tabulated in Tables I-II. These results are verified using the commercial program SAP2000 and its Section Designer module.

In the closed square box cross-section, with respect to the maximum displacements for the $t/a = 0.04$ ratio, the reductions for the next three t/a (0.125, 0.250, 0.375) ratios are 59.9%, 71.5% and 73.4% (Table I). Similarly, in the open square box cross-section, with respect to the maximum displacements for the $t/a = 0.04$ ratio, the reductions for the next three ratios are 96.4%, 99.5% and 99.8% (Table II). It is observed that the open square box sections are more sensitive the changing of the thickness-to-side ratios (Tables I, II). For the maximum displacements of the helicoidal helix, the results of the closed square box section for each t/a ratio are decreased by 99.7%, 96.7%, 84.2%, and 61.2% with respect to the open square box cross-section results (Tables I, II).

TABLE I

THE DISPLACEMENTS, SHEAR FORCES AND MOMENTS OF HYPERBOLOIDAL HELIX HAVING THE THIN-THICK SQUARE BOX SECTIONS

t/a		$(u_z)_{\max}$ ($\times 10^{-3}\text{mm}$)	$(T_z)_{\max}$ ($\times 10^{-4}\text{N}$)	$(M_y)_{\max}$ ($\times 10^{-5}\text{Nm}$)
0.040	this study	1.955	9.983	2.591
	SAP2000	1.961	10.00	2.600
	diff.%	-0.31	-0.17	-0.35

0.125	this study	0.784	9.983	2.591
	SAP2000	0.789	10.00	2.600
	diff.%	-0.64	-0.17	-0.35
0.250	this study	0.557	9.983	2.591
	SAP2000	0.557	10.00	2.600
	diff.%	0.00	-0.17	-0.35
0.375	this study	0.520	9.983	2.591
	SAP2000	0.516	10.00	2.600
	diff.%	0.77	-0.17	-0.35

diff. % = (This study-SAP2000) \times 100/This study)

TABLE II

THE DISPLACEMENTS, SHEAR FORCES AND MOMENTS OF HYPERBOLOIDAL HELIX HAVING THE THIN-THICK OPEN SQUARE BOX SECTIONS

t/a		$(u_z)_{\max}$ ($\times 10^{-3}\text{mm}$)	$(T_z)_{\max}$ ($\times 10^{-4}\text{N}$)	$(M_y)_{\max}$ ($\times 10^{-5}\text{Nm}$)
0.040	this study	653.7	9.983	2.591
	SAP2000	648.1	10.00	2.600
	diff.%	0.86	-0.17	-0.35
0.125	this study	23.55	9.983	2.591
	SAP2000	23.34	10.00	2.600
	diff.%	0.89	-0.17	-0.35
0.250	this study	3.520	9.983	2.591
	SAP2000	3.490	10.00	2.600
	diff.%	0.85	-0.17	-0.35
0.375	this study	1.340	9.983	2.591
	SAP2000	1.330	10.00	2.600
	diff.%	0.75	-0.17	-0.35

diff. % = (This study-SAP2000) \times 100/This study)

B. Dynamic Analysis

The objective of this example is to investigate the effects of the thickness-to-side ratios of the closed and open sections and the boundary conditions on the dynamic behavior of the hyperboloidal helix. The fixed-fixed and fixed-free boundary conditions are employed. The density of material is $\rho = 7850\text{kg/m}^3$. For the fixed-fixed and the fixed free boundary conditions, the first six natural frequency results of the helicoidal helix having the closed and open sections are presented in Tables III-VI. The results are also verified with SAP2000 and its Section Designer module.

In the case of the fixed-fixed boundary condition and the closed square box section, with respect to the fundamental natural frequency for the $t/a = 0.04$ ratio, the reductions for the next three t/a (0.125, 0.250, 0.375) ratios are 6.9%, 16.0% and 22.3% (Table III). Similarly, in the case of the fixed-free boundary condition and the closed square box section, with respect to the fundamental natural frequency for the $t/a = 0.04$ ratio, the reductions for the next three t/a ratios are 6.7%, 15.7% and 22.1% (Table IV). In the case of the fixed-fixed boundary condition and the open closed square box section, with respect to the fundamental natural frequency for the $t/a = 0.04$ ratio, the increases for the next three t/a (0.125, 0.250, 0.375) ratios are 213.3%, 527.2% and 831.2% (Table V). Similarly, in the case of the fixed-free boundary condition and the open closed square box section, with respect to the fundamental natural frequency for the $t/a = 0.04$ ratio, the increases for the next three t/a ratios are 208.1%, 500.0% and 748.6% (Table VI). For both closed and open square box sections, when the influence of the boundary conditions is considered the fundamental natural frequencies

of the fixed-free boundary condition decreased in the range of 78.6%~81.3% with respect to the fixed-fixed boundary condition (Tables III-VI). For the fundamental natural frequency of the hyperboloidal helix having fixed-fixed boundary condition, the results of the open square box section for each t/a ratio are decreased by 94.7%, 82.2%, 60.4%, and 36.4% with respect to the closed square box cross-section results (Tables III,V). For the fundamental natural frequency of the hyperboloidal helix having fixed-free boundary condition, the results of the open square box section for each t/a ratio are decreased by 93.9%, 80.0%, 56.8%, and 33.9% with respect to the closed square box cross-section results (Tables IV,VI).

TABLE III

THE NATURAL FREQUENCIES OF HYPERBOLOIDAL HELIX HAVING THE THIN-THICK SQUARE BOX SECTIONS WITH FIXED-FIXED BOUNDARY CONDITION

t/a		ω (in Hz)					
		1	2	3	4	5	6
0.04	this study	326.3	336.2	359.7	608.4	719.1	765.7
	SAP2000	326.0	335.1	356.2	608.6	717.6	764.4
	diff.%	0.09	0.33	0.97	-0.03	0.21	0.17
0.125	this study	303.8	312.5	338.0	560.3	668.1	711.2
	SAP2000	303.0	311.2	334.0	560.2	665.8	709.6
	diff.%	0.26	0.42	1.18	-0.04	0.34	0.22
0.25	this study	274.1	281.6	307.2	501.6	601.9	640.8
	SAP2000	274.2	281.3	305.3	501.4	601.2	641.1
	diff.%	-0.04	0.11	0.62	0.04	0.12	-0.05
0.375	this study	253.5	260.4	284.9	462.8	556.6	592.7
	SAP2000	254.0	260.5	284.2	462.4	556.6	593.7
	diff.%	-0.20	0.04	0.25	0.09	0.00	-0.17

diff. % = (This study-SAP2000)×100/This study)

TABLE IV

THE NATURAL FREQUENCIES OF HYPERBOLOIDAL HELIX HAVING THE THIN-THICK SQUARE BOX SECTIONS WITH FIXED-FREE BOUNDARY CONDITION

t/a		ω (in Hz)					
		1	2	3	4	5	6
0.040	this study	61.0	61.8	198.1	255.4	322.1	330.0
	SAP2000	60.8	61.6	196.6	255.2	321.6	328.8
	diff.%	0.33	0.32	0.76	0.08	0.16	0.36
0.125	this study	56.9	57.6	186.4	235.3	299.5	307.3
	SAP2000	56.6	57.2	184.5	235.1	298.6	305.7
	diff.%	0.53	0.42	1.18	-0.04	0.34	0.22
0.250	this study	51.4	51.9	169.6	210.7	270.0	277.3
	SAP2000	51.3	51.8	168.9	210.5	270.0	276.8
	diff.%	0.19	0.19	0.41	0.09	0.00	0.18
0.375	this study	47.5	48.0	157.4	194.4	249.7	256.5
	SAP2000	47.5	48.0	157.3	194.2	250.0	256.5
	diff.%	0.00	0.00	0.06	0.10	-0.12	0.00

diff. % = (This study-SAP2000)×100/This study)

TABLE V

THE NATURAL FREQUENCIES OF HYPERBOLOIDAL HELIX HAVING THE THIN-THICK OPEN SQUARE BOX SECTIONS WITH FIXED-FIXED BOUNDARY CONDITION

t/a		ω (in Hz)					
		1	2	3	4	5	6
0.040	this study	17.3	23.0	24.0	49.1	55.6	57.9
	SAP2000	17.3	23.1	23.9	48.9	55.4	58.5
	diff.%	0.00	-0.43	0.42	0.41	0.36	-1.04
0.125	this study	54.2	71.0	72.1	135.1	153.1	175.2
	SAP2000	54.3	71.4	71.8	134.9	152.6	176.6
	diff.%	-0.18	-0.56	0.42	0.15	0.33	-0.80
0.250	this study	108.5	134.8	137.1	261.0	300.0	324.4
	SAP2000	108.6	135.4	136.6	260.8	299.1	326.4
	diff.%	-0.09	-0.45	0.36	0.08	0.30	-0.62
0.375	this study	161.1	183.6	187.1	380.7	423.1	428.2
	SAP2000	161.4	183.8	186.7	381.3	422.0	428.5
	diff.%	-0.19	-0.11	0.21	-0.24	0.26	-0.07

diff. % = (This study-SAP2000)×100/This study)

TABLE VI

THE NATURAL FREQUENCIES OF HYPERBOLOIDAL HELIX HAVING THE THIN-THICK OPEN SQUARE BOX SECTIONS WITH FIXED-FREE BOUNDARY CONDITION

t/a		ω (in Hz)					
		1	2	3	4	5	6
0.040	this study	3.7	3.9	9.6	20.6	21.4	24.9
	SAP2000	3.7	3.9	9.6	20.6	21.3	-
	diff.%	0.00	0.00	0.00	0.00	0.47	-
0.125	this study	11.4	12.0	30.0	63.9	66.2	77.7
	SAP2000	11.4	12.1	30.0	64.0	66.1	-
	diff.%	0.00	-0.83	0.00	-0.16	0.15	-
0.250	this study	22.2	23.3	60.2	122.7	126.9	153.1
	SAP2000	22.2	23.3	60.2	123.1	126.7	-
	diff.%	0.00	0.00	0.00	-0.33	0.16	-
0.375	this study	31.4	32.6	89.8	166.8	175.3	202.4
	SAP2000	31.4	32.6	89.8	167.0	175.1	202.6
	diff.%	0.00	0.00	0.00	-0.12	0.11	-0.10

diff. % = (This study-SAP2000)×100/This study)

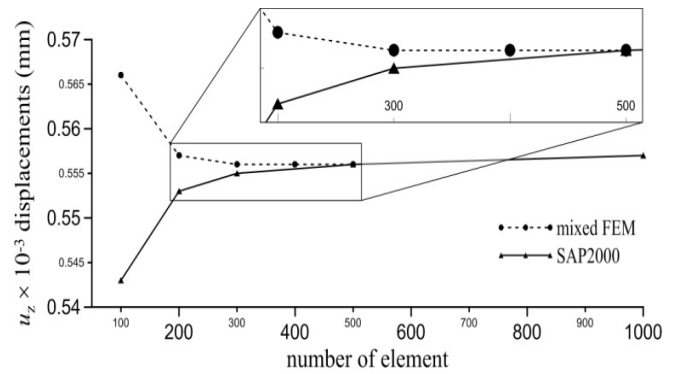


Fig. 2 The convergence analysis for u_z displacement of the hyperboloidal helix having square box cross-section with fixed-free boundary condition

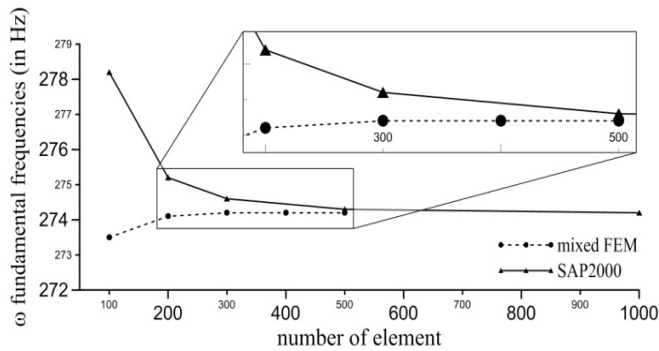


Fig. 3 The convergence analysis for ω fundamental frequency of the hyperboloidal helix having square box cross-section with fixed-fixed boundary condition

IV. CONCLUSIONS

Static and dynamic analyses of hyperboloidal helix having the thin/thick closed and open square box cross-sections are investigated via the mixed FE method. The torsional rigidity of the used cross-sections is determined by the method proposed by the authors [20]. The finite element solutions are compared using the commercial program SAP2000 and its Section Designer module. The percent differences between these finite element models is in range of 0-1.18% in the case of 1000 elements by SAP2000 and 200 elements by the present mixed model for both the static and dynamic analyses, and, the thin/thick closed and open square box sections. The convergence of the static and dynamic analyses of two FE analyses is given in Figs. 2-3. In mixed FE analysis, convergence of the vertical displacement is upper bound and the fundamental natural frequency is lower bound. This difference is due to the used torsional rigidity of the cross-sections, besides the straight SAP2000 elements and the curved elements of the present study. The effects of the closed and the open square box sections that range from thin to thick with four different thickness-to-side ratios and the boundary conditions on the static and the dynamic behavior of the hyperboloidal helix are discussed extensively.

REFERENCES

- [1] M.H. Omurtag and A.Y. Aköz, "The mixed finite element solution of helical beams with variable cross-section under arbitrary loading", *Comput. Struct.*, vol. 43, pp. 325-331, 1992.
- [2] V. Haktanir and E. Kıral, "Statical analysis of elastically and continuously supported helicoidal structures by the transfer and stiffness matrix methods", *Comput. Struct.*, vol. 49, pp. 663-677, 1993.
- [3] W. Busool and M. Eisenberger, "Exact static analysis of helicoidal structures of arbitrary shape and variable cross section", *J. Struct. Eng.*, vol. 127, pp. 1266-1275, 2001.
- [4] V. Yıldırım, "Investigation of parameters affecting free vibration frequency of helical springs", *Int. J. Numer. Methods Eng.*, vol. 39, pp. 99-114, 1996.
- [5] J.E. Mottershead, "Finite elements for dynamical analysis of helical rods", *Int. J. Mech. Sci.*, vol. 22, pp. 267-283, 1980.
- [6] J. Lee, "Free vibration analysis of cylindrical helical springs by the pseudospectral method", *J. Sound Vib.*, vol. 302, pp. 185-196, 2007.
- [7] A.M. Yu, C.J. Yang and G.H. Nie, "Analytical formulation and evaluation for free vibration of naturally curved and twisted beams", *J. Sound Vib.*, vol. 329, pp. 1376-1389, 2010.
- [8] N. Eratli, M. Ermis and M.H. Omurtag, "Free vibration analysis of helicoidal bars with thin-walled circular tube cross-section via mixed

- finite element method", *Sigma Journal of Engineering and Natural Sciences*, vol. 33(2), pp. 200-218, 2015.
- [9] S.A. Alghamdi, M.A. Mohiuddin and H.N. Al-Ghamedy, "Analysis of free vibrations of helicoidal beams", *Eng. Comput.*, vol. 15, pp. 89-102, 1998.
- [10] S. Timoshenko and J.N. Goodier, *Theory of elasticity*, McGraw-Hill, New York, 1951.
- [11] R.J. Roark, *Formulas for Stress and Strain*, McGraw-Hill, New York, 1954.
- [12] N.X. Arutunan and B.L. Abramson, *Torsion of Elastic Bodies* (in Russian), State Publisher, Fizmatgiz, Moscow, 1963.
- [13] C.T. Wang, *Applied Elasticity*, McGraw-Hill, New York, 1953.
- [14] J.F. Elyand and O.C. Zienkiewicz, "Torsion of compound bars-A relaxation solution", *Int. J. Mech. Sci.*, vol. 1, pp. 356-365, 1960.
- [15] L.R. Hermann, "Elastic torsional analysis of irregular shapes", *J. Engng. Mech., ASCE*, vol. 91(6), pp. 11-19, 1965.
- [16] J.L. Krahula and G.F. Lauterbach, "A finite element solution for Saint-Venant torsion", *AIAA Journal*, vol. 7(12), pp. 2200-2203, 1969.
- [17] K. Darılmaz, E. Orakdogan, K. Girgin and S. Küçükarslan, "Torsional rigidity of arbitrarily shaped composite sections by hybrid finite element approach", *Steel and Composite Structures*, vol. 7(3), pp. 241-251, 2007.
- [18] Z.Li, J.M. Ko and Y.Q. Ni, "Torsional rigidity of reinforced concrete bars with arbitrary sectional shape", *Finite Elements in Analysis and Design*, vol. 35, pp. 349-361, 2000.
- [19] J.S. Lamancusa and D.A. Saravanos, "The torsional analysis of bars with hollow square cross-sections", *Finite Element in Analysis and Design*, vol. 6, pp. 71-79, 1989.
- [20] N. Eratli, M. Yılmaz, K. Darılmaz and M.H. Omurtag, "Dynamic analysis of helicoidal bars with non-circular cross-sections via mixed FEM", *Struct. Eng. Mech.*, vol. 57(2), pp. 221-238, 2016.
- [21] E.J. Sapountzakis, "Nonuniform torsion of multi-material composite bars by the boundary element method", *Computers and Structures*, vol. 79, pp. 2805-2816, 2001.
- [22] E.J. Sapountzakis and V.G. Mokedes, "Nonuniform torsion of bars variable cross section", *Computers and Structures*, vol. 82, pp. 03-715, 2004.
- [23] J.T. Oden and J.N. Reddy, *Variational Method in Theoretical Mechanics*, Springer-Verlag, Berlin, 1976.

Study of Geotechnical Characteristics of Miocene marl in the Region of Medea North-South Highway, Algeria

Y. Yongli, M.H. Aissa

Abstract: The purpose of this paper aims for a geotechnical analysis based on experimental physical and mechanical characteristics of Miocene marl situated at Medea region in Algeria. More than 150 soil samples were taken in the investigation part of the North-South Highway which extends over than 53km from Chiffa in the North to Berrouaghia in the South of Algeria. The analysis of data in terms of Atterberg limits, plasticity index and clay content reflect an acceptable correlation justified by a high coefficient of regression which were compared with previous works in the region. Finally approximated equations have been suggested that serves as a guideline for geotechnical design locally.

Keywords: Correlation, Geotechnical properties, Miocene Marl, North-South Highway.

I. INTRODUCTION

THE North-South Highway in Algeria (Chiffa-Berrouaghia section) in an important part which come within the framework of the National Road 01 upgrade (RN°01). The project extends along 53 km, the layout of the road cross plains but the most part through a mountainous region. Thus, topographical and geological conditions along the project are complex and unfavorable which marl formations occupy a very large field. All these factors are a real challenge for the geotechnical practitioners and designers of different construction projects in the region.

In the litterature, we can find several works decaded for marls study and their characterization thus the factors influencing their behavior. O.J. Pejón *et al.* (1997) [1] studied the effect of water on the clay-marl rocks and the contribution of the mineralogy and texture in the swelling process.

Klotz. (1998) [2], as well as Monnet *et al.* (2012) [3] studied the role of wetting-drying cycles on the degradation of marl. But also the influence of freeze-thaw (Rovera *et al.* (1999)) [4].

Extensive studies were carried out on marl in the Algerian Tell (see for example: Bourougaa & Monjengue. (1989) [5], Chebbani & Belaidi. (1997) [6]). Other researchers have shown that the type of marl is a determining factor in the erosion of soils in Algeria (Brahmia. (1993) [7], Kouidri *et al.*

(2010) [8]). Whereas Roose. (1994) [9] showed that the marl is highly vulnerable to gully.

In the geological and geotechnical point of view, many research field can be found in the marly soils of Algeria, including the plaisanciennes marls of Algiers (K. Benallal & K. Ourabia. (1988) [10], D. Chiheb *et al.* (2010) [11], Z. Derriche & G. Cheikh Lounis. (2004) [12]).

F.Z. Aissou & A. Nechnech. (2011) [13] conducted an analysis of the withdrawal swelling potential of the clay marl soils of Plaisancian age in Algiers region, while M.H. Aissa & Kh. Haddouche. (2011) [14] conducted a study of the marly schist formations subjected to landslides.

In the eastern region of Algeria, O. Boudlal *et al.* (2015) [15] conducted a study on the marl in the region of Tizi Ouzou to use as a filling material in roads while Athmania D. *et al.* (2010) [16] also conducted an analysis of clays and marl of Miocene in the Mila region exactly the risk of withdrawal swelling of these formations and also the data from the geotechnical researches in the region (Afès. (1996) [17], A. Mamoune. (2002) [18], Benaïssa & Bellouche. (1999) [19]).

In the target area (Medea), the Miocene marls are very sensitive to erosion[8]. In the literature there is a gap in studies and geotechnical research on Miocene marl of Medea, except a recent study achieved by A. Medjnoun *et al.* (2014) [20] which serves as a reference document for validation of the present study.

This article aims studied the Miocene marl exposed in the region of Medea based on the analysis of the results of laboratory tests, executed as part of geotechnical investigation of the North-South Highway between Chiffa and Berrouaghia, to establish correlations between physical and mechanical parameters of marl in question.

II. GEOLOGICAL SETTING OF THE STUDY AREA

The area between Chiffa and Hamdania begins with medium and lower Cretaceous formations consisting mainly of fractured and weathered schists. The gray marl of Cretaceous age experience a high alteration with exposition to the air in the less steep slopes where water causes very slowly.

Thereafter, we encounter the *Turonian* calcareous formations and calcareous marl of *Vraconian* between Hamdania and Medea.

Marls are greenish, non laminated, hard enough, brecciated, and hard marls which have a violet color with amygdaloïde texture, accompanied by compact calcareous of homogenous grain of the same color (E. Renou. 1842) [21].

Medea region is constituted by a tray, which exceeds altitude of 900m. This tray is formed of tertiary fields [21] of

Y. Yongli, graduated in 1989 from the Guilin School of Geology in China. Actually he is an expert engineer, Senior Geotechnical engineer in the First Highway Consultants Co.Ltd (e-mail: 330629373@qq.com).

M.H. Aissa, graduated in 2011 from the University of Khemis-Miliana in Algeria. Actually he is a PhD student and a Geotechnical engineer in Xi'an China Highway Geotechnical engineering Co.Ltd

Middle Miocene age (*Helvetian*) based on Cretaceous (*Senonian-Cenomanian*). This Helvetian is all most constituted of marl, becomes sandstone in the top and constituting the plate of Medea.

This plate is syncline, oriented N.W-S.E divided into three compartments by faults N.E-S.W with a rejection of 25 meters.

To the South of this plate between Medea and Damiette, a layer of sand and clay separates sandstone in two levels.

Between Medea and Berrouaghia extends the Middle Miocene, characterized by a large amount of marine fossils, and especially by the shells of oyster genres, comb, bucarde, And by various polyparies. As two main formations dominate: *Lower Miocene*:

Formed by a clayey sandstone series, and a series of marl of light gray color, little importante.

Lower Cretaceous (Albian):

Consists of a series of detrital clay and quartzites and another series of reef limestone.

At Berrouaghia city, we encountered a series of *Cenomanian-Turonian-Vracano* formations consists of: Black limestones with Ammonites and Belemnites. Marls with a few large Calcareous shoals at the top. Calcareous rocks with phtanites locally.

Beyond Berrouaghia, the Miocene land gradually fades, except for summits and hills: it gives way to a formation composed of bluish or blackish marl, almost everywhere gypsum, alternating with gray calcareous marl, and generally have layers inclined at 45 degrees [21].

III. TECTONIC CONTEXT OF THE REGION

The tectonic units are Autochton and telliens displaced during the lower Miocene from the North to the South exhibit many lower Cretaceous facies, this superposition followed by postablecloth formations of Miocene age which is the basin of Medea. This tectonisation manifests by folding, faults, and erosions which reveal windows of Tellian tablecloths infra-Miocene.

Towards Medea we encountered marl facies of lower Miocene, and marl and clay of upper Miocene.

IV. SITE CHARACTERISTICS OF MIOCENE MARL

This study is interested in marl formations of Miocene age, which are generally located in the layout of the North-South Highway between PK20 and PK40. (Fig.1).

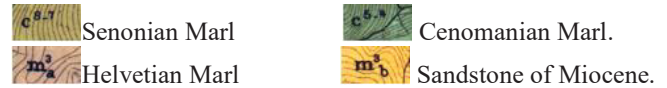


Fig. 1 Location of Miocene Marl in the plan [22]

These marls have a Grey-bluish color, locally in greyish-green and yellowish-green, homogeneous, contain fissures where water circulates, the permeability is low (The permeability coefficient $k = 10^{-1} m/s$), containing a large crustacean fossil and a fragments of fossil. With adding 5% of hydrochloride there will effervescence of the marly rock.

The joints are developed vertically and often there to thin bands of iron oxide, fragile, extremely easy to disintegration, and diagenetic processes are low, also marls have a low wind resistance capacity, the morphology of the terrain is often flat. The slope is less than 20° generally (Fig. 2)



Fig. 2 Overview on the Morphology of Miocene Marn in Medea region.

V. CHARACTERISTICS OF THE MIOCENE MARL IN LABORATORY

V.1. Mineralogical composition of marl:

The determination of the mineralogical composition of Miocene marl is verified by the analysis of the X-ray diffraction spectrum. The results obtained are in Table I:

TABLE I
Mineralogical composition of Marl.

Minerals	Statistical Property	Samples	Maximum	Minimum	Average	Standard
	Number	Value	Value	Value	Value	Deviation
	N	X_m	X_m	X_m	X_m	s
Albite	7	7	3	4	1.4	
Calcite	13	38.9	15	20	6.1	
Dolomite	7	4	1	2	1.1	
Gypsum	1	2	2	2	-	
Orthose	6	8	3	5	1.8	
Quartz	7	26	20	24	2.4	
Illite	7	14	6	10	3.0	
Kaolinite	7	13	8	11	1.8	
Montmorillonite	7	26	18	21	3.1	
Ferruginous Minerals	7	6	6	6	0.5	

Table I reflects a complex mineralogical composition of Miocene Marl. The most abundant clay minerals are: Illite, kaolinite and montmorillonite, totally they can reach 42%, followed by the Quartz silica with 24%, and finally Calcium

carbonate between 38.9% and 15%. The cement material is calcareous.

V.2. Physical properties of marl:

The study of the physical properties of marl Miocene focuses on the particle size, Atterberg limits, soil density (dry and wet) and the void ratio of the soil. The test results are in Table II, note that the liquid limit is measured according to the French standard NF P94-052-1 [23].

TABLE II
PHYSICAL CHARACTERISTICS OF MARL

Statistical Property	Samples Number <i>N</i>	Maximum Value \bar{X}_m	Minimum Value \bar{X}_m	Average Value \bar{X}_m	Standard Deviation <i>s</i>
Physical Property					
Particle size < 2m	150	100.0	72.9	99.2	3.2
Particle size < 0.08m	150	100.0	50.5	87.7	14.4
Particle size < 0.002m	150	64.5	4.2	30.3	15.1
Water content <i>w</i> (%)	150	33.4	9.0	18.3	4.0
Liquid Limit w_L (%)	150	65.0	24.8	43.8	9.7
Plastic Limit w_P (%)	150	31.8	11.6	20.6	3.8
Plasticity Index I_p	150	39.3	8.9	23.2	7.0
Consistency Index I_c	150	1.77	0.82	1.14	0.17
Clays	-	3.69	0.39	0.95	0.53
Activity A_L					
Wet Density	130	2.25	1.83	2.06	0.09
$\rho_n(\frac{M}{c^3})$					
Dry Density	130	2.00	1.54	1.75	0.12
$\rho_d(\frac{M}{c^3})$					
Void Ratio <i>e</i>	130	0.884	0.35	0.579	0.114

The plasticity index I_p is plotted as a function of liquid limit w_L of 150 samples on the plasticity Abacus of Casagrande (Fig. 3). The blue line on the abacus has the following equation: $I_p = 0.73(w_L - 20)$.

Note that the cloud points are above the blue line. For this purpose, the marl is classified as a little plastic clay to a very plastic clay ($A_p - A_L$).

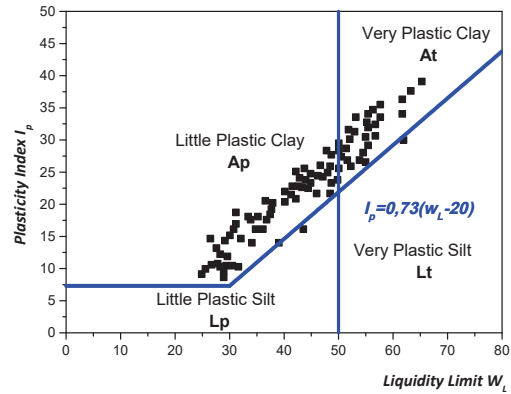


Fig. 3 Plasticity Classification of the Miocene marl

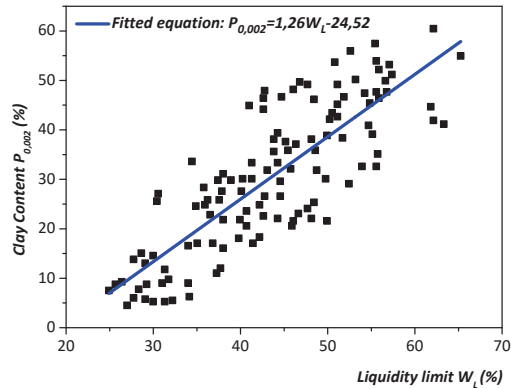


Fig. 4 Clay content as function of liquid limit.

Subsequently, the proportion of clay less than 0.002 mm $P_{0.0}$ is drawn as a function of Liquid limit w_L (Fig. 4). A linear relationship between the liquid limit and the clay content can be seen and this relationship follows this equation: $P_{0.0} = 1.26w_L - 24.52$ with a regression coefficient $R^2 = 0.7063$.

Similarly, the plasticity index I_p is drawn as function of clay content $P_{0.0}$ using data of the present study and the data from the study conducted by [20] for comparison. (Fig. 5) For the present study: $I_p = 0.36P_{0.0} + 11.84$ with a regression coefficient $R^2 = 0.61$

For the comparative study conducted by [20] : $I_p = 0.1P_{0.0} + 21.87$ with a regression coefficient $R^2 = 0.23$

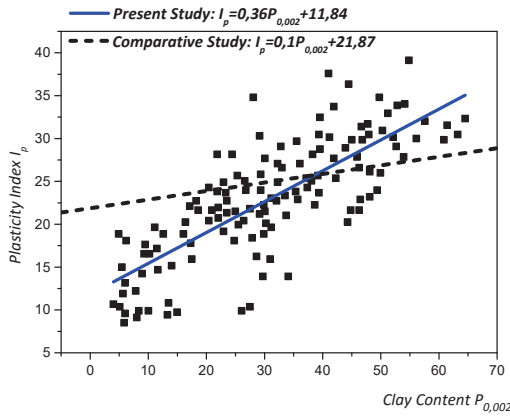


Fig. 5 Plasticity index as function of clay content

V.3. Deformation index of marl:

Statistical analysis of the consolidation test results of all 33 samples is in Table III. The analysis shows that the values are strongly discrete. It should be noted that the consolidation test is based on the French standard XP P 94-090-1 [24]

TABLE III
Consolidation test results of Miocene Marl.

Statistical Property	Samples Number N	Maximum Value X_m	Minimum Value X_m	Average Value X_m	Standard Deviation s
Physical Property					
Preconsolidation pressure P_c (kPa)	33	530	90	237	65.4
Compression index C_c	33	0.198	0.020	0.123	0.048
Swelling coefficient C_g	33	0.072	0.006	0.035	0.016

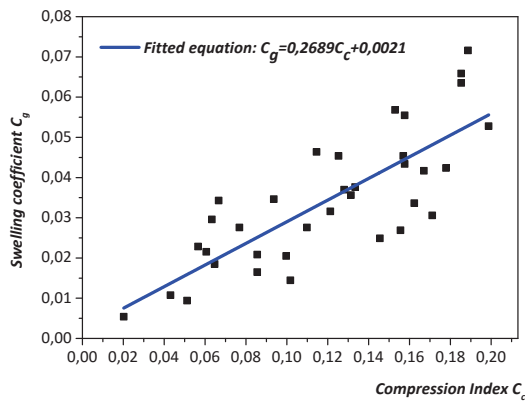


Fig. 6 Swelling coefficient as function of compression index.

The swelling coefficient C_g is drawn as a function of compression index C_c (Fig. 6). The fitted equation is: $C_g = 0.2689C_c + 0.0021$ with $R^2 = 0.63$.

V.4. Mechanical characteristics of marl:

A strength shear tests were performed by using 20 undrained unconsolidated samples of marl and 52 drained consolidated samples of marl. The analysis of Table IV shows that the values of cohesion with the two procedures cited above reflect a wide discretion, whereas the values of the internal friction angle reflect a small discretion.

TABLE IV
Values of Shear Strength Test on the Miocene Marl.

Statistical Property	Samples Number N	Maximum Value X_m	Minimum Value X_m	Average Value X_m	Standard Deviation s
Physical Property					
Undrained Conditions					
Cohesion C (kPa)	20	132	49	89	23
Friction Angle φ ($^\circ$)	20	34.6	16.2	20.4	4.3
Drained Conditions					
Cohesion C' (kPa)	52	177	20	62	31
Friction Angle φ' ($^\circ$)	52	32.9	13.5	22.8	4.2

V.5. Swelling index of marl:

The swelling test was carried out following the French standard NF P94-091 [25]. Statistical analysis of the swelling of test results of all 16 samples is in Table V. The results show that the values are quite discrete.

TABLE V
Swelling index of Miocene Marl.

Statistical Property	Samples Number N	Maximum Value X_m	Minimum Value X_m	Average Value X_m	Standard Deviation s
Property					
Swelling pressure R_g (10^{-2})	16	3.12	0.26	1.78	0.75
Swelling pressure σ_g (kPa)	16	400	46	205	104

VI. DISCUSSION OF THE RESULTS

Through our study, the following notes can be concluded:

According to the plasticity index $I_p = 23.2$, the Miocene marls are plastic.

According to the BRE method (1980) [26], $18 < I_p < 35$ and $30 < P_{0,0} < 60$, the swelling potential is medium to high.

According to the undrained cohesion $C = 89$ kPa, the soil is firm.

According to the compression index $C_c = 0.123$, soil minerals are kaolinites.

According to swelling coefficient $C_g = 0.035$, the swelling risk is high.

Thereafter, correlations are made between the clay content $P_{0,0}$ as function of liquid limit I_p , between plasticity index I_p as function of clay content $P_{0,0}$ in a hand, and between the swelling coefficient C_g as function of compression index C_c in

the other hand. Correlations reflect a linear relationship between parameters with a high regression coefficient R^2 .

For this purpose, equations are suggested:

$$P_{0,0} = 1.26w_L - 24.52 \text{ with } R^2 = 0.7063$$

$$I_p = 0.36P_{0,0} + 11.84 \text{ with } R^2 = 0.61$$

$$C_{gy} = 0.2689C_c + 0.0021 \text{ with } R^2 = 0.63$$

VII. CONCLUSION

Through the statistical analysis of geotechnical results performed on the Miocene marl as part of the recognition of the North-South Highway crossed the Medea region fitted equations, and notes were proposed between the geotechnical parameters with a good accuracy justified by the value of the regression coefficient.

The equations proposed in this study will help to better understand the geotechnical properties of Miocene marl of Medea region, and a fast tool of design when obtaining these settings seems difficult, while there is some guidance and reference for the geotechnical investigation on the local scale.

This work is of paramount importance since it enabled to provide an invaluable data to be served first in future research works in the Medea region and second a way to geotechnical engineers and practitioners in the conception projects.

REFERENCES

- [1] O. J. Pejon, A. Le Roux and D. Guignard. (1997). Comportement à l'eau des Roches Argilo-Marneuses, suivi du Gonflement, Importance de la Minéralogie et des Textures. Bulletin de l'association internationale de géologie de l'ingénieur, Paris N°55, pp.105-119.
- [2] S. Klotz (1998). Caractéristiques Physiques et Mécaniques des Marnes Noires Callovo-Oxfordiennes: Application au Glissement-Coulée de Super-Sauze, Université de Louis Pasteur.
- [3] J. Monnet, D. Fabre and M. Zielibski. (2012). Cycles Gel-Dégel et Altération des Roches Marneuses: Exemple des Terres Noires. Journées Nationales de Géotechnique et de Géologie de l'Ingénieur JNGG2012. Bordeaux 4.
- [4] G. Rovera, Y. Robert, M. Coubat and R. Nedjai. (1999). Erosion et Stades Biorhexistatiques dans les Ravines du Saignon (Alpes de Haute-Provence). Essai de Modélisation Statistique des Vitesses d'Erosion sur Marnes. Colloque « La Montagne Méditerranéenne : Paléoenvironnement, Morphogenèse, Aménagement ». Aix en Provence. pp. 109-115.
- [5] L. Bourougaa, S. Monjengue. (1989). Fixation Biologique et Mécanique des Ravines. Bulletin Réseau Erosion, ORSTOM. Montpellier, No 9 :19-29.
- [6] R. Chebbani, S. Belaidi. (1997). Etude de la Dynamique du Ravinement: Suivi de Deux Couples de Ravines Expérimentales près de Tlemcen. ORSTOM, Montpellier, Bulletin Réseau Erosion 17 : 152-160.
- [7] K. Brahmia. (1993). Essai sur la Dynamique Actuelle dans la Moyenne Montagne Méditerranéenne: Bassin Versant de l'Oued Mina (Zone de Taassalet) Algérie. Thèse de Géographie, Université de Grenoble. France.
- [8] R. Kouidri, K. Bouguerra and M. Guendouz. (2010). Approche Quantitative de l'Erosion Hydrique en Algérie: Bassin Pilote de Souagui (Région de Médéa). Revue scientifique et Technique. LJEE N°16 et 17.
- [9] E. Roose. (1994). Introduction à la GCES. Bull. Pédologie FAO N°70. Rome. 420p.
- [10] D. Chiheb, N. Laradi and S. Haddadi. (2010). Les Marnes du Plaisancien d'Alger, Caractéristiques et Comportement vis-à-vis des instabilités. Séminaire National de Génie Civil SNGC08. Université de Chlef. Algérie.
- [11] K. Benallal, K. Ourabia. (1988). Monographie Géologique et Géotechnique de la région d'Alger (Recueil de Notes). Office des Publications Universitaires, Alger, Algérie.
- [12] Z. Derrich, G. Cheikh Lounis. (2004). Caractéristiques Géotechniques des Marnes Plaisanciennes d'Alger. Bull Eng Geol Environ. 63 :367-378.
- [13] F.Z. Aissiou, A. Nechnech. (2011). Retrait-Gonflement des Marnes Argileuses d'Alger « Etude des risqué naturel ». Séminaire International, Innovation et Valorisation en Génie Civil et Matériaux de Construction INVACO2. Rabat (Maroc).
- [14] M.H. Aissa, Kh. Haddouche. (2011). Analyse et Modélisation d'un Glissement de Terrain. Cas de Sidi Yousef. Alger. Mémoire de Master. Université de Khemis-Miliana. Algérie.
- [15] O. Boudlal, M. Khattaoui, M. Djemai and T. Djebra. (2015). Etude du Comportement Mécanique des Marnes de la Grande Kabylie (Algérie) pour une utilisation dans la Construction Routière. 2^{ème} Congrès Français de Mécanique. Lyon.
- [16] D. Athmania, A. Benaissa, A. Hammadi and M. Bouassida. (2010). Clay and Marl Formation Susceptibility in Mila Province. Algeria. Bull Geotech Geol Eng. 28:805-813.
- [17] M. Afès. (1996). Contribution à la Détermination des Paramètres de Gonflement des Sols et Etude de l'Argile de Mila (Algérie) traitée à la Chaux. Thèse de Doctorat, INSA, Lyon, p300.
- [18] A. Mamoune. (2002). Contribution à la Mesure, Prévion et Modélisation du Comportement des Sols Expansifs. Thèse de Master. Faculté des Sciences de l'Ingénieur, Université Aboubakr Belkaid, Tlemcen, Algérie.
- [19] A. Benaissa, M.A. Bellouche. (1999). Propriétés Géotechniques de quelques Formations Géologiques propices aux Glissement de Terrain dans l'Agglomération de Constantine. Bull Eng Geol Environ. 57(3) : 301-310.
- [20] A. Medjnoun, M. Khatine and R. Bahar. (2014). Caractérisation Minéralogiques et Géotechnique des Argiles Marneuses Gonflantes de la région de Médéa, Algérie. Bull Eng Geol Environ. 73:1259-1272.
- [21] E. Renou. (1842). Exploitation Scientifique de l'Algérie pendant les années 1840, 1841, 1842., Imprimerie Nationale de Paris. France.
- [22] The Detailed Geological Map of the Medea region-Algeria. Leaf No.86, 1896 Edition
- [23] NF P 94-052-1. (1995). Détermination des Limites d'Atterberg. Partie 1: Limite de Liquidité-Méthode de Cone de Pénétration. Association Française de Normalisation (AFNOR).
- [24] XP P94-090-1. (1997). Essai Oedométrique. Partie 1: Essai de Compressibilité sur Matériaux Fins Quasi Saturés avec Chargement par Paliers. Association Française de Normalisation (AFNOR).
- [25] NF P94-091. (1995). Essai de Gonflement à l'Oedomètre: Détermination des Déformations par Chargement de plusieurs Eprouvettes. Association Française de Normalisation 5AFNOR).
- [26] BRE, Building Research Establishment. (1980). Low-Rise Buildings on Shrinkable Clay Soils: Part 1. BRE Digest 240, HMSO, London.

Study of Linear Generator for Vibration Energy Harvesting of Frequency more than 50Hz

Seong-Jin Cho, Jin Ho Kim

Abstract— Energy harvesting is the technology which gathers and converts external energies such as light, vibration and heat which are disposed into reusable electrical energy and uses such electrical energy. The vibration energy harvesting is very interesting technology because it produces very high density of energy and unaffected by the climate. Vibration energy can be harvested by the electrostatic, electromagnetic and piezoelectric systems.

The electrostatic system has low energy conversion efficiency, and the piezoelectric system is expensive and needs the frequent maintenance because it is made of piezoelectric ceramic. On the other hand, the electromagnetic system has a long life time and high harvesting efficiency and it is relatively cheap.

The electromagnetic harvesting system includes the linear generator and the rotary-type generator. The rotary-type generators requires the additional mechanical conversion device if it uses linear motion of vibration. But, the linear generator uses directly linear motion of vibration without a mechanical conversion device and it has uncomplicated structure and light weight compared with the rotary-type generator. Therefore, the linear electromagnetic generator can be useful in using vibration energy harvesting.

The pole transformer systems need electricity sensor system for sending voltage and power information to administrator. Therefore, the battery is essential and its regular maintenance of replacement is required. In case of the transformer of high location in mountainous areas, the person can't easily access it resulting in high maintenance cost.

To overcome these problems, we designed and developed the linear electromagnetic generator which can replace battery in electricity sensor system for sending voltage and power information of the pole transformer. And, it use vibration energy of frequency more than 50 Hz by the pole transformer. In order to analyze the electromagnetic characteristics of small linear electric generator, a commercial electromagnetic finite element analysis program "MAXWELL" was used. Then, through the actual production and experiment of linear generator, we confirmed output power of linear generator.

Keywords—Energy harvesting, Frequency, Linear generator, Experiment.

S. J. Cho is at School of Mechanical Engineering, Yeungnam University, Gyeongsan, CO 38541 Korea (phone: +82-53-810-3835; fax: +82-53-810-4627; e-mail: tjdwls4106@naver.com).

J. H. Kim was with University of California, Berkeley, USA. He is now an associate professor at School of Mechanical Engineering, Yeungnam University, Gyeongsan, CO 38541 Korea (phone: +82-53-810-2441; fax: +82-53-810-4627; e-mail: jinho@ynu.ac.kr).

Suitability Verification of Technological Project through Estimated Cost and Period Information by Technology Development Stage

Bong-Goon Seo, Do-Hyung Park, Daeheon Choi, Seung-Pyo Jun

Abstract— In recent years, the innovative technologies such as big data, artificial intelligence, and IoT have been introduced and developed with huge impacts for all participants in industry. However, industry experience with commercialization of such technologies suggests that most of companies have a great amount of uncertainty in estimating the investment costs and the time required during technology commercialization periods. To strengthen industrial competitiveness and improve the overall technological level of the country, government-funded research and project are very important and the government has a lot of support for SME-led technologies with government-funded research and projects. Generally, companies voluntarily take participate in government-led project, the government evaluates and selects the project in accordance with the objective evaluation system based on the technology proposed by the company. Therefore, the government should be able to confirm how reasonable that the commercialization period and cost required by a company, and will be able to make efficient investments through it. This study proposes a validation system, which confirms that the cost and period of technology commercialization proposed by each individual company based on the R&D data about 10,000 cases of SMEs in South Korea for the last five years. Specifically, if the company proposes a period of commercialization and the costs for the technical characteristics of a particular technology to the government, a system is able to determine whether or not the cost and period suggested by the company is reasonable. The provided system in this study has a great theoretical contribution in terms of being able to check the relationships between the SME technology commercialization status and multiple factors influencing the commercialization. Also, it has a practical contribution in that our findings provide a great guidance on the right selection of government-led projects.

Keywords—R&D, SME, Technology Commercialization, Validation System

Bong-Goon Seo is with the Graduate School of Business IT, Kookmin University, Seoul, Korea (e-mail: bgseo@kookmin.ac.kr).

Do-Hyung park is with the Department of Management Information Systems, Kookmin University, Seoul, Korea (e-mail: dohyungpark@kookmin.ac.kr)

Daeheon Choi is with the College of Business Administration, Kookmin University, Seoul, Korea (e-mail: dhchoi@kookmin.ac.kr).

Seung-Pyo Jun is with Industry Information Analysis Center, Korea Institute of Science and Technology Information, Seoul, Korea (e-mail: spjun@kisti.re.kr)

Surface Erosion and Slope Stability Assessment of Cut and Fill Slope

Kongrat Nokkaew

Abstract—This article assessed the surface erosion and stability of cut and fill slope in the excavation of the detention basin, Kalasin Province, Thailand. The large excavation project was built to enlarge detention basin for relieving repeated flooding and drought which usually happen in this area. However, at the end of the 1st rainstorm season, severely erosions slope failures were widespread observed. After investigation, the severity of erosions and slope failure were classified into five level from sheet erosion (Level 1), rill erosion (Level 2, 3), gully erosion (Level 4), and slope failure (Level 5) for proposing slope remediation. The preliminary investigation showed that lack of runoff control were the major factors of the surface erosions while insufficient compacted of the fill slope led to slopes failures. The slope stability of four selected slope failure was back calculated by using Simplified Bishop with Seep-W. The result show that factor of safety of slope located on non-plasticity sand was less than one, representing instability of the embankment slope. Such analysis agreed well with the failures observed in the field.

Keywords—surface erosion, slope stability, detention basin, cut and fill

Corresponding Author

Kongrat Nokkaew from Kasetsart University , Thailand
e-mail: kongrat.no@ku.th

Synergistic Studies of Multi-Flame Retarders Using Silica Nanoparticles, and Nitrogen and Phosphorus-Based Compounds for Polystyrene Using Response Surface Methodology

Florencio D. De Los Reyes, Magdaleno R. Vasquez Jr., Mark Daniel G. De Luna, Peerasak Paoprasert

Abstract—The effect of adding silica nanoparticles (SiNPs) obtained from rice husk, and phosphorus and nitrogen based compounds namely 9,10-dihydro-9-oxa-10-phosphaphenanthrene-10-oxide (DOPO) and melamine, respectively, on the flammability of polystyrene (PS) was studied using response surface methodology (RSM). The flammability of PS was reduced as the limiting oxygen index (LOI) values increased when the flame retardant additives were added. DOPO exhibited the best retarding property increasing the LOI value of PS by 42.4%. A quadratic model for LOI was obtained from the RSM results, with percent loading of SiNPs, DOPO, and melamine, as independent variables. The observed increase in the LOI value as the percent loading of the flame retardant additives is increased, was attributed both to the main effects and synergistic effects of the parameters, as the LOI response of SiNPs is greatly enhanced by the addition of DOPO and melamine, as shown by the response surface plots. This indicates the potential of producing a cheaper, effective, and non-toxic multi-flame retardant system for the polymeric system via different flame retarding mechanisms.

Keywords—flame retardancy, polystyrene, response surface methodology, rice husk, silica nanoparticle

Corresponding Author

Florencio De Los Reyes from University of Santo Tomas, España,
Manila, Philippines
e-mail: fddelosreyes@ust.edu.ph

Synthesis and Characterization of Hydroxyapatite from Biowaste for Potential Medical Application

Mohammad D.H. Beg*, John O. Akindoyo, Suriati Ghazali and Nitthiyah Jeyaratnam

*Faculty of Chemical and Natural Resources Engineering, Universiti Malaysia Pahang
Lebuhraya Tun Razak, Gambang 26300, Kuantan, Malaysia.*

*Correspondence: M.D.H. Beg, email: dhbeg@yahoo.com; Phone: +6019504590; Fax: +6095492816)

ABSTRACT: Over the period of time, several approaches have been undertaken to mitigate the challenges associated with bone regeneration. This includes but not limited to xenografts, allografts, autografts as well as artificial substitutions like bioceramics, synthetic cements and metals. The former three techniques often come along with peculiar limitation and problems such as morbidity, availability, disease transmission, collateral site damage or absolute rejection by the body as the case may be. Synthetic routes remain the only feasible alternative option for treatment of bone defects. Hydroxyapatite (HA) is very compatible and suitable for this application. However, most of the common methods for HA synthesis are either expensive, complicated or environmentally unfriendly. Interestingly, extraction of HA from bio-wastes have been perceived not only to be cost effective, but also environment friendly. In this research, HA was synthesized from bio-waste: namely bovine bones through three different methods which are hydrothermal chemical processes, ultrasound assisted synthesis and ordinary calcination techniques. Structure and property analysis of the HA was carried out through different characterization techniques such as TGA, FTIR, and XRD. All the methods applied were able to produce HA with similar compositional properties to biomaterials found in human calcified tissues. Calcination process was however observed to be more efficient as it eliminated all the organic components from the produced HA. The HA synthesized is unique for its minimal cost and environmental friendliness. It is also perceived to be suitable for tissue and bone engineering applications.

INTRODUCTION

Bone defects often arise either through traumatic or non-traumatic experiences and most of the medical treatments often administered to victims of bone defects majorly demands artificial bone grafts. Recently, the development of materials whose application is related to bone regeneration and replacement have gained increased attention [1]. A vast number of biomaterials are under investigation as suitable substitute for grafts. Notable among these materials is porous hydroxyapatite (HA) ($\text{Ca}_{10}(\text{PO}_4)_6(\text{OH})_2$), and some other similar calcium phosphate ceramics (such as tricalcium phosphate) [2].

Hydroxyapatite has been specifically reported to possess high biocompatible, osteoconductive, nontoxic, noninflammatory, nonimmunogenetic as well as bioactive properties, which makes it highly suitable for osteointegration [3]. Thus, hydroxyapatite is commonly used in orthopaedic, maxillofacial and dental applications. Preparation of HA from both natural and synthetic sources have been achieved through various techniques as well as from sources which include animal bone, coral exoskeleton and also through chemical synthesis [4]. Some of the methods which have been used to synthesize HA includes emulsion liquid membrane [5], microwave mediated methathesis [6], chemical precipitation [7], hydrolysis [8], expeditious microwave irradiation [9], microemulsion [10] and ultrasonic irradiation [11]. Mechanochemistry technique have also been used to synthesize HA with the help of different reactants such as CaO and CaHPO₄ [12], Ca(NO₃)₂ and (NH₄)₃PO₄ [13], Ca(OH)₂ and H₃PO₄ [14] and Ca(NO₃)₂ and C₆H₁₅O₃P [15]. Furthermore, other researches are based on investigating the influence of different parameters on synthesis of HA through hydrothermal process. The investigated parameters include temperature [16], pH [17] and surfactant [18]. It was found however that most of these synthetic methods are either biologically unsafe or somewhat complicated [19].

Attention is therefore being shifted towards extraction of HA from natural sources most especially due to the economic feasibility, environmental friendliness of this process [3] and the possibility for large scale production [3]. HA bioceramics have been reportedly extracted from some biological wastes such as fish bones, bovine bones as well as the teeth and bones of pig [4]. Most of the early extraction processes of HA from biowastes were majorly achieved through ordinary calcination (thermal decomposition). As research progressed, other methods such as subcritical extraction and alkaline hydrothermal were also exploited for the extraction of HA from biowastes [20]. In a particular research, the three main methods (thermal decomposition, subcritical extraction and alkali hydrothermal technique) were compared for the extraction of HA from bovine bones. It reported that the thermal decomposition method produced HA nanorod rather than nanoparticles which was obtained from the other techniques [20]. However, alkali hydrothermal and subcritical processes were said to produce smaller particle size HA as observed from SEM and FESEM results. Generally from their research, it was reported that the three methods offers the advantage of being simple and cheap, thereby deserving large scale applications. In a similar research, chemical and thermal processes were combined for HA extraction from cortical portions of bovine bones. Result showed that the produced HA has much resemblance with calcified tissues of human. It was suggested that nanoporous structure, chemical constituents and resorbable nature of the HA would be of immense benefit if exploited for bone engineering application [21]. The objective of this study is to synthesize natural HA from cow bones through different approaches such as ultrasonic treatment, hydrothermal treatment as well ordinary calcination techniques. Characterizations such as TGA, XRD and FTIR were used to investigate the properties of the synthesized materials and they were compared with the standard HA.

MATERIALS AND METHODS

Bone preparation

Femur of adult bovine (~3 years old) was purchased from local slaughter house in Jaya Garden, Kuantan Malaysia. The bones were washed carefully to remove fats and other substances adhering to the surface. Cleaning was done in 4% NaOH solution under hydrothermal conditions and the bones were opened up using a jar crusher in order to remove the macroscopic organic parts consisting of proteins collagen e.t.c. After this the bones were washed in hot 1% NaOH solution before it was dried at 150 °C for 24 h. Dried bones were grinded and sieved into fine particles with particle size of about 450 µm.

Synthesis of hydroxyapatite

The natural HA was derived through some chemical and thermal processing of the bone powder. The three different techniques employed are alkaline hydrothermal process, ultrasound assisted alkaline hydrothermal process and calcination process. The materials obtained through these methods were given code names as ALK, ULS and CAL respectively. An untreated bone powder sample referred to as RAW was used as control and its properties were compared with the treated samples. For the three methods, 20 g of the bone powder was used. Ultrasound treatment was conducted using an ultrasound bath (Daihan Ultrasonic Bath; Crest-ultrasonics) the bone powder was soaked in a solution of 1M NaOH at 1:50 for sample and solvent respectively. The beaker was placed in the ultrasound bath set at a temperature 100 °C and the process was continued for 2 h. After treatment, the mixture was filtered and the residue was washed severally using deionized water until pH 7 was attained. Drying was done for 24 h at 105 °C after which the material was grinded and kept for further analysis.

Alkaline hydrothermal treatment was conducted using a heating mantle set at 100 °C and the experiment was conducted for 3 h under reflux on solution containing 1:50 of sample and solvent respectively. After the experiment, filtration, washing, drying and grinding was carried out as described for ultrasound treatment. The obtained material was kept in plastic bags for further analysis. Calcination process was conducted in a furnace at temperature of 850 °C at a rate of 10 °C/min for 1 h [20].

Characterizations

Surface chemistry of the HA was analysed through FTIR analysis. This was used to investigate the presence, appearance and disappearance of functional groups in the HA. It was carried out to understand the possible phase changes as well as determine the deviations of the synthesized HA from stoichiometric HA. The analysis was conducted with the help of an FTIR spectrometer (Nicolet iS5 iD7 ATR; THERMO SCIENTIFIC, Germany), fitted with OMNIC software. The standard KBr technique was used to obtain the IR spectra in a scanning wavelength range of 400-4000 cm⁻¹. X-ray diffraction was performed to deduce the crystalline structure of the HA. Analysis was carried out at a scanning speed of 1deg min⁻¹ over a scanning range of 3-60° and sampling step of 0.02° using an X-ray diffractometer. Thermogravimetric analysis was

performed to investigate the thermal properties of the HA using a TA analyser (TGA Q500 V6.4, Germany). About 5 ± 2 mg sample was placed in a platinum crucible under nitrogen atmosphere at a flow rate of 40 mL min^{-1} . Heating was conducted at $10 \text{ }^\circ\text{C min}^{-1}$ in the range from 25-1000 $^\circ\text{C}$.

RESULTS AND DISCUSSION

Thermal Analysis

The TGA spectra for raw cow bone powder (RAW), hydroxyapatite obtained through alkaline hydrothermal process (ALK), hydroxyapatite obtained through ultrasound-assisted alkaline hydrothermal processes (ULS), and hydroxyapatite obtained through calcination (CAL) (750 $^\circ\text{C}$ for 2 h) are illustrated in Figure 1. The observable weight loss which occurred in the samples is as follows:

From room temperature to around 200 $^\circ\text{C}$ can be attributed to evaporation of residual surface adsorbed water. Whereas this loss was obvious in the spectra of RAW, ULS and ALK, it does not appear in spectra for CAL indicating that it is totally dry as observed by another researcher [20]. Another weight loss can be seen between 250 and 500 $^\circ\text{C}$ which can be attributed to the burning of organic components of the material [22]. The other weight loss from between 600 and 800 $^\circ\text{C}$ could be due to endothermic dissociation of trace CO_3^{2-} . Decomposition of CO_3^{2-} have been reported to occur from about 400-600 $^\circ\text{C}$ in air and 500-890 $^\circ\text{C}$ under nitrogen atmosphere [21], which conforms to the result obtained herein.

On the other hand, it can be generally seen that weight loss for all the samples except CAL was continuous until between 750-800 $^\circ\text{C}$ after which the curves attained balance. As illustrated in Figure 1, after 800 $^\circ\text{C}$, the weight losses for RAW, ULS, ALK and CAL were 35, 14, 12 and 2% respectively. Literature review revealed that the bone generally contains about 30-40% organic components and 60-70% inorganic components [23-25]. The larger weight loss (35%) obtained for RAW can therefore be attributed to presence of larger amount of organic materials compared to other samples. From these results it can be inferred that while hydrothermal processes and other techniques reduced the amount of organic materials in the bone powder, calcination totally removed the organic materials from the bone.

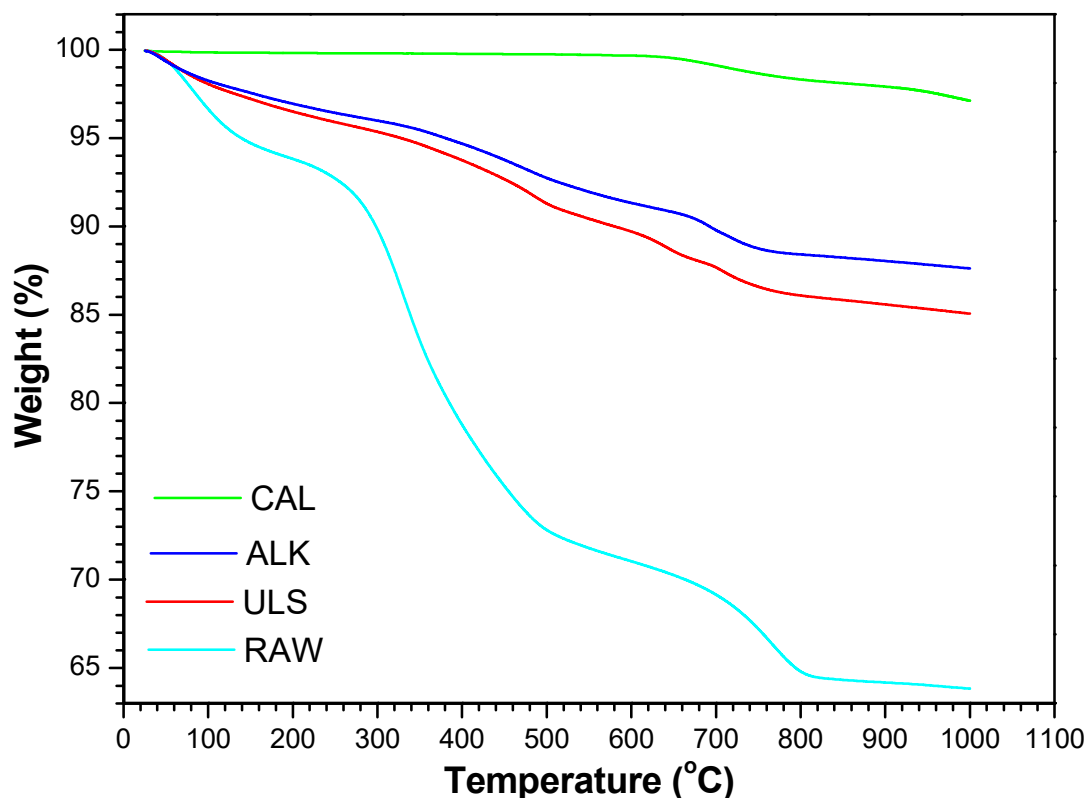


Figure 1: TGA spectra for calcined (CAL), chemical hydrothermal (ALK), ultrasound treated (ULS) and untreated (RAW) bone powder.

XRD analysis

The XRD diffractograms for RAW, ULS, ALK and CAL are illustrated in Figure 2. The spectra were validated against the ICCD standard HA DB card number 01-074-9761. All the peaks associated with the standard HA was found to be present in the spectrum for CAL, ALK and ULS. Thus indicates that all of the treatment methods applied herein are capable of removing collagen and other organic components from the raw bones without necessarily disrupting the molecular skeletal of the HA [26]. Contrary to this, the spectra for RAW was found to be short of certain peaks from the standard spectra. This suggests the presence of certain fibrous collagen in the samples which might have dispersed the X-ray radiations [20]. However, the XRD parameters for the different samples included in Table 1 revealed that only the calcined sample possesses same parameter as the standard HA. This suggests that calcination process is necessary to fully eliminate collagen and other organic materials from the raw bone in order to obtain pure HA.

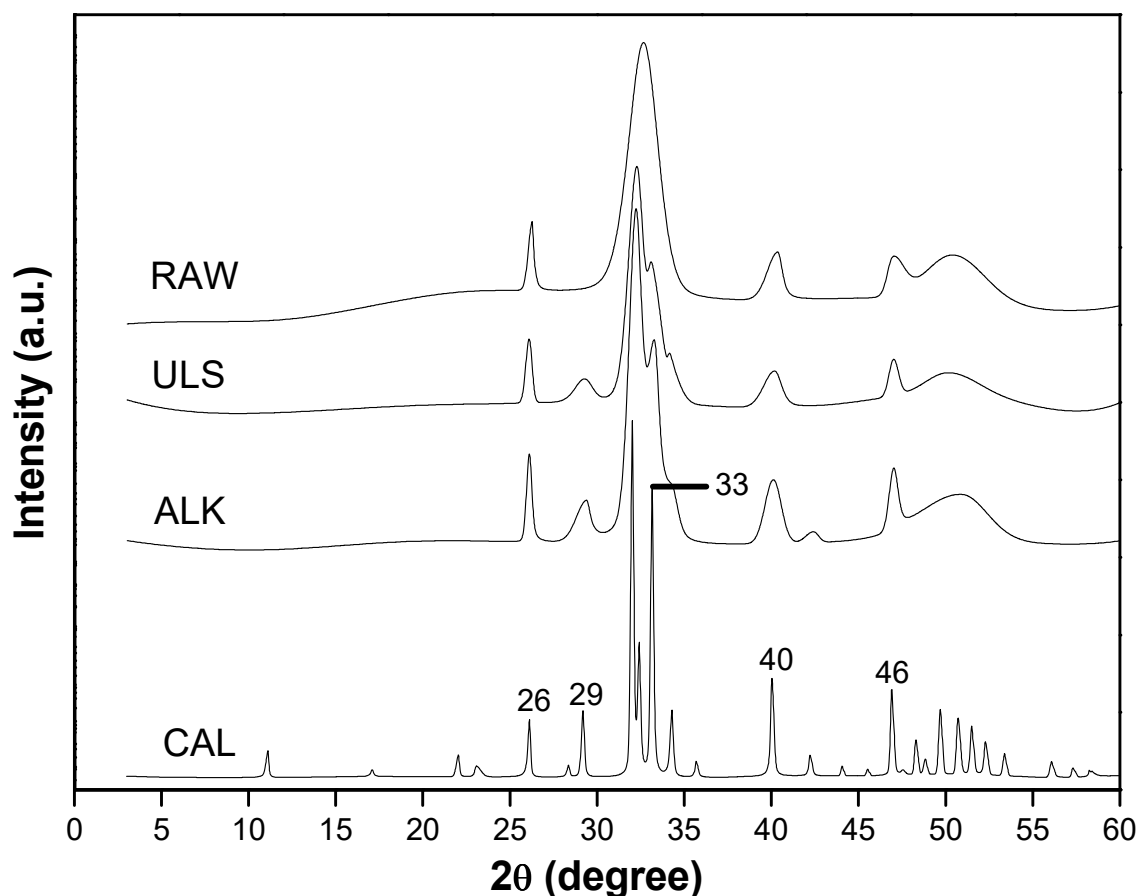


Figure 2: XRD diffractogram for calcined (CAL), chemical hydrothermal (ALK), ultrasound treated (ULS) and untreated (RAW) bone powder.

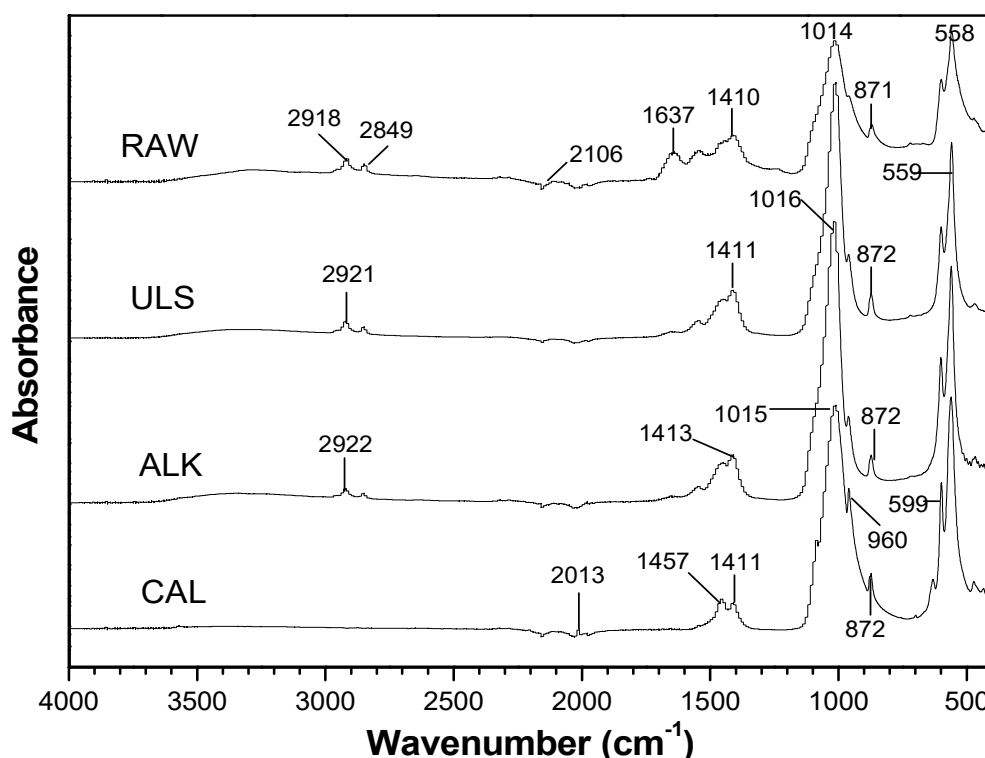
Table 1: XRD parameters for calcined (CAL), chemical hydrothermal (ALK), ultrasound treated (ULS) and untreated (RAW) bone powder

2θ (degree)	Diffraction line Index	d(nm)	ICCD					FWHM				
			CAL	ALK	ULS	RAW	CAL	ALK	ULS	RAW		
26	002	3.41	3.41	3.41	3.42	3.39	0.16	0.16	0.35	0.46	0.35	
29	210	3.06	3.06	3.04	3.05	-	0.18	0.18	0.96	1.17	-	
33	300	2.70	2.70	2.70	2.70	2.74	0.17	0.17	0.74	0.94	2.02	
40	130	2.25	2.25	2.25	2.24	2.23	0.16	0.16	1.09	1.21	1.01	
46	222	1.94	1.94	1.93	1.93	1.93	0.16	0.16	0.58	0.63	1.09	

Fourier transforms infrared spectroscopy

The FTIR spectra for RAW, CAL, ALK and ULS are illustrated in Figure 3. Generally, the characteristic absorbance peaks of apatite phase can be seen from the individual spectrum of each sample. The bands at the upper wavelength from around 3500-3200 cm^{-1} can be attributed to stretching vibrations of bonded hydroxyl groups [27]. This functional group

representation which was also evident around 1637 cm^{-1} in the spectrum for the RAW is perhaps due to the presence of large quantity of surface adsorbed water on the raw bone powder [4]. The presence of this band in the spectrum of the other samples can be associated represents the hydroxyl groups of the HA [28]. At around $2930\text{-}2840\text{ cm}^{-1}$, a low intense band can be seen which is assigned to vibrational stretching of C-H bonds. This band which indicates the presence of organic materials in the sample, was absent from the CAL spectra indicating that the heat treatment was able to eliminate organic components from the bone powder to produce pure HA [28]. The peak at 1015 cm^{-1} and 960 cm^{-1} are attributed to the stretching vibrations of phosphate (PO_4^{3-}) ions whereas deformational vibrations of PO_4^{3-} ions appeared at $605\text{-}550\text{ cm}^{-1}$ [19]. The peaks which appeared at 1457 cm^{-1} and 1410 cm^{-1} suggests the presence of CO_3^{2-} in the synthesized HA. The peak at 872 cm^{-1} is assigned to A type carbonate substitution into the synthesized HA, indicating the presence of surface labile carbonates [4]. From literature, it had been revealed that bones are natural composites made up of collagen and some hydroxycarbonate apatite [23]. Similarly, it had been reported that calcium phosphates including HA exhibits compositional structures which are identical to those of natural bones [29]. Thus the HA synthesized in this study possesses similar chemical properties with the type of biominerals which are present in calcified human tissues.



CONCLUSION

Natural hydroxylapatite was synthesized through three different methods which are alkaline hydrothermal process, ultrasound assisted alkaline hydrothermal process and calcination process. Based on the characterizations conducted, all the three methods were suitable for HA synthesis. However, the only calcination process able to eliminate all the organic components

from the HA. Furthermore, HA obtained through calcination process revealed great similarity with biomaterials which are present in calcified human tissues.

ACKNOWLEDGEMENT

The University Malaysia Pahang is highly acknowledged for supporting this project under the grant RDU140319.

REFERENCES

- [1] J. Zhang, W. Liu, V. Schnitzler, F. Tancret, and J.-M. Bouler, "Calcium phosphate cements for bone substitution: chemistry, handling and mechanical properties," *Acta biomaterialia*, vol. 10, pp. 1035-1049, 2014.
- [2] H. Zhang and B. W. Darvell, "Mechanical properties of hydroxyapatite whisker-reinforced bis-GMA-based resin composites," *Dental materials*, vol. 28, pp. 824-830, 2012.
- [3] S.-C. Wu, H.-C. Hsu, S.-K. Hsu, F.-W. Lin, and W.-F. Ho, "Preparation and characterization of porous calcium-phosphate microspheres," *Ceramics International*, vol. 41, pp. 7596-7604, 2015.
- [4] Q. Liu, J. P. Matinlinna, Z. Chen, C. Ning, G. Ni, H. Pan, *et al.*, "Effect of thermal treatment on carbonated hydroxyapatite: Morphology, composition, crystal characteristics and solubility," *Ceramics International*, vol. 41, pp. 6149-6157, 2015.
- [5] S. Jarudilokkul, W. Tanthapanichakoon, and V. Boonamnuayvittaya, "Synthesis of hydroxyapatite nanoparticles using an emulsion liquid membrane system," *Colloids and Surfaces A: Physicochemical and Engineering Aspects*, vol. 296, pp. 149-153, 2007.
- [6] P. Parhi, A. Ramanan, and A. R. Ray, "A convenient route for the synthesis of hydroxyapatite through a novel microwave-mediated metathesis reaction," *Materials letters*, vol. 58, pp. 3610-3612, 2004.
- [7] Y. Pang and X. Bao, "Influence of temperature, ripening time and calcination on the morphology and crystallinity of hydroxyapatite nanoparticles," *Journal of the European Ceramic Society*, vol. 23, pp. 1697-1704, 2003.
- [8] W.-J. Shih, Y.-F. Chen, M.-C. Wang, and M.-H. Hon, "Crystal growth and morphology of the nano-sized hydroxyapatite powders synthesized from $\text{CaHPO}_4 \cdot 2\text{H}_2\text{O}$ and CaCO_3 by hydrolysis method," *Journal of Crystal Growth*, vol. 270, pp. 211-218, 2004.
- [9] S. Sarig and F. Kahana, "Rapid formation of nanocrystalline apatite," *Journal of crystal growth*, vol. 237, pp. 55-59, 2002.
- [10] G. Guo, Y. Sun, Z. Wang, and H. Guo, "Preparation of hydroxyapatite nanoparticles by reverse microemulsion," *Ceramics international*, vol. 31, pp. 869-872, 2005.
- [11] J. Liu, K. Li, H. Wang, M. Zhu, and H. Yan, "Rapid formation of hydroxyapatite nanostructures by microwave irradiation," *Chemical physics letters*, vol. 396, pp. 429-432, 2004.
- [12] K. Yeong, J. Wang, and S. Ng, "Mechanochemical synthesis of nanocrystalline hydroxyapatite from CaO and CaHPO_4 ," *Biomaterials*, vol. 22, pp. 2705-2712, 2001.
- [13] G. Bezzi, G. Celotti, E. Landi, T. La Torretta, I. Sopyan, and A. Tampieri, "A novel sol-gel technique for hydroxyapatite preparation," *Materials Chemistry and Physics*, vol. 78, pp. 816-824, 2003.
- [14] T. Isobe, S. Nakamura, R. Nemoto, M. Senna, and H. Sfihi, "Solid-state double nuclear magnetic resonance study of the local structure of calcium phosphate nanoparticles synthesized by a wet-mechanochemical reaction," *The Journal of Physical Chemistry B*, vol. 106, pp. 5169-5176, 2002.
- [15] D.-M. Liu, T. Troczynski, and W. J. Tseng, "Water-based sol-gel synthesis of hydroxyapatite: process development," *Biomaterials*, vol. 22, pp. 1721-1730, 2001.
- [16] M. Yoshimura, P. Sujaridworakun, F. Koh, T. Fujiwara, D. Pongkao, and A. Ahniyaz, "Hydrothermal conversion of calcite crystals to hydroxyapatite," *Materials Science and Engineering: C*, vol. 24, pp. 521-525, 2004.

- [17] J. Liu, X. Ye, H. Wang, M. Zhu, B. Wang, and H. Yan, "The influence of pH and temperature on the morphology of hydroxyapatite synthesized by hydrothermal method," *Ceramics international*, vol. 29, pp. 629-633, 2003.
- [18] L. Yan, Y. Li, Z.-X. Deng, J. Zhuang, and X. Sun, "Surfactant-assisted hydrothermal synthesis of hydroxyapatite nanorods," *International Journal of Inorganic Materials*, vol. 3, pp. 633-637, 2001.
- [19] X. Y. Lü, Y. B. Fan, D. Gu, and W. Cui, "Preparation and characterization of natural hydroxyapatite from animal hard tissues," in *Key Engineering Materials*, 2007, pp. 213-216.
- [20] N. A. Barakat, M. S. Khil, A. Omran, F. A. Sheikh, and H. Y. Kim, "Extraction of pure natural hydroxyapatite from the bovine bones bio waste by three different methods," *Journal of materials processing technology*, vol. 209, pp. 3408-3415, 2009.
- [21] R. Murugan, S. Ramakrishna, and K. P. Rao, "Nanoporous hydroxy-carbonate apatite scaffold made of natural bone," *Materials Letters*, vol. 60, pp. 2844-2847, 2006.
- [22] C. Ooi, M. Hamdi, and S. Ramesh, "Properties of hydroxyapatite produced by annealing of bovine bone," *Ceramics international*, vol. 33, pp. 1171-1177, 2007.
- [23] S. Bose, M. Roy, and A. Bandyopadhyay, "Recent advances in bone tissue engineering scaffolds," *Trends in biotechnology*, vol. 30, pp. 546-554, 2012.
- [24] M. Zuber, F. Zia, K. M. Zia, S. Tabasum, M. Salman, and N. Sultan, "Collagen based polyurethanes—A review of recent advances and perspective," *International journal of biological macromolecules*, vol. 80, pp. 366-374, 2015.
- [25] D.-W. Jang, R. A. Franco, S. K. Sarkar, and B.-T. Lee, "Fabrication of Porous Hydroxyapatite Scaffolds as Artificial Bone Preform and its Biocompatibility Evaluation," *Asaio Journal*, vol. 60, p. 216, 2014.
- [26] F. Liu, R. Wang, Y. Cheng, X. Jiang, Q. Zhang, and M. Zhu, "Polymer grafted hydroxyapatite whisker as a filler for dental composite resin with enhanced physical and mechanical properties," *Materials Science and Engineering: C*, vol. 33, pp. 4994-5000, 2013.
- [27] J. O. Akindoyo, M. D. H. Beg, S. Ghazali, and M. R. Islam, "Effects of poly (dimethyl siloxane) on the water absorption and natural degradation of poly (lactic acid)/oil-palm empty-fruit-bunch fiber biocomposites," *Journal of Applied Polymer Science*, vol. 132, 2015.
- [28] K. Haberko, M. M. Bućko, J. Brzezińska-Miecznik, M. Haberko, W. Mozgawa, T. Panz, *et al.*, "Natural hydroxyapatite—its behaviour during heat treatment," *Journal of the European Ceramic Society*, vol. 26, pp. 537-542, 2006.
- [29] G. Fielding and S. Bose, "SiO₂ and ZnO dopants in three-dimensionally printed tricalcium phosphate bone tissue engineering scaffolds enhance osteogenesis and angiogenesis in vivo," *Acta biomaterialia*, vol. 9, pp. 9137-9148, 2013.

Teachers' Gender-Counts a Lot: Impact of Teachers' Gender on Students' Score Achievement at Primary Level

Aqleem Fatimah

Abstract—The purpose of study was to find out the impact of teachers' gender on students' score achievement. Focusing on primary level's teachers & students, a survey research was conducted by using convenient sampling technique. All the students of grade four (1500) and fifty-six teachers (equally divided by gender) from the 50 randomly selected coeducational schools from Lahore were taken as sample. The academic performance was operationalized using a t-test on standardized achievement tests of the students in language, science mathematics and social studies. In addition, all those gender based characteristics of teachers that count a lot in classroom interactions (taking Multi-grade classes, classroom strategies, feedback strategies and evaluation method) that influence students' achievement were also analyzed by using a questionnaire and an observation schedule. The results of the study showed better academic achievement of students (girl & boy) of female teachers comparatively to the students of male teachers. Therefore, as the female teachers' number lacks in Pakistan, the study suggests policy makers to seek guidelines to induct more specialized and professionally competent female teachers because their induction will prove highly beneficial for the betterment of students' score achievement.

Keywords—gender, teacher, competency, score achievement

Corresponding Author

Aqleem Fatimah from Allama Iqbal Open University, Pakistan
e-mail: aqleemkazmi@aiou.edu.pk

The Crack Propagation on Glass in Laser Thermal Cleavage

Jehmning Lin

Abstract—In the laser cleavage of glass, the laser is mostly adopted as a heat source to generate a thermal stress state on the substrates. The crack propagation of the soda-lime glass in the laser thermal cleavage with the straight-turning paths was investigated in this study experimentally and numerically. The crack propagation was visualized by a high speed camera with the off-line examination on the micro-crack propagation. The temperature and stress distributions induced by the laser heat source were calculated by ANSYS software based on the finite element method (FEM). With the cutting paths in various turning directions, the experimental and numerical results were in comparison and verified. The fracture modes due to the normal and shear stresses were verified at the turning point of the laser cleavage path. It shows a significant variation of the stress profiles along the straight-turning paths and causes a change on the fracture modes.

Keywords—Laser cleavage, glass, fracture, stress analysis.

I. INTRODUCTION

SINCE the laser machining has the flexibility for the rapid change of the product design and manufacturing, it is suitable for the process automation in the modern industry. In comparison with the conventional technologies, laser machining is one of the popular applications of the laser materials processing [1]. According to the extraordinary cutting performance of the brittle materials by the laser beam in the laser cleaving process [2], many attempts have been made for the fracture control on brittle materials such as ceramics and glasses by the laser cutting [3]-[7]. Accordingly, the moving path of the beam spot is a key issue to dominate the heat diffusion, temperature and stress distributions on the cleaving area. Very few studies have been made to investigate the effect of the stress profiles on the crack propagation at the turning point in laser cleavage, and however the micro-cracks of the glass substrate were frequently obtained in laser cutting [8]. Since an urgent need of the precise and clean cut for complex shapes and various dimensions of the glass substrates, it is important to control the thermal stress profiles along the moving path on the substrate, especially at the turning paths. Many above characteristics of the laser processing on glass have not been fully investigated yet, and it is possible to improve the processing quality and product yield based on the study on the crack propagation with complex moving paths of the laser beam. The laser thermal cleavage of the glass at straight-turning cutting paths was investigated in this study, and the modes of the crack generation were visualized by the high

speed photography method. The relationships between the cutting path and crack growth will be discussed and compared with the thermal stress fields based on the numerical simulation by FEM.

II. LASER CLEAVAGE EXPERIMENTS

In the laser cleavage of the glass, the experimental arrangement is illustrated in the Fig. 1. A cwTEM₀₀ Nd-YAG laser with a wavelength of 1064 nm and power of 2.5 W was focused through a convex lens to irradiate on a soda-lime glass at a beam spot radius of 0.15 mm. The glass substrate was coated with a carbon film on the upper surface to increase the laser absorption to 79% which has been measured by a laser power meter. A high speed camera with an exposure time of 2 ms and filming speed of 10⁴ frame /sec was used to capture the crack propagation on the glass substrate. On an x-y table with stepping motor controller, the laser cutting process could be achieved at various cutting directions at a constant speed of 5 mm/s.

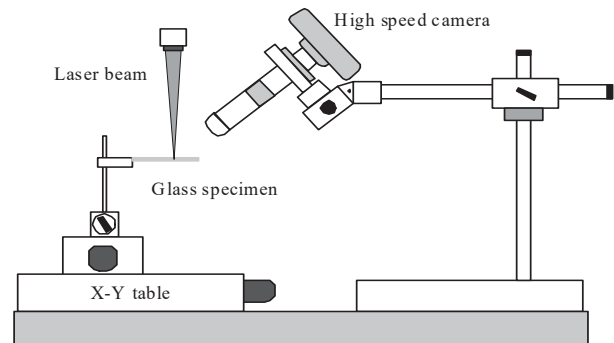


Fig. 1 Experiment set-up

The soda-lime glass specimen with the dimensions of 76 mm x 25 mm x 1 mm was used in the experiment. The physical properties of soda-lime glass were adopted as follows: thermal expansion coefficient of 9.2×10^{-6} m/m°C, density of 2500 kg/m³, average bending fracture strength of 49 MPa [9]. Since the laser beam of 1064 nm wavelength to the soda-lime glass is considered as a high transmittance and approximate 8% will be absorbed [10], therefore the heat affected zone is mainly on the glass surface coated with the carbon film. The path of the laser beam on the specimen could be easily observed due to the carbon film ablated by laser at various cutting paths.

The straight-turning cutting path is illustrated in Fig. 2, where the cutting is from the edge of the glass substrate and turn to an angle of θ^* at point O₂ and the distance between

Jehmning Lin is with the Department of Mechanical Engineering, National Cheng Kung University, Tainan, Taiwan 70101 (phone: 886-6-276-2636; fax: 886-6-235-2973; e-mail: linjem@mail.ncku.edu.tw).

O_1 and O_2 is 5.0 mm. The turning angles θ^* were selected as 30° , 45° , 60° , and 90° in the present study.

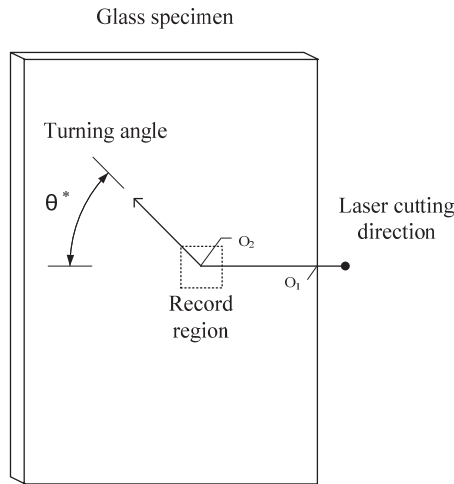


Fig. 2 Illustration of the straight-turning cutting path

Fig. 3 shows the high speed photographs for the laser cutting with various turning angles. It can be found that the thermal cracks do not align with the laser beam near the turning point O_2 , and the crack is slightly behind the laser beam at the turning point. Similar results have been observed off-line in references [4]. There is clear evidence of the micro-cracks crossing the turning points at large angles such as 60° and 90° as shown in Figs. 3 (c) and (d). It can be found that the growth of the straight crack is at a speed close to the laser beam and slightly behind the laser beam. There is a significant deviation of the straight crack to the laser beam path at the turning point, where the micro-cracks abruptly occurred in the cooling stage after the laser passing the turning point.

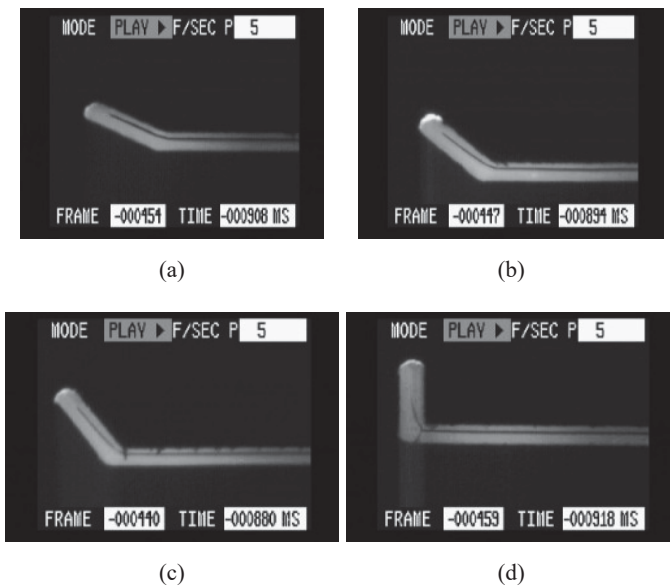


Fig. 3 Photographs from the high speed camera at various turning angles θ^* ; (a) 30° , (b) 45° , (c) 60° , (d) 90°

III. THERMAL STRESS ANALYSIS

The laser beam was applied to the glass cutting as a heat source. The heat was diffused into the glass from laser spot and dissipated into the surroundings. Thus, the stress state was generated on the substrate surface to initiate the cracks, and the crack progressively followed with the laser beam [11]. Since the laser cleaving process includes the temperature distribution, stress field and property variation, all of which are significantly inter-related. In order to simplify the analysis, the problem of the laser cleaving on glass sheets herein will be decoupled by two distinct analytical models: the thermal model and the mechanical model in the thermal-elastic numerical analysis. Using the software ANSYS [12], the element Solid 278 was adopted in the thermal analysis. The domain meshes used for the stress analysis are the same, but the element type was replaced by Solid 185 to calculate the stress and displacement. The temperature dependent properties such as the thermal conductivity, specific heat, Poisson's ratio and Young's modulus of soda-lime glass have been considered in the simulation, and the relationships at various temperatures can be found in the reference [10].

The physical domain of the soda-lime glass specimen is selected with the dimensions of 12 mm x 6 mm x 1 mm in the simulation and illustrated in Fig. 4. Due to the asymmetric cutting path, a fine meshing as illustrated in Fig. 4 (b) around the laser beam was applied to simulate the steep temperature gradients around the heating zone and the number of the meshed elements is 39600. In order to compare the numerical results for various cutting paths, the coordinate system (x_1, y_1, z_1) is for the straight cutting from the point O_1 at the edge of the substrate to the turning point O_2 and the coordinate system (x_1', y_1', z_1') is the cutting path with a turning angle θ^* to the point O_2 as illustrated in Fig. 4 (a). Accordingly, the following assumptions are selected in the numerical simulation:

- 1) The glass properties are homogenous, isotropic and temperature dependent.
- 2) The laser intensity distribution is Gaussian mode.
- 3) The thermal boundaries with free convection in the surrounding air are considered.
- 4) There is no phase change during laser heating.
- 5) The specimen is annealed before laser cleaving, and its initial condition is free of stress.
- 6) The stress-strain relationship of the glass substrate is perfectly elastic.
- 7) Body force has been ignored

There are numerous factors that affect the boundary conditions. The initial temperature of the specimen is assumed to be the ambient temperature of 25°C . The heat convection has been considered from the surface of the glass substrate and the coefficient of the heat convection is quoted as $21 \text{ W/m}^2\text{C}$ [13] on the surfaces including the lower surface of the substrate. The substrate was clamped except for the cutting edge, which was assumed to be free of stress in the analysis. A circular Nd-YAG laser beam with the Gaussian mode intensity is selected and expressed in;

$$I_p(x, y) = \frac{(1-R) \times P}{\pi r_0^2} \times \exp\left[\frac{-2 \times (x^2 + y^2)}{r_0^2}\right] \quad (1)$$

where, I_p is the laser intensity (W/m^2), R is the reflectivity, P is the laser power (W), r_0 is the radius of the laser beam spot (m).

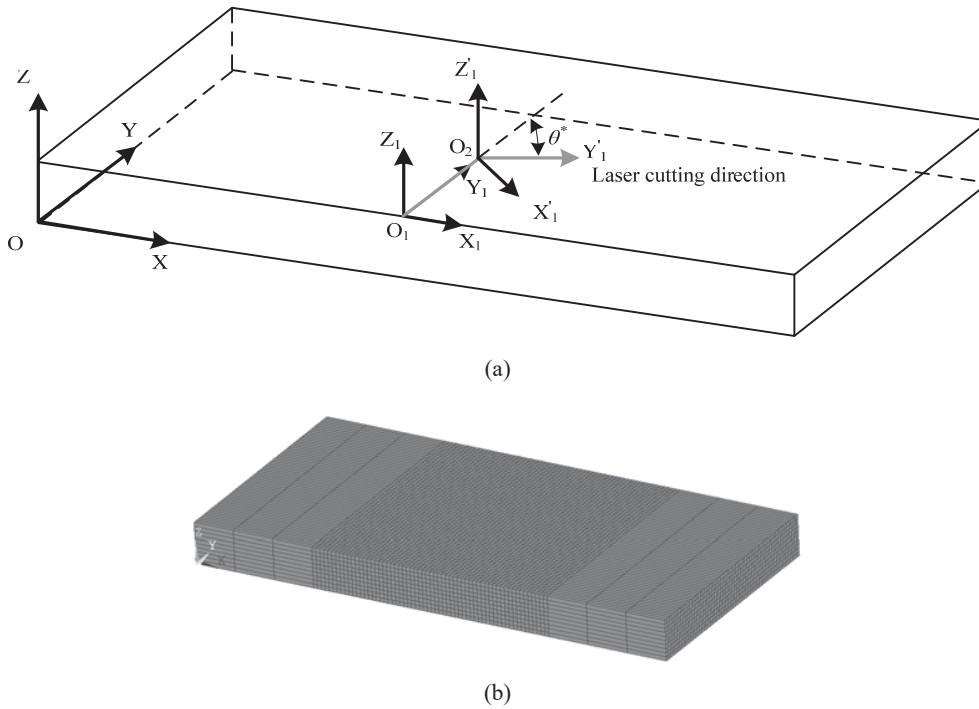
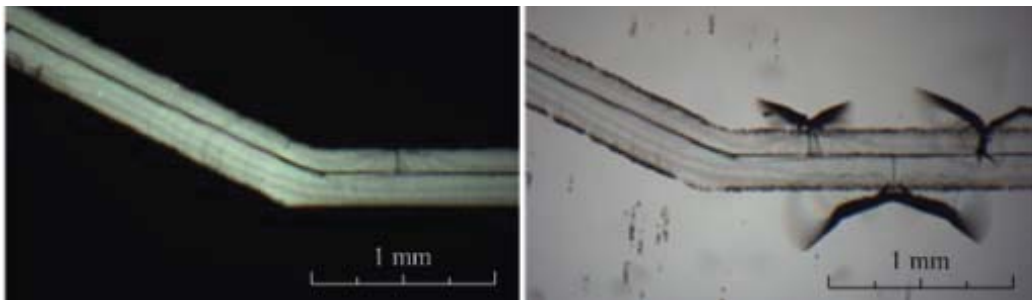


Fig. 4 Physical domain in the numerical simulation; (a) coordinate systems, and (b) meshed grids

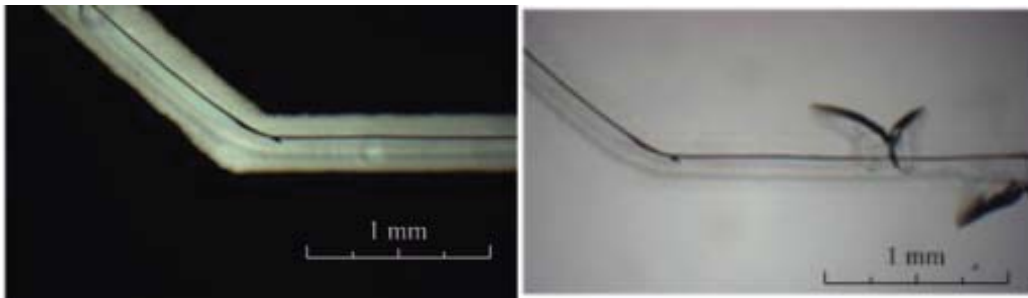
IV. RESULTS AND DISCUSSIONS

According to the experimental results as shown in Fig. 5, a mix mode consisted of the opening and in-plane shear fractures on the side cracking has been considered [4]. Fig. 5 shows that the thermal cracks generate slightly different patterns at various turning angles, but the trends are in a good agreement. There is a round curve near the turning point, and the average radius of the cracking curve is increased with the turning angle. The side crack occurs near the turning point and it is significantly affected by the turning angle of the laser beam. The

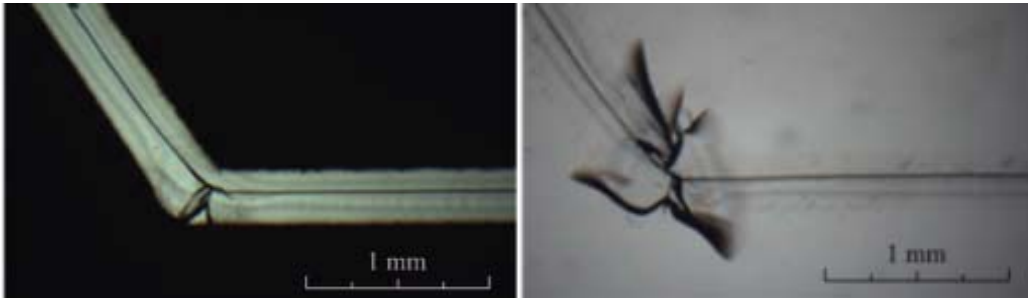
micro-crack will accumulate at the turning point at large angles. The micro-crack might extend backwards to the cutting direction beyond the turning point with an angle larger than 45° in the present study. In the cases of the turning angles of 60° and 90° , it can be found that the crack is irregular and do not follow the cutting path as shown in Figs. 5 (c) and (d). There is no over-cut along the initial direction of the straight-line cutting, the lag between the laser beam and crack is similar to the straight-line cutting after the turning point.



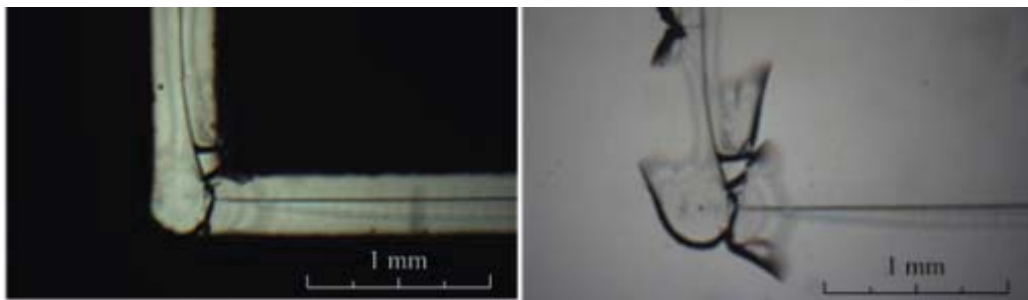
(a)



(b)

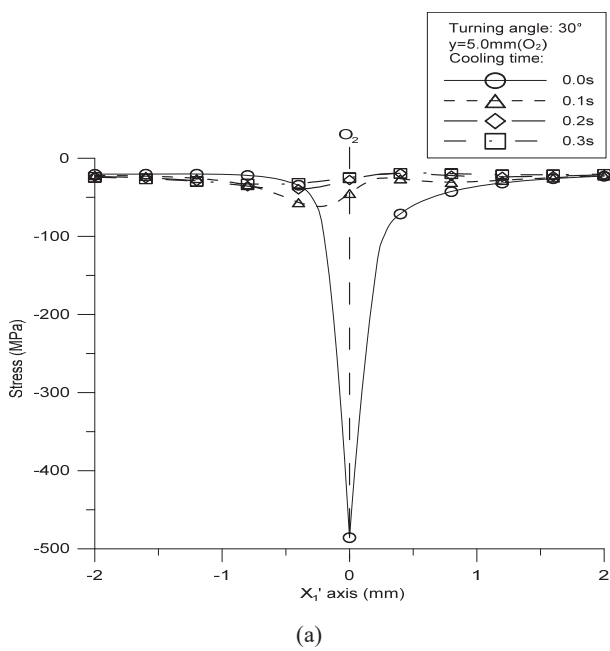


(c)

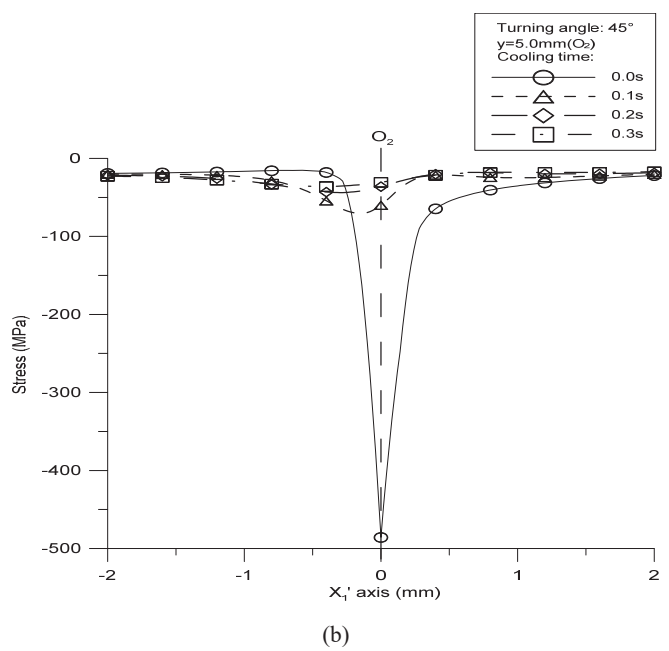


(d)

Fig. 5 Photographs of the cutting paths and side cracks at various turning angles θ^* ; (a) 30° , (b) 45° , (c) 60° , (d) 90°



(a)



(b)

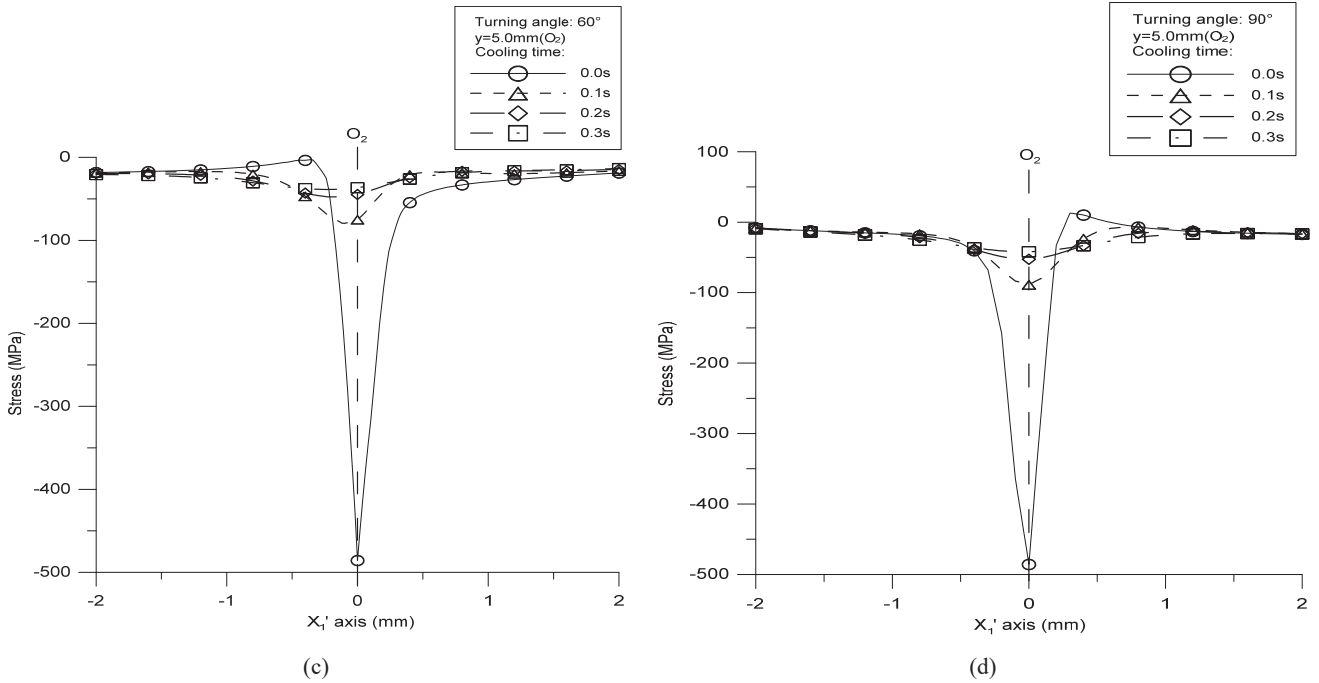
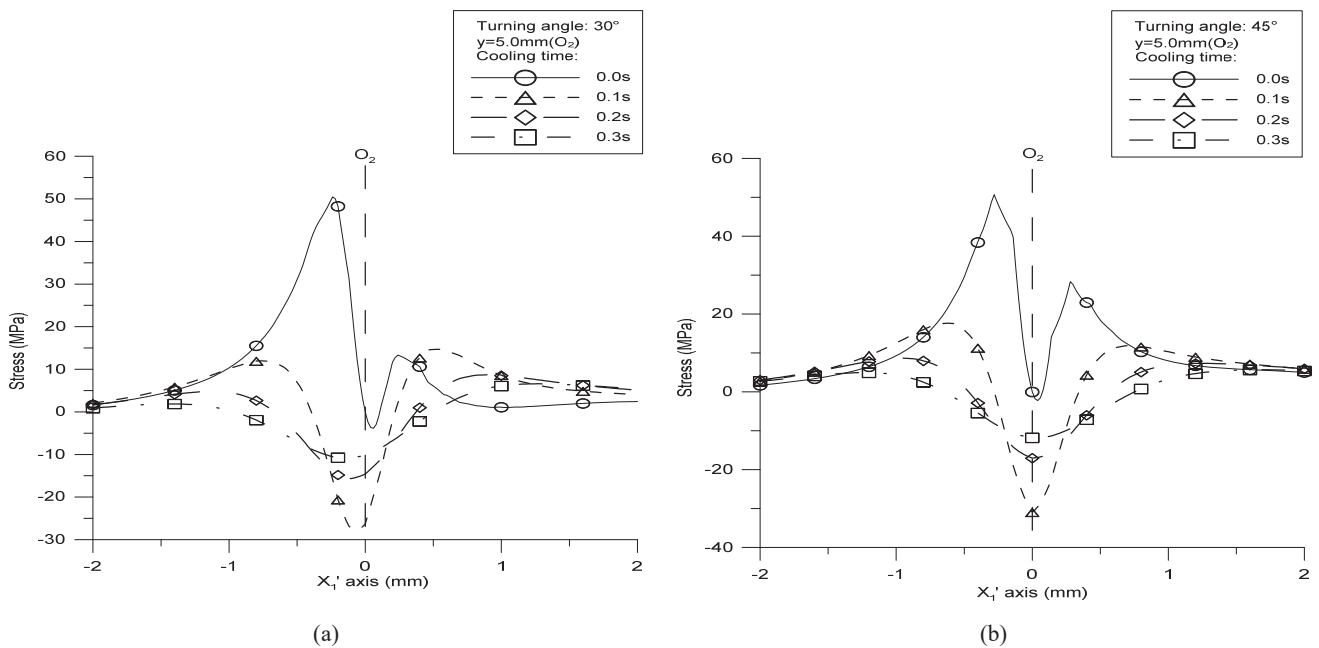


Fig. 6 Distributions of the normal stress σ_{xx} at various turning angles and cooling times

In the cutting with various turning angles, the stress states are shown in Figs. 6 and 7 at the turning point O_2 . There is a tremendous change of the shear stress near the turning point as the laser beam passing in the cooling stage. However, the normal stresses σ_{xx} is almost in the compressive state at the turning point O_2 . Fig. 7 shows a tremendous shift on the shear stress profiles at the turning point in the numerical simulation. Accordingly, the stress contours of the crack formation indicate

that the shear stress σ_{xy} with a corresponding compressive normal stress σ_{xx} dominates the fracture mode as the laser beam passing the turning point O_2 . The side crack could be formed at a large turning angle and cause a failure in the laser cleaving on a glass substrate. Therefore, it is possible to avoid a sharp turning angle and achieve a curvature of the crack in a sequence of cut to prevent the increase of the shear stress.



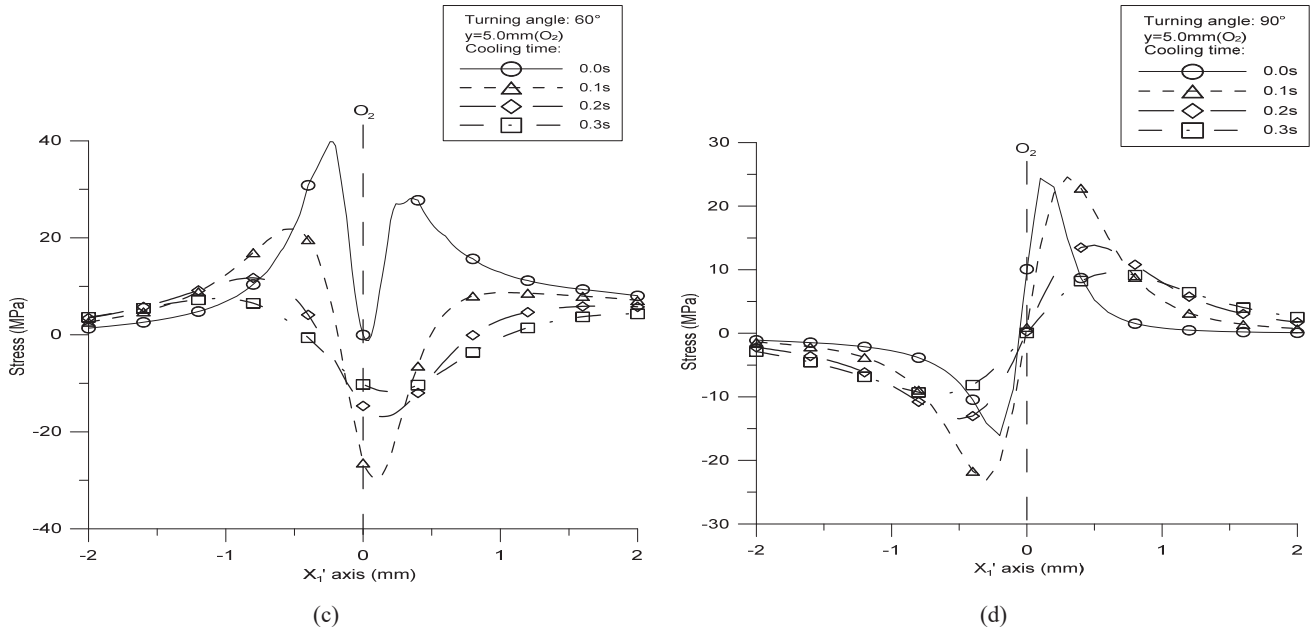


Fig. 7 Distributions of the shear stress σ_{xy} at various turning angles and cooling times

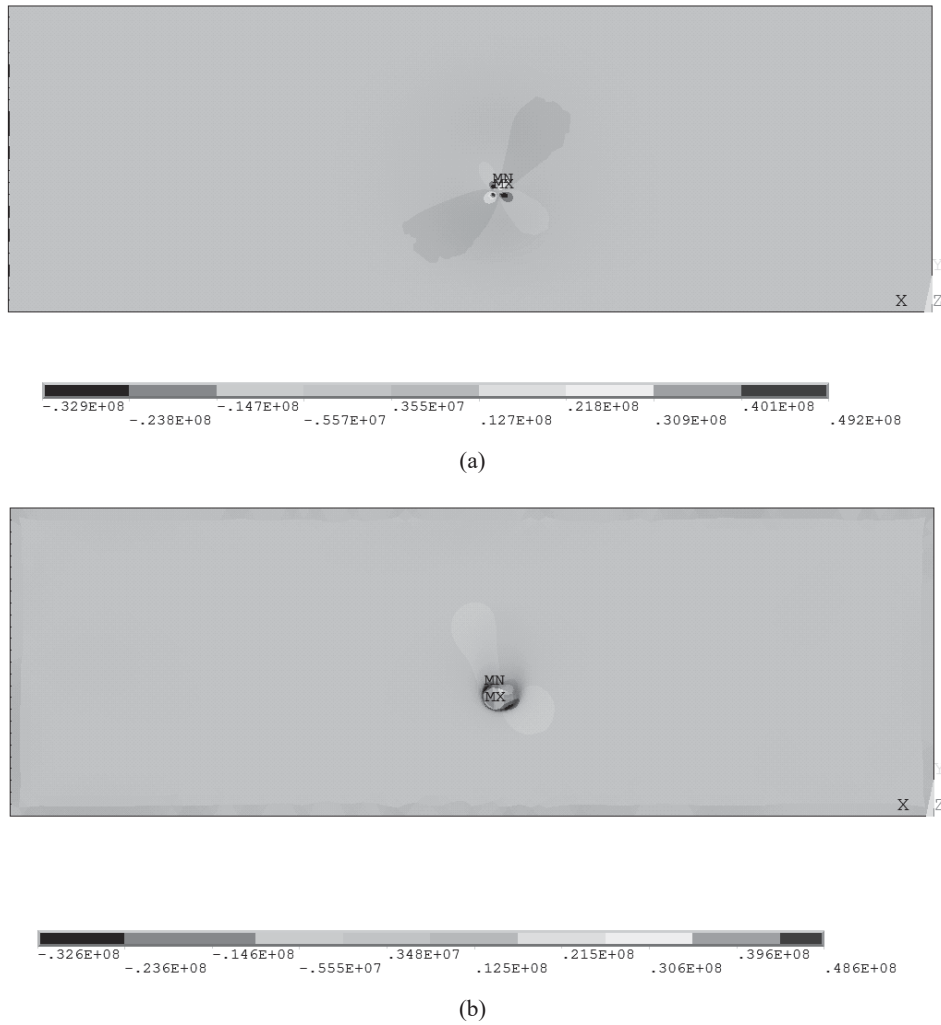


Fig. 8 Shear stress distribution of the laser beam; (a) at the turning point O₂; (b) after the turning point for 0.1 s at $\theta^* = 60^\circ$

Since the shear stress distributions are mainly caused by the geometrical constrains and cutting path around the laser heating zone, Fig. 8 shows the typical profiles of the shear stress σ_{xy} near the turning point O_2 at the turning angles of 60° and 90° , the distorted cracks might form due to the uneven distribution of shear stress at the turning point. Therefore, the crossing crack may randomly appear after the laser passing the turning point O_2 .

[13] FP Incropera, DP. de Witt, Fundamentals of heat and mass transfer. 4th ed. New York: Wiley; 1996.

V. CONCLUSIONS

Under the inspection with high speed photography, the cutting results show that the crack propagation varies with the turning angles. In the laser cleavage of glass, the crack growth does not completely follow the laser beam path; on the cleavage path with various turning angles, the crack will generate a mix fracture mode at the turning point. The stress state may transform to shear stress state and the fracture mode is from opening to in-plane shear mode at a large turning angle. Therefore, the micro-cracks may occur and affect the cutting quality mainly at the turning point in the laser cleavage of glass. A comparison between the numerical and experimental results shows that the control of the crack formation mainly depends on the stress states. The stress distribution would be affected by the turning angles. Therefore, when cutting glasses by laser, there are many parameters that may affect the cutting quality, and the prediction of the stress distribution would be an acceptable method to evaluate the cutting quality and improve the cutting performance.

REFERENCES

- [1] WM. Steen, Laser material processing. Berlin: Springer; 1998.
- [2] RM. Lumley, Controlled separation of brittle materials using a laser. American Ceramic Society Bulletin 1969;48(9):850-4.
- [3] CH. Tsai, CJ. Chen, Application of iterative path revision technique for laser cutting with controlled fracture. Optics and Lasers in Engineering 2004;41:189-204.
- [4] Y. Miyashita, M. Mogi, H. Hasegawa, S. Sujatanod, Y. Mutoh, Study on a Controlling Method for Crack Nucleation and Propagation Behavior in Laser Cutting of Glass. Journal of Solid Mechanics and Materials Engineering 2008;2(12).
- [5] N. Cai, LJ. Yang, Y. Wang, ZG. Tian, Experimental Research of YAG Laser Cutting Soda-lime Glass Sheets with Controlled Fracture. Key Engineering Materials 2010;431-432:507-510.
- [6] S. Nisar, L. Li, MA. Sheikh, AJ. Pinkerton, The effect of continuous and pulsed beam modes on cut path deviation in diode laser cutting of glass. International Journal of Advanced Manufacturing Technology 2010;49(1-4):167-175.
- [7] S. Nisar, L. Li, MA. Sheikh, AJ. Pinkerton, S. Safdar, The effect of laser beam geometry on cut path deviation in diode laser chip-free cutting of glass. Journal of Manufacturing Science and Engineering. Transactions of the ASME 2010; 132(1):0110021-0110029.
- [8] YZ. Wang, JM. Lin, Characterization of the laser cleaving on glass sheets with a line-shape laser beam. Optics and Laser Technology 2007;39:892-899.
- [9] K. Yamamoto, N. Hasaka, H. Morita, E. Ohmura, Three-dimensional thermal stress analysis on laser scribing of glass. Precision Engineering 2008;32:301-308.
- [10] NP. Bansal, RH. Doremus, Handbook of glass properties. Orlando: Academic Press, Inc.; 1986.
- [11] CH. Tsai, CS. Liou, Fracture mechanism of laser cutting with controlled fracture. Journal of Manufacturing Science and Engineering. Transactions of the ASME 2003;125:519-28.
- [12] ANSYS Mechanical APDL Introductory Tutorials. Canonsburg: ANSYS, Inc.; 2012.

The Effects of Weather Events and Land Use Change on Urban Ecosystems: From Risk to Resilience

Szu-Hua Wang

Abstract—Urban ecosystems, as complex coupled human-environment systems, contain abundant natural resources for breeding natural assets and, at the same time, attract urban assets and consume natural resources, triggered by urban development. Land use change illustrates the interaction between human activities and environments factually. However, IPCC (2014) announces that land use change and urbanization due to human activities are the major cause of climate change, leading to serious impacts on urban ecosystem resilience and risk. For this reason, risk assessment and resilience analysis are the keys for responding to climate change on urban ecosystems. Urban spatial planning can guide urban development by land use planning, transportation planning, and environmental planning and affect land use allocation and human activities by building major constructions and protecting important national land resources simultaneously. Urban spatial planning can aggravate climate change and, on the other hand, mitigate and adapt climate change. Research on effects of spatial planning on land use change and climate change is one of intense issues currently. Therefore, this research focuses on developing frameworks for risk assessment and resilience analysis from the aspect of ecosystem based on typhoon precipitation in Taipei area. The integrated method of risk assessment and resilience analysis will be also addressed for applying spatial planning practice and sustainable development.

Keywords—ecosystem, land use change, risk analysis, resilience

Corresponding Author

Szu-Hua Wang from Chinese Culture University, Taiwan
e-mail: szuhuawang@gmail.com

The Efficacy of Emotional Intelligence Training on Anxiety and Quality of Life in Patients with Irritable Bowel Syndrome

Dr. Seyed Ali All Yasin, Dr Hasan Heydari, Banafshe Esmail pour

PhD in Psychology and member of the faculty Islamic Azad University of Khomein

PhD in Psychology and member of the faculty Islamic Azad University of Khomein

Master of Clinical Psychology. Islamic Azad University of Khomein

Abstract

This study aimed to determine the effectiveness of emotional intelligence training on anxiety and quality of life in patients with irritable bowel syndrome. Semi-experimental study design study with pre-test, post-test with control group .The study population was included all patients with irritable bowel syndrome referred to a gastroenterologist and centers and clinics in Tehran in 2016. In order to ensure the diagnosis, the diagnosis of this syndrome all clients by researcher And based on the diagnostic criteria for diagnosis of irritable bowel syndrome were interviewed and then once Ayt willingness to participate in training sessions randomly assigned 18 patients in the experimental group and 18 patients in the control groups. Methods way that, after a pre-test in the experimental group, the experimental group was given emotional intelligence training And the control group were given training to them. Then, after the test was taken from both groups. Tools used in research, the World Health Organization Quality of Life Questionnaire (1989) and Beck Anxiety Inventory, and to analyze the data was used univariate and multivariate analysis of covariance. Finally, the findings show that emotional intelligence training reduces anxiety and its components and also improve the quality of life in patients with irritable bowel syndrome is.

Keywords: education, emotional intelligence, anxiety, quality of life, irritable bowel syndrome

The Methods of Immobilization of Laccase for Direct Transfer in an Enzymatic Fuel Cell

Hoda Khodadadi^a, Ashin Farahbakhsh^{a*}

Department of Chemical Engineering, Quchan Branch, Islamic Azad University, Quchan Iran
Email: afshin.farahbakhsh@gmail.com

ABSTRACT

In this paper we compare five methods of biological fuel cell fabrication by combining a *Shewanella oneidensis* microbial anode and a laccase-modified air-breathing cathode. As a result of bio fuel cell laccase with graphite nanofibers, carbon surface (PAMAN, on the Pt/hpg electrode, graphite sheets MWCNT and with (PG) and (MWCNT) showed, respectively. Describes methods for creating controllable and reproducible bio-anodes and demonstrates the versatility of hybrid biological fuel cells. The laccase-based biocathodes prepared either with the crude extract or with the purified enzyme are able to provide electrochemically active and stable biomaterials. The laccase-based biocathodes prepared either with the crude extract or with the purified enzyme are able to provide electrochemically active and stable biomaterials. When the device was fed with transdermal extracts, containing only 30 μM of glucose, the average peak power was proportionally lower (0.004 mW). The result of bio fuel cell with with graphite nanofibers showed the enzymatic fuel cell reaches 0.5 V at open circuit voltage with both, Ethanol and Methanol and the maximum current density observed for E2 electrode was 228.94 mA/cm².

Keywords:

Enzymatic electrode, Fuel Cell, Immobilization, Laccase

Introduction

According to research by (H. du Toit et al.) in electronic technologies and nanotechnology open up exciting prospects in the field of wearable healthcare devices for a wide range of applications, including non-invasive detection of biomarkers [3]. Enzymatic Bio Fuel Cell (EBFC) utilizes organic molecules as fuel to generate electricity with high efficiency. It employs enzymes to catalyze redox reactions. Replacing traditional noble metal based catalysts with biocatalysts has several advantages; such as comparatively low cost, operation under mild conditions (room temperature and neutral pH) and no emission of greenhouse gases. Being a biological catalyst, enzymes have high specificity and selectivity to the catalysing reaction. These properties

of enzymes allow anodic and cathodic redox reactions to take place in the same chamber and remove the requirement of an ion exchange membrane [2].

Electricity production from renewable and environmentally friendly techniques, and the development of devices capable of meeting the needs of wireless sensors and remote monitoring, has motivated the development of different technologies to use the energy stored in organic compounds such as glucose. In recent decades, enzymatic fuel cells have generated increasing interest because they are devices that have different potential applications such as communications, bioelectronics and medical purposes. In these cells instead of metallic catalysts, enzymatic fuel cells use enzymes as biocatalysts to carry out the oxidation of the substrate at the anode, releasing electrons that travel through an electrical circuit to reach

the cathode. The protons produced by the oxidation of the substrates are combined with an oxidant (commonly oxygen) to form a product (commonly water)[1]. The active site of enzymes are buried in deep pockets that hinder significant electron transfer to the conductive support, primarily because of the electrical insulation of the bio-catalytic site by the surrounding protein shells. To facilitate electron transfer between enzyme and electrode [2].

Laccase is the preferred cathodic enzyme for electro catalytic oxygen reduction reaction because of high open circuit potential (OCP) in comparison to Bilirubin Oxidase and Tyrosinase [2]. The laccases are able to oxidize a wide range of substrates, such aromatic amines and phenols, among others ,they are considered robust and environmentally friendly catalysts for many technological purposes [5]. According research by (H.duToit) the majority of the EFCs implement external electron mediators, either in solution or co-immobilized with the enzyme onto the electrode surface, to improve the electron transfer to the anode. The use of these mediators, however, limits practical ap- plications of EFCs [3].

In this paper we compare the immobilization methods of laccase with graphite sheets MWCNT, pencil graphite (PG) and multi walled carbon nanotubes (MWCNT), graphite nanofibers,Carbon surface (PAMAN) and Pt/Hpg electrode.

Bio fuel cell laccase with graphite sheets MWCNT

The enzymes were immobilized in an oriented fashion on graphite sheets. Before Ax immobilization, the graphite heets electrodes (1cm²) were successively cleaned with dichloride-methane, tetrahydrofuran and water, anddried. Then, then clean graphite electrodes were carboxylated under nitric acid reflux for 2 hat 80 °C. On the other hand,C- WCNT were functionalized with4-azi- doaniline creating anamide bond between the amino group of the 4-azidoaniline and the carboxylic group of C-MWCNT.The functionalization was performed dissolving 5mg of C-MWCNT,5mg of 4-azidoaniline and 5mg of EDC indimethylsulfoxide, and the reaction was kept during 4h.The functionalized nanotubes(ANA MWCNT) were washed three times with 13 ml of phosphatebuffer and centrifugedat 9000 rpmduring 10min.Then,thenzymewas immobilized ontheANA-MWCNTasfollows:Analiquot of 15 ml of AOx was homogenized with 60 ml ofANA-MWCNT,previously sonicated, and incubated during 12h to ensure the formation of the AOx-ANA complex. Once the in cubation was completed,15 ml of Nafion (5%/w/w) were added and homogenized. Twenty-two microliters of the suspension were applied on the graphite electrode and dried under darkness.Theoriented

enzymaticelec- trodes (AOx-ANA-MWCNT)were then washed and storedin phosphate buffer 100mM at pH7.5.The same procedure was performed for control e lectrodes without the addition of 4-azidoa- nile totheC-MWCNT. The oriented laccase electrodes were fabricated also by the “substrate-likelinker” approach with4-(2-aminoethyl) benzoic acid (AEBA)and according to the protocol previously published. The enzymatic fuel cell reaches 0.5V at open circuit voltage with both ,ethanol and methanol, while in short circuit the highest current intensity of250 μ A cm⁻² was obtained with methanol [1].

Bio fuel cell laccase with pencil graphite (PG) and multi walled carbon nanotubes (MWCNT)

Fabrication of E2 electrode (PG/MWCNT/Lac) the PG leads were cleaned and dried in the same way as discussed earlier for the fabrication of electrode E1. The MWCNT (1 mg/ml) was dispersed in DMSO by ultrasonication. The dried PG leads were dipped into MWCNT dispersion and dried in hot air oven at 90 °C. This process was repeated four times to physically adsorb sufficient amount of MWCNT of PG leads. TheMWCNTcoated PG leads were dipped into EDC/NHS (1 mg/ml) solution for 2 h to activate carboxyl groups. The biocathode was fabricated by dipping MWCNT coated PG leads into enzyme solution (3 mg/ml Laccase in 0.1 M phosphate buffer, pH 5.0) and kept at room temperature for 24 h. Finally, the E2 electrodes (PG/MWCNT/Lac) were washed with phosphate buffer (0.1 M) to remove unbound enzymes. When not in use, the electrodes were stored in phosphate buffer at 4°C. The maximum current density observed E2 electrode was 228.94 mAcm⁻² [2].

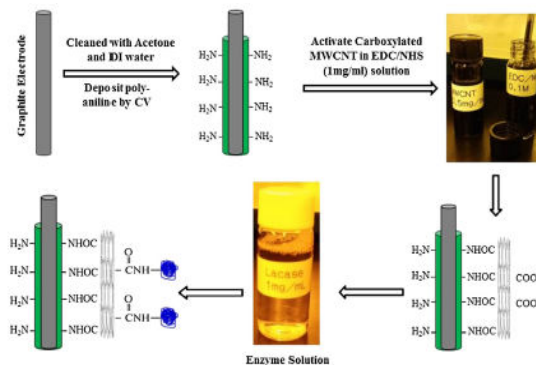


Fig. 1 e Schematic representation of process to fabricate E1 electrode with laccase (PG/PA/MWCNT/Lac) by electro polymerization of polyaniline on pencil graphite leads on which MWCNTs were coated.

Bio fuel cell laccase with graphite nanofibers

S. oneidensis DSP-10 was cultured aerobically in Difco Luria broth containing rifampicin (5 μ g mL⁻¹) at 30 °C, with shaking (120 rpm). Cells were harvested at late stationary phase (OD₆₀₀~ 4) by centrifugation,

Washed (3×) and resuspended in 1X phosphate buffered saline (PBS) to a defined cell density (OD600 = 5; equivalent to $\sim 1 \times 10^9$ cfu/mL). The cell suspension was immobilized to the electrode by CVD of silicon using methodology described previously. Electrodes prepared in this manner are defined Si-biofilm-LB. For natural biofilm formation, electrodes were incubated in growing cultures and recovered from solution at a time equivalent to the late stationary phase of growth (biofilm-LB). *S. oncidensis* DSP-10 was similarly cultured in a defined medium (DM) previously described, containing rifampicin ($5 \mu\text{g mL}^{-1}$) at 30 °C, with shaking (120 rpm) and modified to contain sodium fumarate (30 mM) as a terminal electron acceptor. The culture was incubated in a capped shaker flask to simulate micro-aerobic metabolism; as oxygen is consumed, fumarate acts as an alternative electron acceptor. The resulting culture was harvested at late stationary phase (OD600 \sim 0.3) by centrifugation, washed (3×) and resuspended in PBS. The washed cell suspension was encapsulated onto the electrode as described above and defined Si-biofilm-DM. For natural biofilm formation, electrodes were incubated in growing cultures and recovered from solution at a time equivalent to the late stationary phase of growth (biofilm-DM). As a result, this work describes methods for creating controllable and reproducible bio-anodes and demonstrates the versatility of hybrid biological fuel cells [4].

Bio fuel cell laccase with carbon surface (PAMAN)

The oxidation of the synthetic substrate ABTS was assayed continuously, at 25 °C, by monitoring the formation of the ABTS⁺ radical at 420 nm ($\epsilon_{420 \text{ nm}} = 36,000 \text{ L mol}^{-1} \text{ cm}^{-1}$) in 1 cm path length hermostatted quartz cells using an Ultrospec 5300 pro UV/visible spectrophotometer (Amersham Biosciences). Standard conditions were McIlvaine buffer, pH 4.5, containing 1 mmol L^{-1} ABTS in a final volume of 1 mL. The reaction was initiated by the addition to the cuvette of PyS crude extract or the purified enzyme conveniently diluted in buffer, or the immobilized proteins onto the carbon substrate. The absorbance was recorded for 5 min, and the initial rate was calculated by linear regression during the first minutes of reaction. Controls without enzyme were included in each experiment, to quantify the non-enzymatic oxidation of the substrate. When using the crude or purified enzyme in solution, the experimental conditions (reaction times, enzymatic units) employed were adjusted to guarantee the estimation of initial velocities. The kinetic parameters V_{max} (maximum velocity) and $K_{0.5}$ (apparent affinity constant) were calculated by non-linear regression using the SigrafW software. One enzyme unit (U) was defined as the amount of enzyme that produces $1 \mu\text{mol}$ of ABTS⁺ per minute at the standard conditions. Specific activity was defined as U mg protein^{-1} . Data are reported as the mean \pm S.D. of triplicate measurements, which were considered statistically significant at $P \leq 0.05$. It was observed that both biocathodes tested displayed a very similar loss in power performance as a function of time, reaching 60% of the initial activity after 60 days. Overall, on the basis of the data here obtained, the biocathode containing ABTS entrapped in polypyrrole matrix and PAMAM dendrimers for anchoring of the PyS

laccase is attractive for achieving electrochemical active and stable laccase-based biomaterials [5].

Bio fuel cell laccase and GOX on the pt/hpg electrode

GOx and LAC were used as catalysts at the anode and cathode respectively. APBS solution (pH 7.1) containing 15 mg mL^{-1} of GOx was prepared and placed in a three-electrode set-up with the Pt/hPG electrode used as a working electrode and platinum wire (diameter: 1 mm) and SCE used as a counter and a reference electrode respectively. The GOx immobilization was achieved either by performing a CV scan as previously reported or, to further simplify the immobilization protocol, by applying a fixed potential, in the range of 0.425–0.6 V vs SCE, for one hour. The performance of the GOx/hPG electrode at increasing concentration of glucose was tested by chronoamperometry in a three-electrode set-up, with Pt and SCE as a counter and a reference electrode respectively. The same principle was adopted for the immobilization of LAC. A LAC solution of 2.5 mg mL^{-1} in PBS was prepared and, considering the isoelectric point of LAC from *Rhus vernicifera* (6.8 to 7.4), to develop a negative charge on to the hPG electrode surface, a fixed potential of -0.5 V vs SCE in a three-electrode set-up was applied for a total of 1 hour. When the device was fed with transdermal extracts, containing only $30 \mu\text{M}$ of glucose, the average peak power was proportionally lower (0.004 mW) [3].

Conclusion

Concerning the power density, the methanol was the best substrate reaching $60 \mu\text{W cm}^{-2}$, while with ethanol $40 \mu\text{W cm}^{-2}$ was obtained. The results clearly show that the electrodes with orientated enzyme molecules are better for the current and power. The electroanalysis of both biocathodes confirmed electrocatalytic reduction current. The maximum open circuit potential for E2 electrode was 0.60 V vs Ag/AgCl electrode. For bio fuel cell laccase and GOX on the pt/hpg electrode when the device was fed with transdermal extracts, containing only $30 \mu\text{M}$ of glucose, the average peak power was proportionally lower (0.004 mW). In the bio fuel cell laccase with graphite sheets, demonstrates that changes in the enzyme source can improve the final biocathode performance.

acknowledgment

The authors would like to thank Quchan Islamic Zad University.

References

[1] A. a.arrocha Ulises Cano-Castillo, Sergio A.Aguila, Rafael Vazquez-Duhalt , Enzyme orientation for direct electron transfer in an enzymatic fuel cell with alcohol oxidase and lactase electrodes, Biosensors and Bioelectronics 61(2014)569–574

[2] D. Kashyap, Chulmin Kim , Sung Yeol Kim, Young Ho Kim, Guy Man Kim , Rabat K. Dwivedi, Ashutosh Sharma, Snaked Goel , multi walled carbon nanotube and polyaniline coated pencil graphite based bio-cathode for Enzymatic biofuel cell, i n t e r n a t i o n a l journal o f hydrogen energy 4 0 (2 0 1 5) 9 5 1 5 e9 5 2 2

[3] H.duToit,RazleenRashidi a, DominicW.Ferdani b, Maria BegoñaDelgado-Charro c, CarlM.Sangan d, MirellaDiLorenzo a,n, Generating power from transdermal extracts using a multi-electrode miniature enzymatic fuel cell, Biosensors and Bioelectronics 78(2016)411–417

[4] J. N. royal , Heather R. Luckariftb, Susan R. Sizemoreb, Karen E. Farringtonb,c, Carolin Laua, Glenn R. Johnsonc, Plamen Atanassova,* , Microbial-enzymatic-hybrid biological fuel cell with optimized growth conditions for *Shewanella oneidensis* DSP-10, Enzyme and Microbial Technology 53 (2013) 123–127

[5] S. Aquino Net, A.L.R.L. Zimbardi, F.P. Cardoso L.B. Crepaldi, S.D. Minter J.A. Jorge R.P.M Furrier , A.R. De andrade potential application of lactase from *Pycnoporus sanguineus* in methanol/ O₂ biofuel cells, Journal of Electroanalytical Chemistry 765 (2016) 2–7

The Two Sides of Coin of Peer Review and its Effects on Prospective Mathematics Teachers' Insights Regarding Mathematical Proofs

Ilana Lavy, Atara Shriki

Abstract— In this study we examine the effects of engaging prospective mathematics teachers in peer assessment, as assessors and assesses at the same time, on the development of their assessment skills as regards to geometrical proofs. The research took place within a Method course in which peer assessment activities were employed. Sixteen prospective mathematics teachers participated in the research and had to act both as assessors and assessees. Most of the research literature concerning peer assessment of mathematical products refers to the assessor's or the assessee's point of view separately or to self-assessment. However, in this study we examine the effects of engagement in peer assessment as assessor and assessee at the same time on the PMTs' ability to develop assessment skills in the context of geometrical proof. The phases of research were:

1. The PMTs were asked to solve an identical given problem in which they had to construct geometrical proofs and to submit their solutions by e-mail.

2. The PMTs' solutions were scanned and sent through the course forum mail for evaluation. Each PMT received two anonymous solutions for evaluation and scoring. The PMTs were asked to formulate a list of evaluation criteria, to assign each criterion a numerical weight, and to provide justification for each criterion and weight. In addition, the PMTs had to specifically score the work according to each criterion and explain the underlying reasons for each score. These evaluations were e-mailed to us.

3. Each PMT was e-mailed the two anonymous evaluations and scoring of his or her work and was asked to reflect on them.

4. Using the "What If Not?" (WIN) strategy and based on the initial problem, the PMTs had to start an inquiry process. In this phase, the PMTs were asked to produce a list of the initial problem's attributes, suggest alternatives for each of them, and choose one alternative or a combination thereof for further mathematical investigation. Again, the PMTs e-mailed us their tasks.

5-6. Phases 2 and 3 were repeated, based on the output of work produced in Phase 4.

7. The chosen new problem was solved, including a full written description of the conjectures, solutions, indecisions, and so on.

8-9. In order to enable the PMTs to experience a peer assessment process for unfamiliar problems, Phases 2 and 3 were repeated, based on the output of work produced in Phase 7.

10. Each PMT wrote a summative evaluation and final reflection on the entire process.

Analysis of the research data reveals that during the various phases of the study the prospective teachers developed skills concerning the selection of categories and weights for the assessment of their peers' work. In the criteria set they selected for the peer assessment, they referred to meanings and roles of mathematical proof. In their

reflections, the prospective mathematics teachers also referred to the effects of the peer assessment on their mathematical knowledge, asserting that by being exposed to different solution strategies and new problems they were able to widen their mathematical knowledge.

Keywords— Professional development, peer assessment, geometrical proof, prospective teachers, "what-if-not?" strategy

Ilana Lavy Author is with the Academic College of Yezreel Valley, ISRAEL. (Phone: 972-4-6423519; fax: 972-4-6423517; e-mail: ilanal@yvc.ac.il).

Atara Shriki is with Oranim- Academic College of Education, ISRAEL (e-mail: atrashriki@gmail.com)..

Usage of Internet Technology in Financial Education and Financial Inclusion by Students of Economics Universities

B. Fraćzek

I. INTRODUCTION

Abstract—The paper analyses the usage of the Internet by university students in Visegrad Countries (4V Countries) who study economic fields in their formal and informal financial education and captures the areas of untapped potential of Internet in educational processes. Higher education and training, technological readiness, and the financial market development are in the group of pillars, that are key for efficiency driven economies. These three pillars have become an inspiration to the research on using the Internet in the financial education among economic university students as the group of the best educated people in finance. The financial education is a process that allows for improving the level of financial literacy. In turn, the financial literacy it is the set of financial knowledge, skills, awareness and patterns influencing the financial decisions.. The level of financial literacy influences the level of financial well-being of individuals, determines the scale of saving of households and at the same time gives the greater chance for sustainable and more predictable development of the financial market with the positive impact on economy. The financial literacy is necessary for each group of society but its appropriate level is desirable especially in respect of economics students as future participants of financial markets as well as the experts and advisors in financial decision making. The low level of financial literacy is the great problem of many target groups in both developing and developed countries and the financial education is seen as the best way of improving this situation. Also the financial inclusion plays the special role in enhancing the level of financial literacy in the aspect of education by practice as well as due to interrelation between level of financial literacy and degree of financial inclusion. Despite many initiatives under financial education, the level of financial literacy is still very low. Scientists still search for new ways of solving this problem. One of the proposal is more effective usage of the new technology in financial education, especially the Internet, because of the growing popularity of e-learning and the increasing number of Internet users, especially among young people who are called the Generation Net. Due to special role of the university students studying the economics fields for the future financial markets, students of four universities from Visegrad Countries (Czech Republic, Hungary, Poland and Slovakia) were invited to participate in the survey. The aim of the article is presentation the level and ways of usage the Internet technology in financial education and indication so far unused or underused opportunities.

Keywords—Financial education, financial inclusion, financial literacy, usage of Internet in education.

B. Fraćzek is with the Department of banking and Financial Markets, University of Economics in Katowice, Poland (e-mail: b.fraczek@ue.katowice.pl).

IN the wake of the global financial crisis, the importance of financial education increased all over the world. The financial reality is changing, because of the dynamic development of financial markets as well as due to the increasing transfer of risks to households which are more directly responsible for their financial decisions [1], [2]. In today's world, the financial literacy is important for each target group: For women and men [3], for young and old people [4], [5] for poor and rich, for uneducated and educated, for living in developing as well as in developed countries [6]. The proper level of the financial knowledge and skills is important for both individuals as well as financial markets with the serious impact on the economy [7]. The level of financial literacy touch many aspects of people as individuals and as a community in their daily life. It impacts upon their income, employment, and financial well-being [8], [9]. These effects are far-reaching and affect health, security, housing, food, lifestyle, a child's future literacy abilities. The level of financial literacy determines saving for the future, for retirement and for unforeseen circumstances and emergencies [10], [11].

The range of gained financial literacy skills determines feasibility of basic and complex financial tasks and decision-making. It, in turns, affects households ability to participate in financial markets and it was proven in much research [12], [13], [14]. Financial literacy results in financial efficiency in using the financial products and investing without losses and unnecessary cost (e.g. paying off credit card bills late, choosing the wrong financial product or paying higher interest rates etc.) [15]. But in this point it should be underlined, that the most of people have transactions accounts, but only fraction of them own bonds, stocks and other more sophisticated financial assets [14]. Additional, the financial literacy may better equip people to deal with macroeconomic and financial shocks [16]. The enhancing the financial knowledge and skills directly affects the increasing scale of the financial inclusion [17].

The more involvement of financially educated individuals in the financial markets facilitates to development and the prediction of these markets and benefits for the financial system and the economy. Financially literate consumers are collectively able to influence the ways that financial institutions are managed and at the same time they may influence on the greater competition, innovation and quality of financial products [18]. Better educated financial consumers

understand cyclical changes in the financial markets and in economy and they are more resilient in harsh economic times.

But the fact is that the level of financial education is low [19], [20]. And the situation isn't becoming better. People with the low financial literacy are often marginalized and excluded from financial decision-making.

Much research on the level of financial literacy is conducted among the young people [21], [22]. The lack of financial knowledge and skills make them not prepared for the personal money management [23] and make them responsive to financial advertising. They cannot use their checking accounts and credit cards effectively and they are prone to engage in high-cost credit [24], [25], [26]. These facts threaten their financial security and impact on the quality of their current and future life. Very important is, that the level of financial literacy may repeat itself throughout generations of families. Today's financial world is difficult to understand and assess for people unfamiliar with basic financial and economic concepts. The level of financial literacy of societies doesn't go hand by hand with development of financial markets addicted to the new technology and differences between the level of complexity of financial markets and the knowledge and skills of individual financial consumers increase.

Therefore, effective financial education is needed. Many activities under the financial education don't bring the expected results. The conducted research shows, that even set of financial literacy education programs, mandated by state governments, does not meet the assumed expectations. There are still considered new solutions and at this point it should be underlined the role of modern technology in effective education. The technology supports process of education as well as the assessment of results of this process [27].

Although there is the constant attention paid to the need of financial education directed to the whole of society, the most important target group seems to be the youth. Young people are a very serious group of future financial markets participants. According to demographic data, almost half of all people in the world is under the age of 25 (50,4% in mid of 2016) and individuals between the age of 15 and 24, make up over one-sixth of the world's population (24,3% in mid of 2016) [28]. Therefore the university students population is the target group of the research on the possibility of increasing the efficiency of financial education by using the technological innovations in the educational process in the area of finance.

II. RESEARCH PROBLEM AND METHODOLOGY

With respect to the mentioned insights the aim of this paper is to present situation in the of the Internet by university students of economics fields from Visegrad Group in the process of education with the special emphasis on the financial education. The article underlines the different degrees of usage the Internet in educational processes in finance, taking into account formal, non-formal and informal education.

The following research hypotheses were formulated:

1. The usage of the Internet in education at the university level may increase the efficiency of financial education carried out in the formal as well as non-formal and informal way and at the same time may increase the level of financial literacy and degree of financial inclusion (by proper financial behavior, habits and patterns).

2. The great potential of the Internet is still untapped.

Therefore, the basic research questions are:

- A. What are the main sources of educational contents for university students who study economic fields in 4V Countries?

- B. Is the Internet commonly used in higher education as a whole and what is its role in the financial education?

- C. What are the main methods of e-learning with using the Internet?

- D. Are there in the various 4V Countries the specificity, differences, preferences in using the Internet and/or traditional (paper) forms include educational contents?

- E. Does the using the Internet influence on higher level of financial literacy and financial inclusion?

The two-stages methodology is designed to answer the research questions, verify research hypotheses and achieve the research goals. The first stage was based on the study of the academic and non-academic literature refers to possibility of using the Internet in formal, non-formal and informal education with the special emphasis on the financial education as well as in the realization of the OECD idea of four pillars of the education: learning to know, learning to do, learning to live together, learning to be. Additionally, the descriptive analysis of ways of using the Internet in higher education were conducted. The second stage was an empirical survey. The empirical element of the article is the result of part of the wider survey carried out under research grant among students of economics of the Visegrad countries: the Czech Republic – 362 students of University J. E. Purkyne in Usti nad Labem, Hungary - 203 students of the University of West Hungary in Sopron, Poland - 362 students of University of Economics in Katowice and Slovakia - 274 students of the University of Economics in Bratislava, Faculty of Economics and Business in Kosice. The survey was conducted during April-May 2015. The respondents were all available (during lectures) students of given universities. However, due to the large number of students at the University of Economics in Katowice sample surveys were carried out among students available for lectures.

The universities participated in research can be considered as a typical state universities, where students-respondents are characterized by a number of similar features, including: the structure of gender, differences in the size of the city they come from and differences in the economic/non-economic education of their parents. Therefore it can be assumed that the selected research sample is a miniature of the population of students of economics in countries from Visegrad Group (the countries of Central and Eastern Europe).

The study was carried out taking into account the respondent's country and stage of teaching (I – students starting economics study, students of first year of bachelor study, II - students graduating from economic/financial

education, students of last year of master study).

The sections used in the current paper refer to following areas: basic and extended financial literacy, financial inclusion and the usage the modern technology.

The measurement of financial education efficiency has been taking into account the basic level of financial literacy and uses the questionnaires available in the literature containing concept of simple and compounding interest, inflation, portfolio diversification [20], [29] as well as expanded level of personal finance containing the fundamentals of derivatives market. The degree of financial inclusion is measured by the prism of having account, savings and borrowing the money in formal financial institutions – on the base of World Bank research [30], [31].

In the section refers to the usage the modern technology there were examined: forms, preferences and sources of educational contents (including Internet), forms of e-learning with the special emphasis on the applications of the Internet in education, types of tools used by students under financial education. In the research the descriptive statistics methods are used.

III. THE ROLE OF USING THE INTERNET IN HIGHER EDUCATION IN FINANCE

The Internet plays a significant role in today's lives. It is possible to use it always and everywhere: in schools, colleges, universities, in the workplace, and at home. From the point of view of the financial education it is the medium of the educational contents and the common distribution channel of financial products and services.

Participants of the financial markets need the individual and unique knowledge and skills in many cases. The Internet and other technological innovations may help in both achieving the theoretical knowledge as well as the financial practice (education by practice).

The educational process (teaching and learning) may be carried out in formal, non-formal and informal way [32].

Formal education represents organized, systematic, structured and administered education model according to a given set of laws and norms. The typical for this kind of education a mono-directional methodology is rather poor, ineffective and scarcely creative, that fails to stimulate students and to provide for their active participation in the process. Regardless of the number of students, the same methodology - is adopted. The usefulness of the education for the student's personal and professional growth is negligenced. The formal higher education in the finance comprises mainly studying at the universities. A lot of researchers point to benefits of using the Internet in formal education. They argue that the Internet is used in education because it facilitates learning, teaching and communication [33]. It is also possible to find a great deal of information online at every time. In the finance it may be used to update the financial data and information during lessons and classes under formal education.

In opposite to the formal education the non-formal education is focused on the student and his previously

identified needs and possibilities. It is the intentional from the learner's point of view. The other very important characteristic of the non-formal education is immediate usefulness of the education for the student's personal and professional growth. It is carried out by studying voluntarily with a teacher who assists students with their self-determined interests, by using an organized curriculum. Non-formal education is comprised of a wide variety of educational situations. In today's world very important and popular educational processes, which fall within the scope of non-formal education are "correspondence learning" and "distance learning" in the area of finance as well as "open systems" in the form of online courses in the field of finance, accounting, financial management, sets of educational contents (usually for free) provided by banks, stock exchanges and other stakeholders interested in and responsible for financial education of societies.

The informal education differs from both formal and non-formal education. It doesn't refer to an organized and systematic education and it doesn't include the objectives and subjects usually encompassed by the traditional curricula. From the point of view of students it means the learning resulting from daily life activities related to work, family or even free time. It is not structured (in terms of learning objectives, learning time or learning support) and typically does not lead to certification. It supplements both formal and non-formal education. In the finance area, the informal education – it is the first of all education by practice, by participating in financial markets but also listening to the radio, watching TV, visiting banks and other financial institutions as well as the data analysis during making financial decisions. Most of these activities may be carried out via the Internet.

The Internet facilitates the realization the UNESCO idea of four pillars of the education: learning to know, learning to do, learning to live together, learning to be [34] in the each presented educational way.

Learning to know. Besides using the Internet in access to the educational contents is included in online encyclopedias, books, articles, reports, databases, etc. the Internet allows for deeper drilling the information and greater satisfying the curiosity in learning processes in shorter time. The Internet as the medium helps its users select an item for study and help delve more deeply into a related topic with links to databases and other online sources of knowledge. Very useful may be also freely accessible web search engines like Google Scholar. It facilitates the more effective educational processes in every fields. It should be underlined that pillar learning to know facilitates increasing the low level of financial literacy of various unprivileged group as well as all societies in many countries all over the World. Most of participants of financial markets are uncertain about many concepts and parameters characterizing financial markets, and they learn about these parameters by observing data. This learning is facilitated by the existence of large quantities of financial data available via the Internet. This way of education provides the general teaching and learning together with the deepening knowledge

and at the same time promotes the idea of *life long learning*.

Learning to do. The idea the learning to do was invented in order to acquire both an occupational skill as well as the competence to deal with many situations and work/education in teams. Effective financial education help people to deal with macroeconomic and financial shocks [16]. Considered pillar of education in finance is very strongly related to financial inclusion understood as affordable, timely and adequate access to a wide range of regulated financial products and services and broadening their use by all segments of society [35]. This idea also means young peoples' various financial experiences which may be informal, as a result e.g. participating in financial markets (banking account, payments cards, carrying out transactions at the stock exchanges and forex), or formal and non-formal, involving courses, alternating regular study and work. The using the Internet (mainly Internet account, the information and financial data served via Internet, etc.) in such situations is unquestioned.

Learning to live together. This idea tends to developing an understanding of other people and an appreciation of interdependence - carrying out joint projects, the cooperation and exchange of experience and this way contribute to enhance positive relation among people. It is more and more popular to use Internet platforms to realize many projects, including projects in financial area. It is very popular especially among young people, for whom the Internet environment is well known. Other examples of using the Internet in learning to live together in the area of finance are social networking sites for students, scientists and researchers to share papers, ask and answer the questions, and find collaborators (e.g. Facebook or Research Gate).

Learning to be. This pillar of learning allows to develop one's personality, personal responsibility for own actions and the implementation of own goals. In today's world the Internet helps to appear and exist in many different groups, in society. The financial education, including formal and informal financial education via Internet gives the possibility to be an active investor, to participate in finance forums, to be participant of the financial markets.

At this point it should be noted, that the role of the universities in the education is changed (as a whole), because of the technological and civilization progress. The importance of non-formal and informal learning definitely increases. The "center of gravity" from formal, to non-formal education processes is displacing. Especially in the area of the finance, where the education is necessary for all people, not only for students of economy or finance. The relevant role in these changes plays or may play the Internet. The contemporary concept of teaching is often held in accordance with rule "tell me and I will forget, show me and I may not remember, involve me and I will understand".

The Internet together with other modern technological solutions allow for using described changes in the education for better outcomes of learning and for increasing the chances for carry out all pillars and ideas of education, especially among young people called the Generation Net, and mainly among better educated youth. This group has a greater

predisposition for optimal use the Internet in the process of formal, non-formal and informal education in a conscious and most effective way.

In comparison to traditional learning, learning via Internet make the studying the finance easier and can help in quickly master a financial skills under education by practice at different level of the financial situation complexity. Students may start form the observing the financial data, using financial demos, financial calculators and different analytical tools available in the Internet. They may visit financial forums and discuss many financial problems as the Internet is the great medium of communication.

In addition, the Internet allows for easier contribute to all the Government's objectives for financial education, e.g. to raising standards; improving quality of education, removing barriers to learning and participation in learning, preparing for employment, upskilling in the workplace, and ultimately, ensuring that every learner achieves their full potential.

IV. THE WAYS OF USING THE INTERNET IN HIGHER EDUCATION

The Internet is a one of the most important element of e-learning, which is usually understood as the intentional use of networked information and communications technology in educational processes [36]. There are even the alternative terms for the e-learning in the literature, like online learning, network and web based learning.

The Application of the Internet in Education (AIE) is enormous. In the literature, there are different typologies of AIE [37], which present these great number of possibilities, taking into account e.g. used telecommunication tools, skills level of teachers and learners in computer and telecommunication tools, interaction between the participants of the educational process (types of communication), types of communication methods and the kinds of "pedagogical techniques", teaching methods as well as very wide typologies on the basis of the activity types in all aspects of the educational process.

From the point of view of students (learners) the most important and worth the explanation seem to be the first three typologies.

Students may use the Internet in educational processes by their personal computers (laptops), telephone (smart phone) or other mobile tools (e.g. tablets). This typology may be expanded to applied telecommunication media to collect information on interactive technologies in educational programs (telephone, fax, audio-conference, video-conference, electronic mail, access to databases).

Table 1 presents the most popular Internet tools used in the education assigned to skills level of teachers and learners in their usage.

TABLE I
INTERNET TOOLS FOR ONLINE TEACHING

Internet tools	Skills level of teachers and learners in computer and telecommunication tools			
	L O W	M E D I U M	H I G H	E X P E R T
e-mail, discussion lists				
online lecture notes delivered via the Web				
interactive web tutorials, designed for the course and student interaction				
virtual environments, giving the participants possibility of co-operative activity (like Multi User Dimension, MUD)				

The next typology is focused on types of communication. This criterion may be presented (among others) in accordance with possible combinations of the participants in the communication process, as following:

- *Single communication type* – includes the situations involving an information inquiry (e.g. online resources software: browsers, search systems, Telnet-terminals),
- *One-to-one* – includes bilateral communication (e.g. electronic mail).
- *One-to-multitude* – includes the cases when the information is distributed from one source to many recipients (e.g. listservers, BBS and WWW).
- *Multitude-to-multitude* – includes multilateral multi-directional communication, where all participants in communication have the same status (e.g. www, synchronous and asynchronous teleconferencing, and virtual reality systems with embedded programming language (Multiple User Domains – MUD, MUD Object Oriented – MOO)).

There are in the literature also the typologies of the Internet tools, using in the education under e-learning, with multiple criteria. One of them divides the Internet usage into the four modalities, taking into account educational activities that are carried out by individuals or groups working online or offline, and synchronously or asynchronously [38].

TABLE II
THE APPLICATIONS OF THE INTERNET IN EDUCATION

Individualized self-paced e-learning <i>online</i>	Individualized self-paced e-learning <i>offline</i>
<p>Student is accessing learning resources such as a database or course content online via an Intranet or the Internet.</p> <p>An example: the student studying alone or conducting some research on the Internet or a local network.</p>	<p>Student is using learning resources such as a database or a computer-assisted learning package offline (i.e. after the previous connection to an Intranet or the Internet).</p> <p>An example: a student working alone off a hard drive on gathered materials, (also using CD or DVD).</p>
Group-based e-learning <i>synchronously</i>	Group-based e-learning <i>asynchronously</i>
<p>Groups of students are working together in real time via the Internet or an Intranet.</p> <p>An examples: students engaged in a real-time chat or an audio-videoconference.</p>	<p>Groups of students are working over the Internet or an Intranet, where exchanges among participants occur with a time delay.</p> <p>An example: online discussions via electronic mailing lists.</p>

The Internet and its tools swiftly entered the daily life and was adopted in education. But there are many factors, which influence the effectiveness of the Internet usage in learning and teaching. One of them is the ability of a user to work with information provided via Internet. In the finance area it means having the skills of collecting educational contents, data and information, the proper selection of this data and facts, analyzing the information, dealing with the information and data as well as using many different analytical tools available on the Internet. The second factor which impacts the efficiency of using the Internet in education are skills of intercultural communication in network. It is important during setting different educational materials in international environment as well as during learning by practice at the stock exchange, forex, etc. where a special language with many abbreviations is required. The next factor is adequately prepared teachers who are open to the new ideas, new practices and technologies. The lack of teachers, who are familiar with modern technology and who can benefit from using the Internet as an additional teaching resource is very serious inconveniences. Taking into account the fact that students are usually adaptable to change, are creative and innovative, one of the important challenge is to prepare teachers who can produce these desired student attributes, and teachers who are open to new ideas, new practices and

technologies. It is important in each area of study but analyzing the financial education it is worth to mention that besides required skills level of teachers in computer and telecommunication tools, very important is the practical experience in the financial markets using the Internet technologies.

The usage of the Internet in the financial education meets a lot of needs but also entails some minor inconveniences and threats. The financial education using the information and data available via the Internet is hampered by the huge amount of randomness pervading financial markets. Besides, some programs, scientific articles with educational contents are free to be copied and distributed while others have copyright that limits distribution.

Today anyone can post a multimedia web page and students, often "surf the web" for information. Therefore, skills of the directing and harnessing Internet has become one of the greatest challenges faced by all stakeholders involved in.

V. EMPIRICAL RESEARCH

Having identified main findings on possibility of using the Internet in the financial education, it is important/worth to analyze how it works in practice. The undertaken study should be regarded as preliminary and necessary part of wider research, conducted in order to seek the most effective and the most optimal methods of financial education using the Internet.

At the beginning, it should be highlighted, that for university students the Internet is the great potential, because 100% respondents (students of economics fields in Visegrad Countries) are Internet users. In this point it worth to note, that percentage of Internet users in all population in mid 2016 amounted to 49,2% for the World, 73,9% for Europe, 88,4% for Czech Republic, 80,2% for Hungary, 72,4% for Poland and 82,5% for Slovakia [39].

The first result of research shows, that Internet is very popular source of educational content, notably when it is not directly related to the fields of the studying. The use of the Internet for educational purposes e.g. to getting to know the specifics of a phenomenon, to explaining any concepts, to use dictionaries or virtual encyclopedias etc. is very high.

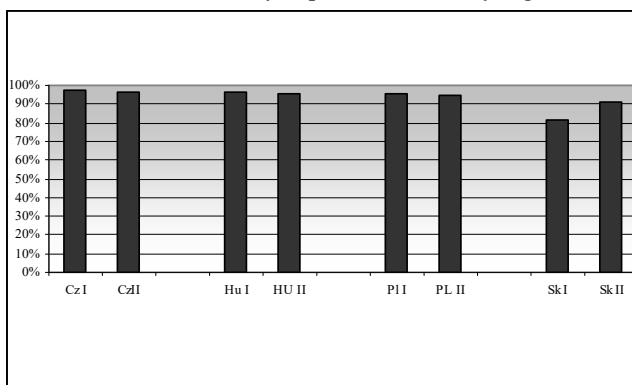


Fig 1. The usage of Internet for educational purposes not directly related to the fields of study

Presented very high Internet usage as a source of knowledge probably follows, that in the fields which are not subject of studying people do not have the appropriate materials and the usage of the Internet is the simplest and the fast way to get the data or the information.

The results of research show, that the use of the Internet as the source of educational content in the studying fields (e.g. economics or finance) is not so high. Fig. 2 presents the scale of Internet usage in financial education in comparison to traditional paper version of materials form lectures, books, reports and etc.

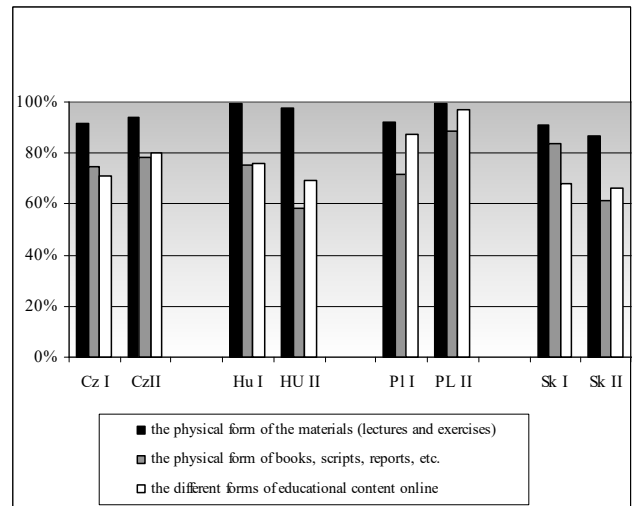


Fig. 2 Usage the different form of educational content (in finance) by students of economics fields

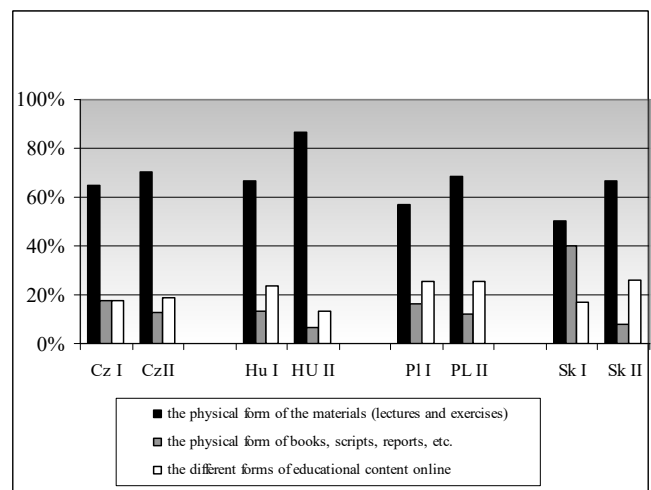


Fig. 3 The most preferred forms of learning under process of financial education

Although almost all (100%) students-respondents declared the usage of Internet as a whole, not all of them use it in educational process during study (chart 2). More detailed research shows the place of Internet as the source of educational content. It turns, that Internet is not favorite form of learning among students-respondents (chart 3). In each country and at every level of study students prefer and use the traditional educational form, source of educational content like

physical form of the materials form lectures and exercises.

As it is described in the theoretical part of the paper in financial education very important is education by practice. Therefore the using the Internet for comparing offers of financial market is examined - e.g. if students want to take the advantage of the financial market's product like bank account, credit card, insurance, investments and other savings and investment products.

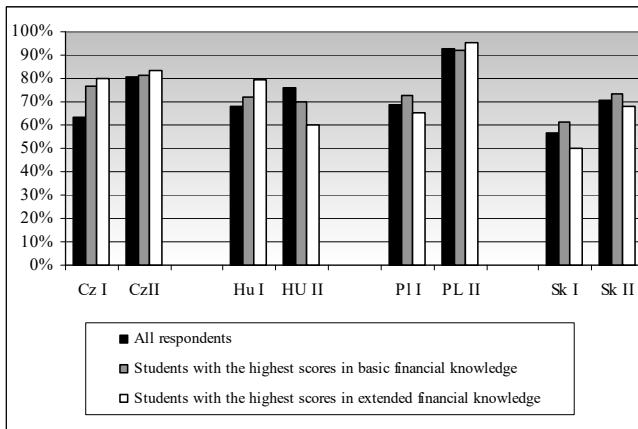


Fig. 4 Using the Internet for comparing offers of financial market – education by practice

Results of this part of research show that students finishing their university financial education (II) use the Internet to compare the financial products more often than students starting their financial education (I). The reason is probably higher knowledge and better understanding after financial education and financial practice during study. But the differences are not significant and they do not meet expectations of the Authors. In addition, in many cases students who achieved the best score in the test on financial education more often use the Internet to find the information about the products of financial markets. This suggests, that the use of Internet may be helpful in more effective financial education.

Examining the usage of Internet in educational process in finance it is worth to explore the popularity of the various applications of the Internet in education described in table 2 in the theoretical part of the paper.

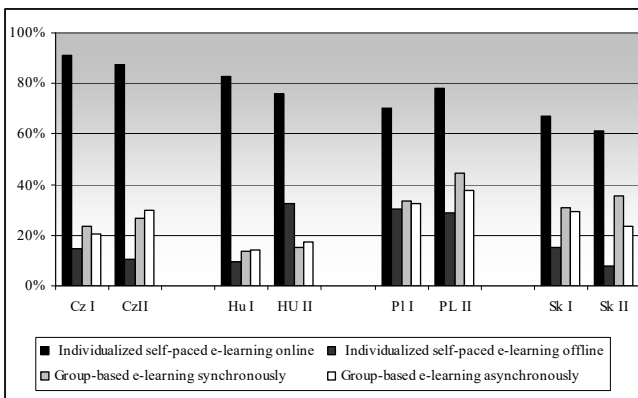


Fig. 5 The usage of various applications of Internet in financial education among the students-respondents (multi-choice question)

Definitely, the most often used form is individualized e-learning online. The research shows that the most of students use the Internet - studying alone on-line and the other applications are used by minority of students. This confirms the untapped opportunities offered by contemporary modern technologies in educational processes. And this time the situation is diverse in particular researched countries.

In the next multi-choice question students pointed the types of Internet possibilities, tools they use in the financial education.

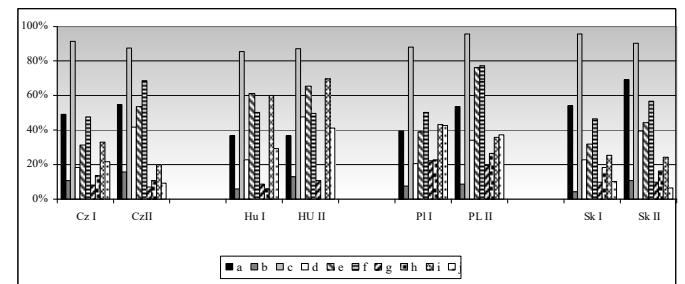


Fig. 6 Internet tools used in the financial education

- E-mailing (Thematic student-to-student correspondence)
- E-mailing questions to the experts
- Google – looking for the information
- Google Scholar (E-books, E-articles)
- Financial portals
- Websites of financial institutions (banks, brokers, stock exchanges, etc.)
- Interactive web tutorials
- Active educational cooperation with other Internet users in virtual environments (discussions, videoconferences)
- Virtual educational content prepared by your teachers
- Virtual educational content of your friend.

The results of research show that most popular is the Google way of searching the Internet for the information. But it should be noted, that the Internet is not an ordinary encyclopedia, It is rather a disorganized database to which everyone can contribute. Therefore users should be equipped in ability and skills of selection and evaluation of searched information.

Specificity of area of financial education causes that the next very important Internet tools are websites of financial institutions like banks, brokers, stock exchanges, etc. as well as the financial portals. These sources of knowledge supply a lot of worth information and educational content under education by practice.

Important finding is that prevailing and most popular Internet tools refer to individual and self education. But Internet also offer the tools facilitate common education many stakeholders, e.g. many students, students and teachers, students and experts, etc. under mailing, discussions, videoconferences. In this group of tools the most popular are and thematic student-to-student correspondence and sometimes virtual educational content prepared by teachers.

The less popular are still interactive web tutorials and questions to the experts. Also the reviewed e-books and e-articles on Google Scholar are used by students very rare.

Next aspect of the research are particular areas, elements of

financial inclusion. Having banking account, saving money in the banks or borrowing money from the banks are the most important aspects of financial inclusion. In the research undertaken the efforts to measure the percentage of all respondents involved in listed areas in comparison to students who realize education by practice.

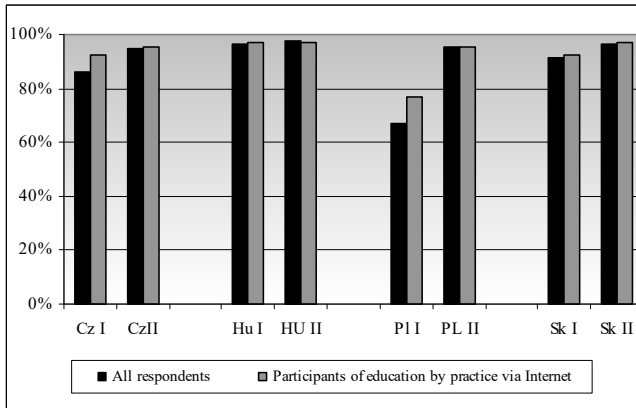


Fig. 7 Having account in formal financial institutions

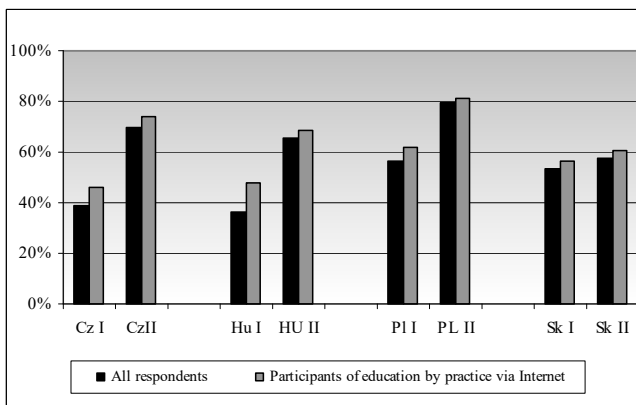


Fig. 8 Savings in formal financial institutions

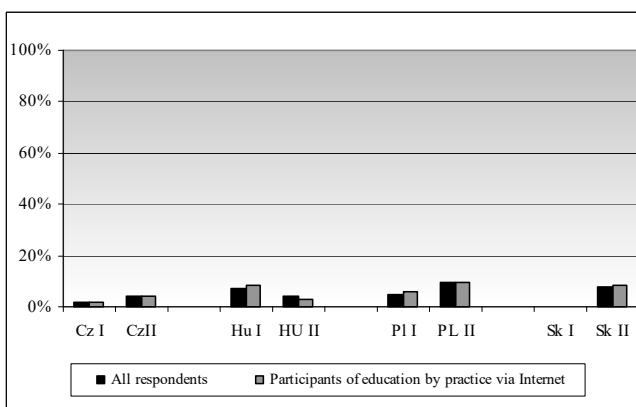


Fig. 9 Borrowing money from the banks

The intention of this aspect of the research was examine and underline the relationship between the education by practice and the real usage the offers of financial market. The results show that although the various level of active participating in particular fields of financial markets (banks offers) education

by practice very often supported by modern technology, facilitates the financial inclusion. And in this moment should be mentioned the interrelation between degree of financial inclusion and the level of financial literacy.

VI. CONCLUSION

Effective education including higher education, technological readiness, and the financial market development are indeed in the group of pillars, that are key for efficiency driven economies [40] and that is why the usage of Internet in financial education at the university level is underlined in current paper. The Internet affords great flexibility its usage in education. This flexibility means access and use the educational content at a time, place and pace that is suitable and convenient to individual students. It is especially important from of education in area of finance, where the information is changing very quickly and where students use high-frequency data.

Conducted research confirms the influence the using of the Internet on the level of financial literacy and on the degree of financial inclusion on the example of 4V Countries. This relationship should be also examined in wider range under the each group of students (in different fields of study). It may help to assign the specificity of using the Internet or other technological innovations to education in different areas. The specificity of different fields of study influencing the level of using the Internet in formal education may reflect on the range and the scale of using the Internet in non-formal and informal education. The research shows that big number of students use the Internet in their informal financial education, including education by practice. But it is unknown the degree of the usage of the Internet in it and probably it is not filled. A very large of possibilities given by the Internet are still not realized in education. The results of research show the level of usage basic tools and techniques used in the Internet e.g. e-mailing in thematic student-to-student correspondence), e-mailing in asking the questions to the experts, Google – looking for the information, Google Scholar – using e-books, e-articles, financial portals, websites of financial institutions (banks, brokers, stock exchanges, etc.), interactive web tutorials, active educational cooperation with other Internet users in virtual environments (discussions, videoconferences), virtual educational content prepared by teachers, virtual educational content of friends and many others. The most popular are the simplest ways of using the Internet in education, e.g. looking for the information in web browsers or e-mailing, while the ways, allowing for achieving the most valuable educational contents like reviewed e-books, e-articles available on Google Scholar or interactive web tutorials are used marginally.

The main goals of contemporary education are intellectual and moral development of students, their critical and creative thinking and their ability to work with information. Therefore, the non-formal and informal education is developed and the Internet plays crucial role in these types of education, especially in education directed to youth as the Generation Net.

The undertaken research, aimed in verifying the possibilities of the Internet usage in learning at the university level, clearly shows that students from researched countries use the Internet in educational process but in unsatisfactory degree and range. The question is: what is the reason? The different preferences in the types of materials/sources used in the formal education is probably results of range and quality of educational contents, their accessibility, specificity of learning in given field of study as well as the ability and skills of searching and verification the information and data. But the reason of unsatisfactory usage the modern technology, including Internet technology may also be lack of developed standards where educational systems using the modern technologies can be utilized in practical academic environment. This problem was underlined many years ago [41] and still is actual.

The education in the finance especially in the area of investment and savings comes to getting to know and understanding the financial concepts and observing data, calculating and analyzing the current data, and also real practice in the finance. In all these aspects the education via the Internet is very helpful and may be carried out in very simply way (by using demos, financial calculators, analytical programs as well as free access to Internet courses and many educational contents).

It should be also paid the attention to the need for complementarily of formal, non-formal and informal education and cooperation between institutions forming and representing all forms of education [42].

ACKNOWLEDGMENTS

B. Frączek thanks International Visegrad Fund for its financial support, which made it possible to integrate the scientists from 4V Countries and conduct the international research under the project titled “Financial knowledge and skills of young future economists in 4V Countries”, ID 21420287.

REFERENCES

- [1] A. Lusardi, “Household Saving Behaviour: The Role of Financial Literacy, Information and Financial Educations Programs”, NBER Working Paper 13824 February 2008, (on line) <http://www.nber.org/papers/w13824.pdf> (Accessed January, 2016).
- [2] P. Muller, S. Devnani, R. Heys, J. Suter, “Consumer Protection Aspects of Financial Services”, European Parliament, Policy Department A: Economic and Scientific Policy, Brussels, 2014, [http://www.europarl.europa.eu/RegData/etudes/etudes/join/2014/507463/IPOL-IMCO_ET\(2014\)507463_EN.pdf](http://www.europarl.europa.eu/RegData/etudes/etudes/join/2014/507463/IPOL-IMCO_ET(2014)507463_EN.pdf), (Accessed 7 July 2016).
- [3] OECD/INFE “Addressing women’s needs for financial education” OECD, (on line) http://www.oecd.org/daf/fin/financial-education/OECD_INFE_women_FinEd2013.pdf, (Accessed February, 2016).
- [4] A. Lusardi, O. Mitchel, V. Cursto, “Financial Literacy among the Young”, The Journal of Consumer Affairs, Vol. 44, No. 2, 2010, (on line) <http://www.councilforeconed.org/wp/wp-content/uploads/2011/11/Financial-Literacy-for-Young-Lusardi.pdf>, (Accessed March, 2016).
- [5] M.S. Finke, J.S. Howe, S.J. Huston, “Old age and the Decline in Financial Literacy”, 2011, (on line) <http://www.tilkingroup.com/textastech.pdf> (Accessed February, 2016).
- [6] Ch. Bumcort, J. Lin, A. Lusardi, “The Geography of Financial Literacy: A Report, Financial Literacy Center”, November, 2011, p.10.
- [7] D. Šoškić, “Financial literacy and financial stability”, Keynote speech, Governor of the National Bank of Serbia, at the Bank of Albania 9th International Conference Building our future through financial literacy, Tirana, 15 September 2011, (Accessed 5 July 2015).
- [8] M.K. Taft, Z.Z. Hosein, S.M.T. Mehrzi, A. Roshan, “The Relation between Financial Literacy, Financial Wellbeing and Financial Concerns”, International Journal of Business and Management; Vol. 8, No. 11, 2013, pp.63-75.
- [9] M. Rooij, A. Lusardi, R. Alessie, Financial Literacy, “Retirement Planning, and Household Wealth”, De Nederlandsche Bank, Working Paper No. 313, August, 2011.
- [10] F. Deufhard, D. Georganakos, R. Inderst, “Financial literacy and savings account returns”, Working Paper Series, European Central Bank, 2015.
- [11] S. Cole, G.K. Shastri, “Smart Money: The Effect of Education, Cognitive Ability, and Financial Literacy on Financial Market Participation”, Harvard Business School and Wellsley College, September 2010, (on line) <http://www.theigc.org/sites/default/files/sessions/cole-lse.pdf> (Accessed January, 2016).
- [12] A. Thomas, L. Spataro, “Financial Literacy, Human Capital and Stock Market Participation in Europe: An Empirical Exercise under Endogenous Framework”, Discussion Papers del Dipartimento di Scienze Economiche – Università di Pisa, 2015, (on line) <http://www.ec.unipi.it/documents/Ricerca/papers/2015-194.pdf> (Accessed February, 2016).
- [13] E. Acquah-Sam, K. Salami, “Knowledge and Participation in Capital Market Activities: The Ghanaian Experience”, International Journal of Scientific Research in Education, June 2013, Vol. 6(2), pp.189-203.
- [14] S. Cole, G.K. Shastri, “If You Are So Smart, Why Aren’t You Rich? The Effects of Education, Financial Literacy and Cognitive Ability on Financial Market Participation”, 2007 (on line) <http://www.bostonfed.org/economic/cprc/conferences/2008/cfrg-october/cole-shastri-rich.pdf>, (Accessed January, 2016).
- [15] C. Bell, D. Goran, J. Hogarth, “Does Financial Education Affect Soldiers’ Financial Behavior?”, Working Paper 2009-WP-08, Networks Financial Institute, 2009.
- [16] L.F. Klapper, A. Lusardi, G.A. Panos, “Financial Literacy and the Financial Crisis”, NBER Working Paper No. 17930, Cambridge, March 2012, (on line) <http://www.nber.org/papers/w17930.pdf> (Accessed March 2016).
- [17] M. Cohen, C. Nelson, “Financial Literacy: A Step for Clients towards Financial Inclusion”, 2011 Global Microcredit Summit, Commissioned Workshop Paper November 14-17, 2011 – Valladolid, Spain, 2011, (on line) http://partnershipsagainstpoverty.org/wp-content/uploads/2013/03/CohenM_Financial_Literacy.pdf (Accessed February, 2016).
- [18] T. Japelli, “Economic Literacy: An International Comparison”, The Economic Journal, November, Vol. 120, Iss. 548, 2010.
- [19] L. Klapper, A. Lusardi, P. Oudheusden, “Financial literacy around the World – insights from S&P Ratings”, 2015 Global Financial Literacy Survey, 2015, (on line) http://media.mhfi.com/documents/2015-Finlit_paper_17_F3_SINGLES.pdf (Accessed 15 June 2016).
- [20] A. Atkinson, F. Messy, “Measuring Financial Literacy: Results of the OECD / INFE Pilot Study”, OECD, Working Papers on Finance, Insurance and Private Pensions, No. 15, OECD Publishing, 2012, pp.446-448.
- [21] OECD (2014), PISA 2012 Results: Students and Money: Financial Literacy Skills for the 21st Century (Volume VI), PISA, OECD Publishing.
- [22] M.S. Sherraden, L. Johnson, B. Guo, W. Elliott, “Financial Capability in Children: Effects of Participation in a School-based Financial Education and Savings Program”. Journal of Family & Economic Issues, 32(3), 2011, pp.385-399.
- [23] NCEE (2016) Survey of the States: Economics and Personal Finance Education in Our Nation’s Schools, National Council on Economic Education’s (NCEE), <http://councilforeconed.org/wp/wp-content/uploads/2016/02/sos-16-final.pdf>, (Accessed July, 2016).
- [24] FINRA Investor Education Foundation (2013) Financial Capability in the United States-Report of Findings from the 2012 National Financial Capability Study. <https://www.federalreserve.gov/pubs/feds/2014/201468/201468pap.pdf>, (Accessed June, 2016).
- [25] L. Mandell, L. Schmid Klein, “The Impact of Financial Literacy Education on Subsequent Financial Behavior”, Journal of Financial Counseling and Planning Volume 20, Issue 1, 2009, pp.15-24.

- [26] N. May, "Undergraduate students and credit cards in 2004: An analysis of usage rates and trends", Wilkes-Barre, PA: Sally May Inc., 2005.
- [27] J.G. Laborda, D.G. Sampson, R.K. Hambleton, E. Guzman, "Guest Editorial: Technology Supported Assessment in Formal and Informal Learning". *Educational Technology & Society*, 18 (2), 2005, pp.1-2.
- [28] Population Pyramids of the World (2015). (on line) <http://populationpyramid.net> (Accessed July, 2016).
- [29] L. Xu, B. Zia, "Financial Literacy around the World", Policy Research Working Paper 6107, The World Bank Development Research Group. 2012, (on line:) http://papers.ssrn.com/sol3/papers.cfm?abstract_id=2094887, (Accessed March, 2016).
- [30] World Bank (2015), "The Little Data Book on Financial Inclusion", The World Bank Group, <https://openknowledge.worldbank.org/bitstream/handle/10986/21636/9781464805523.pdf?sequence=3>, (Accessed March, 2016).
- [31] World Bank (2012), "The Little Data Book on Financial Inclusion", The World Bank Group, <http://data.worldbank.org/sites/default/files/the-little-data-book-on-financial-inclusion-2012.pdf>, (Accessed March, 2016).
- [32] D. Colardyn, J. Bjornavold, "Validation of Formal, Non-Formal and Informal Learning: policy and practices in EU Member States", *European Journal of Education*, Vol. 39, No. 1, 2004, pp. 69-89.
- [33] A. Sayed, M. Mahmoud, M. "Exploring the Process of Integrating the Internet into English Language Teaching", Paper presented at the Academic Conference for Young Researchers in Asyut, Egypt on Apr. 24 2007. EBSCOHost. <http://web.ebscohost.com/webproxy.student.hig.se:2048/ehost/search/advanced>, (Accessed January, 2016).
- [34] UNESCO (1996) 'Learning: The Treasure Within, UNESCO-report' (on line) <http://unesdoc.unesco.org/images/0010/001095/109590eo.pdf> (Accessed January, 2016).
- [35] A. Atkinson, F. Messy, "Promoting Financial Inclusion through Financial Education: OECD/INFE Evidence, Policies and Practice", OECD Working Papers on Finance, Insurance and Private Pensions, No. 34, OECD Publishing, 2013, (on line:) <http://dx.doi.org/10.1787/5k3xz6m88smp-en>, (Accessed January, 2016).
- [36] V.K. Gandhi, "A Review Study on E-Learning for the Empowerment of Teaching and Learning in Higher Education", *Journal of Education and Practice*, Vol 2, No 10, 2011, (on line) <http://iiste.org/Journals/index.php/JEP/article/viewFile/780/683> (Accessed April, 2016).
- [37] A. Khannanov, "Experience of Internet Usage in Education", Analytical Survey(in:) *Internet In Education*, UNESCO Institute for Information Technologies in Education IITE, Moscow 2003, pp.14-16.
- [38] S. Naidu, "E-learning. Guidebook of Principles, Procedures and Practices", CEMCA, New Delhi, 2006, (on line) http://cemca.org.in/ckfinder/userfiles/files/e-learning_guidebook.pdf (Accessed January 2016).
- [39] Internet World Stat (2016). (on line) <http://www.internetworldstats.com/stats.htm>, (Accessed July 2016).
- [40] K. Schwab, K. (Eds.) "The Global Competitiveness Report 2014-2015", World Economic Forum, Geneva 2014, (on line:) http://www3.weforum.org/docs/WEF_GlobalCompetitivenessReport_2014-15.pdf (Accessed March, 2016).
- [41] A. Patel, A., Kinshuk "A Conceptual Framework for Internet based Intelligent Tutoring", (in:) A.Behrooz, (Eds.), "Systems Knowledge Transfer", Volume II, pAce, London, UK, 1997, pp.117-124.
- [42] B. Frączek, "Coordinated actions in the field of financial education as a new approach to improve financial literacy", *International Journal of Business Excellence*, Vol.8 (4), 2015, pp.514-535.

Use of Geometrical Relationship in the Ancient *Vihara* Housing Reclining Buddha Remains of Thailand's *Kamphaeng Phet* World Heritage Site

Svamivastu Vacharee

Abstract— This research investigates the application of geometrical relationship to the ancient religious assembly hall (*Vihara*) housing a reclining Buddha statue of Thailand's *Kamphaeng Phet* Historical Park. The study utilizes the archaeological and wooden roof structure remains of the *Vihara* as the prima facie evidence, supplemented with evidence from other active archaeological sites with architectural kinship as well as Buddhist ideology. At present, the wooden roofs of the *Vihara* fell prey to the elements and there remain only the base, columns and enclosing walls. Unlike typical *Viharas* whose floor plan are of rectangular shape, the floor plan of the *Vihara* housing the reclining Buddha is of square configuration of 25x25m. Further observation has revealed the utilization of large laterite boulders as the principal construction material of the assembly hall (*Vihara*) columns. The laterite columns are of square shape (1x1m) and various heights (H), ranging from 3.50m to 5.50m. The erection of the *Vihara* required a total of 36 laterite columns. The pattern of columns arrangement is of two rows of inner columns, two rows of outer columns and two rows of verandah columns. The space between pairs of the verandah columns was stacked with laterite blocks of varying sizes to form the *Vihara* walls with small openings for ventilation. Upon applying the geometrical relationship-grid system to the *Vihara*, the results reveal that the placement of the columns was deliberately and masterfully undertaken such that the center of the square-shaped *Vihara* is conspicuously spacious so as to accommodate the sacred reclining Buddha statue. The elegance of the *Vihara* demonstrates the ingenious application of geometrical relationship to transforming a space into a structure (i.e. *Vihara*) of architectural and religious significance.

Keywords --- Geometrical Relationship, the religious assembly hall, *Vihara*, Kamphaeng Phet School of Master Builder

Biography

1.Last Name Followed by first Name

Svamivastu Vacharee

2.position/department/organization/country

Senior lecturer, Assoc Prof.

Architectural Department, Faculty of Architecture

King Mongkut's Institute of Technology Ladkrabang.

Chalongkrung Rd. Ladkrabang, Bangkok Thailand 10520

3.Biography (word count should not exceed 50 words)

B.Arch. (KMITL) King Mongkut's Institute of Technology Ladkrabang

M.A. (History of Architecture) Silpakorn University

Over two-decade study of Thai traditional history of architecture based on the application of geometrical relationships by architecture schools of various periods in Thailand in order to enable young architectural students to suitably apply or adapt the acquired knowledge to their modern or future architectural designs and awareness of the role of creative design to the preservation and continuation of Thai architectural identity.

4.Contact information (Address, contact number & email address)

Architectural Department, Faculty of Architecture

King Mongkut's Institute of Technology Ladkrabang.

Chalongkrung Rd. Ladkrabang, Bangkok Thailand 10520

Tel: 66-818325983

Email: vacharee.va@kmitl.ac.th

Utilizing Tornado Code in Signature Based Authentication Technique for Scalable Multimedia Streams over Packet-Lossy Network

Ramin Javadzadeh

raminjavadzadeh@yahoo.com

Abstract— Authentication has turned into a developing issue for video stream over lossy-networks. In spite of the fact that the propelled video coding principles, for example, H.264/AVC effectively decrease the measure of information to be transmitted, the coding reliance gets new difficulties outlining productive stream validation plan. we propose novel plans for scalable multimedia streams over packet-lossy networks. This plan utilizes an advanced digital signature to secure the unity of a range of frames and uses Tornado code to battle packet loss. Test results on H.264 video groupings affirm the adequacy of this strategy decrease calculation time in examination with other error correction codes.

Keywords— Scalable multimedia, authentication, Tornado code, video Stream.

I. INTRODUCTION

video application has gotten to be one of the prevailing applications over Internet, advanced by the fast improvement of the system advances, media coding benchmarks, and the late advances of the online networking system.

For instance, in US, Netflix takes up 33% of Internet Bandwidth [17], also other video applications, for example, YouTube which has 800 million one of a kind guests every month [18].

In the meantime, with the prominence of the cell phones, for example, advanced mobile phones and tablets, more applications are running on the versatile finishes. Today, more than 100 million clients have downloaded mixed media records, and more than 47 million of them do as such all the time [1]. because of the generally clients interest for Diverse video quality, with various gadget abilities, for example, DTV, desktop PC, PDA, and mobile phone, or system data transfer capacity conditions, versatile interactive media coding norms, for example, JPEG-2000 [3] for pictures and MPEG-4 [4] and H.264 adaptable video coding (SVC) [4] for recordings, surfaced as engaging answers for location the pervasiveness of sight and sound applications [1]. We focus on versatile video coding (SVC) strategies that handle incredible adaptability while encountering enormously bring down overheads than conventional techniques [6]. These guidelines produce versatile sight and sound streams made up of a base layer

giving the picture/video at the coarsest quality and one or more upgrade layers that bit by bit enhance the picture/video quality [1]. For instance, the as of late institutionalized versatile augmentation of the H.264/AVC coding standard, known as H.264/SVC [7], bolsters adjusting a video stream along three adaptability measurements: worldly, spatial, and quality (PSNR or loyalty). This three-dimensional versatility model is portrayed in Fig. 1.

Adaptability comprise of three measurements, which are spatial, transient, and quality versatility. Spatial and transient adaptability allude picture size and casing rate, separately. With quality adaptability, the sub stream gives the same spatio-temporal determination as the complete piece stream, for the most part the last versatility alluded to assign to-clamor proportion (SNR) Or fidelity[7].

Adaptable media comprises of one base layer giving the interactive media at the coarsest quality and one or more upgrade layers that bit by bit enhance the sight and sound quality. In the in customary strategies server has sent numerous adaptations of the same substance to cook for various gadgets or system conditions, in versatile sight and sound, source content give a solitary stream for every substance then exchanges the interactive media to intermediaries, where one or more intermediaries perform transcoding—expelling one or more improvement layers (On request), before conveying the transcoded sub streams to end clients. Bundle misfortune is another test that Most of the current arrangements are not versatile over packet_lossy systems. Cutting edge adaptable sight and sound coding gauges are intended to be versatile to bundle misfortune. The security plans for mixed media streams ought to give the same level of strength to bundle misfortune, which is particularly testing to accomplish in light of the fact that cryptographic calculations are amazingly delicate to mistakes [1].

II. RELATED WORKS

The greater part of the current arrangements on sight and sound verification are intended for nonsalable mixed media streams. the work of [8] proposes a plan called Signature Amortization utilizing Information Dispersal Algorithm (SAIDA). SAIDA separates the stream into pieces of n parcels. At that point, it hashes every bundle and connects the

hash values. A change to SAIDA, generally called correspondence overhead diminished SAIDA (cSAIDA), is given in [19] that further brings down the correspondence overhead by playing out the deletion coding twice on the verification information. Habib et al. [9] presented TFDP (Tree-based Forward Digest Protocol) for disconnected from the net P2P gushing, that is, appropriation of effectively recorded media documents. Like SAIDA, bundles are hashed, and parcel hashes are connected and hashed again to shape the review of the square. Not at all like SAIDA, one and only mark is created for the entire stream, in light of the fact that the whole document being spilled is given at first.

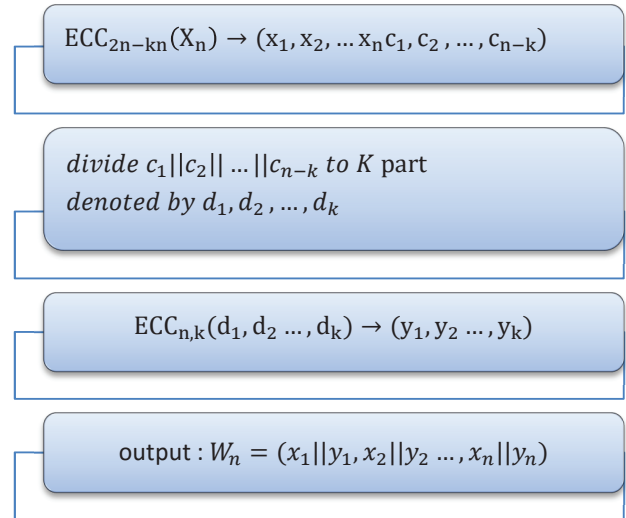
For confirmation of adaptable sight and sound streams, the work of [10] proposes to join the elements of cSAIDA (correspondence effectiveness) and TFDP (calculation proficiency) in planning a validation plan for spilling of pre-encoded streams that calls iTFDP. Alike to cSAIDA, iTFDP partitions information into squares and uses the hash of bundles. The work of [11] utilizes some verification plots that calls SMMA. SMMA utilizes a key for encryption and unscrambling of bundles and hash of took after by a marking operation. The work of [12] presents a crossover validation (HAU) plan. The HAU utilizes both cryptographic verification and substance based confirmation systems to secure trustworthiness and credibility of the SVC code streams. The work of [2] utilizes a confirmation plan for video streams encoded utilizing the general three-dimensional versatility display that permits check of all conceivable sub streams. That can be removed and decoded from the first stream. The assessments demonstrate that this plan is flexible over bundle misfortune rates (10–40%). Adaptable validation taking into account hash trees [13], [14], [15] can be utilized for end-to-end confirmation. all data expected to validate the main layers are install in every layer, this altogether upturns the correspondence overhead [10]. The work of [16] discharged a stream confirmation strategy is proposed for versatile media streams over remote systems. Chart based and ECC-based methodologies are utilized in this technique end by using content-mindful data of media streams, for example, significance separation and coding reliance. Likewise, the outline of structure-kept up marketization for general adaptable media streams is considered.

In synopsis, the present confirmation systems for versatile streams are intended for conventional, and much easier, direct layered recordings.

III. TORNADO STRATEGY

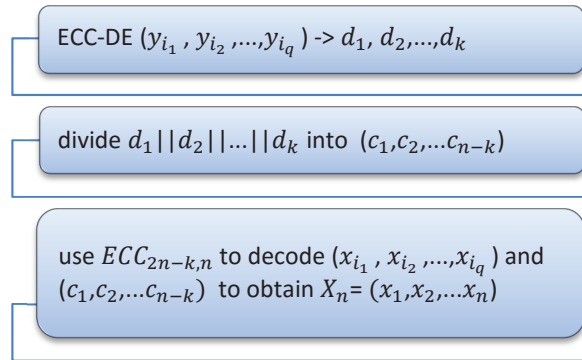
The general thought for accomplishing Erasure redress code is to add some extra (i.e., some additional information) to a parcels, which collectors can use to check unwavering quality of the conveyed bundles, and to recoup parcels. ECC comprises of an encoder module and a decoder module.

A. A. Encoder function $DECS_EN(X_n)$



B. B. Decoder $DECS_DE(Y_q)$:

$x_{i_1}y_{i_1}, x_{i_2}y_{i_2}, \dots, x_{i_n}y_{i_n} = y_q$ this is subset of w_n .



The remarkable benefit of DECS is that, as long as at least k symbols in W_n are received, the DECS decoding ensures that all (x_1, x_2, \dots, x_n) will be recovered.

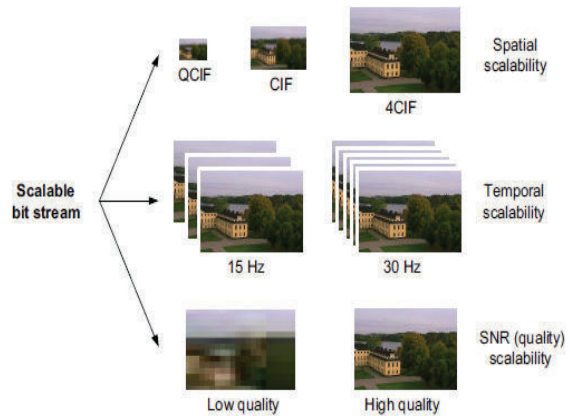


Fig1. three-dimensional versatility model is portrayed

IV. SIGNATURE-BASED AUTHENTICATION SCHEME

multimedia stream is divided into groups of n packets, for each packet is computed hash of top enhancement layer and concatenate with lower layer. For the other enhancement layer is done the same process until reach to the base layer. ECC-EN is applied on the hash of base layer of all packets in individual group of packet and the output is the code words: y_1, y_2, \dots, y_n . In the next step, the hash of base layer of all packets are signed. This signature is divided into k equal length segments. The n code words (s_1, s_2, \dots, s_n) is generated by applying ECC-EN on k segments. The output is concatenation of enhancement layers, their hashes, y_i , s_i and base layer. This output is sent to proxy server and in this step proxy server removes some enhancement layer and again sends modified group of pictures to client. The authentication information which added to the packets (like hashes, ECC-EN, signatures) are used for verifying packets by clients.

C. A. System model

Considered one content source and set of proxies with heterogeneous user with different demand, the source produces protected multimedia streams and forwards them to proxies. Each frame has a base layer and m cumulative enhancement layers, where $m \geq 0$. Without loss of generality, we assume that each network packet carries a complete frame. Hence during the rest of the paper, we use the term frame and packet interchangeably. To keep the description compact, we illustrate our schemes by considering one-dimensional scalability, but they can be easily extended to support multidimensional scalability.

V. B. PROPOSED METHOD

In the proposed method, digital signatures were used for the authentication. While in the packet lossy networks, the probability of packet loss and loss of authentication information is very possible, in this method the error correction code is used in order to recover authentication information in the receiver side. Due to the loss of some of the information, group of picture does not have to throw away. While using error correction code cause increase the computational cost, Tornado code was used as an optimal method.

Proposed model: this schema consists of an authentication algorithm for the source, a transcoding algorithm for the proxies, and a verification algorithm for end users. We pass up The transcoding algorithm in the following.

D. A. Authentication algorithm

Assume that the source creates an interactive media stream with an identifiers_id. The validation is on the gathering of

bundle.

Compute $h_{i,m} = H(L_{i,m})$: for top enhancement layer, $h_{i,j} = H(h_{i,j+1} || L_{i,j})$: $0 \leq j \leq m-1$
 $DEC-EN(h_{1,0}, h_{2,0}, \dots, h_{n,0}) = (h_{1,0} || y_1, h_{2,0} || y_2, \dots, h_{n,0} || y_n)$
 $H = H(h_{1,0}, h_{2,0}, \dots, h_{n,0} || G_{id} || S_{id})$ and $\alpha = Sig_{sk}(H)$
 $\alpha = (\alpha_1, \alpha_2, \dots, \alpha_k)$ and $ECC_{n,k}(\alpha_1, \alpha_2, \dots, \alpha_k) = (s_1, s_2, \dots, s_n)$
 $G' = [P'_1, P'_2, \dots, P'_n]$

$$\begin{aligned} L'_{i,m} &= L_{i,m} \\ L'_{i,j} &= h_{i,j+1} || L'_{i,j}, \text{ for } 0 \leq j \leq m-1 \\ L'_{i,0} &= h_{i,1} || L_{i,0} || y_i || s_i \\ P'_i &= L'_{i,0} || L'_{i,1} || \dots || L'_{i,m} \end{aligned}$$

E. B. Transcoding algorithm.

upon receiving P' , removing some enhancement layer on user demand and has sent P'' to user.

F. C. Verification algorithm.

Because of noisy network, a user may receive q damaged packet of the n packets sent by the proxy, if $q/n \geq$ threshold, then the only job is to save the last packet damaging rate(q/n). Otherwise, user runs the following steps to verify the integrity.

Parse P'' into $m-t+1$ layers: $L_{j,0} || L_{j,1} \dots || L_{j,m-t}$ and $L_{j,0} = h''_{j,1} || L''_{j,0} || y_j || S_j$ and $L_{j,t} = h''_{j,t+1} || L''_{j,t}$: $1 \leq t \leq m-t$

For each enhancement layer compute hash down to base layer

For each packet use hashes on their base layers and the y to recover $(h_{1,0}, h_{2,0}, \dots, h_{n,0})$ with use DECS-DE

Compute $H = H(h_{1,0}, h_{2,0}, \dots, h_{n,0} || G_{id} || S_{id})$
 Recover signature by computing DECS-DE(s_1, s_2, \dots, s_n)
 $= (\alpha_1, \alpha_2, \dots, \alpha_k)$

Then verify the signature with public key, otherwise drop the packet.

VI. CONCLUSION

In the proposed diagram n bundles in gathering were needy to each other. The Tornado code has no effect on security, however it essentially ensures all the hashes so that the client can even now recoup all hashes confirm the parcel regardless of harming. In the late works calculation time through estimation of ECC subject to defer yet with Tornado code calculation overhead decline.

REFERENCES

- [1] H. Deng, Xuhua Ding and Swee-Won Lo, "Efficient authentication and access control of scalable multimedia streams over packet-lossy networks", SECURITY AND COMMUNICATION NETWORKS Security, Wiley Online Library, 2013
- [2] K. Mokhtarian and M. Hefeeda, "End-to-end secure delivery of scalable video streams", Proc. Int. Workshop Network and Operating Systems Support for Digital Audio and Video (NOSSDAV'09), pp. 79-84, 2009
- [3] JPEG 2000 image coding system (ISO 154447) 2004.
- [4] Information technology – coding of audio-visual objects (part 1: systems) (ISO/IEC 14496) 1998.
- [5] Schwarz H, Merpe D, Wiegand T. "Overview of the scalable video coding extension of the H.264/AVC standard". IEEE Transactions on Circuits and Systems for Video Technology 2007; 17(9):1103–1120.
- [6] M. Wien, H. Schwarz, and T. Oelbaum. Performance analysis of SVC. IEEE Transactions on Circuits and Systems for Video Technology, September 2007, 17(9):1194–1203.
- [7] H. Schwarz, D. Marpe, and T. Wiegand. "Overview of the scalable video coding extension of the H.264/AVC standard". IEEE Transactions on Circuits and Systems for Video Technology, September 2007, 17(9):1103–1120.
- [8] Park JM, Chong EKP, Siegel HJ. "Efficient multicast stream authentication using erasure codes". ACM Transactions on Information and System Security 2003; 6(2):258–285.
- [9] HABIB, A., XU, D., ATALLAH, M., BHARGAVA, B., AND CHUANG, J. "A tree-based forward digest protocol to verify data integrity in distributed media streaming". IEEE Trans. Knowl. Data Engin. 2005,17, 7, 1010–1014.
- [10] M. Hefeeda and K. Mokhtarian. "Authentication schemes for multimedia streams: Quantitative analysis and comparison". ACM Transactions on Multimedia Computing, Communications and Applications, 2009.
- [11] H. Yu, "Scalable streaming media authentication", Proc. IEEE Int. Conf. Communications (ICC'04), 2004, vol. 4, pp. 1912-1916.
- [12] Z. Wei, Y. Wu, R. H. Deng, and X. Ding. "A hybrid scheme for authenticating scalable video codestreams". IEEE Trans. on Information Forensics and Security, 2014, 9(4):543--553.
- [13] R. Kaced and J. Moissinac, "Multimedia content authentication for proxy-side adaptation," in Proc. Int. Conf. Digital Telecommunications (ICDT'06), Cote d'Azur, France, Aug. 2006.
- [14] Y. Wu and R. Deng, "Scalable authentication of MPEG-4 streams," IEEE Trans. Multimedia, , Feb. 2006, vol. 8, no. 1, pp. 152–161.
- [15] J. Apostolopoulos, "Architectural principles for secure streaming & secure adaptation in the developing scalable video coding (SVC) standard," in Proc. IEEE Int. Conf. Image Processing (ICIP'06), Atlanta, GA, Oct. 2006, pp. 729–732.
- [16] Yi X, Zheng G, Li M, Ma H, Zheng C (2013) "Efficient authentication of scalable media streams over wireless networks" Multimedia tools and applications, Springer Science, 2013.
- [17] <http://www.adweek.com/news/technology/netflix-takes-third-internetbandwidth-136115>
- [18] http://www.youtube.com/t/press_statistics

Women Learning in Creative Project Based Learning of Engineering Education

Jui-Hsuan Hung, Jeng-Yi Tzeng

Abstract—Engineering education in the higher education is always male dominated. Therefore, women learning in this environment is an important research topic for feminists, gender researchers and engineering education researchers, especially in the era of Gender Mainstreaming. The research topics are from the dialectical discussion of feminism and science development history, gender issues of science education, to the subject choice of female students. These researches enrich the field of gender study in engineering education but lack of describing the detailed images of women in engineering education, including their learning, obstacles, needs or feelings. Otherwise, in order to keep up with the industrial trends of emphasizing group collaboration, engineering education turns from traditional lecture to creative group inquiry pedagogy in recent years. Creative project based learning is one of the creative group inquiry pedagogy which the engineering education in higher education adopts often and it is seen as a gender-inclusive pedagogy in engineering education. Therefore, in order to understanding the real situation of women learning in engineering education, this study took place in a course (Introduction to Engineering) offered by the school of engineering of a university in Taiwan. This course is designed for freshman students to establish basic understanding engineering from four departments (Chemical Engineering, Power Mechanical Engineering, Materials science, Industrial Engineering and Engineering Management). One section of this course is to build a Hydraulic Robot designed by the department of Power Mechanical Engineering. 321 students in the school of engineering took this course and all had the reflection questionnaire. These students are divided into groups of 5 members to work on this project. The videos of process of discussion of five volunteered groups with different gender composition are analyzed and six women of these five groups are interviewed. We are still on the process of coding and analyzing videos and the qualitative data, but several tentative findings have already emerged. (1)The activity models of groups of both genders are gender segregation, and not like women, men never be the ‘assistants’. (2) The culture of the group is developed by the major gender but men always dominate the process of practice in all kinds of gender composition groups. (3)Project based learning is supposed to be a gender-inclusive learning model in creative engineering education but communication obstacles between men and women makes it less women friendly. (4)Gender identity, not professional identity, is adopted by these women while they interact with men in their groups. (5)Gender composition and project based learning pedagogy are not the key factors for women learning in engineering education, but the gender conscience awareness is.

Keywords—Engineering education, gender education, creative project based learning, women learning

J. H. Hung is with Center for Teacher Education, National Tsing –Hua University, Taiwan (e-amil: rashine0518@gmail.com)

J. Y. Tzeng is with Center for Teacher Education, National Tsing –Hua University, Taiwan.

CertifHy: Developing a European Framework for the Generation of Guarantees of Origin for Green Hydrogen

Frederic Barth¹, Wouter Vanhoudt^{*}, Marc Londo, Jaap C. Jansen², Karine Veum², Javier Castro³, Klaus Nürnberger³ and Matthias Altmann⁴

¹ *Hinicio SA, RUE DES PALAIS 44, B-1030 Brussels, Belgium*

² *Sticchting Energieonderzoek Centrum Nederland, WESTERDUINWEG 3, 1755 LE Petten, Netherlands*

³ *Tiv Sud Industrie Service GmbH, WESTENDSTRASSE 199, 80686 Munchen, Germany*

⁴ *Ludwig-Boelkow-Systemtechnik GmbH, Daimlerstr. 15, 85521 Ottoburn Germany*

(*) certifhy@hinicio.com

Hydrogen is expected to play a key role in the transition towards a low-carbon economy, especially within the transport sector, the energy sector and the (petro)chemical industry sector. However, the production and use of hydrogen only make sense if the production and transportation are carried out with minimal impact on natural resources, and if greenhouse gas emissions are reduced in comparison to conventional hydrogen or conventional fuels. The CertifHy project, supported by a wide range of key European industry leaders (gas companies, chemical industry, energy utilities, green hydrogen technology developers and automobile manufacturers, as well as other leading industrial players) therefore aims to: 1. Define a widely acceptable definition of green hydrogen. 2. Determine how a robust Guarantee of Origin (GoO) scheme for green hydrogen should be designed and implemented throughout the EU. It is divided into the following work packages (WPs). 1. Generic market outlook for green hydrogen: Evidence of existing industrial markets and the potential development of new energy related markets for green hydrogen in the EU, overview of the segments and their future trends, drivers and market outlook (WP1). 2. Definition of "green" hydrogen: step-by-step consultation approach leading to a consensus on the definition of green hydrogen within the EU (WP2). 3. Review of existing platforms and interactions between existing GoO and green hydrogen: Lessons learnt and mapping of interactions (WP3). 4. Definition of a framework of guarantees of origin for "green" hydrogen: Technical specifications, rules and obligations for the GoO, impact analysis (WP4). 5. Roadmap for the implementation of an EU-wide GoO scheme for green hydrogen: the project implementation plan will be presented to the FCH JU and the European Commission as the key outcome of the project and shared with stakeholders before finalisation (WP5 and 6). Definition of Green Hydrogen: CertifHy Green hydrogen is hydrogen from renewable sources that is also CertifHy Low-GHG-emissions hydrogen. Hydrogen from renewable sources is hydrogen belonging to the share of production equal to the share of renewable energy sources (as defined in the EU RES directive) in energy consumption for hydrogen production, excluding ancillary functions. CertifHy Low-GHG hydrogen is hydrogen with emissions lower than the defined CertifHy Low-GHG-emissions threshold, i.e. 36.4 gCO₂eq/MJ, produced in a plant where the average emissions intensity of the non-CertifHy Low-GHG hydrogen production (based on an LCA approach), since sign-up or in the past 12 months, does not exceed the emissions intensity of the benchmark process (SMR of natural gas), i.e. 91.0 gCO₂eq/MJ.

CertifHy – European-wide Guarantee of Origin Scheme for Green Hydrogen

Hydrogen – and in particular green hydrogen (green H₂) – as well as technologies linked to hydrogen energy, can help Europe become #1 in renewables and reaching EU target of cutting 80%-95% of greenhouse gas emissions (GHG) by 2050. Therefore, the CertifHy Project Consortium develops the first EU-wide framework for the generation of guarantees of origin (GO) for green hydrogen with the financial support of the European Commission¹. Green hydrogen GOs will boost demand and supply of green hydrogen throughout Europe by the creation of a market for green H₂. It will allow to keep the benefit of green H₂ where it is not produced through decoupling the molecule from the green attribute. This way it is improving the business case for green H₂ as producers will be able to sell the attribute (GO) to consumers willing to pay a premium. We will discuss the roadmap for the implementation of a European-wide framework for green hydrogen in the workshop on 17th June 2016 at the Crowne Plaza hotel in Brussels (from 11 am to 4.15 pm) with key stakeholders from all energy sectors and policy makers. A well-established and transparent market of green hydrogen will uniquely contribute to the realization of Europe's energy transition objectives by decarbonizing the transport sector and energy-intensive industry and enhancing renewable energy use.

Background

The objectives of the CertifHy project are to define a widely acceptable definition of green hydrogen, design a robust GO scheme and propose a roadmap to implement the initiative throughout the EU. The project consortium consisting of Hincio, Energy Research Centre of the Netherland (ECN), Ludwig Bölkow Systemtechnik (DE) and TÜV SÜD designs a framework for a guarantee of origin for green hydrogen within a step-by-step consultation process for European-wide usage of green hydrogen.

A new market for Green Hydrogen

Hydrogen is used in large quantities as chemical feedstock in various industrial applications (including refineries) and could play an important role in transport as well. Global demand for hydrogen is foreseen to reach 50 Mtons by 2025. The market is predicted to grow globally 3,5% per year. Today most of hydrogen is produced from fossil resources. For hydrogen and its applications to be a climate-friendly alternative to fossil fuels, it is necessary to ensure the emission reduction and minimal impact on natural resources in the whole life cycle including the sustainable production of hydrogen using renewable or low-carbon energy sources. It is estimated that about 17% of all hydrogen produce could originate from renewable and low-carbon sources by 2030, representing a market of about 1.7 million tons. In order to allow green hydrogen to be traded, evidence of the green nature of hydrogen will be necessary. Advantage of the GO scheme is that it can be transferred from one to the other holder which allows the consumption of green hydrogen everywhere in Europe independently from its production place. The GO scheme of green hydrogen provides transparency of the market and empowers consumers. By doing this, it boosts commercialization of renewable and low-carbon hydrogen and creates a market pull for hydrogen from sustainable sources. While some consumers require hydrogen produced by renewable energy, others may be satisfied with a low-carbon product. A single GO system can accommodate both needs and can be established at a moderate cost.

¹ CertifHy is funded by FCH JU (Fuel Cells and Hydrogen Joint Undertaking).

Potential impact of Green Hydrogen

Green hydrogen can contribute to realizing EU energy targets by increasing energy security and increasing energy diversity, decarbonizing a wide range of industries and transport, fostering green growth and sustainability. When green hydrogen is produced from renewable electricity through electrolysis, it enhances energy security and improves environmental sustainability at the same time. With EU agreement on at least 80% GHG cut by 2050 the transport sector requires at least 60% decarbonisation. Green and low-carbon hydrogen help to realize energy transition by decarbonizing sectors whose reducing GHG emissions is otherwise difficult, such as industry, heating and cooling, transport and electricity. In the short-term, green hydrogen could replace hydrogen from Steam Reforming of Natural Gas in refineries, thereby decarbonizing traditional fuels such as diesel and gasoline. In the long-term, hydrogen contributes to energy transition as fuel for fuel cell electric vehicles (FCEV) producing zero emissions.

Last but not least, hydrogen is an energy storage enabler and facilitates the further integration of variable renewable energy sources thanks to the flexibility of electricity-to-hydrogen conversion and to the large energy storage capacity.

Workshop "A roadmap for EU wide guarantees of origin for green hydrogen"

Designing a roadmap for the EU-wide implementation of green hydrogen is an important milestone of the output and future of the CertifHy project. We are discussing the roadmap with industry, associations and policy makers in the workshop 'A roadmap for the introduction of guarantees of origin for green hydrogen'. If you are interested in participating, please register for the workshop via email to Magali.perrault@hinicio.com

When: 17th June 2016, 11am – 4.15pm

Where: Crown Plaza Hotel, Le Palace, Rue Gineste 3, 1210 Bruxelles

Information

For further information, feel free to visit www.certifhy.eu or contact us.

Hinicio

Vanessa Wabitsch

Marketing and Communication Coordinator

✉ vanessa.wabitsch@hinicio.com

☎ +32 22 11 34 11, +32 493 69 04 08

CertifHy – Developing a European Framework for the generation of guarantees of origin for green hydrogen

Definition of Green Hydrogen



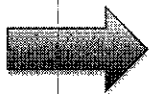
Project supported by the FCH JU



The research leading to these results has received funding from the European Union's Seventh Framework Programme (FP7/2007-2013) for the Fuel Cells and Hydrogen Joint Technology Initiative under grant agreement n° 633107 - Duration: 24 months (Nov 1st 2014 to October 30th 2016)



Agenda



Introduction

- Definition of green hydrogen
 - Criteria for a green H₂ produced by GHG “virtuous” plants
 - Renewable share: definition and illustrations
 - Application of the two GHG thresholds
 - Examples

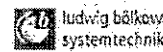
- Q&A

- Objective: Define a widely acceptable definition of green hydrogen; and Determine how an EU wide robust GO scheme should be designed and implemented.

- Consortium



ECN



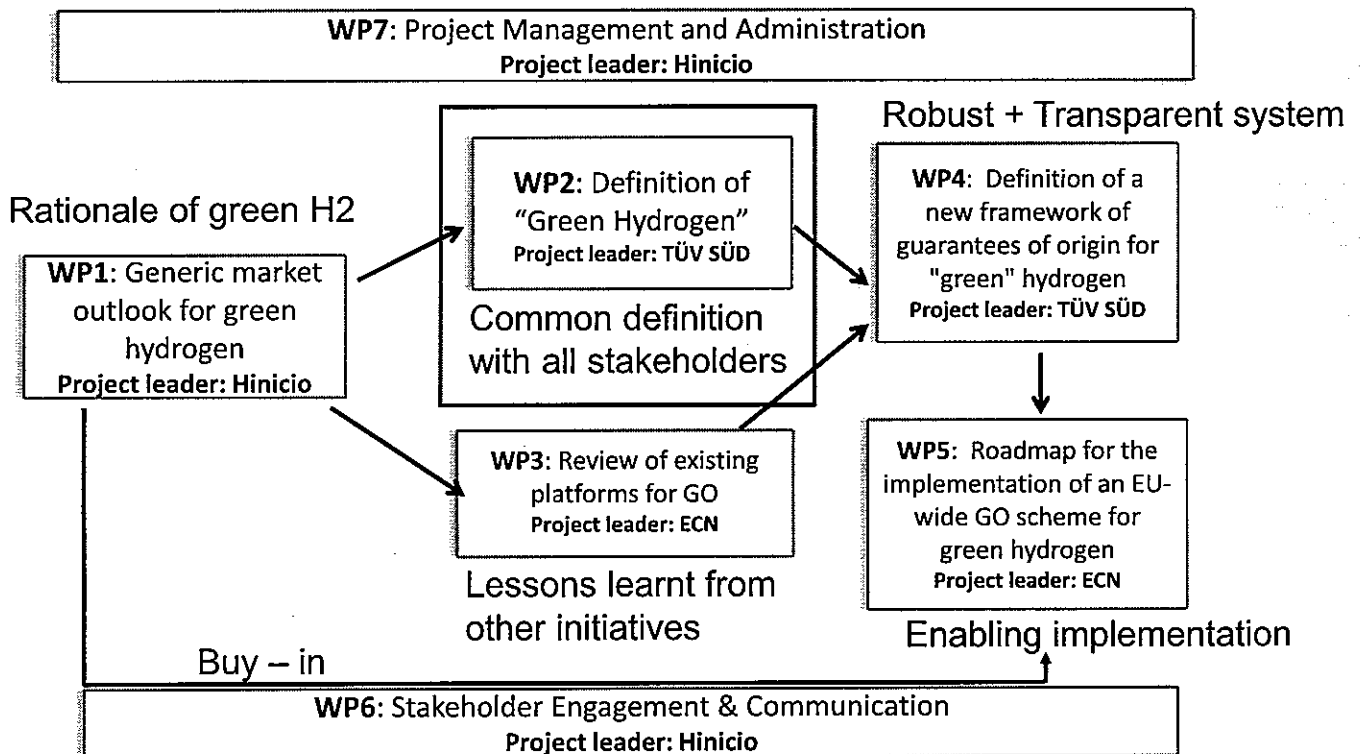
- Affiliated Partners

Step by step consultation process



- Other Partners: Associations, NGO's, Policy Makers,...

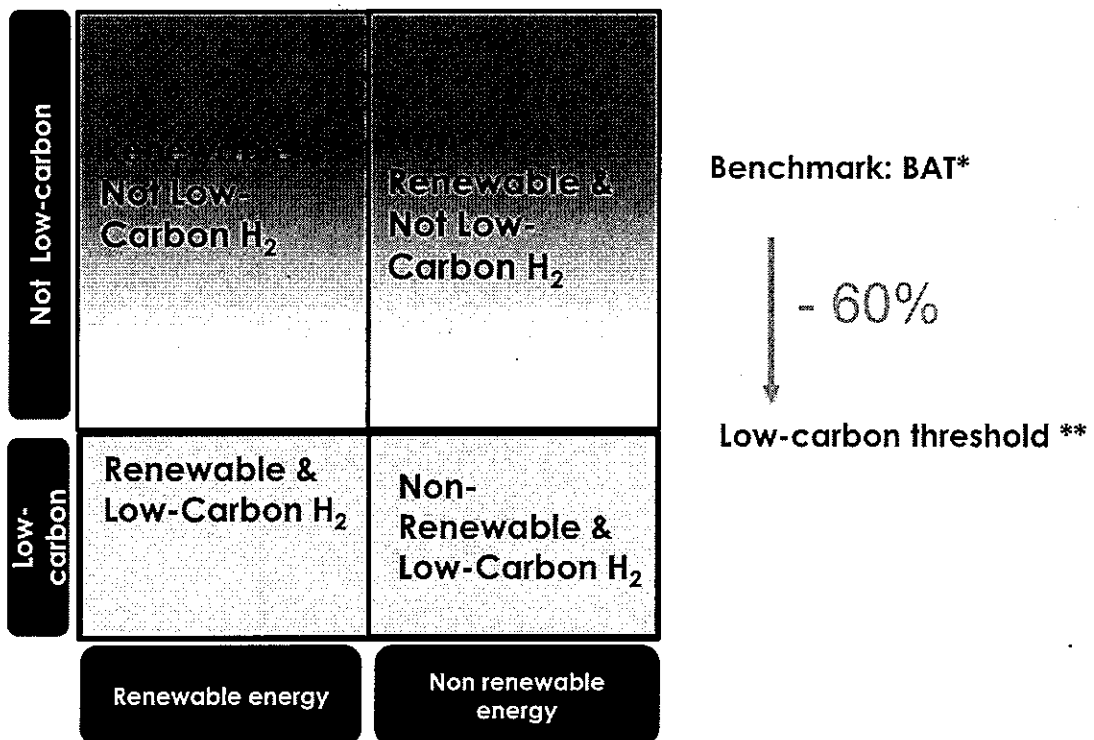
"Supply green H2 where is not produced, improving the business case for green H2"



- Introduction
- Definition of green hydrogen
 - ➔ – Criteria for a green H₂ produced by GHG “virtuous” plants
 - Renewable share: definition and illustrations
 - Application of the two GHG thresholds
 - Examples
- Q&A

5

“Low carbon” defined as a 60% reduction compared to a BAT emission benchmark

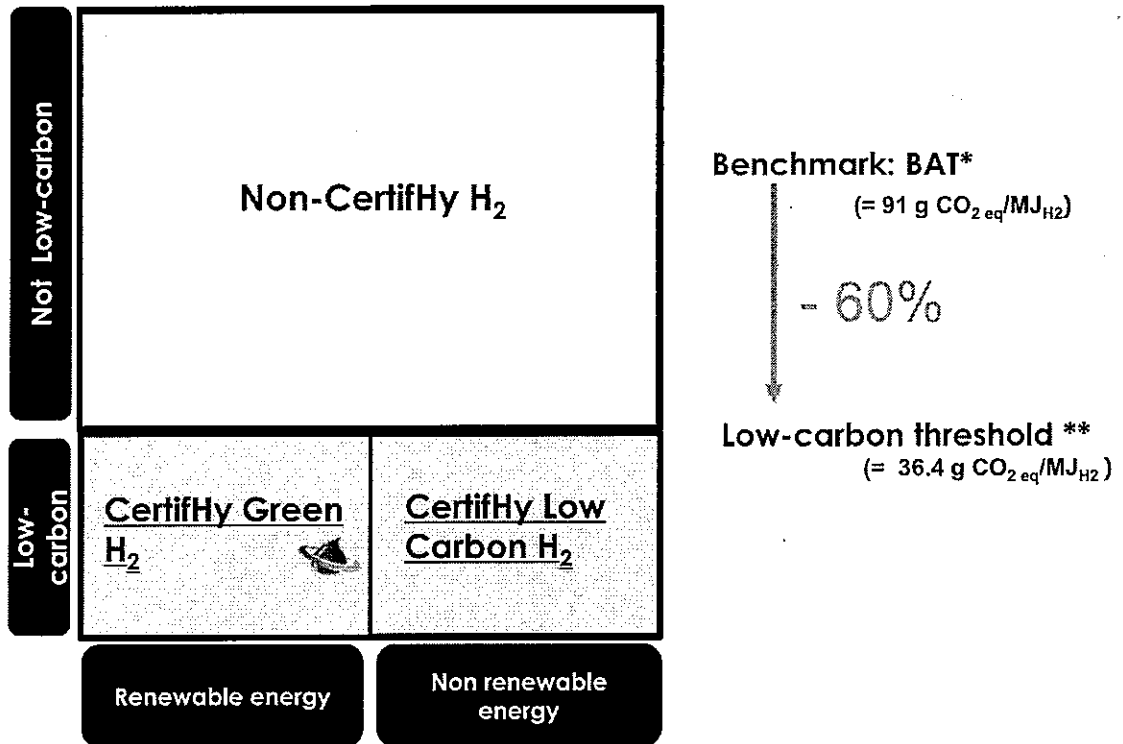


* Best Available Technology = Natural gas steam methane reforming,
= >95% of the provided merchant hydrogen market

** cfr RED reduction requirement for biofuels in 2018

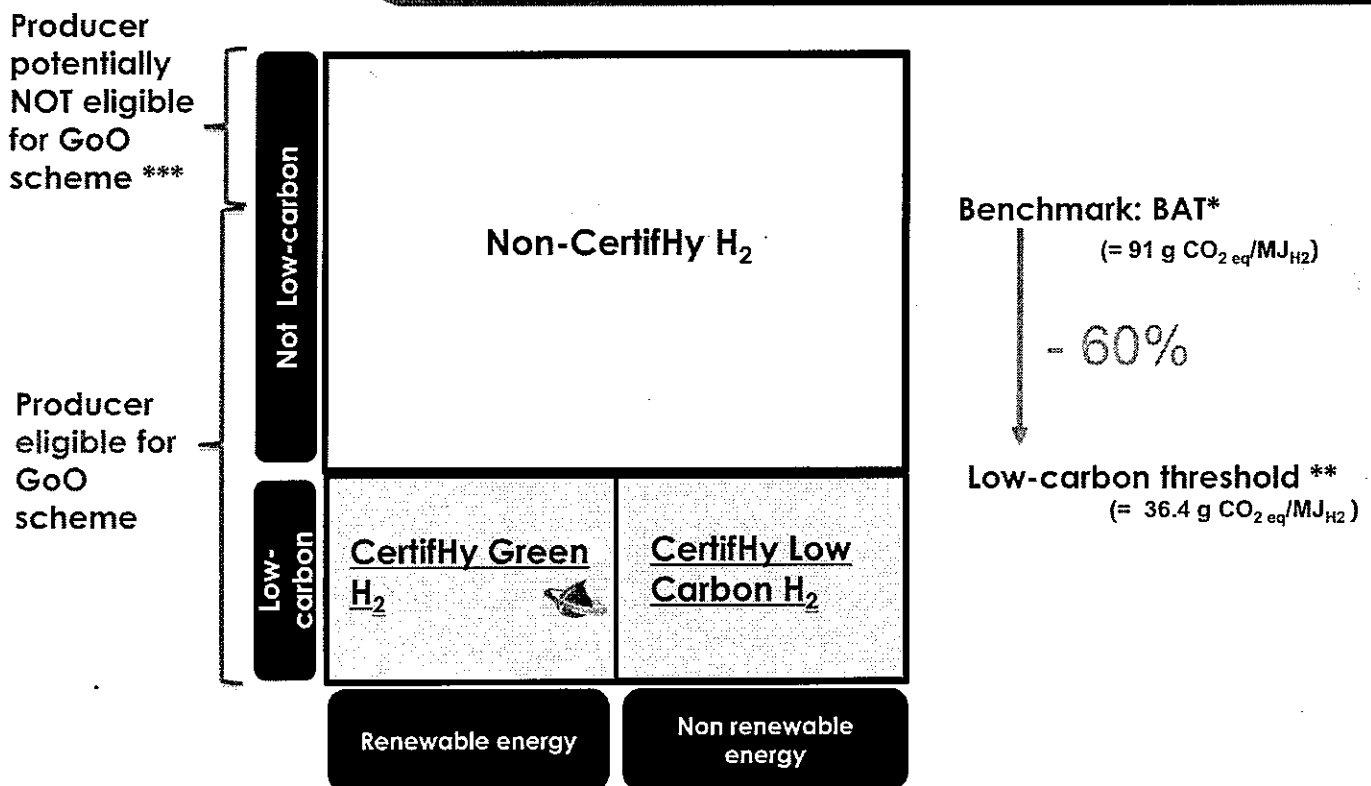
6

As outcome of the consultation process, CertifHy addresses both Renewables and GHG emission targets of hydrogen users

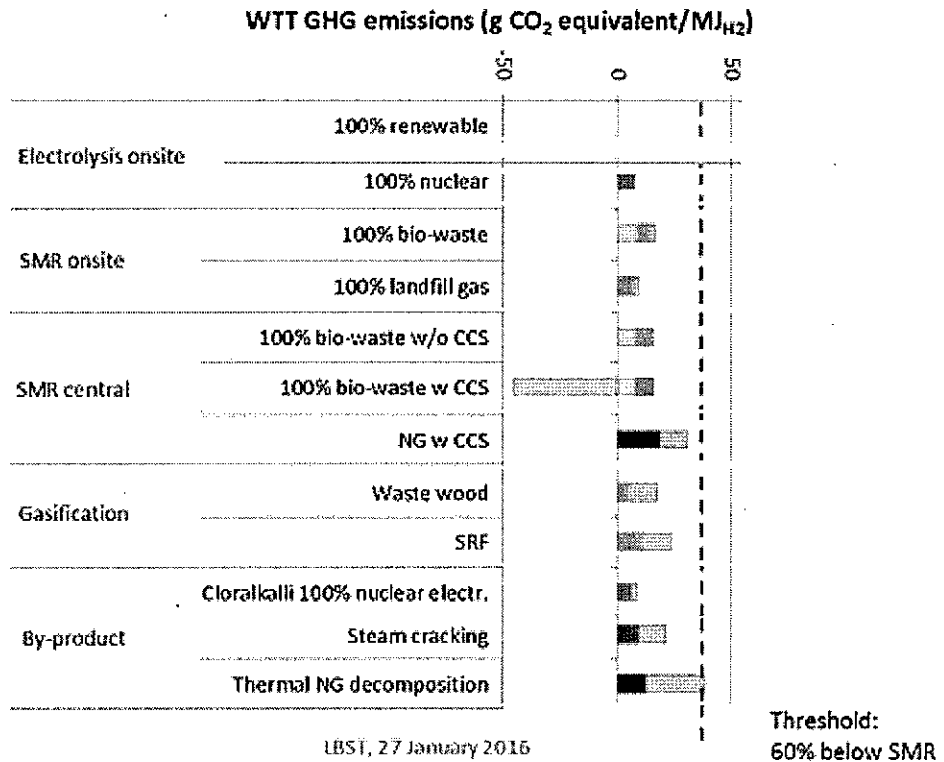
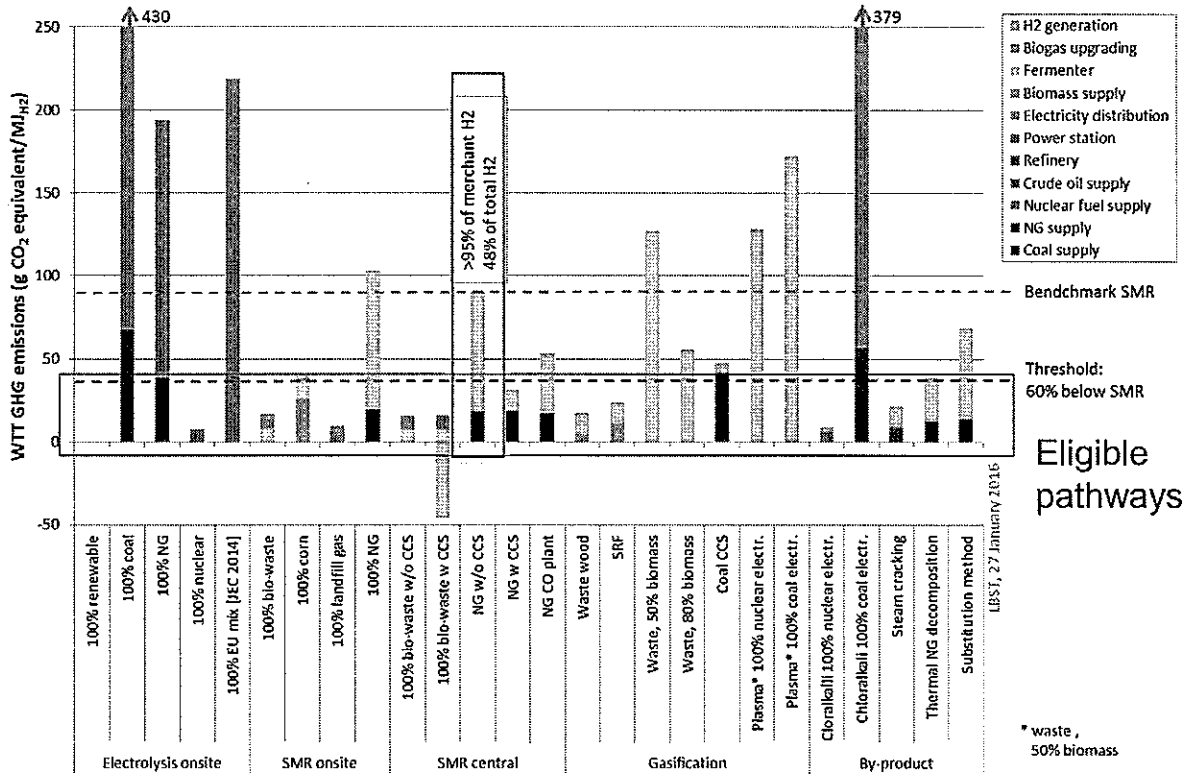


* Best Available Technology = Natural gas steam methane reforming, = >95% of the provided merchant hydrogen market
 ** cfr RED reduction requirement for biofuels in 2018

Excessively high GHG emissions may exclude a plant from participating to the CertifHy GO scheme

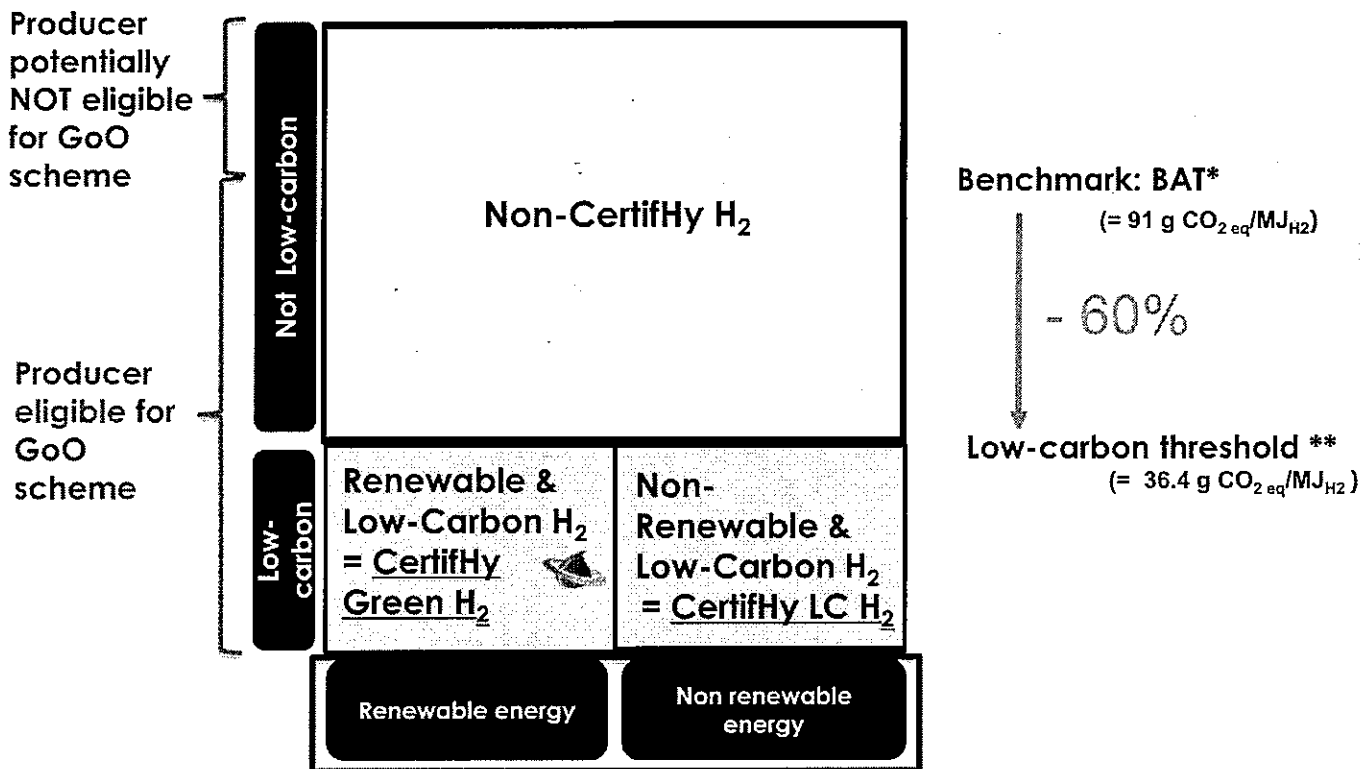


* Best Available Technology = Natural gas steam methane reforming, >95% of the provided merchant H2 market
 ** cfr RED reduction requirement for biofuels in 2018
 *** if GHG content of Non-CertifHy H2 production over the last 12 months is >91gCO2eq/MJ



- Introduction
- Definition of green hydrogen
 - Criteria for a green H₂ produced by GHG “virtuous” plants
 - ➔ – Renewable share: definition and illustrations
 - Application of the two GHG thresholds
 - Examples
- Q&A

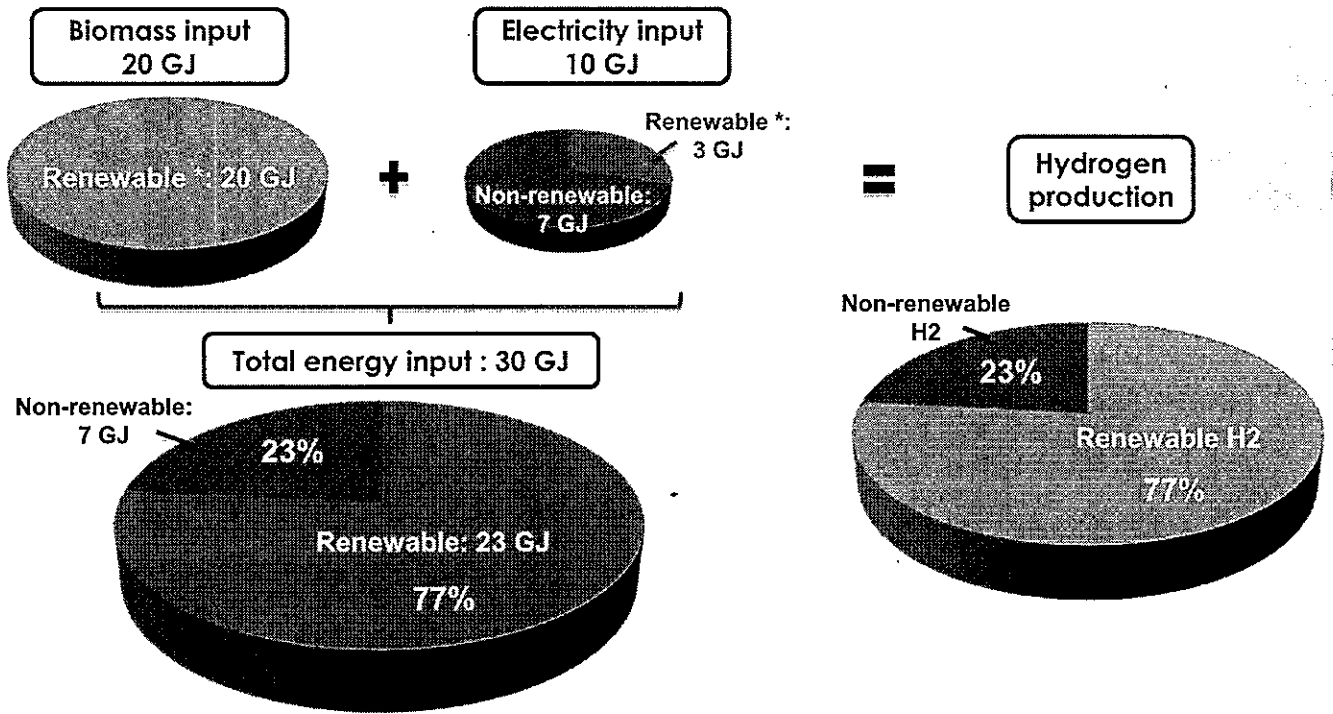
Need to define the amount of Renewable Hydrogen produced by a process using multiple energy inputs



* Best Available Technology = Natural gas steam methane reforming, = >95% of the provided merchant hydrogen market

** cfr RED reduction requirement for biofuels in 2018

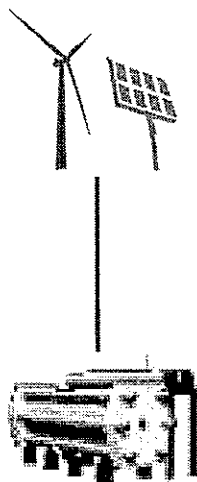
Renewable hydrogen will be as green as the energy used for its production



* Via GO or direct feedstock

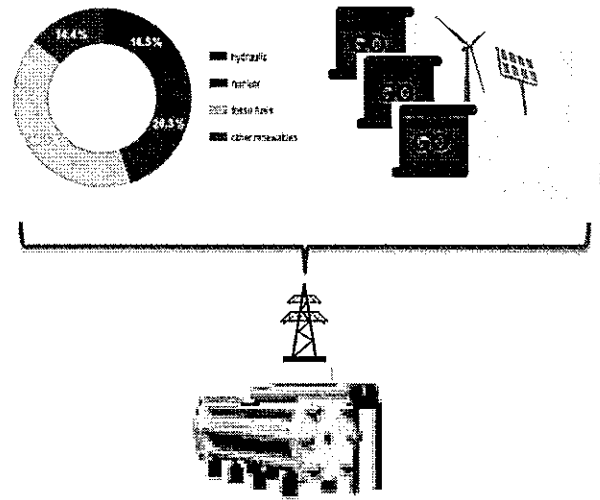
Renewable hydrogen will be as green as the energy used for its production - example Electrolysis

Electrolysis – Direct Connection with Renewable Energy



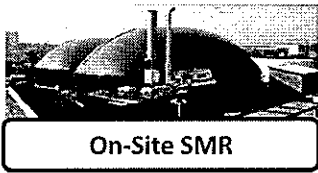
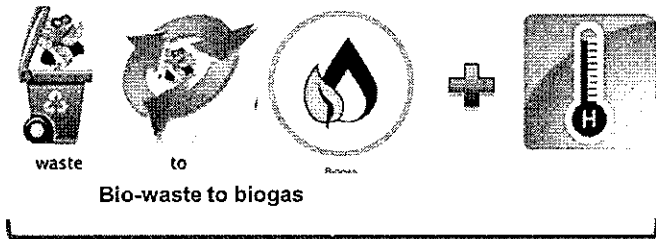
Input	Output
100% Renewable Wind, PV, ..	100% Renewable H2

Electrolysis – Grid Connected: EU mix + RE



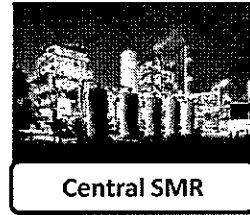
Input	Output
60% Renewable (Wind, PV, Green elec GoO...)	60% Renewable H2
40% EU Mix	

Biogas from bio-waste with non-renewable heat



Input	Output
81% biowaste	81% renewable H2
19% non renewable heat	

Bio-methane from biowaste and Natural Gas

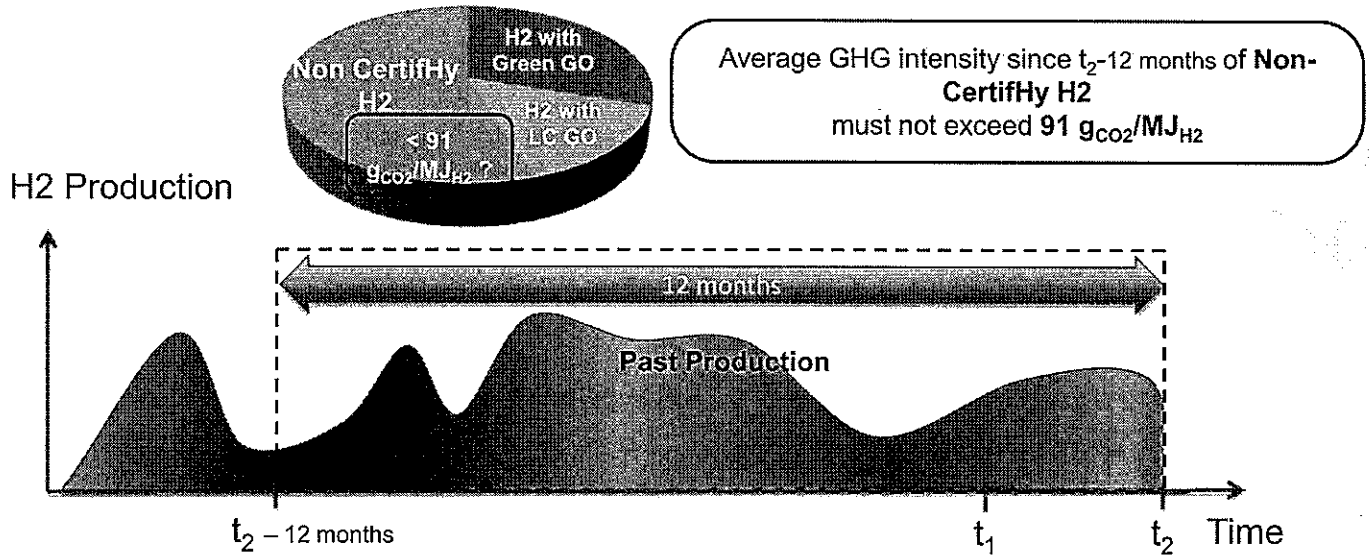


Input	Output
60% bio-methane from bio-waste	60% renewable H2
40% natural gas	

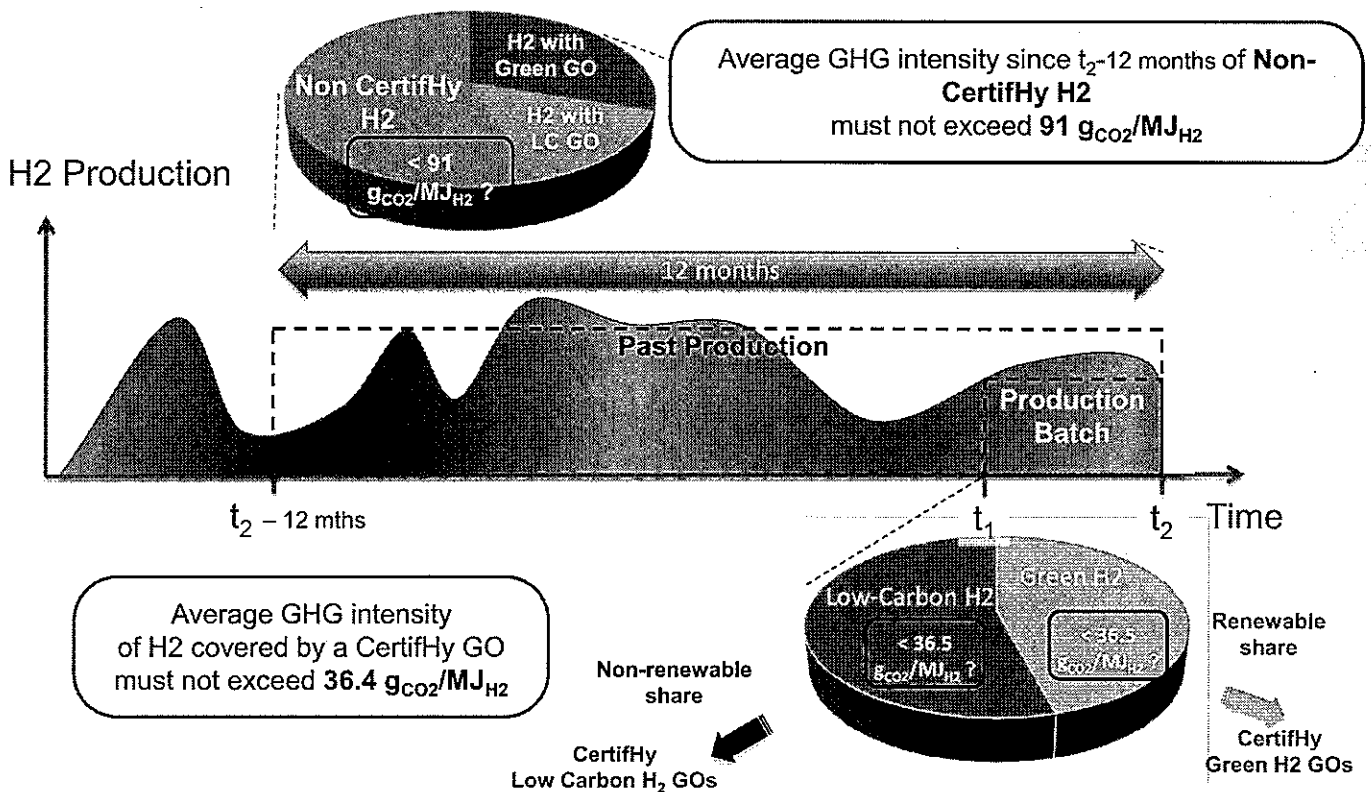
- Introduction
- Definition of green hydrogen
 - Criteria for a green H2 produced by GHG “virtuous” plants
 - Renewable share: definition and illustrations
 - ➔ – Application of the two GHG thresholds
 - Examples

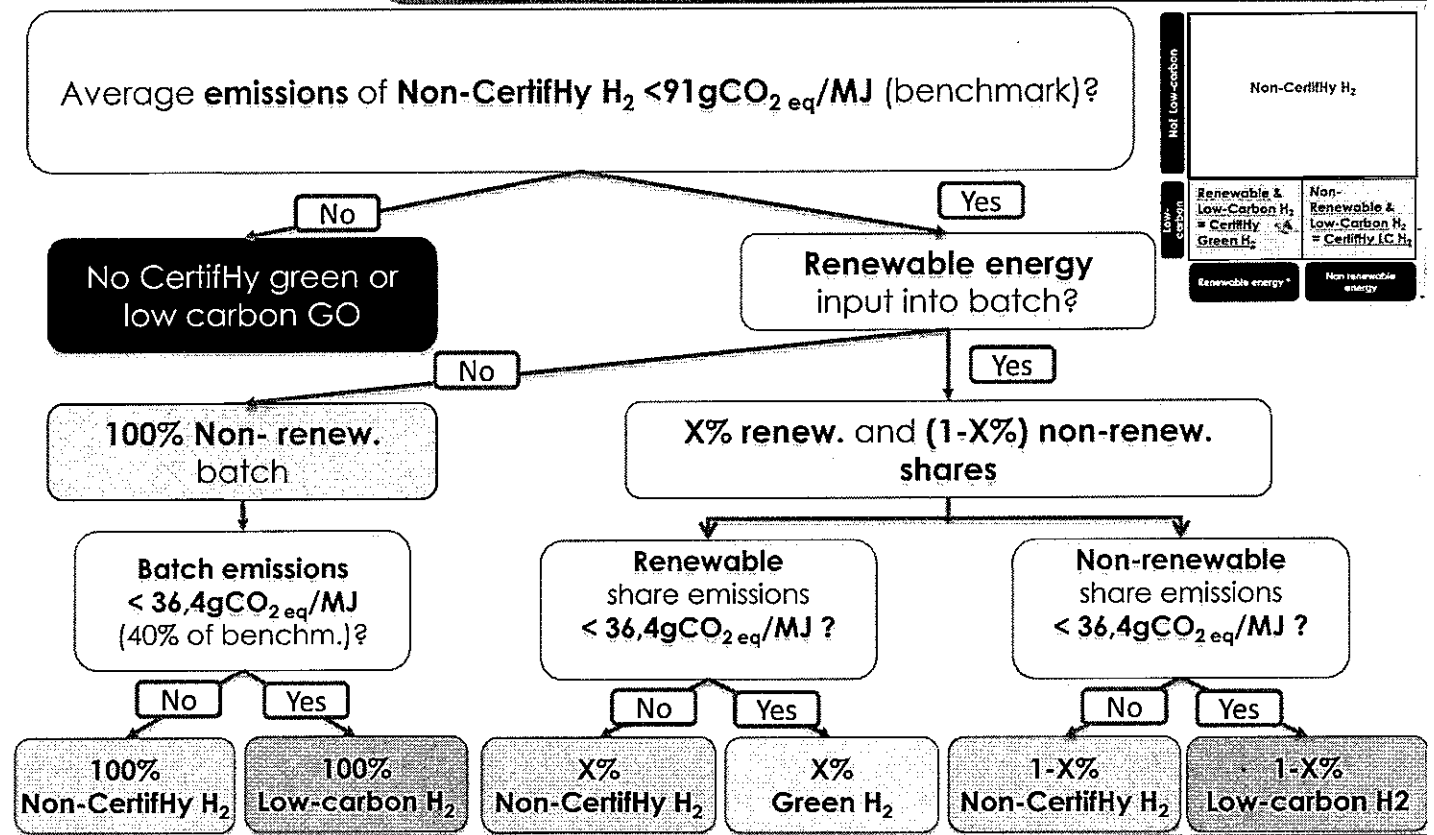
- Annexes

Application of Benchmark threshold on Past Production of the Hydrogen Plant



At the batch level, hydrogen needs to be Low Carbon for producing CertifHy Green or Low-Carbon GOs

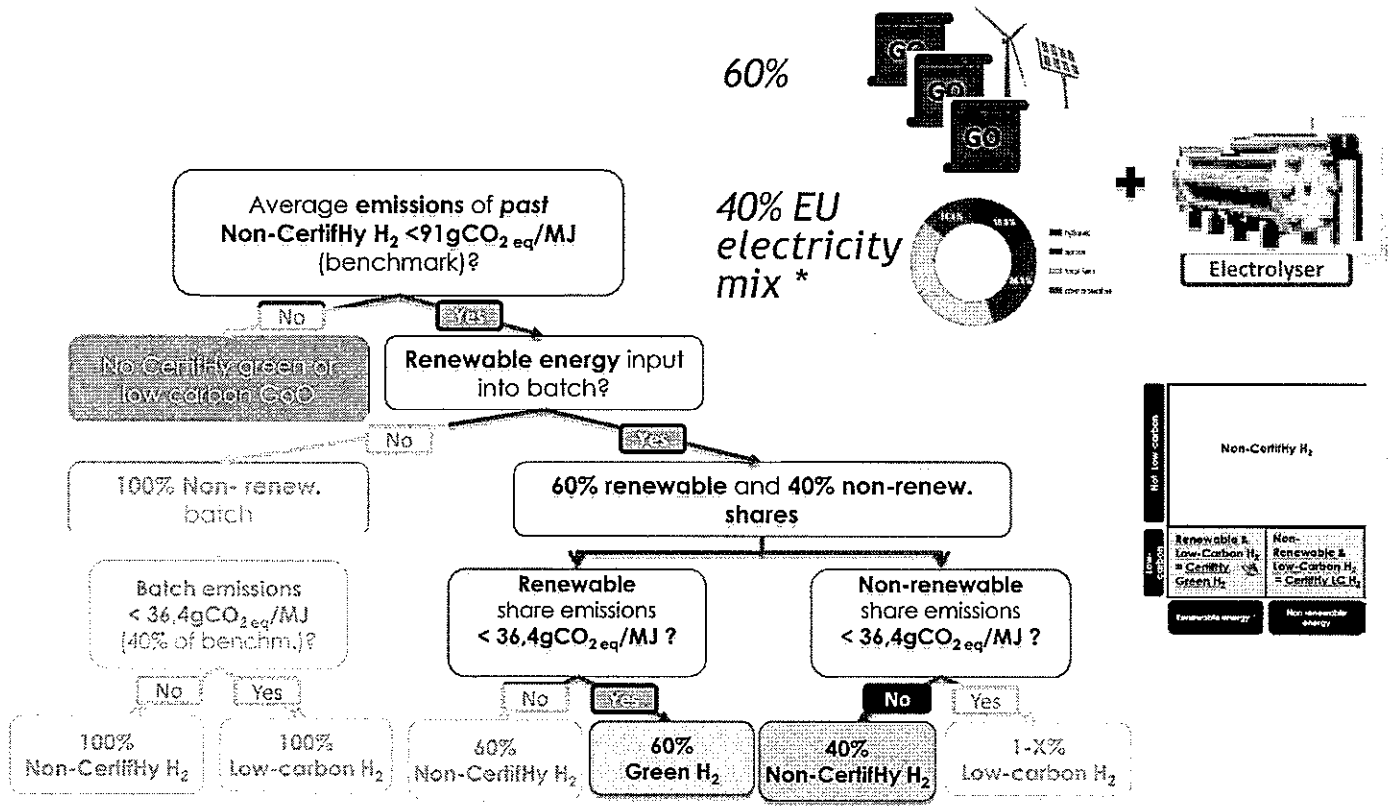




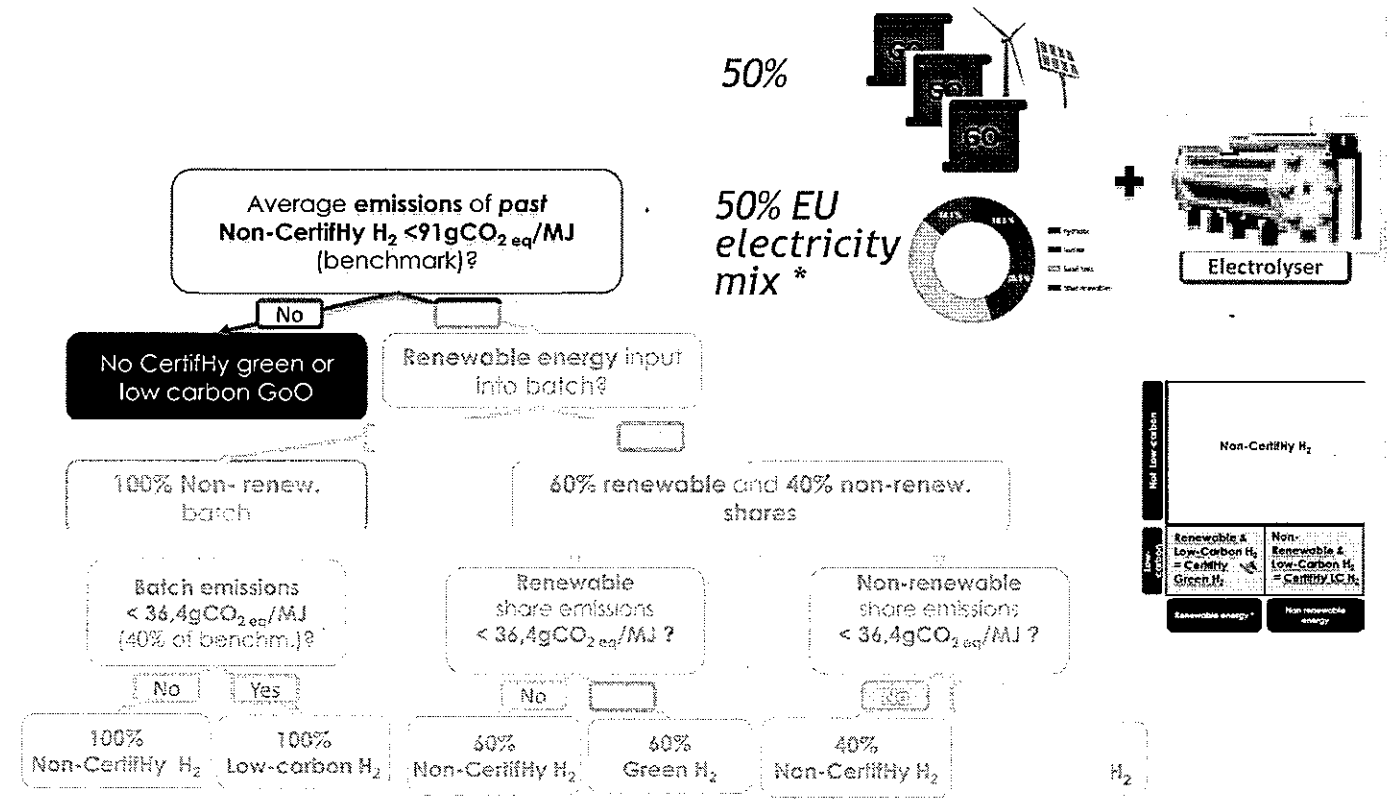
19

- Introduction
- Definition of green hydrogen
 - Criteria for a green H₂ produced by GHG “virtuous” plants
 - Renewable share: definition and illustrations
 - Application of the two GHG thresholds
 - Examples
- ➔
- Benefits expected of green H₂ GoO
- Q&A

20



* GHG content as disclosed by electricity supplier's mix



* GHG content as disclosed by electricity supplier's mix

Depending on the non-renewable energy source used, a minimum amount of Renewable Energy may be needed to keep GHG intensity of non-CertifHy H2 of the plant below benchmark

Carbon intensity (gCO₂/MJH₂) of "Non-CertifHy H2" in function of the electricity mix used

Without inclusion of a renewable share	With inclusion of a renewable share						
	0%	10%	...	50%	60%	70%	80%
EU Mix	217,1				86,8	65,1	43,4
Coal	423,7						84,7
Natural gas	191,5				76,6	57,5	38,3
Nuclear	7,5	7,5	6,8	...	3,8	3,0	2,3
Specific mix	50,0	50,0	45,0	...	25,0	20,0	15,0

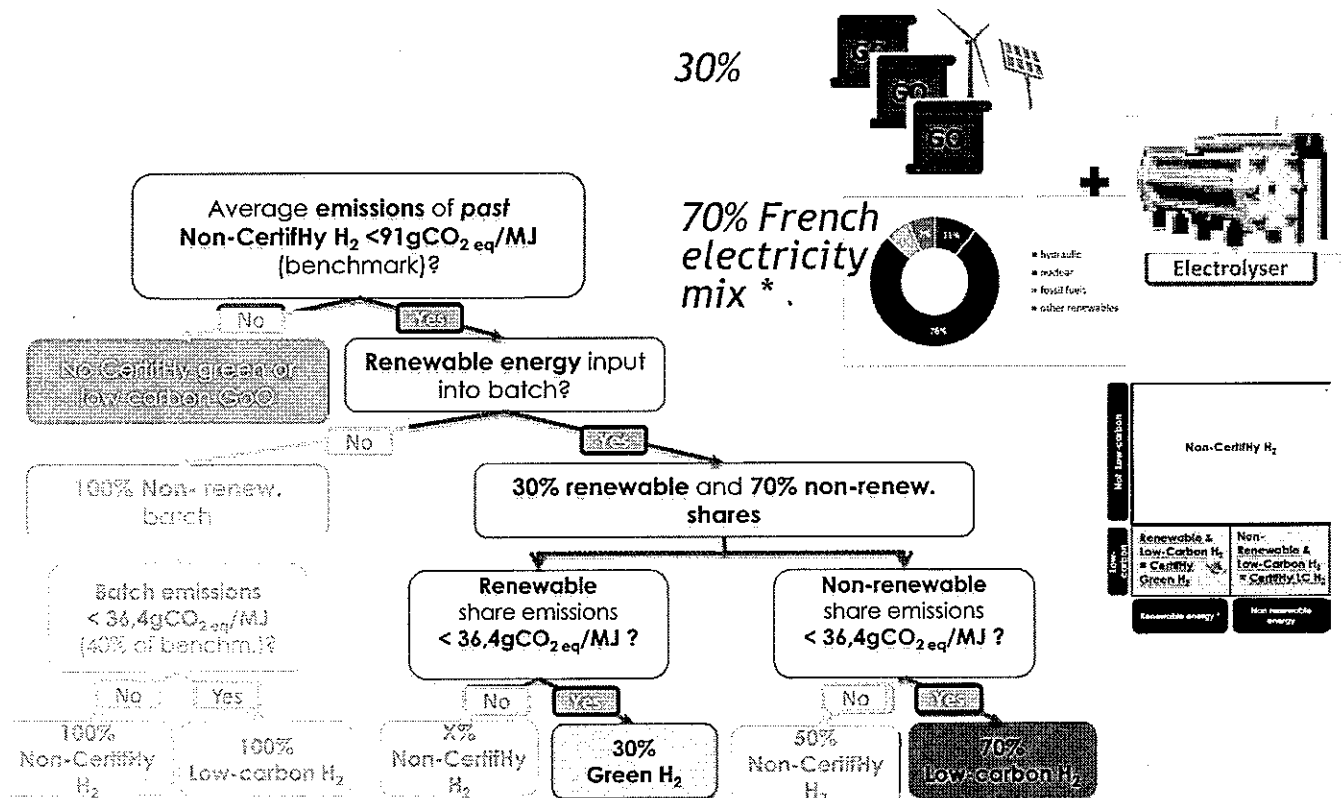
Red : facility is NOT allowed to produce H2 with a CertifHy GoO

Minimum renewable share required in Non-CertifHy H2 for maintaining eligibility to produce CertifHy H2

Non-renew. origin	emissions (gCO ₂ /MJ _{H2})	Min. renewable share required
EU Mix	217,1	58,1%
Coal	423,7	78,5%
Natural gas	191,5	52,5%
Nuclear	7,5	0,0%
Specific mix	50,0	0,0%

Note: PV and Wind are assumed to have zero GHG intensity

CertifHy Green hydrogen process example - electrolysis (3/5)

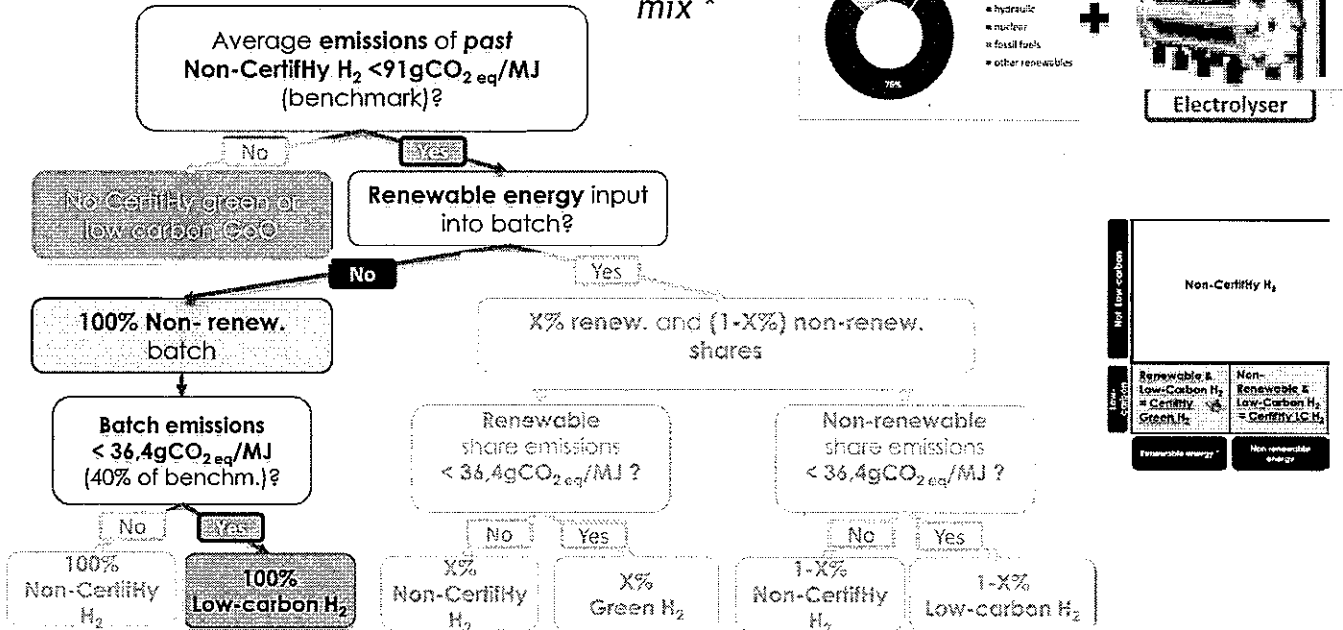
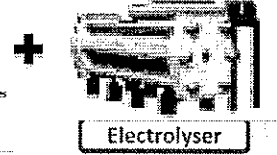


* GHG content as disclosed by electricity supplier's mix

100% French electricity mix *



- hydro
- nuclear
- fossil fuels
- other renewables

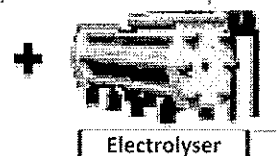


* GHG content as disclosed by electricity supplier's mix

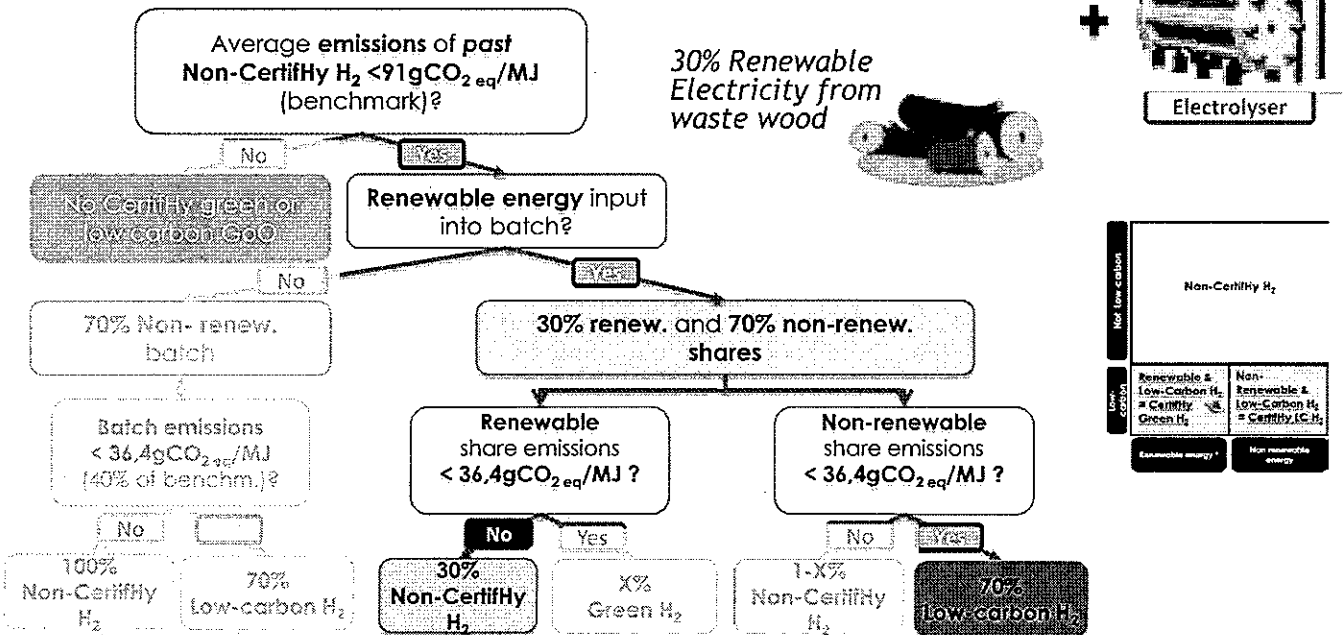
70% French electricity mix *



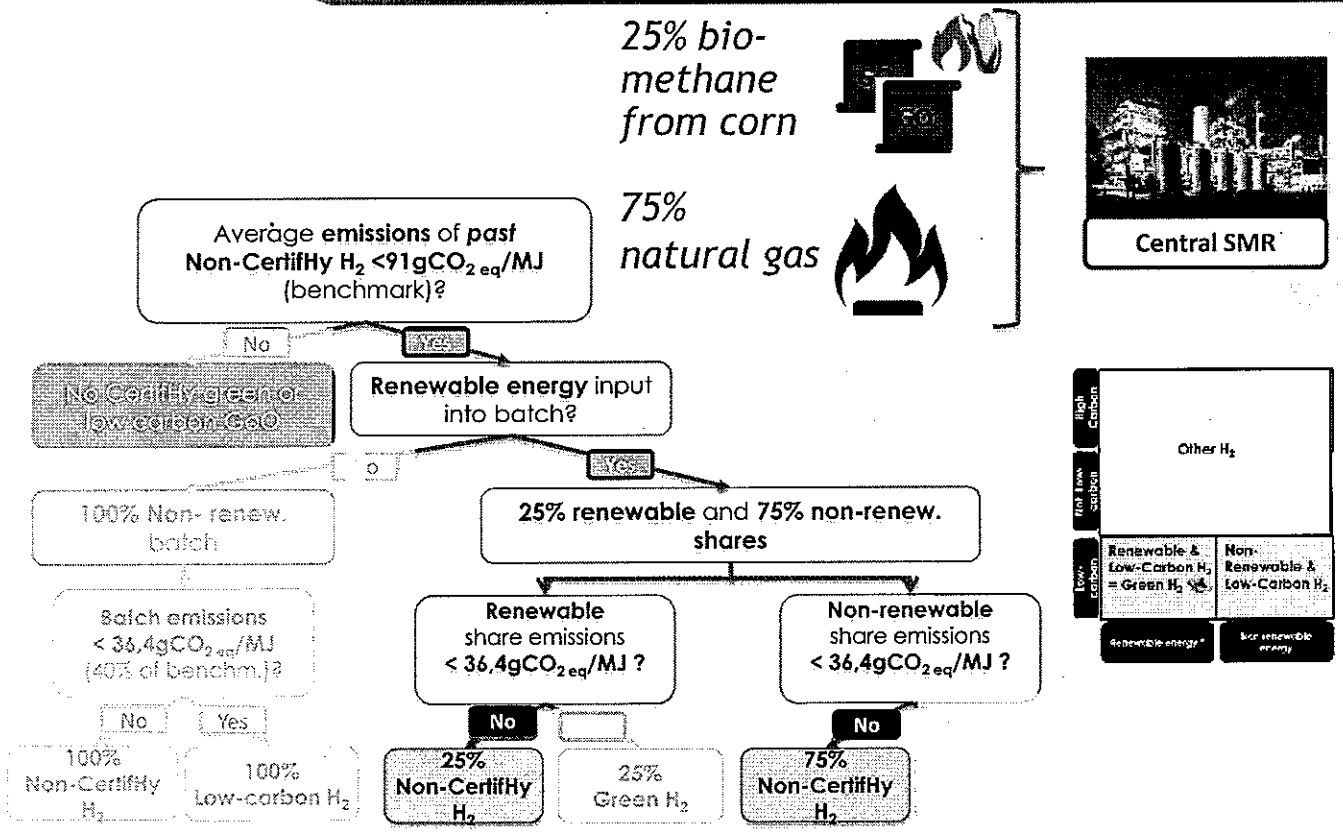
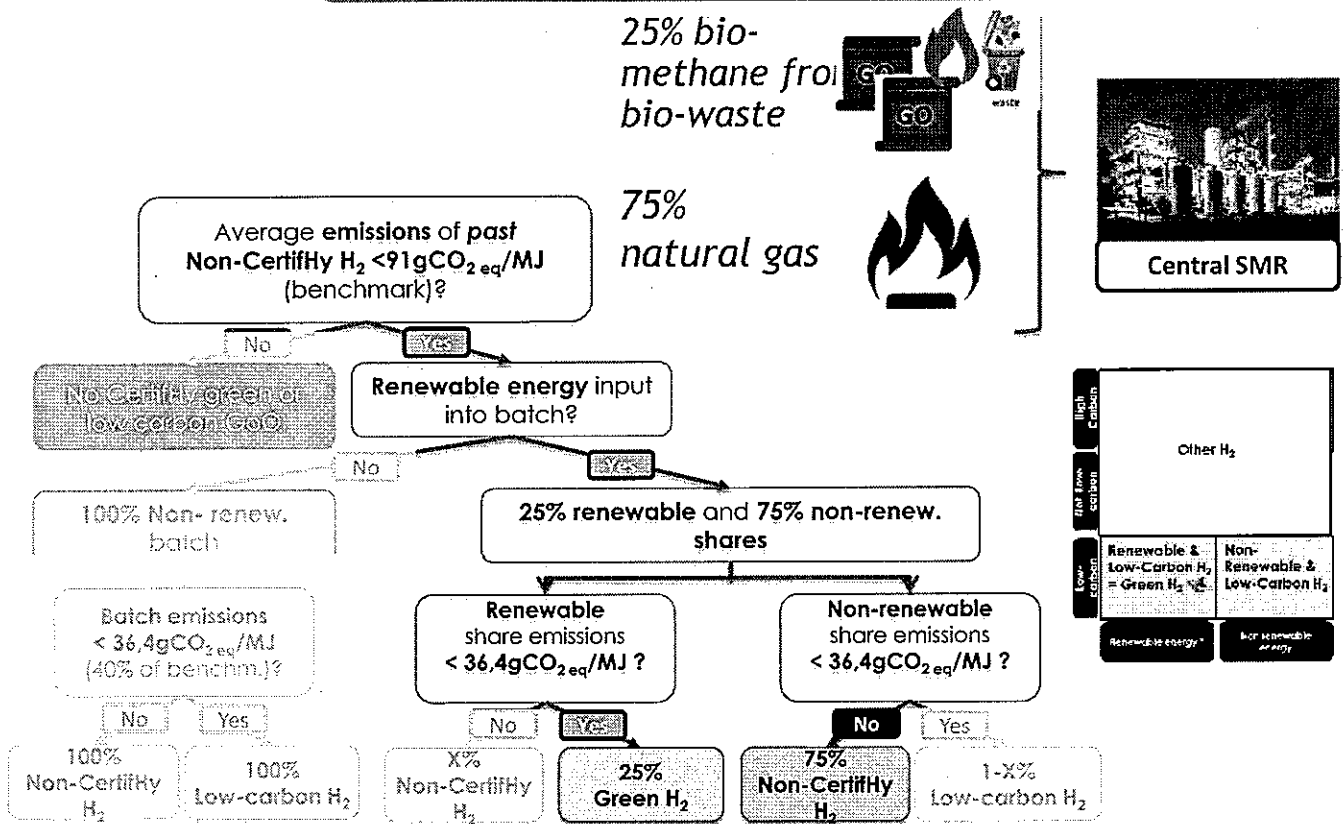
- hydro
- nuclear
- fossil fuels
- other renewables

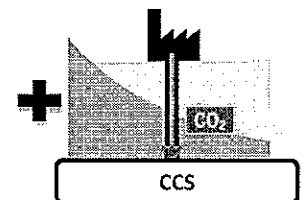
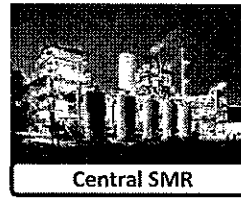


30% Renewable Electricity from waste wood

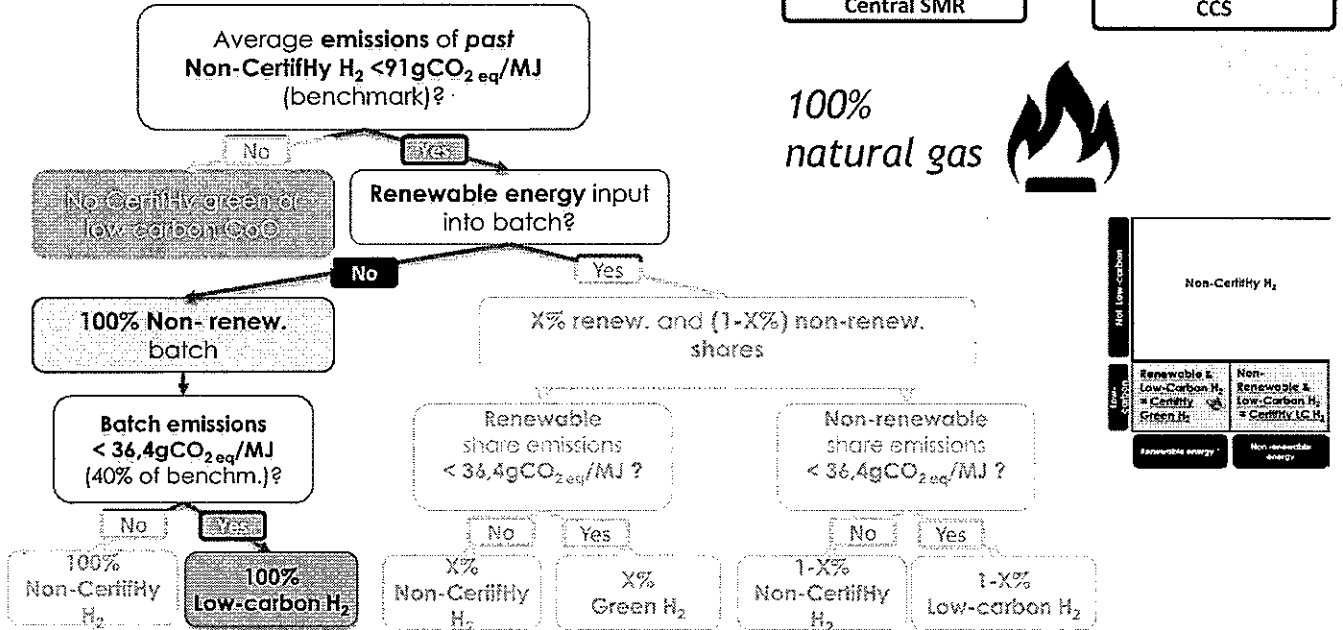


* GHG content as disclosed by electricity supplier's mix





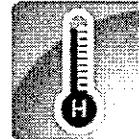
100% natural gas



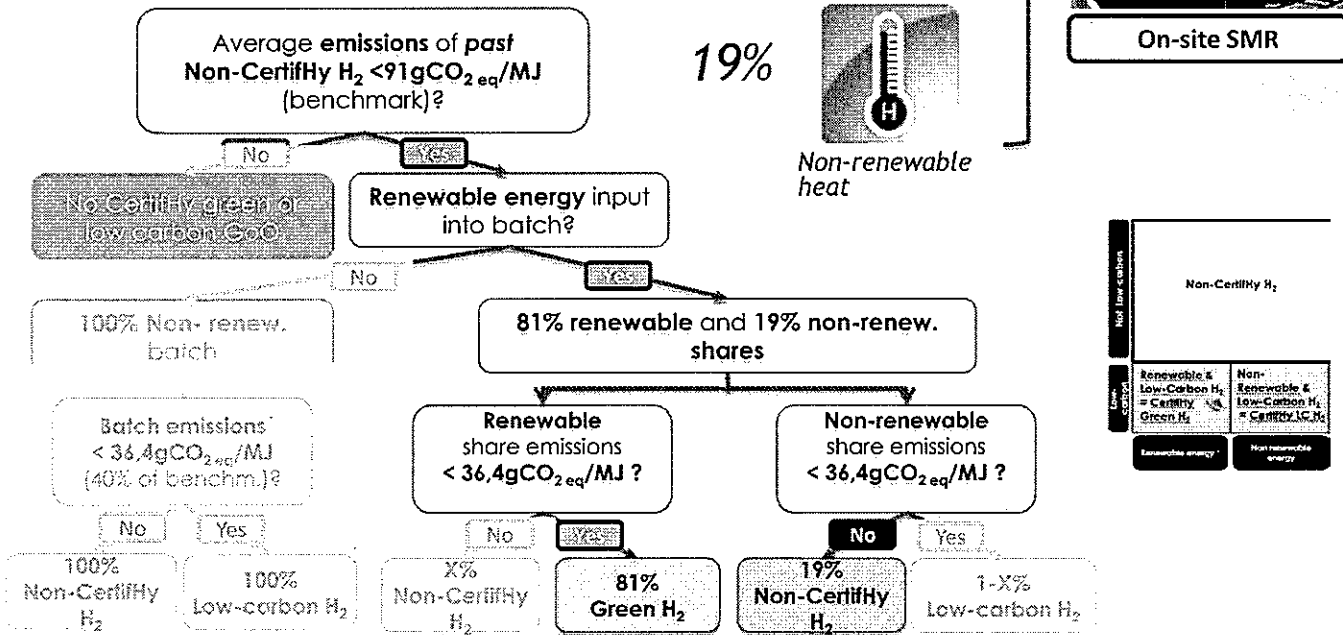
81%

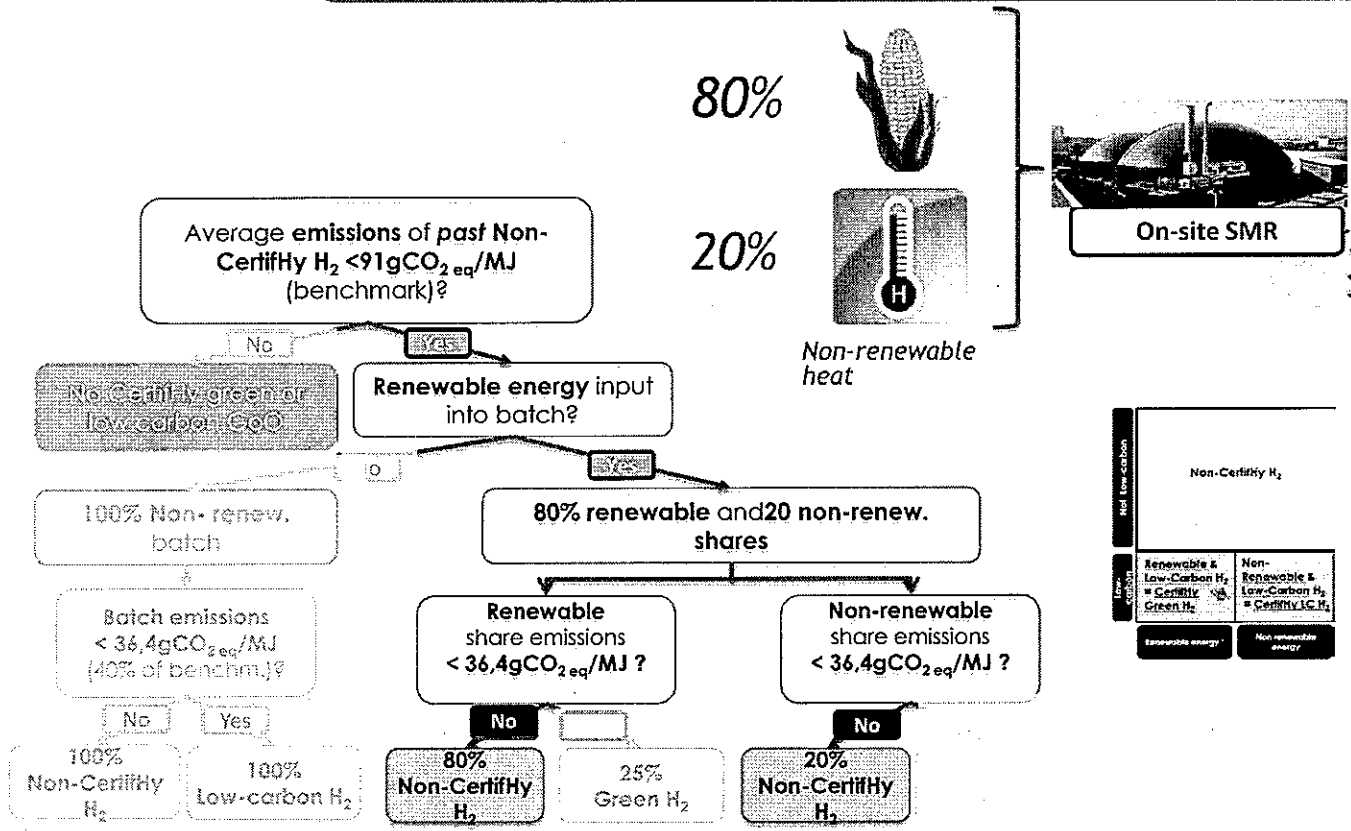


19%



Non-renewable heat





Q&A

Judging Restoration Success of Kamisaigo River Japan

Authors : Rita Lopa, Yukihiro Shimatani

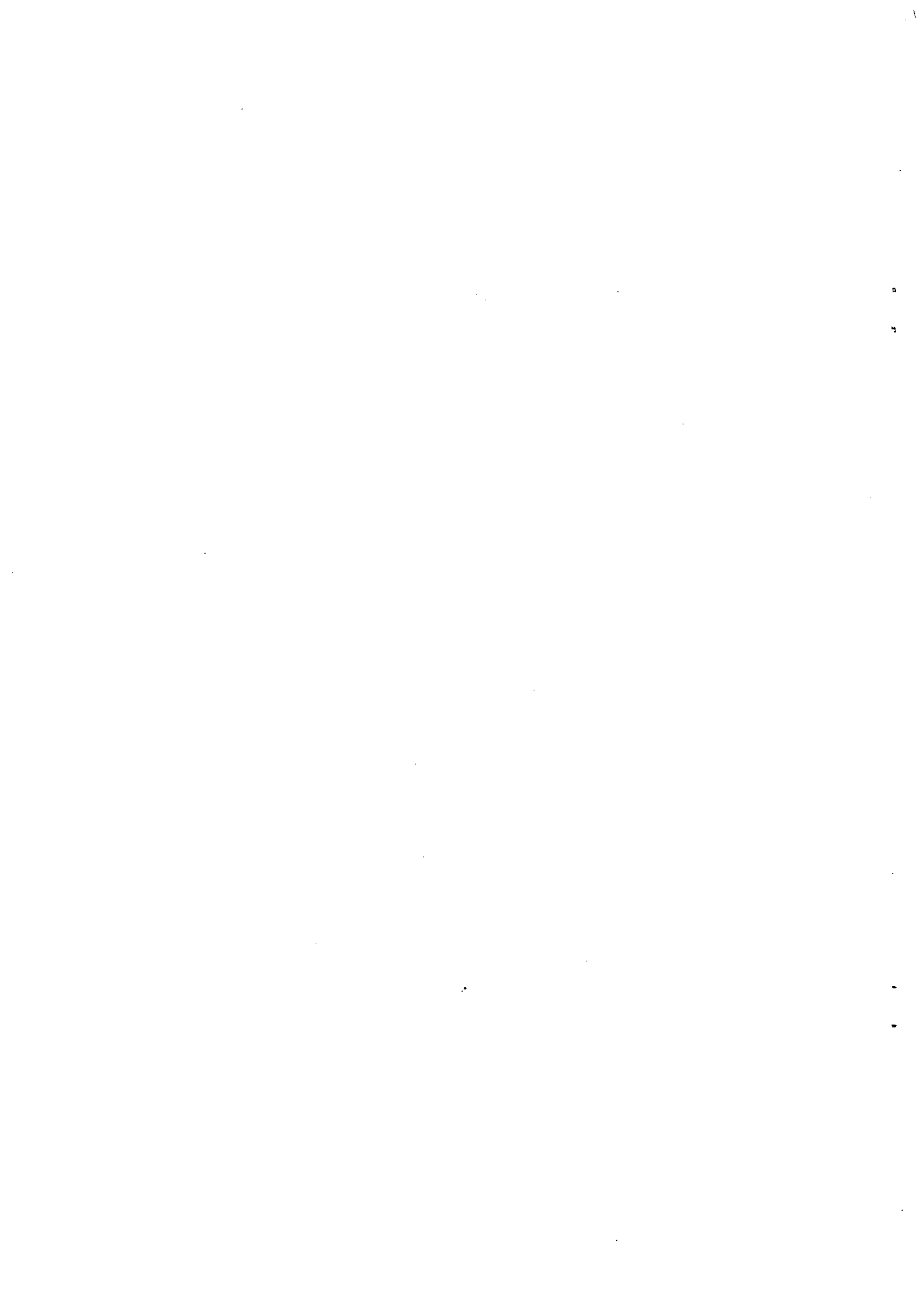
Abstract : The focus of this research is 880m extension development along the Kamisaigo River. The river is flowing tributary of grade 2 rivers Fukutsu City, Fukuoka Prefecture. This river is a small-scale urban river and the river was formerly a straight concrete sea wall construction. The river runs through National Highway No. 3 from the confluence of Saigo River. The study covers the river basin about 326 ha with a catchment area of 20.63 ha and 4,700 m³ capacity regulating pond. The river is not wide, shallow, and has a straight alignment with active (un-vegetated) river channel sinuosity (ratio of river length to valley length) ranging between 1 and 1.3. However, the alignment of the low-flow river channel does have meandering or sinuous characteristics. Flooding is likely to occur. It has become difficult to live in the environment for organisms of the river. Hydrophilic is very low (children cannot play). There is little connection with the local community. Overall, the Kamisaigo River watershed is heavily urbanized and from a morphological, biological and habitat perspective, Kamisaigo River functions marginally not well. For river improvement and maintenance of the Kamisaigo River, the workshop was conducted in the form of planning for the proposed model is presented by the Watershed Management Laboratory. This workshop showed the relationship between citizens, City Government, and University of mutual trust has been established, that have been made landscape, environment, usage, etc.: retaining wall maintenance, hydrophilic zone, landscape zone, nature walks zone: adjacent medical facilities and adjacent to large commercial facilities. Propose of Nature walks zone with point of the design: provide slope that the wheelchair can access and walking paths to enjoy the scenery, and summary of the Kamisaigo River workshop: creating a multi-model study and creation of natural rivers.

Keywords : river restoration, river improvement, natural rivers, Saigo River

Conference Title : ICCEE 2016 : 18th International Conference on Civil and Environmental Engineering

Conference Location : Tokyo, Japan

Conference Dates : September 05-06, 2016




Stream restoration project in Kamisaigo river



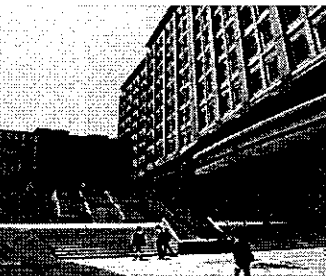
Hironori Hayashi

Department of Geography
Kyushu University

Location of the project site

 KYUSHU UNIVERSITY

About Kyushu University
Research
Schools, Institutes and Faculties
International
Admissions
Campus Life
Alumni
Hospital
Library and Museum



HOME ENGLISH CHINESE KOREAN JAPANESE

Search

News & Topics

- Statement by the IUPUI Council to Jo
- Faculty of Education Research Center
- Kyushu University Wins Researcher's
- Initiative from the members of the
- Institute of Southern Cross University

YouTube

Information and Advisories related to the Great East Japan Earthquake

For International Students & Researchers

Degree Programs in English The NOW to Campus

Map and Contact Us Newsletter Press Release

Kyushu University

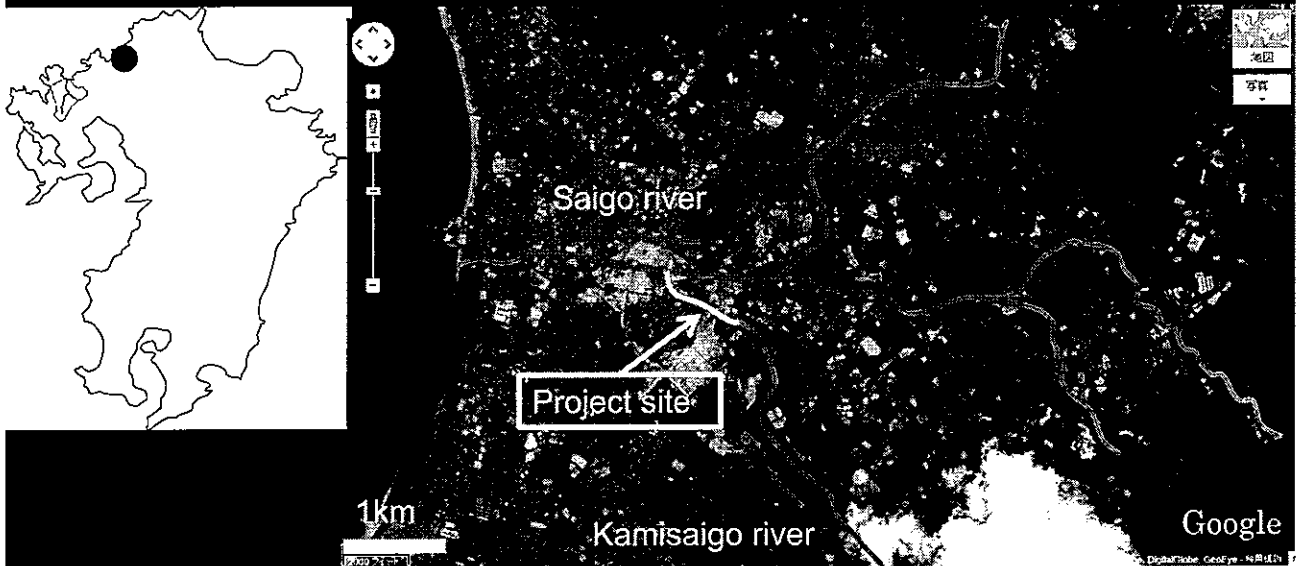


Kyushu Island

Tokyo



Kamisaigo river restoration project



- Kamisaigo river runs through small sized city.

Aerial view around the project site



Kamisaigo river runs through the urbanized area

Issues of the project site



Issues of the project site

- Residents were suffering from floods.
- No vegetation, no fishes, no insects...

- The environment of the project site was not good for residents and aquatic organisms.
- Relationship between residents and river had been disappeared.

Objects of this restoration project

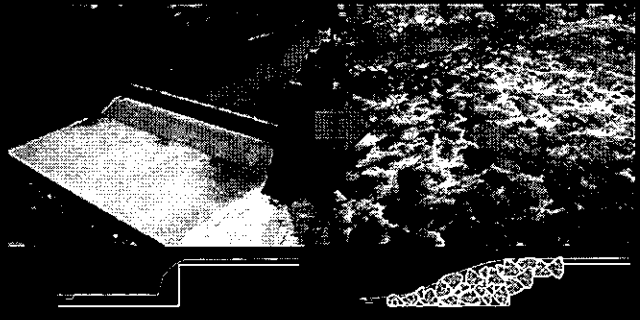
- Flood control
- To restore river environment
- To restore a relationship between river and residents

Design directions

○ Remove concrete revetments



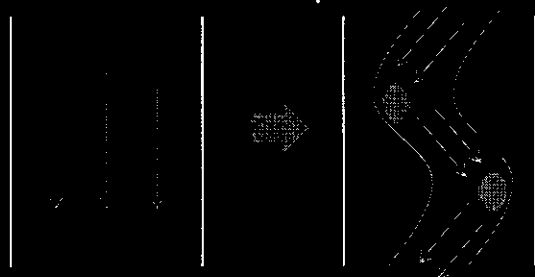
○ Dam removal to restore longitudinal connectivity



○ Broaden out the river width as twice as before to prevent flood

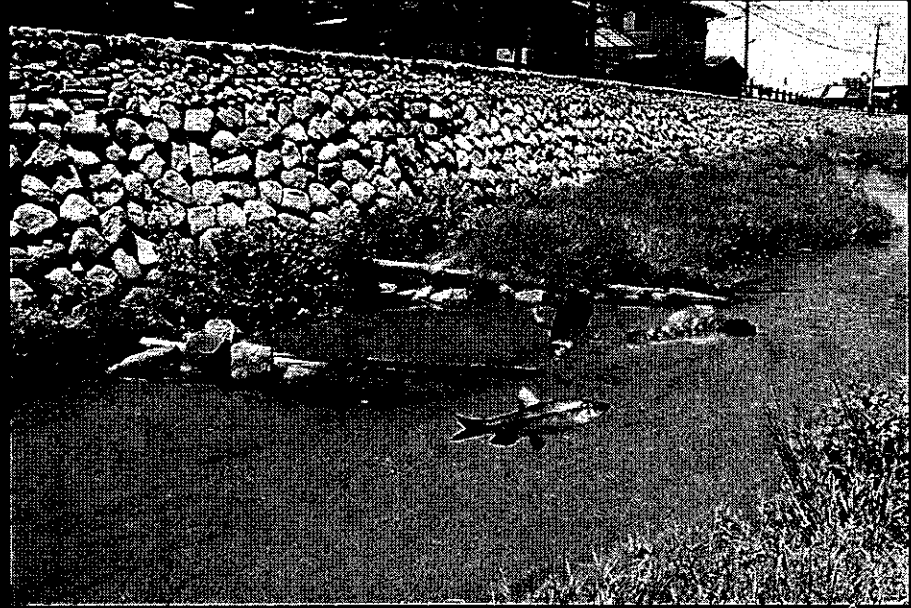


○ Rehabilitate riffle and pool habitats



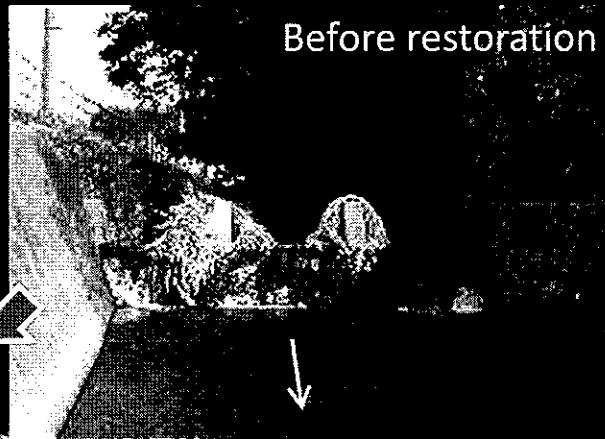
Installed techniques to restore riffle and pool habitat

Log structure



Installed techniques to restore longitudinal connectivity

Rock weir

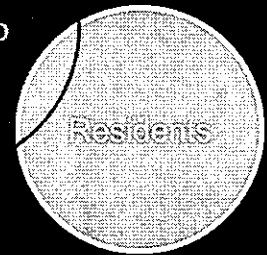


Consensus building with residents

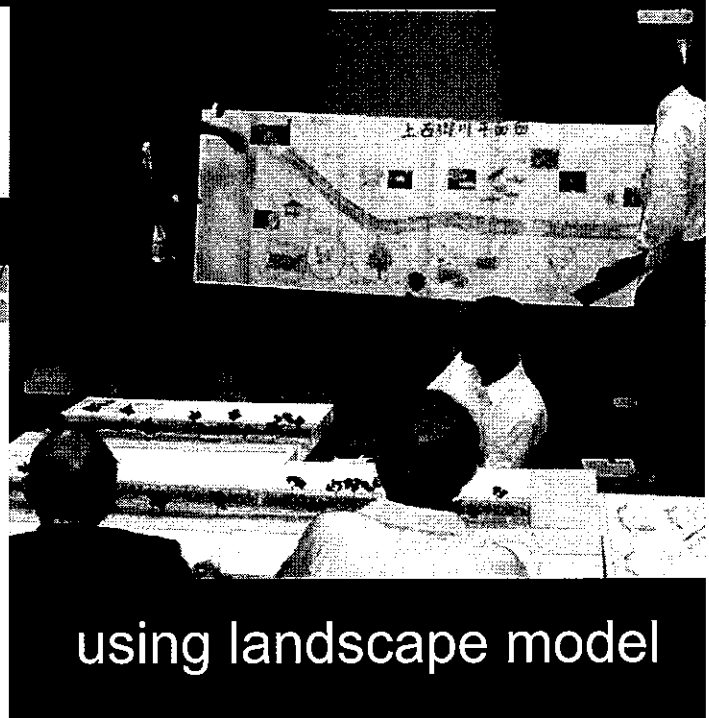
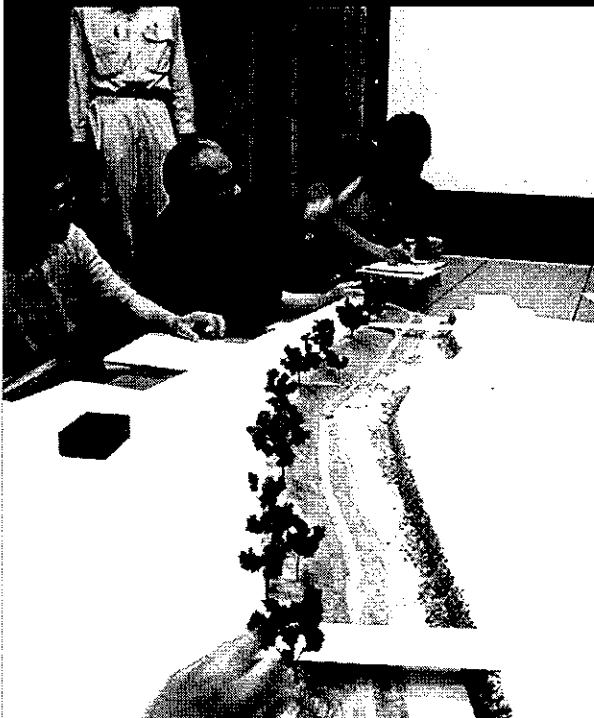
- We conducted workshops with residents over 40 times in past five years to make a consensus about river restoration plan and to make a river maintenance plan .



Workshop



Workshop to discuss restoration plan



Consensus has been made successfully

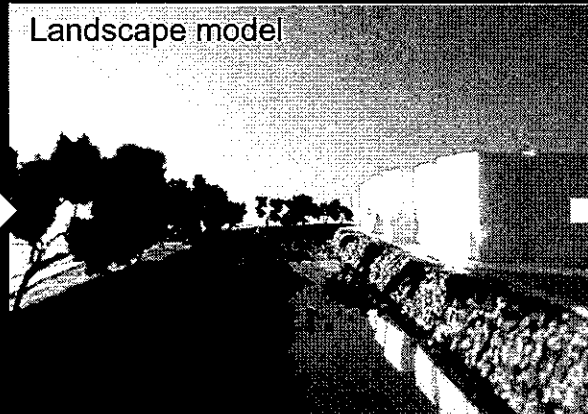


Before and after

Before restoration sep 2009



Landscape model



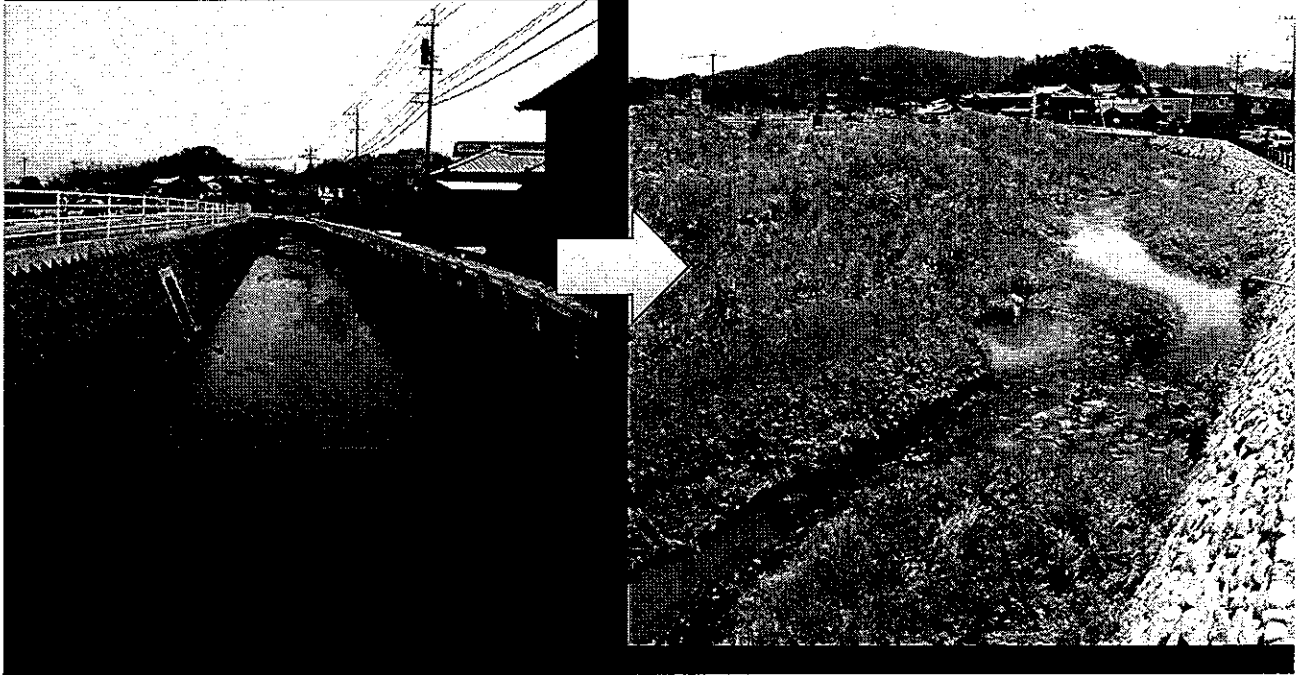
Just after restoration May 2010



About a year after restoration



Restoration work has been completed this year



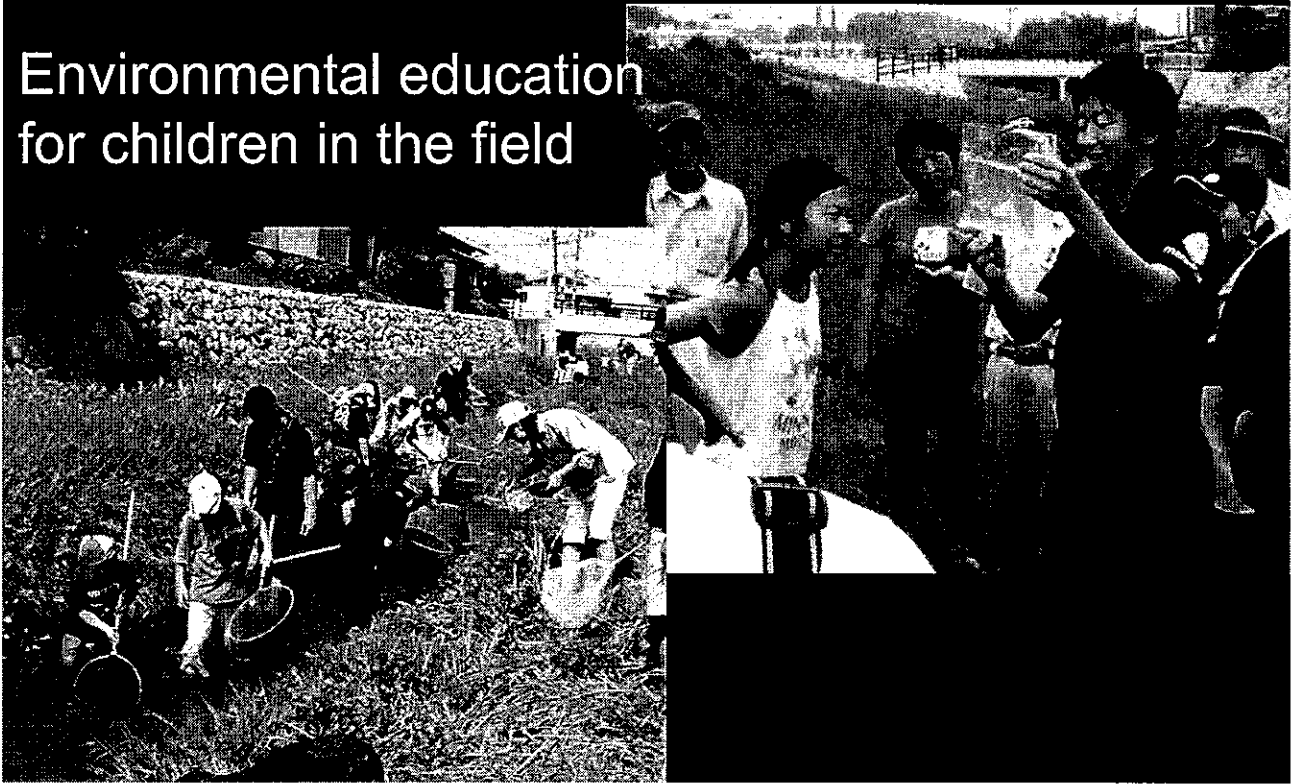
Recent activities



Fish sampling survey to evaluate the restoration works.

Recent activities

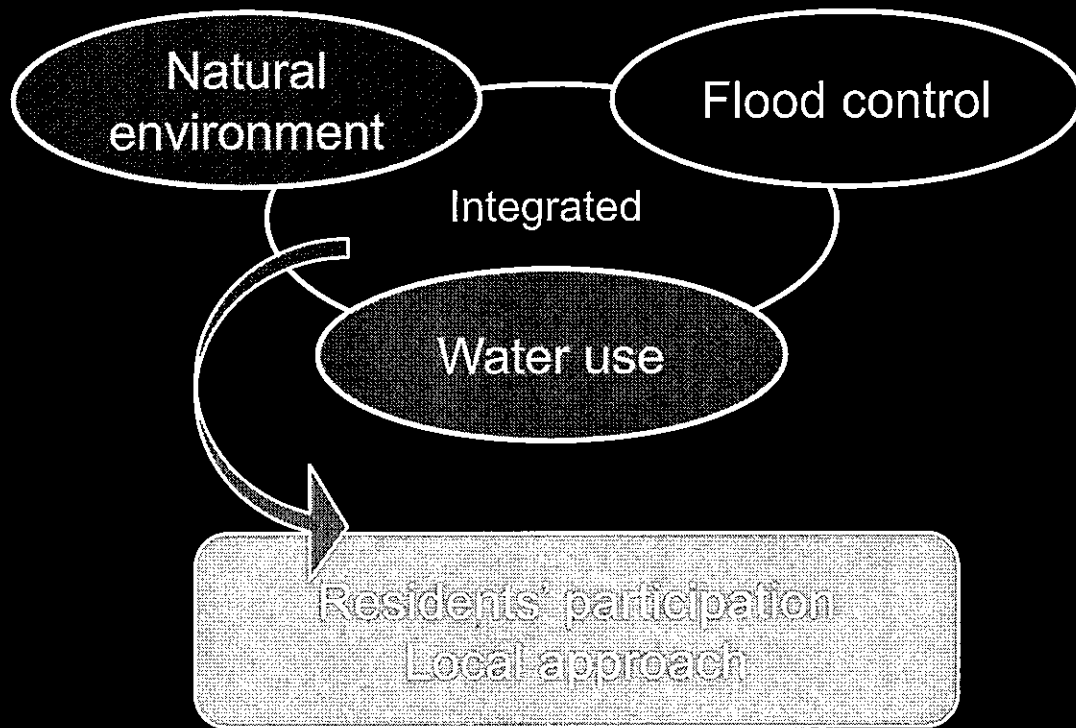
Environmental education
for children in the field



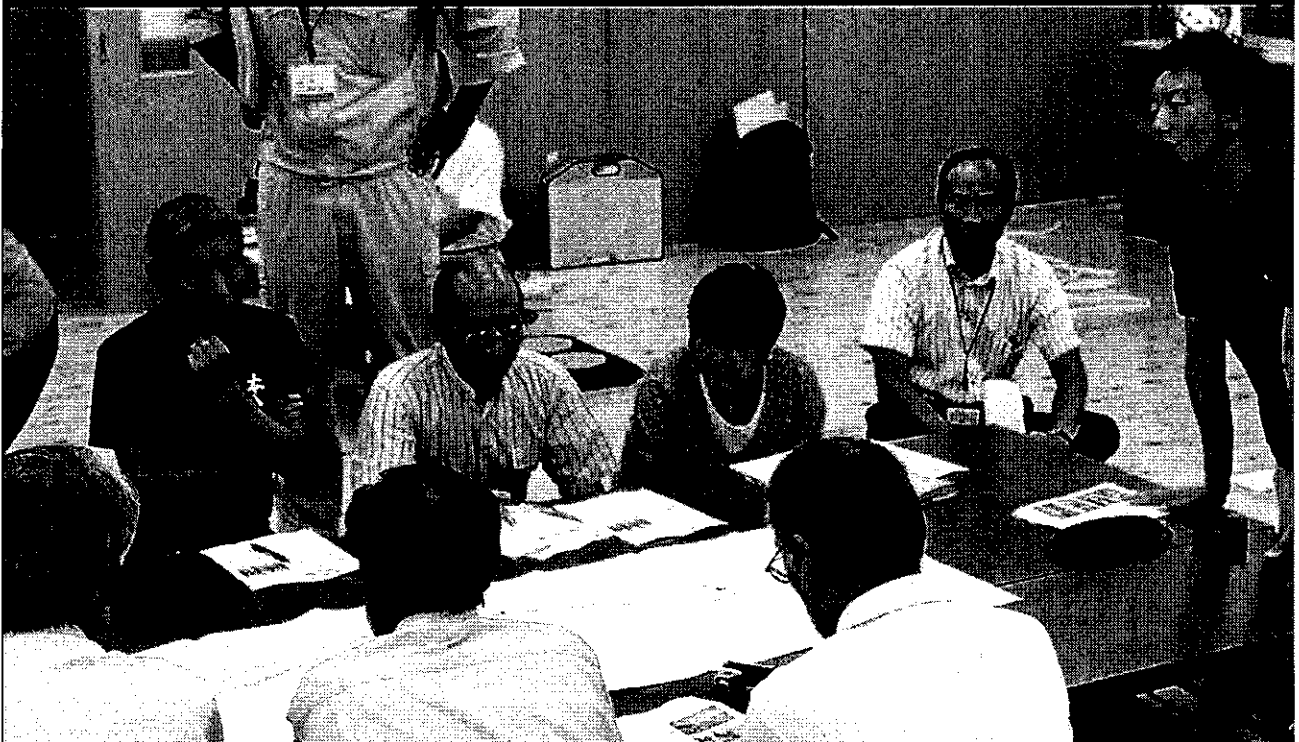
Recent scenery of Kamisaigo river



For sustainable river management



Workshop is still on going . . .





Thank you for your attention!

EVALUATING THE RIVER HEALTH OF PRE- AND POST-RESTORATION IN THE KAMISAIGO RIVER

Rita LOPA¹⁾ Yukihiko SHIMATANI²⁾

Department of Urban and Environmental Engineering, Kyushu University, Fukuoka, Japan

Introduction

Evaluation is important element of river restoration projects. Since 2009 the Kamisaigo River have been installed different types of restoration approaches: A) no meandering, B) artificial riffle and meandering, C) meandering, D) one meter sized rock and meandering which is constructed in 2010, E) one meter sized rock and meandering which is constructed in January 2011, and F) small weir and meandering.

To assess the health of the Kamisaigo River post-restoration successfully or not, an ecological indicator is needed to detect the changing environmental condition. The Fish Biological Health Index (FBHI) scores adequately represent characteristics of river health and used to determine which rivers (or segments of rivers) successful post-restoration.

This study shows how FBHI can be used to monitor and assess river restoration projects to improve future efforts.

Study site

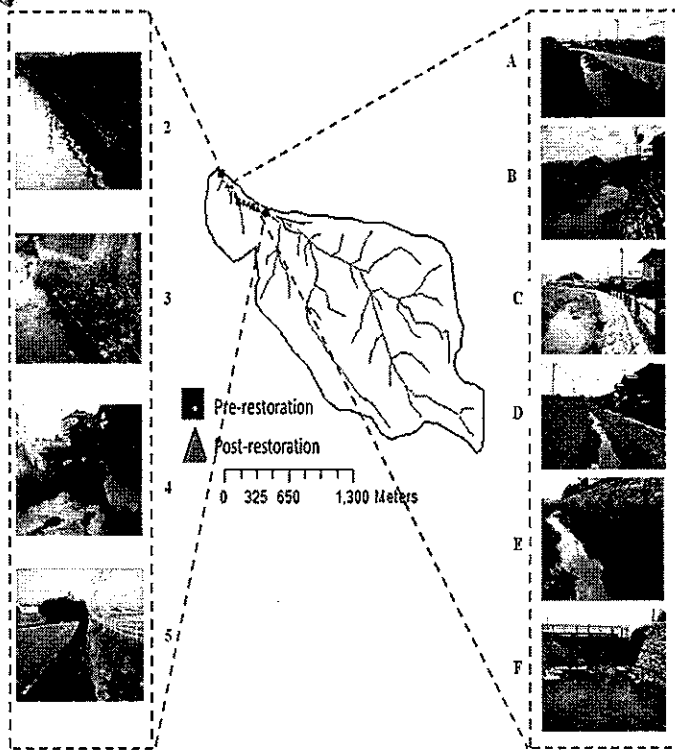


Fig. 1. The Kamisaigo Rivers condition pre- and post restoration

Methods

Monitoring designed

- Twelve sampling sites were designed to collect fish fauna data.
- ◆ October 26th until November 2nd in 2009 for pre-restoration data and
- ◆ November 21st – 30th in 2011 for post restoration data,

Formula

$$FBHI_j = 10 \times N_{ij} / N_j \quad (1)$$

where i is station number (1–6 or A–F), j is metric number (1–14), N_{ij} is the number of species in metric j at station i , and N_j is the number of species in metric j at all stations combined.

Results and Discussion

The Kamisaigo River pre-restoration contains 7 native fish species and no exotic species. Of the 7 native species, appropriate two-seventh (2 species: *Misgurnus anguillicaudatus*, and *Cobitis matsubarae*) are listed as threatened and data deficient in Japan (Environmental Agency of Japan, 1991).

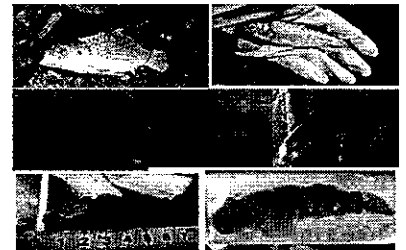


Fig. 4. Fish species in the Kamisaigo River pre-restoration

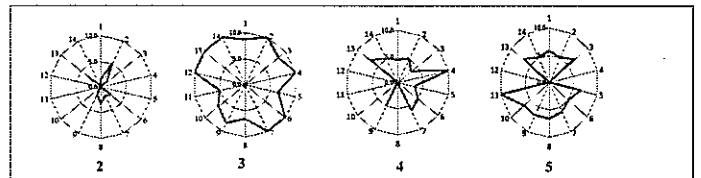


Fig. 5. Fish Biological Health Index pre-restoration

The Kamisaigo River post-restoration contains 11 native fish species and no exotic species. All of the species except *Cyprinus carpio* and *Zacco temmincki* are found on pre-restoration. Of the 11 native species, appropriate two-eleventh (2 species: *Misgurnus anguillicaudatus*, and *Cobitis matsubarae*) are listed as threatened and data deficient in Japan (Environmental Agency of Japan, 1991).

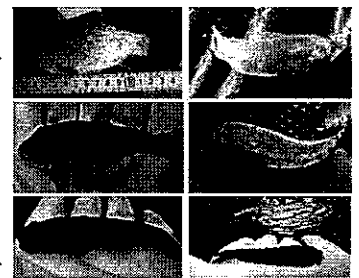


Fig. 6. Additional species post-restoration

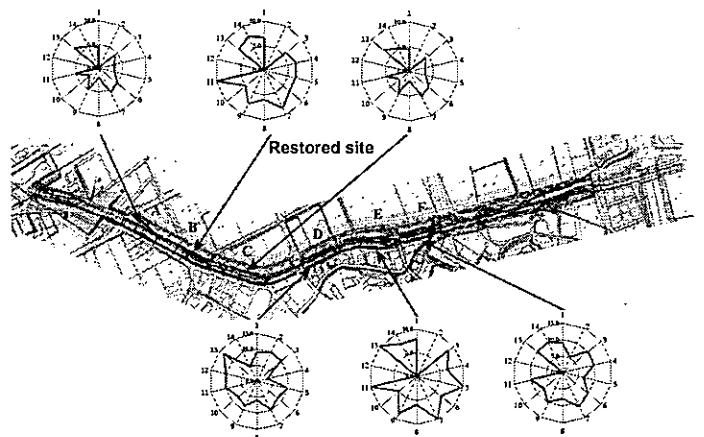


Fig. 7. Fish Biological Health Index post-restoration

Conclusion

- ◆ Compared to pre-restoration conditions, we observed that restoration improved river health improvements in fish diversity.
- ◆ The environmental quality of this river health post-restoration was range in moderate to good conditions in generally based on the FBHI.
- ◆ This study shows how FBHI can be used to monitor and assess river restoration projects to improve future efforts, so we need more research.

Evaluating the river health of pre and post-restoration in the Kamisaigo River

Rita Lopa¹, Yukihiro Shimatani²

*1,2. Department of Urban and Environmental Engineering,
Kyushu University. Japan.*

Abstract

Since 2009 the Kamisaigo River has been restored by the Fukutsu City Government to improve the environmental quality of the river. River restoration measures must be properly installed, monitored, and maintenance to be successful. To assess the health of the Kamisaigo River post-restoration successfully or not, an ecological indicator is needed to detect the changing environmental condition. The Fish Biological Health Index (FBHI) scores adequately represent characteristics of river health and used to determine which rivers (or segments of rivers) successful post-restoration. We calculated 14 regionally developed indices using the ecological features of fish towards several river sites, which included restored sites and control condition in control sites (un-restored sites) in nearby river. The results from several sampling stations indicated that the environmental quality of this river health post-restoration were range in moderate to good conditions in generally. This study shows how FBHI can be used to monitor and assess river restoration projects to improve future efforts.

Keywords: *fish biological health index, river health, restored site, control site.*

1 Introduction

Evaluation is important element of river restoration projects. Evaluating the success of river restoration projects is often limited. Palmer et al. (2005) attempted to define ecologically successful river restoration, and came up with five success criteria, which they called standards for ecologically successful river restoration. These standards include: 1) restoration design should be based on a template of a dynamic, healthy river that could exist at a given site, 2)

measurable ecological improvement, 3) self-sustaining systems resilient to external disturbances, 4) no lasting harm inflicted by the construction of a project, and 5) performance of pre- and post-assessment and public availability of that data.

One way to evaluate projects post-restoration is to compare them to control condition in control sites (un-restored sites) in some nearby rivers. Control site is defined as a sampling site or reach which is as similar as possible to the rehabilitated site in every way, except that it is not rehabilitated (Rutherford *et al.* 2000).

River health is taken to mean the degree of similarity to an un-impacted river of the same type, particularly in terms of its biological diversity and ecological functioning. In other words a healthy river is an un-impacted or pristine state river.

The Fish Biological Health Index (FBHI) is an index for the diversity that can be used to assess the health or condition of an area by counting and classifying some species based on ecological characteristics of fish behaviour and life history that exist in the region.

A new study of European river restoration projects has indicated that their impact on the physical characteristics of rivers depends on the region, river type and restoration approach. In recent years various river restoration projects have been planned or implemented in Japan. Since 2009 the Kamisaigo River has been restored the first and the second stage by the Fukutsu City Government to improve the environmental quality of the river. The first stage restoration involved installing approximately one meter sized rock. The second stage restoration involved installing artificial riffle, weir, and improvement of hydro morphological status by re-meander the river. The purpose of this study is to compare the rate of change every station between restored site and control site by applying FBHI. Our results will contribute to the development of river monitoring, and will enhance conservation efforts.

2 Study Area

Restored site and control site

Investigation were conducted in two sites: the Kamisaigo River as restored site, a small size tributary (second order, the north latitudes of 33°45'24.29 and 33°45'40.16 and east longitudes of 130°29'55.52 and 130°29'25.15) and the Sakura River as control site (second order, the north latitudes of 33°45'40.27 and 33°45'49.86 and east longitudes of 130°30'8.89 and 130°30'21.87)

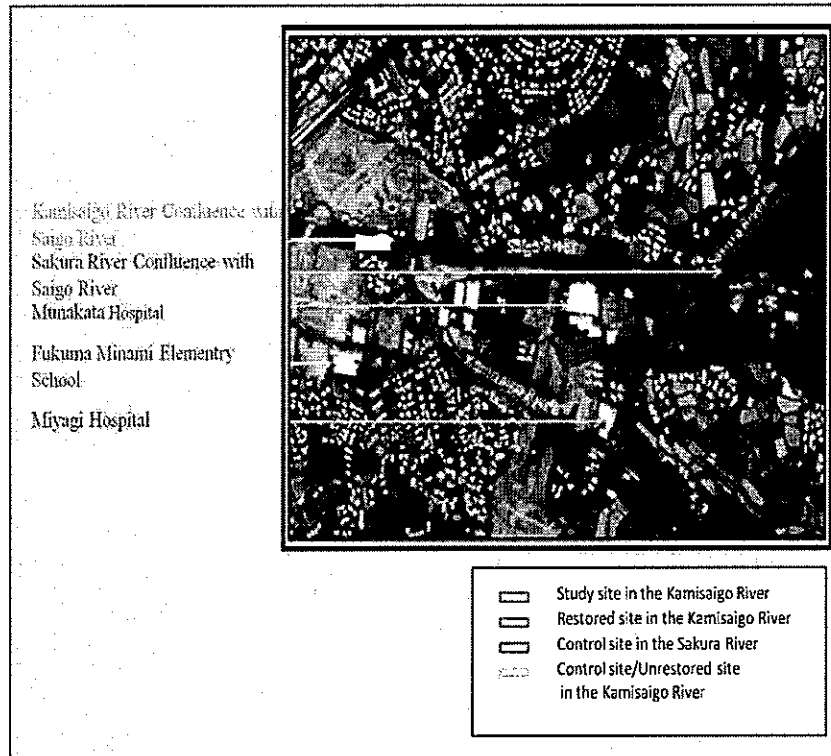


Figure 1. Restored site and control site in Fukuoka, Japan.

during Autumn in 2009 and Autumn in 2011. The restored site and the control sites located at Fukutsu City, in the north of Fukuoka Prefecture Japan, Figure 1.

The land of the city is bordered by mountains on the east and by the sea on the west. The climate and environment is warmed by Tsushima Ocean. Current, it is comparatively warm even in the winter. Total rainfall is approximately 1,500mm a year.

The Kamisaigo River have been restored for creating a more aesthetic natural river habitat, improving the general environment for aquatic organisms and children education, and fostering a strong connection between the local community and the river environment as same as this city's symbol which is corresponded to the basic philosophy of Fukutsu City, 'living in harmony with nature, a city of mutual support'.

Since 2009 the Kamisaigo River have been installed different types of restoration approaches: 1) no meandering, 2) artificial riffle and meandering, 3) meandering, 4) one meter sized rock and meandering which is constructed in 2010, 5) one meter sized rock and meandering which is constructed in January 2011, and 6) small weir and meandering, Figure 2.

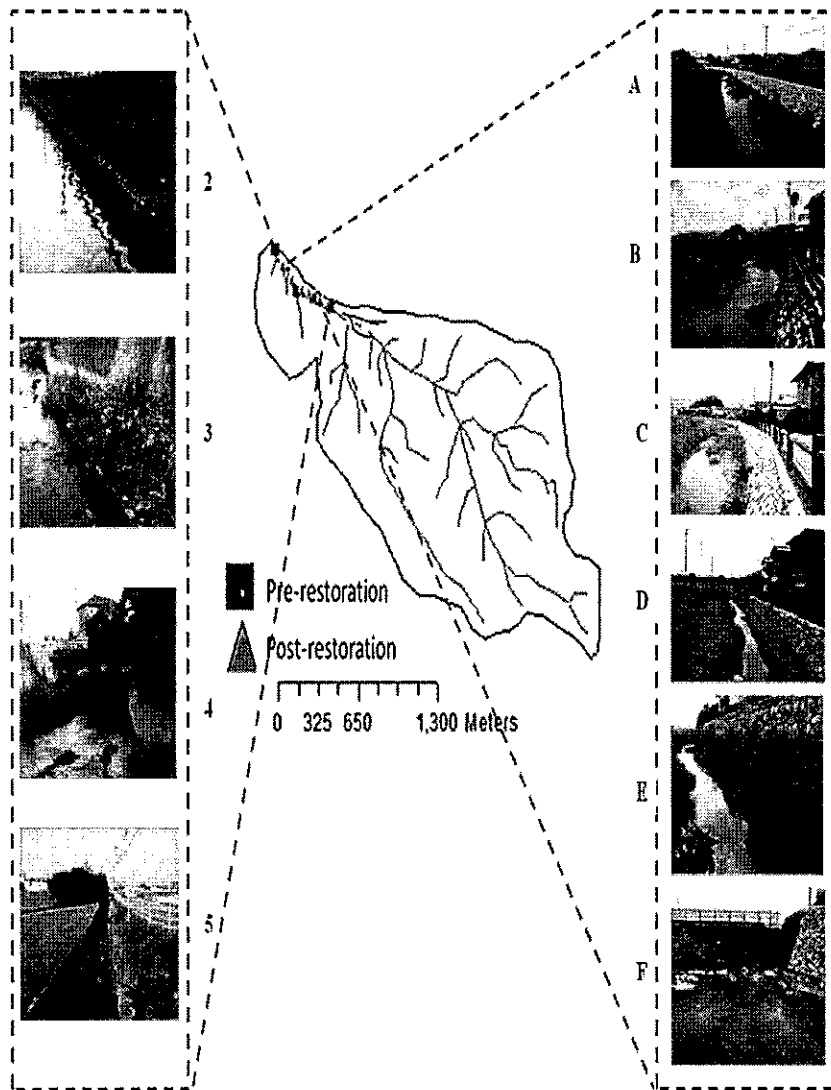


Figure 2. The Kamisaigo River condition pre- and post-restoration

3 Methods

In autumn (October-November) of 2009 and in autumn (November) of 2011, a comprehensive monitoring program was initiated at this site. This monitoring includes fisheries surveys, physical environmental survey, geomorphologic survey and physical biotope mapping/flow ecological mapping (geomorphologic features). Field survey measurements are required to examine actual site

conditions. These surveys will continuously conduct until January 2013. However, in this paper only the autumn data from fisheries surveys and flow ecological mapping will be utilized.

3.1 Fish surveys

Fish assemblages were sampled along the 600 m reach of the river using a backpack electro fisher (LR-20B Smith-Root, Vancouver, WA, USA). There are 10 stretches and we decided to divide every 50 m consist of three part of stretch. We were blocked with (seine) netting to ensure population enclosure. To maximize the capture of fish, we attempted to sample equally four river lines and a variety of habitat types. We associated the fish and the physical environment based on the flow ecology and line transects method (quadrant method). We used intermittent shocking when approaching structures such as downed trees, and patches of vegetation. The fish were measured (total number of fish, length, weight) and released alive.

3.2 Data analysis

The Fish Biological Health Index (FBHI) is an index for the diversity that used to assess the health or condition of these sites by counting and classifying some species based on ecological characteristics of fish behaviour and life history that exist in the region. The index was composed of the following 14 indicators based on ecological characteristics of fish behaviour and life history; (1) native species, (2) endangered species, (3) freshwater species, (4) diadromous species, (5) swimming species, (6) bottom-dwelling species, (7) species that live usually in flow areas, (8) species that live usually in calm areas, (9) mainstream species, (10) floodplain species, (11) species that spawn in aquatic vegetation, (12) species that spawn on muddy bottoms, (13) species that spawn on gravel bottoms, and (14) species that spawn on rocky bottoms. These metrics are typically evaluated with respect to criteria such as the environmental significance of the site and data availability. The fish species are listed and scored against criteria developed from high-quality historical data. To verify sampling efficacy, we compared our species list with lists developed by Kyushu University and, where available, those from previous fish collections.

The Fish Biological Health Index (FBHI) was calculated using the following equation:

$$FBHI_{ij} = 10 \times N_{kij} / N_{sj} \quad (1)$$

where i is station number (1–6), j is metric number (1–14), N_{kij} is the number of species in metric j at station i , and N_{sj} is the number of species in metric j at all stations combined.

The FBHI scores adequately represent characteristics of river health and used to determine which rivers (or segments of rivers) successful post-restoration. The overall FBHI was calculated in three steps: (1) each $FBHI_{ij}$ was calculated, (2) the mean of each metric was calculated ($\frac{\sum_{k=1}^6 FBHI_{kj}}{6}$), and (3) the $FBHI_j$ of each metric was averaged to give the $FBHI_{ij}$ of each station.

4 Results and Discussion

Fish species richness was assessed at several river sites, which included restored sites and control sites. *Zacco platypus* is very common fish in Kyushu Island. The Kamisaigo River pre-restoration contains 7 native fish species and no exotic species, Table 1. Of the 7 native species, appropriate two-seventh (2 species: *Misgurnus anguillicaudatus*, and *Cobitis matsubarae*) are listed as threatened and data deficient in Japan (Environmental Agency of Japan, 1991). The Kamisaigo River post-restoration contains 11 native fish species and no exotic species, Table 2. All of the species except *Cyprinus carpio* and *Zacco temmincki* are found on pre-restoration. Of the 11 native species, appropriate two-eleventh (2 species: *Misgurnus anguillicaudatus*, and *Cobitis matsubarae*) are listed as threatened and data deficient in Japan (Environmental Agency of Japan, 1991).

Table 1. Fish species collected from the Kamisaigo River pre-restoration

Species	Japanese name	Station 2	Station 3	Station 4	Station 5
<i>Cyprinus carpio</i>	koi				1
<i>Zacco platypus</i>	oikawa		24	62	11
<i>Zacco temmincki</i>	kawamutsu		2		
<i>Misgurnus anguillicaudatus</i>	dojou		3		
<i>Cobitis matsubarae</i>	yamatoshimadojou	31	6	4	28
<i>Odontobutis obscura</i>	donko		4		4
<i>Rhinogobius sp.CB</i>	shimayonobori		1	5	
Total species		1	6	3	4
Population		31	40	71	44

Table 2. Fish species collected from the Kamisaigo River post-restoration

Species	Japanese name	Station A	Station B	Station C	Station D	Station E	Station F
<i>Carassius auratus langsdorfi</i>	gimbuna		2		1	1	1
<i>Zacco platypus</i>	oikawa	1	325	566	332	215	174
<i>Phoxinus oxycephalus</i>	takahaya				1	2	
<i>Pseudogobio esocinus</i>	kamatsuka	3	11	6	28	93	49
<i>Misgurnus anguillicaudatus</i>	dojou				1		
<i>Cobitis matsubarae</i>	yamatoshimadojou				1		1
<i>Odontobutis obscura</i>	donko	20	21	15	26	27	12
<i>Gymnogobius petschiliensis</i>	sumiukigori		2				
<i>Gymnogobius urotaenia</i>	ukigori					1	4
<i>Rhinogobius sp.CB</i>	shimayonobori	1	3	2	14	38	113
<i>Rhinogobius sp.OR</i>	toyoshinobori						4
Total species		4	6	4	8	7	8
Population		25	364	589	404	377	358

According to Nakajima et al. (2010) the spawning ground and habitat condition could be considered as one of the factor in shaping the fish assemblage because by understanding the natural behaviour and fish life history, the distribution pattern of selected species can be predicted. Subsequently, we assess the species-richness component of diversity and the health of resident taxonomic groupings and habitat guilds of fishes by fish metrics, Table 3 and 4.

Table 3. Fish assemblage metric based on ecological characteristics of fish behaviour and life history in the Kamisaigo River pre-restoration

Species	Metric 1 native species	Metric 2 endangered	Metric 3 fresh water	Metric 4 diadromous fish	Metric 5 swimming bottom species	Metric 6 flow area	Metric 7 calm area	Metric 8 main stream	Metric 9 flood plain	Metric 10 aquatic vegetation	Metric 11 spawn in muddy bottom	Metric 12 spawn in gravel bottom	Metric 13 spawn in rock bottom	Metric 14
<i>Cyprinus carpio</i>	0		0		0		0	0	0	0				
<i>Zacco platypus</i>	0		0		0	0		0				0		
<i>Zacco temminckii</i>	0		0		0	0		0				0		
<i>Misgurnus anguillicaudatus</i>	0	0	0		0		0	0			0			
<i>Cobitis maculata</i>	0	0	0		0	0		0				0		
<i>Odonobutis obscura</i>	0		0		0	0	0	0	0	0				0
<i>Rhinogobius sp. CB</i>	0			0	0	0		0						0
Total	7	2	6	1	3	4	5	3	6	3	2	1	3	2

Table 4. Fish assemblage metric based on ecological characteristics of fish behaviour and life history in the Kamisaigo River post-restoration

Species	Metric 1 native species	Metric 2 endangered	Metric 3 fresh water	Metric 4 diadromous fish	Metric 5 swimming bottom species	Metric 6 flow area	Metric 7 calm area	Metric 8 main stream	Metric 9 flood plain	Metric 10 aquatic vegetation	Metric 11 spawn in muddy bottom	Metric 12 spawn in gravel bottom	Metric 13 spawn in rock bottom	Metric 14
<i>Carassius auratus longidorsis</i>	0		0		0		0	0	0	0				
<i>Zacco platypus</i>	0		0		0	0		0				0		
<i>Puntius carcephalus</i>	0		0		0	0		0				0		
<i>Pseudogobio esocinus</i>	0		0		0	0		0				0		
<i>Misgurnus anguillicaudatus</i>	0	0	0		0		0	0			0			
<i>Cobitis maculata</i>	0	0	0		0	0		0				0		
<i>Odonobutis obscura</i>	0		0		0	0	0	0	0	0				0
<i>Gymnogobius pseudohieris</i>	0			0	0	0	0	0						0
<i>Gymnogobius unicolor</i>	0		0	0	0	0	0	0						0
<i>Rhinogobius sp. CB</i>	0			0	0	0		0						0
<i>Rhinogobius sp. OR</i>	0		0	0	0	0	0	0	0					0
Total	11	2	9	4	3	8	10	6	10	4	2	1	4	5

From the FBHI results, the pre-restoration/un-restored site which is station 3 has recorded the highest FBHI value while station 2 has recorded the lowest FBHI results, Figure 3. It was suggested that the high FBHI value at station 3 is associated with variety in ecological flow (42% runs and glide, 42% slack shallow and 16% scour pools), and some vegetation were present. It was observed that the variety of habitat condition such as a run, glide and pool could contribute in shaping the fish composition in this area. This condition was suggested as the best condition for fish species to live because it provided various kinds of velocity and depth magnitude (Kehmier et al. 2007) and the species richness was high at locations with greater vegetation cover and preserved riparian forest (Cetra & Petrere, 2007).

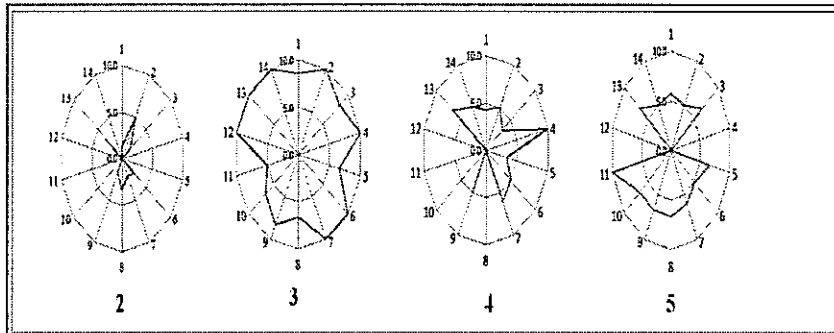


Figure 3. Fish Biological Health Index pre-restoration

On the other hand, low FBHI value at Station 2 was associated with the entirely of slow-current shallow habitats (slacks or shallows) with uniform conditions. Overhanging vegetation, root wads, and aquatic vegetation were absent. The low percentage of vegetation has led to decreases of insectivore and herbivores species because the food chain for these species was disturbed and loss. At the same time, it also affected the species that depended on the vegetation to spawn, because there are no places to lays and attached their eggs.

Meanwhile the post-restoration/restored site which is station D has recorded the highest FBHI value while station A and C have recorded the lowest FBHI results, Figure 4 and Table 5. It was suggested that the high FBHI value at station D is associated with one meter sized rock and meandering which is restored two years ago. At this reach river, a formerly straightened reach (100 m long) was re-meandered in 2010 as the first stage restoration in the Kamisaigo River and was consisted of runs with spaced pools and presents low water turbidity. Aquatic vegetation is restricted to a narrow belt and domestic sewage is present at low levels. It was observed that the one meter size rock can break fast-moving currents and provide a resting area for fish, because fish can hold behind it.

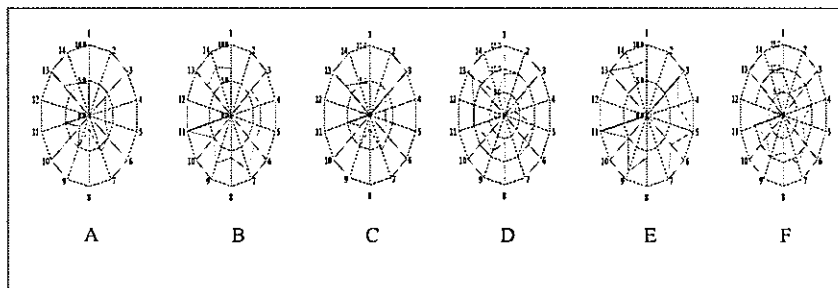


Figure 4. Fish Biological Health Index post-restoration

Some studies have shown the importance of big rock and meandering channels for fish populations. Common examples of habitat enhancement are the placement of materials, such as large pieces of wood or boulders into the stream channel, or manipulation of the channel itself to improve habitat for fish and/or other aquatic organisms. Boulder clusters were one of the more effective techniques. Successful stream restructuring in Oregon was reported by Armantrout (1991), with boulder structures proving most durable (Bruce R. Ward, 1997). Meanwhile, the report "Final Biological Assessment and Evaluation for East Fork Indian Creek Stream Restoration Project" made by Tom Biebighauser (2009) has suggested that constructed in-stream features using large woody debris and rock would improve bank stability and create aquatic habitat. Fukushima (2001) demonstrated that spawning habitats of Sakhalin taimen (*Hucho perryi*) were closely associated with meandering channels in small streams. Nicol et al. (2004) reported that fish abundances were higher in tightly curving meander bends than in gently curving meander bends in a large Australian river, the Murray River. Thus, by combining between installing one meter sizes rock and meandering in the Kamisaigo River have proved that it was the best technique approaches to improve the fish fauna.

Despite station C was associated with meandering, it was recorded as low FBHI. In this reach, the river was consisting of variety in ecological flow (pools 10%, runs 25%, glides 55% and slow-current shallow habitats (slacks or shallows) 10%. Unfortunately, it was observed that meandering could not affect the fish composition in this area. Likewise, station A was associated with no meandering; it was recorded as low FBHI. In this reach, the river was consisting of variety in ecological flow (runs 30%, glides 35% and slow-current shallow habitats (slacks or shallows) 35%. These designs perhaps have inappropriate. It should be considered further for revision with another design or still need time for monitoring, because this is the monitoring data that are not quite a year early post-restoration.

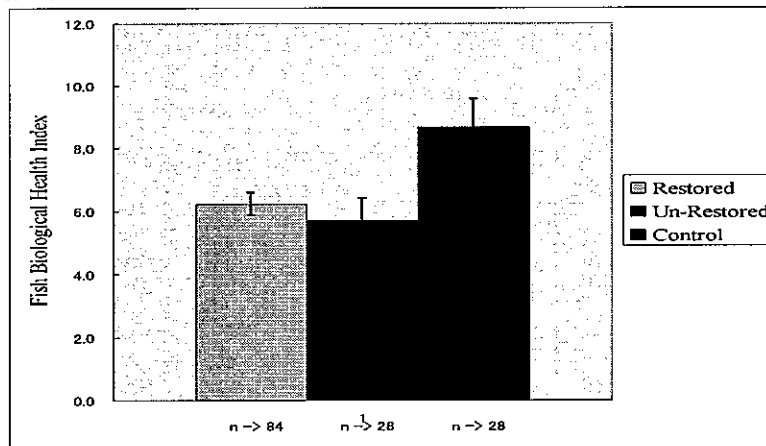


Figure 5. Fish Biological Health Index Comparison

Table 5. Analysis result of the metric of Fish Biological Health Index which was verified with those developed by Kyushu University

Metric	Indicator	Restored sites						Control Sites			
		Station A	Station B	Station C	Station D	Station E	Station F	Un-restored Ct-A	Un-restored Ct-B	Station Ct-C	Station Ct-D
Metric 1	native species	4.4	6.7	4.4	8.9	7.8	8.9	5.6	6.7	7.8	7.8
Metric 2	endangered	0.0	0.0	0.0	10.0	0.0	5.0	5.0	5.0	10.0	10.0
Metric 3	freshwater	4.3	5.7	4.3	10.0	8.6	10.0	7.1	7.1	10.0	10.0
Metric 4	diadromous species	3.3	6.7	3.3	3.3	6.7	10.0	0.0	6.7	0.0	3.3
Metric 5	swimming	3.3	6.7	3.3	10.0	10.0	6.7	13.3	10.0	16.7	16.7
Metric 6	bottom species	5.0	6.7	5.0	8.3	6.7	10.0	1.7	5.0	3.3	5.0
Metric 7	flow area	5.7	8.6	5.7	10.0	10.0	11.4	4.3	7.1	7.1	7.1
Metric 8	calm area	2.0	6.0	2.0	6.0	6.0	8.0	6.0	4.0	8.0	10.0
Metric 9	main stream	5.0	7.5	5.0	8.8	8.8	10.0	6.3	7.5	7.5	7.5
Metric 10	floodplain	2.5	5.0	2.5	7.5	5.0	7.5	7.5	2.5	10.0	12.5
Metric 11	spawning plant raw	5.0	10.0	5.0	10.0	10.0	10.0	15.0	5.0	20.0	15.0
Metric 12	spawning muddy bottom	0.0	0.0	0.0	10.0	0.0	0.0	0.0	0.0	0.0	10.0
Metric 13	spawning gravel bottom	6.7	6.7	6.7	13.3	10.0	10.0	6.7	10.0	10.0	10.0
Metric 14	spawning rock bottom	5.0	7.5	5.0	5.0	7.5	10.0	0.0	5.0	2.5	5.0

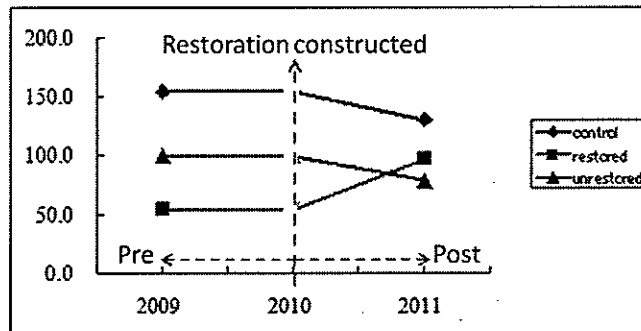


Figure 6. Graph of river health (pre-post restoration) based on FBHI

The analysis results performed that restoration improve fish diversity in the Kamisaigo River, Figure 5 and 6. Eleventh introduced species were identified, representing more than 50% of the increasing native and threatened species. This study showed that fish assemblage metric based on ecological characteristics of fish behaviour and life history was most accurate in predicting the river health.

5 Conclusion

The environmental quality of this river health post-restoration was range in moderate to good conditions in generally based on the FBHI. For pre-restoration condition, the highest FBHI values were recorded in station 3 and the lowest FBHI values were recorded in station 2. Meanwhile for post-restoration condition, the highest FBHI values was recorded in station D which is characterized by one meter sizes rock and meandering, the lowest FBHI values was recorded in station A which is characterized by no meandering. Compared that restoration improved river health improvements in fish diversity. This study shows how FBHI can be used to monitor and assess river restoration projects to improve future efforts, so we need more research. Future studies should examine more closely the ecological flow of this river. Monitoring and adaptive management should support overall success of this project.

6 Acknowledgements

We thank River Restoration Centre for giving us the opportunity to write this opinion paper. This work was presented at the April 19th 2012 River Restoration Centre 13th Annual Network Conference in Nottingham University, England. This work was supported by a grant from the Japan Bank International Corporation and the Watershed Management Laboratory, Department of Urban and Environmental Engineering, Kyushu University.

7 References

- [1] Bruce R. Ward, Using Boulder Clusters to Rehabilitate Juvenile Salmonid Habitat, Watershed Restoration Technical Circular No. 9: 10-1-10-10 Ministry of Environment, Lands and Parks, Vancouver, 1997.
- [2] Cetra, M and Petre, J.R., M, Associations between fish assemblage and riparian vegetation in the Corumbataí River Basin (SP) Journal of Biology,

67(2): 191-195, 2007.

[3] J.L. Pretty, S.S.C. Harrison, D.J. Shepherd, C. Smith, A.G. Hildrew and R.D. Hey, River rehabilitation and fish population: assessing the benefit of instream structures, *Journal of Applied Ecology*, 40: 251-265, 2003.

[4] Jun Nakajima, Yukihiro Shimatani, Rei Itsukushima and Norio Onikura, Assessing riverine environments for biological integrity on the basis of ecological features of fish, *Advanced in river engineering*, Vol.16, p.449-454, 2010.

[5] M.A. Palmer, E.S. Bernhardt, J.D. Allan, P.S. Lake, G. Alexander, S. Brooks, J. Carr, S. Clayton, C.N. Dahm, Standard for ecologically successful restoration, *Journal of Applied Ecology*, 42 : 208-217, 2005.

[6] Michio Fukushima, Salmonid Habitat- Geomorphology Relationships in Low-Gradient Streams, *Ecology*, 82(5) :1238-1246, 2001.

[7] Rita Lopa, Yukihiro Shimatani, Hironori Hayashi and Jun Nakajima, Applying a fish biological integrity index for restoration plan in small sized river: a case study in the Kamisaigo River, *Water Resources Management*, Vol.VI, p.113-124, 2011.

[8] Rutherford I, Jerie K and Marsh N, A rehabilitation manual for Australian Streams, Volume 2, Cooperative Research Centre for Catchment

[9] Simon J Nicol, Jason A Lieschke, Jarod P Lyon, and John D. Koehn, Observation on the distribution and abundance of carp and native fish, and their responses to a habitat restoration trial in the Murray River, Australia *New Zealand Journal of Marine and Freshwater Research*, 38: 541-551, 2004.

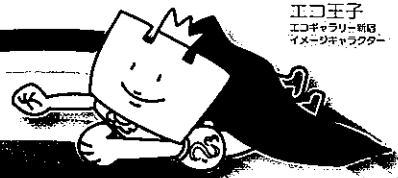
[10] Tom Biebighauser, Final Biological Assessment and Evaluation for East Fork Indian Creek Stream Restoration Project, USDA Forest Service Southern Region, 2009.



平成28年度 新宿区「環境絵画展」

エコ王子
エコギャラリー新宿
イメージキャラクター

こども環境絵画 コンテスト



作品
テーマ

環境問題や環境保全、新宿区の理想的な環境

をテーマに、環境絵画を募集します！

応募資格

新宿区在住・在学の小・中学生と家族の方（※ただし、ファミリーの部は未就学児も応募可能）

区長賞

全作品から1点

賞状と副賞（図書カード）

金賞

各区分ごとに1点

賞状と副賞（図書カード）

銀賞

各区分ごとに1点

賞状と副賞（図書カード）

銅賞

各区分ごとに2点

賞状と副賞（図書カード）

努力賞

各区分ごとに若干数

賞状

◆昨年度の受賞作品

平成27年度は、計412点ものご応募をいただきました。その中で、審査会を経て30点が受賞しました。

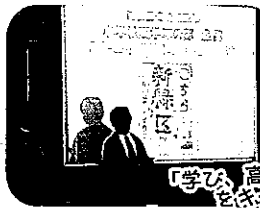


▲平成27年度 新宿区「環境絵画展」
区長賞 佐藤 一真（西新宿中学校1年）

8月29日(月)
応募締切!

応募者全員に
素敵な参加賞を
プレゼント!

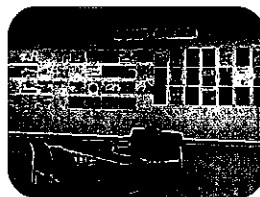
◆昨年度『新宿こども環境シンポジウム』（表彰式）の様子



「学び、高め、広げようエコの環」をテーマに、受賞者が集まり発表が表彰式となりました。

◆応募・受賞作品の活用（展示発表）

ご応募いただいた全作品は、エコギャラリー新宿で開催される『新宿区環境絵画・環境日記展2016』で展示させていただきます。また、昨年度は受賞作品を新宿パークタワーや損保ジャパン日本興亜本社ビルでの巡回展示も行ない、多くの方に見ていただきました。さらに、新宿区が発行するカレンダー『平成29年 新宿区エコ・チェックダイアリー』に掲載される予定です。



▲『新宿区環境絵画・環境日記展2015』



▲新宿パークタワーでの展示



▲損保ジャパン日本興亜本社ビルでの展示

2016年10月
新宿区エコ・チェックダイアリー
『新宿区エコ・チェックダイアリー』
にも受賞作品が掲載されます!

【お問い合わせ・応募先】

エコギャラリー新宿（新宿区立環境学習情報センター・新宿区立区民ギャラリー）【担当：加藤】

〒160-0023 新宿区西新宿2-11-4 新宿中央公園内 / TEL：03-3348-6277 / E-mail：info@shinjuku-ecocenter.jp

【主催】新宿区、NPO 法人新宿環境活動ネット 【協賛】東京ガス株式会社 中央支店

※このチラシは、再生紙を使用しています。

新宿の花・みどりいっぱい 写真を募集しています



平成28年12月15日から1ヶ月間、新宿区立区民ギャラリーで開催する
「新宿の花・みどりいっぱい写真展」に展示します

応募要項:

- ①応募作品: 1. 我が家の花・みどりを題材としたもの、2. 我が家のみどりのカーテンを題材としたもの(みどりのカーテンプロジェクト報告書に使用した写真でも可)、3. 街や公園で見かけた花・みどりを題材としたもので、いずれも平成27年以降に新宿区内で撮影された写真
※単に花や植物のクローズアップではなく、花・みどりがある風景としての写真を募集します
- ②作品サイズ: 2L以上A4サイズ程度のプリントとします(組み写真可、写真データでの応募は不可)
- ③募集期間: 平成28年10月15日(土)から11月15日(火)
- ④提出方法: 作品に応募票を添えて期限内に郵送が直接持ち込みしてください。
- ⑤応募資格: 新宿区に在住・在学・在勤の方
- ⑥肖像権等: 第三者の承諾が必要な場合は、応募者の責任において承諾を得てください
- ⑦著作権等: 応募作品の著作権者は撮影者となりますが、使用権は主催者が有し写真展のほか、広報・啓発などに使用する場合があります。尚、応募作品の返却はいたしません
- ⑧写真展: 平成28年12月15日(木)から29年1月15日(日)年末年始を除く
- ⑨表彰: 優秀作品(若干名)を新宿エコウィングランナーで表彰します

提出先: 〒160-0023 東京都新宿区西新宿2-11-4 (新宿中央公園内)
新宿区立環境学習情報センター 新宿の花・みどりいっぱい写真展係
電話: 03-3348-6277 FAX: 03-3344-4434

この印刷物は再生紙を使用しています

切り取り線

新宿の花・みどりいっぱい写真展

応募票

※印の項目は必須です

フリガナ		年齢	歳	性別	男・女
氏名 ※					
住所 ※	(〒 -)				
連絡先	TEL ※	e-mail		@	
撮影場所 ※		撮影日 ※	平成	年	月
注1: 応募者は、応募時点で本応募要項に記載する条件に同意したものとします。 注2: 被写体の肖像権等には充分ご注意ください、承諾を得てから応募してください。 ※但し、人物が小さく写っているなど顔が特定できないものは承諾なしで結構です。					
本人の承諾の有無 有り 無し (どちらかに○を付けてください。)					
作品タイトル ※					
メッセージ ※	以下に「作品に添えるメッセージ」をお願いします。 (150字程度)				

- ◎複数作品応募の場合は応募票をコピーしてお使いください。なお応募票はホームページからもダウンロードできます
- ◎ご応募の際、写真の裏面にも必ず「お名前」「タイトル」をご記入ください。サインペンなど筆先の柔らかいものをご使用ください

